Petrogenesis of mineralized horizons in the Offset and Creek zones, Lac des Iles Complex, N. Ontario

Justin Jonsson

A thesis submitted in partial fulfillment of the requirements for the Degree of Master of Science (Geology)

Lakehead University, Thunder Bay, Ontario

April 2023

Abstract

The Lac des Iles Complex is a Neoarchean polyphase mafic-ultramafic complex located in the Marmion terrane of the Superior Province, 85 km north of Thunder Bay, Ontario, Canada. The intrusive complex can be subdivided into two discrete subcomplexes: the ultramafic-dominated North Lac des Iles Complex and the mafic-dominated South Lac des Iles Complex (SLDIC). The SLDIC has been subdivided into the gabbronorite, breccia, norite, and diorite domains. To date, economic Pd-rich mineralization has been discovered in both the breccia and norite domains and occurs proximal to the contacts between the breccia and gabbronorite domains and between the breccia and norite domains. The objectives of this study were to i) evaluate the mechanisms of formation of the mineralized horizons near the contact between the breccia and norite domains in the Offset and Creek zones of the SLDIC, and ii) assess the tectonic setting in which the SLDIC formed.

The breccia and norite domains are both composed of varitextured, brecciated, and equigranular leucocratic to melanocratic norites and gabbronorites, and their altered equivalents. The breccia domain contains a greater proportion of brecciated and varitextured rocks, whereas the norite domain contains a greater proportion of equigranular rocks. All pre-alteration lithologies are essentially plagioclase-orthopyroxene cumulates with minor quantities of interstitial clinopyroxene, biotite, magnetite, chalcopyrite, pentlandite, and pyrrhotite. Variable degrees of hydrothermal alteration are indicated by the presence of tremolite-actinolite and talc (after pyroxene), chlorite and white mica (after plagioclase), and pyrite (after pyrrhotite). Although the breccia and norite domains are mineralogically similar, the breccia domain is generally more leucocratic (i.e., higher plagioclase/pyroxene ratio) than the norite domain.

Neodymium isotopic evidence indicates that the Offset and Creek Zone magmas were crustally contaminated. ε_{Nd} values of 19 analyzed samples range from +0.38 to -3.47 (median = -2.13), which is consistently more negative than the ε_{Nd} value of +2.24 expected in an uncontaminated mantle-derived magma that crystallized at ~2.7 Ga. The crustal contaminant that imparted the negative ε_{Nd} values is unlikely to be the tonalitic gneiss that hosts the SLDIC, given that the ε_{Nd} value of the one reported tonalitic gneiss sample is -1.77. The lack of correlation between ε_{Nd} and geochemical or spatial variations suggests that crustal contamination was not the cause of the geochemical variability observed within the Offset and Creek Zones. Samples from both the breccia and norite domains have similar trace-element chemistry, including enriched LILE/LREE patterns, flat HREE patterns, and pronounced negative Nb anomalies. Although these characteristics can be caused by assimilation of crustal material,

it appears more likely that they are the result the melting of a depleted mantle source in a magmatic arc. Evidence for this includes low Nb/Yb ratios, high Ba/Th ratios, low Th content, and the lack of correlation between geochemical variability and Nd isotopic variability.

Evidence from S isotopes of sulfide minerals and whole-rock geochemistry suggests that the addition of crustal S was not necessary in the formation of the Pd-rich mineralization within the Offset and Creek zones. $\delta^{34}S$ values of 54 sulfide crystals from 17 samples range from -0.37‰ to +3.28‰ VCDT (median = +1.11‰), with values from 52 of 54 crystals falling in the expected range of mantle-derived sulfur (0 ± 2‰). Based on the association of low Cu/Pd and S/Se ratios with high Pd values, Offset and Creek zone ores formed at high R factors, which were likely high enough to cause the PGE enrichment without incorporation of crustal sulfur. The greater quantity of Pd-enriched sulfide mineralization in the Offset Zone compared to the Creek Zone appears to have been due to a greater amount of sulfide liquid in the Offset Zone that also underwent higher R factors, and the distribution of sulfide liquid and magma flow in the SLDIC was likely influenced by primary structural constraints on the geometry of the intrusion. No evidence was found for significant remobilization of sulfide minerals or chalcophile elements, including the PGEs.

The spatial relationship of the breccia and norite domains of the SLDIC is consistent with a single parent magma that separated via flow differentiation into a more melanocratic, orthopyroxene-rich core (norite domain) and a more leucocratic, plagioclase-rich rim (breccia domain). After the breccia and norite domains had partially crystallized, later magma pulses then intruded into the intrusive complex, equilibrating with the partially crystallized rocks and imparting geochemical heterogeneity but not brecciation. At the latest stages of crystallization, when the breccia and norite domains were nearly and/or completely solidified, additional magma pulses largely confined to the breccia domain were emplaced near the major feeder structures (Shelby Lake structure and to a lesser extent, the Roby Central structure) and imparted varitextured and brecciated textures.

The major, early magma pulse that formed the breccia and norite domains was likely sulfur-saturated, but did not carry a large quantity of sulfide and was therefore not the main source of mineralization. The proximity of brecciation and mineralization to the major feeder structures suggests that the latest-stage magmas remobilized sulfides from depth into their present-day orientation near the breccia-norite domain boundary, primarily into the breccia domain. Heat from these late magma pulses resulted in the portion of the norite domain closest to the domain boundary to crystallize at a late stage, resulting in gravitational settling of sulfide liquid through the domain boundary and into the portion of the norite domain proximal to the contact.

Acknowledgments

First and foremost, thank you to Dr. Peter Hollings for his patience and guidance throughout the process of completing this project. The encouragement, constructive criticism, and commitment to helping me accomplish my goals were invaluable.

I would like to thank Dr. Lionnel Djon and Impala Canada for the conception of this research project and for the project funding. Thanks go out to Dr. Djon and the entire team at the Lac des Iles mine for access to the mine site, drill core, pulps and rejects, and cutting facilities that were necessary for undertaking my work.

Thank you to Dr. Matthew Brzozowski and Dr. Wyatt Bain for their assistance in interpreting my data and helping to scrutinize my conclusions. Thank you to Kristi Tavener and Dr. Jonas Valiunas for preparing the excellent thin sections and sulfur isotope sample blocks. Thank you to Dr. Laure Martin at the University of Western Australia for conducting the sulfur isotope analyses, and to Dr. Dominique Weis at the University of British Columbia for conducting the neodymium isotope analyses.

This study was funded by Lakehead University, Impala Canada, and a National Sciences and Engineering Research Council (NSERC) Collaborative Research and Development Grant. Additional support was provided by the Society of Economic Geologists Canada Foundation and the Bernie Schnieders Memorial Scholarship Fund. Thank you to all who were involved in providing financial support to this project.

Thank you to all of my colleagues at the Resident Geologist Program of the Ontario Geological Survey for supporting me through the process of finishing this project. Special thanks in this regard go out to Robert Cundari, Mark Puumala, and Dorothy Campbell.

Thank you to all the faculty and fellow students in the Lakehead University Department of Geology for fostering such a great environment to learn and work in. Special thanks to the great friends I've made in the department for humouring the impromptu geology discussions and venting sessions, most notably Tianna Groeneveld, Jordan Peterzon, Vicky Currie, Spencer Killins, and Sergio Bautista. You guys are the best.

Last but not least, thank you to my family for the unwavering support. Thank you to my parents for always having something insightful to offer, regardless of if the phone call home was for good news or to complain about my research problems. Thank you to my siblings Braden and Haley for being such good friends, providing good distractions and a reason to always look forward to the visits home.

Table of Contents

List of Figures

List of Tables

Chapter 1 – Introduction

The Lac des Iles Complex is a Neoarchean (2.689 Ga; D.W. Davis cited in Stone et al., 2003) polyphase intrusive body comprising two discrete intrusive complexes, the ultramafic-dominated North Lac des Iles Complex and the mafic-dominated South Lac des Iles Complex (SLDIC). The SLDIC has been subdivided into four separate lithological domains, known as the gabbronorite, breccia, norite, and diorite domains (Decharte et al., 2018). The SLDIC is host to several zones of PGE-rich magmatic sulfide mineralization, generally hosted within – 10-200 m thick, steeply dipping zones of <5% sulfide that occur in proximity to the contact between certain lithological domains, namely at the breccia-gabbronorite and breccia-norite domain boundaries. The largest of these are the Roby and Offset Zones which, when including satellite zones to the Offset Zone, comprise all of the economic mineralization within the Lac des Iles Complex (2022 Mineral Reserves: 40.4 Mt @ 1.90 g/t Pd, 0.18 g/t Pt, 0.14 g/t Au, 0.06% Ni, 0.06% Cu; Impala Platinum Holdings Limited, 2022).

The general processes by which nickel-copper-platinum group element (PGE)-enriched sulfide systems form are relatively well understood; a sulfide liquid separates from a silicate magma, is enriched in metals via interaction with the silicate magma and crystallizes in a relatively small and concentrated area (Naldrett, 1999). Systems valued dominantly for PGE content are less common than those primarily valued for Ni and Cu, and commonly occur as sulfide-poor, stratiform, reef-style horizons within layered igneous complexes (Naldrett, 2010). The deposits within the SLDIC are sulfide-poor and spatially associated with the lithological contact between cumulate mafic igneous units; however, they differ from most PGE-enriched

systems in a number of ways. For example, they are steeply dipping, irregularly distributed, commonly associated with magmatic brecciation, and strongly enriched in Pd relative to other PGEs. Different deposits show diverging geochemical trends, including S/Se and Cu/Pd ratios, suggesting that different parts of the intrusive complex may have undergone different magmatic and/or post-magmatic processes. In addition, a majority of global Ni-Cu-PGE-mineralized systems are derived from mantle plume-associated magmatism occurring with rift settings and cratonic margins (Naldrett, 2004). A minority of Ni-Cu-PGE deposits are interpreted to have formed in continental arc settings, including the Aguablanca (Tornos et al., 2006), Selebi-Phikwe (Maier et al., 2007), and Sally Malay (Sproule et al., 1999) deposits. Several past studies have suggested that the Lac des Iles Complex formed within a continental arc setting (Brugmann et al., 1997; Barnes and Gomwe, 2010; Djon et al., 2018), whereas other authors have interpreted a mantle plume settling (Hinchey et al., 2005).

Early open-pit and underground mining were focused on the Roby and northern/central portions of the Offset Zone, which are hosted entirely within the breccia domain near the contact with the unmineralized gabbronorite domain. Underground development and mining of the southern Offset Zone in the last ~10 years has resulted in recognition of significant economic mineralization at the breccia-norite domain boundary. The location of other mineralized zones within the SLDIC at the breccia-norite domain boundary (e.g., North VT Rim, Creek Zones) has raised questions as to the petrogenesis of these mineralized zones (e.g., Decharte et al., 2018; Djon et al., 2018). This study focused on the southern Offset Zone and the Creek Zone as type examples of this mineralization setting within the SLDIC.

Despite continued exploration and academic research, developing a comprehensive deposit model for Lac des Iles has been challenging. Uncertainty remains regarding the source of the magma, the source of the sulfur within the system, and the physical processes by which PGE enrichment and sulfide distribution occurred. This study focused on addressing two major questions:

1) What are the petrogenetic processes responsible for the formation of the breccia and norite domains of the South Lac des Iles Complex and the presence of PGE-rich magmatic sulfide mineralization proximal to the breccia-norite domain contact?
2) What are the tectonic processes that influenced the genesis and evolution of the magma that crystallized into the South Lac des Iles Complex?

Chapter 2 – Regional Geology

2.1 - Superior Province

The Superior Province of the Canadian Shield is the largest Archean craton in the world (Fig. 2.1), spanning ~1 572 000 km^2 of south-central Canada and the northern United States (Thurston, 1991). The Superior Province is bound by Paleoproterozoic orogenies to the north, west, and east (Churchill Province), to the south (Southern Province), and by a Mesoproterozoic orogeny (Grenville Province) to the southeast (Card & Ciesielski, 1986). The Superior Province is dominantly composed of belt-shaped, generally east-trending granite-greenstone, metasedimentary, and plutonic terranes, which preserve a record of continental accretion during the 2.72-2.68 Ga Kenoran orogeny (Card, 1990; Percival et al., 2006). The Superior Province has remained largely stable since ~2.6 Ga, providing an excellent record of cratonic evolution likely reaching back to ~3.6 Ga and possibly further (Skulski et al., 2000; Percival et al., 2012).

The Superior Province has historically been subdivided into subprovinces based on lithology, regional structure, geophysical characteristics, and ages of rocks and geological events (Douglas, 1973; Goodwin, 1978). Card & Ciesielski (1986) developed a classification scheme in which four litho-tectonic subprovince types were recognized: volcano-plutonic, metasedimentary, plutonic, and high-grade gneiss. Researchers in recent years have shifted toward a hierarchical classification scheme with subdivisions based partially on historical subprovincial boundaries but also incorporating recent mapping, higher-precision

geochronology, and modern interpretations of structure and geophysical characteristics (Percival, 2007; Stott et al., 2010).

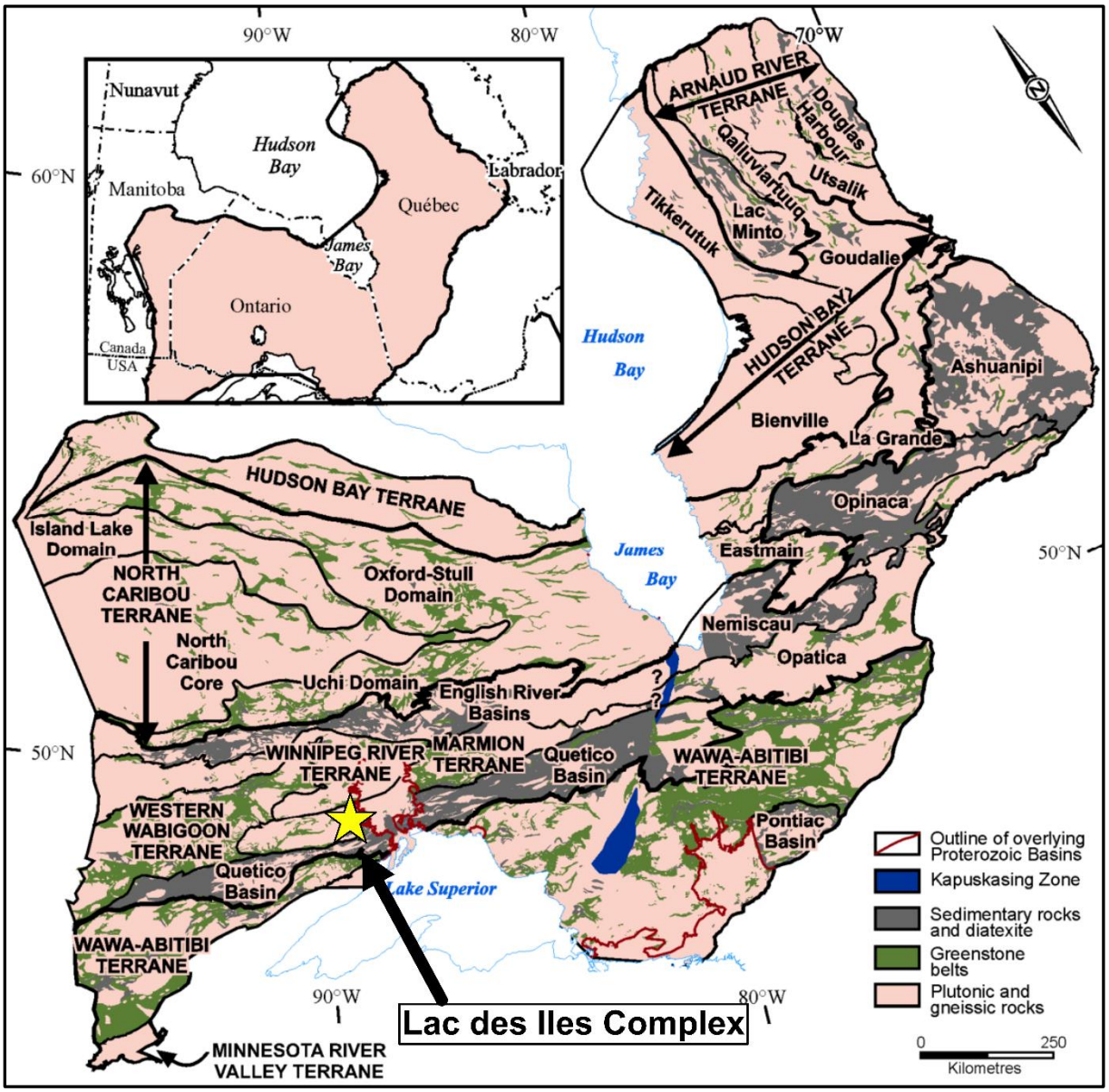

Figure 2.1 – Terrane map of the Superior Province (modified from Stott et al., 2010).

Stott et al. (2010) proposed a revised terrane map of the Superior Province (Fig. 2.1) that recognized four levels of groupings: superterranes, terranes, domains, and tectonic assemblages. A superterrane is an amalgamation of two or more terranes that assembled prior

to Neoarchean assembly of the Superior Province, although the existence of superterranes within the Superior Province remains a subject of debate (Parks et al., 2006; Stott et al., 2010). A terrane is defined as a tectonically bounded region with internal characteristics distinct from those in adjacent regions prior to Neoarchean assembly of the Superior Province (Stott et al., 2010). A domain is typically a younger, lithologically distinct part of a terrane, featuring juvenile crust or sharing a common basement (Stott et al., 2010). A tectonic assemblage is defined as being distinct in lithology, age, and tectonic setting, and is composed of one or more stratigraphic groups of formations (Stott et al., 2010).

The major subprovince categories delineated by Card and Ciesielski (1986) are largely still recognizable within the hierarchical system developed by Stott et al. (2010). Volcano-plutonic units such as the Wawa-Abitibi and Wabigoon terranes and the Uchi domain are dominantly composed of anastomosing belts of greenschist-grade supracrustal rocks that flank domiform syn- and post-orogenic felsic plutons (Thurston and Chivers, 1990; Stott, 1997; Percival et al., 2012). Metasedimentary basins such as the English River, Quetico, and Opinaca typically consist of greenschist- to amphibolite-facies metaturbidites and metagreywackes as well as post-orogenic granitoid plutons (Card and Ciesielski, 1986; Percival et al., 2012). Plutonic units, including the Berens River domain and the Winnipeg River terrane, are characterized by abundant granitic plutonism, lesser enclaves of mafic volcanism and plutonism, and a general scarcity of supracrustal rocks (Card and Ciesielski, 1986). High-grade gneiss units such as the Kapuskasing Structural Zone and the Pikwitonei domain comprise complexly deformed belts of supracrustal and plutonic origin, broadly metamorphosed to upper-amphibolite to granulite-facies gneisses (Card and Ciesielski, 1986; Card, 1990).

The assembly of the Superior Province occurred via crustal accretion during the Kenoran orogeny (Stockwell, 1972; Stott, 1997). Recent models recognize five discrete accretional events within the Kenoran orogeny (2.72-2.68 Ga), each exhibiting similar sequences of magmatism, sedimentation, deformation, metamorphism, and plutonism (Percival et al., 2006). Each orogeny involved the collision and subduction of one or more major volcano-plutonic/plutonic terranes or accreted groups of terranes, and most resulted in the formation of a corresponding regional sedimentary basin (Percival et al., 2006).

2.2 - Marmion terrane

The Marmion terrane is a relatively small, granitoid-dominated terrane of the western Superior Province, composed of large granitoid batholiths along with later plutonic rocks and supracrustal sequences including minor greenstone belts (Fig. 2.2). The area comprising the Marmion terrane has historically been categorized as part of the plutonic-dominated central portion of the extensive east-trending Wabigoon terrane, located between the Quetico and English River basins (Card and Ciesielski, 1986; Card, 1990). More recently, the Marmion terrane has been re-interpreted as a discrete crustal block, with Nd model ages and zircon inheritance patterns that are distinct from the Winnipeg River terrane to the north (an area formerly classified as the north-central Wabigoon terrane) and the western Wabigoon terrane to the west (Tomlinson et al., 2004; Stott et al., 2010). Tomlinson et al. (2004) placed the boundary between the Marmion and eastern Wabigoon terranes in the region obscured by Proterozoic rocks of the Nipigon Embayment, suggesting the eastern Wabigoon terrane was potentially coeval to the Marmion terrane or partially derived from re-worked Marmion terrane rocks. This is supported by zircon inheritance patterns and Nd model ages, but the scarcity of

exposed basement rock in the eastern Wabigoon terrane makes it difficult to make a direct comparison (Tomlinson et al., 2004).

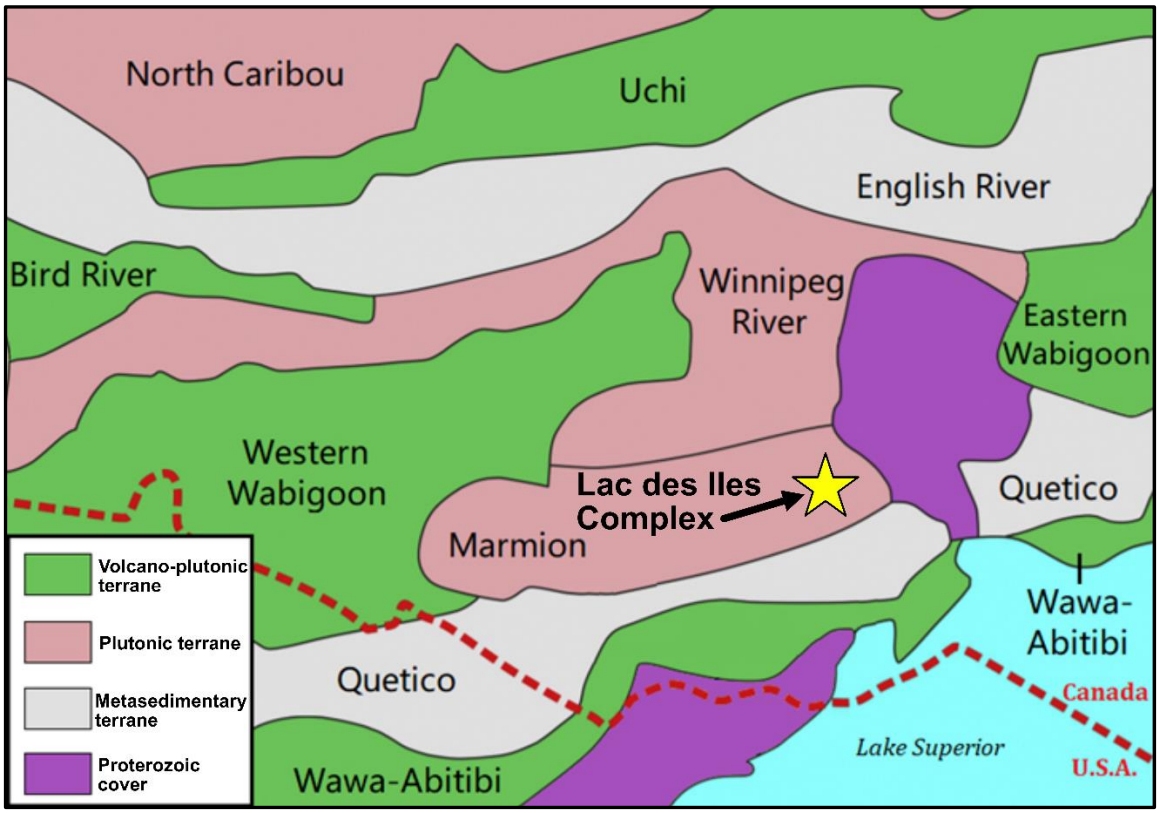

Figure 2.2 – Map of terrane subdivisions showing the location of the Marmion terrane within the Superior Province (modified from Stott et al., 2010 and Sotiriou et al., 2018).

Card (1990) interpreted the ~3000 km^2 Marmion batholith as a basement block upon which later supracrustal rocks were accreted, though he argued these later assemblages were likely allochthonous due to interpreted tectonic boundaries and a lack of isotopic and geochemical evidence. It has more recently been recognized that the ~3 Ga Marmion batholith and coeval volcanic sequences, which represent the oldest crust in the area formerly classified as the central Wabigoon, likely served as a nucleus around which autochthonous accretion of the Marmion terrane occurred (Tomlinson et al., 2003; Stone and Davis, 2006). Stone and Davis (2006) used geochronology and improved mapping to identify nine lithotectonic domains

within the Marmion terrane and proposed a model in which the proto-continent developed via periodic accretion of arc-derived magmatic and crustal material until at least ~2.73 Ga. Tomlinson et al. (2004) suggested that magmatism in the Winnipeg River and Marmion terranes at 2.93-2.87 Ga is consistent with collision between the terranes at that time, prior to accretion of additional domains on the southern and eastern margins of the Marmion terrane. The Marmion terrane was accreted onto the developing Superior Province during the Central Superior orogeny (2.71-2.70 Ga), a phase of the Kenoran orogeny in which the western Wabigoon was also accreted onto the southern margin of the Winnipeg River terrane (Percival et al., 2006). The 2.695 Ga Shebandowan orogeny, which accreted the Wawa-Abitibi terrane onto the southeastern edge of the Superior Province, generated the sediments of the Quetico basin directly south of the Marmion terrane (Percival et al., 2006).

2.3 – Lac des Iles suite

The Lac des Iles suite is a series of 1-10 km wide, sub-circular to ovoid mafic to ultramafic intrusions arranged in a ~30 km-wide circle within the Marmion terrane, near its southern margin with the Quetico basin. The Lac des Iles suite includes the Buck Lake, Demars Lake, Dog River, Legris Lake, Taman Lake, Tib Lake, and Wakinoo Lake intrusions, as well as the Lac des Iles Complex (Fig. 2.3). Several of these intrusions host PGE-rich magmatic sulfide mineralization, including the economic Pd-rich mineralization that occurs in the South Lac des Iles Complex, which has been primarily mined for Pd along with secondary Pt, Au, Cu, and Ni (Decharte et al., 2018). The Lac des Iles suite intrusions are composed of a range of mafic rocks including leucogabbro, hornblende gabbro, gabbronorite, and norite; ultramafic rocks are rare aside from in the layered North Lac des Iles Complex (Sutcliffe and Smith, 1988). U-Pb

geochronology on zircons has yielded ages for the South Lac des Iles Complex of 2689.0 ± 1.0 Ma and 2693.3 ± 1.3 Ma, and for the North Lac des Iles Complex of 2687.0 ± 1.6 Ma (D.W. Davis cited in Stone et al., 2003; Heaman and Easton, 2006; Heaman and Easton, unpublished). Similar methods have yielded ages of 2685.9 ± 1.6 Ma for the Tib Lake intrusion and 2.690 ± 0.9 Ma for the nearby Shelby Lake batholith (D.W. Davis cited in Stone et al., 2003).

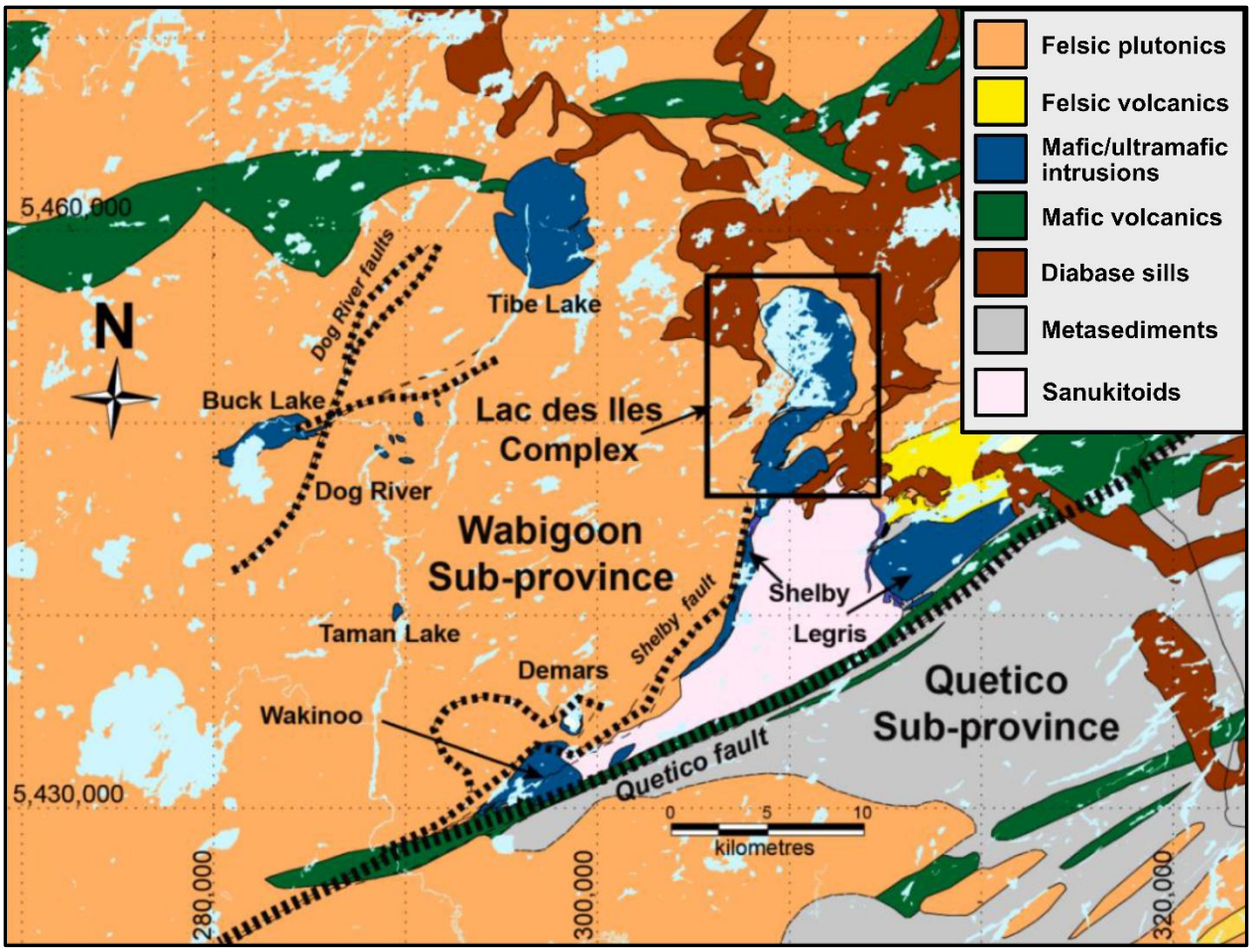

Figure 2.3 – Map of Lac des Iles suite intrusions (in dark blue) (modified from Djon, 2017).

Several different interpretations have been offered for the origin of the Lac des Iles suite. Brugmann et al. (1997) suggested a continental arc affinity based on neodymium isotope ratios and trace element geochemistry, noting enrichment in large ion lithophile elements (LILE) and light rare earth elements (LREE) and depletion in high field strength elements (HFSE). Additionally, Brugmann et al. (1997) noted that the Lac des Iles suite's sub-circular shape, composite lithology, and petrological characteristics resemble those of subduction-related Alaskan-type intrusions. Barnes and Gomwe (2010) interpreted the parent magma to have been of calc-alkaline continental arc affinity, noting orthopyroxene and plagioclase compositions similar to those expected in arc-related andesitic rocks. Alternatively, Hinchey et al. (2005) suggested a potential ocean-island or seamount setting, as they interpreted the parental magma to be similar to an enriched mid-ocean ridge basalt. Several authors have noted the proximity of the deposits to the Quetico-Marmion/Wabigoon boundary, as well as the importance of major regional faults on the emplacement of the suite (Gupta and Sutcliffe, 1990; Stone et al., 2003).

2.4 – Lac des Iles Complex

The Lac des Iles Complex is the largest intrusive complex of the Lac des Iles suite and can be divided into two discrete bodies, referred to as the North and South Lac des Iles Complexes (Fig. 2.4). The complex is situated along the NE-trending Shelby Lake fault, which is a splay of the terrane-bounding Quetico fault and is interpreted to be a potential feeder structure (Stone et al., 2003). Based on limited drill core and field exposures of the intrusive contact between the two bodies, the North Lac des Iles Complex is currently interpreted to postdate the South Lac des Iles Complex (Djon et al., 2017). The North Lac des Iles Complex is a ~4.5 x 6 km

composite intrusive body, made up a several stacked, gently dipping, saucer-shaped intrusive bodies (Sutcliffe and Sweeny, 1986). Ultramafic rocks including websterite, olivine websterite, pyroxenite, and wehrlite dominate the complex, along with lesser mafic rocks such as gabbronorite (Djon et al., 2018). The North Lac des Iles Complex can be further subdivided into the Northern Ultramafic Centre, which shows distinct cyclic cumulate layering, and the Southern Ultramafic Centre, which is less well understood but appears to be concentrically zoned and demonstrates cyclicity at least on a local scale (Sutcliffe and Sweeny, 1986; Djon et al., 2018). Djon et al. (2017) proposed a model in which two continuously interacting magmas crystallized alternately, resulting in macro-layering that controlled the reef-style PGE-Ni-Cu mineralization seen in the North Lac des Iles Complex. Though several mineral occurrences are recognized within the North Lac des Iles Complex, no economic deposits are currently recognized, and known mineralization is generally considered too narrow and low-grade to be a major focus of exploration (Decharte et al, 2018; Djon et al., 2018).

The ~2 x 6 km South Lac des Iles Complex (SLDIC) has historically been divided into three discrete, contiguous mafic intrusions, known as the Mine Block, South Lac des Iles, and Camp Lake Intrusions (Fig. 2.4). Recently, Impala Canada geologists have re-interpreted the geology of the SLDIC based on compilation and interpretation of geochemical, geophysical, and lithological characteristics, and developed a new model (Fig. 2.5) that comprises three discrete magmatic episodes, the boundaries of which are somewhat different from the three discrete intrusions defined in the previous model (Decharte et al., 2018).

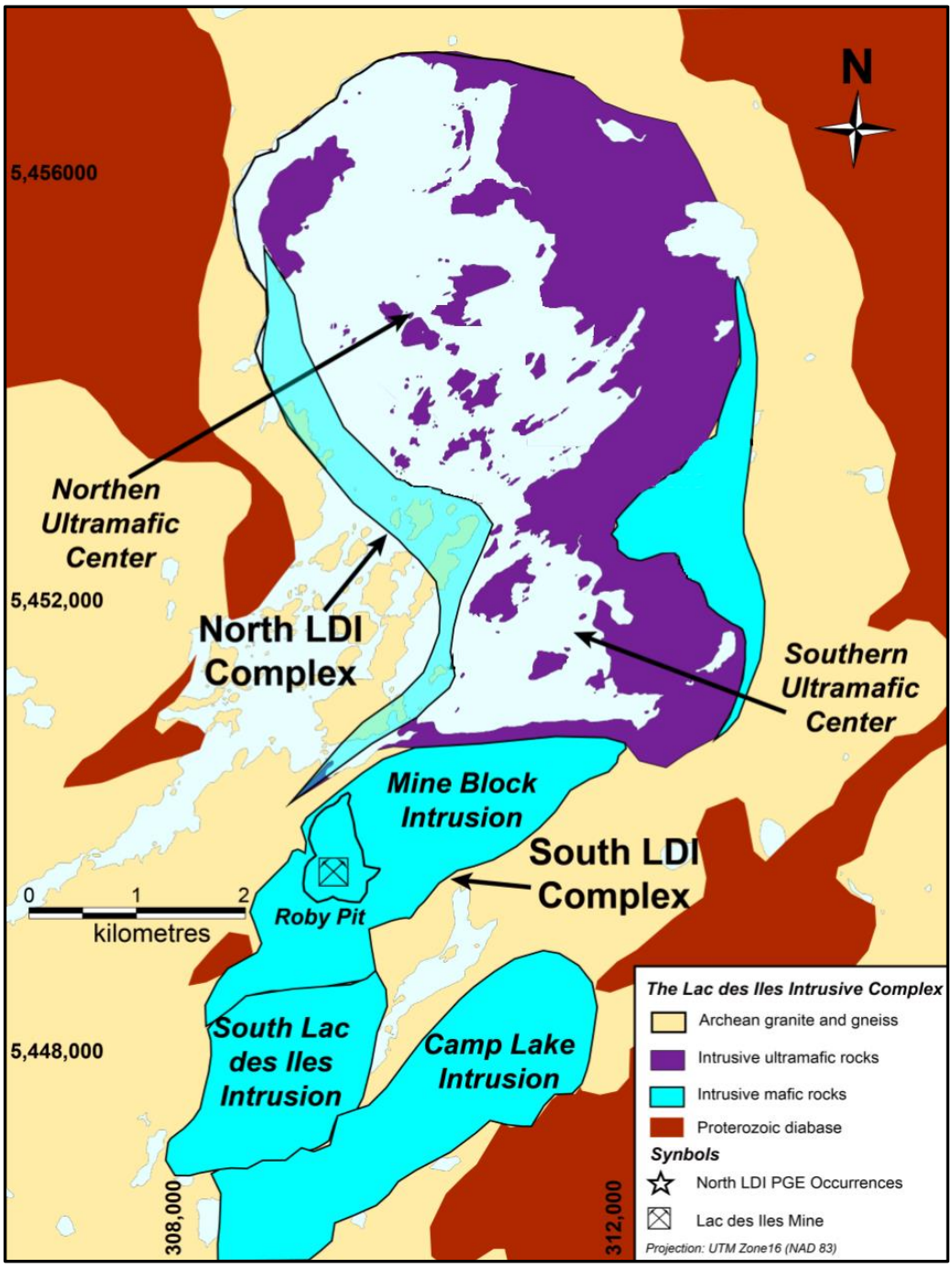

Figure 2.4 – Map of the Lac des Iles Complex, with historical subdivision of the South Lac des Iles Complex into three discrete intrusions (modified from Djon, 2017).

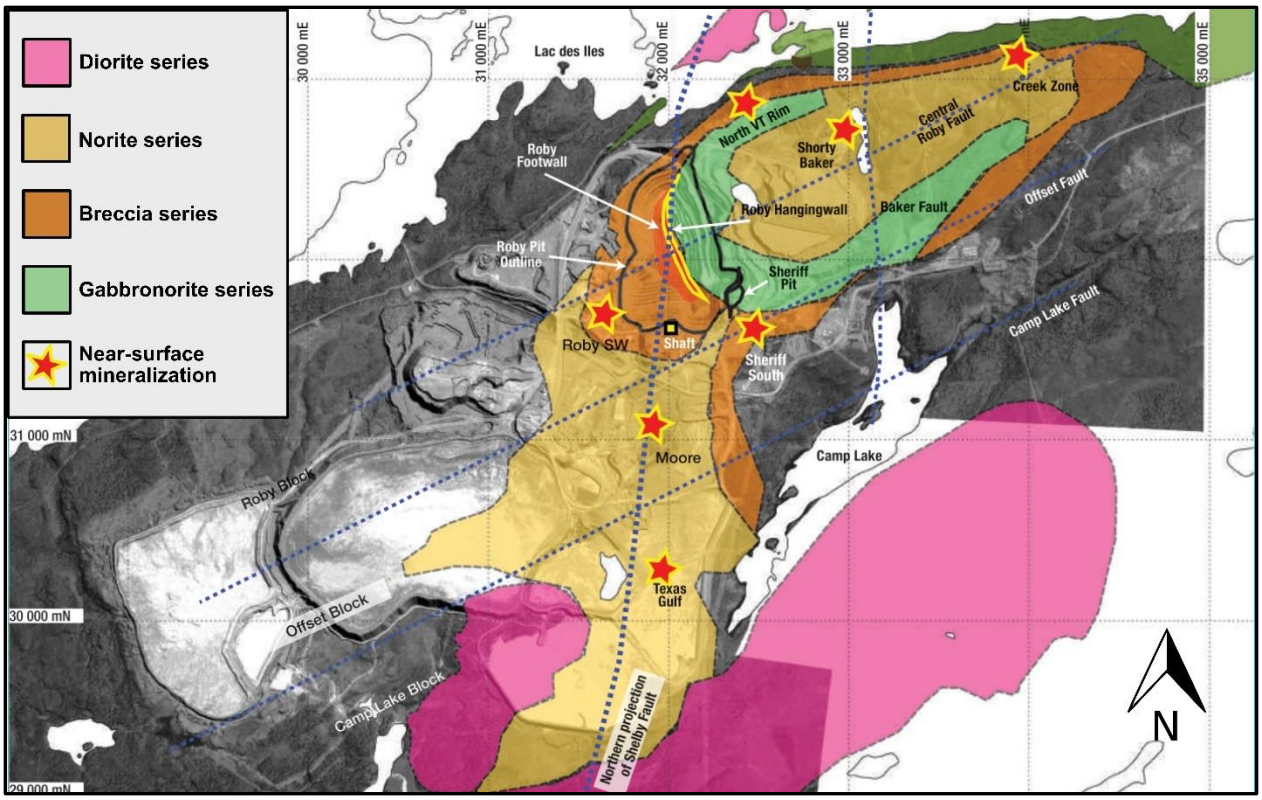

Figure 2.5 – Map of the South Lac des Iles Complex, with updated geologic subdivisions (modified from Impala Platinum Holdings Limited, 2022).

The earliest of the three magmatic episodes in the refined model for the South Lac des Iles Complex comprises equigranular gabbronorite and magnetite gabbronorite and is termed the gabbronorite series (Decharte et al., 2018). The gabbronorite series makes up a relatively small portion of what was formerly termed the Mine Block Intrusion and lacks significant mineralization. The second magmatic episode comprises a structurally complex, texturally chaotic suite of variably altered mafic rocks referred to as the breccia and norite series, making up the majority of the former Mine Block and South Lac des Iles Intrusions (Decharte et al., 2018). The area formerly referred to as the Mine Block Intrusion hosts all known economic mineralization within the Lac des Iles Complex, whereas the area formerly comprising the South Lac des Iles Intrusion consists of norite series lithologies and hosts only sporadic low-grade

mineralization. The third and final phase of magmatism consists mostly of hornblende gabbro and diorite and is termed the diorite series (Decharte et al., 2018). The diorite series comprises the entirety of the former Camp Lake Intrusion and a minority of the former South Lac des Iles Intrusion, and hosts only a few low-grade PGE-Ni-Cu occurrences.

The portion of the breccia and norite series formerly known as the Mine Block Intrusion is dominantly composed of massive to varitextured, leucocratic to melanocratic gabbronorites and norites and altered equivalents, namely metagabbronorite and chlorite-actinolite schist (Brugmann et al., 1989; Sutcliffe et al., 1989; Lavigne and Michaud, 2001; Barnes and Gomwe, 2011). The norite series is dominantly equigranular and not brecciated, with composition ranging from leuconorite to melanocratic norite to gabbronorite (Decharte et al., 2018). The breccia series is similar in bulk composition but generally more leucocratic than the norite series, and is very texturally heterogeneous, with extremely variable grain size and widespread magmatic brecciation containing lithic fragments of highly variable size and geometry (Lavigne and Michaud, 2001; Decharte et al., 2018). Pyroxene-plagioclase adcumulates dominate both the breccia and norite series, in which orthopyroxene is always the dominant pyroxene (Barnes and Gomwe, 2011). Although olivine is not observed in any rocks of the former Mine Block Intrusion, it may have been a minor pre-alteration component of some metagabbronorite and chlorite-actinolite schist units, based on whole-rock geochemistry (Barnes and Gomwe, 2011).

PGE-Ni-Cu mineralization within the SLDIC is hosted in zones of <3% disseminated sulfide minerals. A sulfide assemblage of pyrrhotite+chalcopyrite+pentlandite±pyrite is observed in fresh rocks, whereas assemblages of chalcopyrite+pyrite±pentlandite and chalcopyrite+pyrite±millerite are seen in altered rocks (Djon and Barnes, 2012). Palladium is

dominantly hosted in small platinum group mineral grains proximal to sulfide disseminations, as well as within pentlandite and to a lesser extent millerite (Djon and Barnes, 2012). The Roby and Offset zones account for the majority of PGE-Ni-Cu mineralization recognized in the SLDIC (Decharte et al., 2018). They are steeply dipping, 50-400 m wide zones of chlorite-actinolite schist and metagabbronorite with 0-3% sulfide, offset by a fault but interpreted to have originally been part of a continuous ore zone (Duran et al., 2016). A longitudinal view of the geological domains directly surrounding the Offset zone is presented in Figure 2.6. Several other PGE occurrences are present in the South Lac des Iles Complex, mostly occurring proximal to contacts between the breccia and norite series, largely within a few hundred metres of the Roby/Offset zones or near the northern rim of the South Lac des Iles Complex (Decharte et al., 2018).

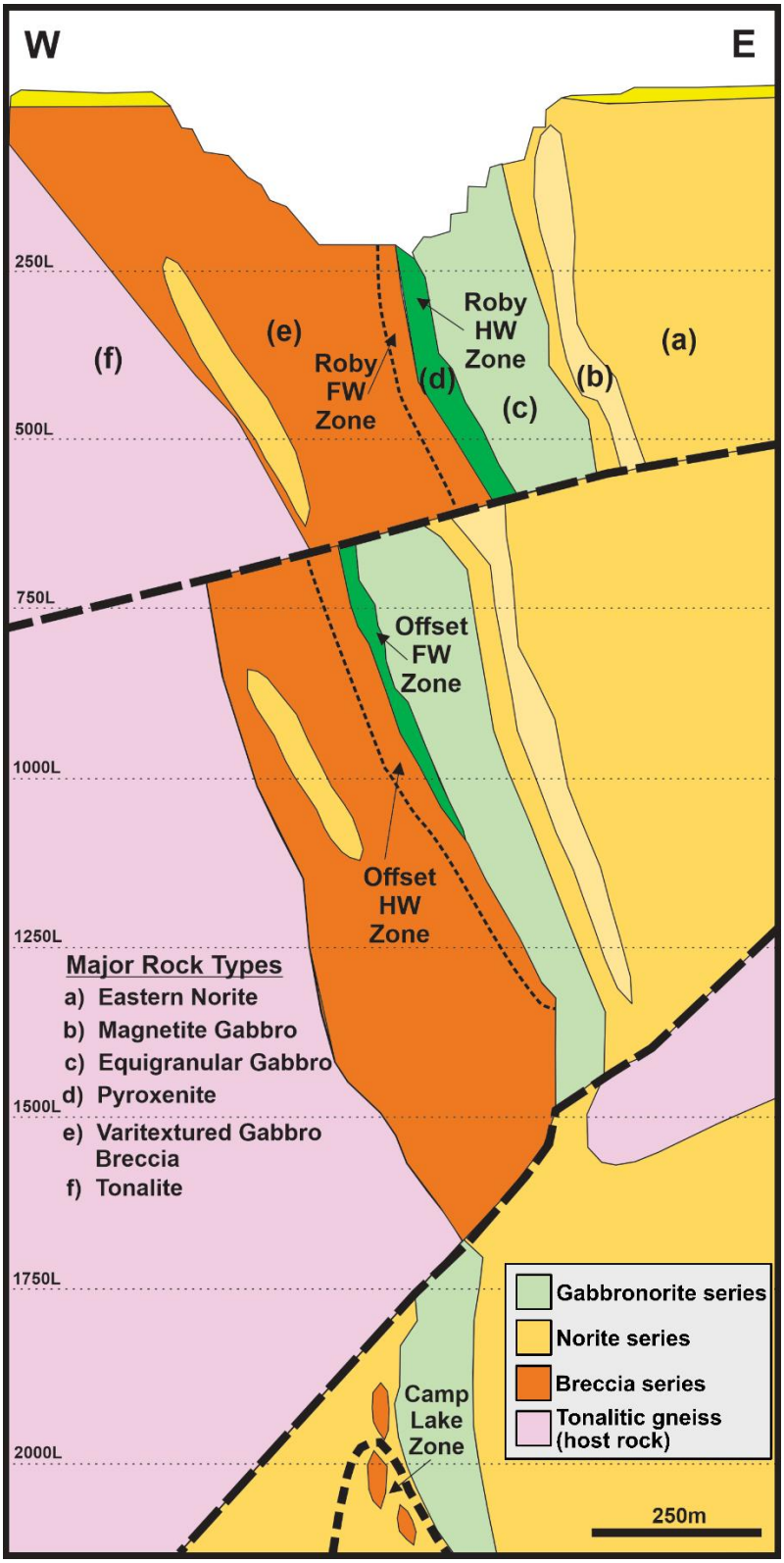

Figure 2.6 – Cross section of geological domains of the Roby and Offset zones and surrounding lithologies, looking north (elevation in metres below surface). Image provided by Impala Canada.

Several characteristics of the SLDIC are not commonly seen in other PGE-rich magmatic sulfide deposits, including the broad, steeply dipping ore zones, the extremely high Pd/Pt (typically >10) and Pd/Ir ratios (>10,000 in highest-grade zones), and increasing Pd/Pt ratios at higher Pd grades (Barnes and Gomwe, 2011; Djon et al., 2018). Several models have been developed to explain the conditions by which the SLDIC and its deposits formed, most of which invoke multiple stages of magmatism and many of which invoke some degree of PGE redistribution by hydrothermal fluids. Brugmann et al. (1989) developed a model by which volatile-rich evolved magma remelted earlier-crystallizing portions of the intrusive complex, resulting in Pd enrichment as well as varitextured and brecciated textures. Several other authors (Lavigne and Michaud, 2001; Hinchey et al., 2005, Barnes and Gomwe, 2011; Peck et al., 2016) have argued that brecciation was generated by later pulses of relatively primitive magma. Hinchey et al. (2005) and Barnes and Gomwe (2011) suggested that Pd enrichment in the SLDIC occurred via re-entrainment of earlier-formed sulfides from depth into their current position by later pulses of magma.

Although most models involve some degree of collection of PGEs by a magmatic sulfide liquid, the importance of late-stage PGE transport via hydrothermal fluids has been debated. The presence of the highest-grade Pd mineralization within chlorite-actinolite schist, along with the low sulfur content and general lack of correlation between Pd and S in this zone, has led some to suggest that relatively low-temperature hydrothermal fluids carried Pd into the chlorite-actinolite schist (Hinchey et al., 2005; Barnes and Gomwe, 2011), which occurred after the SLDIC was entirely or almost entirely crystallized. This hydrothermal fluid has been proposed to be thiosulfide-bearing (Barnes and Gomwe, 2011) or carbonic (Hanley and

Gladney, 2011). In contrast, other models propose that the concentration of PGEs in the high-grade chlorite-actinolite schist predated low-temperature hydrothermal alteration, either by magmatic (Decharte et al., 2018) or high-temperature hydrothermal processes (Schisa et al., 2015), with some authors (Djon and Barnes, 2012; Boudreau et al., 2014) noting the general lack of correlation between PGE enrichment and hydrothermal alteration.

Open-pit mining operations at Lac des Iles commenced in 1993, and underground operations began in 2006. The Roby and Offset Zones are and have been the primary focus of underground mining operations, with the Roby Zone also being historically mined via open pit. In recent years, underground mining has expanded into satellite deposits of the Offset Zone, including the B2, B3, and C Zones, and open-pit mining has intermittently been undertaken on the Twilight Zone via the Sherriff open pit (Decharte et al., 2018). Production from the Lac des Iles mine to June 30, 2022, amounts to 69.08 Mt at 1.91 g/t Pd and 0.14 g/t Pt, for a total of 4.28 Moz Pd and 329.3 koz Pt (Campbell et al., 2023). Proven and probable mineral reserve figures as of June 30, 2022, are 40.4 Mt @ 1.90 g/t Pd, 0.18 g/t Pt, 0.14 g/t Au, 0.06% Ni, and 0.06% Cu, for a total of 2.48 Moz Pd, 230 koz Pt, and 180 koz Au (Impala Platinum Holdings Limited, 2022). Measured and indicated mineral resource figures (exclusive of mineral reserves) as of June 30, 2022, are 39.2 Mt at 1.86 g/t Pd, 0.19 g/t Pt, 0.13 g/t Au, 0.07% Ni, and 0.06% Cu for a total of 2.57 Moz Pd, 260 koz Pt, and 180 koz Au (Impala Platinum Holdings Limited, 2022).

Chapter 3 – Methods

3.1 – Sampling

Sample collection took place at the Lac des Iles mine in July and August of 2020. Four drill holes, drilled between 2017 and 2019 and stored at the Lac des Iles core storage facility, were sampled for the study. Locations of the drill holes within the South Lac des Iles Complex are shown in Figure 3.1. Two hundred and ten drill core samples were taken for this study. Of these samples, 83 were selected for thin section preparation. A total of 163 samples were selected for whole rock geochemistry, 16 of which were from drill core and 147 of which were from previously assayed pulp/reject material.

3.2 – Petrography

Eighty-five polished thin sections were prepared at the Lakehead University lapidary facility, including 83 samples from the South Lac des Iles Complex and two from the tonalitic gneiss host rock. Thin sections were analyzed under transmitted and reflected light. Photomicrographs were acquired using an Olympus SC180 camera mounted on an Olympus Bx51 microscope. Complete petrographic descriptions are provided in Appendix A.

3.3 – Geochemistry

One hundred and sixty-three rock samples were submitted for whole rock geochemical analysis to ALS Geochemistry in Thunder Bay. Five blank samples (unmineralized quartzose sandstone) and nine certified reference material samples were added to the submission for quality control, for a total of 177 samples. Three different certified reference materials

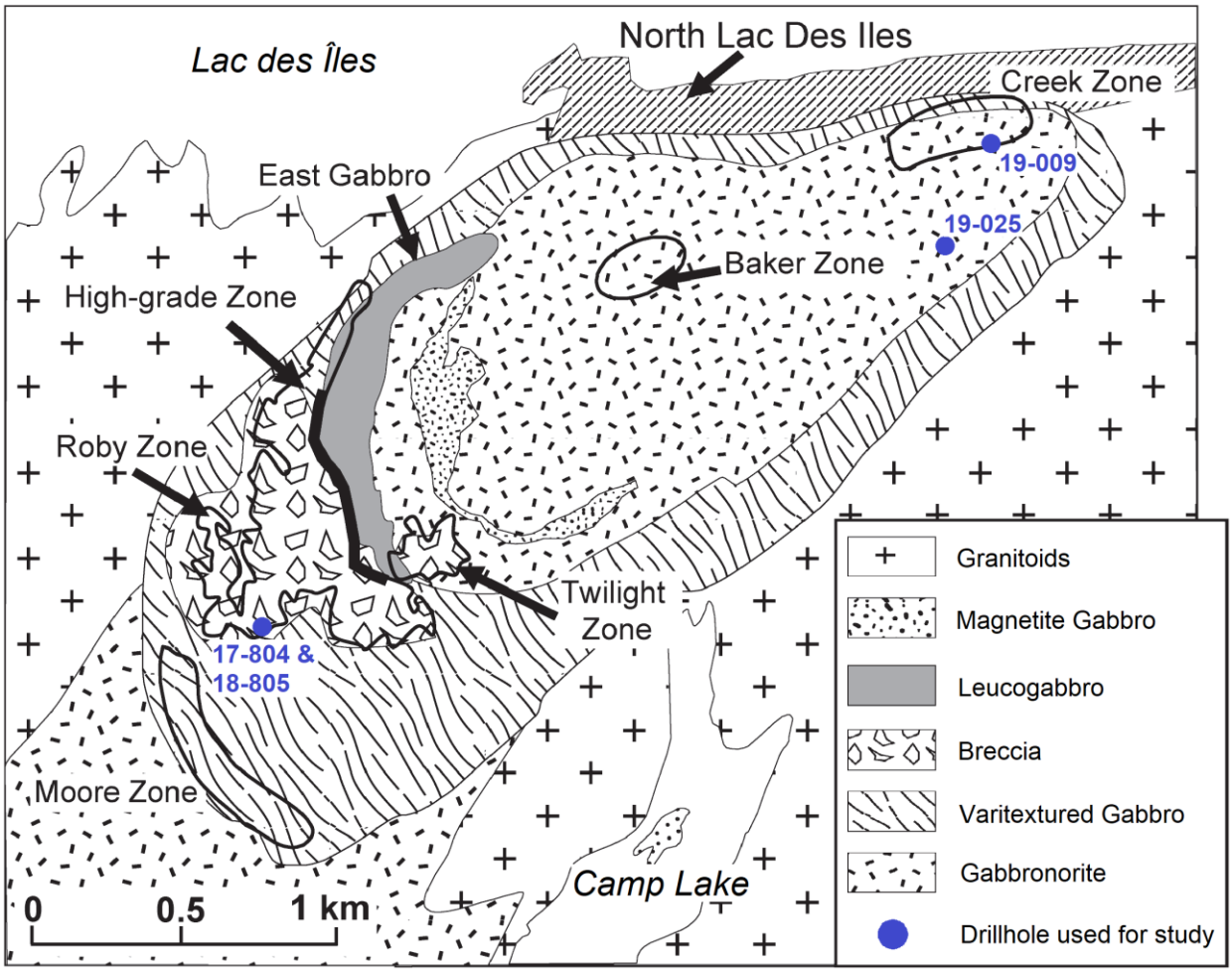

Figure 3.1 – Locations of drill holes used for study (modified from Duran et al., 2016).

prepared by CDN Resource Laboratories Ltd. were used: CDN-PGMS-27, CDN-ME-10, and CDN-ME-1208. Samples were crushed and then pulverized in a steel ball mill until 85% of the sample passed through a 75-micron screen, followed by closed-vessel four-acid digestion. Major element analysis was conducted via inductively coupled plasma atomic emission spectroscopy (ICP-AES). Trace elements were measured via inductively coupled plasma mass spectrometry (ICP-MS) following a lithium borate fusion preparation. Gold and platinum group elements were analyzed using a combination of fire assay and ICP-MS. Certain trace elements (As, Bi, Hg, In, Re, Sb, Se, Te, Tl) were analyzed via X-ray fluorescence (XRF). Loss on ignition was measured

gravimetrically following heating to 1000°C. Full results of geochemical analyses are provided in Appendix B.

3.4 – Sulfur isotopes

Twenty samples containing disseminated sulfide minerals were selected from drill core for sulfur isotope analysis. Eighteen of these samples were collected from drill holes from the Offset South, B3 Zone, and Creek Zones of the South Lac des Iles Complex, and two samples were taken from tonalitic gneiss country rock. Sample mounts were prepared by cutting ~5x5 mm blocks from drill core, which were mounted in 2.5 cm-wide epoxy pucks. Sample preparation was undertaken in the Lakehead University lapidary facility.

Samples were analyzed for their ^{32}S, ^{33}S, ^{34}S, and ^{36}S content via in situ secondary ion mass spectrometry (SIMS). Analyses took place in October of 2021 at the Centre for Microscopy, Characterization, and Analysis at the University of Western Australia, using a CAMECA IMS 1280 large-geometry ion microprobe. Resin mounts with polished samples were trimmed to 1 cm of the side of the mount to accommodate a standard block containing matrix-matches standards within the SIMS sample holder. Samples and standard blocks were cleaned in ethanol and deionized water and sputter-coated with a ~20 nm Au coat to prevent charging during analysis.

Each sample surface was sputtered over a 10 x 10 µm area, using a 10kV Gaussian Cs^+ beam with an intensity of ~2.5 nA and a total impact energy of 20 keV. Secondary ions were admitted in the double-focusing mass spectrometer within a 75 µm entrance slit and focused within the centre of a 3000 µm field aperture (x 130 magnification). Energy was filtered using a

30 eV band pass with a 5 eV gap toward the high-energy side. All isotopes were collected simultaneously: ^{32}S, ^{33}S and ^{34}S in Faraday cup detectors fitted with 10^{10} Ω (L'2, ^{32}S) and 1011 Ω (L1, ^{33}S and H1, ^{34}S) resistors, and ^{36}S in an electron multiplier (H2), all operating at a mass resolution of ~2500. The $^{32}S^{1}H$ and ^{33}S peaks were not completely resolved under these conditions; to account for this, the magnetic field was offset slightly to the low-mass side to avoid interference from $^{32}S^{1}H$ on the ^{33}S peak. The magnetic field was regulated using nuclear magnetic resonance control. Each analysis includes a pre-sputtering over a 15 x 15 µm area for 30 seconds, followed by the automatic centering of the secondary ions in the field aperture. Each analysis then consists of a 30 four-second cycles acquisition. The analytical session was monitored for drift using two bracketing standards every 5-6 sample analyses Matrix-matched reference materials with established sulfur isotope values and uncertainties were used to correct for instrumental mass fractionation and drift. Reference materials for pyrite ("Sierra"), chalcopyrite ("Nifty-b"), pyrrhotite ("Alexo"), and pentlandite ("VMSO") were used (reference material values can be found in LaFlamme et al., 2016). Corrections for instrumental mass fractionation were performed according to the process outlined in Kita et al. (2019).

Sulfur isotope fractionation is expressed in "delta" (δ) and "cap delta (Δ) notation, in permil (‰) units relative to Vienna Canyon Diablo troilite. Data processing follows the procedure outlined in LaFlamme et al. (2016). Multiple analyses were performed on each analyzed crystal, from which a mean value was calculated for each set of analyses. Error is expressed as two standard deviations from the calculated mean of all analyses performed on a single sample. Full results of sulfur isotope analyses are provided in Appendix C.

3.5 – Neodymium isotopes

Nineteen powdered rock samples from the South Lac des Iles complex were selected for Sm-Nd isotope analysis. Analyses took place in August of 2021 at the Pacific Centre for Isotopic and Geochemical Research at the University of British Columbia. Samples were dissolved using high-pressure dissolution, and analysis was performed via multi-collector inductively coupled mass spectrometry (MC-ICP-MS). Two MC-ICP-MS machines were employed: a Nu Plasma 1700 instrument was used for most analyses, and a Nu Plasma NP214 instrument fitted with high sensitivity sampling/skimmer cones was used for analyses of samples with lower Nd concentrations. Isotope analyses were carried out following the methodology outlined in Weis et al. (2006). Neodymium isotopic compositions were measured in static mode with relay matrix rotation on a double Re-Ta filament. Replicate analyses (repeat analysis of the same chemically prepared solution) and duplicate analyses (analysis of a separate solution prepared from the same sample) were performed as a quality control measure. Two reference standards of known trace element and Nd isotopic composition were used for external calibration: G-3, a granite standard developed by United States Geological Survey, and JNdi-1, a neodymium oxide standard developed by Tanaka et al. (2000). Data were normalized to $^{146}Nd/^{144}Nd = 0.7219$ using an exponential law, to correct for instrumental mass fractionation. Reported values were corrected for mass bias and instrumental drift via sample-standard bracketing normalization against established Nd isotopic values of the standard JNdi-1. Rare earth and high field strength element concentrations of all samples were measured using thermal ionization mass spectrometry. Results are reported in terms of isotopic ratios ($^{143}Nd/^{144}Nd$ and $^{144}Nd/^{145}Nd$). Full results of neodymium isotope analysis are included in Appendix D.

Chapter 4 - Results

4.1 – Field observations

Detailed drill core logging was carried out on parts of four diamond drill holes, with a total of 733 m logged (Table 4.1). Drill core logging was focused on sections of drill holes that encompassed various degrees of Pd enrichment and included the boundary between the breccia and norite domains of the South Lac des Iles Complex. Despite the lithological domain names commonly used by Impala Canada geologists, namely “breccia”, “norite”, and “gabbronorite”, all domains are primarily composed of leucocratic to melanocratic gabbronorite and norite, dominantly made up of adcumulate plagioclase and pyroxene and their alteration products. The breccia domain is dominantly made up of varitextured rocks and the distribution of brecciated zones is variable; brecciation is widespread in some areas, but is not observed in large portions of the drill holes used in this study. In this study, established field terms used by Impala Canada geologists are used to refer to lithological domain names, whereas rock descriptions adhere to IUGS classification.

Table 4.1 – Locations of diamond drill holes analyzed in this study. Locations in NAD83 Zone 16U.

Drill hole Number	Easting (UTM)	Northing (UTM)	Collar Elevation (m)	Azimuth	Dip	Length (m)	Logged Interval (m)	Zone
17-804	309284	5449298	-294	137.7	-34.7	498.0	117-360	Offset South
18-805	309284	5449298	-292	157.7	13.2	369.4	60-260	B3
19-009	311475	5450607	494	15.3	-46.9	281.0	20-110	Creek
19-025	311404	5450349	517	346.1	-61.3	578.0	320-520	Creek

In unaltered zones, both lithological domains are composed of >95% plagioclase and pyroxene, along with minor biotite, chalcopyrite, pyrrhotite, pentlandite, and magnetite. Unaltered zones comprise a small minority of the intervals logged for this study; in the majority of all logged lithologies, the primary mafic assemblage has been partially to completely replaced by a chlorite-actinolite-white mica-dominated alteration assemblage. Due to the preservation of primary textures and the textural similarity across varying degrees of alteration, the assumption was made for logging purposes that altered rocks were originally plagioclase-pyroxene cumulates. Aside from Fe-rich enstatite (bronzite) in some weakly to moderately altered portions of the norite domain, which has a characteristic high reflectivity and semi-translucent appearance, orthopyroxene and clinopyroxene were not visually distinguishable from each other in hand sample. Based on IUGS classification, some of the samples in this study are norites and some are gabbronorites, and there is no consistent spatial distribution of the two rock types between the breccia and norite domains (discussed in Chapter 4.2). Due to the difficulty in distinguishing orthopyroxene and clinopyroxene in hand sample and the fact that the differences between gabbronorites and norites in this study are based on small differences in clinopyroxene content, gabbronorites and norites are collectively referred to as "gabbronorite" in this section.

4.1.1 – Offset Zone

Two drill holes, DH# 17-804 and DH# 18-805, were selected from the southern part of the Offset Zone (Fig. 4.1). The holes were drilled from the same underground drill pad and both collared into breccia domain rocks, followed by norite domain lithologies to the end of the logged interval. DH# 17-804 was chosen from the Offset South Zone and DH# 18-805 was

chosen from the B3 Zone, which is located to the southwest of and contiguous with the Offset South Zone. The two drill holes selected from the Offset Zone include mineralized intercepts where elevated Pd content (>25 m drill hole intervals of >2.5 ppm Pd) is proximal to the breccia-norite domain boundary, within both the breccia and norite domains in DH# 17-804 and within the norite domain in DH# 18-805. In contrast to the drill holes analyzed in this study, mineralization in the northern and central parts of the Offset Zone primarily occurs within chlorite-actinolite schist and varitextured/brecciated gabbronorite and norite of the breccia domain, along the contact with the "gabbronorite" domain (Fig. 4.1). The gabbronorite domain

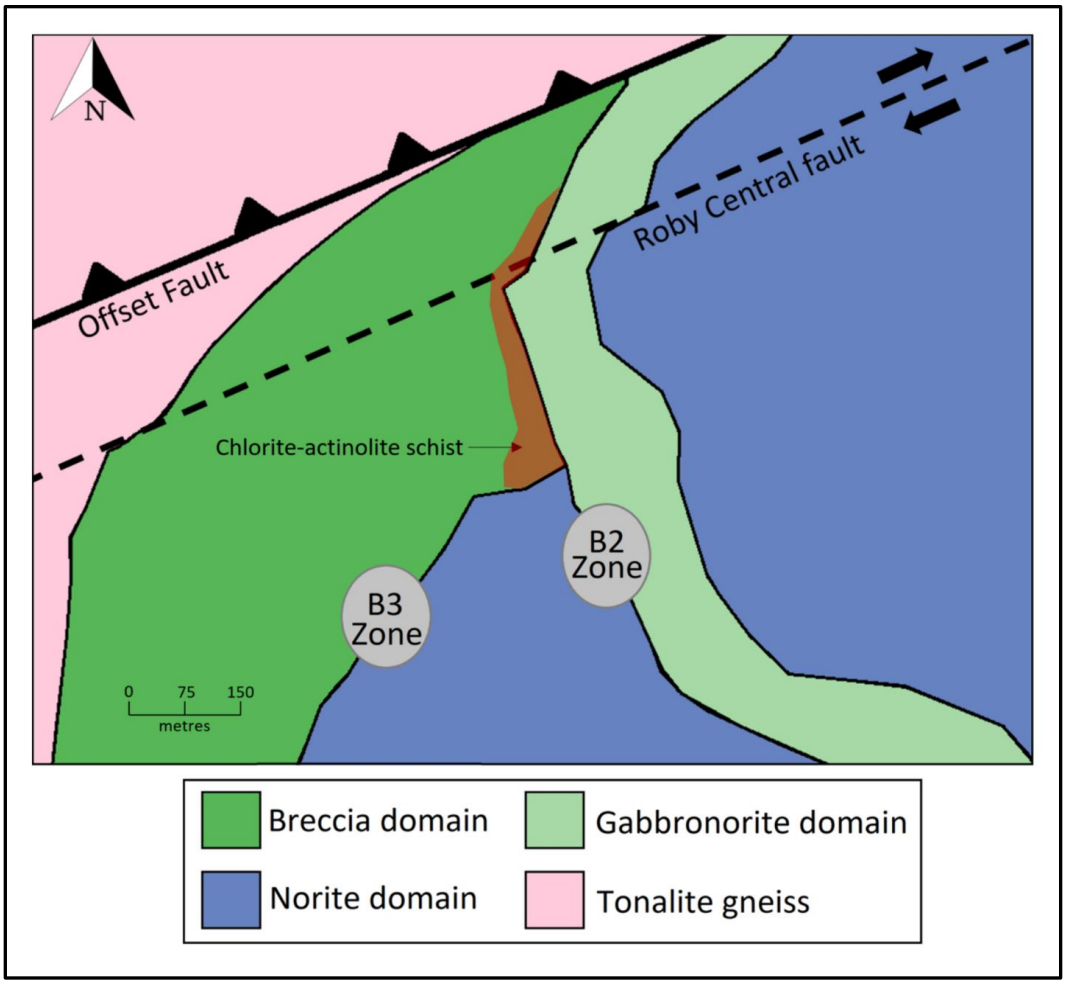

Figure 4.1 – Plan view of lithological domains within Offset Zone at 800 "mine level" (300 m below sea level) (modified from Decharte et al., 2018).

is composed of foliated, massive, medium-grained gabbronorite, and does not contain economic Pd enrichment or significant sulfide mineralization. The chlorite-actinolite schist has been interpreted by previous workers to have originally been olivine gabbronorite to gabbronorite in composition, and has been pervasively altered and completely replaced by chlorite-actinolite±talc (Barnes and Gomwe, 2011). Focusing on the Offset South and B3 Zones, where significantly increased alteration intensity is not associated with increased Pd content, minimizes the effect of alteration on interpretation of primary magmatic textures and geochemistry.

4.1.1.1 – Breccia domain within the Offset Zone

The two Offset Zone drill holes (Fig. 4.2), DH# 17-804 (Offset South Zone) and DH# 18-805 (B3 Zone), were drilled from the same underground drill pad and both collared into breccia domain rocks. The main rock type observed is varitextured gabbronorite (Fig. 4.3A), consisting of 55-60% plagioclase and 40-45% pyroxene, of which the pyroxene has mostly been replaced by chlorite and actinolite in most areas. Biotite was intermittently observed, comprising up to 2% of the rock, and trace to 5% pyrrhotite-chalcopyrite-pentlandite±pyrite is also present. Plagioclase and pyroxene crystals are subhedral to anhedral and similar in size, ranging from fine (crystals <2 mm in size) to pegmatitic (crystals >1 cm in size). Plagioclase crystals are commonly observed partially encircling smaller pyroxene crystals. Plagioclase is dominantly light grey to white (Fig. 4.3B), appearing grey-purple to white in areas of least alteration (Fig. 4.3C). Pyroxene is occasionally brown-grey but more commonly appears dull green due to alteration.

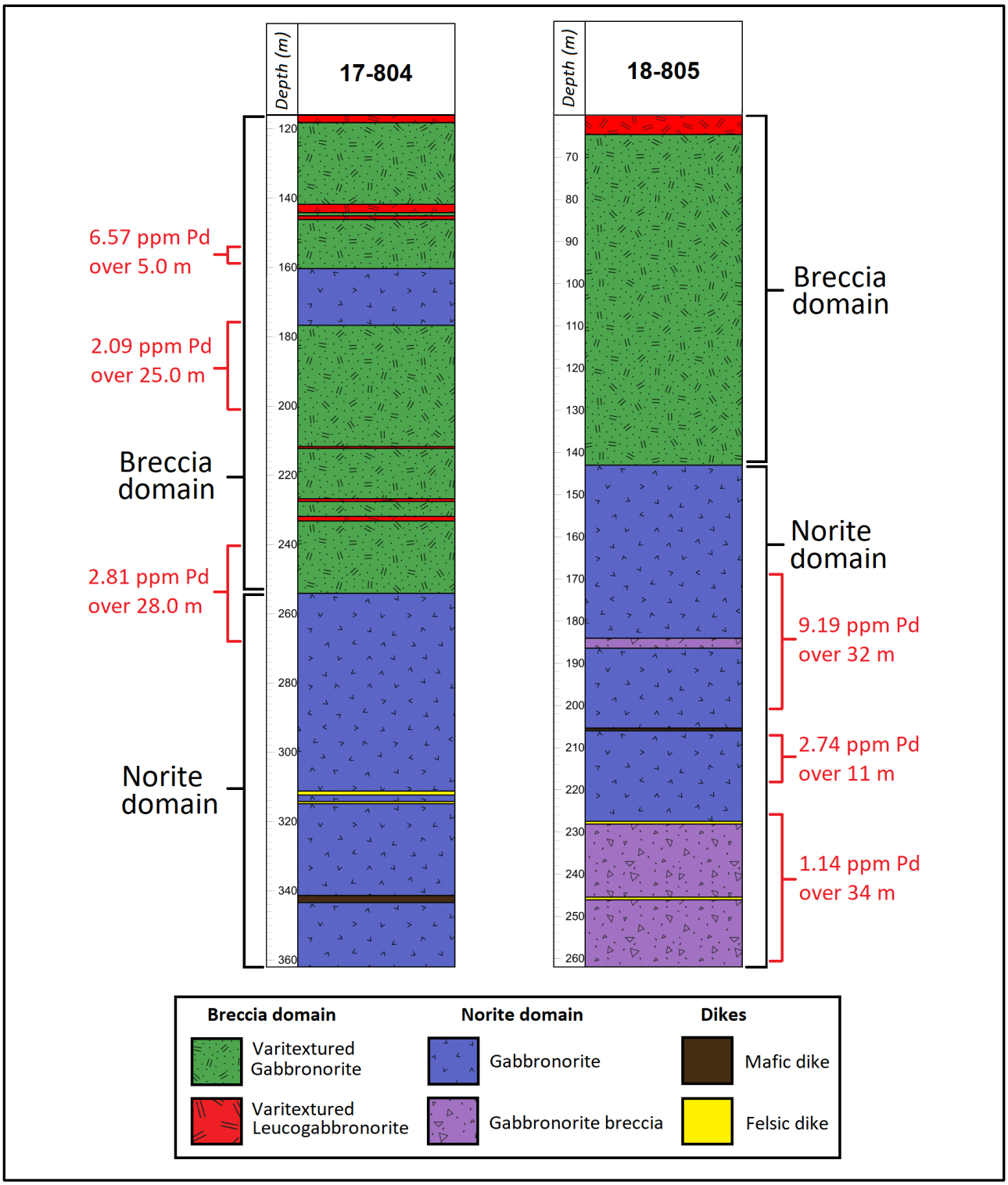

Figure 4.2 – Lithologies of logged intervals of diamond drill holes from the Offset Zone.

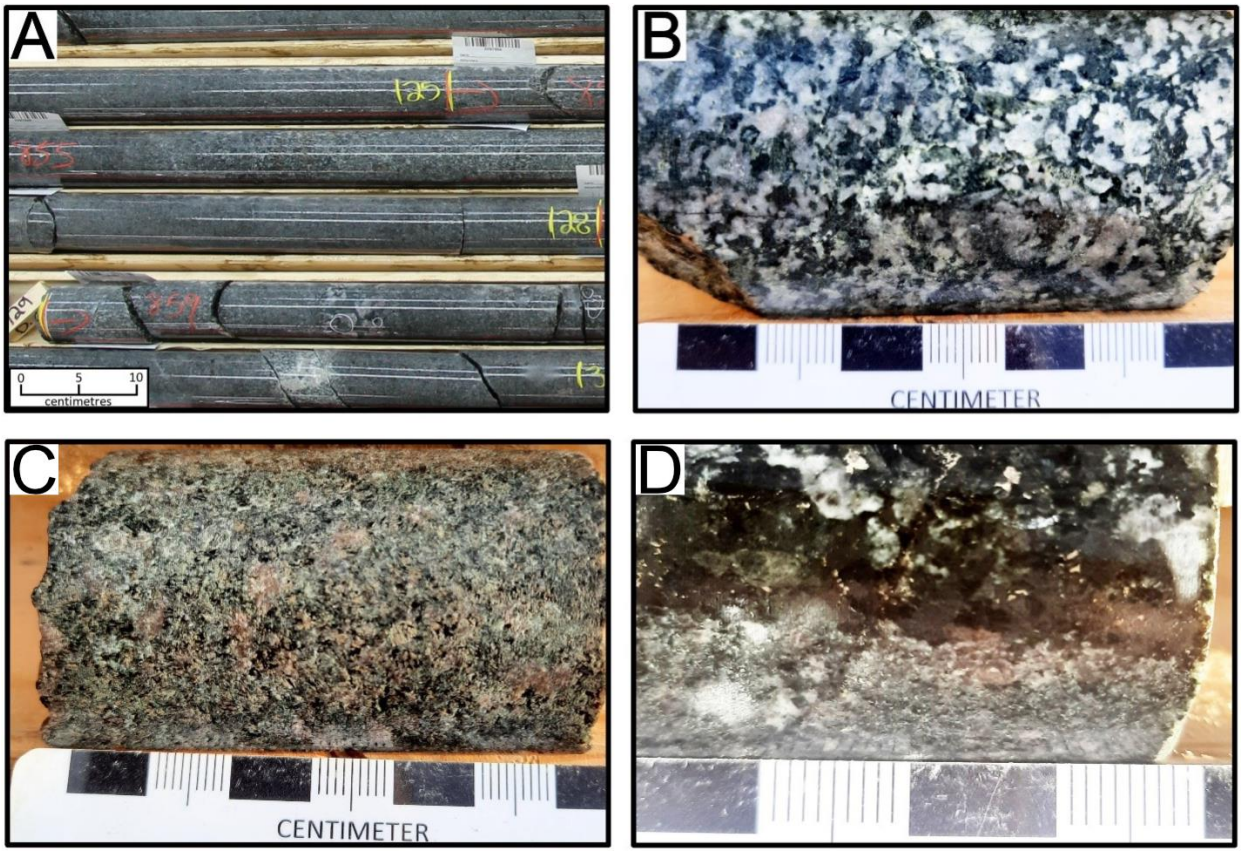

Figure 4.3 – Varitextured gabbronorite from the breccia domain of the Offset Zone. A) Representative sample of varitextured gabbronorite from DH# 18-805. B) Typical alteration intensity; plagioclase is albitized and pyroxene is completely replaced by chlorite and actinolite. C) Sample of less altered rock; plagioclase is unaltered and pyroxene is rimmed by chlorite and actinolite. D) Palladium-rich varitextured gabbronorite in DH# 17-804.

The other major rock type observed within the breccia domain is leucogabbronorite (Fig. 4.4A). Both Offset Zone drill holes intersected intervals of alternating gabbronorite and leucogabbronorite that comprise ~10% of the total logged interval. Leucogabbronorite consists of 65-75% plagioclase and 25-35% pyroxene prior to alteration, along with 0-5% pyrrhotite-chalcopyrite-pentlandite±pyrite. Intervals of leucogabbronorite are 10 cm to 1.5 m in length, and are similar in texture and alteration style/intensity to surrounding gabbronorite aside from their coarse to pegmatitic grain size. Boundaries between the gabbronorite and

leucogabbronorite are commonly gradational over the scale of a few centimetres, with some sharp and generally straight boundaries also observed.

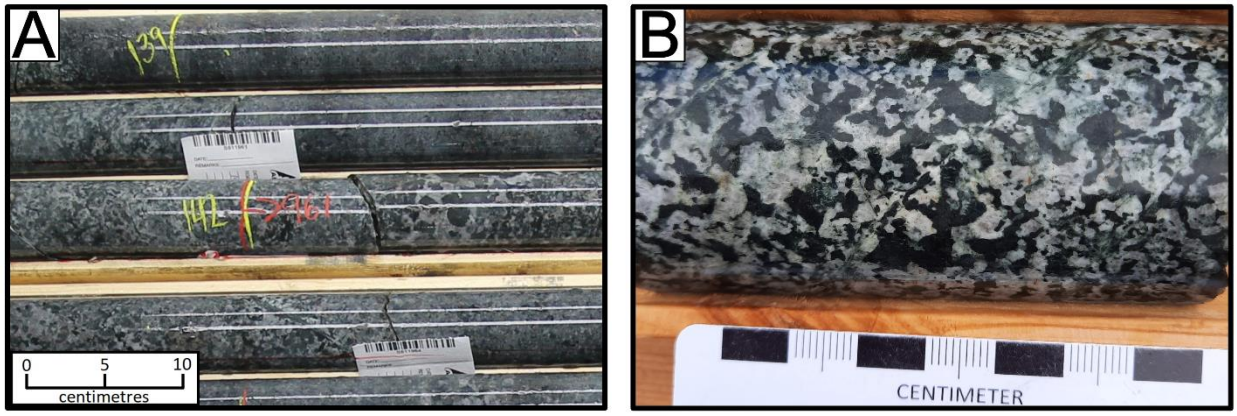

Figure 4.4 – Breccia domain rocks of the Offset Zone. A) Representative sample of varitextured leucogabbronorite/gabbronorite breccia from DH# 17-804. B) Characteristic example of "varitextured" texture.

Sulfide minerals most commonly occur in trace quantities as fine polysulfide disseminations in which mineralogy, especially the difference between pyrrhotite and pentlandite, was difficult to determine in hand sample. In areas of stronger alteration in which pyroxene has been completely replaced by chlorite and actinolite, the sulfide assemblage is dominated by pyrite and chalcopyrite. Intermittent zones (<50 cm) of 1-5% interstitial to blebby pyrrhotite-chalcopyrite-pentlandite±pyrite was observed throughout the breccia domain, typically alongside coarse-grained to pegmatitic silicates. Multiple <5 m intervals of 1-2% finely disseminated to blebby sulfide are present in DH# 17-804 (Fig. 4.3D) including several within a 25 m interval averaging 2.09 ppm Pd (176.0-201.0 m), representing the highest Pd grade within the breccia series in the studied drill holes. Increased sulfide mineral content (1-2%) was also observed in a 4.1 m section directly above the domain boundary contact. Magnetic

susceptibility within the breccia domain is low to locally moderate, generally between 0.5 $x10^{-3}$ to 3.0 $x10^{-3}$ kappa and increasing locally to up to ~50.0 $x10^{-3}$ kappa. Magnetite was not observed in drill core hand samples.

Gabbronorite within the breccia domain has commonly been referred to by previous workers and Impala Canada geologists as "varitextured", as the grain size of plagioclase and pyroxene varies considerably, ranging from fine-grained to pegmatitic and changing substantially in size over the scale of a few centimetres to a few metres (Fig. 4.4B). Grain size variations are almost always gradational, aside from sharp contacts bounding some pegmatitic zones. Sulfide minerals typically occur as fine disseminations within intervals of fine- to coarse-grained silicates, and usually as 2-10 mm blebs in coarse-grained to pegmatitic sections. Proportions of plagioclase and pyroxene typically remain constant regardless of grain size aside from in pegmatitic intervals, which are slightly more plagioclase-rich on average (~60-65% plagioclase). In both Offset Zone drill holes, grain size variations are generally less common and smaller in magnitude closer to the domain boundary contact. Grain size generally coarsens with depth in DH# 17-804, but not in DH# 18-805.

Breccia domain rocks in the Offset Zone are massive aside from occasional <40 cm zones of weakly aligned plagioclase and a single 1.2 m interval of weakly developed layering of anorthosite and gabbronorite. Intervals that can clearly be identified as brecciated comprise ~2% of the total logged interval. Breccia clasts within these intervals are <20 cm in size and consist of leucogabbronorite and/or pyroxene-bearing anorthosite with 60-90% plagioclase with sharp, irregular contacts with the surrounding gabbronorite (Fig. 4.5A). Due to the compositional similarity of some breccia clasts to the surrounding rock and to

leucogabbronorite pegmatitic intervals, it is possible that some “pegmatites” of leucogabbro with sharp, straight boundaries may in fact be clasts. Depending on the conditions under which brecciation occurred, it is also possible that some zones of compositional/textural variation may actually be clasts in which the margins were resorbed and equilibrated with surrounding magma. A 17.1 m interval was observed in DH# 17-804 that bears textural and compositional similarity to the norite domain; due to the relative similarity of the two lithologies and the undulating nature of the contact, it is possible that this interval represents a contact embayment, a large clast, or is actually a more pyroxene-rich lithology within the breccia domain. The nature of the domain boundary contact is somewhat obscured in both drill holes, by alteration in DH# 17-804 and by a minor fault in DH# 18-805. The contact in DH# 17-804 appears to be sharp and undulating (Fig. 4.5B), and in DH# 18-805 the contact appears gradational over a ~50 cm area with a subtle sharp contact on the bottom end (Fig. 4.5C).

Quartz-albite-biotite dikes crosscut breccia domain rocks in both drill holes. These dikes are typically 5-15 cm wide, oblique to drill core axis, and frequently occur as clusters over the scale of several metres (Fig. 4.6A). Quartz-albite veins are also present, which are <3 cm in width and most commonly proximal to and sometimes crosscutting the felsic dikes. Volumetrically insignificant quartz-carbonate veinlets (<1 cm in diameter) were occasionally observed, rarely extending across the width of a piece of drill core and generally proximal to zones of structural discontinuity such as dikes, quartz-albite veins, and contacts between gabbronorite and leucogabbronorite (Fig. 4.6B, C). Dikes and veins each constitute less than 2% of total logged intervals, and are barren of sulfide minerals and magnetite.

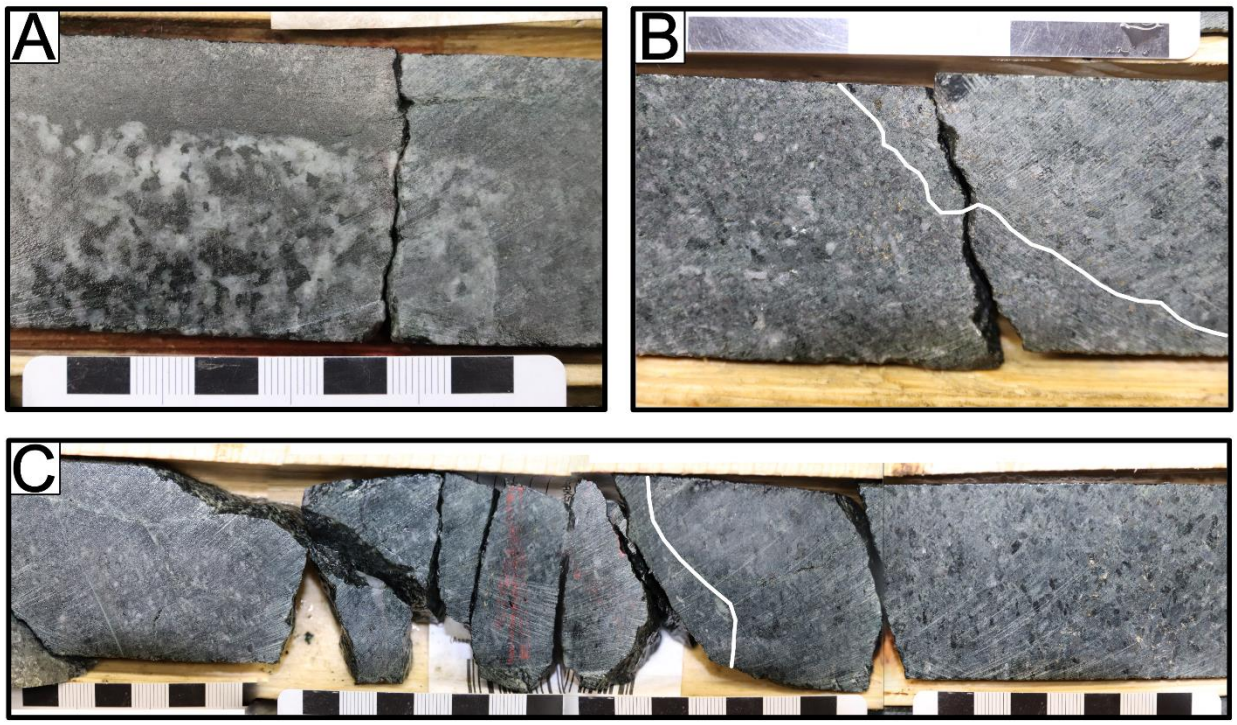

Figure 4.5 – Contact relationships within the Offset Zone. A) Leucogabbronorite clast within gabbronorite of the Offset Zone in DH# 17-804. B) Domain boundary contact between breccia and norite domains in DH# 17-804. C) Domain boundary contact between breccia and norite domains in DH# 18-805. Contacts delineated by white lines.

The degree of alteration appears to be fairly consistent within the breccia series. Plagioclase is generally not visibly altered aside from zones of "bleaching" adjacent to veins and faults, with thin rims of white mica alteration surrounding plagioclase crystals in the areas of strongest alteration. The dominance of white plagioclase within the breccia domain of the Offset Zone, in comparison to the norite domain of the Offset Zone and both domains within the Creek Zone, suggests that pervasive albite alteration of plagioclase may have occurred. Pyroxene is mostly to completely replaced by fine-grained pseudomorphs of chlorite and actinolite in all except the least altered areas, where chlorite-actinolite alteration occurs as rims. Variably orientated veinlets of fine-grained chlorite-actinolite are present throughout, consistently <2 mm in width (4.6D). Quartz-albite veins are commonly surrounded by <50 cm-

wide epidote-albite alteration haloes. Strong chlorite-actinolite-white mica alteration was observed in a 2 m area directly adjacent to the contact with the norite domain in DH# 17-804, but no increase in alteration was observed at the contact in DH# 18-805.

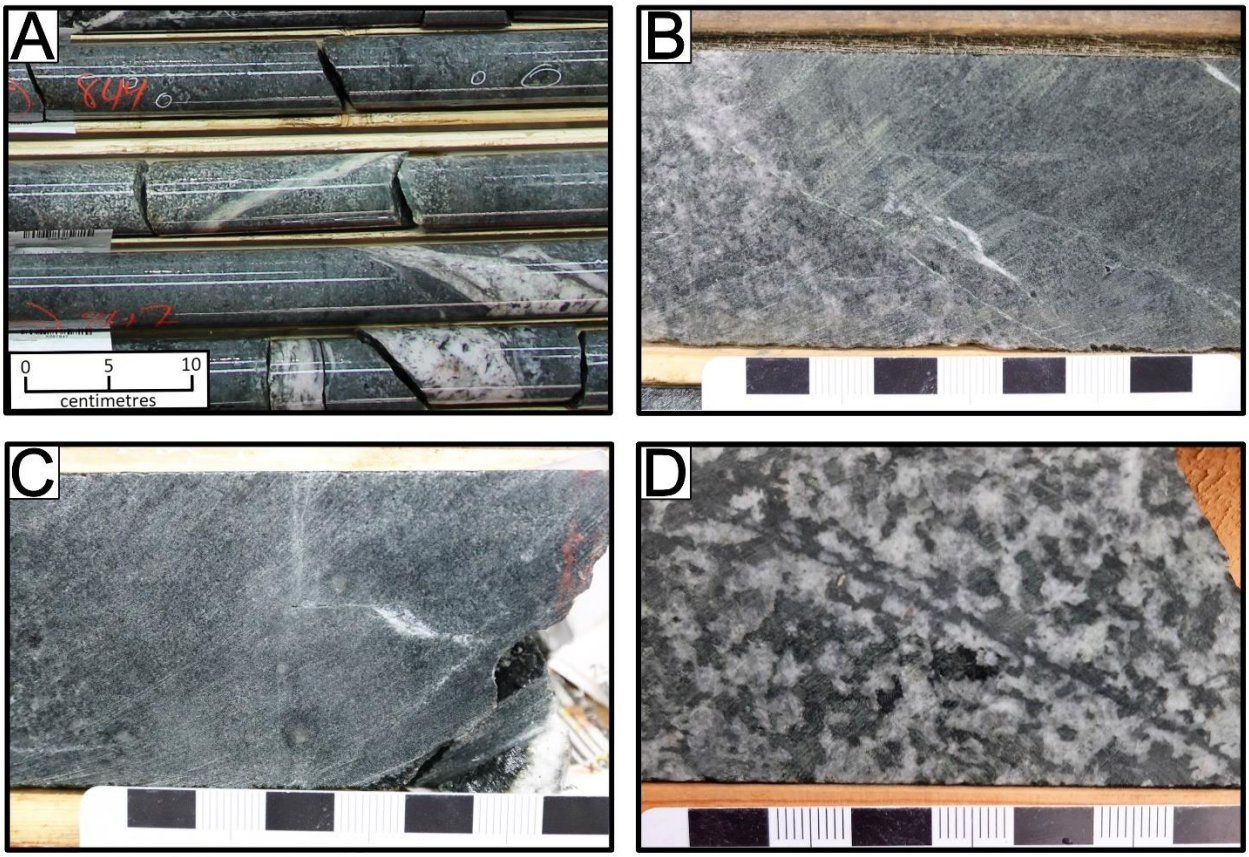

Figure 4.6 – A) Characteristic swarm of quartz-albite-biotite dikes from the Offset Zone in DH# 18-805. B & C) Quartz-carbonate veinlets associated with gabbronorite-leucogabbronorite contacts. D) Chlorite-actinolite veinlet crosscutting varitextured gabbronorite in DH# 17-804.

4.1.1.2 – Norite domain within the Offset Zone

Norite domain rocks were observed in both drill holes from the Offset Zone. The norite domain begins at 254.1 m in DH# 17-804 (Offset South Zone) and at 142.9 m in DH# 18-805 (B3 Zone), extending to the end of the logged intersection in both drill holes. Massive, equigranular gabbronorite comprises the majority of the intercept in both drill holes, consisting of 45-50%

plagioclase and 50-55% pyroxene prior to alteration (Fig. 4.7A/B). Plagioclase is most commonly purple-grey, appearing grey-white in areas of strongest alteration, whereas pyroxene is most typically dark grey-brown. Up to 3% biotite was also observed, as well as trace to 2% pyrrhotite-chalcopyrite-pentlandite±pyrite. Up to 2% magnetite over <2 m intervals was intermittently observed in DH# 17-804, but magnetite was not observed in hand sample in DH# 18-805. Pyroxene has been replaced by chlorite and actinolite to a variable degree in the majority of observed rocks,

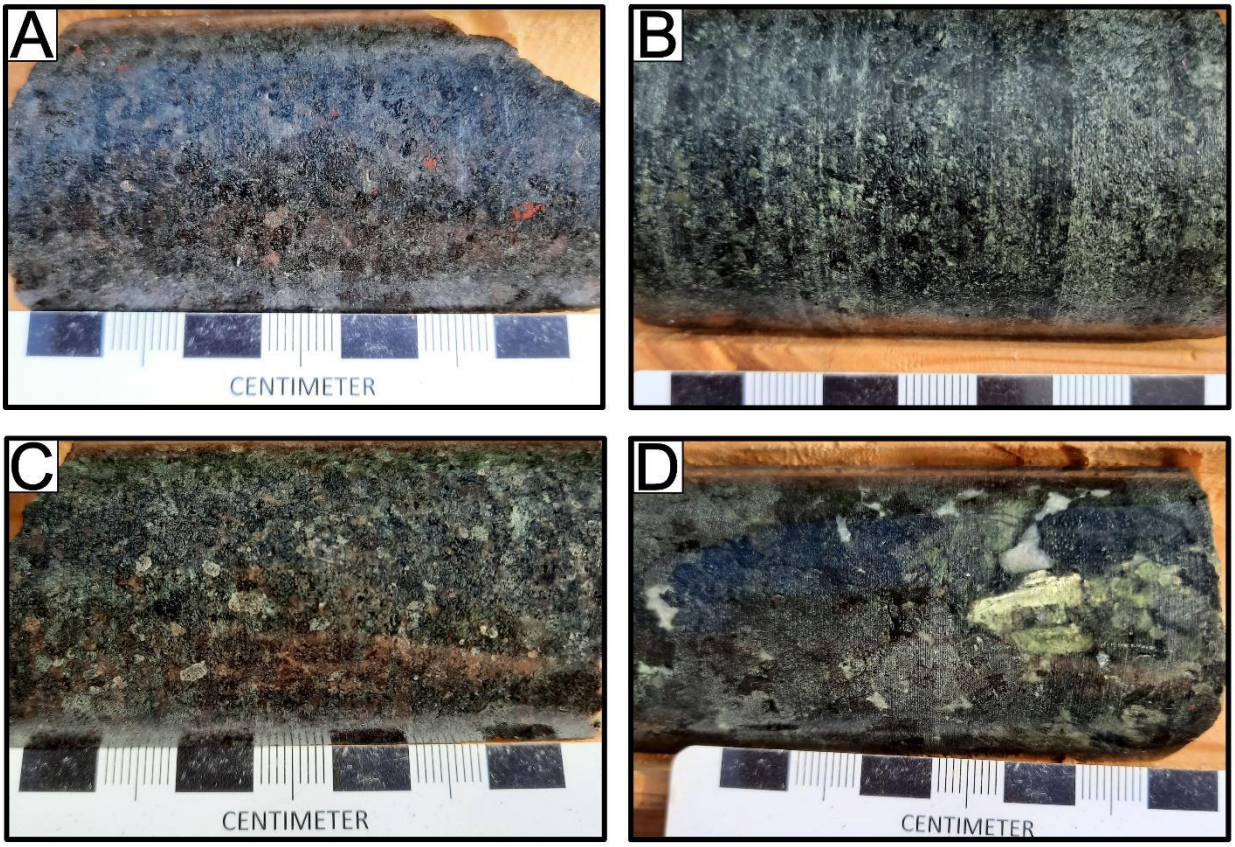

Figure 4.7 – Gabbronorite from the norite domain of the Offset Zone. A) Weakly altered gabbronorite from DH# 18-805. B) Strongly altered gabbronorite from DH# 17-804. C) Gabbronorite with visible Fe-rich enstatite (bronzite) from DH# 18-805. D) Pegmatitic gabbronorite with visible bronzite from DH# 18-805.

ranging from thin alteration rims to complete replacement. In most areas with a low degree of alteration, orthopyroxene can be recognized as making up >80-90% of the pyroxene present, occurring as Fe-rich enstatite (bronzite) that can be identified by its submetallic lustre (Fig. 4.7C/D). Otherwise, orthopyroxene and clinopyroxene are indistinguishable in hand specimen.

Sulfide minerals are dominantly present at trace quantities, increasing locally to <2% over <1 m intervals. The most significant sulfide intercept in the norite domain of DH# 17-804 is a 5.2 m interval located directly below the contact with the breccia domain. A 32.3 m interval of 1-2% disseminated sulfide minerals in DH# 18-805, centered 41 m below the breccia-norite domain boundary contact, was observed in the area containing the highest Pd grades of studied drill holes within the norite domain. Magnetic susceptibility within the norite domain is slightly higher than seen in the breccia domain, typically ranging from 1.0 $x10^{-3}$ to 5.0 $x10^{-3}$ kappa. Local elevations of magnetic susceptibility of up to ~20-40 $x10^{-3}$ kappa are seen throughout both drill holes, and in each drill hole a single zone that includes ~1-2 pyrrhotite yields magnetic susceptibility of up to 150.0 $x10^{-3}$ kappa. No magnetite was observed in hand samples from either drill hole.

Heterolithic breccia comprises the lower 32 m of the logged interval of DH# 18-805 (Fig. 4.8A). This interval is interpreted to be part of the norite domain, based on the presence of bronzite in least altered rocks, the compositional similarity of non-leucocratic rocks to typical norite domain lithologies, and interpretations of other drill holes in the area by Impala Canada geologists. Lithology of this section ranges from leucogabbronorite to melanogabbronorite, with 40-65% plagioclase and 35-60% pyroxene prior to alteration. The proportions of leucogabbronorite and melanogabbronorite within this interval increase and decrease with

depth, respectively. Contacts between compositionally distinct zones are generally sharp and undulating (Fig. 4.8B), though jagged, irregular contacts were also observed. Gradations in composition and grain size are observed at a minority of these contacts, occurring over the scale of less than a few centimetres (Fig. 4.8C).

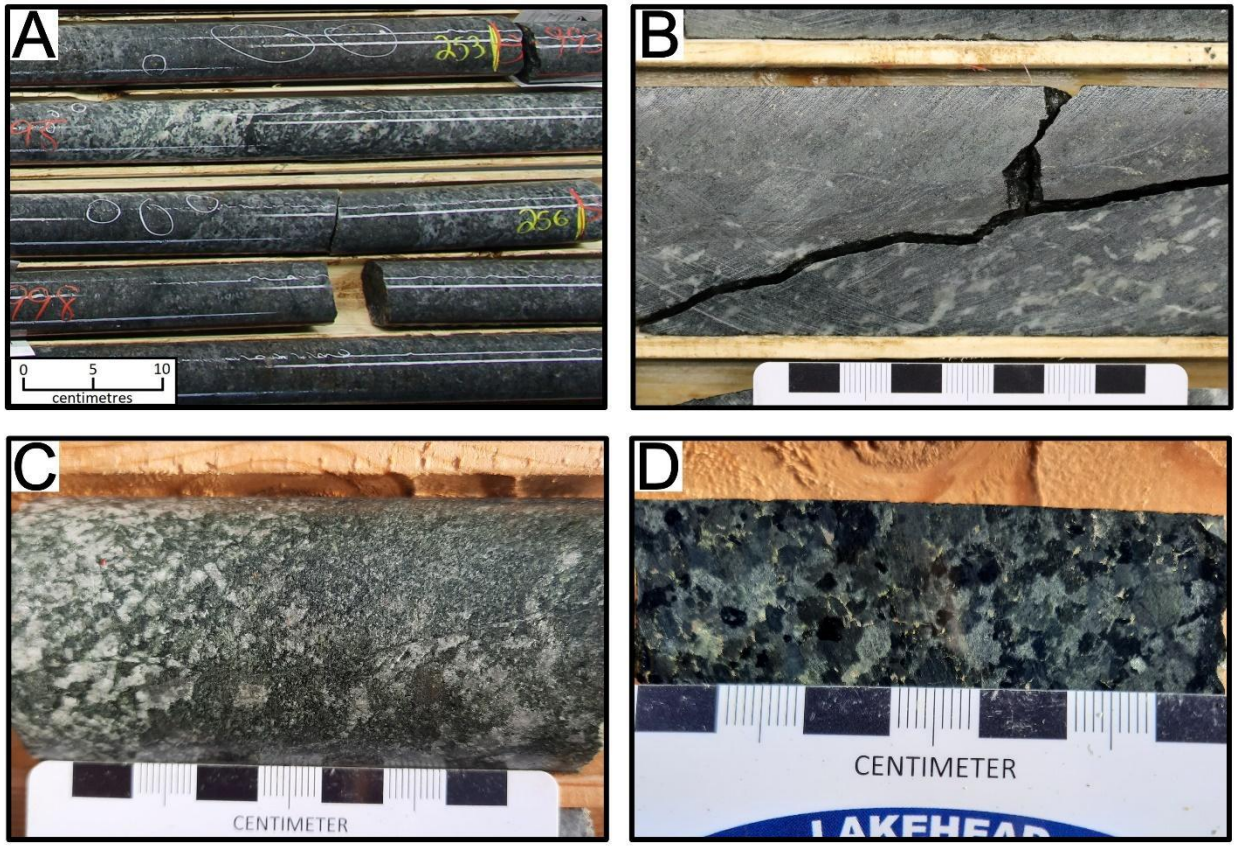

Figure 4.8 – Heterolithic breccia from the norite domain of DH# 18-805. A) Representative sample of gabbronorite breccia from the norite domain. B) Sharp contact between melanogabbronorite and gabbronorite. C) Gradational contact between leucogabbronorite and gabbronorite. D) Interstitial sulfide mineralization within gabbronorite.

Aside from the interval of heterolithic breccia, most rocks in the norite domain have an equigranular, massive texture, lacking the changes in grain size seen in the breccia domain. Grain size is medium to coarse, and plagioclase and pyroxene crystals are subhedral to anhedral. Sulfide minerals are generally present as fine disseminations, and as small interstitial

polysulfide accumulations in more sulfide-rich zones (Fig. 4.8D). Variations in grain size were observed intermittently in DH# 18-805, most commonly as a change from medium-grained to pegmatitic. These intervals are texturally similar to the varitextured gabbronorite of the breccia domain but are compositionally very similar to the surrounding norite domain rocks.

Quartz-albite-biotite dikes and aphanitic mafic dikes were observed in both drill hole intersections of the norite domain. The felsic dikes are compositionally similar to those intersecting rocks of the breccia domain but are generally larger, most commonly 40-80 cm in width and comprising 2% of logged intervals within the breccia domain. Mafic dike intervals are 0.2-2.0 m in width and make up 3% of total logged intervals. Quartz±albite veinlets were observed less frequently than in the breccia domain, typically 0.2-2.0 cm in width and within tens of metres of the domain boundary contact, becoming less frequent with depth and constituting <1% of the logged intervals.

Alteration intensity within the norite domain is more variable and generally less intense than in the breccia domain. Plagioclase crystals generally appear unaltered aside from zones of "bleached" alteration surrounding veins and dikes. Pyroxene ranges from unaltered to completely replaced by chlorite-actinolite, most commonly partially altered to rims and pseudomorphs of dull green-grey chlorite-actinolite, which is generally darker in colour than seen in the breccia domain. Zones of weaker and stronger alteration are typically 10-50 m in length, with the contacts between them usually being gradational over 0.5-2.5 m. Aside from a 1.8 m interval of strong alteration directly below the domain boundary contact in DH# 17-804, no correlation between alteration and proximity to the contact was observed.

4.1.2 – Creek Zone

Two drill holes, DH# 19-009 and DH# 19-025, were selected for detailed logging from the Creek Zone (Fig. 4.9). Both Creek Zone drill holes were drilled from the surface and collared into the norite domain, followed by breccia domain lithologies and ending in ultramafic rocks of the North Lac des Iles Complex. Because the South Lac des Iles Complex was the focus of this study, North Lac des Iles Complex lithologies were not sampled or analyzed in detail.

A major purpose of studying drill holes from the Creek Zone was to determine the processes that resulted in Pd enrichment along the contact between the breccia and norite domains in the eastern part of the South Lac des Iles Complex that hosts the Creek Zone, and to compare those results to the better studied western part of the intrusive complex that hosts all known economic Pd mineralization. Additionally, these drill holes were selected to compare relatively mineralized and unmineralized areas hosted in similar lithologies in the Creek Zone. DH# 19-025 contains a mineralized intercept averaging 1.06 ppm Pd over 36 m (Fig. 4.10), which is among the best Pd intercepts encountered by Impala Canada in the Creek Zone. DH# 19-009 includes only a short intersection of increased Pd content located adjacent to the domain boundary contact.

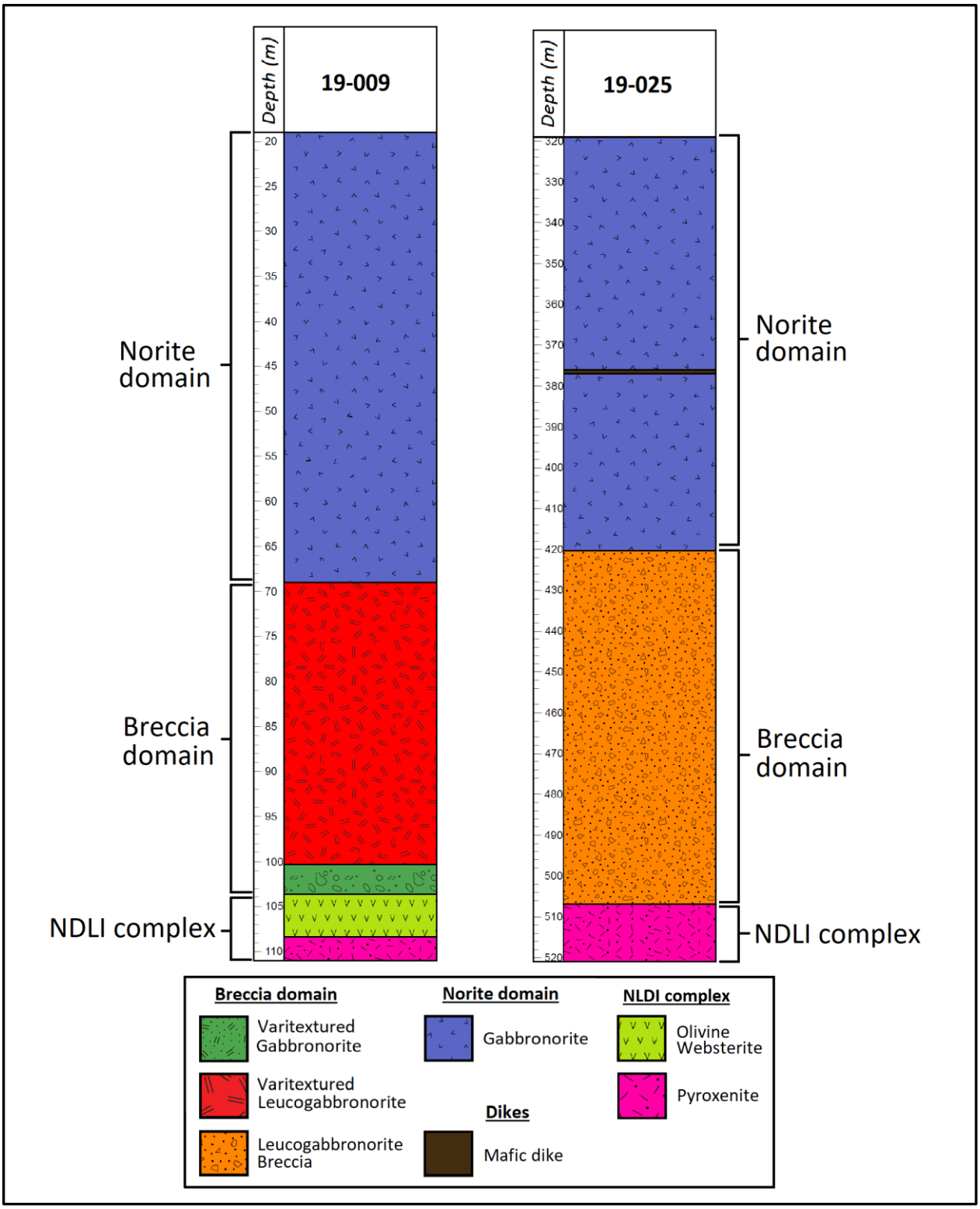

Figure 4.9 – Lithologies of logged intervals of diamond drill holes from the Creek Zone.

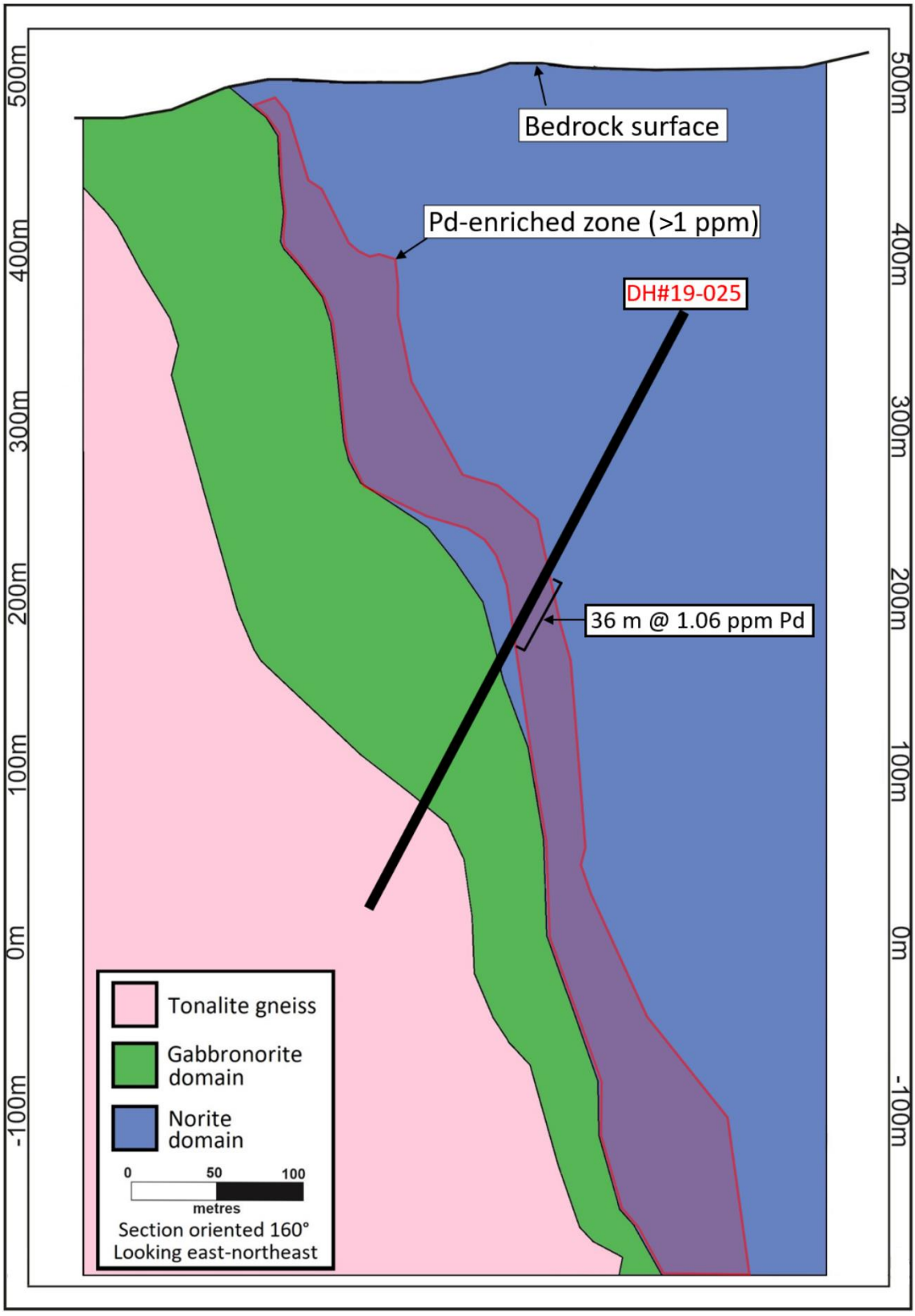

Figure 4.10 – Cross-section view of Creek Zone mineralization and the location of DH# 19-025.

4.1.2.1 – Breccia domain within DH# 19-025

Breccia domain rocks within DH# 19-025 comprise varitextured gabbronorite/ leucogabbronorite breccia. 65% of this interval is made up of varitextured gabbronorite, consisting of 50-60% plagioclase and 40-50% pyroxene, which have been partially altered to a chlorite-actinolite-dominated assemblage (Fig. 4.11A/B). Intervals of varitextured gabbronorite in DH# 19-025 are visually similar to those seen in the Offset Zone, with a similar adcumulate texture, subhedral to anhedral crystals, and varitextured appearance in which grain size is commonly variable over a scale of a few centimetres to a few metres. Plagioclase colour ranges from purple-grey in the least altered areas to white-grey in areas of stronger alteration, commonly with white rims and grey centres of crystals. Pyroxene appears dull green-grey as the result of alteration.

Intervals of varitextured leucogabbronorite make up 35% of the breccia domain in DH# 19-025 (Fig. 4.11C/D), generally decreasing in quantity with depth but present throughout the entire logged interval. Leucogabbronorite is composed of 65-75% plagioclase and 25-35% pyroxene prior to alteration, alongside trace finely disseminated sulfide minerals. In contrast to the dominance of pegmatitic crystals within leucogabbronorite observed in the Offset Zone, 60% of leucogabbronorite intervals within DH# 19-025 are composed of crystals <1 cm in size, the other 40% being pegmatitic. Regardless of the dominant crystal size in a given interval, these intervals display local variations in grain size and texture that is characteristic of varitextured breccia domain rocks. The contacts bounding leucogabbronorite intervals are generally sharp and straight to somewhat undulating, with gradational contacts over the scale of <20 cm also observed. Glomerophyric “popcorn texture” was commonly observed within the

leucogabbronorite, with pyroxene and especially plagioclase crystals occurring in clusters rather than being evenly distributed.

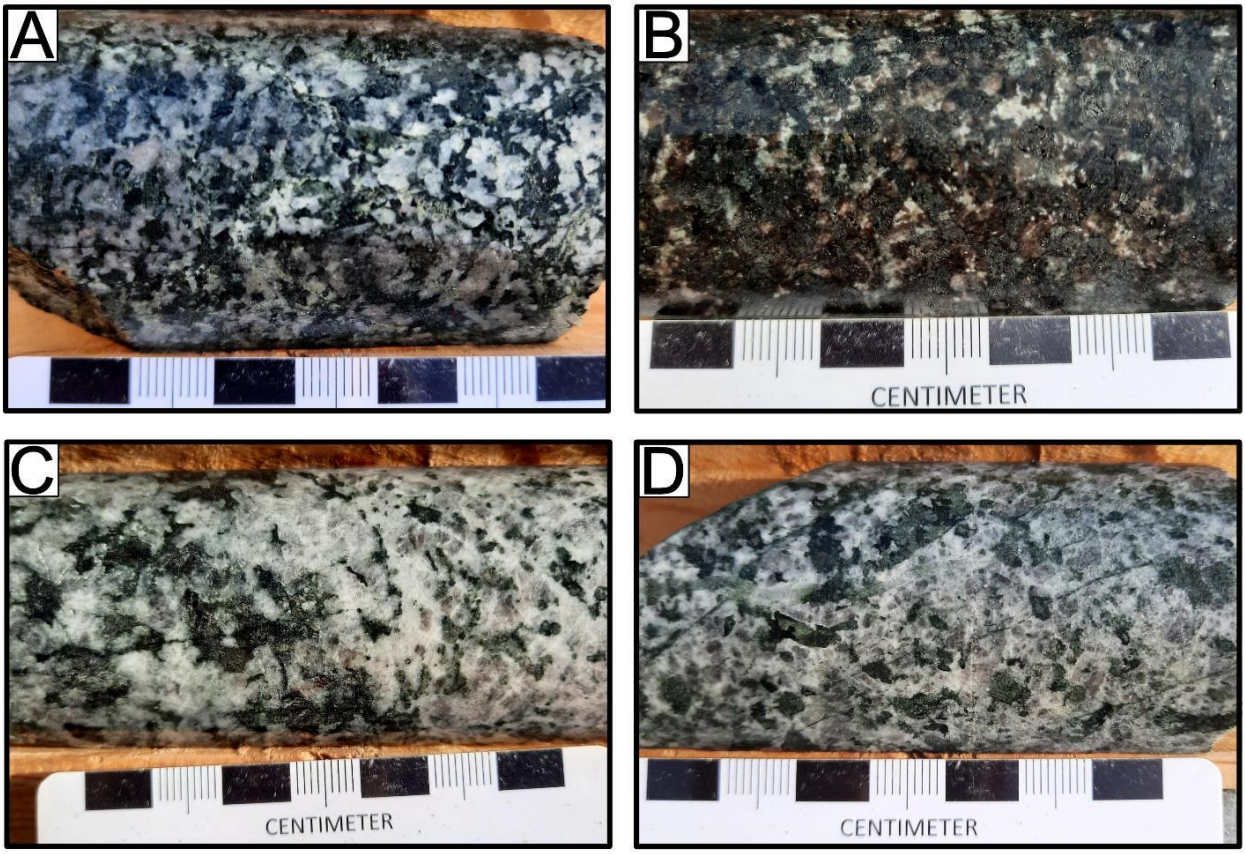

Figure 4.11 – Breccia domain rocks from DH# 19-025. A) Typical texture and alteration intensity of varitextured gabbronorite. B) Interval of weakly altered varitextured gabbronorite. C) Contact between leucogabbronorite and gabbronorite. D) Typical texture and alteration intensity of varitextured leucogabbronorite.

Finely disseminated to interstitial pyrrhotite-chalcopyrite-pentlandite-pyrite makes up 0.5-1.0% of a 12.6 m interval directly below the domain boundary contact (Fig. 4.12A/B), with the same assemblage observed as fine disseminations at trace quantities through the rest of the domain. Magnetic susceptibility within the breccia domain of DH# 19-025 averages slightly higher than seen in the breccia domain of logged Offset Zone drill holes, generally between 0.5 $x10^{-3}$ kappa and 10.0 $x10^{-3}$ kappa, and locally increasing to up to 80-95 $x10^{-3}$ kappa in a few

sections of weakly altered pegmatitic gabbronorite. No magnetite was observed within hand samples of the breccia domain of DH# 19-025.

The overall structure of the brecciated domain in DH# 19-025 is difficult to discern, as is the exact nature of the relationship between brecciated clasts and host rock. Due to the seemingly random orientation of leucogabbronorite intervals and the irregular nature of the majority of contacts bounding leucogabbronorite, with combinations of straight/jagged/ gradational boundaries commonly seen bounding individual intervals (Fig. 4.12C/D), these intervals are interpreted to be clasts rather than co-magmatic intrusions. Clasts of leucogabbronorite range from 20 cm to 21.5 m in length, with individual leucogabbronorite clasts commonly interrupted by <20 cm intervals of gabbronorite and melanocratic gabbronorite, bound by sharp contacts. Quartz-albite-biotite dikes and quartz-albite veins, of similar character to those in the Offset Zone, each make up ~1% of the logged interval, generally occurring within and adjacent to zones of brecciation. The contact between the breccia and norite domains in DH# 19-025 occurs as a 7 m zone of alternating lithologies from both domains. The presence of alternating lithologies at the domain contact may represent an oblique drill hole section of an undulating contact, or the intrusion of magma from one domain into rocks of the other domain.

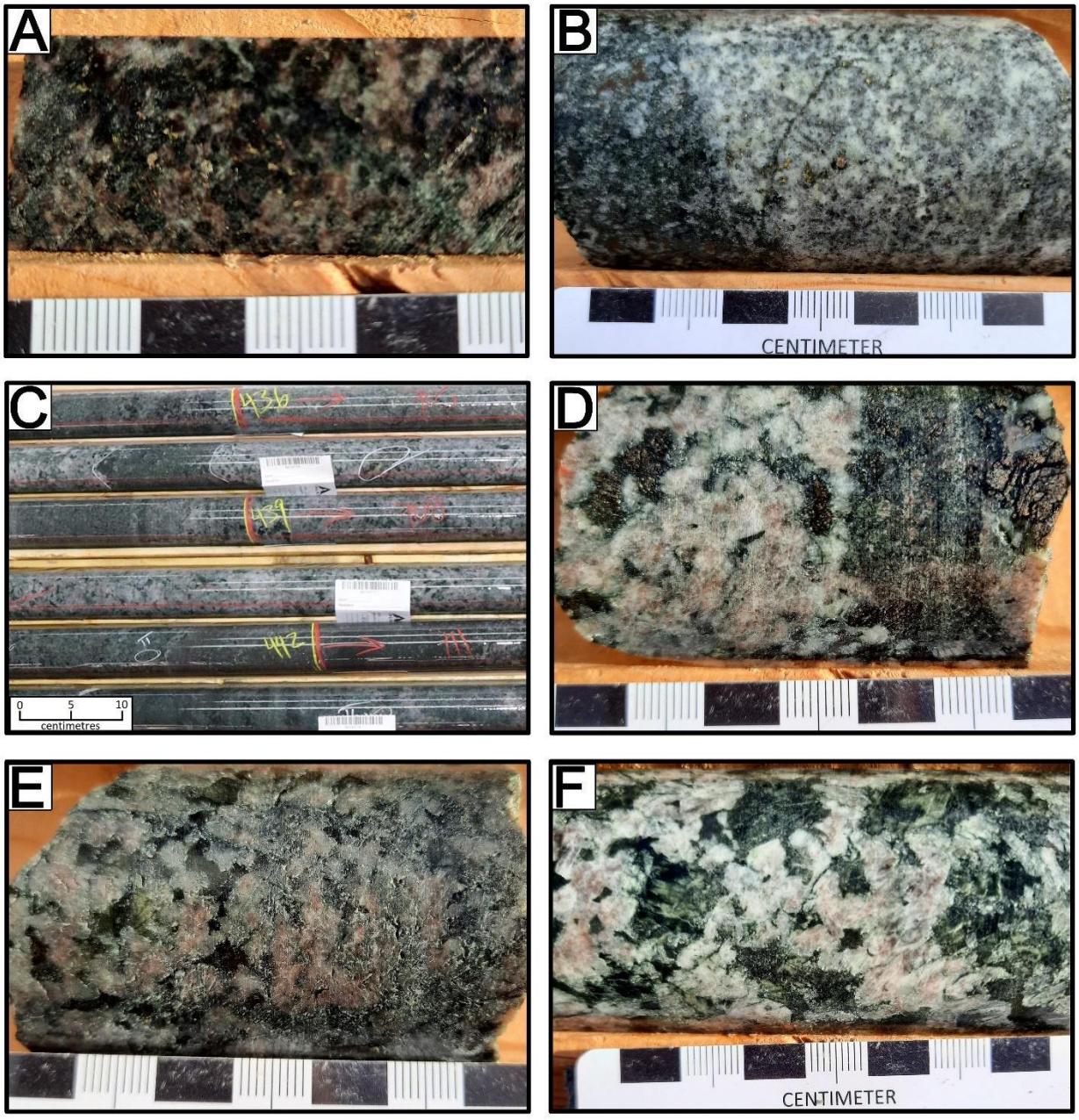

Figure 4.12 – Breccia domain rocks from the Creek Zone. A) Sulfide mineralization in pegmatitic gabbronorite. B) Sulfide mineralization at a gabbronorite-leucogabbronorite contact in DH# 19-025. C & D) Representative samples of breccia domain rocks in DH# 19-025. E) Weakly altered glomerophyric leucogabbronorite from DH# 19-009. F) Typical texture and alteration intensity of glomerophyric leucogabbronorite from DH# 19-009.

Intensity of alteration within the breccia domain of DH# 19-025 is more consistent and generally weaker than seen in the breccia domain of the Offset Zone. Plagioclase appears to be largely unaltered; pre-alteration crystal boundaries and cleavage faces are discernible throughout. Pyroxene ranges from unaltered to completely replaced by chlorite and actinolite, and higher degrees of pyroxene alteration are mostly present in leucocratic intervals. Pyroxene is most commonly partially to completely altered to a dull grey-green. Fine-grained chlorite-actinolite veinlets (0.5-2.0 mm wide) are present, with similar appearance and in similar quantity to those seen in the Offset Zone. No association between alteration intensity and depth or proximity to the domain boundary contact was observed.

4.1.2.2 – Breccia domain within DH# 19-009

The breccia domain interval in DH# 19-009 is made up of coarse-grained to pegmatitic varitextured leucogabbronorite (Fig. 4.12E/F). Variations in grain size are similar to those in other areas in the breccia domain, but the magnitude of variation is less and <5 mm crystals are very rarely observed. Glomerophyric “popcorn texture” is observed in the majority of rocks within this interval, comprising 65-80% plagioclase and 20-35% pyroxene prior to alteration. Sulfide minerals were not observed aside from a 70 cm interval of 2% interstitial pyrite and trace very finely disseminated chalcopyrite. Magnetic susceptibility is similar to breccia domain rocks of the Offset Zone and generally lower than observed in DH# 19-025, most commonly ranging from 0.5 $x10^{-3}$ kappa to 2.0 $x10^{-3}$ kappa and reaching a maximum of just 3.1 $x10^{-3}$ kappa. No magnetite was observed within hand samples of the breccia domain in DH# 19-009. The contact between the breccia and norite domains in DH# 19-009 appears to be sharp, though

the exact nature cannot be discerned due to the presence of a 4 cm mafic dike at the domain boundary.

The degree of alteration within DH# 19-009 is variable and generally increases with depth, aside from at the upper contact with the norite domain where alteration is stronger. In general, the degree of alteration is less than in the Offset Zone and similar to the generally weak alteration observed in the breccia domain of DH# 19-025. Plagioclase is mostly unaltered, and is dominantly purple-grey in less altered intervals and white within areas of stronger alteration. Pyroxene alteration ranges from rims to complete replacement by chlorite and actinolite. Quartz-carbonate veinlets (0.3-2.0 cm wide) with epidote and/or hematite alteration haloes present over a 3 m interval below the domain boundary contact, and occasional <2 mm chlorite-actinolite veinlets were observed. Aside from these, no veins or dikes are observed within the breccia domain in DH# 19-009.

4.1.2.3 – Norite domain within the Creek Zone

Both drill holes from the Creek Zone collared into rocks of the norite domain. Equigranular, massive gabbronorite comprises the majority of both intersections (Fig. 4.13), interrupted in both drill holes by intermittent <1m sections in which grain size is locally variable but composition is the same as surrounding intervals. The composition of the norite domain rocks within the Creek Zone are generally similar to those observed in the Offset Zone, comprising 45-55% plagioclase and 45-55% pyroxene prior to alteration. Relative quantities of plagioclase and pyroxene remain similar throughout the entire logged interval in DH# 19-009. In DH# 19-025, plagioclase/pyroxene proportion decreases slightly at 379 m, shifting from an

average of 55% plagioclase/45% pyroxene to 45% plagioclase/55% pyroxene. As seen in the Offset Zone, plagioclase is most commonly purple-grey and pyroxene is dark grey-brown, whereas grey-white plagioclase and dark green alteration products of pyroxene are observed in areas of strongest alteration. Biotite was intermittently observed, composing 0-2% of the total rock. Pyrrhotite-chalcopyrite±pentlandite±pyrite was present as trace disseminations and <1 m zones of 0.1-2% interstitial/disseminated sulfide throughout the majority of both drill holes. From 373.4-388.2 m in DH# 19-025, 1-2% disseminated to blebby pyrrhotite-chalcopyrite-pentlandite-pyrite was observed (Fig. 4.13F). Increased sulfide content was also seen directly adjacent to the domain boundary contact in DH# 19-025, present as 1% pyrrhotite-chalcopyrite-pentlandite-pyrite. Pyrite was the only sulfide mineral observed in DH# 19-009, occurring as trace disseminations as well as very rare <1 cm blebs.

A single short interval of disseminated magnetite was encountered in both drill holes; 5% coarsely disseminated magnetite was seen over a 35 cm area directly above the domain boundary contact in DH# 19-009, and 3% finely disseminated magnetite was observed within a 2.5 m interval in DH# 19-025. Magnetic susceptibility within DH# 19-025 was most commonly between 5.0 $x10^{-3}$ kappa and 30.0 $x10^{-3}$ kappa, decreasing to <3.0 $x10^{-3}$ kappa in the most strongly altered portions. Magnetic susceptibility within DH# 19-009 was variable depending on alteration intensity. In the more strongly altered upper part of the drillhole, magnetic susceptibility ranges from 0.7 $x10^{-3}$ kappa to 27.4 $x10^{-3}$ kappa, and ranges from 40.0 $x10^{-3}$ kappa to 70.0 $x10^{-3}$ kappa in the less altered lower part of the norite domain.

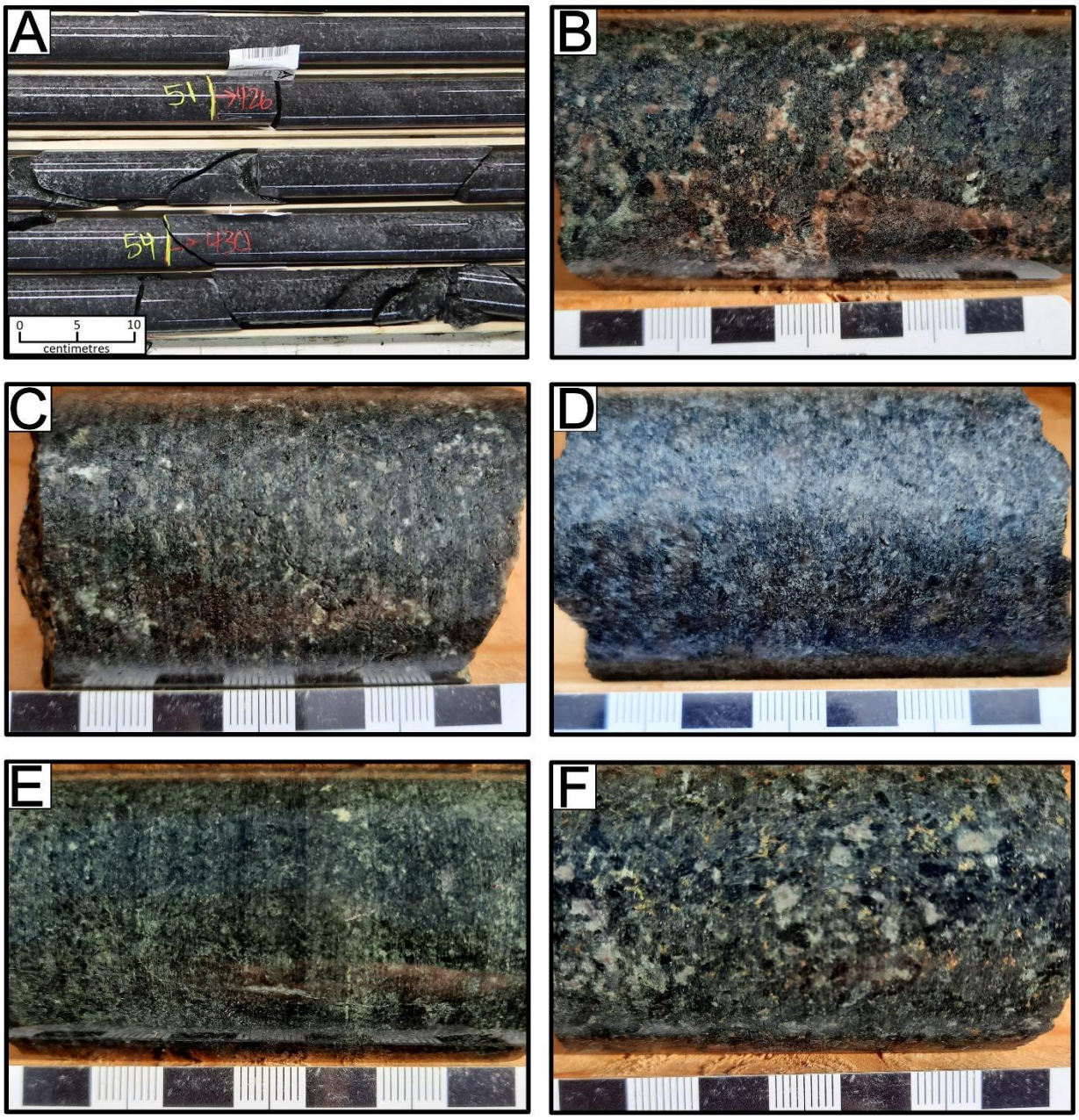

Figure 4.13 – Norite domain rocks from the Creek Zone. A) Representative drill core intersection of norite domain gabbronorite in DH# 19-009. B) Weakly altered gabbronorite from DH# 19-009. C) Moderately altered gabbronorite from DH# 19-009. D & E) Strongly altered gabbronorite from DH# 19-009 & DH# 19-025. F) Sulfide mineralization in altered gabbronorite from DH# 19-025.

Norite domain rocks within the Creek Zone generally have a similar texture and structure to those seen in the Offset Zone. Both Creek Zone drill holes are almost entirely equigranular and massive, lacking grain size variability seen in rocks of the breccia domain. Short intervals of local grain size variability were present in both Creek Zone drill holes, in which crystal size ranges from medium-grained to pegmatitic within <50 cm intervals. A few <10 cm zones are present in both drill holes where pyroxene appears to be weakly aligned (Fig. 4.14A); these zones are located adjacent to quartz-carbonate or chlorite-actinolite veinlets are most likely due to the alignment of the pyroxene alteration products, chlorite and actinolite. Brecciated rocks were not observed within the norite domain of the Creek Zone. Several 1-5 cm-wide layers of anorthosite, consisting of 90% plagioclase and 10% pyroxene, were observed within a 30 cm interval in DH# 19-025 (3.14B/C). An interval of intermittent fracturing and local faulting was observed at 22.8-35.0 m in DH# 19-009, characterized by increased alteration intensity and several rubble zones consisting of heavily fractured drill core, fault gouge, and occasional slickensides (3.14D/E/F). The angle of broken drill core is variable throughout the interval, most commonly 35-40 degrees to drill core axis.

Dikes and veins were less common than in the Offset Zone. One 15 cm-wide felsic dike and one 70 cm-wide mafic dike were seen in DH# 19-025, whereas no dikes were observed within the norite domain in DH# 19-009. Quartz±albite veinlets (1-10 mm in diameter) were observed in DH# 19-025, occurring in random orientation and in lesser quantity than in the Offset Zone, comprising <0.5% of the total logged interval. An increased number of quartz±albite veinlets were observed in a 7 m interval directly adjacent to the domain boundary contact, making up 1% of the logged interval. 1-5 mm chlorite-actinolite veinlets were present

in both drill holes, encompassing <0.5% of the total logged interval and occurring in random orientation, commonly in clusters over the span of <50 cm.

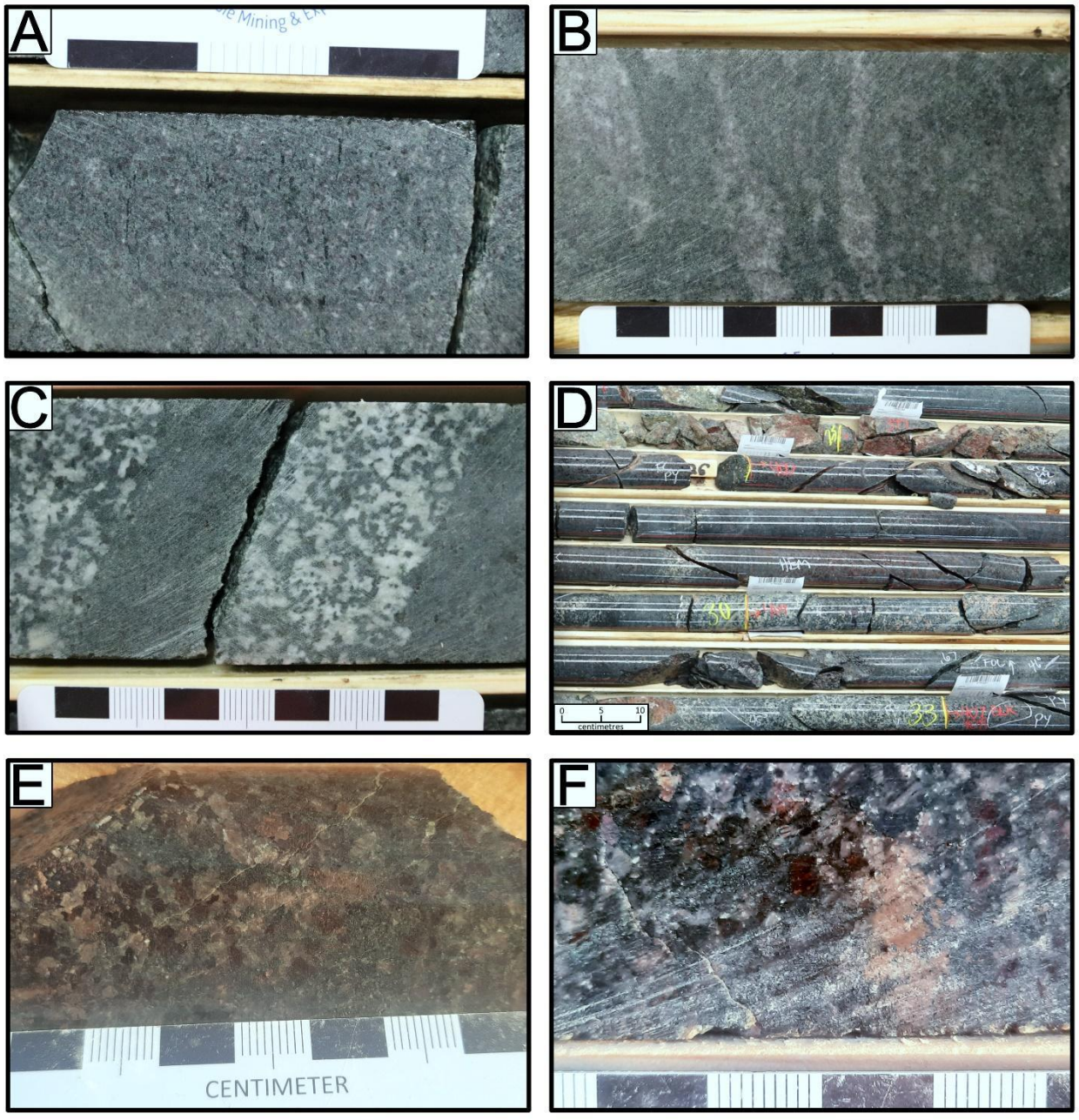

Figure 4.14 – Norite domain rocks from the Creek Zone. A) Aligned pyroxene alteration products in DH# 19-025. B) Anorthosite layers within gabbronorite in DH# 19-025. C) Leucogabbronorite layers within gabbronorite in DH# 19-025. D) Portion of fractured zone in DH# 19-009. E & F) Hematite-altered gabbronorite from fractured zone in DH# 19-009.

Alteration within the norite domain of the Creek Zone is generally less intense than the breccia domain of the Creek Zone and both domains of the Offset Zone. Plagioclase is generally unaltered, whereas pyroxene ranges from unaltered to completely replaced, most commonly partially altered to rims of dark green-grey chlorite and actinolite. In DH# 19-025, alteration is locally increased over several 0.5-3.0 m intervals in which pyroxene in completely replaced by chlorite and actinolite that is lighter in colour than surrounding areas, and a minority of plagioclase crystals are altered to albite. This increased degree of alteration is seen in a 3 m interval directly above the domain boundary contact in DH# 19-025. In DH# 19-009, pervasive alteration of pyroxene to lighter-coloured chlorite/actinolite and minor albite alteration of plagioclase were observed in the top portion of the logged intersection to 40.8 m, whereas only rims of chlorite and actinolite around pyroxene crystals were observed from 40.8 m to the domain boundary contact. Alternating zones of pervasive hematite and pervasive albite-potassic-chlorite-actinolite alteration were observed within the faulted zone intersected in DH# 19-009. A second zone of pervasive hematite alteration is observed at 58.8-61.0 m in DH# 19-009. No increase in alteration intensity with proximity to the domain boundary contact was observed in DH# 19-009.

4.2 - Petrography

Petrographic data was collected at Lakehead University via transmitted and reflected light microscopy. Mineral identification and modal percentage estimations were conducted by visual interpretation. Detailed descriptions of all samples are included in Appendix A.

As described in Section 4.1, two lithological domains (breccia and norite) were identified in each of the four logged drillholes. As this study was focused on characterizing the nature of the area proximal to the domain boundary contacts, sampling density for petrographic analysis was increased in the area around the contacts and decreased with distance from the contacts. Additionally, because the main focus area of this project was the Offset Zone, a larger number of samples were analyzed from the Offset South Zone (n = 29) and the B3 Zone (n = 40) than the Creek Zone (n = 14). Between the four studied drillholes, a total of 37 samples were petrographically analyzed from the breccia domain, and 46 samples were analyzed from the norite domain. In addition, two polished thin sections of tonalitic gneiss were prepared for the purpose of performing sulfur isotope analysis of pyrite. Petrographic analysis of these two samples was not performed.

All analyzed samples are plagioclase-pyroxene adcumulates that have been partially to completely altered to secondary silicate minerals. Of the samples that are mostly made up of unaltered or weakly altered primary magmatic minerals, all samples are primarily composed of plagioclase, orthopyroxene, and clinopyroxene, with up to 3% biotite, up to 6% oxides, and trace hornblende sometimes present as accessory phases. Sulfide minerals are present in all samples and range from trace quantities to 4% of a given sample. In 57 of 83 samples, >90% of

pyroxene is altered to a hydrous mineral assemblage; most of these samples have >99% alteration of pyroxene. Due to the lack of discernible differences between orthopyroxene and clinopyroxene in these samples, IUGS classification was not attempted in samples in which >90% pyroxene is altered. Of the samples that contain <90% alteration of pyroxene, all samples are either norites or gabbronorites.

Attempts were made to estimate the pre-alteration proportion of plagioclase and pyroxene in all samples. Based on petrographic relationships (especially the presence of certain minerals as partial pseudomorphs of partially altered primary crystals), most of the minerals present in the samples could be categorized primarily as alteration products of plagioclase (white mica, epidote, quartz; Fig. 4.15A) or pyroxene (tremolite-actinolite, talc, anthophyllite; Fig. 4.15B). Due to this, the pre-alteration mineral proportions are assumed to be broadly correct, but may be imprecise on the order of several percentage points, especially in the most intensely altered samples (Fig. 4.15C).

In estimating pre-alteration mineral percentages, alteration minerals were categorized as products of the minerals they are commonly associated with (Appendix A), despite the fact that some of the alteration minerals were observed replacing multiple magmatic minerals. Chlorite is generally present as an alteration product of plagioclase, but commonly also occurs as a minor component of alteration aggregates occurring after pyroxene (Fig. 4.15D). In a few samples, more chlorite was seen as an alteration product of pyroxene than of plagioclase. Tremolite-actinolite and talc are present as alteration products of both orthopyroxene and clinopyroxene. Pyroxene alteration minerals are listed in Appendix A as alteration products of the primary mineral that the majority of the alteration mineral is associated with. Due to the

presence of some of these alteration minerals as products of multiple magmatic minerals, some discrepancies are present between pre-alteration and post-alteration mineral percentages in Appendix A.

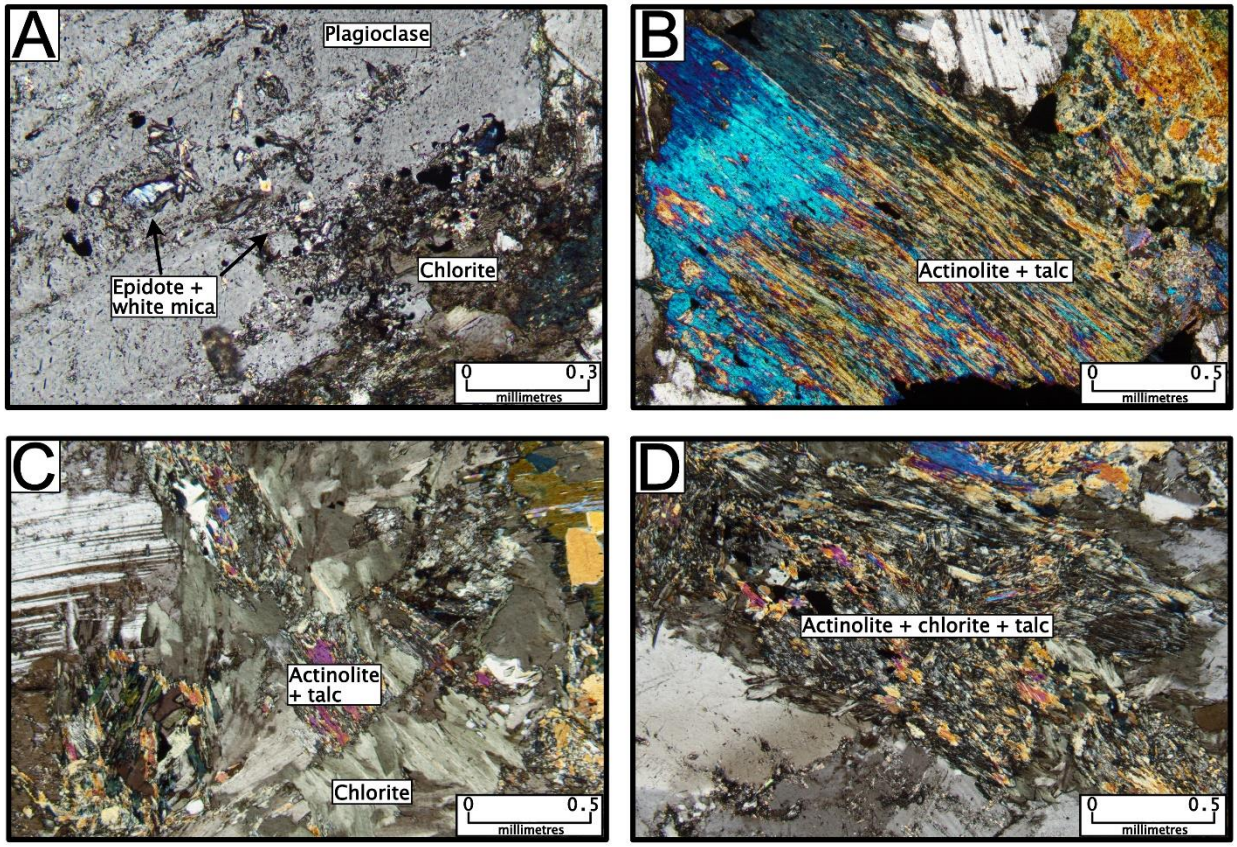

Figure 4.15 – Examples of alteration styles from the study area. Photos taken under cross-polarized light. A) Plagioclase partially altered to white mica+chlorite+epidote (Sample JJ-TS-011). B) Pyroxene completely altered to actinolite+talc (Sample JJ-TS-189). C) Intensely altered portion of sample in which pre-alteration crystal boundaries are difficult to discern (Sample JJ-TS-072). D) Pyroxene completely altered to actinolite+chlorite+talc (Sample JJ-TS-071).

4.2.1 – Breccia domain within the Offset Zone

Thirty-one samples were petrographically analyzed from the breccia domain of the Offset Zone. Eighteen of these samples were from DH# 17-804 from the Offset South Zone, and 13 were from DH# 18-805 from the B3 Zone. Sampling density varied throughout the drillholes,

with increased density in Pd-enriched zones as well as in proximity to the geological domain boundary with the adjacent norite domain.

Sampling in the Offset South Zone was focused on two zones of Pd enrichment intersected in the breccia domain by DH# 17-804 (Fig. 4.16); an upper mineralized zone averaging 2.09 ppm Pd over 25.0 metres wholly within the breccia domain, and a lower mineralized zone averaging 2.81 ppm Pd over 28.0 metres spanning the contact between the breccia and norite domains (2.00 ppm Pd over 14.0 m in the portion in the breccia domain). Samples were taken every 5 metres in the upper mineralized zone, and every 2 metres in the lower mineralized zone. Other samples in the breccia domain of DH# 17-804 were taken at irregular spacing to encompass relatively leucocratic and melanocratic zones within the drill hole, and to encompass less Pd-enriched material located directly above the Pd-enriched zone at the domain boundary contact.

Sampling in the B3 Zone was focused on the area directly above the contact with the norite domain boundary (Fig. 4.17), as no major zone of Pd enrichment was encountered in the breccia domain of DH# 18-805. Samples from DH# 18-805 were largely taken at regular intervals, with samples taken every 2 metres for 12 metres above the contact, with wider spacing between samples with greater distance from the boundary contact.

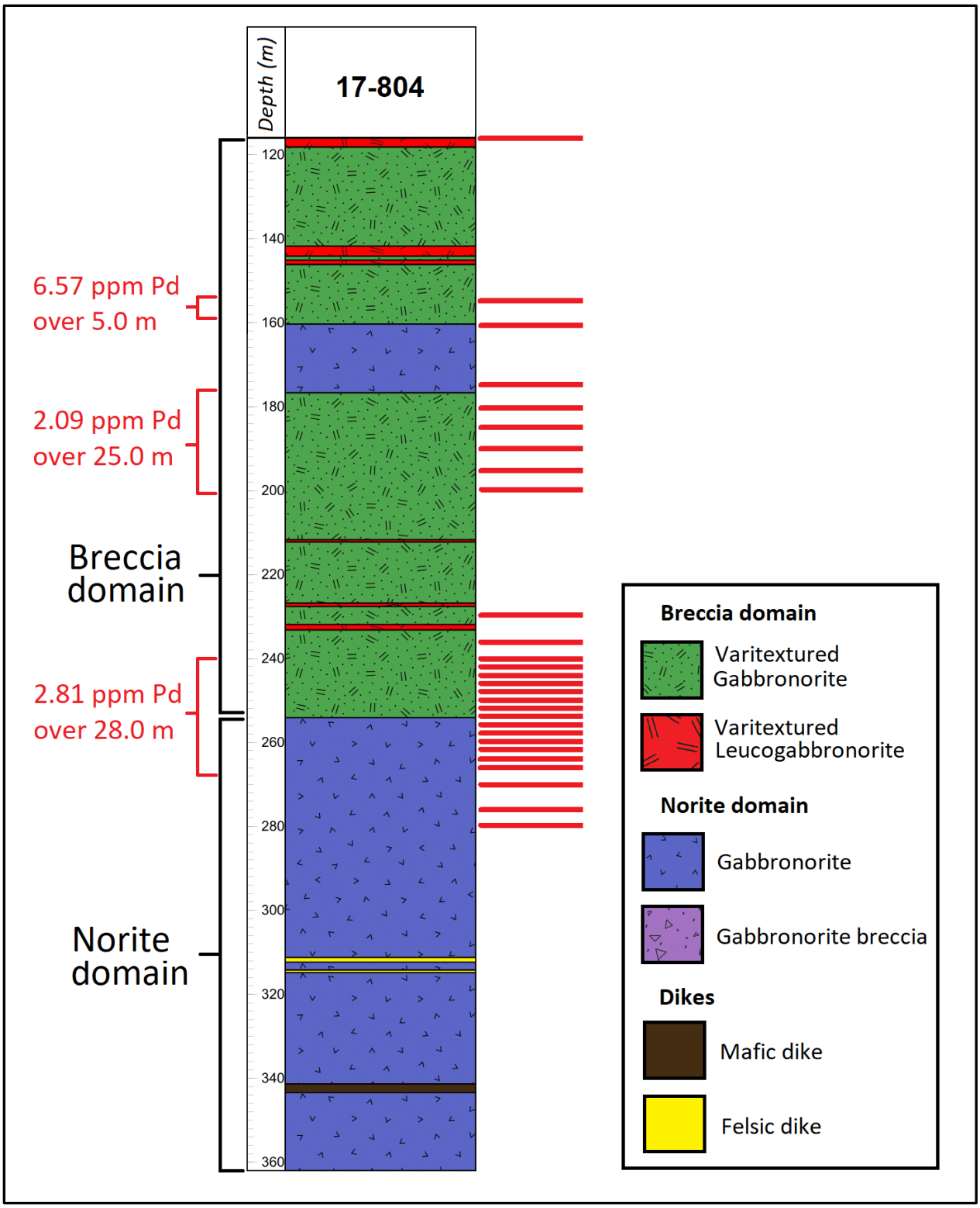

Figure 4.16 – Sample locations for petrographic analysis from DH# 17-804, denoted by red lines (assay results provided by Impala Canada).

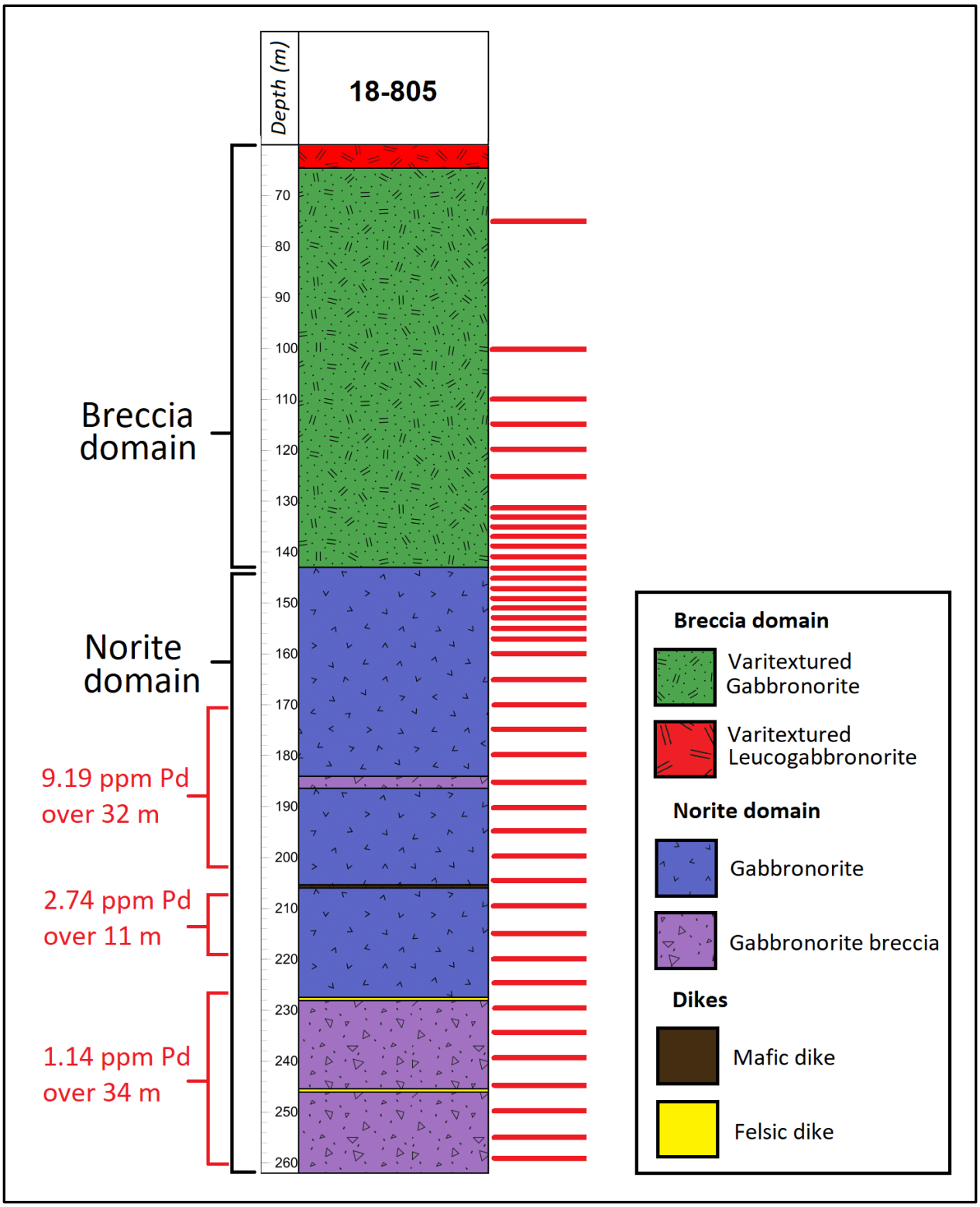

Figure 4.17 – Sample locations for petrographic analysis from DH# 18-805, denoted by red lines (assay results provided by Impala Canada).

Due to the degree of alteration of pyroxene, it was not possible to determine the pre-alteration proportion of orthopyroxene and clinopyroxene in most samples. As result, the majority of these samples cannot be classified via IUGS classification. Of the eight samples that have <90% alteration of pyroxene, seven plot within the gabbronorite field and one plots on the boundary between gabbronorite and norite (Fig. 4.18).

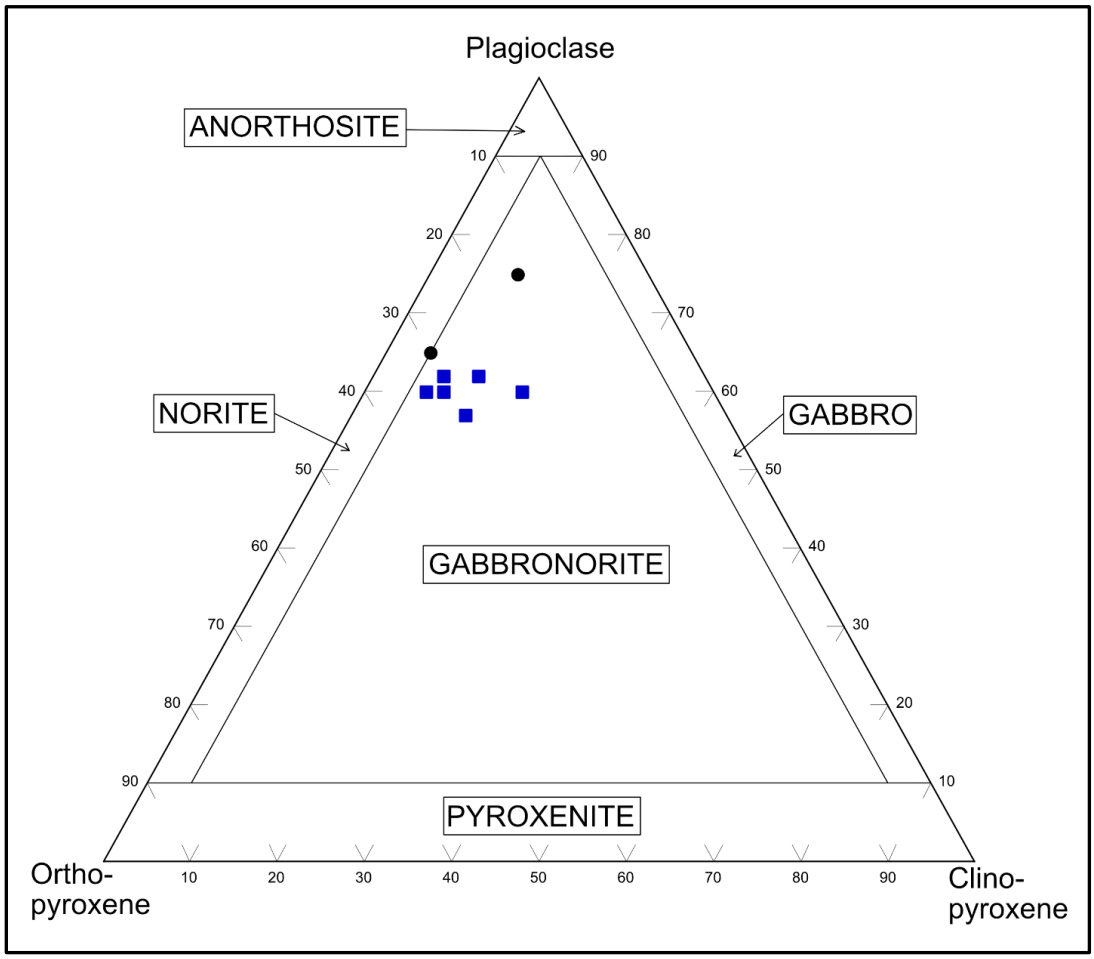

Figure 4.18 – Ternary diagram of plagioclase, orthopyroxene, and clinopyroxene content of samples from the breccia domain of the Offset Zone (Offset South Zone = black circles. B3 Zone = blue squares).

4.2.1.1 – Breccia domain within the Offset Zone – Crystal proportions and properties

Most of the samples from the breccia domain of the Offset Zone have similar textures, crystal size, and pre-alteration proportions of plagioclase and pyroxene. Biotite is the only other magmatic silicate mineral observed and is present in almost all samples. The primary texture is fairly well preserved in the majority of samples (Fig. 4.19A, B) due to the low degree of plagioclase alteration and the tendency of alteration minerals to pseudomorph magmatic minerals. Plagioclase and pyroxene crystals both show significant variation in size, with crystals ranging from <0.1 mm to ~30 mm in size. Local poikilitic texture is common (Fig. 4.19C, D), in which larger crystals (usually plagioclase or clinopyroxene) partially to completely encircle smaller crystals (usually plagioclase and/or orthopyroxene).

Plagioclase is the dominant mineral present in almost all samples, generally making up 55-65% of the rock prior to alteration. Crystals are usually anhedral to rarely subhedral, aside from smaller crystals that are encircled by other crystals, which are commonly subhedral to rarely euhedral (Fig. 4.20A). Smaller to average-sized crystals (<3 mm) are typically equant, whereas >3 mm crystals range from equant to tabular. In several samples, lath-shaped crystals are present, partially to completely surrounded by pyroxene or other plagioclase crystals (Fig. 4.20B). Overall, average crystal size is quite variable from sample to sample, including in areas of denser sample spacing. In general, the average crystal size of most samples ranges from 0.8-2.5 mm. Average plagioclase crystal size shows no spatial variation in the B3 Zone, whereas samples distal from the domain boundary contact in the Offset South Zone generally have a larger crystal size than those that are closer (<25 m) to the contact. The maximum crystal size in a sample is generally ~5 mm, with plagioclase crystals up to 30 mm in size seen in a pegmatitic

sample from the Offset South Zone. Aside from the one pegmatitic sample, minimum crystal size of plagioclase is consistently <0.3 mm, with the smallest crystals typically encircled by plagioclase or pyroxene crystals, as well as at junctions between several crystals.

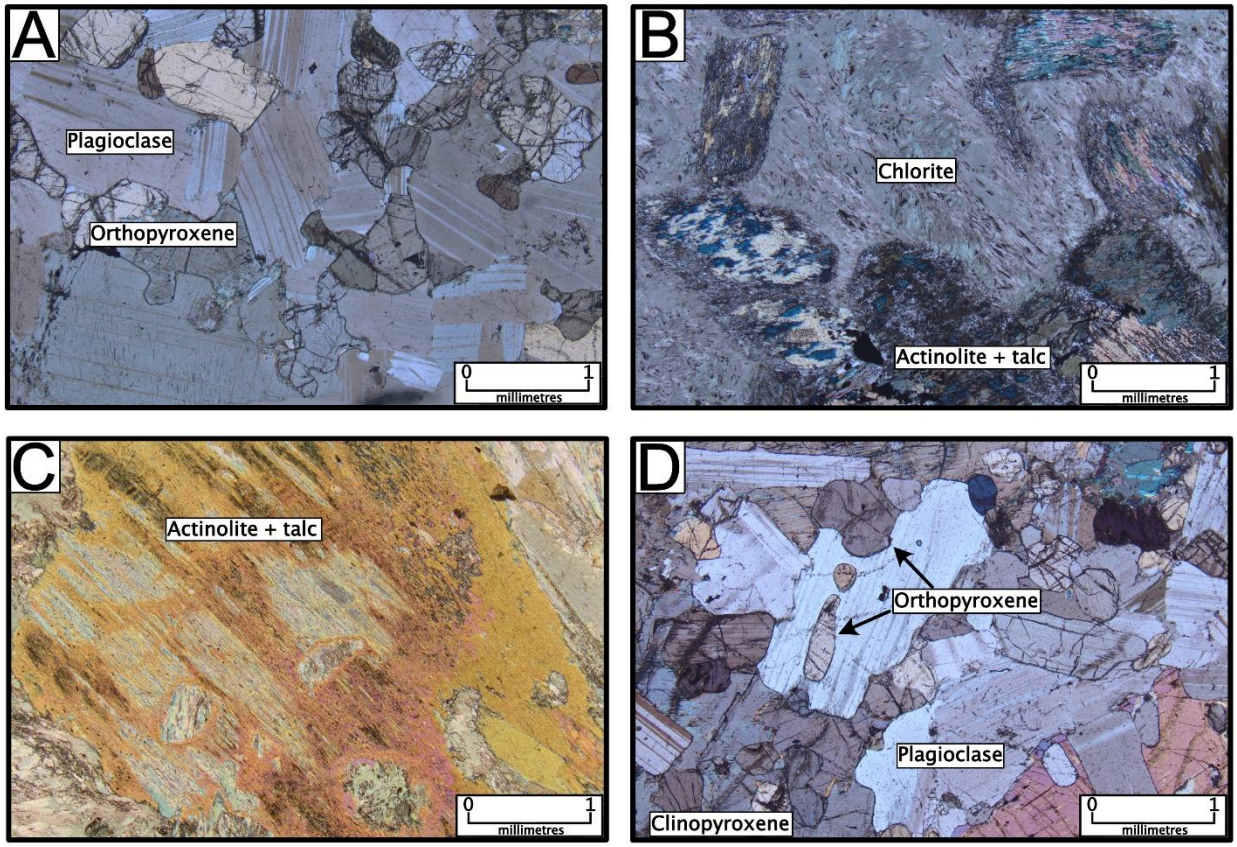

Figure 4.19 – Examples of textures from breccia domain of Offset Zone. Photos taken under cross-polarized light. A) Typical texture of unaltered sample (Sample JJ-TS-079). B) Typical texture of strongly altered sample, in which pre-alteration crystal boundaries are discernible (Sample JJ-TS-017). C) Poikilitic texture in which oikocryst and chadacrysts are completely altered (Sample JJ-TS-082). D) Typical poikilitic texture (Sample JJ-TS-080).

Boundaries between plagioclase crystals are typical of textural equilibration, with curved boundaries present in every sample (Fig. 4.21A) and triple junctions present in some samples. Plagioclase crystals commonly occur in clusters made up of several crystals of different sizes (Fig. 4.21B). Weak deformation twinning was observed in <5% of crystals in most samples (Fig. 4.21C). Plagioclase crystals are commonly weakly fractured, with fractures filled in most

cases by alteration minerals. A greater number of fractured crystals and crystals showing deformation twinning are present in samples that are less strongly altered. Strong recrystallization is present in one sample, in which 10% of the plagioclase in the sample is present as clusters of <0.1 mm crystals with polygonal triple junctions (Fig. 4.21D), occurring mostly as rims or within fractures in otherwise largely unaltered plagioclase crystals.

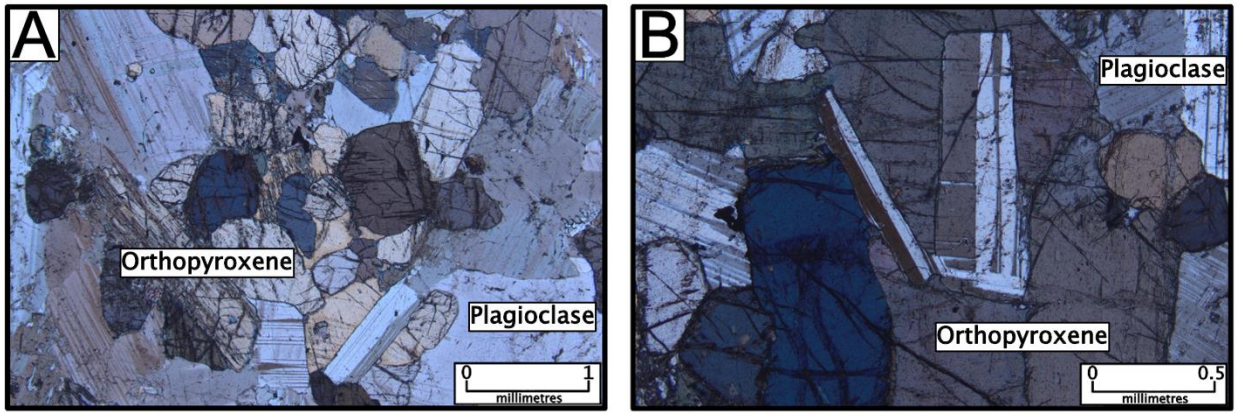

Figure 4.20 – Plagioclase morphology. Photos under cross-polarized light. A) Anhedral cumulate plagioclase, as well as subhedral plagioclase surrounded by orthopyroxene (Sample JJ-TS-080). B) Orthopyroxene enclosing lath-shaped and tabular plagioclase (Sample JJ-TS-079).

Pyroxene makes up the significant minority of most samples prior to alteration (generally 35-45%), and is the dominant mineral in two samples. The majority of altered pyroxene crystals that are pseudomorphed have similar shape, size, and habit to unaltered orthopyroxene, implying that orthopyroxene was the dominant pyroxene in these samples. Where alteration does not obscure crystal shape/habit, crystals were anhedral to subhedral and generally equant. Smaller crystals that are enclosed by plagioclase or other pyroxene are commonly euhedral (Fig. 4.22A). Larger (>2.5 mm) crystals are commonly anhedral and elongate. Maximum crystal size is typically ~5.0 mm, with crystals up to 15 mm in size seen in two pegmatitic samples from the Offset South Zone. Pyroxene crystals sometimes occur in

clusters (Fig. 4.22B). but most commonly do not, and do not display the equilibrated texture seen in plagioclase. Average crystal size of orthopyroxene/altered pyroxene is generally smaller than plagioclase, most commonly 1-2 mm. Unaltered pyroxene crystals are usually heavily fractured and commonly display good cleavage (Fig. 4.22C).

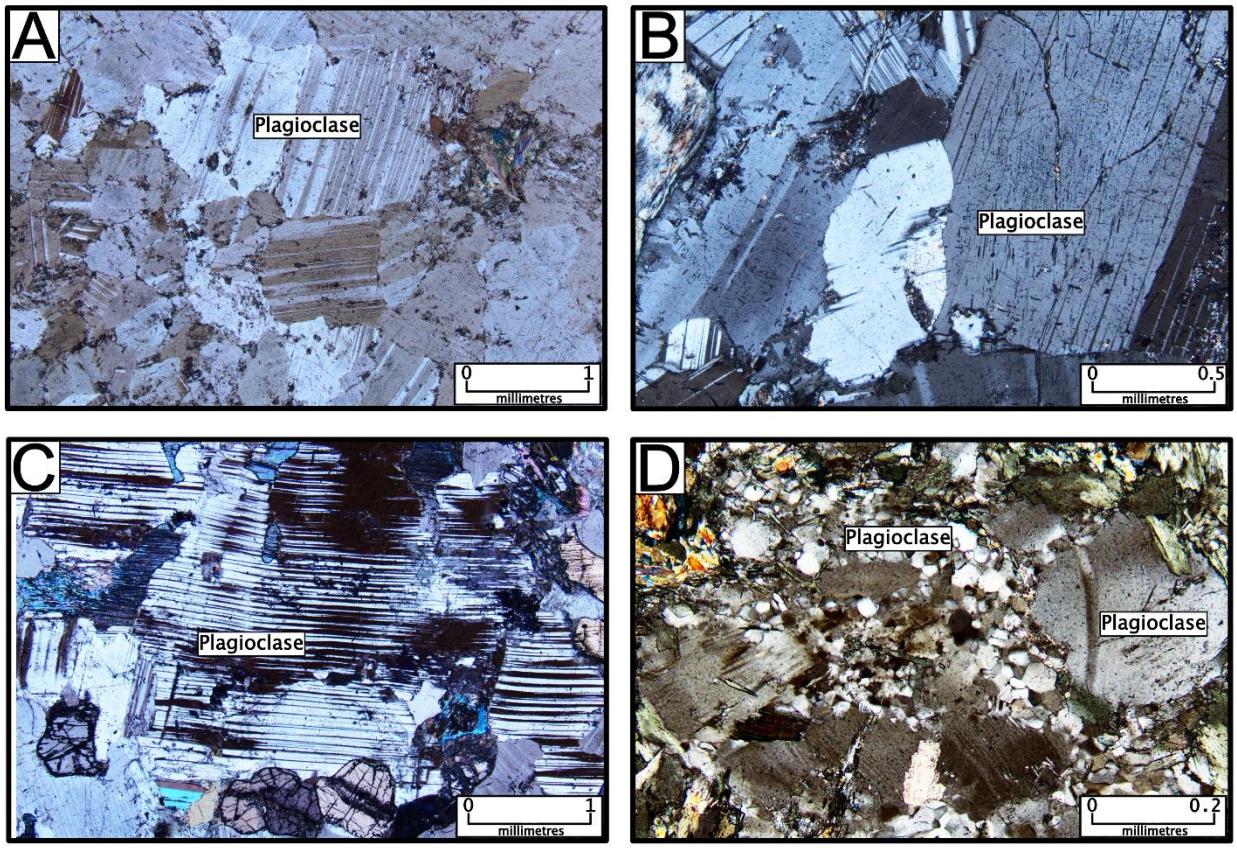

Figure 4.21 – Relationships between plagioclase crystals. Photos taken under cross-polarized light. A) Curvilinear boundaries of equilibrated plagioclase crystals (Sample JJ-TS-001). B) Plagioclase crystals of varying sizes occurring adjacent to each other (Sample JJ-TS-025. C) Deformation twinning in plagioclase (Sample JJ-TS-077). D) Recrystallized, very fine-grained plagioclase present in contact with magmatic plagioclase (Sample JJ-TS-071).

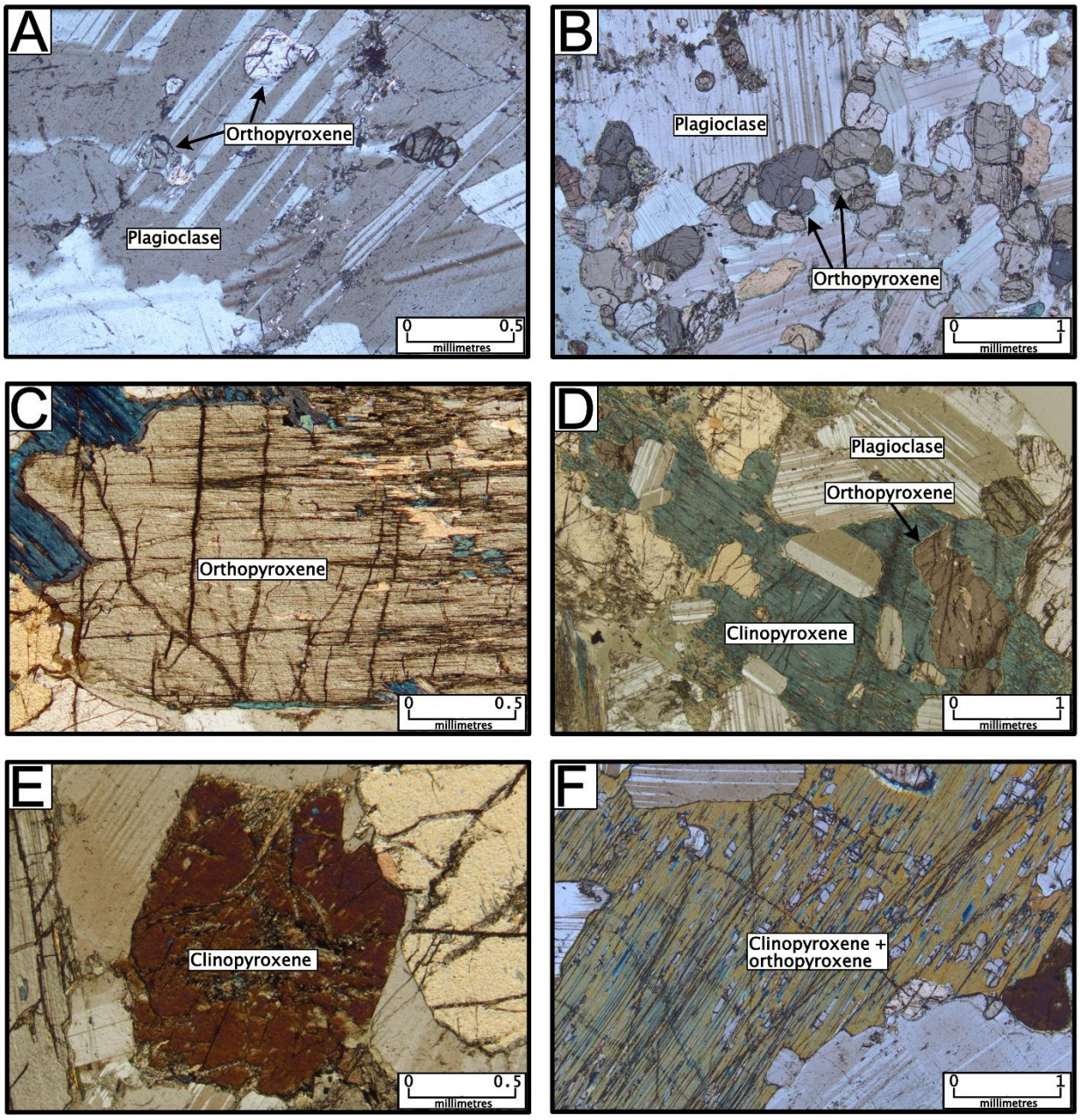

Figure 4.22 – Examples of pyroxene crystal morphology. Photos taken under cross-polarized light. A) Subhedral to euhedral orthopyroxene crystals completely surrounded by plagioclase (Sample JJ-TS-018). B) Clusters of orthopyroxene crystals (Sample JJ-TS-026). C) Typical unaltered orthopyroxene crystal, with heavy fracturing and good cleavage. D) Poikilitic texture, in which plagioclase and orthopyroxene are partially to completely surrounded by clinopyroxene (Sample JJ-TS-041). E) Equant, subhedral clinopyroxene crystal alongside orthopyroxene and plagioclase F) Orthopyroxene crystals exsolved from clinopyroxene.

Clinopyroxene crystals, in samples in which they are discernible, generally range in size from <2 mm to >10 mm. In all samples with identifiable clinopyroxene, the majority of crystals are significantly larger than plagioclase and orthopyroxene crystals, most commonly >5 mm in size. These crystals are anhedral and irregularly shaped, and always partially to completely enclose smaller crystals of plagioclase and orthopyroxene (Fig. 4.22D). In most samples with identifiable clinopyroxene, a minority of clinopyroxene crystals are <2 mm, equant, and generally subhedral (Fig. 4.22E). Elongate, very fine (<0.2 mm) orthopyroxene crystals are commonly present along cleavage planes of clinopyroxene crystals, appearing to be the product of exsolution (Fig. 4.22F).

Biotite is present in 28 of 31 samples analyzed from the breccia domain of the Offset Zone. Based on textural evidence, almost all biotite present in these samples appears to be primary, as crystals are typically elongate, platy, and sometimes occur in "books" that are characteristic of magmatic crystals (Fig. 4.23A, B); characteristics of secondary biotite such as very fine-grained aggregates or randomly oriented/pseudomorphic crystals were not observed. However, in moderately to strongly altered samples, these crystals of biotite that appear magmatic commonly occur within aggregates of alteration minerals such as chlorite and tremolite-actinolite (Fig. 4.23C, D). Biotite would generally be expected to be a product of alteration when in direct contact with these minerals, and as such, it is possible that some biotite present in these samples is secondary.

Sulfide minerals are present in every sample from the Offset Zone, ranging in quantity from <0.1% to 4%. Sulfide mineral proportion does not directly correlate to Pd enrichment. Although sulfide mineral proportion is generally higher in zones of Pd enrichment, several

samples in Pd-enriched zones contain comparable quantities of sulfide minerals to samples from outside of these zones. Pyrite and chalcopyrite are present in every sample from the Offset Zone, whereas pyrrhotite and pentlandite are present in a majority of samples. In most samples, sulfide minerals are commonly present as both interstitial polymineralic aggregates and finely disseminated monomineralic crystals. Interstitial crystals are composed of chalcopyrite and one or both of pyrite and pyrrhotite, with pentlandite commonly also present (Fig. 4.24A, B). Pyrite and/or pyrrhotite are typically the most volumetrically significant

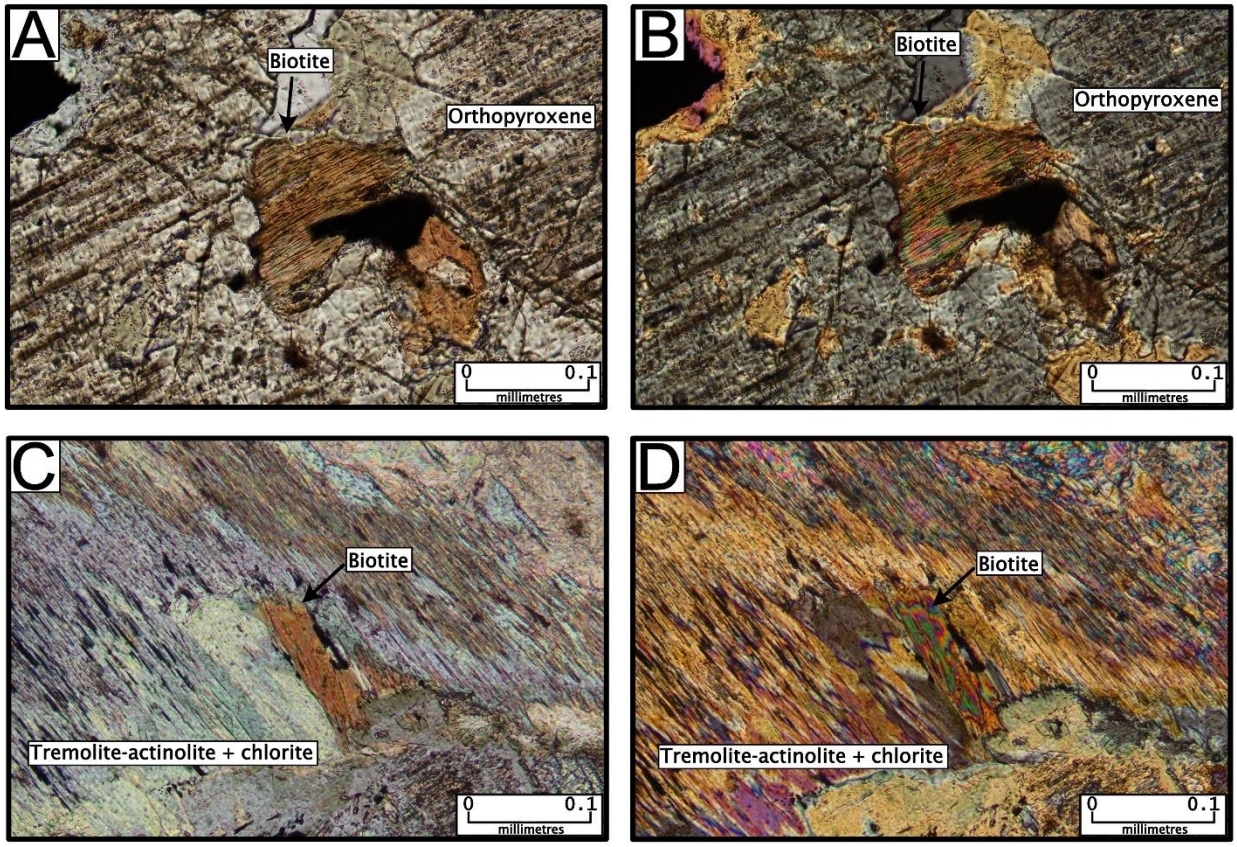

Figure 4.23 – A) Typical magmatic biotite crystal, under plane-polarized light (Sample JJ-TS-011). B) Typical magmatic biotite crystal, under cross-polarized light (Sample JJ-TS-011). C) Biotite crystal enclosed by alteration minerals, under plane-polarized light (Sample JJ-TS-009). D) Biotite crystal enclosed by alteration minerals, under cross-polarized light (Sample JJ-TS-009).

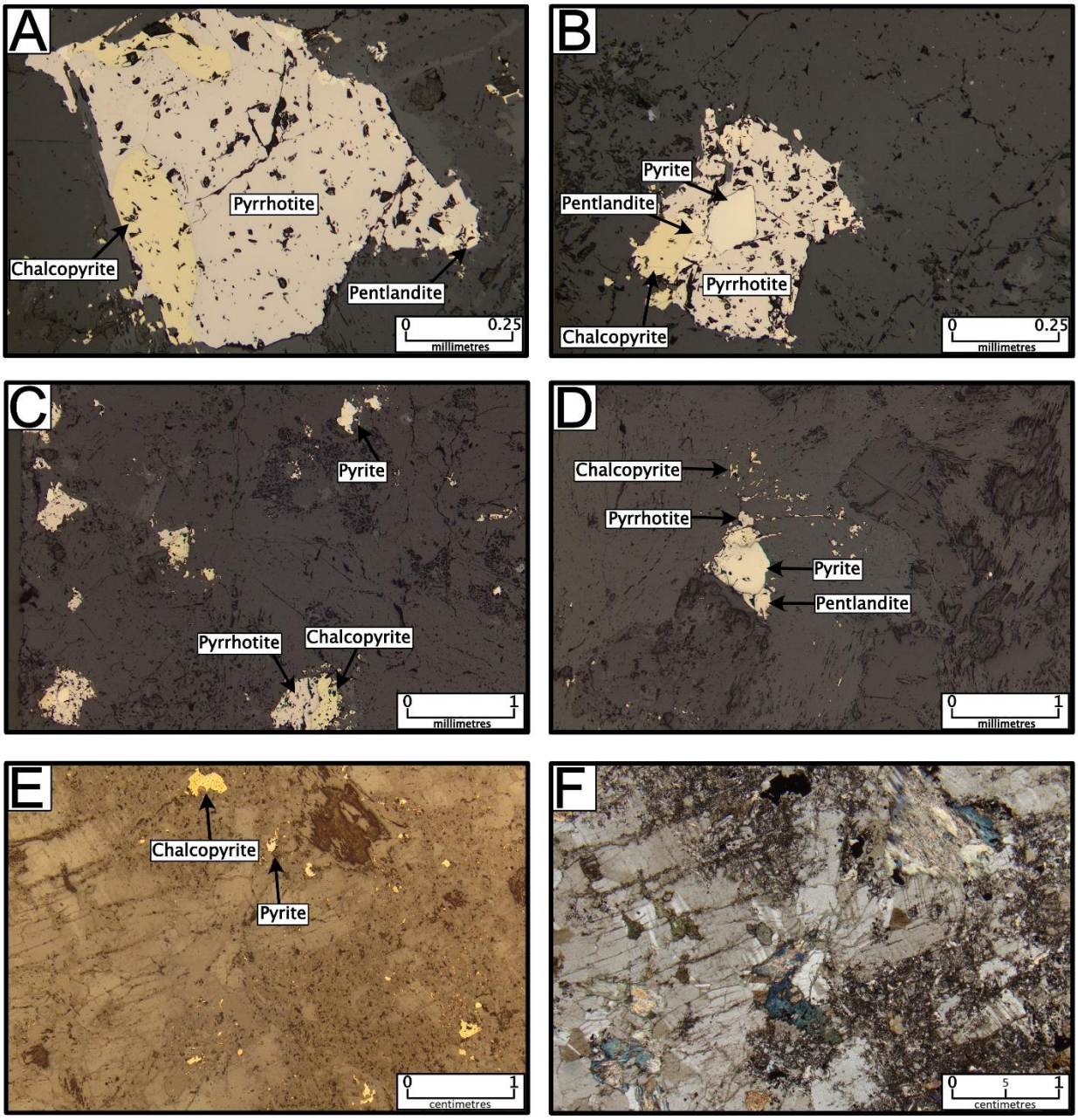

Figure 4.24 – Examples of sulfide mineral textures. Photos taken under reflected light, except for 4.24F which was taken under cross-polarized light. A) Interstitial polysulfide crystal composed of pyrrhotite, chalcopyrite, and pentlandite (Sample JJ-TS-016). B) Interstitial polysulfide crystal composed of pyrrhotite, pyrite, chalcopyrite, and pentlandite. C) Cluster of interstitial polysulfide crystals surrounded by disseminated monosulfide crystals (Sample JJ-TS-068). D) Polysulfide crystals surrounded by disseminated monosulfide crystals (Sample JJ-TS-032). E) Disseminated monosulfide crystals associated with silicate alteration minerals (Sample JJ-TS-068). F) Disseminated monosulfide crystals associated with silicate alteration minerals (Sample JJ-TS-068).

component. Interstitial crystals are typically 0.1-2.0 mm in size and irregularly shaped, and multiple crystals commonly occur in <2 cm clusters. Disseminated monomineralic crystals are typically very fine grained (<0.05 mm), composed of pyrite, chalcopyrite, or rarely pyrrhotite. These monomineralic crystals most commonly occur as <2 cm haloes around interstitial crystals and are commonly also disseminated throughout samples, most commonly in association with silicate alteration minerals (Fig. 4.24C, D).

Oxide minerals are present in nearly half of all samples from the breccia domain of the Offset Zone (15 out of 31). Magnetite is the dominant oxide mineral, occurring most commonly as 0.1-1.0 mm interstitial crystals. These crystals typically occur in proximity (<1 cm) to clusters of sulfide minerals (Fig. 4.25A), though they occur independent of sulfide minerals in a minority of samples. Magnetite also occasionally occurs as very finely disseminated (<0.05 mm) crystals present in silicate alteration mineral aggregates. In two samples, a darker-coloured grey mineral can be seen as elongate crystals (appearing to be exsolved from magnetite) and/or irregular partial rims; this mineral is interpreted to be ilmenite (Fig. 4.25B).

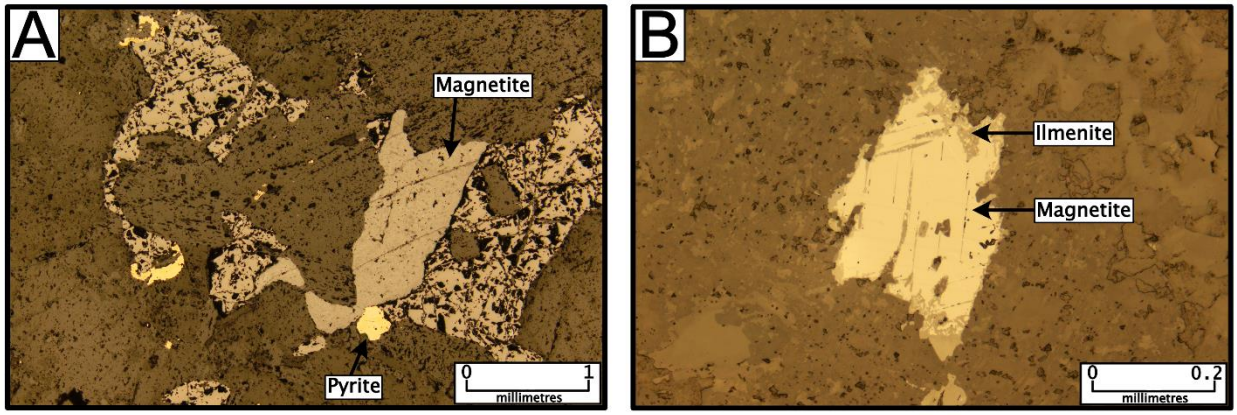

Figure 4.25 – Examples of oxide mineral textures. Photos taken under reflected light. A) Magnetite crystals in contact with sulfide minerals (Sample JJ-TS-017). B) Crystal primarily composed of magnetite with partial rim/exsolved crystals of ilmenite (Sample JJ-TS-033).

4.2.1.2 – Breccia domain within the Offset Zone – Alteration

Based on visual estimates, the mean proportion of plagioclase that has been replaced by alteration minerals in samples from the breccia domain of the Offset Zone is 15-20%. This data is skewed by two samples in which plagioclase has been completely or almost completely altered; nearly half (15 out of 31) of samples contain <10% altered plagioclase. Alteration intensity of plagioclase generally scales with alteration intensity of pyroxene; samples in which a significant amount of pyroxene is unaltered generally contain nearly completely unaltered (<2% of sample) plagioclase. The degree of plagioclase alteration in samples with >99% altered pyroxene ranges from 1-100%, and is most commonly between 10-20%. Alteration intensity of different crystals within the same sample is relatively homogeneous, with increased alteration in crystals surrounded by pyroxene or present in more pyroxene-rich areas (Fig. 4.26A, B).

White mica and chlorite are the most common alteration minerals present after plagioclase. Where plagioclase is weakly altered, white mica is generally the dominant alteration mineral and occurs either as monomineralic aggregates or in aggregates with minor chlorite and/or epidote (Fig. 4.26C). These are typically very fine-grained and most commonly occur as <0.1 mm patches, as fracture fill, and as partial rims. Muscovite is occasionally present as rare <0.2 mm platy crystals in these white mica-dominated alteration zones. Chlorite is typically present as a monomineralic very fine- to fine-grained aggregate in weakly altered samples, occurring as partial rims most commonly where plagioclase is in contact with altered pyroxene. Where plagioclase is strongly to completely altered, chlorite is the dominant alteration mineral, typically occurring as fine-grained aggregates alongside white mica (Fig.

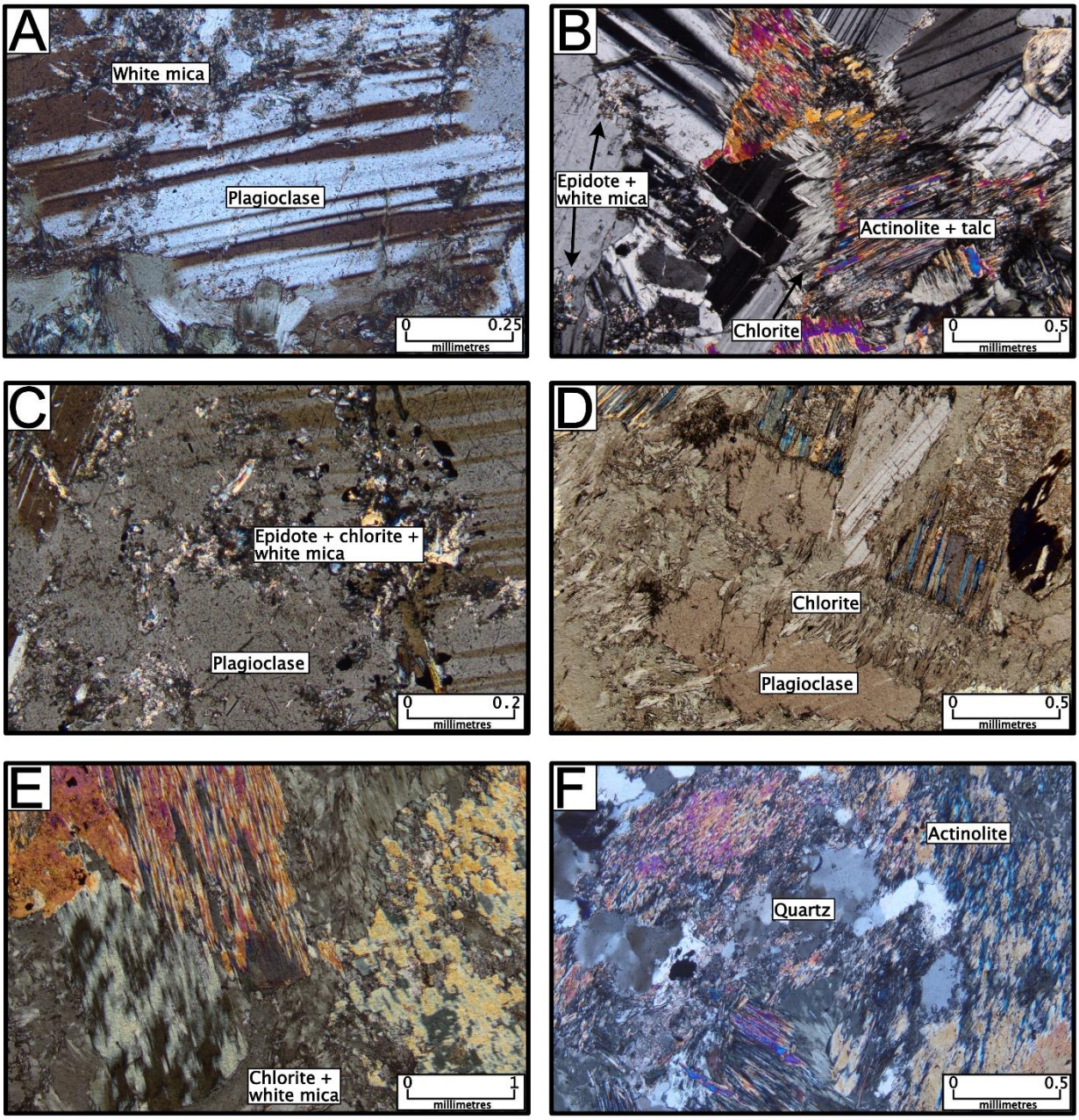

Figure 4.26 – Alteration styles and mineralogy occurring after plagioclase. Photos taken under cross-polarized light. A) Plagioclase crystal weakly altered to white mica (Sample JJ-TS-015). B) Plagioclase crystal from the same sample as 4.24A, with similar white mica alteration within crystal and chlorite alteration present at crystal margin with altered pyroxene (Sample JJ-TS-015). C) Plagioclase crystal weakly altered to patches of white mica+chlorite+epidote (Sample JJ-TS-011). D) Plagioclase altered to complete chlorite rims (Sample JJ-TS-014). E) Sample in which plagioclase is completely altered to chlorite and minor white mica (Sample JJ-TS-033). F) Polycrystalline quartz aggregate occurring between tremolite-actinolite aggregates (Sample JJ-TS-017).

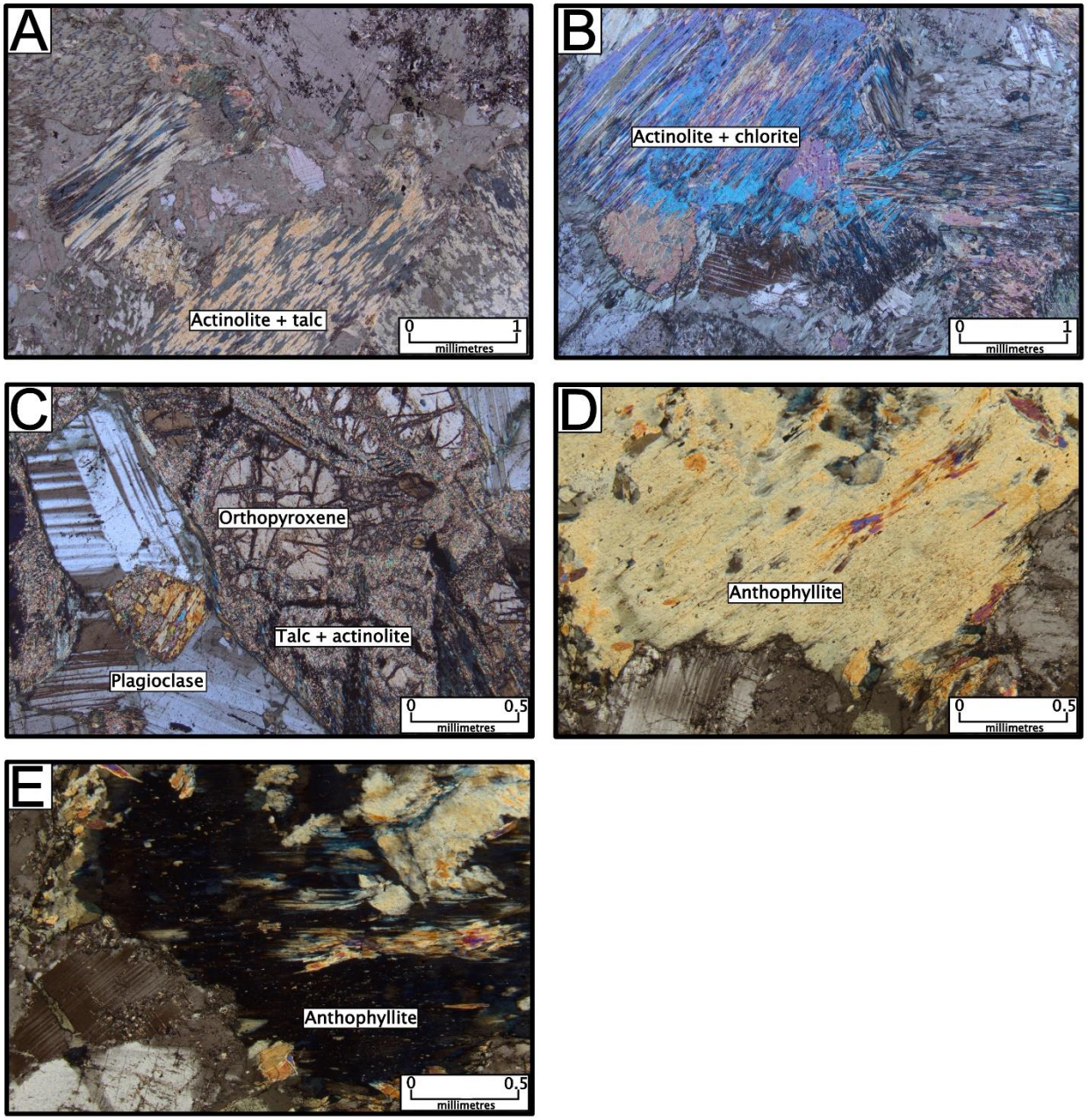

Figure 4.27 – Alteration styles and mineralogy occurring after pyroxene. Photos taken under cross-polarized light. A) Pyroxene crystals completely altered to tremolite-actinolite (Sample JJ-TS-029). B) Pyroxene crystals completely altered to tremolite-actinolite and chlorite (Sample JJ-TS-015). C) Orthopyroxene crystal moderately altered to talc and minor tremolite-actinolite (Sample JJ-TS-081). D) Anthophyllite crystal inclined from extinction angle (Sample TS-JJ-071). E) Anthophyllite crystal showing parallel extinction (Sample TS-JJ-071).

4.26D, E). Epidote is present as an alteration product of plagioclase in most samples, typically in trace amounts and never exceeding 1% of a sample. <1% quartz occurs in a few strongly altered samples, within veinlets and as <2 mm polycrystalline aggregates with mosaic texture (Fig. 4.26F). Trace carbonate occurs in two strongly altered samples, occurring as a minor component of veinlets.

Tremolite-actinolite and talc are the most common alteration products of pyroxene, with fine-grained aggregates of tremolite-actinolite being by far the most common alteration product, occurring as monomineralic aggregates or alongside very fine-grained talc and sometimes chlorite (Fig. 4.27A, B). Tremolite-actinolite is less commonly present as discrete crystals, commonly displaying simple twinning. Talc is a minor alteration product in samples with strongly altered pyroxene, whereas it is the dominant alteration product of orthopyroxene in several weakly altered samples (Fig. 4.27C). Chlorite is sometimes present as a minor component of very fine- to fine-grained aggregates of tremolite-actinolite±talc. Anthophyllite is an uncommon alteration product (Fig. 4.27D, E), occurring as discrete crystals sometimes showing simple twinning, and never exceeding 2% of a total sample.

4.2.1.3 – Breccia domain within the Offset Zone – Spatial variation

Minimal systematic spatial variability was observed in the pre-alteration composition of samples from the breccia domain of the Offset Zone. Relative proportions of plagioclase and pyroxene vary from sample to sample, but no variation was observed to be associated with distance from the domain boundary contact in either drill hole (Figs. 4.28, 3.29). Clinopyroxene was only discernible in two of nineteen samples from the Offset South Zone, so downhole

variability was not determined in this zone. In the B3 Zone, six of the seven samples closest to the domain boundary contact (spanning 11.6 m) contain discernible clinopyroxene. In those samples, clinopyroxene proportion increases modestly with proximity to the contact; the three most distal samples average 8% clinopyroxene, whereas the three most proximal samples average 14% clinopyroxene. Biotite and magnetite show no spatial variability. Sulfide mineral quantities show no spatial variability aside from general association with greater Pd enrichment.

No spatial variability in alteration style or alteration mineralogy was observed in either drillhole from the breccia domain of the Offset Zone, though some downhole variation in alteration intensity was observed (Figs. 4.28, 4.29) In both the Offset South Zone and the B3 Zone, the sample closest to the domain boundary contact (<2 m away) is more intensely altered than the samples directly above it. Aside from this, alteration intensity was variable throughout the Offset South Zone, with no consistent spatial variability observed. Similarly, each of the most weakly altered samples (dominantly unaltered pyroxene) occur within <5 m of samples of typical alteration intensity (dominantly unaltered plagioclase and altered pyroxene). Each of the most strongly altered samples (dominantly altered plagioclase) also occur within <5 m of samples of typical alteration intensity. Samples distal to the domain boundary contact in the B3 Zone show consistent alteration intensity, with completely altered pyroxene and almost unaltered to weakly altered plagioclase. Aside from the sample adjacent to the domain boundary contact, the other six samples taken within <12 m of the contact in the B3 Zone show the weakest alteration intensity of all samples taken in the Offset Zone.

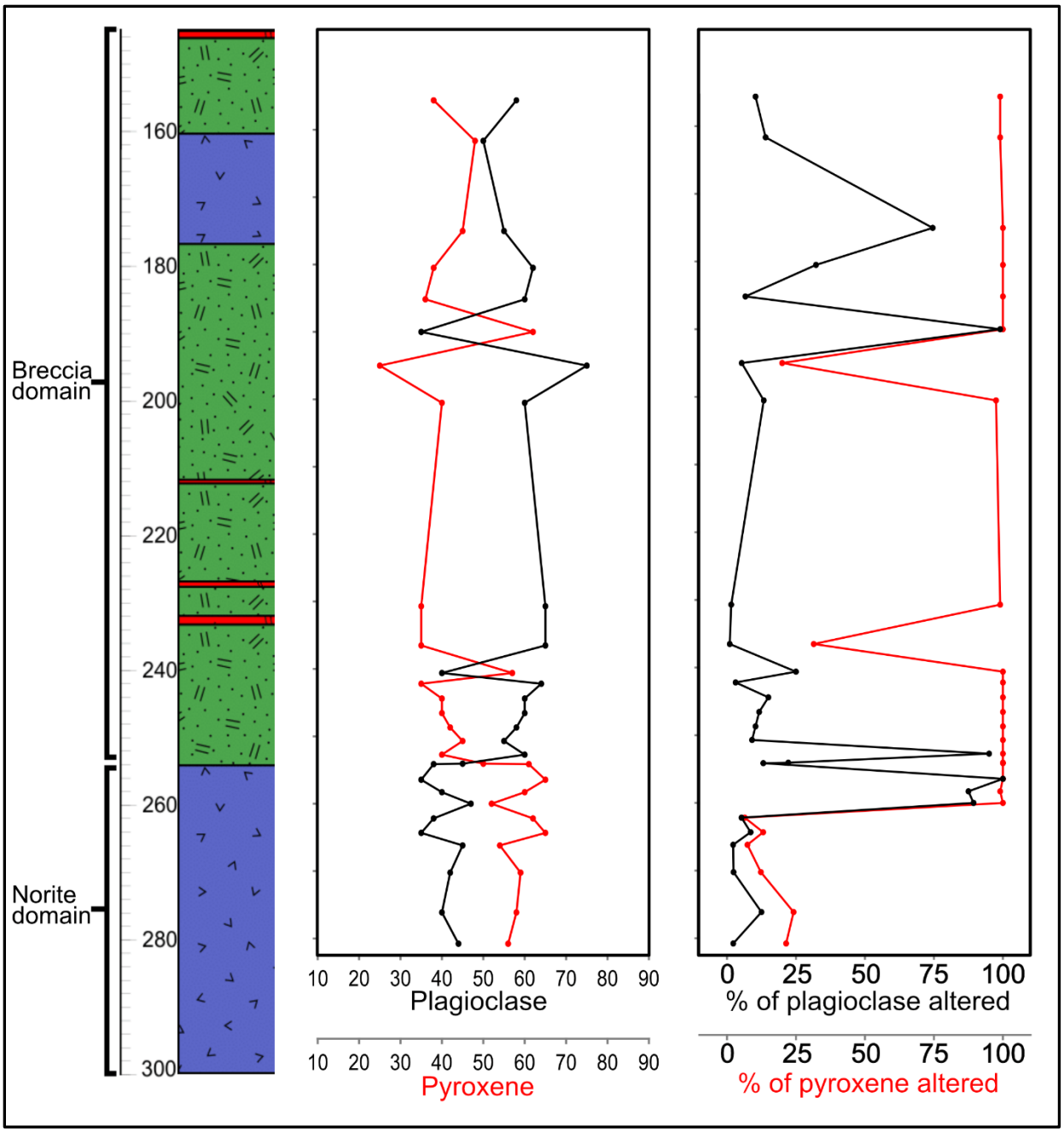

Figure 4.28 – Downhole plot of DH# 17-804 showing estimated pre-alteration proportion of plagioclase and pyroxene in each sample, and percentage of each mineral that has been replaced by alteration minerals.

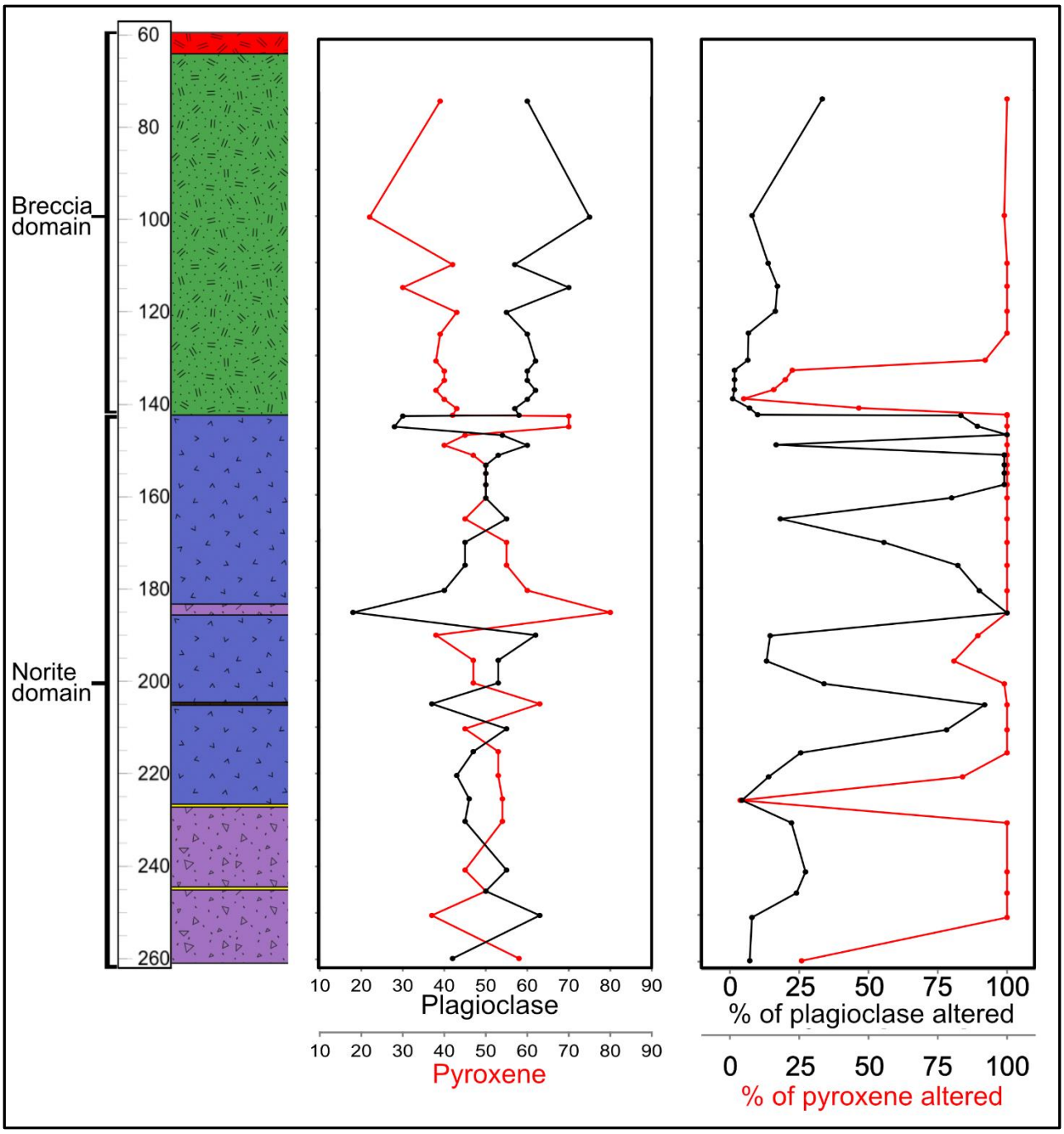

Figure 4.29 – Downhole plot of DH# 18-805 showing estimated pre-alteration proportion of plagioclase and pyroxene in each sample, and percentage of each mineral that has been replaced by alteration minerals.

4.2.2 – Norite domain within the Offset Zone

Thirty-eight samples were petrographically analyzed from the norite domain of the Offset Zone. Eleven of these samples were from DH# 17-804 from the Offset South Zone, and 27 were from DH# 18-805 from the B3 Zone. Sampling density varied throughout the drillholes, generally concentrated adjacent to the geological domain boundary with the adjacent breccia domain.

Sampling in the Offset South Zone was conducted over a 26 m area adjacent to the domain boundary contact in DH# 17-804 (Fig. 4.16). The area directly adjacent to the domain boundary contact is the only portion of the norite domain of this drill hole that is significantly enriched in Pd, averaging 3.61 ppm Pd over 14.0 m. This zone of enrichment is part of a larger zone extending into the breccia domain, averaging 2.81 ppm Pd over the entire 28.0 m interval. Samples were taken every 2 metres within the mineralized zone. Three other samples were taken at a 5 metre spacing directly below the mineralized zone.

Sampling in the B3 Zone encompassed the entire logged interval of the norite domain in DH# 18-805 (Fig. 4.17). The entirety of the norite domain in the logged interval of this drill hole is Pd-enriched, including a 32 m zone averaging 9.19 ppm Pd. Samples were taken every 2 metres in a 14 m area directly adjacent to the domain boundary contact. Samples were taken every 5 metres throughout the rest of the logged interval.

It was not possible to determine the pre-alteration proportion of orthopyroxene and clinopyroxene in most samples due to the complete or near-complete alteration of pyroxene, and as such, the majority of these samples cannot be classified via IUGS classification. Of the

ten samples that have sufficient unaltered pyroxene to classify, five plot within the gabbronorite field, three plot within the norite field, two plot on the boundary between gabbronorite and norite (Fig. 4.30).

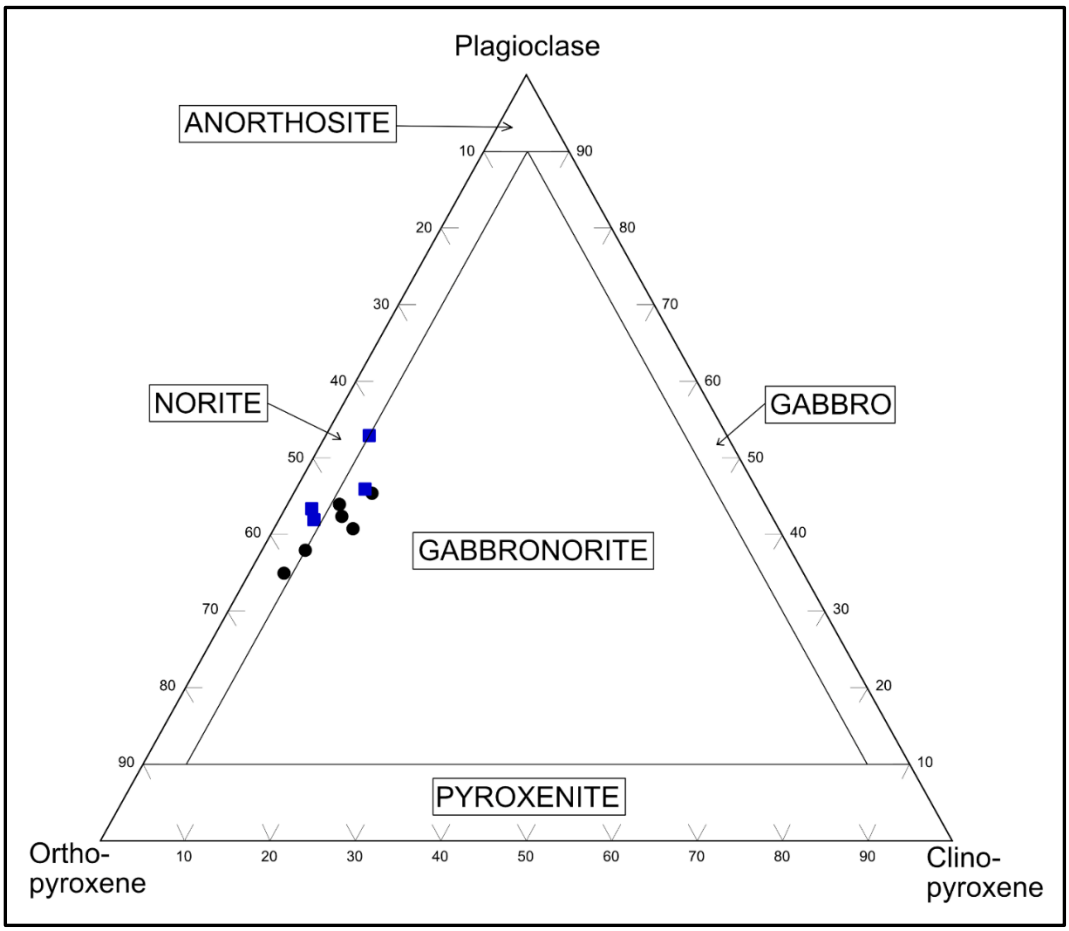

Figure 4.30 – Ternary diagram of plagioclase, orthopyroxene, and clinopyroxene content of samples from the norite domain of the Offset Zone (Offset South Zone = black circles. B3 Zone = blue squares).

4.2.2.1 – Norite domain within the Offset Zone – Crystal proportions and properties

The majority of samples from the norite domain of the Offset Zone have relatively similar texture and crystal size. Although less significant variations in crystal size are seen in the norite domain than in the breccia domain of the Offset Zone, crystal size of plagioclase and pyroxene is typically quite variable within a single sample (Fig. 4.31A), with very fine- to medium-grained crystals present in the majority of samples. Biotite is the only other commonly observed primary silicate mineral, and hornblende is observed in two samples from the Offset South Zone. Primary texture is consistently massive and unfoliated. One sample that has been completely altered is moderately foliated; all other samples are unfoliated, including other samples that are completely altered. Primary texture is fairly well preserved in the majority of samples, though there are several samples in which primary texture is difficult to determine, as pseudomorphing is not as prevalent in samples that have been completely or almost completely replaced by alteration minerals (Fig. 4.31B). Poikilitic texture is common, though less prevalent than seen in the Offset Zone.

Plagioclase makes up the significant minority of the pre-alteration mineral proportion in most samples, most commonly comprising 40-50% of the rock prior to alteration. Plagioclase is the dominant mineral in 10 of 38 samples, comprising <55% of the rock in seven samples and 60-63% of the rock in the other three. As seen in the breccia domain of the Offset Zone, crystals are usually anhedral to rarely subhedral (aside from smaller crystals encircled by other crystals that are typically subhedral to euhedral), and typically equant to less commonly tabular. Lath-shaped plagioclase crystals observed in several samples from the breccia domain were not observed in the norite domain. Distribution of plagioclase crystal size is relatively similar to that

seen in the breccia domain, with the largest difference in the norite domain being that less variation is present within each individual sample. There is no systematic downhole variation from sample to sample in either drill hole; the only observed trend is that average crystal size is generally slightly larger in more plagioclase-rich samples. Average crystal size of most samples ranges from 1.0-2.0 mm. Maximum crystal size in a sample ranges from 4.0 to 8.0 mm, and minimum crystal size is generally <0.2 mm, with a minority of samples containing no observed <1.0 mm crystals.

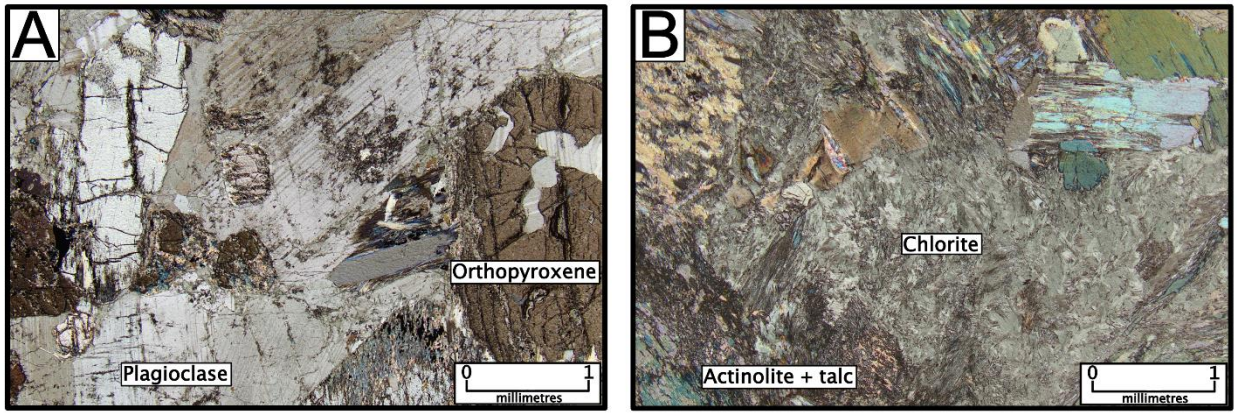

Figure 4.31 – Textures from the norite domain of the Offset Zone. Photos taken under cross-polarized light. A) Plagioclase and pyroxene of variable size (Sample JJ-TS-039). B) Alteration obscuring primary texture (Sample JJ-TS-089).

Similar to the breccia domain of the Offset Zone, boundaries between plagioclase crystals typify textural equilibration. Curvilinear boundaries are present in every sample in which plagioclase has not been completely altered, and triple junctions are present in a minority of samples, typically between very fine-grained crystals. Plagioclase crystals sometimes occur in clusters made up of several crystals, though this is less common than in the breccia domain. Clusters of plagioclase crystals are more prevalent in samples with a higher proportion of plagioclase. <5% of crystals in most samples show deformation twinning, with a

minority of samples having no observable deformation twinning. Crystals are commonly weakly fractured, with fractures commonly filled by alteration minerals. Two samples from the B3 Zone in which >80% of plagioclase has been replaced by alteration minerals contain very heavily fractured plagioclase crystals (Fig. 4.32A). Plagioclase in these samples, along with one other sample from the B3 Zone, also displays widespread deformation twinning and undulose extinction.

Pyroxene constitutes the majority of the pre-alteration mineral proportion in most samples from the norite domain of the Offset Zone, most commonly making up 50-60% of the rock prior to alteration. As in the breccia domain, the majority of well-pseudomorphed pyroxene crystals have a similar shape, size, and habit to orthopyroxene, implying that orthopyroxene was the dominant pyroxene pre-alteration. Orthopyroxene crystals, where unaltered, are typically subhedral and equant, whereas the largest crystals in a sample (typically >3 mm) are more commonly anhedral and elongate/tabular. In approximately half of the samples, crystals are commonly present in <10 mm clusters consisting of >90% pyroxene (Fig. 4.32B). Average crystal size is most commonly 0.7-2.0 mm, with crystals typically slightly smaller and showing less variation in size than plagioclase crystals in the same sample. Maximum crystal size in a sample ranges from 2.0 mm to 9.0 mm.

Clinopyroxene is present in all samples from the norite domain of the Offset Zone in which >10% of pyroxene is unaltered. The proportion of clinopyroxene in samples in which it can be discerned is generally lower than in the breccia domain of the Offset Zone, with all samples in the norite domain containing <10% clinopyroxene. Clinopyroxene crystals in the norite domain are typically smaller than those seen in the breccia domain; >8 mm crystals are

only seen in 3 of 10 clinopyroxene-bearing samples, and the majority of crystals are of similar size to the larger plagioclase and orthopyroxene crystals (Fig. 4.32C). Aside from size, characteristics of clinopyroxene crystals in the norite domain are generally similar to those in the breccia domain. Crystals are most commonly anhedral and irregularly shaped, partially to completely enclosing adjacent plagioclase and orthopyroxene crystals. A minority of clinopyroxene crystals in most samples are subhedral and equant, and significantly smaller than the irregularly shaped crystals (typically 1-2 mm). As in the breccia domain, <0.2 mm elongate orthopyroxene crystals are present along cleavage planes of clinopyroxene, appearing to have been exsolved.

Biotite is the main primary interstitial phase observed in the norite domain of the Offset Zone. Biotite is present in a majority of samples (25 of 38), which is less than seen in the breccia domain. Biotite is observed at a similar quantity in the norite domain as in the breccia domain, typically composing <0.1% to 0.5% of the sample. Weaker alteration is generally associated with a greater proportion of biotite, though degree of alteration shows no correlation with the presence or absence of biotite. Similar to in the breccia domain, the majority of biotite appears to be primary, occurring as platy crystals and/or "books" of crystals. A minority of biotite in several samples occurs as very fine- to fine-grained aggregates, appearing to be the product of alteration and/or remobilization.

Hornblende is present in trace quantities in two samples from the norite domain, one from each of the Offset South Zone and the B3 Zone. Two ~0.5 mm crystals were observed in the Offset South Zone sample (Fig. 4.32D) that have been partially altered to talc+chlorite+tremolite, and thus appear to be primary. Several <0.7 mm crystals were

observed in the B3 Zone sample in a strongly altered, mosaic textured area in which other minerals show polygonal triple junctions; it is possible that these crystals are actually a different dark-coloured secondary amphibole.

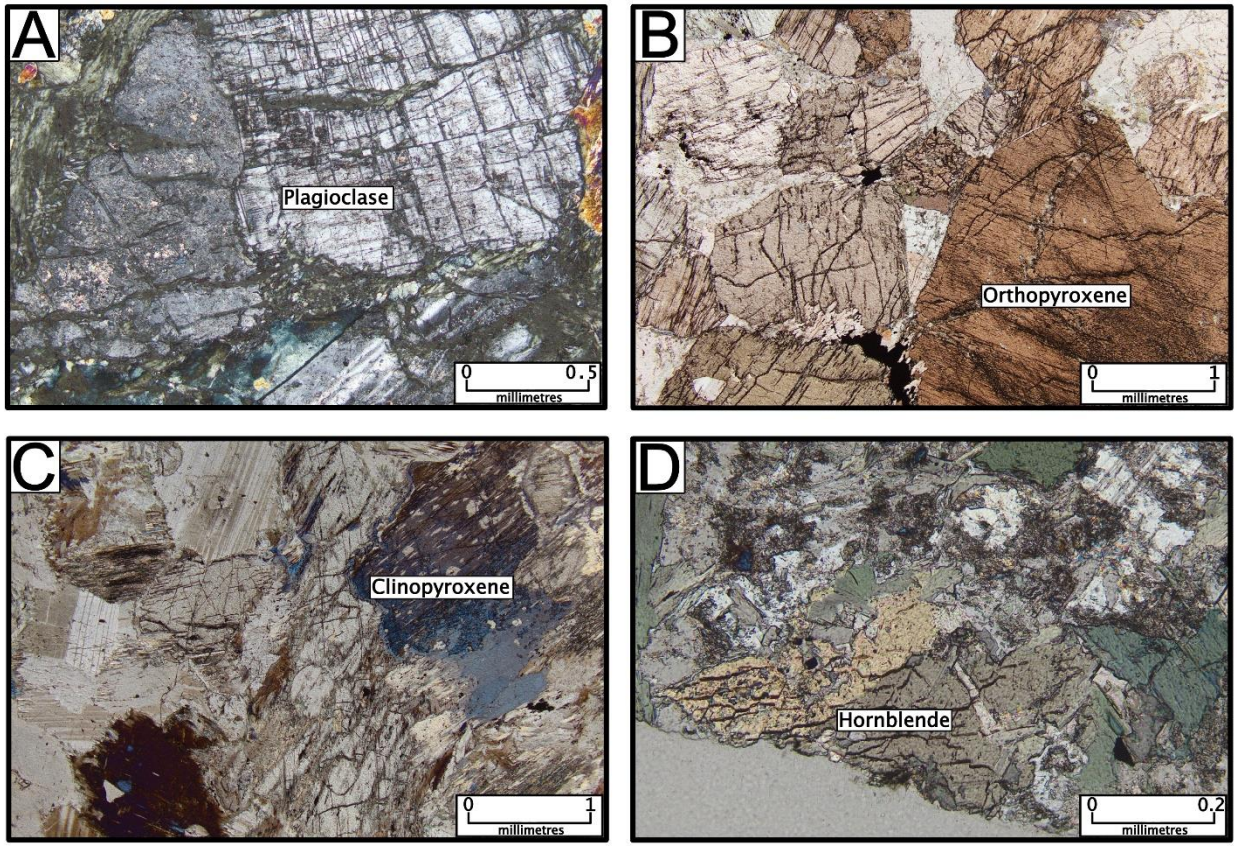

Figure 4.32 – Mineral textures from the norite domain of the Offset Zone. Photos taken under cross-polarized light. A) Heavily fractured plagioclase in strongly altered sample (Sample JJ-TS-083). B) Cluster of cumulate orthopyroxene (Sample JJ-TS-040). C) Clinopyroxene crystals of similar size to orthopyroxene and plagioclase (Sample JJ-TS-098). D) Hornblende crystals (Sample JJ-TS-034).

Sulfide minerals are present in every sample from the norite domain of the Offset Zone, ranging in quantity from <0.1% to 2%. Pyrite and chalcopyrite are present in every sample in at least trace quantities. Pyrrhotite and pentlandite are each present in roughly half of all samples (18 out of 38 and 21 out of 38 samples, respectively). Pyrrhotite and/or pentlandite are absent

in a majority of samples that contain <0.5% sulfides, and most samples in which they are absent are strongly altered (pyroxene is completely altered and plagioclase is mostly or completely altered). Morphology and distribution of sulfide crystals is similar to the breccia domain; sulfides are present as interstitial chalcopyrite±pentlandite±pyrite±pyrrhotite crystals (typically >0.2 mm) and very finely disseminated monosulfide chalcopyrite and pyrite crystals (typically <0.1 mm). As in the breccia domain, disseminated crystals commonly occur as clusters and commonly form haloes around interstitial crystals.

Oxide minerals, typically magnetite, are present in 33 of 38 samples from the norite domain of the Offset Zone. Magnetite typically occurs at trace quantities as <0.1 mm finely disseminated crystals, most commonly occurring along cleavage planes of silicate alteration aggregates. In samples with >0.1% magnetite, <0.5 mm interstitial crystals are also present. In three samples, a darker-coloured grey mineral interpreted to be ilmenite can be seen as randomly oriented, elongate crystals in aggregate with magnetite.

4.2.2.2 – Norite domain within the Offset Zone – Alteration

The visually estimated mean proportion of plagioclase that has been replaced by alteration minerals in the norite domain of the Offset Zone is 45-50%. This is significantly higher than the mean alteration proportion of 15-20% seen in the breccia domain. Plagioclase has been completely or near completely altered in 7 of 38 samples in the norite domain, whereas 8 of 38 samples contain <10% altered plagioclase. Plagioclase alteration intensity displays a weak correlation with pyroxene proportion in a sample; all samples with >65% pyroxene contain dominantly altered plagioclase (Fig. 4.33A) and all samples with <40% pyroxene contain

dominantly unaltered plagioclase (Fig. 4.33B), but no correlation is seen in samples with 40-65% pyroxene. Similar to the breccia domain, samples in which plagioclase is completely or near completely altered always contain completely altered pyroxene, though several samples with completely altered pyroxene also contain dominantly unaltered plagioclase. As in the breccia domain, alteration intensity of different crystals within a single sample is relatively homogenous, with increased alteration intensity adjacent to pyroxene and adjacent to veinlets.

The alteration style of plagioclase in the norite domain is very similar to in the breccia domain. White mica and chlorite are the most common alteration minerals (Fig 4.33C), with white mica being dominant in weakly altered samples and chlorite being dominant in moderately to strongly altered samples. White mica dominantly occurs as very fine-grained aggregates, commonly in aggregate with chlorite and/or epidote. Chlorite is typically present as fine-grained aggregates where it is the dominant alteration mineral, occurring with or without minor white mica. Epidote was observed in approximately half of all samples, never exceeding trace quantities and always in aggregates with white mica±chlorite. Quartz was observed in eight samples, never exceeding trace quantities and only present in veinlets and/or samples in which plagioclase has been completely altered.

The alteration style of pyroxene is also very similar to that seen in the breccia domain. Tremolite-actinolite, talc, and chlorite are the only observed alteration products of pyroxene in the norite domain (Fig. 4.33D). Tremolite-actinolite and talc are present in every sample, most commonly occurring as fine-grained polymineralic aggregates, usually alongside chlorite. Tremolite-actinolite is the most substantial alteration product, typically making up >90% of

pyroxene alteration products. Talc typically makes up 5-10% of pyroxene alteration products, replacing up to ~30% of pyroxene in the most talc-rich samples.

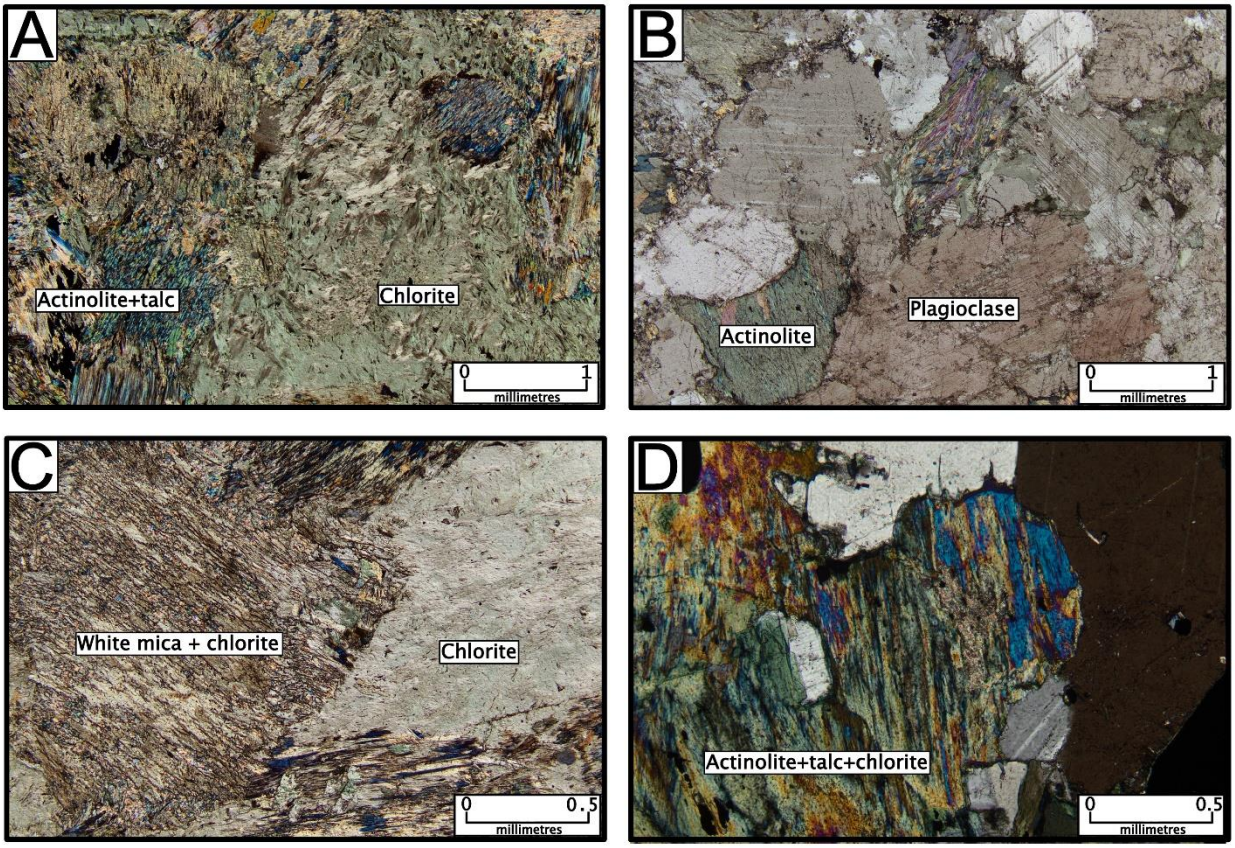

Figure 4.33 – Alteration in the norite domain of the Offset Zone. Photos taken under cross-polarized light. A) Typical completely altered plagioclase in pyroxene-rich sample (Sample JJ-TS-096). B) Typical weakly altered plagioclase in pyroxene-poor sample (Sample JJ-TS-110). C) Plagioclase crystals altered to white mica+chlorite (left) and only chlorite (right) (Sample JJ-TS-036). D) Pyroxene altered to actinolite+talc+chlorite (Sample JJ-TS-086).

4.2.2.3 – Norite domain in the Offset Zone – Spatial variation

Some differences are present between the pre-alteration composition of samples from the Offset South Zone (DH# 17-804) and B3 Zone (DH# 18-805). Pyroxene is always the dominant pre-alteration mineral in samples from the Offset South Zone (Fig. 4.28), making up >50% of the pre-alteration content in all samples. In contrast, 10 of 27 samples from the B3

Zone contain more plagioclase than pyroxene prior to alteration (Fig. 4.29). No downhole spatial trend is evident in plagioclase/pyroxene content of either sample. In the B3 Zone, two samples closest to the domain boundary contact have higher pre-alteration pyroxene content (~70%) than all other samples from the B3 Zone except for one. No increase in pyroxene content is observed adjacent to the domain boundary contact in the Offset South Zone. Of the six samples in the Offset South Zone in which clinopyroxene is discernible, the two samples closer to the domain boundary contact have slightly lower clinopyroxene content (4-5%) than the four distal samples (6-9%). No spatial variation in clinopyroxene content was observed in the four clinopyroxene-bearing samples from the B3 Zone. Similar to the breccia domain, no spatial variability in biotite or magnetite content was observed, and sulfide content showed no spatial variation aside from with Pd content.

Some spatial variations of alteration intensity were recognized in the norite domain of the Offset Zone. In the Offset Zone South, the five samples taken closest the domain boundary are mostly altered, with completely or near completely altered pyroxene and plagioclase alteration ranging from 10-100%. In contrast, the five samples more distal to the domain boundary contact were all weakly altered, with >75% of pyroxene and >85% of plagioclase unaltered in all samples. Alteration intensity was not observed to correlate with pyroxene content in the Offset South Zone. In the B3 Zone, downhole variation or association of alteration with the domain boundary contact was not observed. Alteration intensity is generally stronger in the B3 Zone, with 23 of 27 samples containing >90% altered pyroxene. Alteration intensity of plagioclase in the B3 Zone was observed to generally increase with increased pyroxene content.

4.2.3 – Breccia domain within the Creek Zone

Six samples were petrographically analyzed from the breccia domain of the Creek Zone. Three samples were analyzed from each of the two Creek Zone drill holes, DH# 19-009 (Fig. 4.34) and DH# 19-025 (Fig. 4.35). Due to the limited number of samples taken from the breccia domain of the Creek Zone, sampling was focused on covering the entire zone at somewhat regular spacing, while also encompassing differences in mineralogy proportions, alteration intensity, and sulfide mineral proportions. One sample in DH# 19-025 was taken proximal to the domain boundary contact. In each of the two drill holes, one sample was taken from the zone of Pd enrichment, and two samples were taken in the portion of the drill hole that is not Pd-enriched. The pre-alteration proportion of orthopyroxene and clinopyroxene could not be determined in any of the six samples from the breccia domain of the Creek Zone, as pyroxene has been completely replaced by alteration minerals in all six samples. As such, IUGS classification of these samples was not possible.

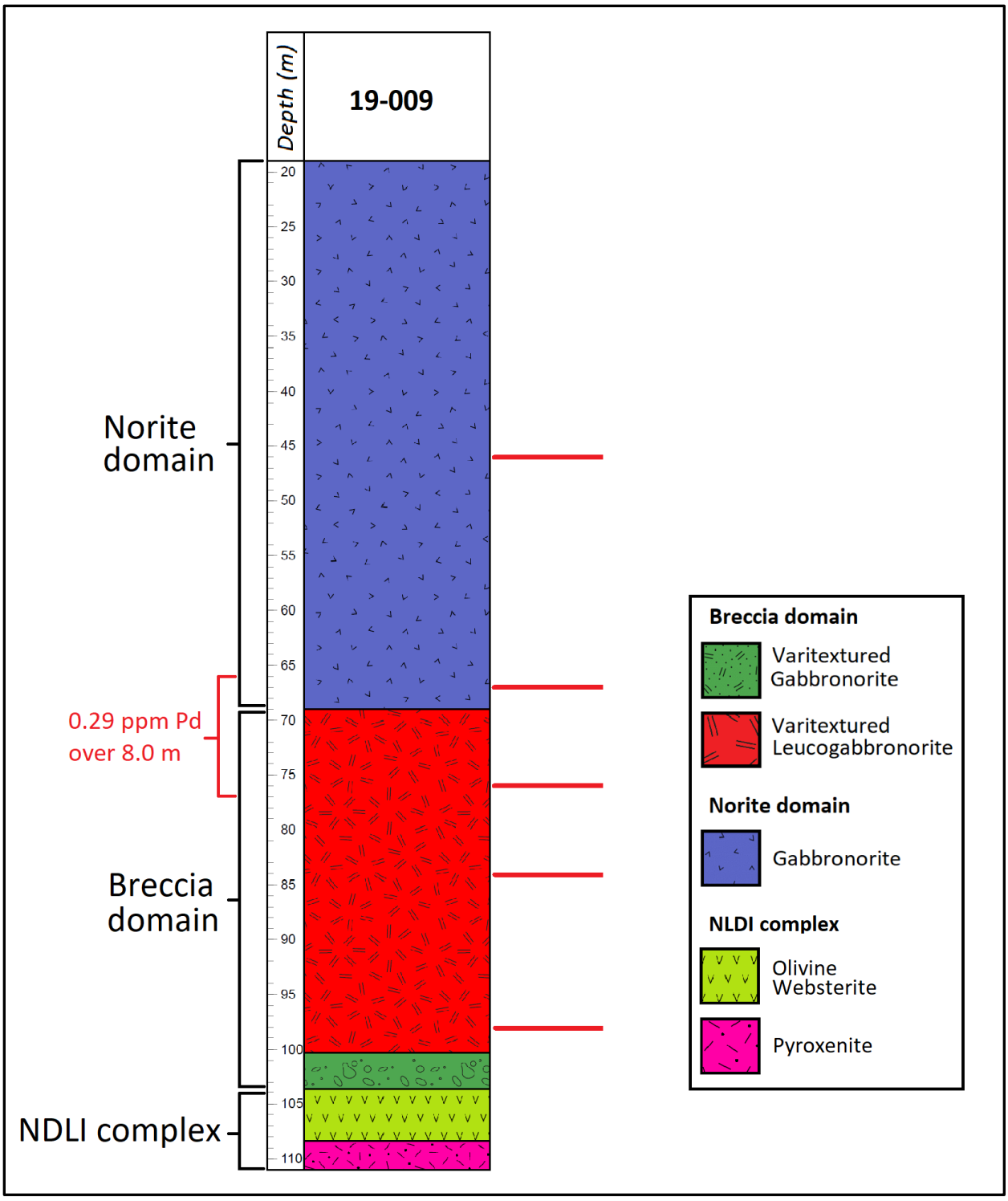

Figure 4.34 – Sample locations for petrographic analysis from DH# 19-009, denote by red lines (assay results provided by Impala Canada).

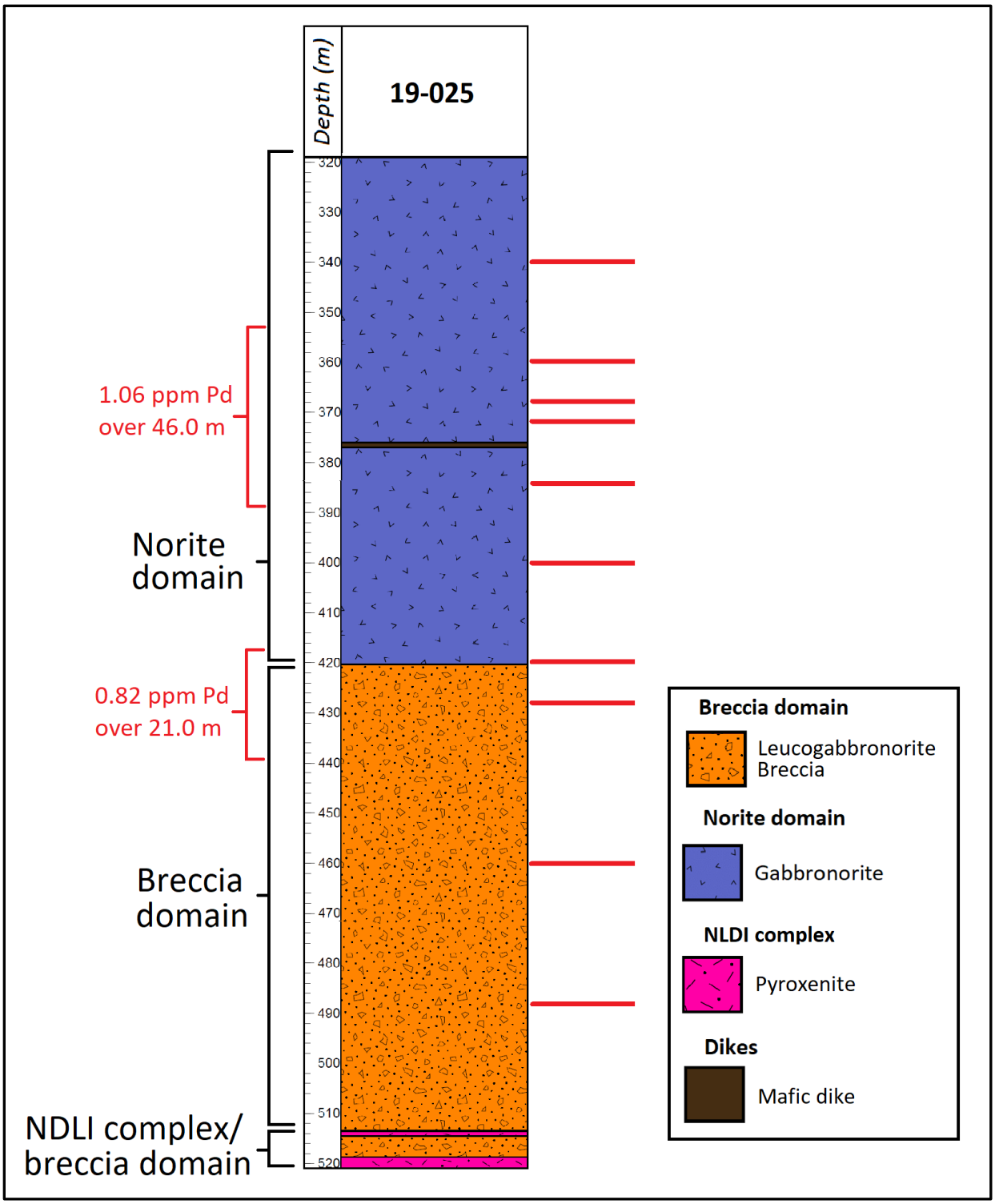

Figure 4.35 – Sample locations for petrographic analysis from DH# 19-025, denoted by red lines (assay results provided by Impala Canada).

4.2.3.1 – Breccia domain with the Creek Zone – Crystal proportions and properties

The size of pre-alteration plagioclase and pyroxene crystals in samples taken from the breccia domain of the Creek Zone is generally larger and shows greater variation than seen in the breccia domain samples from the Offset Zone. Very fine- to medium-grained crystals are present in all samples, and coarse to pegmatitic crystals are present in four of six samples. The proportion of pre-alteration plagioclase and pyroxene is more variable than in the Offset Zone, though this is biased by the presence of two samples taken at the boundary between small-scale plagioclase cumulate and pyroxene cumulate zones (Fig. 4.36A, B). As in the Offset Zone, the pre-alteration texture is generally well preserved due to the pseudomorphing of pyroxene and the relatively low degree of alteration of plagioclase. Unlike the Offset Zone, biotite was not observed in any of the breccia domain samples from the Creek Zone, nor was any other accessory mineral. Local poikilitic texture, in which larger crystals of plagioclase and/or altered pyroxene enclose smaller crystals of plagioclase and/or altered pyroxene, was observed in three of six samples.

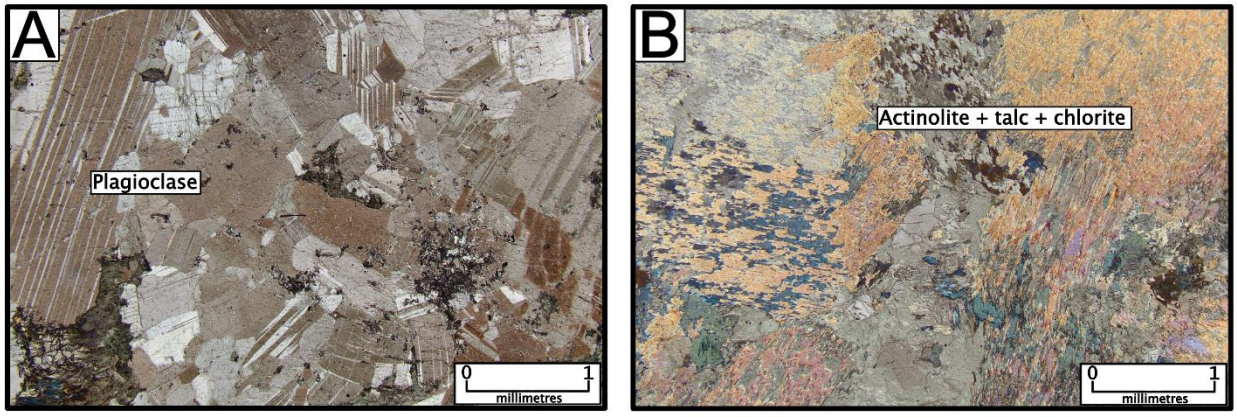

Figure 4.36 – Cumulate zones in the breccia domain of the Creek Zone. Photos taken under cross-polarized light. A) Area of cumulate plagioclase (Sample JJ-TS-140). B) Area of cumulate pyroxene, replaced by alteration minerals (Sample JJ-TS-140).

Plagioclase is the primary mineral present in all samples, making up 55-70% of samples prior to alteration. Crystals are most commonly anhedral and equant, with a minority of crystals in most samples anhedral to subhedral and tabular. Polygonal triple junctions are seen in very fine-grained crystals making up a minority of plagioclase present in DH# 19-025. Average plagioclase crystal size ranges from 1 mm in finer-grained samples to 8 mm in the coarsest-grained samples. Maximum crystal size in a sample ranges from 4-15 mm, whereas minimum crystal size is consistently <0.5 mm in all samples. As seen in the Offset Zone, plagioclase boundaries are curved and appear to be texturally equilibrated. A majority of crystals in all samples are weakly to moderately fractured, with deformation twinning in a minority of samples, affecting <5% of crystals where present.

Pyroxene, which has been completely replaced by alteration minerals in all samples, comprises the substantial minority of all samples from the breccia domain of the Creek Zone, making up 30-45% of all samples. Similar to the Offset Zone, altered pyroxene in the majority of samples has been pseudomorphed and most pyroxene appears to have had similar characteristics to orthopyroxene observed in less altered samples, appearing equant and anhedral to subhedral. In two of six samples from the breccia domain of the Creek Zone, ~25% of pseudomorphed pyroxene appears to have been anhedral, irregularly shaped, and wrapping around adjacent crystals, characteristics which imply that these crystals were clinopyroxene. In all samples, an insufficient quantity of pseudomorphed crystals were present to infer the pre-alteration proportions of orthopyroxene and clinopyroxene. Average pre-alteration crystal size is difficult to determine, but generally appears to range from 1.5 mm to 7 mm. Maximum pre-alteration crystal size in a sample ranges from 3 to 20 mm. Minimum pre-alteration crystal size

is generally not discernible due to the degree of alteration, though <0.5 mm pre-alteration crystals are discernible in several samples.

Sulfide minerals were observed in every sample from the breccia domain from the Creek Zone, constituting <0.5% of the sample in all cases. Pyrite is present in all six samples, and was the only observed sulfide mineral in three of those samples. Chalcopyrite was observed in the other three samples, typically in roughly equal proportion to pyrite where present. Pentlandite is present in two samples and pyrrhotite is present in one sample, each present in only trace quantities. In all samples, very finely disseminated monosulfide pyrite and chalcopyrite are the dominant sulfide mineral style. The two pentlandite-bearing samples, both from DH# 19-025, also contain rare interstitial polysulfide aggregates.

Magnetite was the only oxide mineral observed in the breccia domain of the Creek Zone, present in trace quantities in four of six samples. Magnetite crystals are always <0.2 mm, present as interstitial crystals between primary silicates in two samples, and present as very finely disseminated aggregates associated with altered silicates in the other two samples.

4.2.3.2 – Breccia domain within the Creek Zone – Alteration

The visually estimated mean proportion of plagioclase replaced by alteration minerals in the breccia domain of the Creek Zone is 25-30%. Unlike the trend seen in both lithological domains in the Offset Zone, no association was observed between plagioclase alteration intensity and proportion of plagioclase/pyroxene in a sample. Because all samples from the breccia domain of the Creek Zone contain completely altered pyroxene, no correlation can be made between pyroxene alteration intensity and plagioclase alteration intensity. Two samples

from the breccia domain of the Creek Zone are taken at the boundary of adjacent zones containing >80% pyroxene and >80% plagioclase, respectively. In these samples, >90% of the plagioclase present in the pyroxene-rich zones has been replaced by alteration minerals. In the plagioclase-rich portions of these samples, plagioclase shows typical alteration intensity of other samples from the breccia domain of the Creek Zone. Aside from these two samples, alteration intensity of plagioclase within a single sample is relatively consistent.

The alteration style of plagioclase in the breccia domain of the Creek Zone is similar to that seen in both domains of the Offset Zone, with chlorite and white mica being the most prevalent plagioclase alteration minerals in all samples. The largest observed difference between the breccia domains of the Creek and Offset Zone is the lack of white mica-dominated alteration; whereas white mica is dominant in some weakly altered samples in the breccia domain of the Offset Zone, chlorite is the most voluminous plagioclase alteration mineral in all samples from the breccia domain of the Creek Zone. Epidote was observed in three of six samples, ranging from trace quantities to 2% of the total rock. As in both domains of the Offset Zone, alteration of plagioclase occurs as very fine-grained irregular patches/fracture-filling white mica±chlorite±epidote, and fine-grained partial to complete rims of typically monomineralic chlorite.

Pyroxene has been completely replaced by alteration products in the breccia domain of the Creek Zone. Alteration style of pyroxene is very similar to that seen in completely altered samples from both domains of the Offset Zone. Very fine- to fine-grained tremolite-actinolite±talc±chlorite is present in all samples, with tremolite-actinolite being the most prevalent pyroxene alteration mineral in all cases. Talc typically makes up 2-5% of pyroxene

alteration products. Talc-dominant alteration aggregates, seen in some weakly altered samples from the breccia domain of the Offset Zone, were not observed in the breccia domain of the Creek Zone.

4.2.4 – Norite domain within the Creek Zone

Eight samples were petrographically analyzed from the norite domain of the Creek Zone. Six samples were analyzed from DH# 19-009, and two samples were analyzed from DH# 19-025. More samples were taken from DH# 19-009 due to focus of this study on characterizing Pd-enriched zones, as Pd enrichment is present in DH# 19-009 and not present in DH# 19-025. Of the six samples taken from DH# 19-009, four were taken from the zone of Pd enrichment (1.06 ppm Pd over 46.0 m), whereas the other two were taken on either side of the Pd-enriched zone. Of the two samples analyzed from DH# 19-025, one sample was taken from near the domain boundary contact and the other was taken distal from the contact.

Pre-alteration proportion of orthopyroxene and clinopyroxene was discernible in seven of eight samples from the norite domain of the Creek Zone, including all six samples from DH# 19-009 and one of two samples from DH# 19-025. These seven samples were categorized via IUGS classification; four samples plot in the gabbronorite field and three samples plot in the norite field (Fig. 4.37).

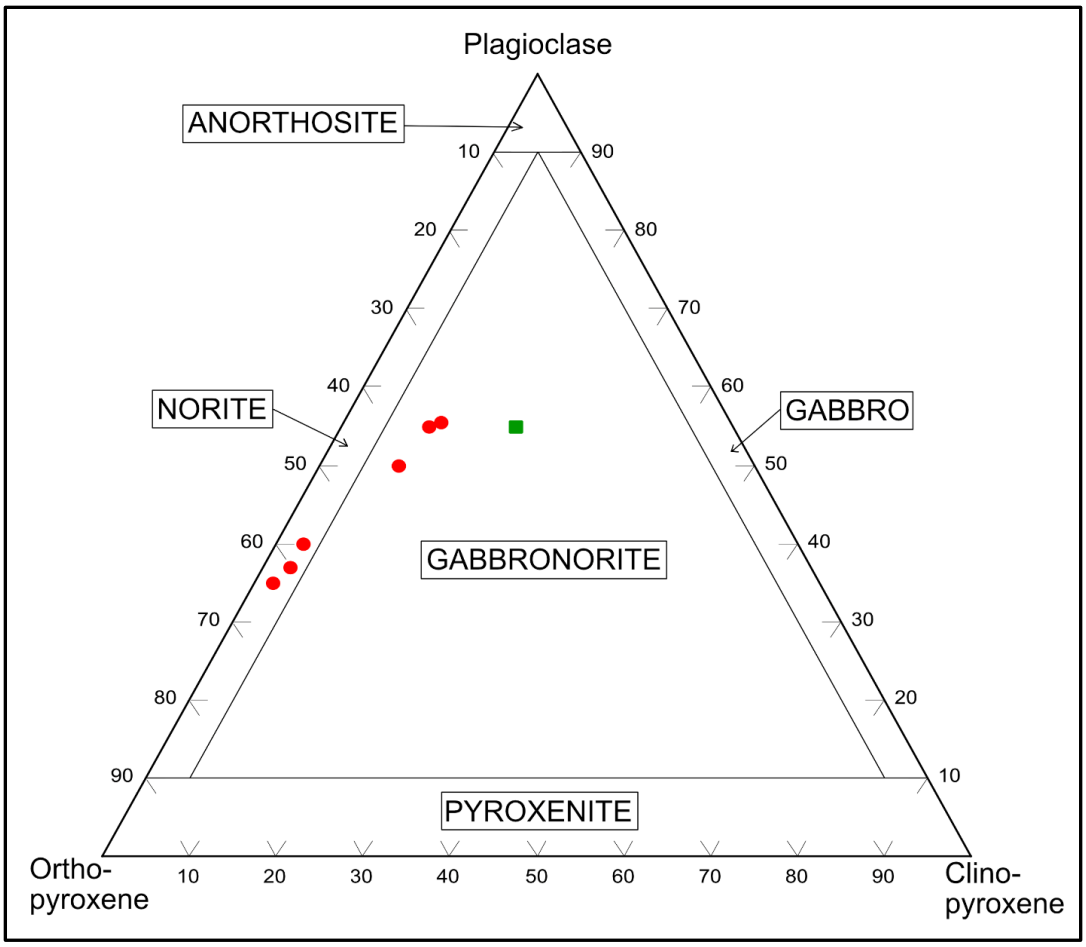

Figure 4.37 – Ternary diagram of plagioclase, orthopyroxene, and clinopyroxene content of samples from the norite domain of the Creek Zone (DH# 19-009 – red circles. DH# 19-025 – green square).

4.2.4.1 – Norite domain within the Creek Zone – Crystal proportions and properties

Similar to the norite domain of the Offset Zone, pre-alteration crystals in samples from the norite domain of the Creek Zone are generally smaller and show less variation in size (in a single sample and between samples) than crystals in samples from the breccia domain. Crystal size is still typically quite variable within a single sample; very fine- to medium-grained crystals are present in all samples, and coarse-grained crystals are also present in three of eight samples. Pre-alteration proportion of plagioclase and pyroxene is more variable than seen in

the norite domain of the Offset Zone, and pre-alteration crystal morphology is very well preserved in all samples. Biotite was the only observed accessory mineral, present in three of eight samples. Local poikilitic texture is observed in all samples, with clinopyroxene and rarely plagioclase/orthopyroxene present as oikocrysts and plagioclase/orthopyroxene present as chadacrysts.

Plagioclase makes up 35-55% of the pre-alteration mineral assemblage in samples from the norite domain of the Creek Zone, including four of eight samples in which it is the most common mineral. This is a higher rate of plagioclase-dominant samples than seen in the norite domain of the Offset Zone, where 10 of 38 samples contained >50% plagioclase. As in all other samples in this study, plagioclase is texturally equilibrated with common curved boundaries. In one sample from DH# 19-009, the majority of plagioclase is <0.5 mm and mosaic textured, possibly the result of recrystallization. Aside from this sample, average plagioclase crystal size ranges from 1-3 mm. Minimum crystal size is always 0.2 mm or less, and maximum crystal size ranges from 3 to 7 mm. A majority of plagioclase crystals are weakly fractured in all samples, and deformation twinning was observed in 4 of 8 samples.

Pyroxene constitutes 42-65% of the pre-alteration proportion of samples from the norite domain of the Creek Zone. Orthopyroxene is the dominant pyroxene in all samples, and is generally equant and subhedral to less commonly elongate and anhedral. Average orthopyroxene crystal size ranges from 1 to 3 mm. Minimum crystal size is always <0.2 mm and maximum crystal size ranges from 3 to 7 mm. Clinopyroxene is typically anhedral and irregularly shaped, and makes up the minority of pyroxene in all samples, typically at a slightly higher

proportion than seen in the Offset Zone. One sample from DH# 19-009 contains 20% clinopyroxene, which is the highest amount seen in any sample in this study.

Biotite was observed in trace quantities in three of eight samples from the norite domain of the Creek Zone. In one sample, biotite is present as very fine-grained aggregates alongside chlorite, appearing to be the product of alteration. In the other two samples, biotite is present as <0.2 mm platy crystals, appearing to be primary magmatic.

Sulfide minerals are present in all samples from the norite domain of the Creek Zone, ranging from trace quantities up to 4% of the sample. In six of eight samples, <0.5% sulfide content is present. Pyrite was observed in all eight samples, and chalcopyrite was observed in all samples except one. Pentlandite and pyrrhotite were observed in four and three samples, respectively. Sulfides in the two samples with the highest sulfide content (1% and 4%) are dominantly present as interstitial polysulfide aggregates dominated by pyrrhotite and chalcopyrite (Fig. 4.38A). Sulfide proportion in all other samples is dominated by pyrite and chalcopyrite, typically present as very finely disseminated crystals.

Oxide minerals were observed in all samples from the norite domain of the Creek Zone, ranging in proportion from <0.1% to 6% of a sample. In five of six samples, magnetite was the only observed oxide mineral, ranging from trace amounts to 1% of the rock. In one sample from DH# 19-009, 5% magnetite and 1% ilmenite are present, with ilmenite occurring as randomly oriented exsolution crystals within a minority of magnetite crystals (Fig. 4.38B). In all samples, oxide crystals are interstitial to primary silicate minerals. In a majority of samples, the majority of oxide crystals are spatially associated and/or in contact with sulfide crystals.

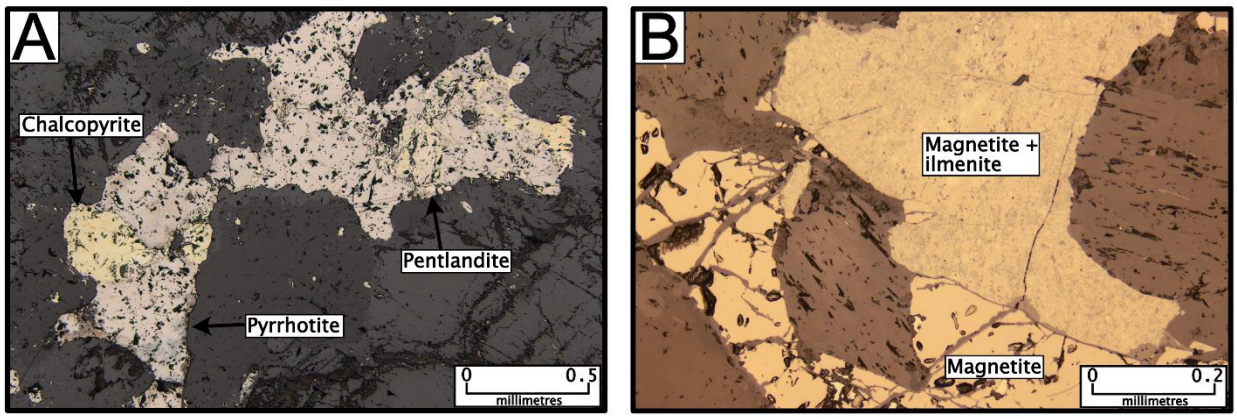

Figure 4.38 – Opaque mineral textures in the norite domain of the Creek Zone. Photos taken under reflected light. A) Polysulfide aggregate composed of pyrrhotite+chalcopyrite+ pentlandite (Sample JJ-TS-133). B) Oxide mineral texture; lower magnetite crystal flanked by upper crystal of ilmenite very finely exsolved within magnetite (Sample JJ-TS-189).

4.2.4.2 – Norite domain within the Creek Zone – Alteration

Based on visual estimations, the mean percentage of plagioclase that has been altered in the norite domain of the Creek Zone is ~10%, with alteration proportion never exceeding 20%. This is significantly lower than the average of 45-50% seen in the norite domain of the Offset Zone. A weak correlation between plagioclase alteration percentage and pyroxene proportion in a sample is observed, though the association is not as strong as seen in the Offset Zone. A moderate correlation between plagioclase alteration intensity and pyroxene alteration intensity is observed. In one sample from DH# 19-025, plagioclase has a greater alteration intensity than pyroxene, which was not observed in any other samples analyzed in this study. Alteration intensity of different plagioclase crystals within a single sample is generally fairly consistent aside from samples in which <10% of plagioclase is altered; in these samples, a significant minority of plagioclase crystals appear completely unaltered, which was generally not observed in the Offset Zone.

Plagioclase alteration in the norite domain of the Creek Zone is similar to other samples in which plagioclase has been weakly altered, with chlorite and white mica present as the dominant alteration minerals. Unlike weakly altered samples from the norite domain of the Offset Zone, white mica is not the dominant alteration mineral; white mica and chlorite are present in roughly equal proportions in all samples (Fig. 4.39A) except one, in which chlorite is dominant. The alteration style is quite similar to that seen in all other samples analyzed in this study, with most crystals altering to irregular very fine-grained patches of white mica±chlorite±epidote and partial rims of fine-grained chlorite.

Mean visually estimated alteration proportion of pyroxene in the norite domain of the Creek Zone is 25-30%. This data is skewed by one sample in which pyroxene has been completely altered, and two samples in which ~50% of pyroxene has been altered; in the five other samples, <15% of pyroxene has been replaced by alteration minerals. Tremolite-actinolite and talc are present as alteration products in all samples, typically as very fine-grained to fine-grained aggregates. Anthophyllite was observed in one sample, present as <1 mm crystals in trace quantities. In a majority of samples, tremolite-actinolite and talc are present in roughly equal proportions (Fig. 4.39B), with talc being clearly dominant in one sample and tremolite-actinolite clearly dominant in two samples. This is in contrast to the norite domain of the Offset Zone, which is more strongly altered and contains a much higher proportion of tremolite-actinolite, but is generally in line with the higher proportion of talc seen in more weakly altered samples throughout the samples analyzed for this study.

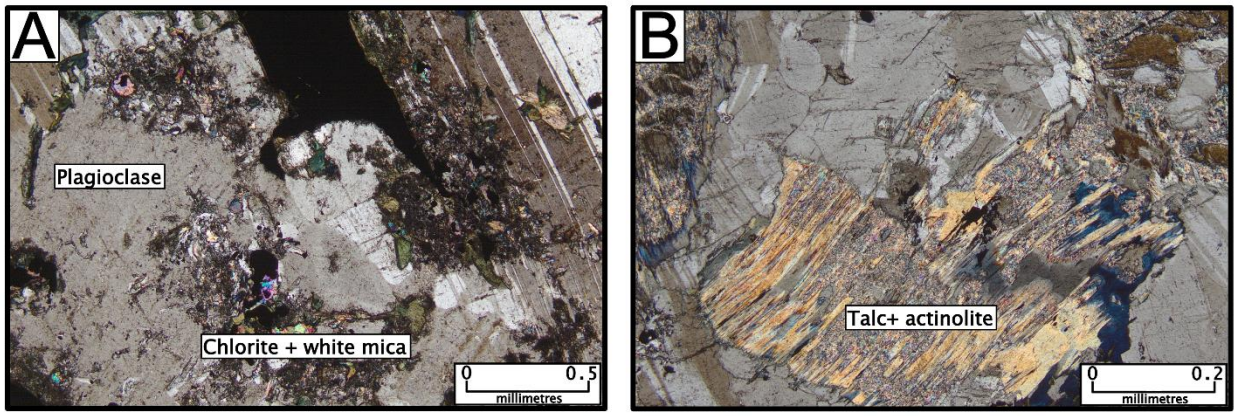

Figure 4.39 – Alteration mineral textures in the norite domain of the Creek Zone. Photos taken under cross-polarized light. A) Moderately altered plagioclase crystal, with chlorite and white mica present in roughly equal proportion (Sample JJ-TS-189). B) Completely altered pyroxene crystal, with actinolite and talc present in roughly equal proportion (Sample JJ-TS-138).

4.2.4.3 - Creek Zone – Spatial variation

Very little downhole variability was observed in either lithological domain in either drill hole from the Creek Zone. Spatial variation in pyroxene, plagioclase, sulfide, and magnetite content was not observed in either lithological domain. Of the eight samples from the norite domain of the Creek Zone, the only sample with completely altered pyroxene was taken adjacent to the domain boundary contact of DH# 19-009. Aside from this, no increase between alteration intensity and proximity to the domain boundary contact (observed in both breccia domain intersections and one of two norite domain intersections in the Offset Zone) is present in the Creek Zone drill holes. Downhole variability in alteration intensity is not present in either drill hole from the Creek Zone.

Due to the relatively low number of samples analyzed from the Creek Zone compared to the Offset Zone, spatial analysis of these samples is inherently more difficult. Assessment of spatial variability was based on only three samples from the breccia domain from each of the

two Creek Zone drill holes, and of two and six samples from the norite domain of these drill holes. As such, the observed lack of spatial variation in these samples does not preclude the existence of a more subtle spatial variation that was not captured by sampling.

4.3 – Whole rock geochemistry

Geochemical characteristics were determined using trace and major element concentrations. Geochemical data used for this study is included in Appendix B. Due to the cumulate nature of the rocks, trace element and major oxide relationships may not be completely representative of the original magma. Some samples provided by Impala Canada were largely or completely composed of late mafic dikes, late felsic dikes, and/or lithologies of the North Lac des Iles Complex. Due to the focus of this project on studying the South Lac des Iles Complex, these samples were excluded from analysis.

All samples analyzed for whole rock geochemistry were half core samples of NQ-size drill core. A sample was taken for whole rock geochemistry at 77 of the 82 locations that a sample was taken for petrography. Due to the larger number of whole rock geochemistry samples than petrography used in this study, many whole rock geochemistry samples have no corresponding thin section for the sample location. All whole rock geochemistry samples are drill core intervals of 60 cm in length or greater, and the large majority (483 of 490) of samples were taken over one metre intervals. Although shorter sample intervals would have made it easier to correlate geochemical results with petrographic observations, shorter samples would make geochemical interpretation less reliable due to the tendency of the intrusion to be locally heterogenous, brecciated, and varitextured. Additionally, the majority of samples submitted for

geochemical analysis were previously crushed pulps and rejects of metre-long samples that had previously been submitted for assay by Impala Canada.

4.3.1 – Offset Zone

A total of 357 samples from the Offset Zone were used in this study. This includes 20 samples submitted for this study from previously assayed pulp/reject material, and 341 samples previously analyzed by Impala Canada. Of these samples, 52 are from DH# 17-804 from the Offset South Zone, and 305 are from DH# 18-805 from the B3 Zone. The samples have been grouped into units based on drill core logging and petrographic analysis.

Of the samples from the Offset South Zone, 25 samples are from the breccia domain and 27 samples are from the norite domain. Two of the samples from the breccia domain of the Offset South Zone are from the area logged as varitextured leucogabbronorite, and the other 23 samples are from the area logged as varitextured gabbronorite. All 27 samples from the norite domain of the Offset South Zone are from the area logged as equigranular gabbronorite. Samples from the Offset South Zone were taken in two metre intervals in a 70.7 m area surrounding the domain boundary contact (230-300.7 m), and every 5 m in a 85 m area directly above the more densely sampled portion (145-230 m).

Of the samples from the B3 Zone, 143 samples are from the breccia domain and 162 samples are from the norite domain. Five of the samples from the breccia domain of the B3 Zone are from the area logged as varitextured leucogabbronorite, and the other 137 samples are from the area logged as varitextured gabbronorite. Eighty-one of the samples from the norite domain of the B3 Zone are from the area logged as equigranular gabbronorite, and 81

samples are from the area logged as gabbronorite breccia. All samples from the B3 Zone were previously analyzed by Impala Canada and the results provided for this study. Sampling covers the entirety of a 307 m interval from the top of the drillhole.

Downhole plots of major element content of samples from DH# 17-804 and DH# 18-805 are presented in Figures 4.40 and 4.41. Many of the samples included in this study from DH# 18-805 were from outside of the logged interval. Using drill core photographs and logs provided by Impala Canada, it was confirmed that the samples above the logged area are from the breccia domain and that the samples below the logged area are from the norite domain.

Generalized trends in major element oxide content are present in the Offset Zone. In both Offset Zone drill holes, CaO, Na_2O, and Al_2O_3 content is higher in the breccia domain, whereas MgO, MnO, and Fe_2O_3 content is higher in the norite domain. In the Offset South Zone, concentration of these elements is more variable in the breccia domain and less variable in the norite domain. The opposite trend is observed in the B3 Zone, in which major element concentrations are less variable in the breccia domain than in the norite domain. The major element content of the breccia domain is fairly similar in the B3 Zone and the Offset South Zone. The major element content of the norite domain in the B3 Zone, however, is less mafic (higher CaO, Na_2O, and Al_2O_3 content, lower MgO and MnO content) than the norite domain in the Offset South Zone, and is roughly intermediate to the breccia and norite domains of the Offset South Zone.

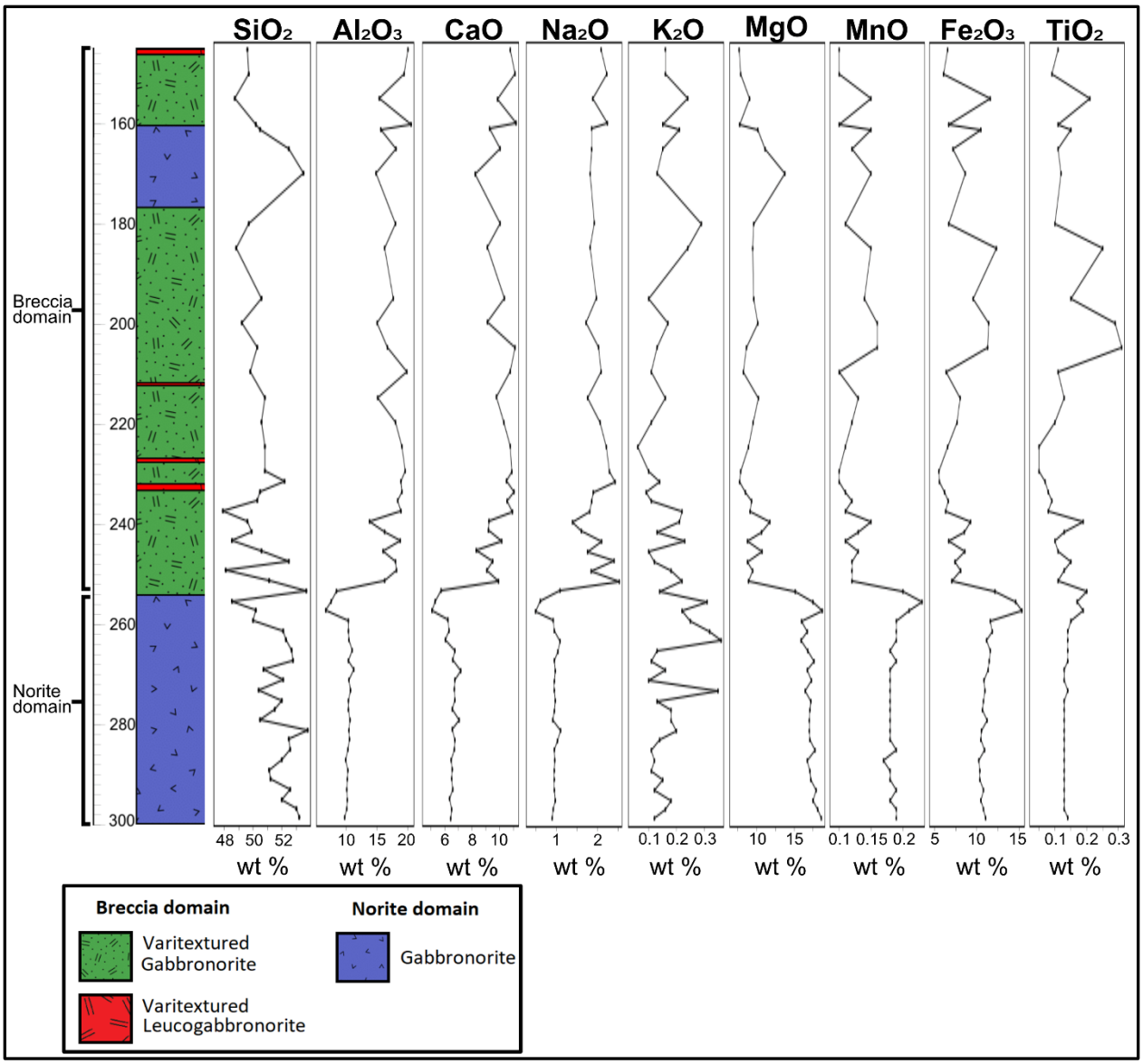

Figure 4.40 – Downhole plots of major elements in samples from DH# 17-804 (Offset South Zone).

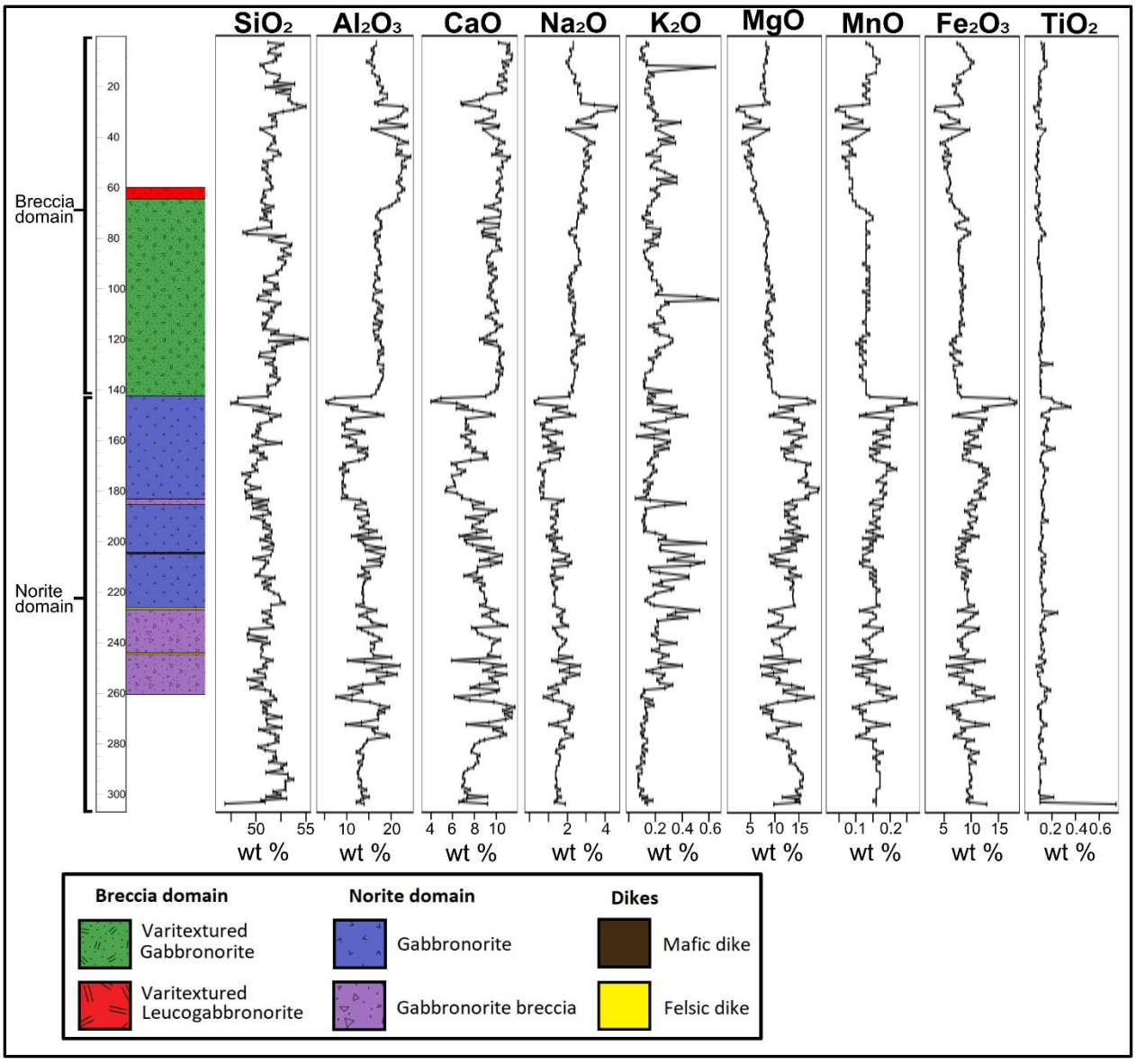

Figure 4.41 – Downhole plots of major elements in samples from DH# 18-805 (B3 Zone).

Representative samples from the major lithologies of the breccia and norite domains of the Offset South and B3 Zone were plotted on primitive mantle-normalized plots (Figs. 4.42, 4.43). In general, samples from the Offset Zone display weakly enriched light rare earth element (LREE) profiles; median primitive mantle-normalized La/Sm_N is 2.82 in the norite domain and 2.72 in the breccia domain. Heavy rare earth element (HREE) profiles are most commonly flat to

and slightly fractionated; median primitive mantle-normalized Gd/Yb_N is 0.96 in the breccia domain and 0.81 in the norite domain. Negative Nb anomalies are present in all samples and are typically quite pronounced. Positive Eu anomalies are present in all samples from the breccia domain and a majority of samples from the norite domain, with larger anomalies

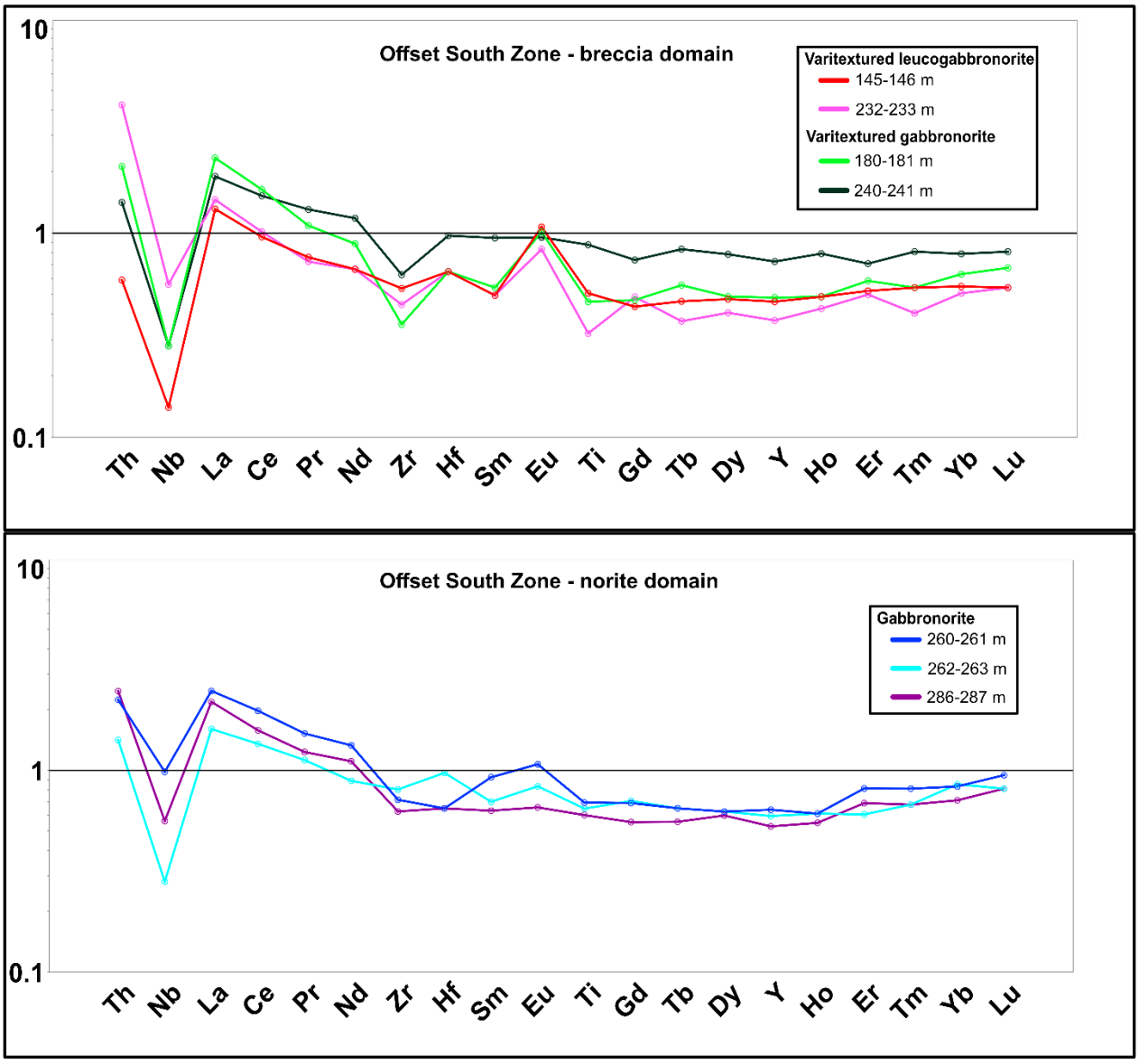

Figure 4.42 – Primitive mantle-normalized plots of representative samples of major rock types from the breccia and norite domain of the Offset South Zone. Normalizing values from Sun and McDonough (1989).

typically present in the breccia domain. Negative Zr-Hf anomalies are present in a majority of samples, with no correlation observed between zone or lithological domain and the presence or magnitude of Zr-Hf anomaly.

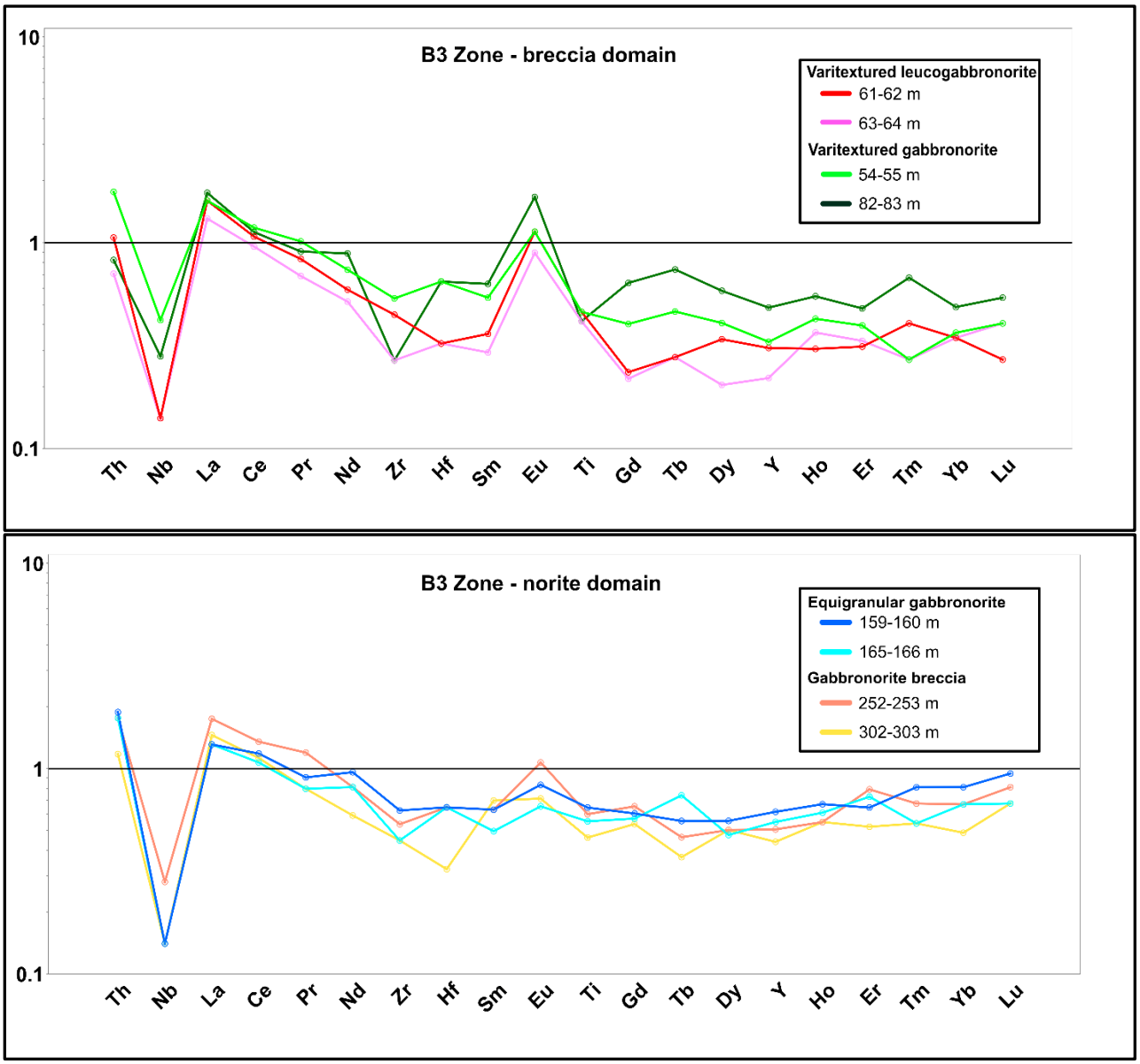

Figure 4.43 – Primitive mantle-normalized plots of representative samples of major rock types from the breccia and norite domain of the B3 Zone. Normalizing values from Sun and McDonough (1989).

Downhole plots of Gd/Yb_N and La/Sm_N were constructed for both drill holes to assess for spatial variation (Fig. 4.44). Gd/Yb_N does not show any downhole variability, but anomalously low values directly below the domain boundary contact are present in both drill holes. In addition, the highest observed Gd/Yb_N value observed in the Offset Zone is present directly above the domain boundary contact of the Offset South Zone. La/Sm_N shows a spatial trend in parts of both drillholes. In the Offset South Zone, the highest observed La/Sm_N of the norite domain is present directly below the domain boundary contact; below this, La/Sm_N reverts to a low value and generally increases with depth through the norite domain. In the B3 Zone, La/Sm_N displays a generally increasing trend from 113-243 m; this interval includes the domain boundary contact.

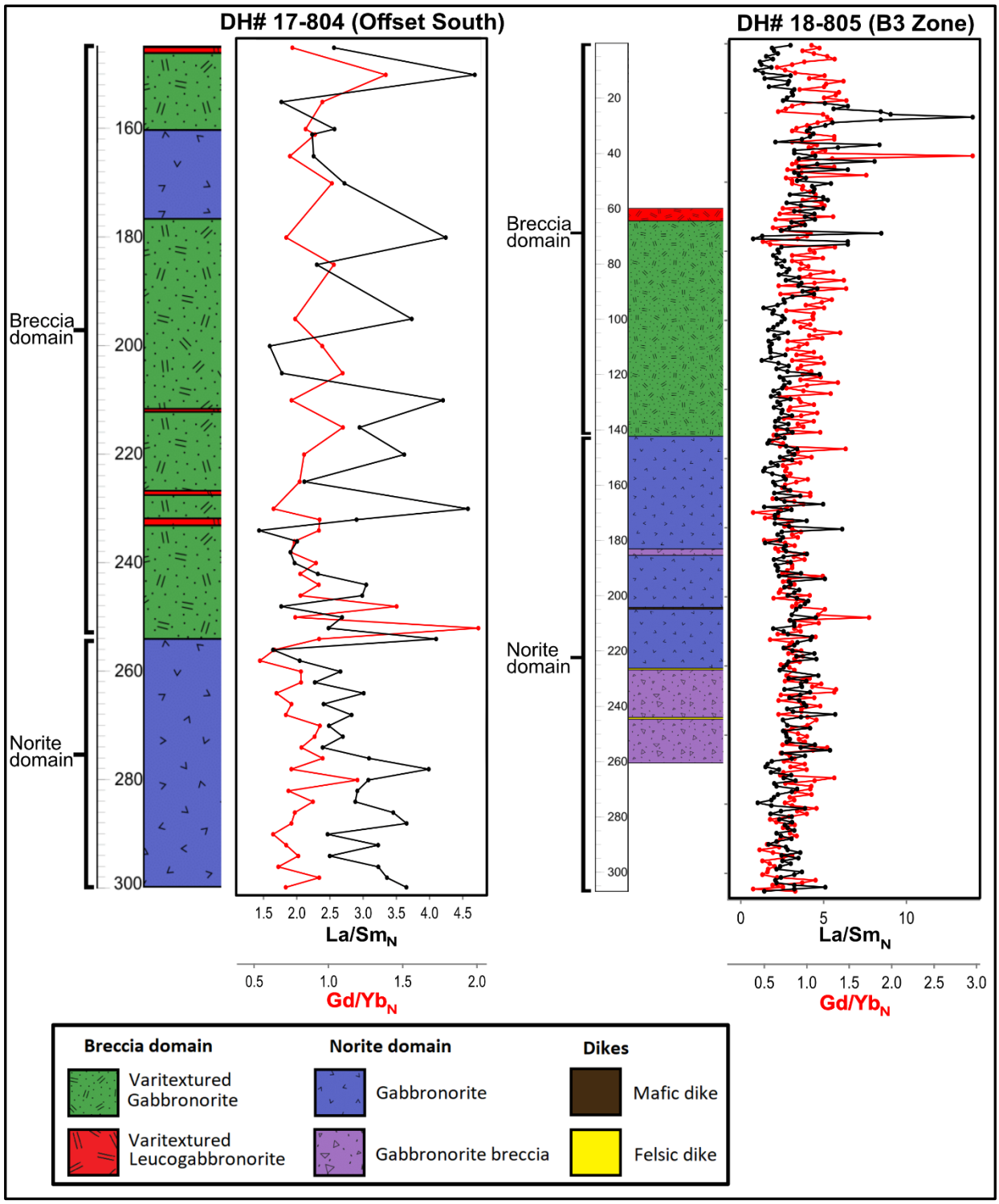

Figure 4.44 – Downhole La/Sm$_N$ vs Gd/Yb$_N$ plots of samples from Offset Zone drill holes. Normalizing values from Sun and McDonough (1989).

4.3.2 – Creek Zone

A total of 133 Creek Zone samples were taken from drill core and previously assayed pulp/reject material and analyzed for geochemical composition. Of these samples, 41 are from DH# 19-009 and 92 are from DH19-025. The samples have been grouped into units based on drill core logging and petrographic analysis. Of the samples from DH# 19-009, 16 samples are from the breccia domain and 25 samples are from the norite domain. All samples from the breccia domain of DH# 19-009 are from the area logged as varitextured leucogabbronorite, and all samples from the norite domain of DH# 19-009 are from the area logged as equigranular gabbronorite. Of the samples from DH# 19-025, 43 samples are from the breccia domain and 50 samples are from the norite domain. All samples from the breccia domain of DH# 19-025 are from the area logged as varitextured gabbronorite breccia and all 49 samples from the norite domain of DH# 19-025 are from the area logged as equigranular gabbronorite.

Downhole plots of major element content of samples from DH# 19-009 and DH# 18-805 are presented in Figures 4.45 and 4.46. Comparison of major element content between the two lithological domains shows a clear relationship in DH# 19-025, but not in DH# 19-009. Relationships between all major elements in DH# 19-025 follow the same trends observed in the Offset Zone; Al_2O_3, Na_2O, and CaO content are elevated in the breccia domain, and Fe_2O_3, MnO, and MgO are elevated in the norite domain. In DH# 19-009, average Al_2O_3 content is slightly higher in the breccia domain than the norite domain (18.6% vs. 16.3%), but CaO is essentially the same and Na_2O is actually lower in the breccia domain (1.56% vs. 2.25%). Fe_2O_3 and MnO content is higher in the norite domain, but MgO content is higher in the breccia domain.

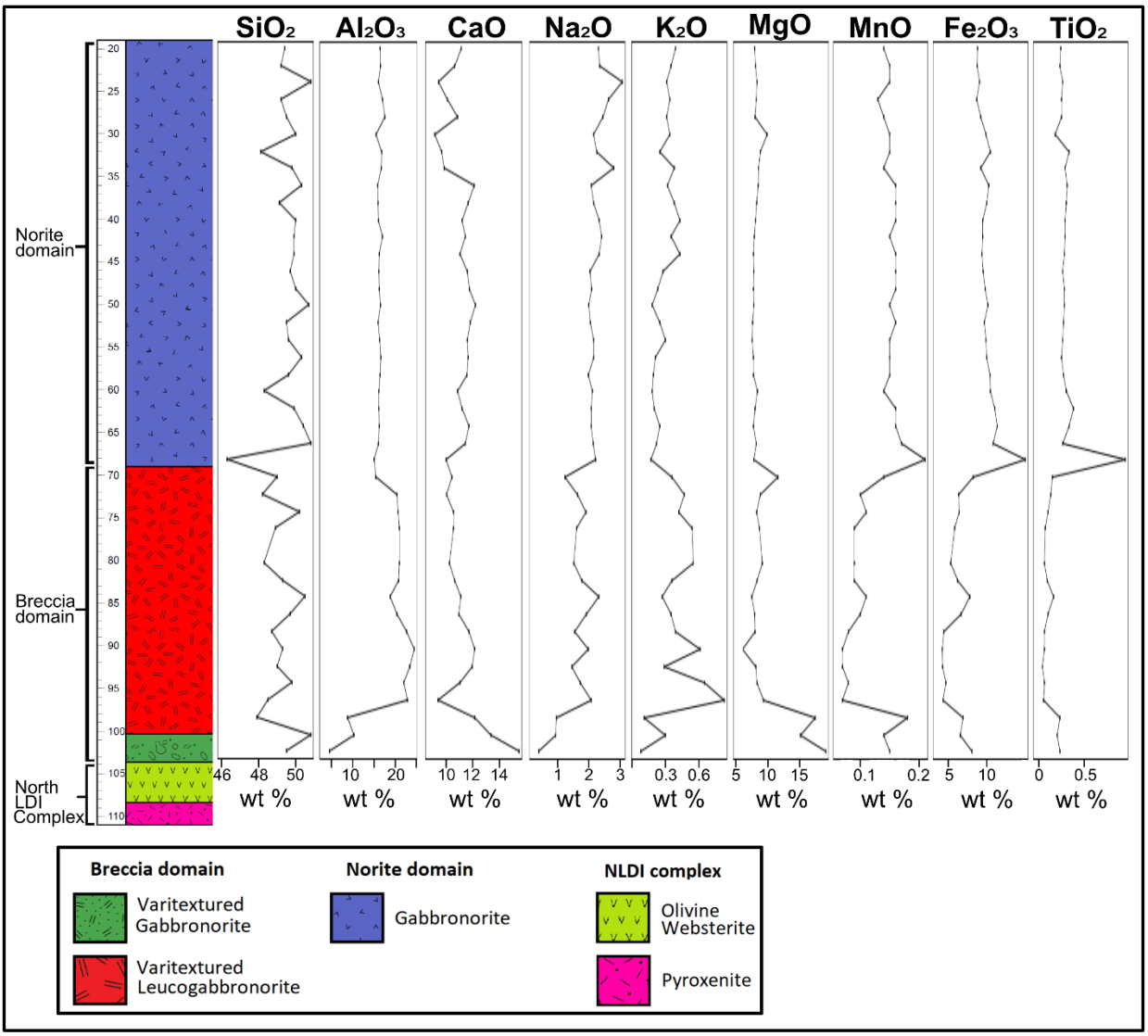

Figure 4.45 – Downhole plots of major elements in samples from DH# 19-009 (Creek Zone).

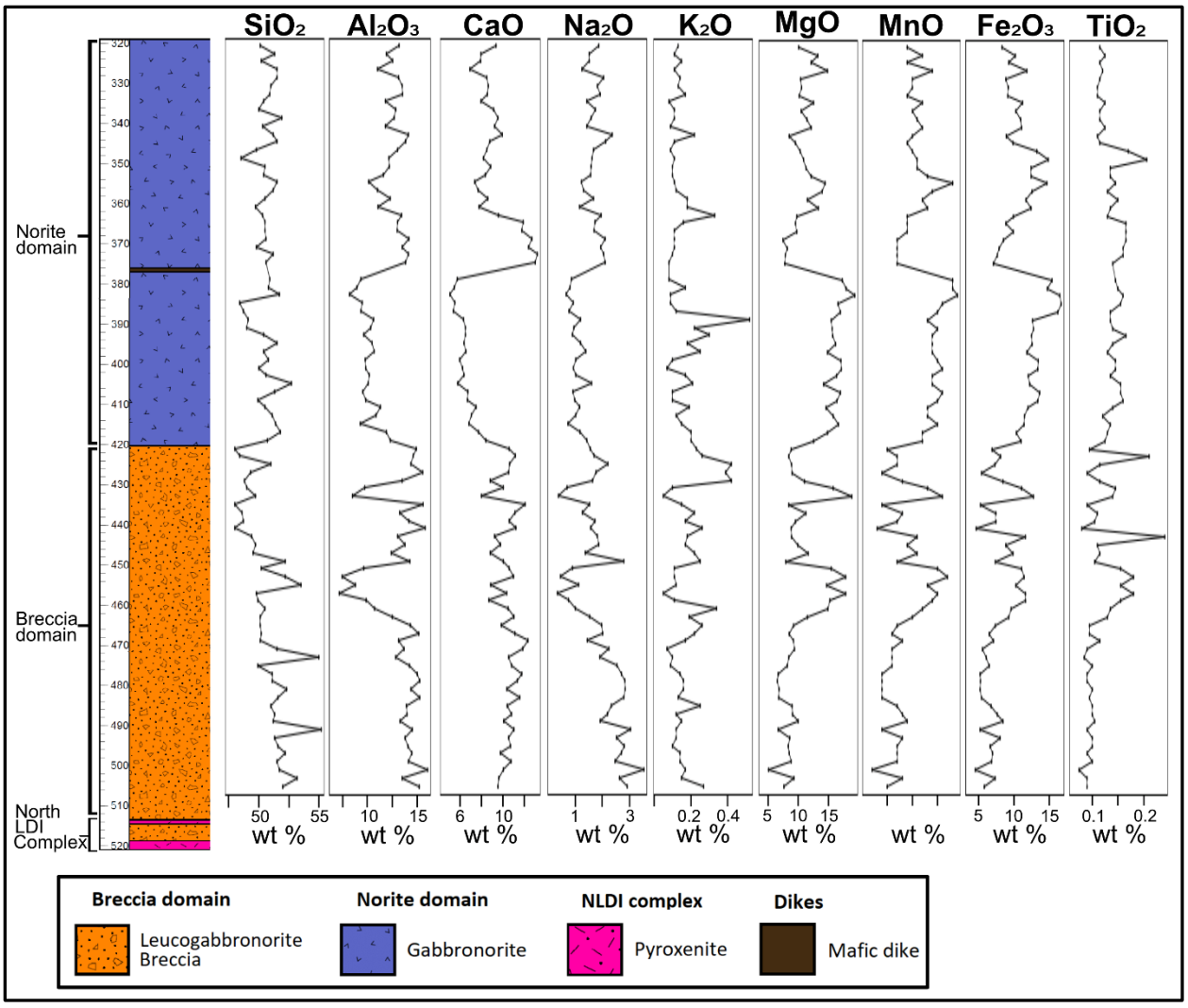

Figure 4.46 – Downhole plots of major elements in samples from DH# 19-025 (Creek Zone).

Representative samples from the major lithologies of the breccia and norite domains of the Creek Zone were plotted on primitive mantle-normalized plots (Fig. 4.47), with similar general trends observed as in the Offset Zone. LREE profiles show weak enrichment, with a slightly gentler slope (median La/Sm_N of 1.88 in the norite domain, 2.21 in the breccia domain) than observed in the Offset Zone. HREE profiles are typically flat, with a median Gd/Yb_N of 1.13 in the breccia domain and 1.00 in the norite domain. Negative Nb anomalies are present in all samples. Negative Zr-Hf are present in a majority of samples from both domains, whereas

positive Eu anomalies are present in all samples from the breccia domain and most samples from the norite domain.

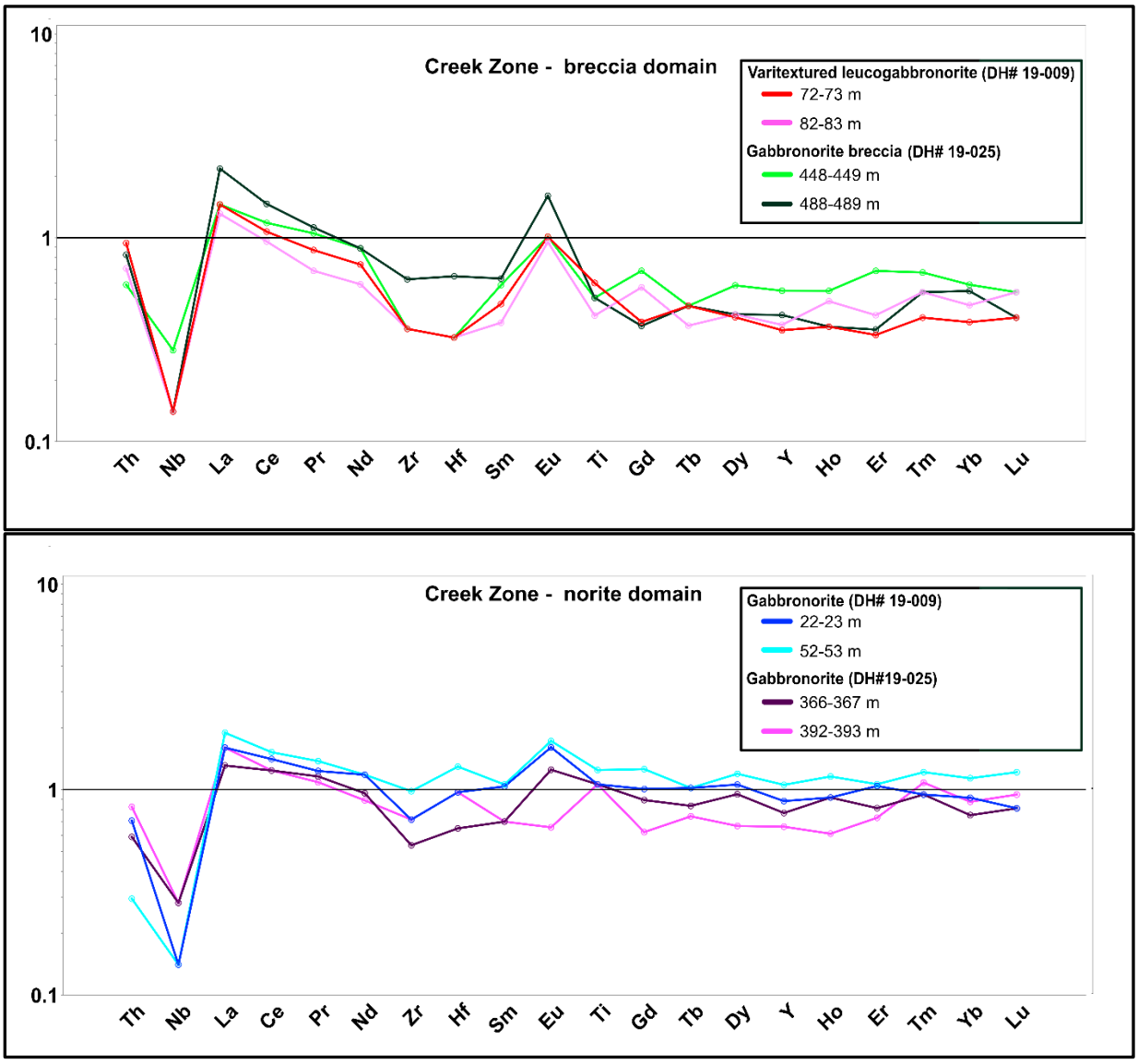

Figure 4.47 – Primitive mantle-normalized plots of representative samples of major rock types from the breccia and norite domain of the Creek Zone.

As in the Offset Zone, the lightest LREEs (La, Ce, Pr) are enriched relative to primitive mantle in the majority of samples from both domains of the Creek Zone. Concentration of other REEs in both domains of DH# 19-009 and the breccia domain of DH# 19-025 show similar trends

to the Offset Zone, in which heavier LREEs (Sm, Nd) and HREEs are depleted in a majority of samples. In the norite domain of DH# 19-009, however, Sm, Nd, and all of the HREEs are slightly enriched relative to primitive mantle in most samples.

Downhole plots of Gd/Yb_N vs La/Sm_N are presented in Figure 4.48. In DH# 19-009, Gd/Yb_N shows a relatively constant downhole value throughout, whereas ranges of both variables show a smaller degree of variability in the norite domain of this drill hole than in any other domain/drill hole analyzed in this study. A sharp increase in Gd/Yb_N and decrease in La/Sm_N is observed in the three samples of the breccia domain adjacent to the contact with the North Lac des Iles Complex. In DH# 19-025, the lowest Gd/Yb_N values are observed in a ~40 m section of the norite domain directly above the domain boundary contact, which roughly corresponds to the highest-$MgO/MnO/Fe_2O_3$ portion of the norite this drill hole. Other than this, no consistent spatial variations in La/Sm_N and Gd/Yb_N were observed.

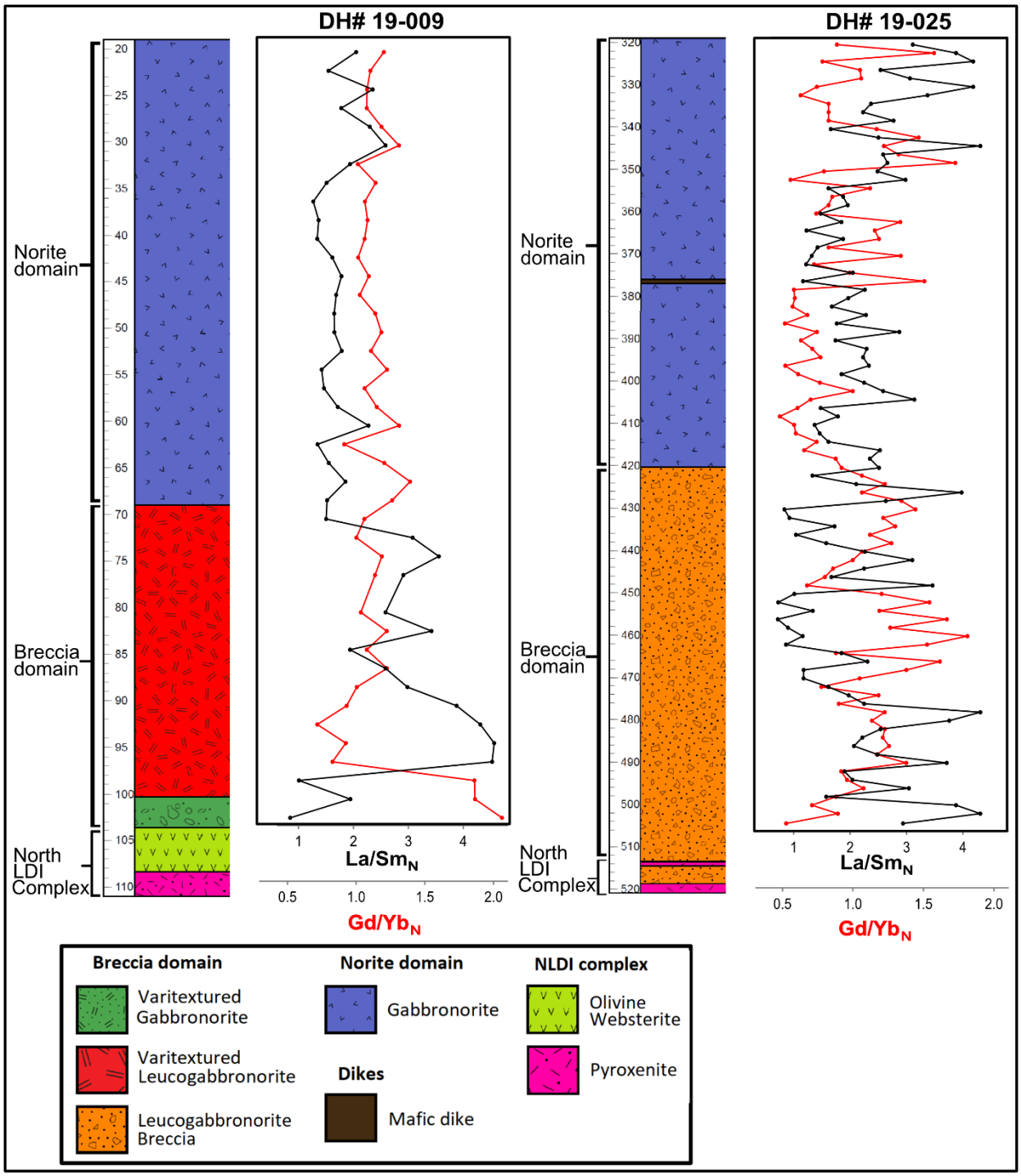

Figure 4.48 – Downhole La/Sm$_N$ vs Gd/Yb$_N$ plots of samples from Creek Zone drill holes. Normalizing values from Sun and McDonough (1989).

4.4 – Sulfur isotopes

Twenty samples were analyzed for sulfur isotope values. Results of sulfur isotope analyses are presented in Table 4.2. Samples were selected to reflect a broad range of rock types, alteration intensity, and Pd content. Sulfur isotope analysis was undertaken to evaluate the source of sulfur in sulfide minerals and to determine if any variability is present between or within different zones and lithological domains. Results were reported as quantities of ^{32}S, ^{33}S, ^{34}S, and ^{36}S as well as calculated values of $\delta^{33}S$, $\delta^{34}S$, $\delta^{36}S$, $\Delta^{33}S$, and $\Delta^{36}S$. ^{36}S was not analyzed in all samples due to issues with laboratory equipment. Full sulfur isotope analysis data is included in Appendix C. In most of the samples, analysis was performed on a representative crystal of each sulfide mineral present (pyrite, pyrrhotite, pentlandite, and/or chalcopyrite), as long as crystal was large enough for analysis were present. In a few cases, multiple crystals of the same sulfide mineral were analyzed in a single sample to test for variability between different crystals. Each individual crystal was analyzed at multiple points (8 to 15), and the mean value of the results from a single crystal was taken as the value for that crystal.

Eleven of the 20 analyzed samples were taken from the Offset Zone, 7 were taken from the Creek Zone, and two were taken from tonalitic gneiss country rock. Of the Offset Zone samples, seven were taken from the Offset South Zone (five from the breccia domain, two from the norite domain) and three were taken from the B3 Zone (one from the breccia domain, three from the norite domain). Of the Creek Zone samples, five were taken from DH# 19-025 (three from the norite domain, two from the breccia domain), and two were taken from DH# 19-009 (one from each the breccia and norite domains). In total, nine samples were analyzed from each of the breccia and norite domains.

Table 4.2 – ^{34}S, $\Delta^{33}S$, and $\Delta^{36}S$ results (NP = analysis not performed).

Drill hole	Depth (m)	Domain	Assemblage	Analyzed Mineral	$\delta^{34}S$ (‰)	$\delta^{34}S$ error	$\Delta^{33}S$ (‰)	$\Delta^{33}S$ error	$\Delta^{36}S$ (‰)	$\Delta^{36}S$ error
17-804	155.63	Breccia	Py-Po-Pn-Ccp	Pyrite	**1.49**	1.43	**-0.09**	0.04	**0.25**	0.26
17-804	155.63	Breccia	Py-Po-Pn-Ccp	Chalcopyrite	**0.81**	0.30	**-0.07**	0.05	**0.33**	0.33
17-804	155.63	Breccia	Py-Po-Pn-Ccp	Pyrrhotite (1)	**1.54**	0.51	**-0.04**	0.09	**0.14**	1.74
17-804	155.63	Breccia	Py-Po-Pn-Ccp	Pyrrhotite (2)	**1.48**	0.21	**-0.02**	0.06	**0.31**	0.25
17-804	185.16	Breccia	Py-Po-Pn-Ccp	Pyrite	**1.15**	1.50	**-0.09**	0.07	**0.18**	0.37
17-804	185.16	Breccia	Py-Po-Pn-Ccp	Chalcopyrite	**1.11**	0.15	**-0.08**	0.05	**0.32**	0.36
17-804	185.16	Breccia	Py-Po-Pn-Ccp	Pyrrhotite (1)	**1.72**	0.25	**-0.05**	0.06	**0.46**	0.27
17-804	185.16	Breccia	Py-Po-Pn-Ccp	Pyrrhotite (2)	**1.63**	0.18	**-0.03**	0.09	**0.49**	0.33
17-804	185.16	Breccia	Py-Po-Pn-Ccp	Pentlandite	**0.50**	1.00	**-0.08**	0.07	**0.22**	0.46
17-804	195	Breccia	Py-Po-Pn-Ccp	Pyrrhotite (1)	**1.18**	0.29	**-0.05**	0.10	**NP**	NP
17-804	195	Breccia	Py-Po-Pn-Ccp	Pyrrhotite (2)	**0.97**	0.34	**-0.07**	0.06	**NP**	NP
17-804	195	Breccia	Py-Po-Pn-Ccp	Pyrrhotite (3)	**1.12**	0.18	**-0.04**	0.08	**NP**	NP
17-804	195	Breccia	Py-Po-Pn-Ccp	Chalcopyrite (1)	**0.88**	0.44	**-0.11**	0.08	**0.28**	0.41
17-804	195	Breccia	Py-Po-Pn-Ccp	Chalcopyrite (2)	**0.81**	0.53	**-0.08**	0.06	**0.38**	0.42
17-804	195	Breccia	Py-Po-Pn-Ccp	Chalcopyrite (3)	**0.35**	1.02	**-0.08**	0.07	**0.48**	0.50
17-804	195	Breccia	Py-Po-Pn-Ccp	Pentlandite (1)	**-0.01**	0.71	**-0.07**	0.07	**0.68**	0.27
17-804	195	Breccia	Py-Po-Pn-Ccp	Pentlandite (2)	**0.20**	0.58	**-0.08**	0.10	**0.27**	0.42
17-804	240.61	Breccia	Py-Pn-Ccp	Pyrite	**0.69**	0.59	**-0.06**	0.06	**0.54**	0.54
17-804	240.61	Breccia	Py-Pn-Ccp	Chalcopyrite	**0.37**	0.52	**-0.08**	0.06	**0.54**	0.72
17-804	240.61	Breccia	Py-Pn-Ccp	Pentlandite (1)	**3.03**	1.04	**-0.09**	0.08	**0.16**	0.37
17-804	240.61	Breccia	Py-Pn-Ccp	Pentlandite (2)	**3.28**	1.28	**-0.07**	0.22	**0.23**	0.45
17-804	250.7	Breccia	Py-Po-Pn-Ccp	Pyrite	**1.15**	1.23	**-0.08**	0.08	**NP**	NP
17-804	250.7	Breccia	Py-Po-Pn-Ccp	Chalcopyrite	**0.30**	1.51	**-0.07**	0.04	**0.07**	0.52
17-804	250.7	Breccia	Py-Po-Pn-Ccp	Pentlandite	**1.13**	2.31	**-0.06**	0.10	**0.00**	0.51
17-804	258.29	Norite	Py-Po-Pn-Ccp	Pyrite	**0.90**	0.75	**-0.08**	0.06	**NP**	NP
17-804	258.29	Norite	Py-Po-Pn-Ccp	Chalcopyrite	**0.46**	0.28	**-0.07**	0.04	**-0.08**	0.52
17-804	258.29	Norite	Py-Po-Pn-Ccp	Pentlandite	**-0.37**	0.79	**-0.06**	0.05	**-0.25**	0.65
17-804	266.19	Norite	Py-Po-Pn-Ccp	Chalcopyrite (1)	**0.93**	0.49	**-0.06**	0.07	**0.33**	0.51
17-804	266.19	Norite	Py-Po-Pn-Ccp	Chalcopyrite (2)	**0.70**	0.19	**-0.06**	0.07	**0.44**	0.28
17-804	266.19	Norite	Py-Po-Pn-Ccp	Pyrrhotite	**0.80**	0.22	**-0.03**	0.05	**NP**	NP
18-805	100.22	Breccia	Py-Po-Pn-Ccp	Pyrite	**1.29**	1.37	**-0.06**	0.07	**0.06**	0.40
18-805	100.22	Breccia	Py-Po-Pn-Ccp	Chalcopyrite (1)	**1.19**	0.15	**-0.07**	0.06	**0.01**	0.34
18-805	100.22	Breccia	Py-Po-Pn-Ccp	Chalcopyrite (2)	**1.19**	0.34	**-0.08**	0.07	**0.06**	0.47
18-805	100.22	Breccia	Py-Po-Pn-Ccp	Pyrrhotite (1)	**1.16**	0.81	**-0.04**	0.06	**0.42**	0.47
18-805	100.22	Breccia	Py-Po-Pn-Ccp	Pyrrhotite (2)	**1.19**	0.19	**-0.06**	0.06	**-0.10**	0.56
18-805	170.22	Norite	Py-Po-Pn-Ccp	Pyrite	**0.37**	0.56	**-0.06**	0.04	**NP**	NP
18-805	185.32	Norite	Py-Po-Pn-Ccp	Pyrite	**0.43**	0.30	**-0.07**	0.11	**NP**	NP
18-805	259.81	Norite	Py-Po-Pn-Ccp	Pyrite	**1.29**	0.57	**-0.10**	0.04	**NP**	NP
18-805	259.81	Norite	Py-Po-Pn-Ccp	Chalcopyrite	**1.12**	0.28	**-0.06**	0.08	**NP**	NP
18-805	259.81	Norite	Py-Po-Pn-Ccp	Chalcopyrite	**1.07**	0.15	**-0.06**	0.04	**NP**	NP
19-025	360.54	Norite	Py-Ccp	Pyrite	**1.63**	0.16	**-0.06**	0.06	**NP**	NP
19-025	384.86	Norite	Py-Po-Pn-Ccp	Chalcopyrite	**0.93**	0.23	**-0.07**	0.07	**NP**	NP
19-025	384.86	Norite	Py-Po-Pn-Ccp	Pyrrhotite	**1.14**	0.22	**-0.07**	0.07	**NP**	NP
19-025	384.86	Norite	Py-Po-Pn-Ccp	Pentlandite	**0.02**	0.57	**-0.04**	0.12	**1.01**	0.73
19-025	400.44	Norite	Py-Po-Pn-Ccp	Chalcopyrite	**1.24**	0.49	**-0.06**	0.06	**NP**	NP
19-025	400.44	Norite	Py-Po-Pn-Ccp	Pentlandite	**0.95**	0.46	**-0.08**	0.05	**NP**	NP
19-025	432.44	Breccia	Po-Pn-Ccp	Chalcopyrite	**1.85**	0.53	**-0.08**	0.08	**NP**	NP
19-025	488.3	Breccia	Py-Po-Pn-Ccp	Pyrite	**1.13**	0.84	**-0.08**	0.07	**NP**	NP
19-025	488.3	Breccia	Py-Po-Pn-Ccp	Pyrrhotite (1)	**1.06**	0.58	**-0.03**	0.04	**NP**	NP
19-025	488.3	Breccia	Py-Po-Pn-Ccp	Pyrrhotite (2)	**1.15**	0.24	**-0.03**	0.05	**NP**	NP
19-009	68	Norite	Py-Ccp	Pyrite	**0.90**	0.63	**-0.06**	0.07	**NP**	NP
19-009	68	Norite	Py-Ccp	Chalcopyrite	**-0.29**	0.17	**-0.06**	0.06	**NP**	NP
19-009	84	Breccia	Py-Ccp	Pyrite (1)	**1.64**	0.26	**-0.05**	0.06	**NP**	NP
19-009	84	Breccia	Py-Ccp	Pyrite (2)	**1.58**	0.30	**-0.08**	0.06	**NP**	NP
N/A	N/A	Tonalitic gneiss	Py	Pyrite	**2.40**	0.74	**-0.08**	0.05	**NP**	NP
N/A	N/A	Tonalitic gneiss	Py	Pyrite	**1.84**	0.53	**-0.10**	0.07	**NP**	NP

Downhole plots of $\delta^{34}S$ values are included in Figure 4.49. $\delta^{34}S$ values range from -0.37‰ to +3.28‰, with all values falling in the expected range of mantle-sourced sulfur (0 ± 2‰; Seal, 2006), except for two pentlandite crystals from the same sample at 240.61 m depth of the Offset South Zone, which have values of +3.03‰ and +3.28‰. No significant difference in $\delta^{34}S$ value is seen in the breccia vs. norite domains (median values of 1.15 and 0.90‰, respectively) or in the Offset vs. Creek Zones (median values of 0.95 and 1.14‰, respectively). No systematic differences in $\delta^{34}S$ values are observed when comparing different sulfide assemblages or proximity to the domain boundary contact. Median values of analyses of chalcopyrite (+0.90‰), pyrrhotite (+1.16‰), and pyrite (+1.22‰) are relatively similar, whereas pentlandite (+0.20‰) has a slightly less positive median value. The difference in $\delta^{34}S$ values in different crystals in the same sample ranges from quite low (<0.10‰ in three samples) to moderate (>1.00‰ in five samples). The two tonalitic gneiss country rock samples yield slightly higher values (2.40 and 1.84‰) than most samples from the South Lac des Iles Complex. Error values for all analyzed samples are low and support the reliability of the data.

$\Delta^{33}S$ values range from -0.02 to -0.11‰, which is within the range of mass-dependent fractionation (0 ± 0.2‰; Farquhar and Wing, 2003). No correlation between $\Delta^{33}S$ and lithological domain, zone, or distance from the domain boundary contact was observed. Tonalitic gneiss country rock samples have similar values (-0.08 and -0.10) to samples from the South Lac des Iles Complex. $\Delta^{33}S$ error values are very low and support the reliability of the data. $\Delta^{36}S$ values were collected to aid in the interpretation of $\Delta^{33}S$ values if a mass-independent signature was observed. Because that is not the case, $\Delta^{36}S$ values are not relevant for interpretation of the data set.

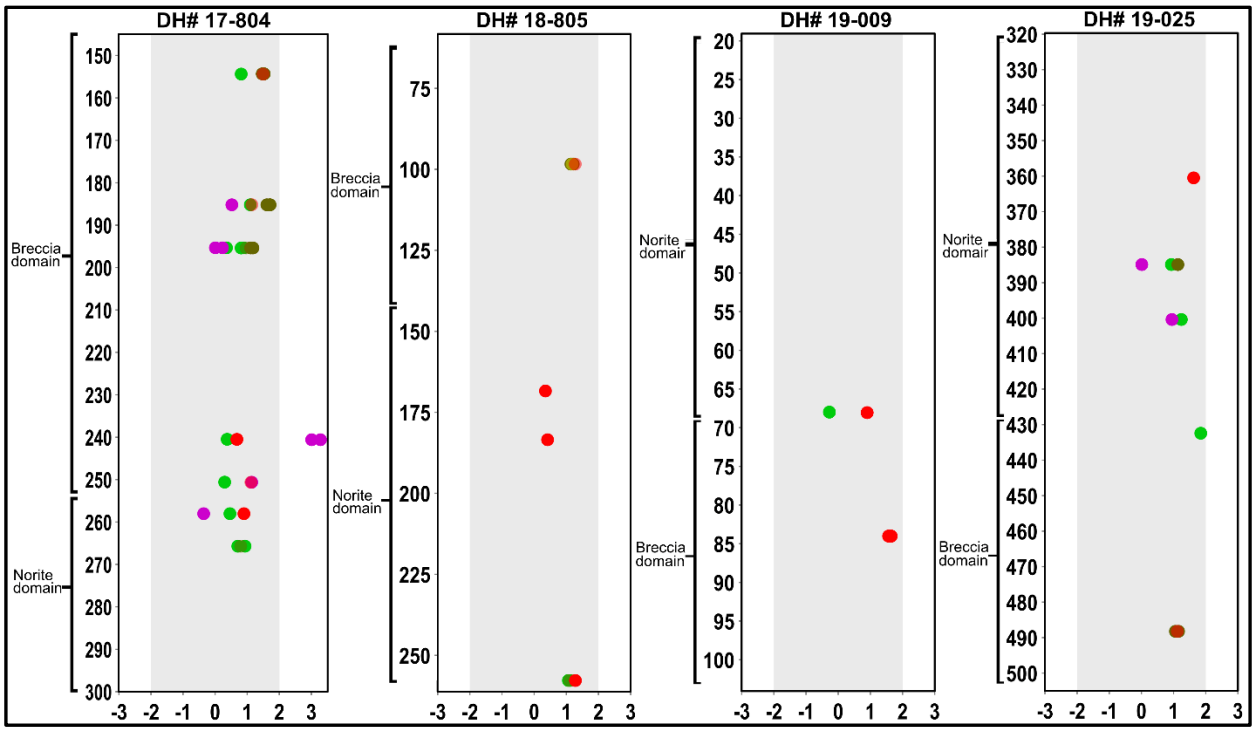

Figure 4.49 – Downhole plots of $\delta^{34}S$ values of all analyzed crystals. Green = chalcopyrite, purple = pentlandite, brown = pyrrhotite, red = pyrite. Grey boxes represent mantle values (Seal, 2006).

4.5 – Neodymium isotopes

Neodymium isotope analysis was performed on nineteen samples. Results from Nd isotope analysis are included in Table 4.3. Samples were chosen to represent a broad range of rock types, Pd grades, and variations in rare earth element concentrations and patterns. Samples were taken from the Offset South and both Creek Zone drill holes, but not the B3 Zone. This was done to better assess downhole variation in single drill holes. The Offset South Zone was chosen over the B3 Zone because there is less geochemical variability in the Offset South Zone, making each sample more representative of the zone and individual domains in that drill hole. Nine samples were analyzed from the Offset South Zone, and ten samples were analyzed from the Creek Zone. Of the Offset South Zone samples, five were taken from the breccia domain and four were taken from the norite domain. Of the Creek Zone samples, five

were taken from DH# 19-025 (four from the norite domain, one from the breccia domain), and five were taken from DH# 19-009 (three from the norite domain, two from the breccia domain). In total, 11 samples from the norite domain and eight samples from the breccia domain were submitted for analysis.

Results are reported in terms of $^{143}Nd/^{144}Nd$ and $^{144}Nd/^{145}Nd$ isotopic ratios (full results presented in Appendix D). ε_{Nd} values were calculated using an age of 2689.0 Ma (D.W. Davis cited in Stone et al., 2003), using the method outlined by DePaolo (1981). This is the most recent age date from the western South Lac des Iles Complex, which includes the Offset Zone. The most recent published age date for the eastern South Lac des Iles Complex, which includes the Creek Zone, is 2693.3 Ma (Heaman and Easton, 2006). These results are concordant with the most recent age date for the Lac des Iles Complex in general, which is 2687.0 Ma and was acquired from the North Lac des Iles Complex by Heaman and Easton (2018, unpublished).

ε_{Nd} values range from 0.38 to -3.47, with 18 of 19 samples yielding a negative value. In all drill holes for which ε_{Nd} was measured, no systematic variability is observed between lithological domains or within individual drill holes. ε_{Nd} is somewhat less variable in the Creek Zone than in the Offset Zone, with 8 of 10 Creek Zone samples falling between -1.89 and -2.93.

Table 4.3 – ε_{Nd} results.

Drill hole	Depth from	Depth to	Domain	ε_{Nd}
17-804	145	146	Breccia	**0.38**
17-804	155	156	Breccia	**-3.27**
17-804	185	186	Breccia	**-2.10**
17-804	200	201	Breccia	**-1.79**
17-804	240	241	Breccia	**-2.47**
17-804	258	259	Norite	**-0.44**
17-804	266	267	Norite	**-2.25**
17-804	280	281	Norite	**-3.47**
17-804	298	299	Norite	**-1.09**
19-025	334	335	Norite	**-2.13**
19-025	364	365	Norite	**-1.29**
19-025	384	385	Norite	**-1.89**
19-025	398	399	Norite	**-2.28**
19-025	482	483	Breccia	**-2.09**
19-009	22	23	Norite	**-2.50**
19-009	46	47	Norite	**-0.79**
19-009	64	65	Norite	**-2.93**
19-009	70	71	Breccia	**-2.53**
19-009	76	77	Breccia	**-2.32**

Chapter 5 - Discussion

5.1 – Source of the South Lac des Iles Complex magma

Constraining the source of the magma that formed the breccia and norite domains of the South Lac des Iles Complex is important for developing a deposit model and characterizing the Pd-rich mineralization associated with the contact between the two domains. The tectonic setting of the intrusive complex and the degree of crustal contamination are the most significant factors to be evaluated when considering the magma source. The majority of the world's significant Ni-Cu-PGE deposits are located in rift-related settings in which large quantities of magma were generated via high degrees of partial melting in extensional environments (Naldrett, 2004). In contrast, a minority of Ni-Cu-PGE deposits (e.g. Aguablanca, Huangshan, Sally Malay, Selebi-Phikwe, Xiarihamu) are interpreted to have formed in collisional environments where slab subduction triggered a smaller degree of partial melting in the upper mantle (Sproule et al., 1999; Tornos et al., 2006; Maier et al., 2007; Zhang et al., 2017; Lu et al., 2019).

5.1.1 – Source of the South Lac des Iles Complex magma – Previous work

The magma that formed the South Lac des Iles Complex has been variably argued to have been sourced from either a subduction setting or a mantle plume. Brugmann et al. (1997) presented the case for a continental arc affinity, based on Nd isotopes, enrichment of LILEs and LREEs, depletion of HFSEs, and proximity to the boundary between the Quetico and Marmion terranes. Brugmann et al. (1997) also noted several characteristics of the Lac des Iles Complex that are similar to subduction-associated Alaskan-type intrusions, including the composite

lithology, sub-circular shape of the South Lac des Iles Complex (SLDIC), and petrological characteristics (including the presence of two-pyroxene gabbros, olivine/clinopyroxene-dominant ultramafic cumulates in the North Lac des Iles Complex, and hornblende-rich mafic rocks in the South Lac des Iles Complex). Barnes and Gomwe (2010) also argued for a subduction-related setting, interpreting orthopyroxene and plagioclase compositions in the SLDIC as being representative of a parental continental arc-related calc-alkaline andesite. Djon et al. (2018) examined samples from the Offset Zone of the SLDIC (as well as the North Lac des Iles Complex) and argued that the enrichment in LILEs, negative Nb anomalies, and positive Pb anomalies in the Lac des Iles Complex are similar to those seen in arc basalts.

In contrast, Hinchey et al. (2005) modeled the SLDIC magma as being derived by high degrees of partial melting of a moderately depleted mantle source in a mantle plume setting. They interpreted the REE concentrations of the modeled SLDIC parent magma as similar to enriched mid-ocean ridge basalts (E-MORB). Hinchey et al. (2005) calculated the primitive melt content of MgO in melanocratic rocks of the Roby Zone of the SLDIC to be 8.9% MgO, but they argued that this was likely impacted by pre-emplacement fractional crystallization of olivine and that the primary melt would have had an MgO composition of ~17.3% MgO. This modeled primary MgO content is near the lower boundary for komatiites and picrites, which are sourced via high degrees of partial melting of the depleted mantle and are unrelated to continental arcs (Arndt et al., 2008).

5.1.2 – Source of the South Lac des Iles Complex magma - Whole rock geochemistry

Systematic differences in trace element content are observed in magmas generated in different tectonic environments. Although the following processes and categories were formulated to describe volcanic rocks, they are also commonly used to classify intrusive rocks such as those that make up the Lac des Iles Complex. Ocean island basalts (OIBs) are consistently observed to have higher incompatible element contents and greater enrichment of LILEs/LREEs relative to HFSEs/HREEs than upper mantle-sourced volcanic rocks such as arc and mid-ocean ridge basalts (MORBs; Sun and McDonough, 1989; Hofmann, 1997; Pearce, 2008). This difference in composition occurs mainly because OIBs form as the result of mantle plumes derived from partial melts of the lower mantle (up to >1000 km depth), which has not been depleted via episodic melting and is thus enriched in incompatible elements compared to the upper mantle (Hofmann, 1997). Conversely, arc basalts are generated via melting of the upper part of the mantle (<100 km depth), which has been progressively depleted of incompatible elements via episodes of partial melting throughout the Earth's history (Hofmann, 1997).

Although MORBs and arc basalts melt similar parts of the mantle, the magmas that they generate have different characteristics due to the influence of the subducting slab in melt generation. Arc basalts are comparatively enriched in LILEs and LREEs, which are highly mobile in fluids that are generated from the subducting slab and are incorporated into the melting mantle (Saunders, 1991). HFSEs are not mobile in subduction-related fluids; their content in arc magmas is therefore thought to represent the composition of the melting mantle wedge rather than the influence of the subducting slab, resulting in negative HFSE anomalies compared to the enriched LILEs and LREEs (Pearce and Peate, 1995). Because no known economic Ni-Cu-PGE

deposits are associated with MORBs (Schulz et al., 2010), the focus of this section is to delineate between an OIB and arc setting and to determine the influence of crustal contamination.

Primitive mantle-normalized plots of incompatible elements were constructed using average compositions of samples taken for this study (Fig. 5.1A-C). Limited variability in average incompatible element content is seen between the Creek and Offset Zones and between the breccia and norite domains. LILEs (Cs, Rb, Ba, K, Sr, Eu) and LREEs are weakly to moderately enriched relative to primitive mantle, whereas HREEs show a generally flat pattern. HFSEs (Ta, Nb, P, Zr, Hf, Ti) range from undepleted to depleted, with Nb being the only HFSE that is consistently strongly depleted (median Nb/Nb* = 0.09). No systematic Ti anomalies were observed, with a median Ti/Ti* of 0.89, a large spread of values (0.04 to 14.70), and a slightly lower average Ti/Ti* observed in the breccia domain than the norite domain. Zirconium-hafnium anomalies are weakly negative to nonexistent, with Zr generally showing a slightly more negative anomaly than Hf.

Primitive mantle-normalized plots of five samples of tonalitic gneiss country rock are included in Figure 5.1D. Four samples were taken by Wyatt Bain in the summer of 2022, and one sample was reported by Brugmann et al. (1997). Fractionated LREE curves and negative HFSE anomalies are seen in all samples. Flat HREE patterns are present in four samples, whereas one sample has a depleted HREE curve. Most of the incompatible elements are consistently more abundant in all tonalitic gneiss samples than in the Offset and Creek Zones, except for HREEs, whose content ranges from similar to greater than the South Lac des Iles Complex samples. Niobium anomalies are present in all samples (Nb/Nb* = 0.08-0.46), ranging from similar to less pronounced than those present in South Lac des Iles Complex samples.

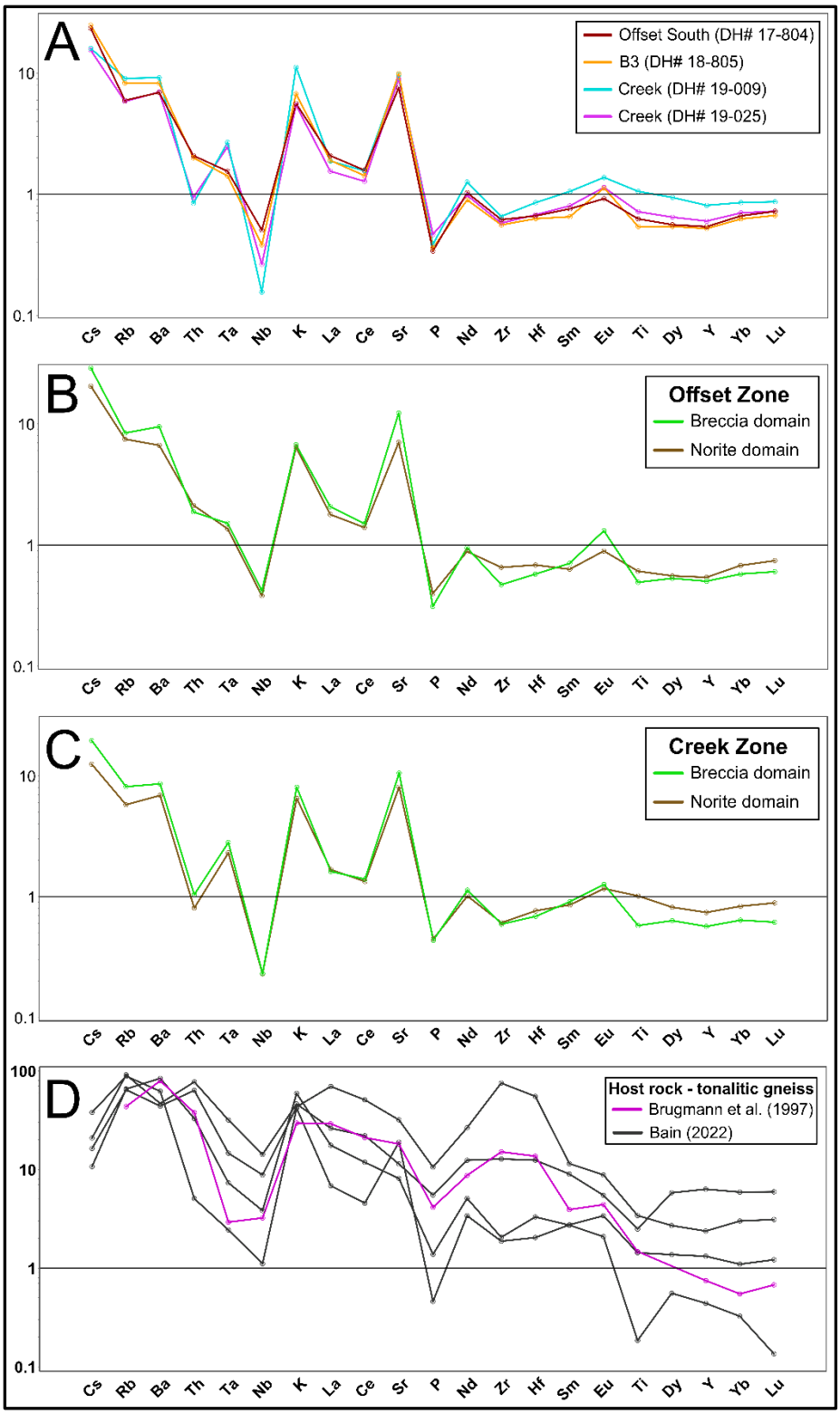

Figure 5.1 – Primitive mantle-normalized plots of incompatible elements. A) All samples from each studied drill hole. B) Breccia and norite domains of Offset Zone. C) Breccia and norite domains of Creek Zone. D) Samples of tonalitic gneiss host rock. Note the different Y-axis scale in D. Normalizing values from Sun and McDonough (1989).

The broad range of values in the tonalitic gneiss samples indicates that the gneissic complex has a heterogenous composition. Despite this, the similarity in incompatible element trends between tonalitic gneiss samples can be used to make assessments of its possible assimilation into the Lac des Iles magma. Values of some incompatible elements/elemental ratios in the South Lac des Iles Complex are between expected mantle values and values observed in the tonalitic gneiss, which could be taken as potential evidence for assimilation of the tonalitic gneiss as the mechanism for incompatible element enrichment of the South Lac des Ilex Complex magma. Values of some elements/elemental ratios in the South Lac des Iles Complex samples (medians of Th = 0.08 ppm, Zr = 5 ppm, Gd/Yb_N = 0.92, Ti/Ti* = 0.89) could reasonably be derived via contamination of a mantle-derived magma by rocks with similar composition to the tonalitic gneiss samples (Th = 0.43-6.57 ppm, Zr = 21-842 ppm, Gd/Yb_N = 1.10-3.57, Ti/Ti* = 0.02-0.32). However, the presence of similar or lower values of some elemental ratios in the tonalitic gneiss (La/Sm_N = 2.49-7.43, Ba/Th = 49.6-1009.3) compared to the South Lac des Iles Complex samples (medians of La/Sm_N = 2.59, Ba/Th = 608.8) suggest that incompatible element enrichment of the Lac des Iles magma cannot solely be explained by contamination by the tonalitic gneiss. Additionally, the lesser magnitude of Nb anomalies in the tonalitic gneiss compared to the South Lac des Iles Complex samples suggests that country rock assimilation is an unlikely candidate for generation of the negative Nb anomalies in the South Lac des Iles Complex. Based on these observations, it is likely that the trace element contents of the samples in this study were generated either by involvement of a component other than the tonalitic gneiss, which could be 1) subduction-derived fluids or 2) rocks with different composition to that of the tonalitic gneiss. Because the tonalitic gneiss is the sole host rock to

the Lac des Iles Complex, the second scenario is difficult to assess as it would involve rocks of unknown characteristics assimilated at depth.

One way to discriminate magma source and help discern the processes that may have modified the trace element content of the magma (e.g., subduction, crustal contamination, fractional crystallization) is to plot samples on a diagram of Th/Yb vs. Nb/Yb (Pearce and Peate, 1995; Pearce, 2008). Ytterbium is used as a normalizing factor because its abundance is not significantly modified by fractional crystallization, partial melting, or enrichment processes that occur after magma is generated (Pearce, 1983). Thorium and niobium are used because they display similar enrichment in mantle-derived magmas, but behave differently in arc settings, as Th is effectively transferred from a slab source via the fluid whereas Nb is not (Pearce and Peate, 1995). Additionally, all three elements are relatively immobile during alteration and metamorphism (Pearce and Peate, 1995).

Samples from this study are plotted on a Th/Yb vs. Nb/Yb diagram in Figure 5.2. The grey “mantle array” represents the relative proportions of Th and Nb (normalized to Yb) in mantle-derived magmas. Samples plotting above the mantle array indicate enrichment in Th relative to Nb due to either crustal assimilation/fractional crystallization or by modification of the mantle by slab-derived fluids. The composition of the tonalitic gneiss that hosts the Lac des Iles Complex and the average composition of Archean continental crust are also plotted on these diagrams; if a mantle-derived magma were enriched in Th relative to Nb strictly via crustal assimilation, the samples would plot between the mantle array and these compositions. This is clearly not the case in the samples from the breccia and norite domains of the South Lac des Iles Complex, which have a lower Nb/Yb content than if they were modified strictly by

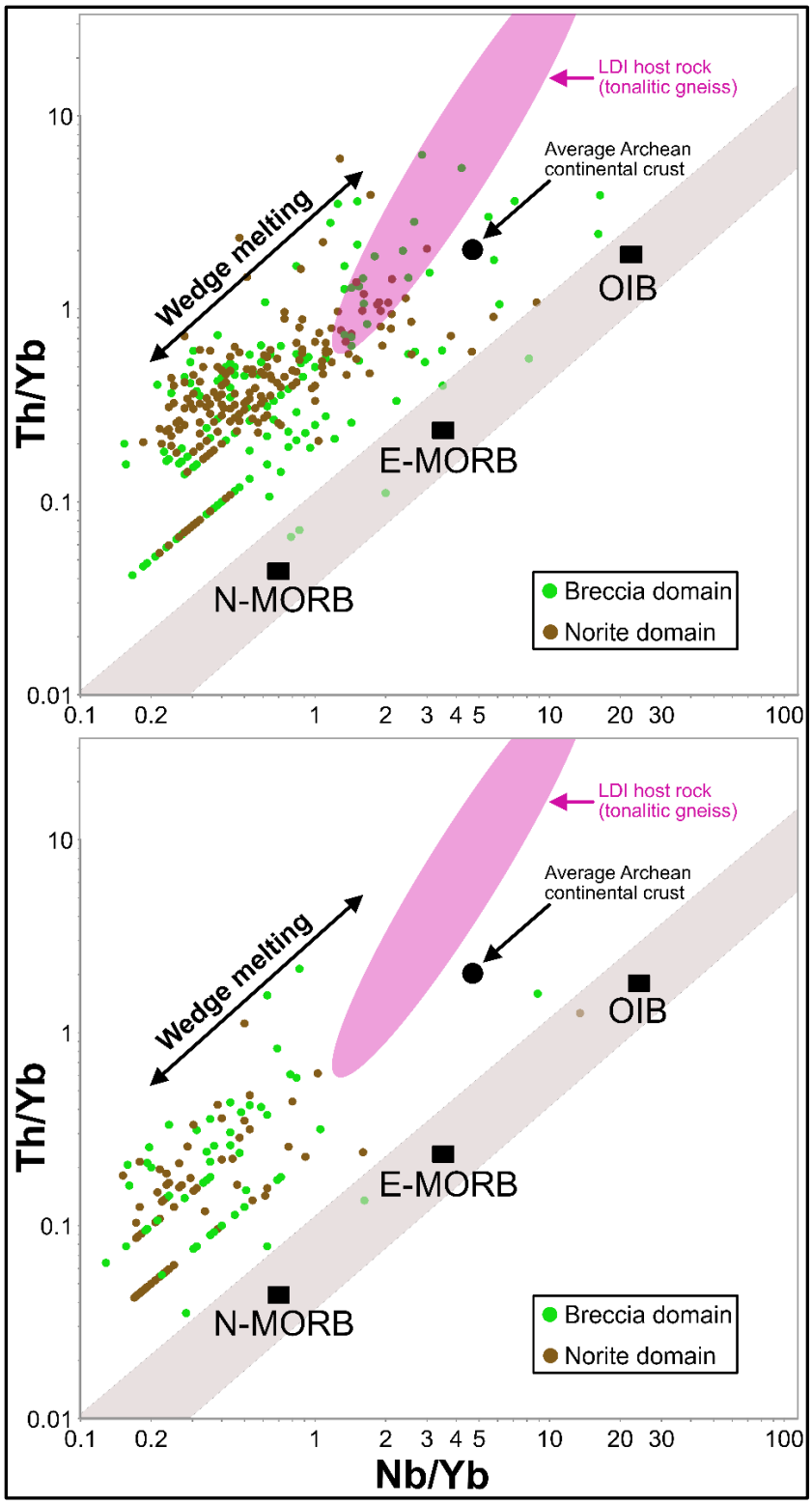

Figure 5.2 – Bivariate plot of Th/Yb vs. Nb/Yb for A) Offset Zone samples and B) Creek Zone samples. Mantle array (in grey) from Pearce et al. (2008). N-MORB, E-MORB, OIB compositions from Sun and McDonough (1989). Average Archean continental crust composition from Rudnick and Fountain (1995). Tonalitic gneiss composition from Bain (2022) and Brugmann et al. (1997).

crustal contamination. Conversely, the modification of a mantle-derived magma by subduction zone processes would result in increasing Th/Yb relative to Nb/Yb with increasing input of slab-derived fluids. In this case, samples would plot between the mantle array and the "wedge melting" field in Figure 5.2. This is consistent with the data from this study; the majority of samples plot directly above the more depleted portion of the mantle array, suggesting that a subduction-influenced depleted mantle source is plausible. Samples from the Offset Zone show a wider range of Th/Yb and Nb/Yb values than samples from the Creek Zone, in which most samples have Th/Yb < 1 and Nb/Yb < 2. This could indicate that the Creek Zone may have undergone a lesser and less variable degree of crustal contamination, and/or been generated via the melting of a more depleted source.

An enriched, OIB-like parent magma for the breccia and norite domains of the South Lac des Iles Complex would be difficult to reconcile with the trends observed in Figure 5.2; although a large degree of crustal contamination of an OIB source could produce the Th/Nb ratios seen in the South Lac des Iles Complex, the Th/Yb and Nb/Yb ratios in that case would be much higher than is observed in these samples. Several other characteristics of the trace element content of these samples are inconsistent with an OIB source; OIBs typically display strong enrichment in LREEs (rather than weak to moderate), fractionated HREEs (rather than flat), and total incompatible element contents many times higher than primitive mantle (Sun and McDonough, 1989), none of which were observed in this study.

The formation of negative Nb anomalies has been explained by two different and contrasting processes. The classical view is that Nb anomalies occur via the retention of Nb-bearing oxide minerals (sphene, rutile, ilmenite, titanomagnetite), amphiboles, and/or mica in

the mantle during arc-related fluid movement and magmatism (Green and Pearson, 1986; Ionov and Hofmann, 1995). The more widely accepted view is that HFSEs, including Nb, Ta, and Ti, are immobile in slab-derived fluids and that their content in arc magmas represent that of the depleted mantle wedge (McCollough and Gamble, 1991). In this interpretation, the negative HFSE anomalies seen in arc magmas are the result of enrichment in fluid-mobile LILEs and LREEs relative to HFSEs, rather than retention of HFSEs in the residual mantle (McCollough and Gamble, 1991). Regardless of the mechanism, negative Nb anomalies are a feature of arc magmas and are not observed in MORB and OIB magmas.

Negative Nb anomalies can also be acquired when magmas of any origin assimilate continental crust, which is broadly Nb-depleted and LREE-enriched. If Nb anomalies were derived from crustal contamination rather than subduction-related processes, the strength of the niobium anomaly should correlate to the degree of LREE enrichment, as greater amounts of assimilation would proportionally increase LREEs and relatively deplete Nb. To test this, Nb/Nb* (size of Nb anomaly) is plotted against La/Sm, which is a proxy for degree of LREE enrichment (Fig. 5.3). Depleted mantle (represented by N-MORB), average Archean continental crust, and composition of tonalitic gneiss host rock are also plotted. If crustal contamination caused the high La/Sm and low Nb/Nb* of the samples in this study, they would be expected to plot between depleted mantle and crustal compositions. The samples plot to the left of the average Archean continental crust, and below, within, and/or to the left of the tonalitic gneiss. Coupled with the lack of correlation between Nb/Nb* and La/Sm, this further suggests that crustal contamination was not the main cause of the Nb anomalies.

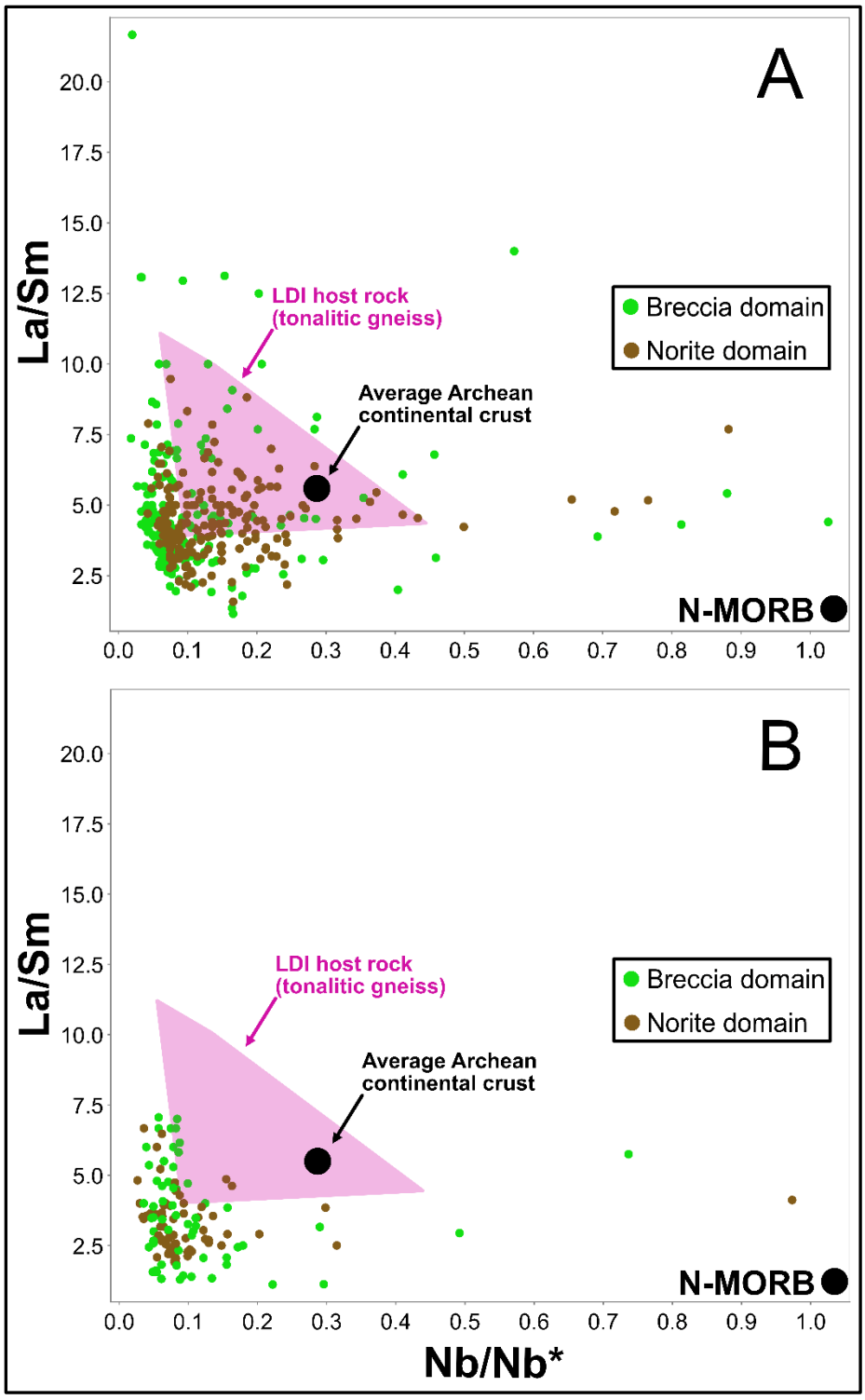

Figure 5.3 – Bivariate plot of La/Sm vs. Nb/Nb for A) Offset Zone samples and B) Creek Zone samples. N-MORB composition from Sun and McDonough (1989). Average Archean continental crust composition from Rudnick and Fountain (1995). Lac des Iles host rock composition from Brugmann et al. (1997) and Bain (2022).*

Enrichment in LILEs is a common characteristic of arc-derived magmas that is not observed in unmodified mantle-derived magmas (Sun and McDonough, 1989). Despite this, mantle-derived magmas can become enriched in LILEs via late-stage hydrous alteration or crustal contamination. The variable degree of alteration of the sample suite used in this study provides a good basis for testing whether LILE enrichment is due to late-stage/post-emplacement alteration. Visually estimated alteration intensity ranges from 3% to 100% replacement of magmatic silicate minerals (plagioclase, orthopyroxene, clinopyroxene) by alteration minerals (dominantly chlorite, white mica, tremolite-actinolite, talc). Loss on ignition and visually estimated alteration intensity are plotted on Figure 5.4. A positive correlation is observed, which suggests that loss on ignition is a good proxy for alteration intensity.

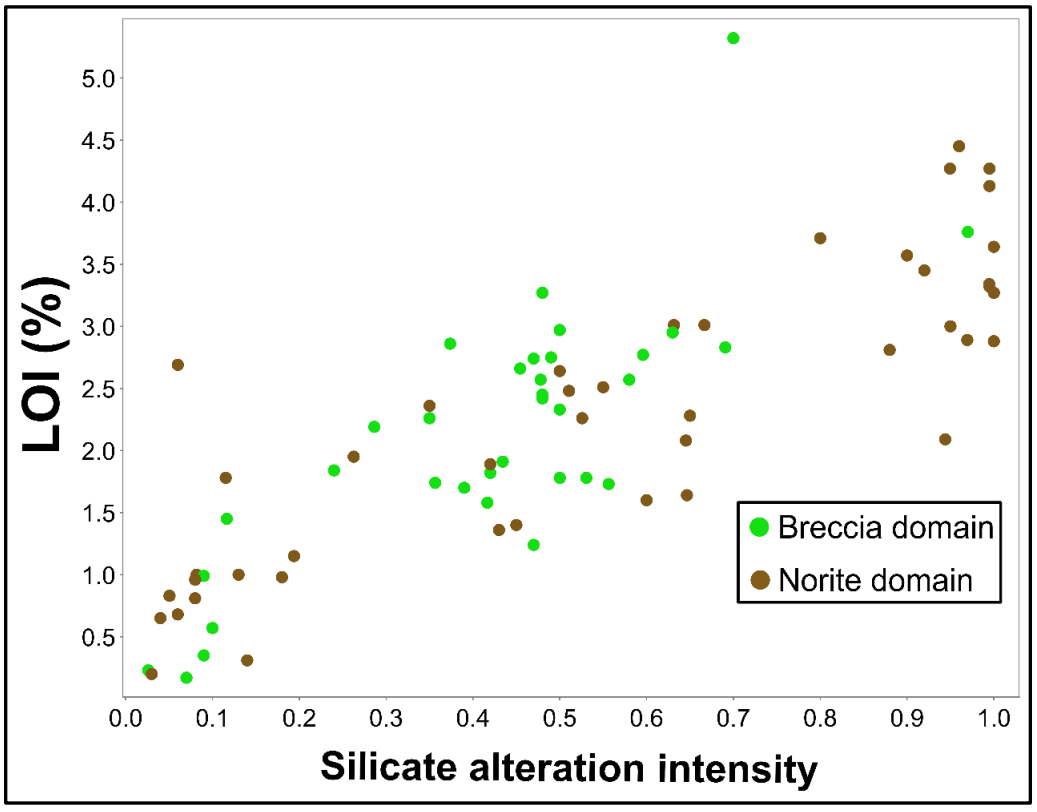

Figure 5.4 – Bivariate plot of loss on ignition (LOI) vs. visually estimated proportion of silicate mineralogy that has been replaced by alteration minerals.

Loss on ignition is plotted against LILEs (Cs, Rb, Ba) in Figure 5.5A-C. Although the correlation between loss and ignition (and therefore alteration intensity) and Rb and Cs suggests that these elements were enriched by alteration to some degree, only a weak correlation is observed between Ba and alteration intensity. Additionally, samples with very low loss on ignition have Ba and Cs contents that are significantly higher than the primitive mantle, suggesting that these elements were enriched prior to alteration.

The mechanism of LILE enrichment can be evaluated in part by looking at the Ba/Th ratio (Breeding et al., 2004). Ba/Th ratios are lower in mantle-derived magmas (<90; Sun and McDonough, 1989) and average Archean continental crust (113; Rudnick and Fountain, 1995) than arc-derived magmas, which are enriched due to the mobility of Ba in subduction-related fluids. The Ba/Th ratios of arc-derived magmas are highly variable, commonly up to ~400 and less commonly as high as 2000 or more (Turner et al., 1996; Hawkesworth et al., 1997; Turner et al., 2003; Pearce et al., 2005). Loss on ignition is plotted against Ba/Th ratio in Figure 5.5D. The Ba/Th ratios of the samples analyzed in this study are variable and are generally very high (median = 608.75, highest value = 6560), and are not correlated with alteration intensity. These values are significantly higher than typical Ba/Th ratios in arc basalts (Turner et al., 1996; Pearce et al., 2005) and subduction-related mafic/ultramafic intrusive rocks (Yuan et al., 2010; Zhao and Zhou, 2008); in all of these studies, the authors invoke Ba/Th ratios of <350 as being high enough to indicate arc-related fluid influence. The high Ba/Th ratios are unlikely to be due to the assimilation of the continental crust, as Ba/Th ratios in very weakly altered/unaltered samples are higher than average continental crust (113; Rudnick and Fountain, 1995) as well as tonalitic gneiss host rock (299).

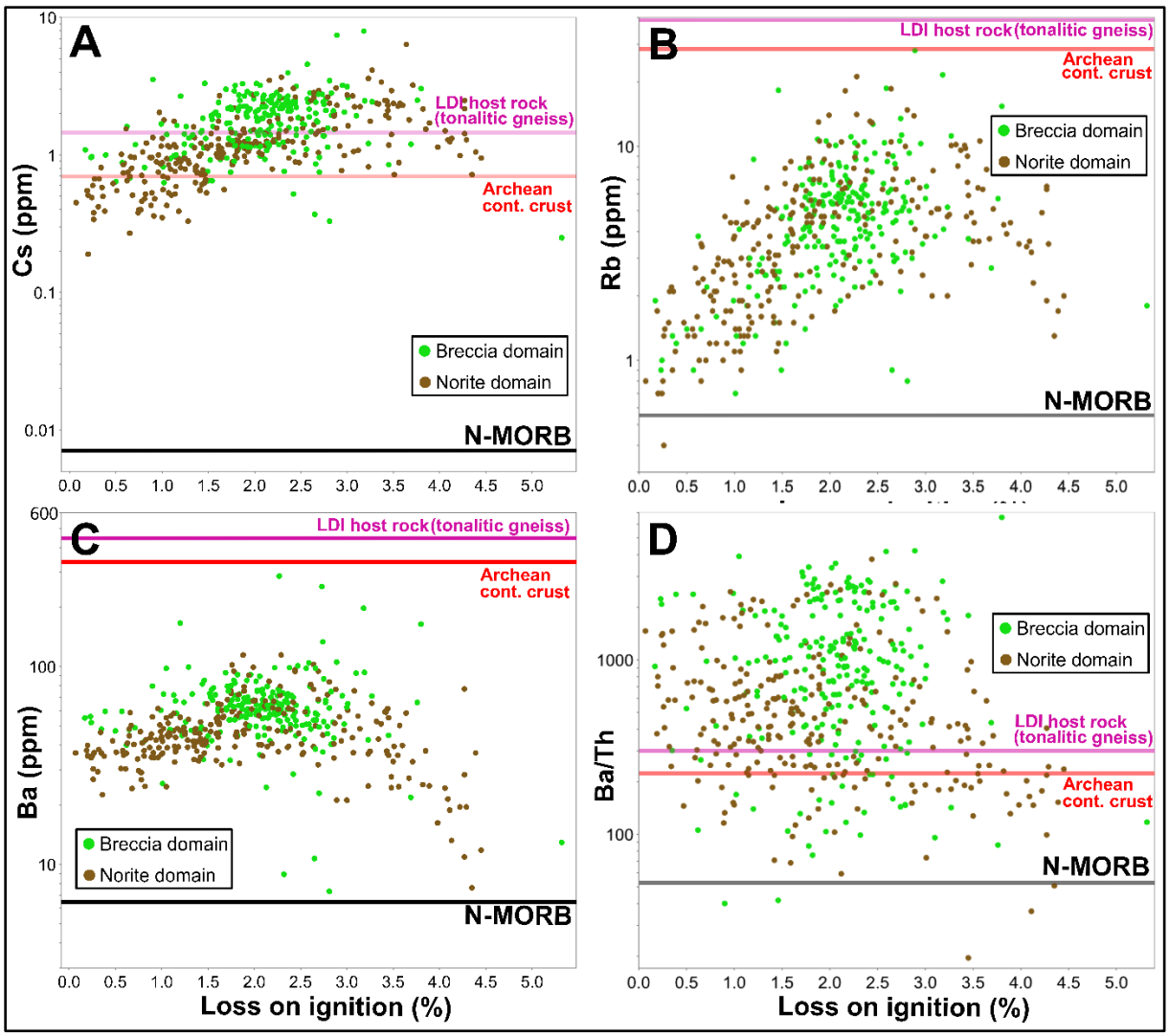

Figure 5.5 – Bivariate plots of loss on ignition (LOI) vs. Cs, Ba, Rb, and Ba/Th. Black lines represent depleted mantle (N-MORB) values (from Sun and McDonough, 1989). Red lines represent average Archean continental crust values (from Rudnick and Fountain, 1995). Pink lines represent average of tonalitic gneiss host rock samples (from Brugmann et al., 1997 and samples collected by Bain, 2022)

Ba/Th is plotted against Th in Figure 5.6. The high Ba/Th ratios (median = 609) and low Th content (median = 0.08 ppm) of the samples in this study are not consistent with an OIB- or MORB-like magma source, as average OIBs contain 4 ppm Th and a Ba/Th ratio of 87.5, and average N-MORBs (depleted mantle) contain 0.12 ppm Th and a Ba/Th ratio of 52.5 (Sun and McDonough, 1989). Thorium values of the samples in this study are similar to average depleted

mantle, which had to have been subsequently modified. This modification is unlikely to solely be via crustal assimilation, as average Archean continental crust is estimated to contain 3.0 ppm Th and Ba/Th of 113 (Rudnick and Fountain, 1995), and the average content of tonalitic gneiss host rock samples is 3.7 ppm Th and Ba/Th of 299. Despite the fact that there potentially has been some enrichment in Ba by late-stage hydrous fluids, the presence of very high Ba/Th ratios in the least altered rocks suggests that slab-derived fluid input was the most significant influence on the high Ba/Th within the breccia and norite domains of the South Lac des Iles Complex.

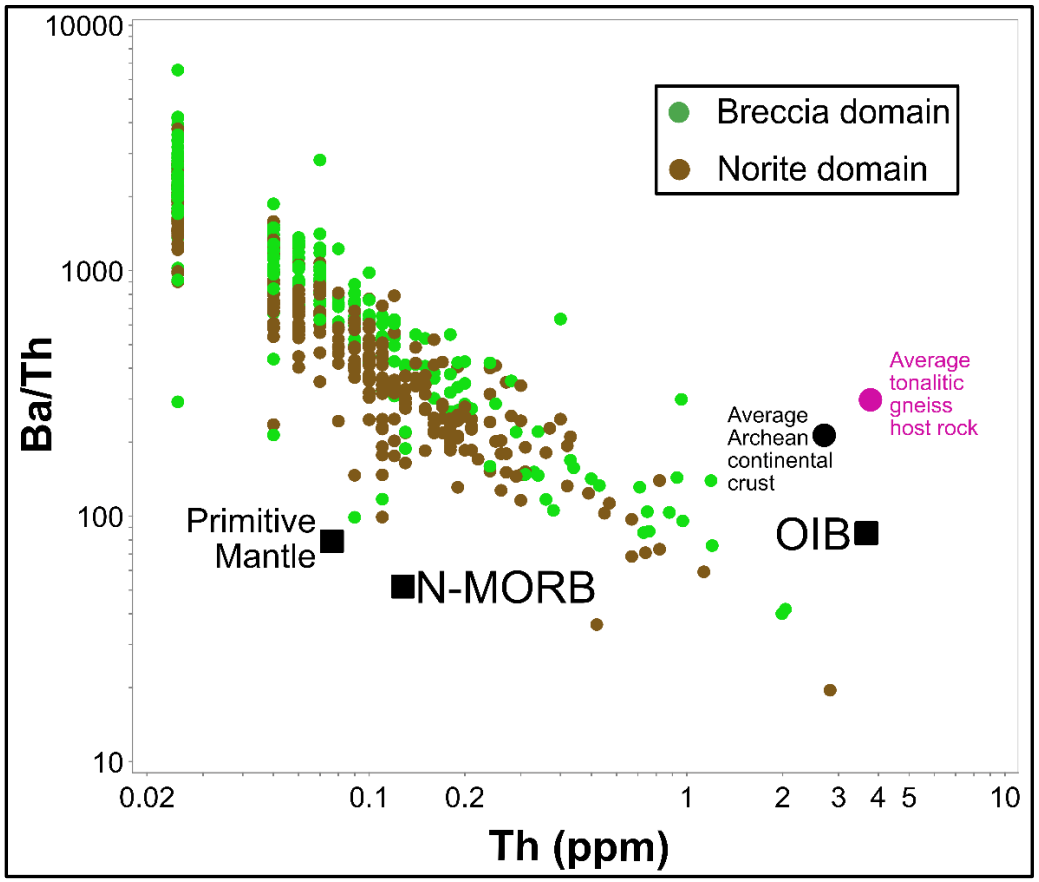

Figure 5.6 – Logarithmic bivariate plot of Ba/Th vs. Th content. Average MORB and OIB values from Sun and McDonough (1989). Average Archean continental crust composition from Rudnick and Fountain (1995).

5.1.3 – Source of the South Lac des Iles Complex magma – Neodymium isotopes

Neodymium isotopic ratios are commonly used to investigate processes that affected the composition of a magma. Because episodic partial melting over time has depleted Nd in the mantle relative to Sm (Dickin, 2005), and because ^{147}Sm decays to ^{143}Nd, the $^{143}Nd/^{144}Nd$ content of an intrusive rock can be used to extrapolate Sm/Nd content of a magma at the time of crystallization and to make inferences about the processes that modified its composition (DePaolo and Wasserburg, 1976; DePaolo, 1988). Epsilon Nd (ε_{Nd}) is an expression that is commonly used to quantify the variation in the Nd isotope content in a rock from the calculated expected Nd content of a mantle-derived magma of a given age (DePaolo, 1981). ε_{Nd} of the primitive mantle is 0; progressive Sm/Nd fractionation has resulted in an increasingly positive ε_{Nd} of the mantle and an increasingly negative ε_{Nd} of older continental crust over time (DePaolo, 1981). As a result, interaction of a mantle-derived magma with older continental crust will produce a more negative ε_{Nd} value than would be produced without crustal contamination.

The ε_{Nd} values of the 19 samples analyzed for this study range from +0.38 to -3.47. Eighteen of 19 samples have negative values, and the ε_{Nd} of 14 of 18 samples are between -1 and -3. Median values are similar between the breccia (-2.21) and norite (-2.13) domains, as well as between the Offset (-2.10) and Creek (-2.23) Zones. ε_{Nd} is somewhat less variable in the Creek Zone than the Offset Zone; the two most extreme values are both from the Offset Zone, whereas 8 of 10 Creek Zone samples fall between -1.89 and -2.93. Following the method outlined in DePaolo (1981), a depleted mantle source from 2689 Ma (age of the Lac des Iles Complex) would have a ε_{Nd} value of +2.24. An uncontaminated mantle source is incompatible

with the ε_{Nd} values of the samples analyzed in this study, as even the most positive values of the samples in this study are too low to be derived from a strictly mantle-sourced magma.

Primitive mantle-normalized plots of the samples taken for Nd isotope analysis are presented in Figure 5.7. Trace element patterns of the samples are generally similar to the sample set as a whole. To assess the connection between trace element patterns and crustal contamination, Offset Zone samples were selected to include a range of Nb depletion, including two samples with minimal Nb anomalies that also do not contain positive Eu anomalies. The sample with the least pronounced Nb anomaly (Nb/Nb* = 0.72) has the lowest ε_{Nd} of all analyzed samples (-3.47), whereas the other sample lacking a strong negative anomaly (Nb/Nb* = 0.66) has an ε_{Nd} value of -1.09. If the pre-contamination magma was not depleted and Nb anomalies were due to crustal contamination, it would be expected that the strength of the anomaly would correlate with more negative ε_{Nd} values. The absence of this relationship further suggests that Nb anomalies were derived from subduction-related processes rather than crustal contamination.

Because the Lac des Iles Complex is hosted in tonalitic gneiss of the granitoid-dominated Marmion terrane, it would be reasonable to assume that a felsic plutonic lithology is the most likely crustal contaminant. ε_{Nd} is plotted against La/Sm, Nb/Nb*, Ba/Th, and SiO_2 in Figure 5.8. Felsic plutonic rocks generally have high La/Sm and low Nb/Nb*, so if crustal contamination was the main factor that caused the enrichment in LREEs and LILEs, ε_{Nd} would be expected to correlate with La/Sm and Nb/Nb*. Correlation with Ba/Th would also be expected if crustal contamination was the main cause of the high Ba/Th ratios. No relationship between ε_{Nd} and these variables is observed in Figure 5.8, suggesting that the magma already had enriched LREE

and LILE content and negative Nb anomalies when crustal material was assimilated, and that crustal material did not significantly alter the La/Sm, Nb/Nb*, or Ba/Th ratios.

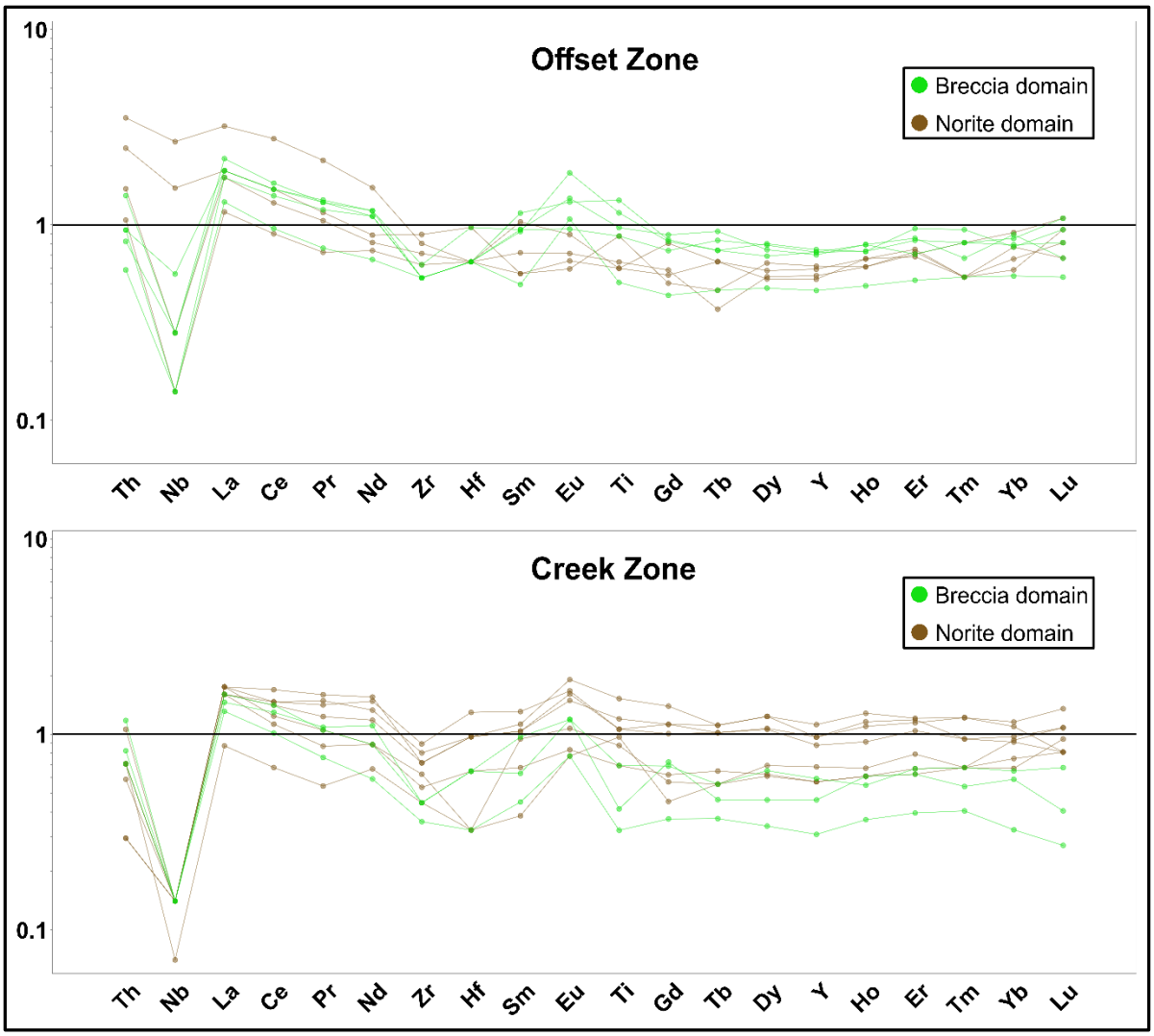

Figure 5.7 – Primitive mantle-normalized plots of samples taken for Nd isotope analysis from the A) Offset Zone and B) Creek Zone. Normalizing values from Sun and McDonough (1989).

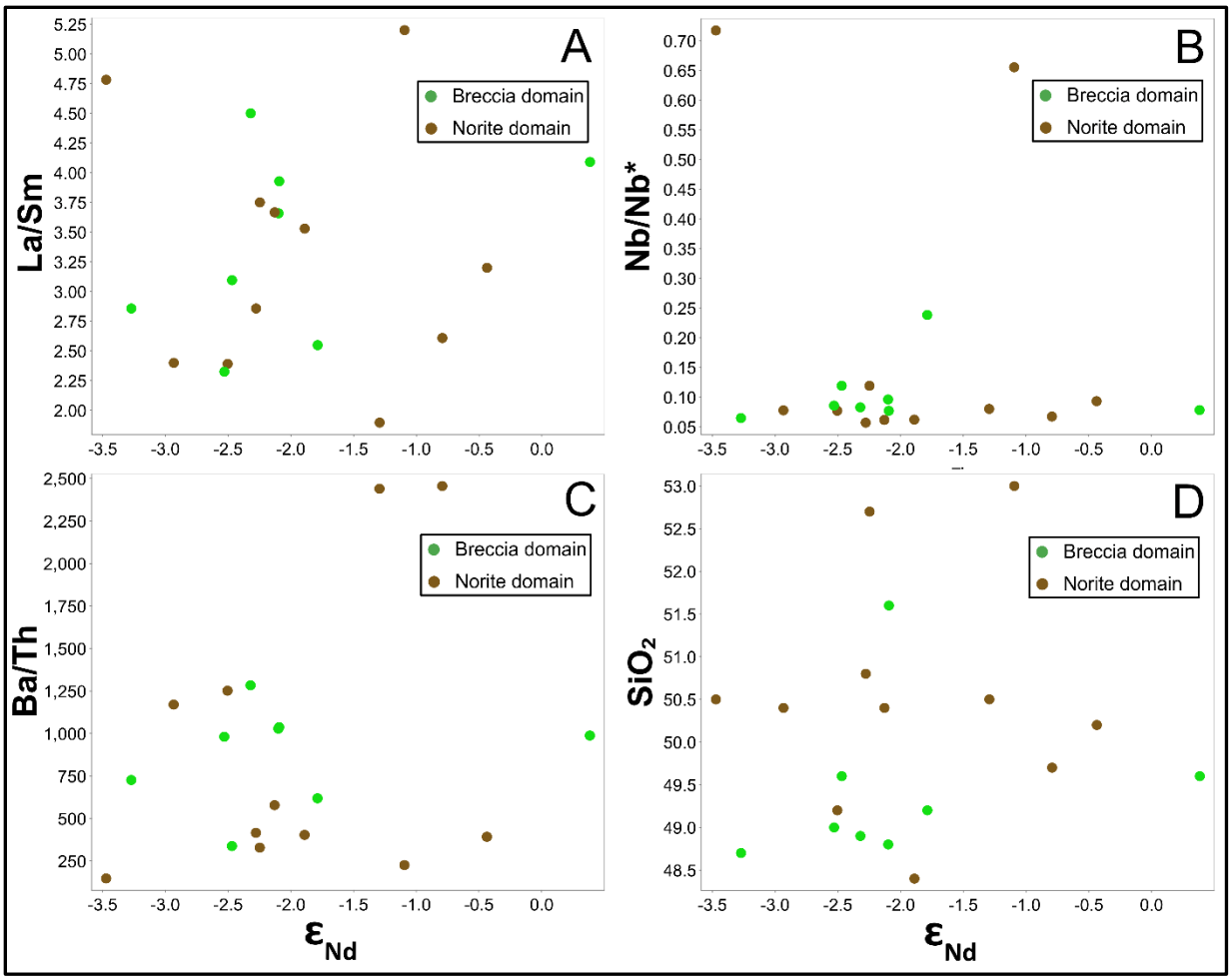

Figure 5.8 – Bivariate plots of ε_{Nd} vs. A) La/Sm, B) Nb/Nb, C) Ba/Th, D) SiO_2.*

Downhole plots of ε_{Nd} for the three sampled drill holes are presented in Figure 5.9. No clear systematic variations in ε_{Nd} are apparent between lithological domains or with proximity to the domain boundary contact. The ε_{Nd} content of the Offset Zone drill hole (DH# 17-804) is slightly more variable than the two Creek Zone drill holes. Association between ε_{Nd} and Pd content is not observed between Pd-mineralized and Pd-unmineralized holes (DH# 17-804 and 19-025 intersect Pd-enriched zones, DH# 19-009 does not), nor on the scale of individual samples.

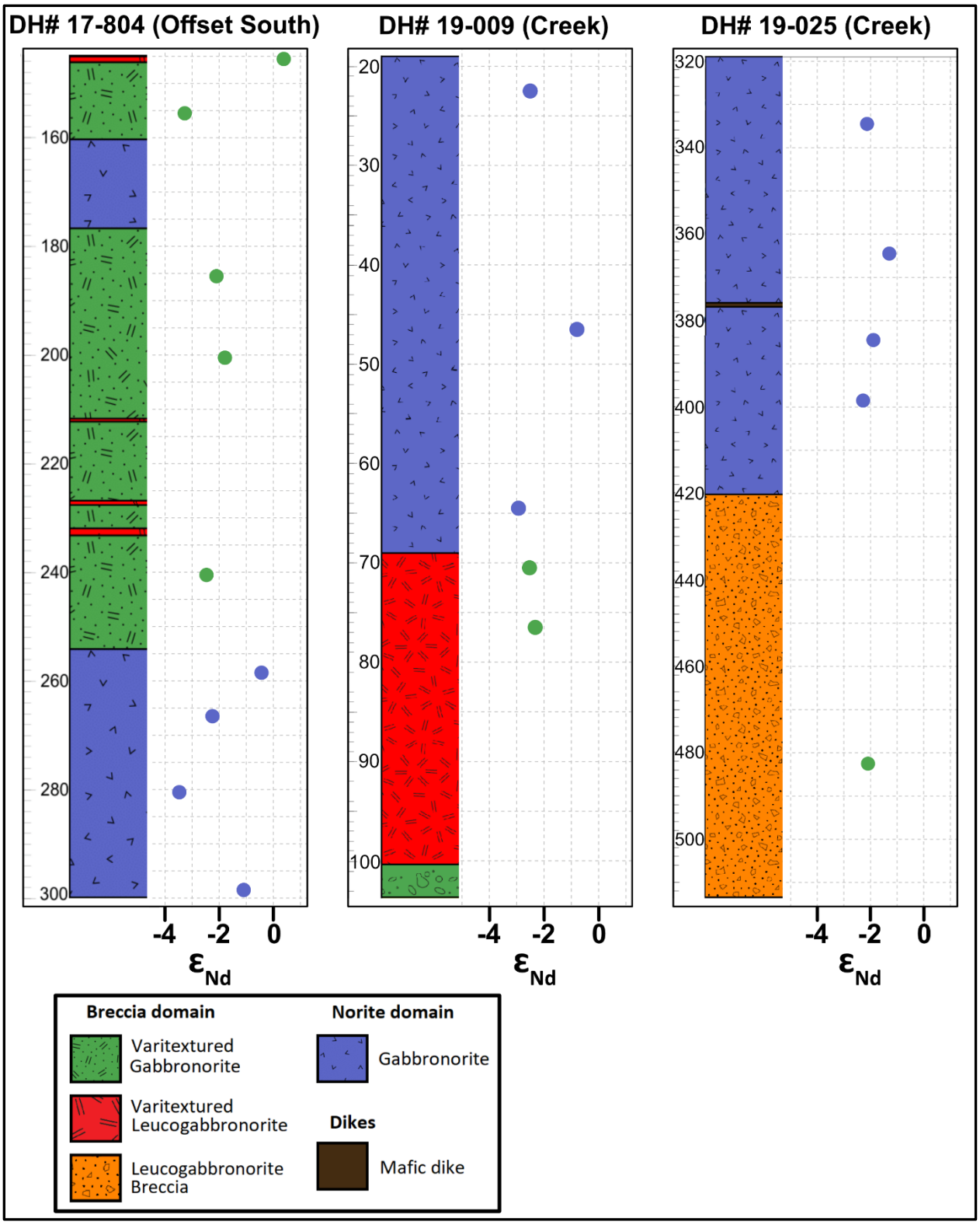

Figure 5.9 – Downhole plots of ε_{Nd}. Green dots = breccia domain, blue dots = norite domain.

5.1.4 – Source of the South Lac des Iles Complex magma – Comparisons

One prior study has evaluated Nd isotope characteristics of the Lac des Iles Complex (Brugmann et al., 1997). This previous study included seven samples from the South Lac des Iles Complex, all of which were taken from the Roby Zone and surface outcrops from the western South Lac des Iles Complex. Brugmann et al. (1997) used an emplacement age of 2738 Ma to calculate ε_{Nd}, which is significantly older than the currently accepted age of 2689 Ma. Due to this discrepancy, ε_{Nd} of samples taken by Brugmann et al. (1997) were recalculated using an age of 2689 Ma. The recalculated ε_{Nd} values range from -0.52 to +2.14, which is broadly similar to the range calculated in the original study (0.0 to +1.9). The authors interpreted this range of values as being indicative of a relatively low degree of crustal contamination, and that the scatter in the results was due to the combined effects of assimilation and crystal fractionation. No major petrological differences exist between the Roby and Offset Zones, which are interpreted to be structurally offset portions of an originally continuous mineralized zone.

Brugmann et al. (1997) reported whole rock geochemical and neodymium isotope results of one sample of the tonalitic gneiss hosting the Lac des Iles Complex. Using the currently accepted age of the Lac des Iles Complex, ε_{Nd} of the tonalitic gneiss sample from Brugmann et al. (1997) was recalculated to be -1.77. As this sample has a lower ε_{Nd} than all samples from the Lac des Iles Complex analyzed by Brugmann et al. (1997), they invoked the tonalitic gneiss as a potential source of crustal contamination. Because this value is less negative than the median value of all samples from the Lac des Iles Complex analyzed in this study, it is likely that the principal crustal contaminant that imparted the negative ε_{Nd} values was not the tonalitic gneiss. However, it is difficult to make definite conclusions based on the

ε_{Nd} of only one country rock sample, as it is possible that the tonalitic gneiss has heterogeneous and potentially more negative ε_{Nd} values that were not observed by Brugmann et al. (1997).

Brugmann et al. (1997) invoked a low degree of crustal contamination of the Lac des Iles magma by the tonalitic gneiss, based on the slightly more negative ε_{Nd} values of the tonalitic gneiss compared to their samples from the South Lac des Iles Complex. It is possible, though, that crustal contamination occurred at depth instead of or in addition to contamination by adjacent country rocks. Based on the consistently negative ε_{Nd} values observed in this study, crustal contamination had to have occurred, and the contaminant must have had a ε_{Nd} value more negative than the lowest value (-3.47) observed in this study. The contaminant must have either had 1) a strongly negative ε_{Nd} value, but only a minor amount was assimilated so as not to have materially changed the trace element content of the magma, or 2) a strongly to potentially more moderately negative ε_{Nd} and a similar trace element profile to the Lac des Iles magma, potentially with a higher degree of assimilation.

Either situation must account for the high Ba/Th and low Th, Nb/Ta and Nb/Yb values seen in the samples in this study, all of which are not commonly seen in crustal rocks, including the tonalitic gneiss host rocks (Rudnick and Fountain, 1995; Brugmann et al., 1997). A contaminant with a strongly negative ε_{Nd} value would necessitate a crustal source that is significantly older than the Lac des Iles Complex. Tomlinson et al. (2004) reported a zircon inheritance age of 2.95 Ga from the Heaven Lake greenstone belt, located in the Marmion terrane approximately 20 km from the Lac des Iles Complex. Model ages in other parts of the terrane as old as 3.05 Ga have also been reported (Tomlinson et al., 2004), which is 360 million years older than the age of the Lac des Iles Complex. ε_{Nd} values as low as -6.86 were also

obtained in the Marmion terrane, in granodiorites of the Obonga Lake greenstone belt (Tomlinson et al., 2004). Though these rocks are distant from the Lac des Iles Complex and thus not a potential direct contaminant, these results indicate that significantly negative ε_{Nd} values are present in some Marmion terrane rocks, and thus could occur at depth and be a potential contaminant for the Lac des Iles magma.

Assimilation of a contaminant with more moderately negative ε_{Nd} values, at a higher degree of assimilation, would require the contaminant to have a trace element profile similar to that of the Lac des Iles magma. The most likely candidate for this would be other arc-derived rocks, which were sufficiently older than the Lac des Iles Complex to have ε_{Nd} values more negative than mantle-derived rocks. Arc-derived rocks are the most likely contaminant because they could have similar trace element contents (high Ba/Th and Th/Yb, low Th and Nb/Yb) to the South Lac des Iles Complex. The tonalitic gneiss country rock is an unlikely candidate for derivation of the negative ε_{Nd} values, due to the less negative ε_{Nd}, lower Ba/Th, higher Nb/Yb, and higher Nb/Nb* in the tonalitic gneiss samples than in the majority of South Lac des Iles Complex samples. However, this assessment is based on an ε_{Nd} value of only one sample of tonalitic gneiss and whole rock geochemistry of only five samples. If the ε_{Nd} values of the tonalitic gneiss are actually heterogenous and more negative in some areas than the sample assessed in this study, it is possible that a moderate degree of assimilation of the tonalitic gneiss could produce the ε_{Nd} values of the Lac des Iles Complex samples without significantly affecting the trace element content that appears to rule out a high degree of country rock assimilation.

5.2 – Source of sulfur and genesis of ore zones

Assessing the source of sulfur is an important consideration in evaluating the history of the South Lac des Iles Complex magma and the genesis of the Pd-rich mineralization present within the intrusive complex. Evidence for crustal sulfur addition is present in a majority of magmatic Ni-Cu-PGE deposits, and has been suggested by some authors to be a necessary component in their formation (Naldrett, 1999; Keays and Lightfoot, 2010). Other authors have argued that formation of magmatic sulfide ores containing only mantle-derived sulfur is possible (Maier, 2005; Seat et al., 2009; Ripley and Li, 2013). Ni-Cu-PGE ore formation without external sulfur addition appears to require interaction of an immiscible sulfide liquid with large quantities of magma, and is considered relatively uncommon due to the generally small amounts of sulfide liquid produced and the fact that sulfide saturation would usually occur late in the magma evolution, after which large degrees of sulfide liquid-silicate magma interaction are less likely (Ripley and Li, 2013). Despite these constraints, evidence for the formation of magmatic sulfide deposits without external sulfur addition appears to be present in several systems, including PGE-rich, sulfide-poor systems such as the Panton intrusion (Beinlich et al., 2020) and the Sonju Lake intrusion (Park et al., 2004), as well as moderately sized systems in which Ni and Cu are the main economic metals of interest such as the Nebo-Babel deposit (Seat et al., 2009) and several mineralized intrusions in the Central Asian orogenic belt (Wei et al., 2019). Ripley and Li (2013) argue that it is possible to produce deposits containing <30 Mt of sulfide (e.g. Lac des Iles) via triggering of sulfide saturation by processes other than the addition of crustal sulfur. These processes include the introduction of volatiles to the magma, fractional

crystallization, assimilation of siliceous crustal rocks with negligible sulfide content, and mixing of magmas.

Sulfur isotopic analysis is commonly used as a method of constraining the source of sulfur in magmatic Ni-Cu-PGE deposits. The relative proportions of the four stable isotopes of sulfur (^{32}S, ^{33}S, ^{34}S, and ^{36}S) in the mantle and in uncontaminated mantle-derived magmas are well characterized and can be explained via mass-dependent fractionation. Surficial processes, however, can fractionate sulfur isotopes in a manner that is independent of their mass and therefore distinguishable from mantle-derived rocks. The degree of mass-independent fractionation is small and is commonly expressed in "delta notation" ($\delta^{XX}S$) , which measures the degree of deviation of the ^{XX}S:^{32}S ratio from that expected during mass-dependent fractionation (Seal, 2006). The "capital delta" notation ($\Delta^{XX}S$) is used to express the deviation of two $\delta^{XX}S$ values, and is most commonly used to express the difference of $\delta^{33}S$ or $\delta^{36}S$ values from $\delta^{34}S$ (Seal, 2006). $\delta^{XX}S$ and $\Delta^{XX}S$ are expressed in permil (‰), typically in relation to the Vienna Canyon Diablo Troilite ("VCDT") standard, which is interpreted to be representative of the sulfur isotope content of the primitive mantle (Ault and Jensen, 1962; Seal, 2006).

With few limited exceptions, the $\delta^{34}S$ content of mantle-derived rocks is considered to be 0 ± 2‰ VCDT (Seal, 2006). Magmatic sulfide systems with sulfur isotope values that deviate significantly from this value are considered to have assimilated crustal sulfur, as mass-independent sulfur isotope fractionation processes only operate on Earth's surface (Seal, 2006; Ripley and Li, 2013). However, $\delta^{34}S$ values of sulfide within the mantle range do not necessarily preclude crustal sulfur addition, for two reasons. The first reason is that large degrees of sulfide liquid-silicate magma interaction, commonly expressed as "R factor", can reset $\delta^{34}S$ values via

sulfur isotope exchange (Ripley and Li, 2003; Brzozowski et al., 2021). By this process, $\delta^{34}S$ values that may have been mass-independent after crustal assimilation can be modified via isotopic equilibration with S-bearing magma to mass-dependent values by the time sulfide crystallization occurs. The second reason is that crustal rocks may have mass-dependent $\delta^{34}S$ values that are not distinguishable from mantle-derived rocks (Seal, 2006). This is especially relevant for rocks from the early to middle Archean, which formed prior to the existence of biological processes responsible for the majority of sulfur isotope fractionation processes and sometimes therefore have mass-dependent $\delta^{34}S$ values (Grassineau et al., 2005). By the Neoarchean, surficial biological processes were operating at a significant enough degree to consistently generate mass-independent $\delta^{34}S$ values in crustal rocks (Grassineau et al., 2005).

In rocks older than 2.45 Ga, mass-independent fractionation signatures of $\Delta^{33}S$ (>0 ± 0.2‰ VCDT) and $\Delta^{36}S$ (>0 ± 0.4‰ VCDT) are observed, interpreted to be the result of photochemical reactions occurring in the oxygen-poor Archean atmosphere (Farquhar and Wing, 2003). Therefore, mass-independent $\Delta^{33}S$ and $\Delta^{36}S$ values in rocks older than 2.45 Ga can provide evidence for crustal sulfur assimilation in systems in which mass-dependent $\delta^{34}S$ values are observed. Initially mass-independent $\Delta^{33}S$ and $\Delta^{36}S$ values may be diluted, however, by the same sulfur isotope exchange processes at high R factors that can obscure initially mass-independent $\delta^{34}S$ values. In general, analysis of multiple sulfur isotopes provides a stronger basis for the evaluation of crustal sulfur addition via assimilation of Archean rocks than evaluation of $\delta^{34}S$ alone (Farquhar and Wing, 2003; Shahabi Far et al., 2018).

Sulfur/Se ratios are another tool that are commonly used to help constrain the processes by which magmatic Ni-Cu-PGE deposits are formed, due to the variability of S/Se in

crustal rocks, the mobility of sulfur relative to selenium, and the tendency of Se to partition into sulfide liquid. Estimates of average mantle S/Se values range from 3100 (Lorand et al., 2003) to 3300 (McDonough and Sun, 1995; Hattori et al., 2002), with a range of 2850-4350 expected in unmodified mantle-derived rocks (Eckstrand and Hulbert, 1987). Sulfur/Se ratios above this range are most commonly attributed to assimilation of S-rich crustal rocks and/or low R factors whereas values below mantle range may be generated via sulfur loss via hydrothermal fluids, assimilation of S-poor crustal rocks, or by Se upgrading at high R factors (Queffurus and Barnes, 2015). Low S/Se ratios in some settings have also been explained via low degrees of partial melting and/or a mantle source that has been previously depleted by episodic partial melting (Hattori et al., 2002; Hinchey and Hattori, 2005). Other factors that are less commonly invoked to explain non-mantle S/Se values (Queffurus and Barnes, 2015) are either not applicable to the South Lac des Iles Complex (high-grade metamorphism, serpentinization, supergene weathering, difference in Se compatibility between monosulfide and intermediate solid solutions) or are outside the scope of this study (refertilization of mantle lithosphere, Se retention during partial melting).

Copper/Pd ratios are also commonly used to estimate the R factor of Ni-Cu-PGE-mineralized systems, with lower Cu/Pd corresponding to higher R factors. This is due to the extremely chalcophile character of Pd and its ability to partition into sulfide liquid much more effectively than moderately chalcophile Cu, whose content in sulfide is more limited by the amount of sulfur present (Maier et al., 1998). Cu/Pd ratios may also be modified by early segregation of sulfides (Barnes et al., 1993), assimilation of Cu-bearing rocks, or by hydrothermal alteration (Polovina et al., 2004).

5.2.1 – Source of sulfur and genesis of ore zones – Previous work

Two previous studies have assessed the sulfur isotope composition of the South Lac des Iles Complex. Hinchey and Hattori (2005) reported $\delta^{34}S$ values from 16 mineral separates from the Roby and Twilight Zones, with results ranging from 0.00-1.52‰ VCDT. The similarity of these results to the expected mantle range of 0 ± 2‰, as well as petrographic and geochemical evidence, led Hinchey and Hattori (2005) to conclude that mineralization was of primary magmatic origin and that negligible contribution of country rock sulfur occurred. Additionally, the authors interpreted that $\delta^{34}S$ values of pyrite comparable to or lower than co-existing chalcopyrite was indicative of the two minerals forming at different phases, in isotopic disequilibrium.

Duran et al. (2016) characterized the sulfur isotope composition of sulfide-rich pods in the Roby, Offset, and Baker Zones. All samples examined by Duran et al. (2016) had $\delta^{34}S$ values within the mantle range of 0 ± 2‰ VCDT. Two pyrite-rich samples from the Baker Zone had $\delta^{34}S$ values between +1 and +1.5‰ VCDT, and S/Se ratios well above mantle range. All other samples examined by Duran et al. (2016) had $\delta^{34}S$ values between -1 and +1‰ VCDT, most of which had S/Se ratios within mantle range. Based on these results, as well as whole rock geochemical and textural evidence, Duran et al. (2016) concluded that sulfide-rich pods were formed via magmatic processes and that sulfur addition via hydrothermal fluids may have contributed to the higher $\delta^{34}S$ and S/Se values of the pyrite-rich samples from the Baker Zone.

Several previous studies have evaluated the geochemical characteristics of the Roby and/or Offset Zone mineralization and provided contrasting models for its origin. Hinchey and

Hattori (2005) and Djon et al. (2018) argued that the low S/Se values in the Roby/Offset Zones are representative of a strongly depleted mantle source from which sulfur had been previously depleted relative to Se. Duran et al. (2015) reported S/Se values of sulfide-rich pods from the Roby, Offset, and Baker Zones that were similar to typical mantle values, suggested that these values reflected the parent magma, and suggested that low S/Se values in the more typical disseminated sulfide mineralization could be the result of late-stage sulfur loss. Duran et al. (2016) interpreted high Pd/Se and Ir/Se ratios of disseminated sulfide mineralization from the Roby and Twilight Zones as being representative of high R factors. Hinchey et al. (2005) suggested that low Cu/Pd ratios in the chlorite-actinolite schist of the Roby Zone were generated via fractional crystallization of the early gabbronorite domain that segregated the low Cu/Pd sulfides at depth before it elevated and was emplaced. In this model, the magma that formed the breccia and norite domains later passed through the same magma conduit and incorporated the residual low Cu/Pd sulfide liquid. Djon et al. (2018) observed variable Cu/Pd ratios within the North Lac des Iles Complex, including low values in the Sutcliffe Zone similar to those seen in the Offset and Creek Zones of the South Lac des Iles Complex. Djon et al. (2018) invoked high R factors as the cause of the low Cu/Pd ratios in the Sutcliffe Zone.

Sulfur isotope analyses in the Offset Zone have only been performed on the sulfide-rich pods, and no sulfur isotope analyses have been reported for the disseminated sulfide zones that host the majority of the mineralization in the Offset Zone. Additionally, no sulfur isotope analyses have been reported for samples from the Creek Zone, or of the tonalitic gneiss that hosts the Lac des Iles Complex.

5.2.2 – Source of sulfur and genesis of ore zones – Sulfur isotopes, S/Se, and Cu/Pd

The potential for mass-independent fractionation of ^{33}S and ^{36}S should be considered before evaluating sulfur sources based on $\delta^{34}S$ alone. $\delta^{33}S$ is plotted against $\delta^{34}S$ in Figure 5.10. The slope of the line of best fit (0.5156) is nearly identical to the slope of 0.515 expected in the case of mass-dependent fractionation (Seal, 2006). $\Delta^{33}S$ values range from -0.02 to -0.11, which is entirely within the typical range of mass-dependent fractionation (0 ± 0.2‰ VCDT; Farquhar and Wing, 2003). These values allow for the possibility of entirely mantle-derived sulfur, but do not preclude the possibility of crustal sulfur assimilation. If there was a significant crustal source of sulfur, it would be expected to have a mass-independent $\Delta^{33}S$ signature due to the age of the Lac des Iles Complex, but that signature could have been masked by high R factors. Based on these results, ^{33}S and ^{36}S values do not provide significant value in determining the magma history, and sulfur source can therefore be evaluated using $\delta^{34}S$ alone.

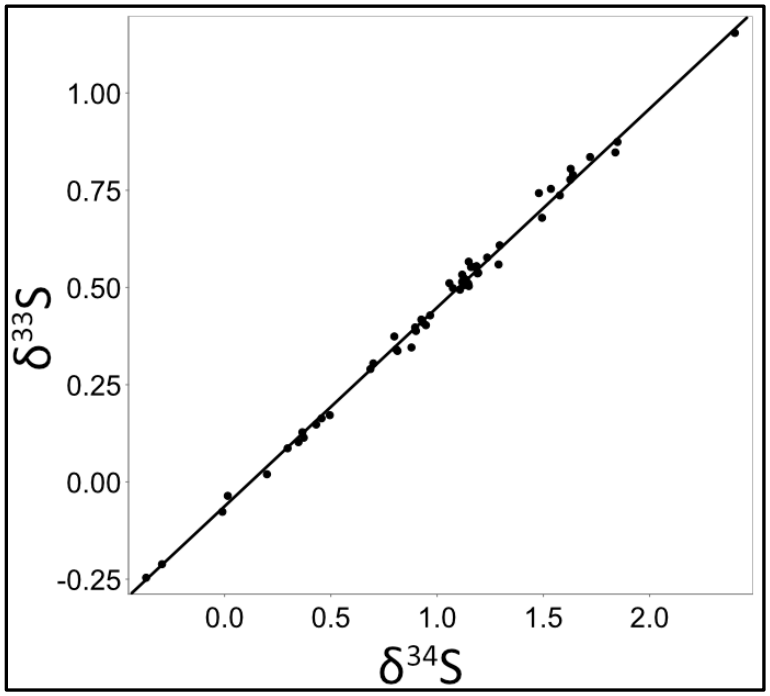

Figure 5.10 – Bivariate diagram of $\delta^{34}S$ and $\delta^{34}S$ of all analyzed samples. Slope of line = 0.5156.

Pyrite crystals from tonalitic gneiss country rock were analyzed for sulfur isotope content, yielding $\delta^{34}S$ values of +2.40‰ and +1.80‰, and $\Delta^{33}S$ values of -0.08‰ and -0.10‰. The similarity of these values to the mantle range presents challenges in solely using sulfur isotope analysis to constrain the presence of sulfur derived from the tonalitic gneiss, as even significant assimilation of crustal sulfur from the country rocks would not produce sulfur isotope values in the South Lac des Iles complex that are significantly different from mantle values. The majority of sulfur isotope analyses in this study yielded $\delta^{34}S$ values that fall between the tonalitic gneiss and the average mantle content (0‰). Therefore, based on sulfur isotope analysis alone, the influence of sulfur derived from the tonalitic gneiss can neither be proven nor ruled out.

The similarity of sulfur isotope values between the breccia and norite domains and between the Offset and Creek zones (Fig. 4.49) suggests that processes that affected sulfur isotope composition were generally similar in all domains and zones analyzed in this study. Variation of $\delta^{34}S$ values of primary sulfide minerals observed in this study are in general agreement with sulfur fractionation factors commonly observed in sulfides crystallizing at equilibrium from a magma, in which $\delta^{34}S$ values of pyrrhotite, chalcopyrite, and pentlandite are expected to decrease in sequential order (Li and Liu, 2006; LaFlamme et al., 2016). Differences between median values of pyrrhotite (+1.16‰) and pentlandite (+0.20‰) are similar to the relationship expressed by LaFlamme et al. (2016; $\delta^{34}S_{pyrrhotite\text{-}pentlandite}$ = 0.7-1.0 ± 0.5‰), whereas median $\delta^{34}S$ values of chalcopyrite (0.90‰) fall between pyrrhotite and pentlandite, as expected. The similarity of values between minerals that crystallize from monosulfide solid solution (pyrrhotite and pentlandite) and those that crystallize from intermediate solid solution

(chalcopyrite) suggests that sulfur isotope fractionation between monosulfide and intermediate solid solutions, which is observed in some magmatic sulfide systems, did not occur in the Offset and Creek Zones of the South Lac des Iles Complex.

When comparing individual samples rather than median values, ranges of $\delta^{34}S$ values are somewhat more variable in some samples than others (Fig. 4.49), suggesting that there may have been some local modification of $\delta^{34}S$ values, which can occur via hydrothermal alteration. However, the lack of a systematic difference suggests that there has not been systematic change in $\delta^{34}S$ values by hydrothermal fluids. Pyrite is present as a secondary mineral, replacing pyrrhotite and possibly pentlandite to a lesser degree, and is commonly observed in contact with chalcopyrite±pentlandite. The similarity of median $\delta^{34}S$ values in pyrite (+1.22‰) to those in pyrrhotite (+1.16‰) further suggests that hydrothermal activity has not systematically changed the sulfur isotope content of samples in this study.

Bulk-rock S/Se and Cu/Pd ratios are plotted against $\delta^{34}S$ in Figures 5.11 and 5.12. Aside from one sample from 68 m depth in DH# 19-009 in which one chalcopyrite and one pyrite crystal were analyzed, all samples analyzed for sulfur isotope content yield S/Se ratios that are lower than the mantle range of 2850-4350 (Eckstrand and Hulbert, 1987). Cu/Pd ratios of most samples are below the mantle range of 1000-10000 (Barnes et al., 1993), with 5 of 18 samples plotting within the mantle range. No correlation is present between $\delta^{34}S$ and S/Se or Cu/Pd ratios. If the more positive $\delta^{34}S$ values were the result of heterogenous incorporation of crustal sulfur by the Lac des Iles magma, a positive correlation between S/Se and $\delta^{34}S$ would be expected. The generally below-mantle S/Se and Cu/Pd values suggest that systematic sulfur loss and/or Se upgrading occurred, as well as Cu loss and/or Pd upgrading.

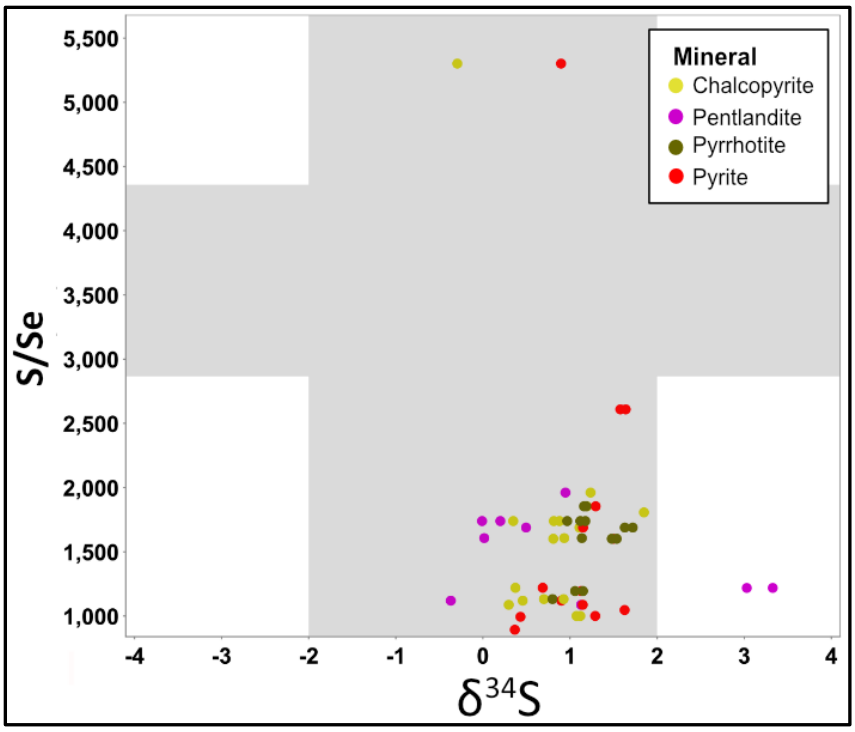

Figure 5.11 – Bivariate plot of $\delta^{34}S$ and S/Se ratios. Grey boxes represent mantle values of $\delta^{34}S$ (from Seal, 2006) and S/Se (from Eckstrand and Hulbert, 1987).

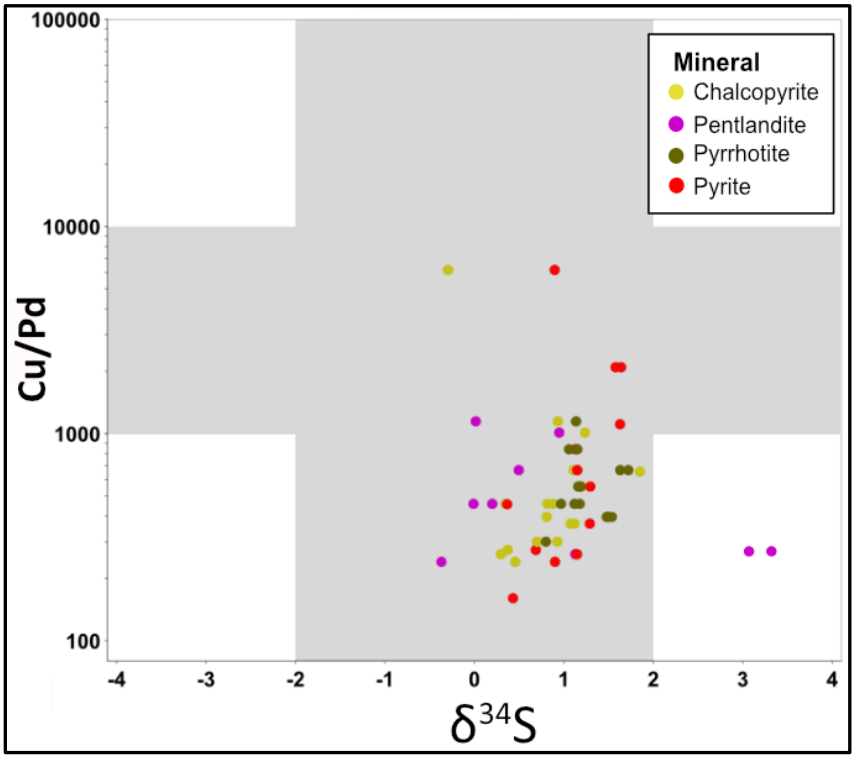

Figure 5.12 – Bivariate plot of $\delta^{34}S$ and Cu/Pd ratios. Grey boxes represent mantle values for $\delta^{34}S$ (from Seal, 2006) and Cu/Pd (from Barnes et al., 1993).

S/Se ratios for all samples in this study are plotted against Pd and Cu/Pd in Figures 5.13 and 5.14, and downhole plots of S/Se and Cu/Pd ratios are included in Figures 5.15 and 5.16. In all drill holes, the majority of samples have S/Se ratios below the mantle range, with a minority of samples plotting within and/or above the mantle range. The majority of samples in the two Offset Zone drill holes have Cu/Pd ratios below mantle range, whereas the Creek Zone drill holes have a greater proportion of samples within mantle range, or slightly above in the case of DH# 19-009.

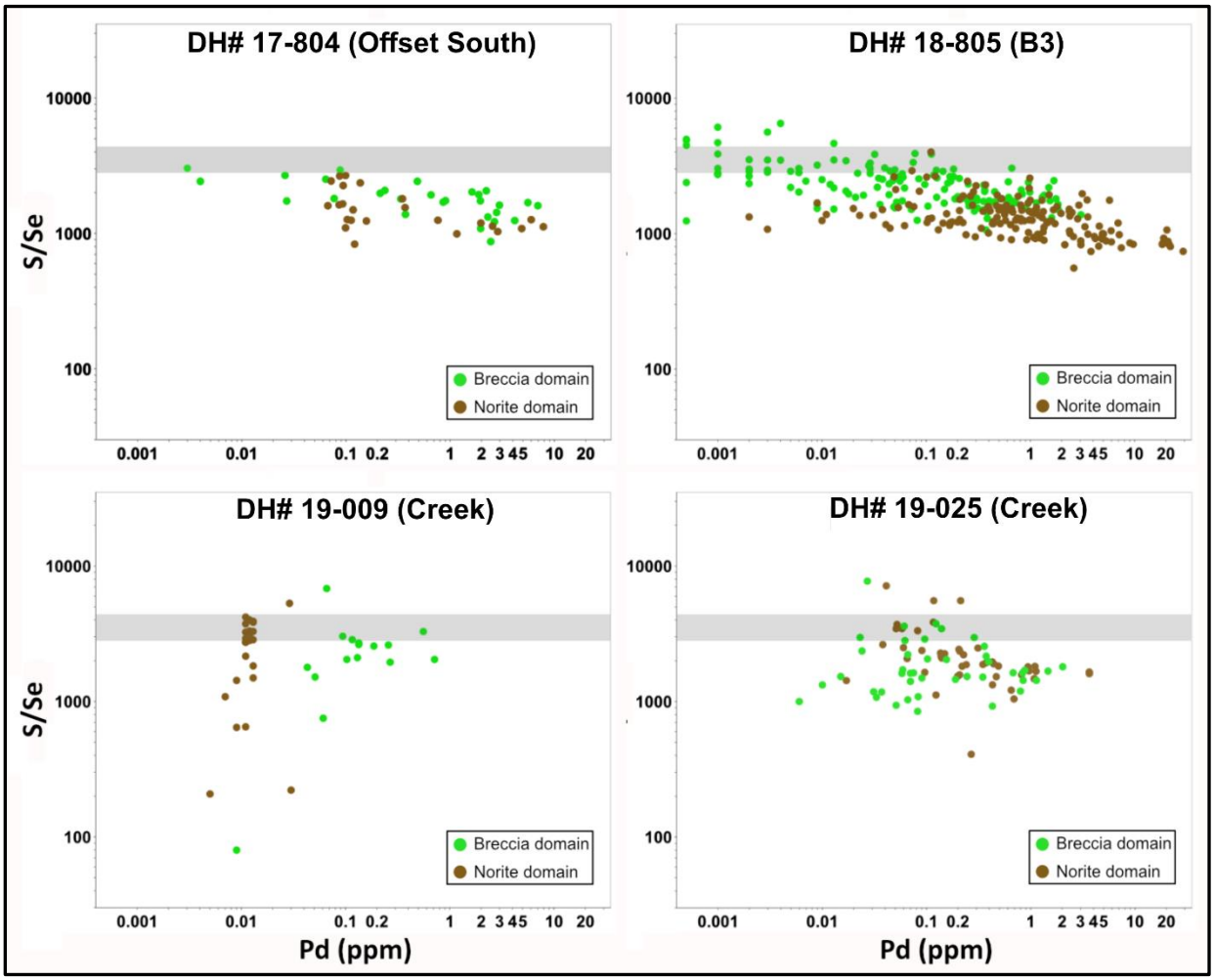

Figure 5.13 – Bivariate plots of S/Se and Pd. Grey boxes represent mantle values of S/Se (from Eckstrand and Hulbert, 1987).

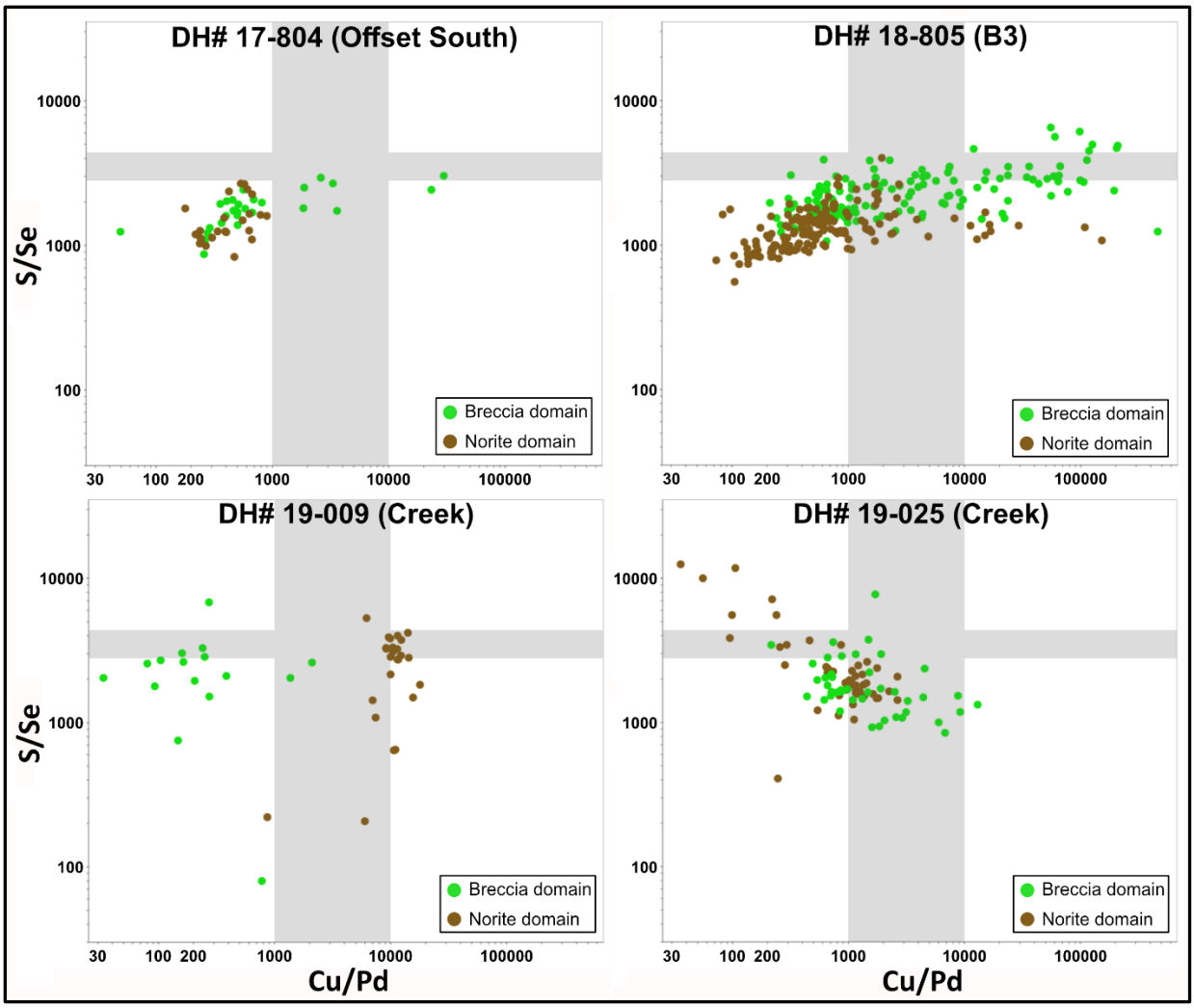

Figure 5.14 – Bivariate plot of S/Se and Cu/Pd ratios. Grey boxes represent mantle values for S/Se (from Eckstrand and Hulbert, 1987) and Cu/Pd (from Barnes et al., 1993).

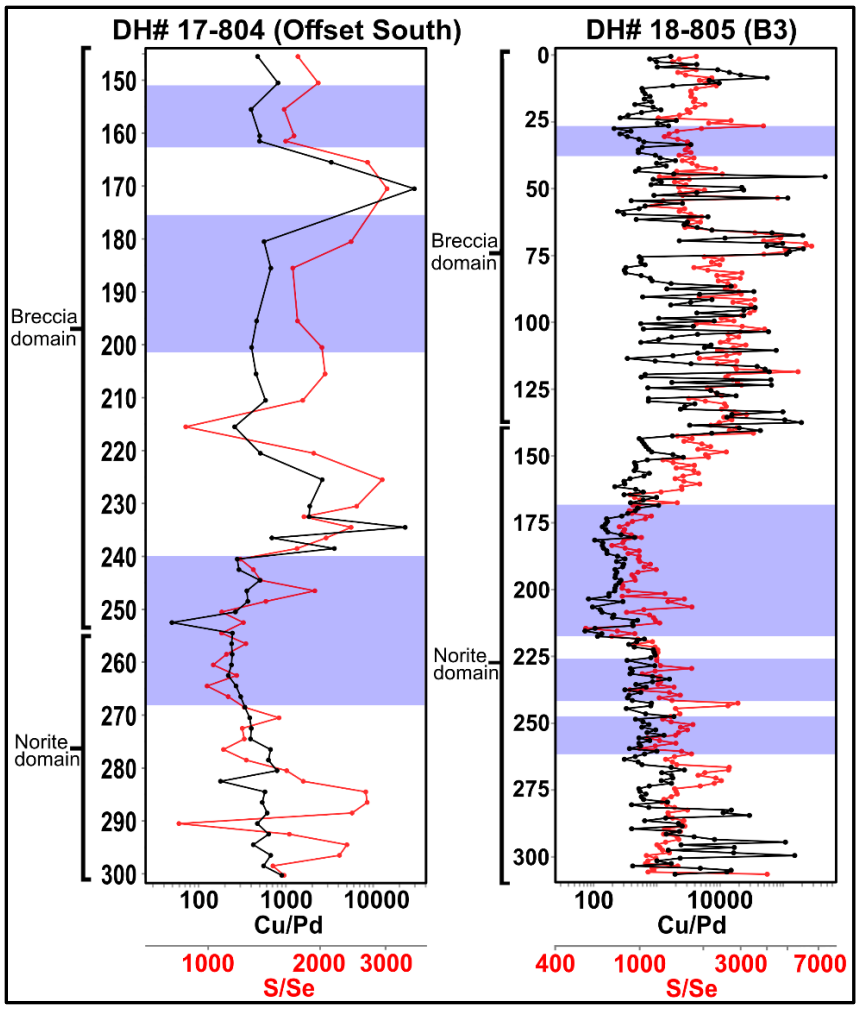

Figure 5.15 – Downhole plots of Cu/Pd and S/Se ratios of Offset Zone drill holes. Zones of significant Pd enrichment (>10 m averaging > 1 ppm Pd) shown as blue boxes.

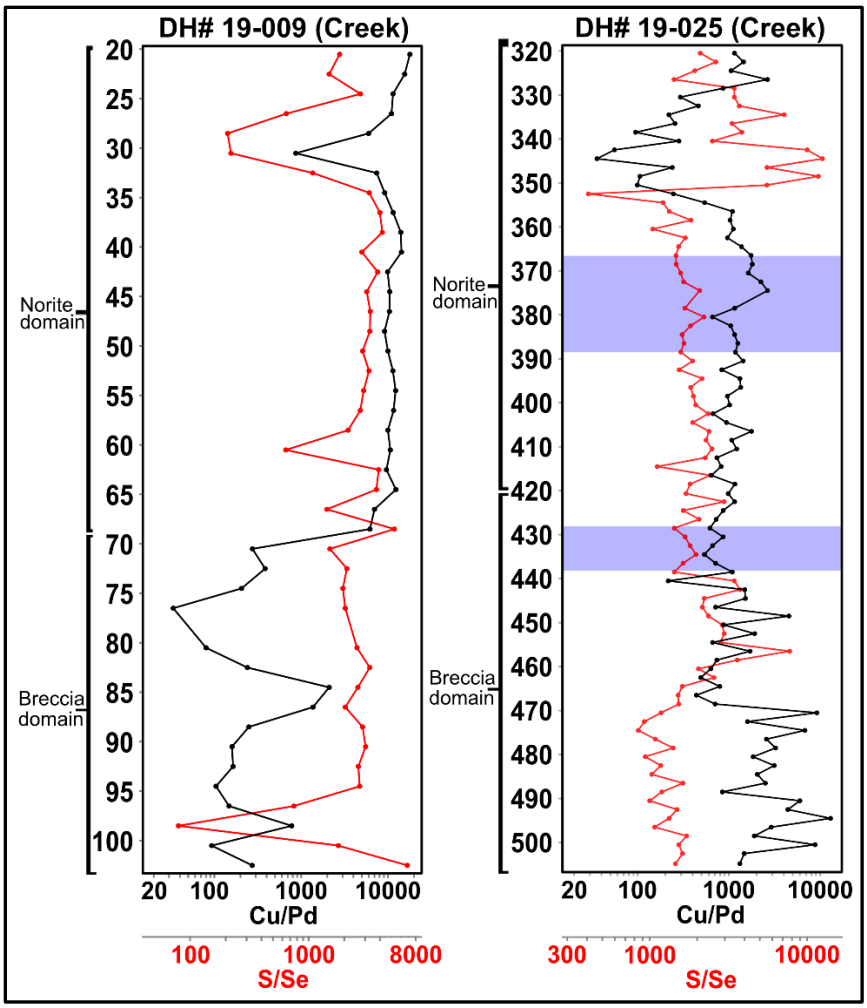

Figure 5.16 – Downhole plots of Cu/Pd and S/Se ratios of Offset Zone drill holes. Zones of significant Pd enrichment (>10 m averaging > 1 ppm Pd) shown as blue boxes.

5.2.3 – Source of sulfur and genesis of ore zones – Assessing variability

Association between low S/Se, low Cu/Pd, and high Pd content is present in the two Offset Zone drill holes (Fig. 5.15). The most Pd-enriched intervals of both DH# 17-804 (2.81 ppm Pd from 240-268 m depth) and DH# 18-805 (6.73 ppm Pd from 169-218 m depth) correspond with the lowest Cu/Pd and S/Se ratios in those drill holes. Accordingly, relatively linear relationships are present between Pd and S/Se and Cu/Pd in the Offset Zone (Figs. 5.13, 5.14).

High R factors are the most likely mechanism by which this relationship can be explained. Although other mechanisms could potentially explain either low S/Se or low Cu/Pd individually, no other explanation is viable for their association. Hydrothermal alteration could result in both low S/Se (via sulfur loss) and low Cu/Pd (via Cu loss and/or Pd gain), but several lines of evidence suggest that this has not occurred. Loss on ignition, which is a good proxy for alteration intensity in the samples in this study (Fig. 5.4), does not correlate with S, Cu, S/Se, or Cu/Pd (Fig. 5.17). Palladium gain via hydrothermal fluids is also unlikely, as Pd and Pt show

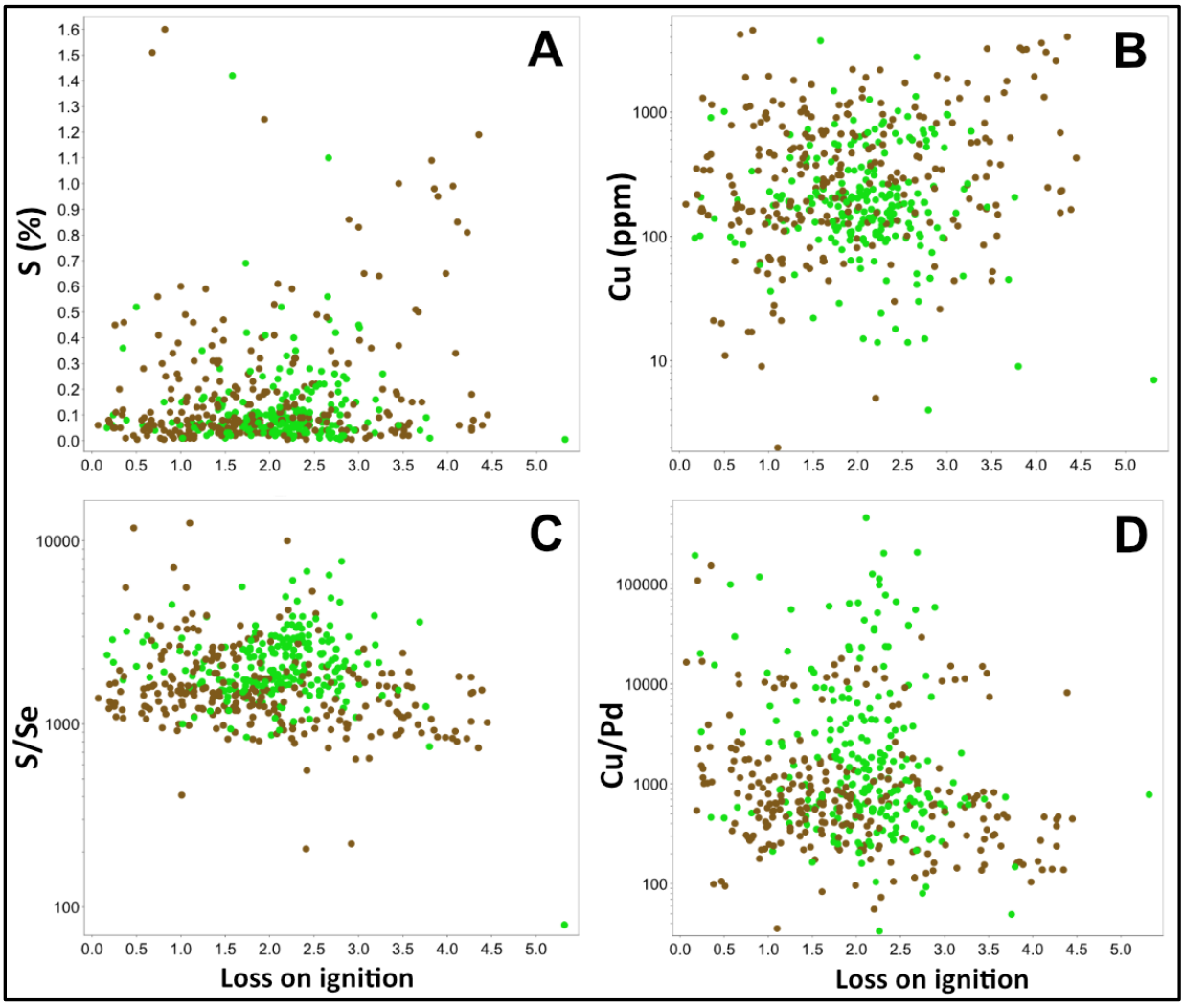

Figure 5.17 – Bivariate plots of loss on ignition vs. A) sulfur (%), B) Cu (ppm), C) S/Se, and D) Cu/Pd in all samples.

proportional enrichment (Fig. 5.18); if significant hydrothermal remobilization of PGEs occurred, a strong correlation between Pd and Pt would not be expected as Pd is more hydrothermally mobile than Pt (Cousins and Vermaak, 1976; Seabrook et al., 2004). Additionally, Cu/Pd vs. Pd plots (Fig. 5.19) show a negative correlation at lower Pd content and a more horizontal distribution at higher Pd content. This relationship is expected in systems in which R factor controls the relationship between PGEs and Cu (Barnes et al., 1993); if significant Cu was removed, vertical trends would be expected, representative of varying Cu content at similar degrees of Pd enrichment. These results are in agreement with the results of Djon and Barnes (2012), who reported similar Pd/Pt ratios to this study, and showed that Pd content does not change in sulfide assemblages representative of different degrees of alteration. Finally, Cu and Ni contents in assay show a good correlation as is expected in primary magmatic

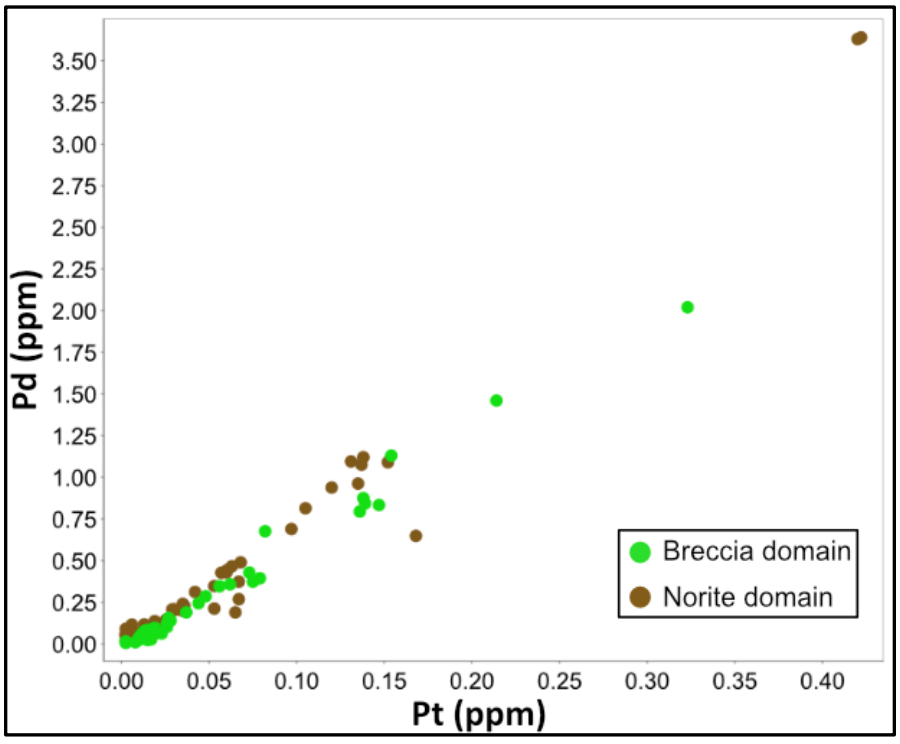

Figure 5.18 – Bivariate plot of Pt vs Pd in all samples.

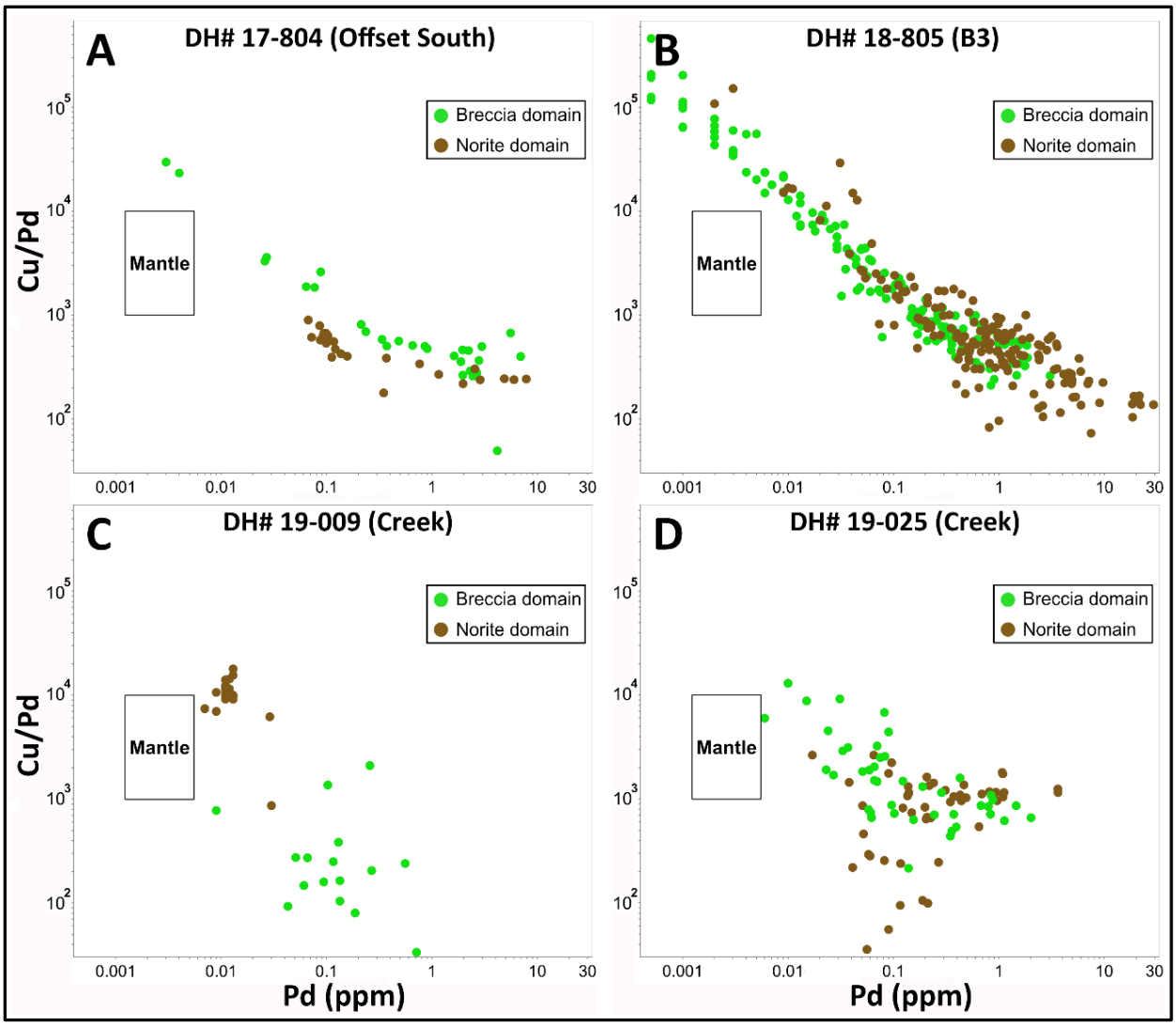

Figure 5.19 – Cu/Pd vs. Pd in all samples.

assemblages (Fig. 4.20). Although some variability can be seen in the most Cu- and Ni-rich samples, the generally strong correlation between Cu and Ni suggests that systematic Cu loss did not occur. Collectively, these results suggest that hydrothermal alteration was not the cause of low Cu/Pd and S/Se in the Offset Zone, and that Pd was not significantly remobilized by hydrothermal fluids.

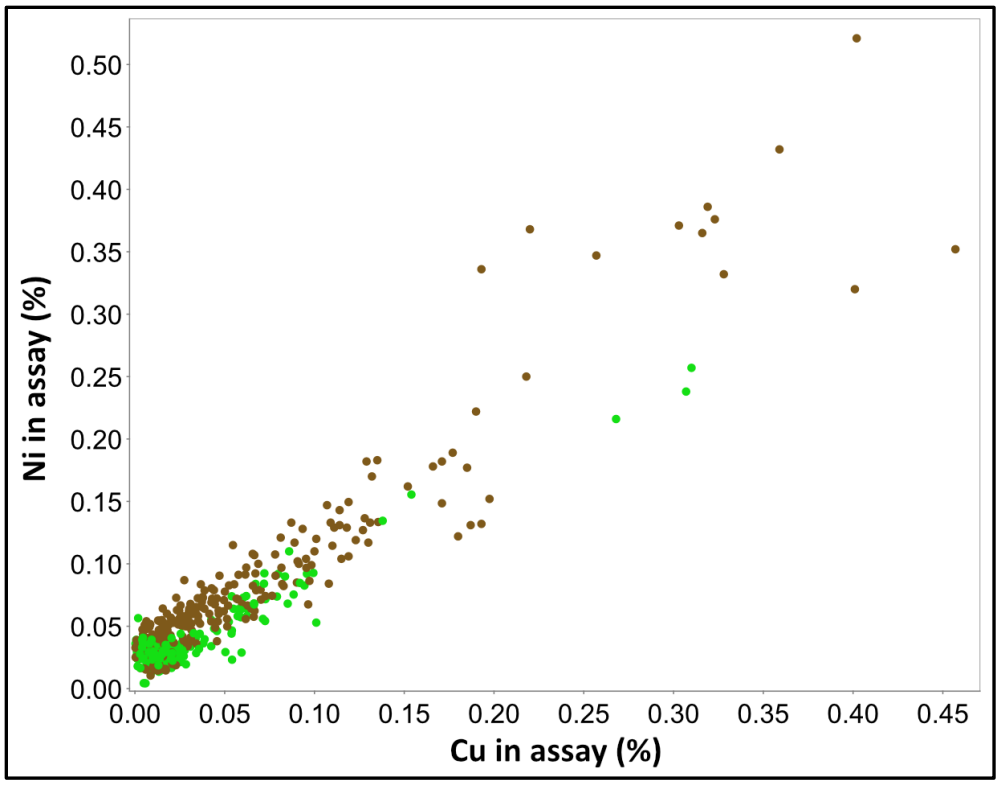

Figure 5.20 – Bivariate plot of Cu vs Ni (assay) in all samples.

Low S/Se ratios could also be generated by the assimilation of sulfur-poor crustal rocks, but this is not plausible as a singular explanation in the Offset Zone due to the high Pd grades. The crustal rocks would then need to have the very unlikely dual characteristic of high Pd grades and sulfur content significantly lower than the relatively sulfur-poor South Lac des Iles Complex, and/or the magmatic sulfide liquid would have had to have already been enriched in Pd via high R factors. The possibility of a mantle source with low S/Se ratios invoked by Hinchey and Hattori (2005) would not explain the low Cu/Pd ratios in the samples in this study. If the mantle source did have S/Se ratios below the typical mantle range, either 1) high R factors also occurred and generated the low Cu/Pd ratios, which would also upgrade Se relative to S and mask the pre-upgrading ratio or 2) high R factors did not occur, and Cu was lost during

hydrothermal alteration. The latter case is implausible because systematic Cu loss does not appear to have occurred.

The relationship between S/Se, Cu/Pd, and Pd is less clear in the Creek Zone than in the Offset Zone. In contrast to the relationship seen in the Offset Zone, the two main zones of Pd enrichment in the Creek Zone drill holes analyzed in this study (DH# 19-025; 1.34 ppm from 366-388 m depth, and 1.02 ppm from 428-437 m depth) show no correlation with low Cu/Pd and S/Se ratios (Fig. 4.13, 4.14, 4.16). Despite this, the majority of samples within this zone have Cu/Pd and S/Se ratios below and/or at the lower end of the mantle range. Accordingly, it is possible that the entire zone at ~360-440 m with relatively constant Cu/Pd and S/Se ratios (Fig. 5.16) underwent similar R factors, but that the sulfide liquid was irregularly distributed and only the Pd-rich zones had enough sulfide present to incorporate a significant quantity of Pd. The generally higher Cu/Pd and S/Se ratios observed in the Creek Zone drill holes compared to the Offset Zone drill holes may also indicate that mineralization in the Creek Zone was produced by relatively lower R factors.

In contrast to the relationship seen in the Offset Zone, DH# 19-025 from the Creek Zone actually shows a well-defined inverse correlation between Cu/Pd and S/Se ratios (Fig. 5.16), including discrete zones of high S/Se and Cu/Pd (332-351 m depth), and low S/Se and high Cu/Pd (470-505 m depth). Several possible mechanisms could have generated the inverse relationship between Cu/Pd and S/Se in DH# 19-025. Variable incorporation of crustal rocks could be a factor; if sulfur-bearing country rocks were assimilated and equilibrated with a magma that already contained an immiscible sulfide liquid enriched in Pd via high R factor, high S/Se ratios could be generated without significantly modifying the low Cu/Pd ratios. A potential

candidate for this process is the tonalitic gneiss country rocks, which contain sulfur in the form of pyrite as well as negligible Cu and Pd. Only a minor addition of crustal sulfur by this process would be necessary to generate the high S/Se, low Cu/Pd zone in DH# 19-025 (332-351 m depth), as sulfur content in this zone is very low (0.005-0.02%). The lowest Cu/Pd ratios in DH# 19-025 could also have been generated via Cu loss, as these samples display a roughly vertical trend in the plot of Cu vs Cu/Pd (Fig. 5.19), which would be expected if variable Cu loss occurred in a zone that experienced a similar degree of Pd enrichment via R factor.

The high Cu/Pd, low S/Se zone in DH# 19-025 (470-505 m depth) is unlikely to have been generated via Cu loss or by MSS/ISS fractionation; Cu/Ni ratios (representing MSS/ISS fractionation) and Cu content in this zone are similar to the drill hole as a whole. If high R factors did not occur in this area, it would necessitate S/Se ratios of the parent magma lower than typical mantle values, as suggested by Hinchey and Hattori (2005). It is also possible that high R factors did occur, but that the magma was Pd-depleted (possibly via prior Pd segregation into sulfide in a different part of the intrusive complex) and therefore did not impart significant Pd into the sulfides in this area. Although the high Cu/Pd, low S/Se zone in DH# 19-025 is near the contact of the Creek Zone with the ultramafic North Lac des Iles Complex, interaction with the ultramafic complex is an unlikely influence due to the low MgO content (5.10-9.98%) seen in this zone.

The downhole variability of Cu/Pd and S/Se in the majority of drill holes suggests that the processes that modified these ratios were variable, even on the metre-scale. In contrast, the norite domain of DH# 19-009 has Cu/Pd and S/Se ratios that are very similar in the majority of samples (Figs. 5.14, 5.16). Palladium values within this zone are also quite low, consistently

<0.1 ppm. It is possible that this zone represents a primary magma that has not undergone significant Pd enrichment by R factor. S/Se ratios of the majority of samples are within the mantle range, and all except one sample have Cu/Pd ratios that are within or slightly above mantle range (Fig. 5.14).

5.2.4 – Source of sulfur and genesis of ore zones – Summary

The correlation between Pd content and S/Se and Cu/Pd ratios in Pd-rich portions of the Offset Zone, and the lack of evidence for systematic Cu or sulfur loss, suggests that high R factors are the dominant mechanism by which Pd-rich zones in the Offset Zone formed. Other potential mechanisms that can cause low S/Se and/or Cu/Pd ratios (Cu and/or S loss via hydrothermal alteration, MSS/ISS fractionation, mantle source with low S/Se) are only partially viable and necessitate the presence of high R factors to explain the relationship between Pd, S/Se, and Cu/Pd.

The origin of Pd-rich mineralization in the Creek Zone is more enigmatic than the Offset Zone, due to the lack of correlation between Pd, S/Se, and Cu/Pd. Below-mantle Cu/Pd and S/Se ratios in Pd-enriched horizons in DH# 19-025 suggest that Pd mineralization was probably generated by silicate magma-sulfide liquid interaction, but the lack of mineralization in areas with similar Cu/Pd and S/Se to the mineralized zones is not easily explained by the data available for this study. It is possible that overall sulfide liquid content was lower in the Creek Zone than in the Offset Zone, which limited the ability of Pd to accumulate in the Creek Zone. Higher Cu/Pd and S/Se ratios of mineralized horizons in the Creek Zone compared to the Offset

Zone could be the result of lower R factors, which may help explain the less voluminous and less Pd-rich character of mineralization in the Creek Zone.

$\delta^{34}S$ values in the typical mantle range within the Offset and Creek Zone reported in this study are consistent with results reported by Hinchey and Hattori (2005) from the Roby and Twilight Zones and by Duran et al. (2016) from sulfide-rich pods. These authors interpreted these results to be representative of mantle-derived sulfur. Based on other geochemical parameters evaluated in this study and the generally sulfide-poor nature of the Lac des Iles orebodies, the Offset and Creek Zones seem to satisfy the parameters outlined by Ripley and Li (2013) for genesis of PGE-rich magmatic sulfide mineralization without significant crustal sulfur. Despite this, the similarity of $\delta^{34}S$ values in the Offset/Creek Zones to those in the tonalitic gneiss host rocks means that the presence of crustal sulfur cannot be ruled out. Regardless of the presence or absence of crustal sulfur, the lack of $\delta^{34}S$ variation between the breccia and norite domains, between the Offset and Creek Zones, and between mineralized and unmineralized rocks suggest that the variable influence of crustal sulfur did not affect the presence or endowment of mineralization in the Offset and Creek Zones.

If crustal sulfur was incorporated, three possible scenarios could be invoked: 1) the contaminant had a similar sulfur isotope content to the mantle, such as the host tonalitic gneiss, 2) the sulfur isotope signature of the contaminant was not similar to the mantle, but the degree of incorporation was so small that it did not change the sulfur isotope signature of the magma, or 3) the sulfur isotope signature of the contaminant may or may not have been similar to the mantle, but the sulfur isotope values were diluted to mantle values via high R factors. $\delta^{34}S$ can be reset to mantle values at R factors of >10,000 (Brzozowski et al., 2021), which are

reasonable values given the low Cu/Pd ratios seen in this study. If this were the case, however, it would be expected that samples with S/Se and Cu/Pd ratios similar to the mantle would have non-mantle $\delta^{34}S$ values, which are not observed. Therefore, the third scenario listed above is unlikely. The second scenario listed above is possible, but is not relevant to formation of Pd-rich mineralization because most of the sulfur in this scenario would still be mantle-sourced. Therefore, it can be inferred that the sulfur in the Offset and Creek Zones was 1) wholly derived from the mantle, or 2) partially derived from a source with similar $\delta^{34}S$ signature to the mantle (such as the host tonalitic gneiss) and homogenized in the magma so that variable crustal sulfur did not influence the formation of mineralization.

5.3 – Formation of the breccia and norite domains

The prevailing view is that the South Lac des Iles Complex formed via three compositionally distinct phases of magmatism (Decharte et al., 2018). In this model, initial magmatism produced the gabbronorite series, a second phase of magmatism produced the breccia and norite series, and a final phase of magmatism produced the diorite series. The gabbronorite and diorite series do not contain economic mineralization and were not the focus of this study. As such, the focus of this section is to evaluate the geochemical differences and/or similarities of the breccia and norite series and determine their relationship and formation history.

5.3.1 – Formation of the breccia and norite domains – Historical work

Previous studies did not thoroughly assess differences in the breccia and norite domains. Although some prior studies do include a relatively small number samples from the

norite domain, the majority of these studies discuss differences and similarities of the different parts of the breccia domain (e.g. Brugmann et al., 1989; Lavigne and Michaud, 2001; Hinchey and Hattori, 2005; Hinchey et al., 2005; Barnes and Gomwe, 2011). The studied breccia domain units in these studies typically comprise chlorite-actinolite schist, magmatic breccia, and/or varitextured gabbronorite. The norite domain has come into greater focus since mining and systematic exploration of the Offset Zone began ~10 years ago, as the southern portion of the Offset Zone, including the B2, B3, and C-Zones, hosts significant Pd mineralization within equigranular gabbronorites of the norite domain (Decharte et al., 2018). Prior to exploration of the Offset Zone, significant economic mineralization had not been recognized in the norite domain.

The majority of prior studies have invoked models in which the equigranular portions of the breccia and norite domains formed via typical fractional crystallization processes, and in which the varitextured and brecciated portions of the breccia domains formed via the influence of late-stage volatile-rich evolved magma (Brugmann et al., 1989) or influx of later magma pulses (Lavigne and Michaud, 2001; Hinchey et al., 2005; Barnes and Gomwe, 2011). In the majority of studies in which the gabbronorite domain has been evaluated, it has been argued to have formed via an earlier stage of magmatism than the breccia and norite domains (Hinchey and Hattori, 2005; Barnes and Gomwe, 2011; Decharte et al., 2018). Schisa et al. (2015) provided an alternative model in which high-temperature magmatic fluids imparted the leucocratic character of the gabbronorite domain via dissolution of plagioclase from the chlorite-actinolite schist of the breccia domain, which resulted in the melanocratic character of the schist.

5.3.2 – Formation of the breccia and norite domains – Paragenesis

No differences were observed between the paragenesis of the breccia and norite domains and between the Offset and Creek Zones. Although there are compositional and textural differences between the two domains (the breccia domain contains more plagioclase, less pyroxene, greater compositional variability, and higher degree of brecciated and varitextured rocks than the norite domain), no differences were observed in the proportion, distribution, or crystallization history of any other primary or secondary minerals. No differences in paragenesis or average composition were observed between the Offset and Creek Zones.

In both the norite and breccia domains, plagioclase and orthopyroxene both commonly occur as subhedral to anhedral crystals (Figs. 4.20, 4.21, 4.22). Local poikilitic textures are present in most samples from both domains, though in all samples these textures are seen in only a small minority (typically <2%) of crystals. Poikilitic textures are present as subhedral to euhedral plagioclase and orthopyroxene chadacrysts that are partially to completely encircled by larger crystals of plagioclase, orthopyroxene, and/or clinopyroxene (Figs. 4.19, 4.22). The presence of plagioclase and orthopyroxene as chadacrysts suggests that plagioclase and orthopyroxene both began crystallizing early in the solidification of the magma. Plagioclase equilibration textures, including curvilinear boundaries, polygonal triple junctions, and anhedral/irregularly shaped crystals are present in all samples in which crystal boundaries are not obscured by alteration (Figs. 4.21, 4.36) This suggests that plagioclase was crystallizing throughout the solidification history of the magma. Curved, equilibrated boundaries were also observed in orthopyroxene (Fig. 5.21), though they were not present in every sample and were

less widespread than those seen in plagioclase. This, along with the generally subhedral shape of orthopyroxene, indicates that it crystallized throughout most of the solidification of the magma, though crystallization appears to have stopped earlier than plagioclase in some areas due to the absence of equilibration textures and anhedral crystals in some samples. No spatial variation in the timing of cessation of orthopyroxene crystallization was observed.

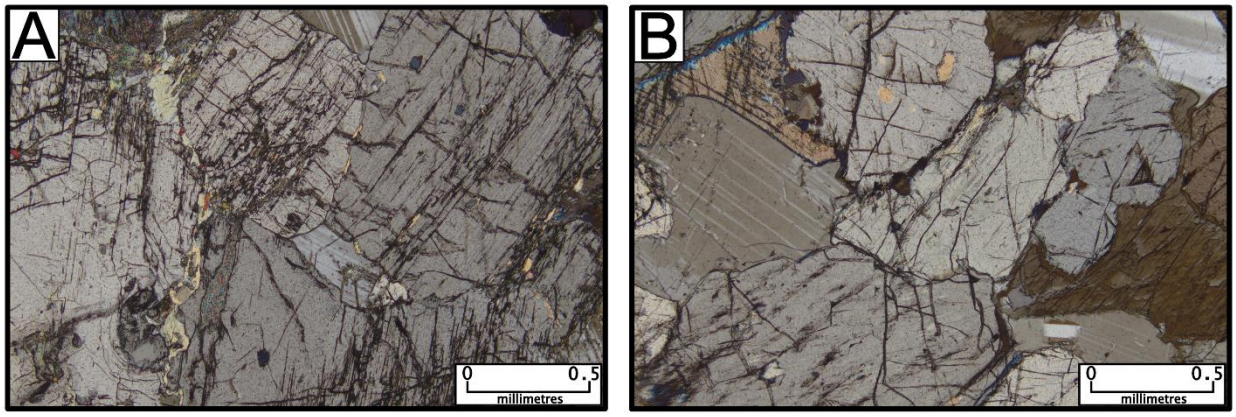

Figure 5.21 – Curvilinear boundaries between orthopyroxene crystals in A) Sample JJ-TS-041 and B) Sample JJ-TS-105. Photos taken under cross-polarized light.

In contrast to plagioclase and orthopyroxene, the large majority of clinopyroxene crystals in both domains are irregular and anhedral, with ameboid/“blob”-shaped crystals making up the large majority of observed clinopyroxene in most samples (Fig. 4.22D). These irregularly shaped crystals are generally much larger than adjacent plagioclase and orthopyroxene, and are dominantly present as oikocrysts partially to completely surrounding several plagioclase and/or orthopyroxene crystals. In most samples, smaller equant and subhedral clinopyroxene crystals of similar size to adjacent plagioclase and orthopyroxene make up a minority of the clinopyroxene present (Fig. 4.22E). These results suggest that clinopyroxene was an early crystallizing phase in at least some areas, though at a much lower proportion than plagioclase and orthopyroxene. Most of the clinopyroxene had to have

crystallized at a later stage; due to the irregular ameboid shape and poikilitic texture of the majority of crystals, this had to have occurred at a stage at which most of the magma had been solidified. The large size of most clinopyroxene crystals and absence of small, anhedral crystals suggests that they did not crystallize from very late-stage trapped interstitial magma, and thus had to have formed early enough that the magma was still freely equilibrating with crystals.

Biotite and hornblende are the only other magmatic silicate minerals observed in the samples in this study, with biotite present in a majority of samples and hornblende present in only two samples. The pre-alteration biotite proportion is difficult to estimate due to its apparent presence as both a primary mineral (Fig. 4.23A, B) and an alteration product (Fig. 4.23C, D), but it appears to always make up <2% of the pre-alteration assemblage, usually occurring at only trace quantities. Primary biotite crystals are typically <0.5 mm; the small size of the biotite crystals suggests that they crystallized at a late stage of the solidification of the magma.

Secondary silicate minerals are observed in varying quantities in all samples in this study. The hydrous nature of the alteration assemblage and the association of stronger alteration with higher loss on ignition (Fig. 5.4) suggests that alteration occurred via hydrothermal processes. The highly variable distribution of degree of alteration between rocks of similar composition suggests that regional metamorphism is not the principal cause of alteration. In samples with a low degree of alteration (>90% of magmatic silicate proportion is unaltered), plagioclase alters to white mica+chlorite+epidote (Figs. 4.26A, B, C, 4.33B), whereas an assemblage of chlorite+white mica±quartz (Figs. 4.26D, E, F, 4.33A, C, 4.39A) was observed in samples with a moderate to high degree of alteration. As such, white mica and chlorite

occurred as reaction products through the entire alteration history, but chlorite became much more volumetrically significant as the reaction progressed. Epidote was an early-stage reaction product but was destroyed in later stages, whereas quartz only formed as a late-stage alteration product. Pyroxene was observed to have altered to the same assemblage of tremolite-actinolite+talc±anthophyllite in all samples (Figs. 4.27, 4.33D, 4.36B). The pyroxene alteration assemblage does not change appreciably with increased alteration intensity, as tremolite-actinolite is the most volumetrically significant pyroxene alteration product in almost all samples.

Sulfide minerals were observed in all samples analyzed in this study. In samples in which primary igneous silicate minerals are mostly preserved, pyrrhotite, chalcopyrite, and pentlandite are dominant and occur as fine disseminations to small interstitial blebs. The maximum size of sulfide aggregates is larger in samples with higher sulfur content, though relatively fine disseminations are generally present in both sulfide-poor (<0.1% sulfides) and more sulfide-rich (>2% sulfides) samples (Figs. 4.24A, C, 4.38A). The irregular and anhedral shape of sulfide blebs and lack of sulfide inclusions within primary silicate crystals suggests that sulfide crystallization occurred at a relatively late stage, after a large degree of the silicate magma had already been crystallized. The common presence of sulfide aggregates up to 5 mm in size in more sulfide-rich samples (>2% sulfide) requires there to have been enough room between silicate crystals to accommodate the maximum size of sulfide crystals, meaning that sulfide crystallization could not have occurred at a very late stage in only small interstices between silicate minerals. Pentlandite predominantly occurs as relatively coarse aggregates at the margins of pyrrhotite crystals, and sometimes occurs as coarse, irregular exsolution

products from pyrrhotite (Fig. 5.22A-C). Exsolution lamellae ("flames") of pentlandite within pyrrhotite are very rare (Fig 5.22D). The pentlandite textures suggest that crystallization of

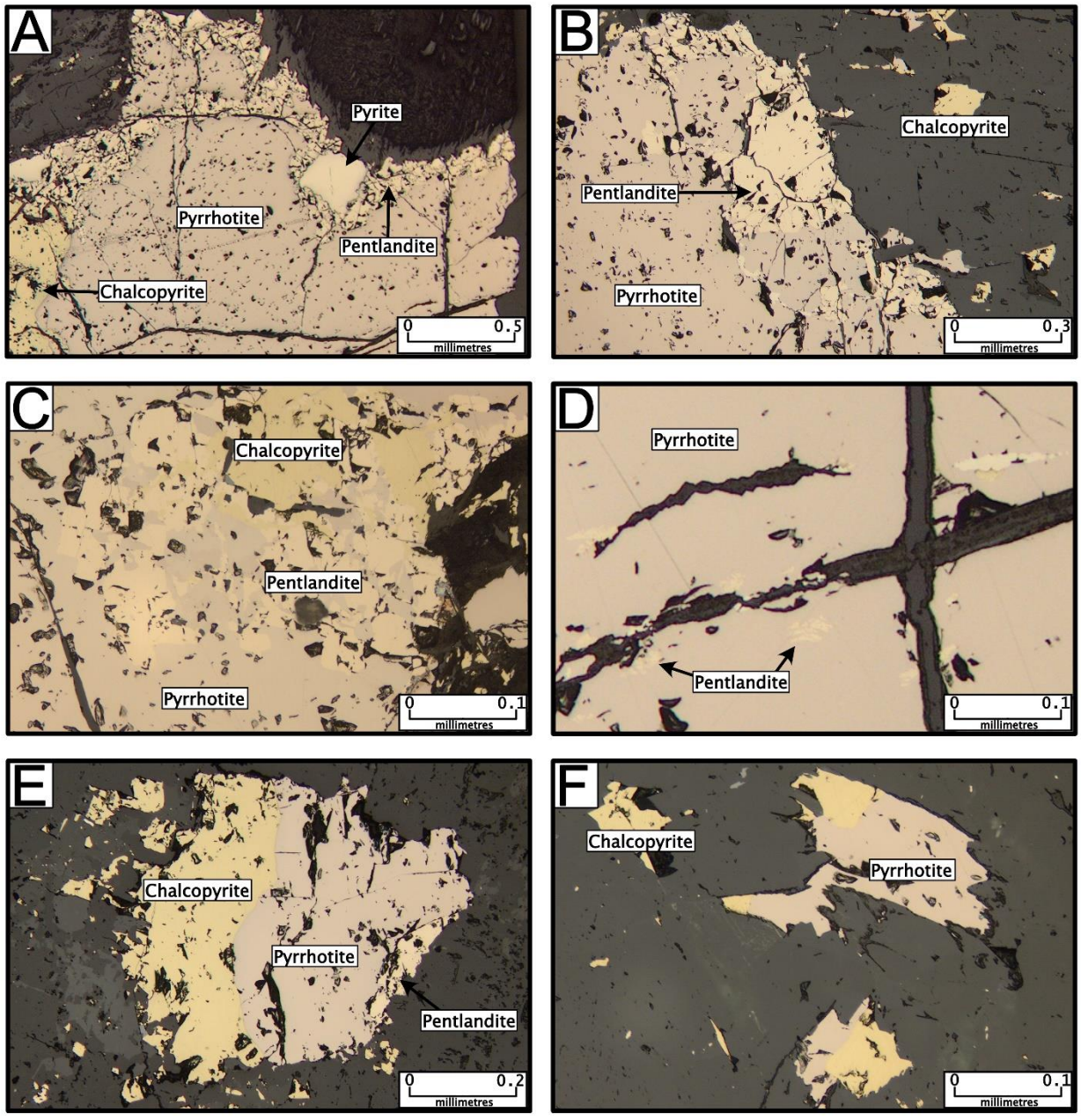

Figure 5.22 – Magmatic sulfide textures. Photos taken under reflected light. A) Pentlandite crystals at the margin of pyrrhotite crystal (Sample JJ-TS-018). B) Pentlandite crystals at the margin of pyrrhotite crystal (Sample JJ-TS-093). C) Pentlandite coarsely exsolved from pyrrhotite (Sample JJ-TS-141). D) Pentlandite finely exsolved from pyrrhotite (Sample JJ-TS-018). E) Smooth, curved boundary between pyrrhotite and chalcopyrite (Sample JJ-TS-068). F) Smooth, curved boundaries between pyrrhotite and chalcopyrite (Sample JJ-TS-084).

pentlandite from monosulfide solution was not a low-temperature process (i.e. above 250° C), and that the cooling rate was slow enough so that supersaturation of Ni in the monosulfide solution did not occur (Durazzo and Taylor, 1982; Kelly and Vaughan, 1983). In samples with a low degree of alteration, chalcopyrite has smooth, wavy boundaries with adjacent pyrrhotite (Fig. 5.22E, F) and occurs only in blebs, suggesting that it crystallized from intermediate solid solution and that remobilization did not occur in weakly altered samples. Pyrite is present in very small quantities in some weakly altered samples, occurring within magmatic sulfide blebs and appearing to replace pyrrhotite.

In moderately to strongly altered samples, the dominant sulfide assemblage is pyrite+chalcopyrite+pentlandite. Pyrrhotite content is variable, with pyrrhotite typically present in moderately altered samples and typically absent in strongly altered samples. The texture of the sulfide minerals in more strongly altered samples is variable. In samples that contain both pyrite and pyrrhotite, replacement of pyrrhotite by pyrite typically occurs in situ (Fig. 5.23A) and the morphology of the sulfide blebs is generally similar to weakly altered samples. The textural relationship and roughly inverse proportion of pyrite and pyrrhotite suggest that pyrite replaced pyrrhotite in areas of stronger hydrothermal alteration. In more strongly altered samples that contain little to no pyrrhotite, pyrite crystals typically occur as larger anhedral to subhedral crystals as well as fine disseminations. Chalcopyrite and pentlandite both occur as very fine disseminations in strongly altered samples (Fig. 5.23B) and as larger crystals/aggregates in proximity to and/or contact with pyrite crystals. Larger chalcopyrite and pentlandite crystals in strongly altered samples bear textural resemblance to chalcopyrite and pentlandite in weakly altered samples (Fig. 5.23C, D). Pyrite and chalcopyrite were also

observed as very thin, elongate crystals within aggregates of silicate alteration products, most commonly tremolite-actinolite. These textures suggest that local remobilization and disaggregation of sulfides has occurred. However, no evidence is present for large-scale remobilization of sulfide minerals.

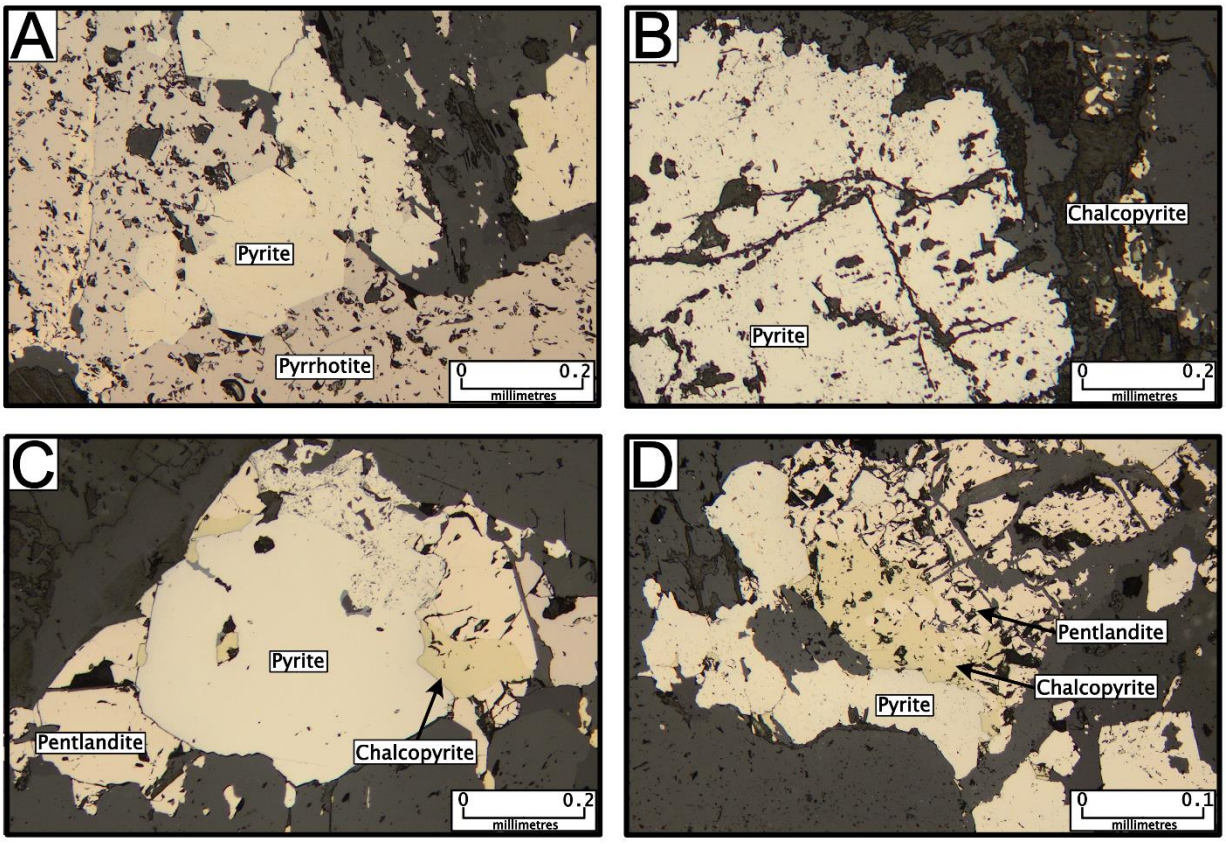

Figure 5.23 – Sulfide textures in altered samples. Photos taken under reflected light. A) Pyrite partially replacing pyrrhotite in situ (Sample JJ-TS-155). B) Pyrite crystal adjacent to very finely disseminated chalcopyrite (Sample JJ-TS-123). C) Pyrite-chalcopyrite-pentlandite bleb (Sample JJ-TS-032). D) Pyrite-chalcopyrite-pentlandite aggregate (Sample JJ-TS-027).

Magnetite was the most commonly observed oxide mineral, and is present as anhedral, irregularly shaped crystals. Ilmenite is present in a minority of samples, occurring as very fine exsolution lamellae from magnetite or less commonly as discrete crystals in contact with magnetite. The anhedral shape of oxide crystals suggests that they crystallized after the silicate

magma had largely crystallized. The similarity of shape and maximum size of oxides to sulfide blebs suggests that oxides crystallized at a generally similar period in magma evolution. No evidence is present for hydrothermal remobilization of oxides.

Based on the above interpretations, the paragenesis of samples analyzed in this study is summarized in Figure 5.24. Orthopyroxene and plagioclase are ubiquitous in the early crystallization of the magma, with clinopyroxene also present as a minor early crystallizing phase in some locations. In the late stages of magmatic crystallization, plagioclase and orthopyroxene continue to crystallize with orthopyroxene becoming less significant in the latest stages of crystallization. Clinopyroxene, biotite, magnetite, ilmenite, chalcopyrite, pentlandite, and pyrrhotite are dominantly or entirely late crystallizing phases. Chlorite, white mica, tremolite-actinolite, talc, anthophyllite, and pyrite were produced at varying quantities at all stages of alteration. Epidote was only produced in early stages of alteration, whereas quartz only formed in late stages.

This paragenesis only encompasses minerals that were observed in this study, and there are likely other minor phases present that were not observed. Apatite (Boudreau et al., 2014; Schisa et al., 2015), millerite (Barnes and Gomwe, 2011; Boudreau et al., 2014) and platinum group minerals (Boudreau et al., 2014; Djon et al., 2018) have been reported to a high degree of confidence in previous studies of the Lac des Iles Complex. These minerals have previously been observed to occur as very fine-grained crystals in only trace quantities where present, and may have been too small to observe using a light microscope. Millerite may not have been present in the samples in this study as it is only observed in areas of very strong alteration (Barnes and Gomwe, 2011), of which only a few samples were taken for this study.

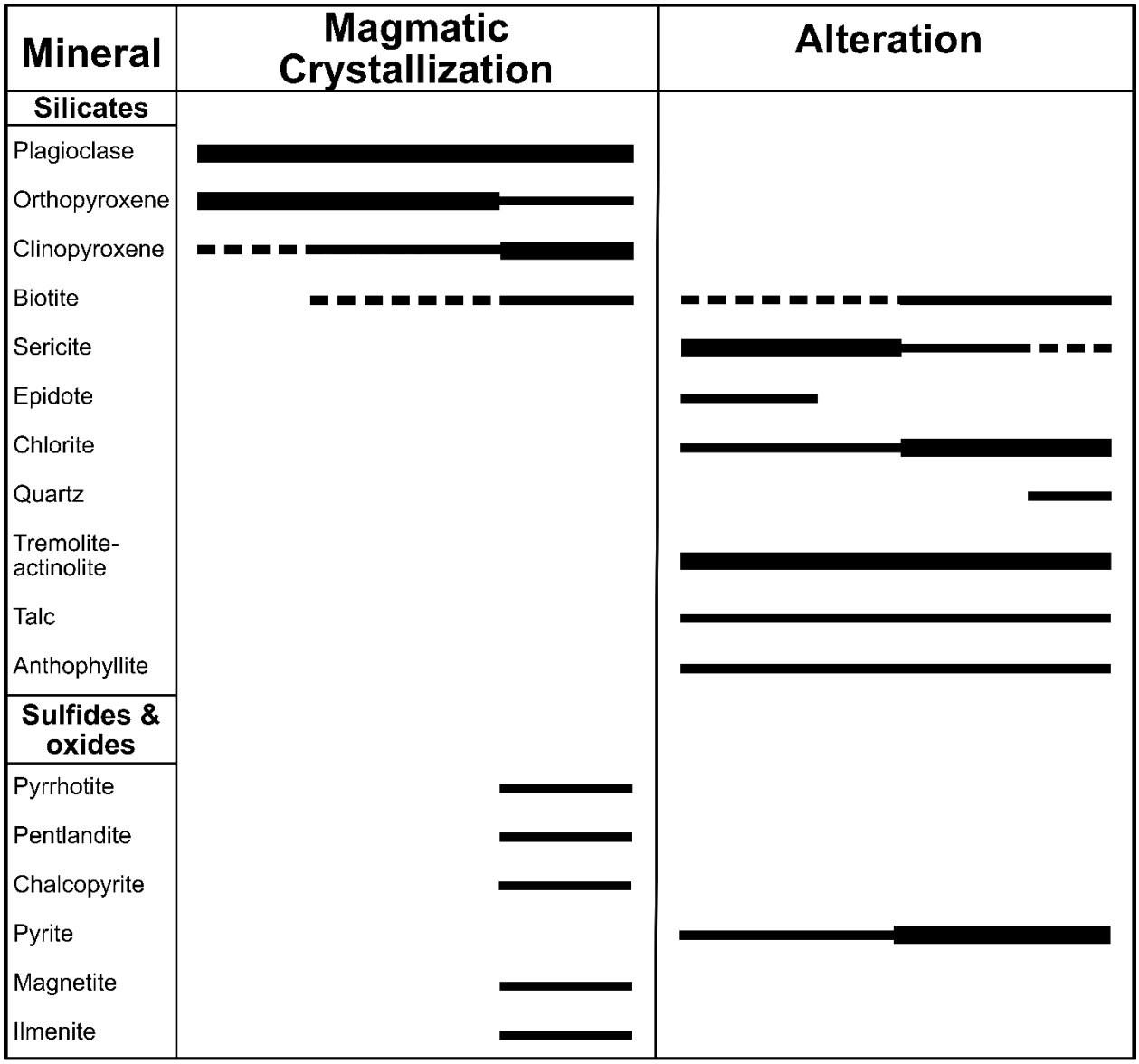

Figure 5.24 – Paragenesis of the breccia and norite domains of the Lac des Iles Complex.

5.3.3 – Formation of the breccia and norite domains – Petrologic model

The weight of geochemical evidence suggests that the breccia and norite domains crystallized from magmas with similar chemistries. This is indicated by the similarity in incompatible element content (Figs. 5.1, 5.2, 5.3, 5.6), Nd isotope content (Fig. 5.9), sulfur isotope content (Fig. 4.49), Pd/Pt ratios (Fig. 5.18), and Cu/Ni ratios (Fig. 5.20). Some elements

(Al, Ca, Co, Fe, Ga, Mg, Mn, Na, Sc, Sr, and Zn) show inconsistent but broadly systematic variability between lithological domains, in which Al, Ca, Ga, Na, and Sr are generally higher in the breccia domain and Co, Fe, Mg, Mn, Sc, and Zn are generally higher in the norite domain. These variations can be explained by the more plagioclase-rich character of the breccia domain and the more pyroxene-rich character of the norite domain (Fig. 5.25). The visually estimated plagioclase/pyroxene ratio correlates with Al_2O_3, CaO, Na_2O, Ga, and Sr. Aluminum,

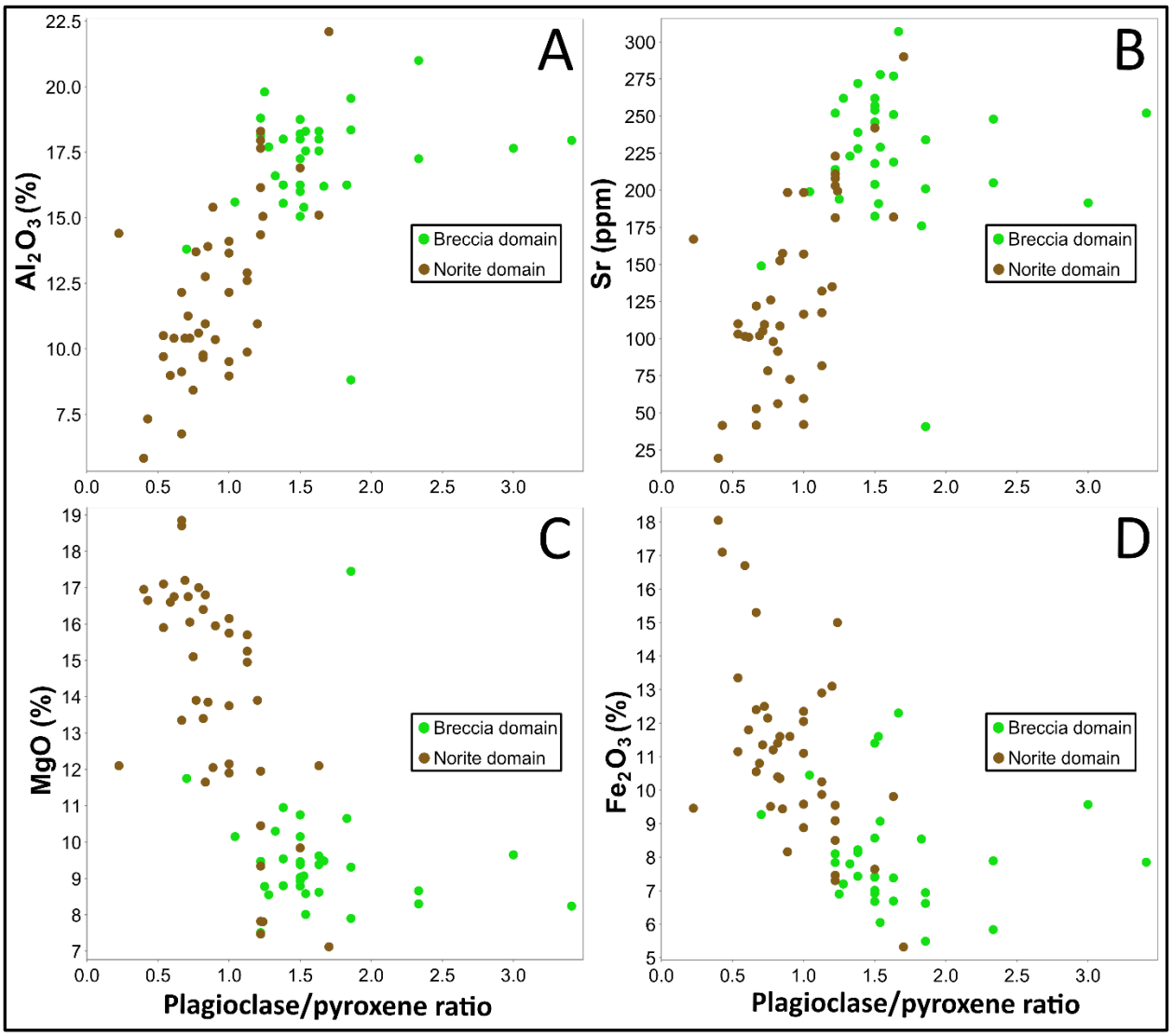

Figure 5.25 – Bivariate plots of visually estimated pre-alteration plagioclase/pyroxene ratio against A) Al_2O_3, B) Sr, C) MgO, D) Fe_2O_3.

Ca, and Na are major constituents of plagioclase but occur in lower quantities in pyroxene, whereas Ga and Sr readily substitute for Al^{3+} and Ca^{2+} in plagioclase, respectively (Vincent and Nightingale, 1974; Blundy and Wood, 1991). A negative correlation is present between the plagioclase/pyroxene ratio and Fe_2O_3, MgO, MnO, Co, Sc, and Zn. Iron and Mg are major constituents of pyroxene and occur in negligible quantities in plagioclase, whereas Mn, Co, Sc, and Zn can substitute for Fe and/or Mg in pyroxene (Morimoto et al., 1989).

Despite the generally more plagioclase-rich composition of the breccia domain and the generally more pyroxene-rich composition of the norite domain, there is a large degree of compositional heterogeneity in both domains. Downhole plots of Al_2O_3 and MgO (elements that show the strongest correlation with plagioclase and pyroxene, respectively), show that there is not a direct relationship between the lithological domain and the plagioclase/pyroxene content (Fig. 5.26), and varying degrees of compositional heterogeneity show no association with brecciation or textural differences. This is typified by the Al_2O_3 and MgO content in the norite domain of the two Creek Zone drill holes, DH# 19-009 and DH# 19-025; the intercepts appear texturally similar in drill core and petrographic section, but DH#19-025 shows significant compositional variation whereas DH#19-009 is relatively compositionally homogenous through the entire norite domain intersection.

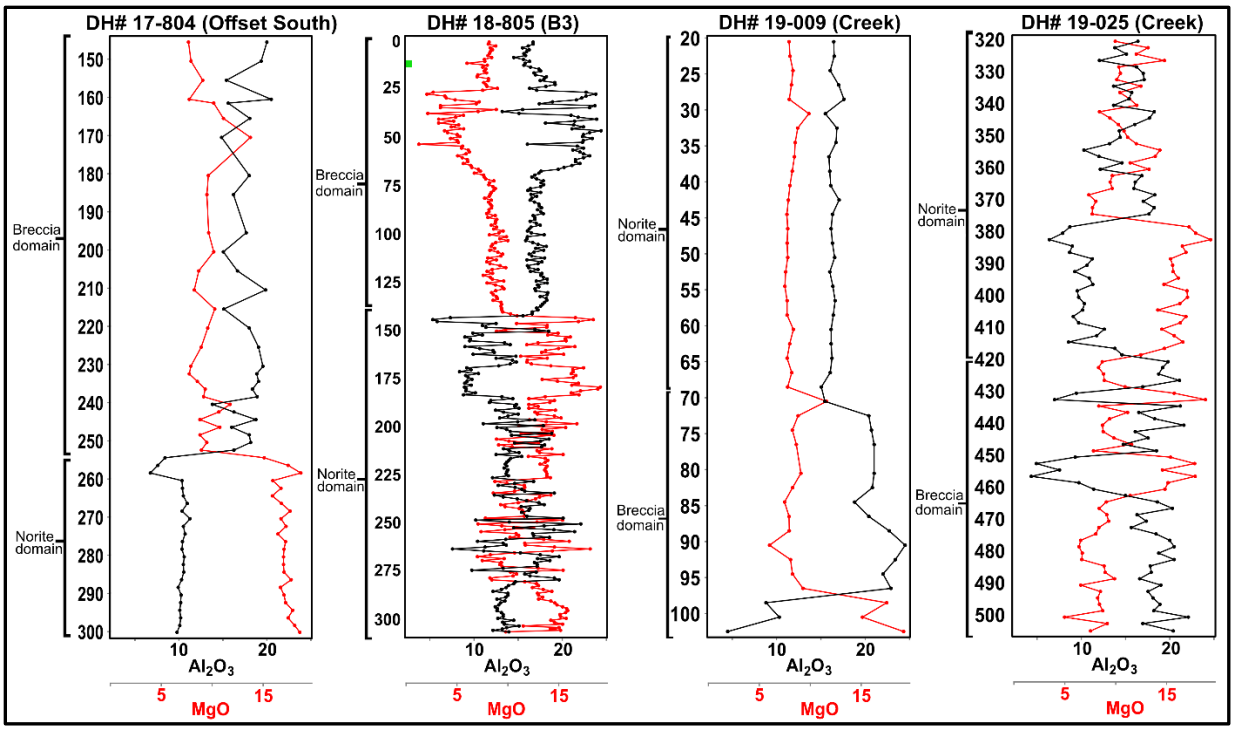

Figure 5.26 – Downhole plots of Al_2O_3 and MgO in all studied drill holes.

Fractional crystallization and gravitational settling of crystals is a common magmatic process that frequently results in compositional variation of an intrusion. In some systems, fractional crystallization of silicates has been proposed as the main mechanism by which sulfur saturation occurs and PGE/Au-rich sulfide mineralization is formed, such as in the Sonju Lake intrusion (Park et al., 2004) and the Skaergaard intrusion (Andersen et al., 1998). Gravitational settling of crystals is not a viable process to explain compositional differentiation in the South Lac des Iles Complex, as contacts between lithological domains are vertical rather than horizontal. Additionally, the fact that the South Lac des Iles Complex is in contact with the layered, upright, and roughly coeval North Lac des Iles Complex provides evidence that the South Lac des Iles Complex is currently in a similar orientation as when it formed. Although early fractional crystallization and gravitational settling can be disrupted by later magma pulses,

resulting in more heterogeneity than intrusions that form as the result of crystallization within a closed-system magma chamber, this does not appear to have occurred in the South Lac des Iles Complex. Fractional crystallization and gravitational settling results in gradational, systematic geochemical trends that are not broadly observed in the drill holes analyzed in this study. Inconsistent gradational trends in some elements (Al, Co, Fe, Ga, Mg; Fig. 4.26) are observed in parts of one or both of the breccia domain intercept (0-104 m depth) of DH# 18-805 (B3 Zone) and the norite domain intercept (378-417 m depth) of DH# 19-025 (Creek Zone), suggesting that fractional crystallization may be a factor influencing local geochemical variation in limited portions of both the breccia and norite domains and both the Offset and Creek Zones. Despite this, the lack of consistent gradational variation suggests that this was not a major process affecting compositional variation within or between studied lithological domains of the Lac des Iles Complex, and does not appear to have influenced distribution of mineralization nor the separation of the breccia and norite domains.

The combination of fractional crystallization and gravitational settling that produces well-defined vertical compositional variation is characteristic of low-energy magma systems, in which magma crystallizes in an essentially closed systems without influx of new pulses from below, or outflow of magma to higher levels of the crust. However, if fractional crystallization occurs under high-energy conditions, such as in a continuously flowing vertical magma conduit, broad lateral compositional variability can be produced via magmatic flow differentiation (Bhattacharji and Smith, 1964). In these systems, early-forming crystals are entrained in flowing magma and move toward the centre of the magma body (Bhattacharji and Smith, 1964; Komar, 1972); models for some systems involve remobilization of fractionally crystallized phases from a

deeper staging chamber (de Waal et al., 2004). As crystallization continues, lateral portions of the intrusion represent more evolved portions of the parent magma. Flow differentiation has been invoked as a mechanism of lateral lithological variability in Ni-Cu-PGE sulfide-mineralized intrusions including the western and central parts of the Jinchuan intrusion (Chai and Naldrett, 1992), the Baimazhai intrusion (Wang et al., 2006), and the Kalatongke intrusions (Zhang et al., 2009). Of particular relevance to this study is the suggestion that the concentric lithological zonation commonly seen in Alaskan-type intrusions can be explained via flow differentiation (Himmelburg and Loney, 1995; Farahat and Helmy, 2006; Helmy et al., 2014). Although early models suggest that crystal segregation via flow differentiation is only applicable in relatively narrow (<100 m) dikes (Barriere, 1976), it has more recently been argued that this process can operate in much larger magma systems (Himmelburg and Loney, 1995; Farahat and Helmy, 2006; Koenders and Petford, 2023).

Sutcliffe and Sweeny (1986) and Brugmann et al. (1997) noted several similarities between the South Lac des Iles Complex and Alaskan-type intrusions. Similar to the pattern seen in Alaskan-type intrusions, the South Lac des Iles Complex contains a more mafic lithological unit at the centre of the intrusive complex (norite domain) and a more felsic lithological unit at the margins (breccia domain). Although the South Lac des Iles Complex does not contain the ultramafic lithologies that are common in Alaskan-type intrusions, it seems reasonable that the same mechanisms of petrologic differentiation can operate in any high-energy, vertically flowing magmatic system, regardless of the parent magma composition.

Aside from the Lac des Iles suite of intrusions, the other major mafic-ultramafic intrusive suite associated with the accretion of the Wawa terrane to the Wabigoon terrane in the

Shebandowan orogeny are the Quetico intrusions (MacTavish, 1999; Pettigrew and Hattori, 2006). The Quetico intrusions have been dated at 2688+6/-5 (Samuels Lake intrusion; McNicoll and Pettigrew cited in Pettigrew and Hattori, 2006), which overlaps with the age of the Lac des Iles Complex. Similar to the South Lac des Iles Complex, several of the Quetico intrusions, including the Samuels Lake, Kawene, Chief Peter, and Plateau Lake Intrusions, are made up of lithologies that grade from more mafic at the core to less mafic at the periphery of the intrusion (MacTavish, 1999; Pettigrew and Hattori, 2006). All four of the above listed Quetico intrusions contain disseminated sulfide mineralization, which is PGE-rich and relatively Ni-Cu-poor in all except the Plateau Lake intrusion. Similar to the South Lac des Iles Complex, mineralization is hosted adjacent to internal lithological contacts in the Kawene and Chief Peter intrusions (MacTavish, 1999). It appears reasonable to suggest that the Quetico intrusions and the South Lac des Iles Complex formed via generally similar petrogenetic processes, in which a depleted mantle source with considerable geochemical influence from the subducting slab was melted, resulting in high-energy, vertical magma systems in which concentrically zoned intrusive complexes formed.

The presence of only mafic lithologies in the South Lac des Iles Complex compared to the mafic-ultramafic composition of the Quetico intrusions suggests that different pre-emplacement petrological processes operated. The mafic lithologies of the South Lac des Iles Complex could be the result of magmatic differentiation at depth, or of parent magma generation via a lower degree of partial mantle melting than the Quetico intrusions. The presence of high Ni tenors in sulfide within South Lac des Iles Complex mineralization seems to preclude the early segregation of olivine and/or clinopyroxene, which would preferentially

assimilate Ni. As such, a low degree of partial melting of the mantle seems more reasonable. This interpretation is consistent with an arc andesite as the parent magma for the South Lac des Iles Complex, as has been previously suggested (Barnes and Gomwe, 2010). Pettigrew and Hattori (2006) suggested that the considerable proportion of ultramafic rocks seen within the Quetico intrusions could be the result of steep slab subduction during the Shebandowan orogeny and coincident melting of the depleted mantle in front of the steepened slab. The mafic lithologies within the South Lac des Iles Complex could be the result of a relatively lower degree of partial melting than the Quetico intrusions, possibly due to the influence of a more shallowly subducting slab beneath the Lac des Iles Complex.

The large-scale separation of the breccia and norite domains via flow differentiation does not account for local heterogeneity, in which large variations in the plagioclase/pyroxene proportion are observed over relatively small distances. If flow differentiation was the mechanism by which the breccia and norite domains separated, later-stage influxes of generally compositionally similar magma are the most likely scenario by which internal compositional variability of lithological domains was generated. These magma influxes had to have been occurring episodically both while the South Lac des Iles Complex was still a crystal mush (to account for compositional variability in equigranular, equilibrated areas such as the majority of the norite domain intercepts observed in this study) as well as when the South Lac des Iles Complex was completely or almost completely crystallized (to account for magmatic brecciation). The nature of the later magma pulses were at least partially more pyroxene-rich compared to the rocks the intrusive complex as a whole, as evidenced by the melanocratic nature of the breccia matrix in the Roby Zone (Hinchey et al., 2005). The dominance of

brecciated and heterogeneous lithologies within the portion of the breccia domain near the contact with the norite domain suggest that the greatest amount of late-stage, post-crystallization magma influx occurred along the breccia-norite domain boundary contact and was preferentially focused on the breccia domain. Additionally, some degree of late-stage,

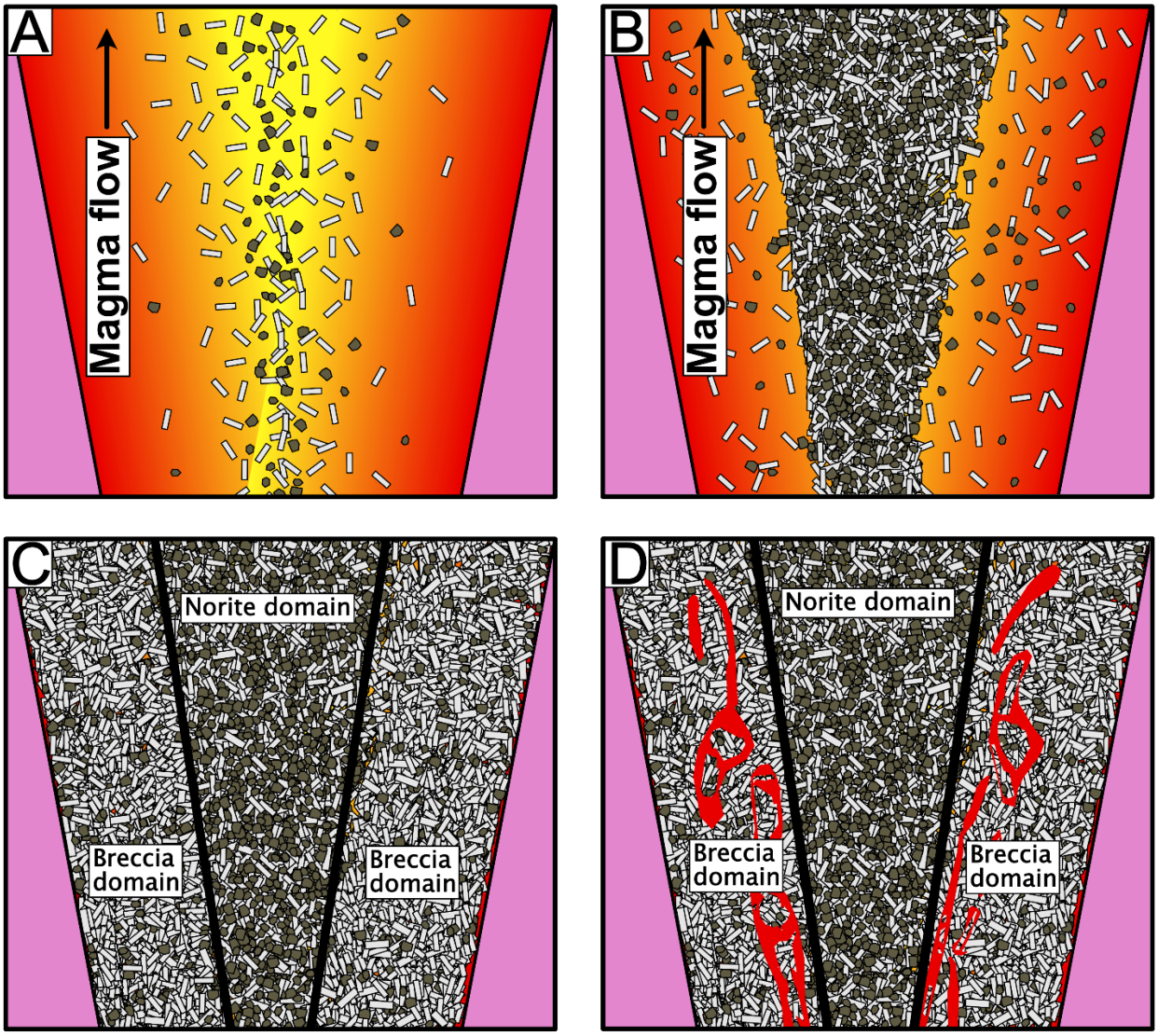

Figure 5.27 – Model for the formation of the breccia and norite domains. A) Early forming crystals concentrate toward the centre of the vertically flowing magma conduit. B) The relatively orthopyroxene-rich accumulation of these early forming crystals forms the norite domain. C) The relatively plagioclase-rich accumulation of later forming crystals forms the breccia domain. D) Late-stage magmatic influx results in brecciation and textural heterogeneity, concentrated in the breccia domain near the contact with the norite domain.

brecciating magma influx had to have also occurred within the norite domain, as evidenced by the interval of brecciated rocks observed within DH# 18-805 (B3 Zone) of this study.

5.4 – Petrogenesis of contact-associated mineralization

Any model for the formation of the Lac des Iles Complex ores must explain 1) the unusual Pd enrichment, typified by the high ratios of Pd to all other PGEs (Pd/Pt = ~10, Pd/Ir = ~10,000; Brugmann et al., 1989; Djon et al., 2018), 2) the presence of mineralization in both strongly altered rocks (chlorite-actinolite schist) and weakly altered rocks (gabbronorites), and 3) the occurrence of highest-grade mineralization in the chlorite-actinolite schist. Although the chlorite-actinolite schist-hosted mineralization was not assessed in this study, assessing models that have been invoked for its formation are helpful in developing a model for the formation of mineralization in the breccia and norite domains.

5.4.1 – Petrogenesis of contact-associated mineralization – Historical work

Brugmann et al. (1989) invoked a model in which hydrothermal fluids partially remelted the crystallized breccia domain, scavenging Pd, Pt, and Au and transporting them upwards. The authors used this model to explain the high Pd/Ir and Pd/Pt ratios of the orebodies by suggesting that Ir, Os, Ru, and to a lesser extent Pt were retained in silicates and/or oxides at a higher degree than Pd during partial remelting.

Barnes and Gomwe (2011) developed a model in which a sulfide liquid was segregated and crystallized in a structural trap in a feeder chamber below the South Lac des Iles Complex, during the formation and solidification of the barren gabbronorite domain and during the early stages of the crystallization of the breccia and norite domains. In this model, a sulfur-

undersaturated magma later passed over the sulfides at depth, partially dissolving the sulfide and preferentially assimilating Cu, Pd, S, and Au. The authors suggested that this magma was then injected into the partially crystallized breccia and norite domains, mixing with the partially crystallized magma and forming the varitextured gabbro and magmatic breccia of the breccia domain. Although this model provides a seemingly reasonable mechanism of formation for mineralization in the magmatic breccia, varitextured gabbronorite, and chlorite-actinolite schist, it does not fully explain Pd enrichment within gabbronorite of the breccia and norite domains that is not varitextured or brecciated.

Schisa et al. (2015) studied halogen content of apatite to develop a model that accounted for high Pd/Pt and Pd/Ir ratios in all economically mineralized lithologies and domains of the Lac des Iles Complex. The authors invoked the enrichment of Cl in apatite in weakly altered rocks as evidence for a Cl-rich hydrothermal fluid that preferentially remobilized Pd in comparison to other PGEs. A main difference between this and other models is that in this model, hydrothermal mobilization of Pd is a high-temperature process that occurred while there was still a significant liquid magma component to the breccia and norite domains, and thus caused Pd enrichment in all economically mineralized zones. This contrasts with the low-temperature hydrothermal processes invoked by other workers that would have occurred after the breccia and norite domains were mostly or completely solidified.

5.4.2 – Petrogenesis of contact-associated mineralization – Genetic model

Nd isotopic data (Section 5.1.3) and S isotopic data (Section 5.2.2) indicate that there is no association between crustal sulfur or overall crustal contamination and mineralization within

either the Offset or Creek Zones. Therefore, variable crustal assimilation cannot explain the formation of mineralized horizons. As discussed in Sections 5.1 and 5.2, variable hydrothermal alteration also cannot explain the distribution of ore zones, as there is strong evidence that that mineralization in the Offset and Creek Zones is associated with primary magmatic sulfides. The similarity of geochemical trends between and within the breccia and norite domains also preclude the mixing of discrete magmas as a formation mechanism of mineralization.

Decharte et al. (2018) discussed a model in which the proximity of major mineralized zones to the Shelby Lake (i.e., Offset Zone) and Roby Central (i.e. Offset and Creek Zones) structures is reflective of these structures being the expressions of magmatic feeder conduits that transported the Lac des Iles magma. In this model, PGEs and Au were preferentially incorporated in sulfides that crystallized proximal to the feeder structures, and sulfides that crystallized as the magma was moving outwards into the periphery of the intrusive complex were less PGE-rich. Pd/S ratio and Pd content are plotted in Figure 5.27; if Pd concentration is solely a function of PGE enrichment in sulfides crystallizing proximal to the feeder structures, Pd/S ratio should decrease with distance from the lithological contacts, which occur near the interpreted feeder structures in the area of the Offset and Creek Zones. This relationship between Pd/S and Pd is inconsistent; a gradational and correlative relationship is observed in the Pd-mineralized norite domain of DH# 17-804 (Offset South Zone), but direct relationships are not observed in any other drill holes.

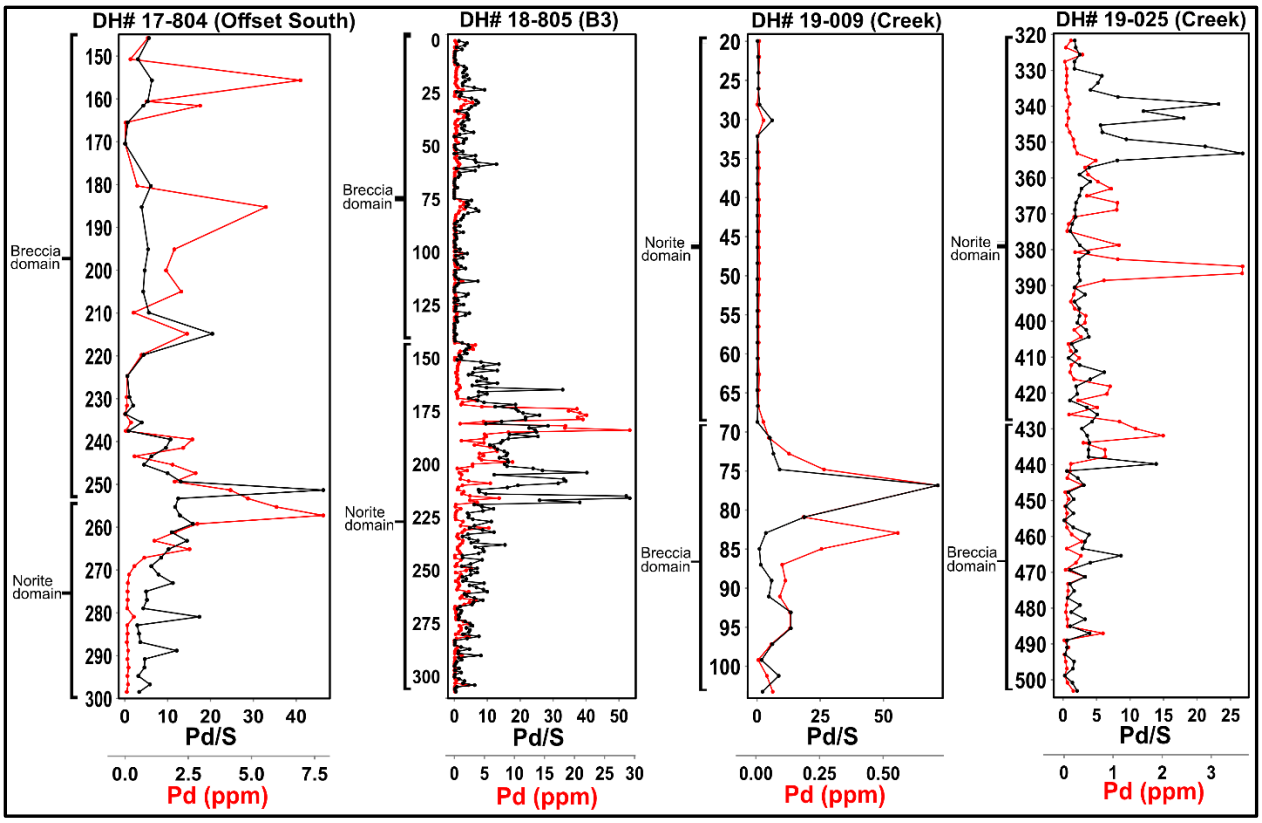

Figure 5.28 – Downhole plots of Pd (ppm) and Pd/S ratio for all studied drill holes.

Phenocryst sorting of a sulfur saturated magma via flow differentiation should result in the concentration of sulfides in the central part of the differentiating intrusion, as the early-forming sulfides are denser than the magma that is entraining them (Chai and Naldrett, 1992; Wang et al., 2006). Despite this, PGE-rich sulfide mineralization associated with internal lithological contacts is observed in several Alaskan-type intrusions, including the Kawene, Chief Peter, and Salt Chuck intrusions (Himmelburg and Loney, 1995; MacTavish, 1999). Flow differentiation alone cannot explain the presence of internal contact-associated mineralization such as that within the South Lac des Iles Complex, which is concentrated along the boundary of the breccia and norite domains. The scarcity of late-stage interstitial silicate phases has led previous authors to suggest that late-stage interstitial silicate magma was exfiltrated from the

South Lac des Iles Complex (Barnes and Gomwe, 2011; Djon et al., 2018). If solidification of the norite domain occurred slightly earlier than the breccia domain, it may be possible that late-stage interstitial fluid could have first been expelled from the norite domain laterally into the breccia domain, before being expelled from the breccia domain into country rocks or upward into the now-eroded portion of the crust. If this occurred, it could be possible that sulfide minerals in the norite domain could have been melted by this fluid or still have been in liquid phase, and been moved laterally toward the contact between the norite and breccia domains. This model, however, does not sufficiently explain how sulfide liquid could become re-entrained and re-deposited in the magmatic, equilibrated assemblages observed in the samples in this study. The textures of the primary magmatic sulfide disseminations, including the close relationship between whole rock Cu and Ni content and the roughly 2:1:1 ratios of pyrrhotite:chalcopyrite:pentlandite seen in most disseminations, appears to argue against late-stage magmatic remobilization of sulfide minerals.

Decharte et al. (2018) noted the proximity of the major mineralized zones to the Shelby Lake and Roby Central structures (Fig. 5.28), which are interpreted to have been the major feeder structures to the South Lac des Iles Complex that have been re-activated as later-stage faults. The most widespread brecciation in the South Lac des Iles Complex is located in the western part of the breccia domain, in proximity to the Shelby Lake structure. Strong brecciation is also observed in the Baker Zone, which is located along the Roby Central structure. Although the compositional heterogeneity distal from the domain boundary contact seems to indicate that some later-stage stage magmatic pulses were not concentrated along these structures, the distribution of brecciation suggest that the latest magmatic pulses were

largely concentrated along the feeder structures and did not significantly infiltrate the rest of the intrusive complex.

The model provided by Barnes and Gomwe (2011), in which a sulfide liquid segregated at depth before remobilization by later magma pulses into the South Lac des Iles Complex, is generally consistent with the data observed in this study. This model provides a reasonable mechanism by which the lowest Cu/Pd and S/Se ratios and highest Pd/S ratios are associated with the highest Pd grades, as magma flowing past a sulfide liquid trapped at depth would partition PGEs into the sulfide liquid. In this case, the physical behaviour of sulfide minerals during flow differentiation of the breccia domain is not relevant to ore formation because most of the sulfide minerals were introduced by late magmatic phases that occurred when the breccia and norite domains were largely to completely crystallized.

The presence of mineralization in the norite domain could then be the result of gravitational crystal settling of sulfides through the breccia-norite domain contact. Known mineralization within the norite domain (Offset Zone, North VT Rim, Creek Zone) is only located in areas where the norite domain is to the south and/or the east of the adjacent breccia domain. If the South Lac des Iles Complex was dipping steeply toward the northwest at the time of emplacement, rather than its current near-vertical orientation, gravitational crystal settling from the breccia domain into the norite domain could have occurred. Late-stage magmatic activity concentrated proximal to the feeder chamber would generate heat, potentially causing the portion of the norite domain closest to the domain boundary contact to not fully crystallize until very late in the magmatic evolution; this could provide the necessary space for sulfide minerals mobilized by late-stage magmatism to percolate through the domain boundary

contact before becoming trapped at the interface between the partially crystallized and fully crystallized portions of the norite domain. The lateral movement of sulfides away from the feeder structure could result in PGE-rich sulfide mineralization crystallizing closer to the contact and PGE-poor mineralization crystallizing at further distances, as suggested by Decharte et al. (2018) and observed in DH# 17-804. However, the absence of this relationship in other drill holes in this study suggests that this process did not occur in all mineralized zones, or that if it did, the distribution of PGEs may have been modified by later magma pulses.

In the drill holes analyzed in this study, Pd-enriched zones proximal to the breccia-norite domain boundary contact in the Offset Zone are associated with high Pd/S ratios, whereas Pd-enriched zones distal from the contacts have similar Pd/S ratios to their surrounding rocks. These zones also have higher Cu/Pd and S/Se ratios than zones of Pd enrichment at domain boundary contacts. As a result, the generation of local Pd enrichment at greater distances from the domain boundary contact appears to be due to the entrainment by magma pulses of sulfide minerals with lower R factors than contact-associated mineralization. If progressive magma pulses were entraining sulfides from the same trapped sulfide source at depth, this suggests that magma pulses that infiltrated portions of the South Lac des Iles Complex distal from the breccia-norite domain boundary contact occurred earlier than magma pulses that infiltrated the area directly surrounding the domain boundary contact. This observation supports the idea that the latest stage of magmatism was focused on the breccia-norite domain boundary contact, and could conceivably have provided heat that kept the boundary of the norite domain semi-liquid and thus potentially permeable for sulfides to percolate through.

Pd-enriched zones from the Creek Zone have higher Cu/Pd and S/Se ratios than samples of similar Pd enrichment from the Offset Zone, which likely indicates that Creek Zone orebodies underwent lower R factors than those in the Offset Zone. Creek Zone orebodies are both smaller (i.e., lower amounts of sulfide) and less Pd-rich than those in the Offset Zone. The cryptic relationship between Cu/Pd, S/Se, and Pd grades in DH# 19-025 may also indicate that contamination by tonalitic country rocks was greater in the Creek Zone, though it does not appear to have been a significant factor influencing mineralization.

The smaller size and lower Pd tenor of Creek Zone deposits may be due to primary structural constraints; the Offset Zone occurs near the junction of the Shelby Lake and Roby Central structures, whereas the Creek Zone occurs along the Roby Central structure but ~2 km from the Shelby Lake structure. The Shelby Lake structure is interpreted to be a major, crustal-scale splay off of the terrane-bounding Quetico fault and is thought to be the main structural conduit that the Lac des Iles magma exploited as it rose through the crust (Decharte et al., 2018). The Roby Central structure is interpreted to have had relatively significant but secondary influence on the primary morphology of the South Lac des Iles Complex, and may or may not have been a secondary magmatic feeder structure (Decharte et al., 2018). The lesser degree of widespread brecciation in the Creek Zone compared to the Offset Zone, along with the lesser overall sulfide content, suggests that late-stage magmatism that entrained PGE-rich sulfides along the breccia-norite domain boundary contact may have been less voluminous along the Roby Central structure than it was along the Shelby Lake structure, resulting in a lesser quantity of PGE-enriched sulfides being emplaced in the Creek Zone. Additionally, if sulfides were remobilized from depth into a Creek Zone in a similar manner to in the Offset Zone, but from a

different reservoir of sulfides at depth (i.e., two discrete pools of segregated sulfides beneath each of the Shelby Lake and Roby Central structures), the higher Cu/Pd and S/Se ratios in the Creek Zone could be the result of lesser silicate-sulfide interaction at depth due to lower magma volumes flowing through the Roby Central structure.

Chapter 6 - Conclusions

All samples analyzed in this study are gabbronorites or norites and their altered equivalents, with most samples falling near the compositional boundary between gabbronorite and norite. Both the breccia and norite domains within both the Offset and Creek Zones crystallized via similar parageneses. In all studied areas, orthopyroxene and plagioclase were the dominant early crystallizing phases, with clinopyroxene also present as a minor early crystallizing phase in some areas. As crystallization progressed, plagioclase remained a major crystallizing phase, the proportion of orthopyroxene decreased, and that of clinopyroxene generally increased despite being only a minor phase in some areas. Biotite, magnetite, chalcopyrite, pentlandite, and pyrrhotite were volumetrically minor, late-crystallizing phases. Distribution of post-crystallization hydrothermal alteration was variable, altering plagioclase to a white mica+chlorite+epidote assemblage at early stages and a chlorite+white mica±quartz assemblage at late stages. Alteration of pyroxene was broadly more intense than the alteration of plagioclase and occurred as a tremolite-actinolite+talc±anthophyllite assemblage at all stages of alteration. Pyrrhotite was variably altered to pyrite, with greater degrees of alteration generally occurring alongside higher silicate alteration intensity.

Geochemical evidence indicates that the South Lac des Iles Complex formed in a magmatic arc setting. This evidence includes enriched LREE patterns, flat HREE patterns, enrichment of LILEs, and depletion of HFSEs, especially Nb. These characteristics can sometimes be generated via crustal contamination of a mantle-derived magma; however, the high Ba/Th and low Yb-normalized Nb/Th ratios of the samples in this study are consistent with melting of

a depleted mantle source in a magmatic arc setting, regardless of the influence of crustal contamination.

Neodymium isotope content indicates that crustal contamination of the South Lac des Iles Complex magma has occurred. ε_{Nd} values of samples in this study (+0.38 to -3.47; median value of -2.13) are uniformly more negative that the ε_{Nd} value of +2.24 expected in a mantle-derived magma that crystallized at ~2.7 Ga, indicating that crustal rocks with negative ε_{Nd} values had to have been incorporated into the magma. No systematic differences in Nd isotope content were observed between the Offset and Creek Zones, between the breccia and norite domains, or between mineralized and unmineralized zones. This lack of correlation suggests that differential crustal contamination between different zones or lithological domains did not occur, and that variable crustal contamination did not affect the presence of sulfide minerals or economic mineralization. The lack of correlation between ε_{Nd} values and elemental concentrations suggests that the crustal contaminant was uniformly mixed in the South Lac des Iles Complex magma.

Available geochemical data for the tonalitic gneiss country rock suggests that it was not the principal crustal contaminant. The similar La/Sm and Nb/Nb* of South Lac des Iles Complex samples to the tonalitic gneiss country rock preclude the trace element characteristics of the South Lac des Iles Complex as being caused by the assimilation of the tonalitic gneiss. ε_{Nd} of one sample of tonalitic gneiss reported by Brugmann et al. (1997) is -1.77, which is not consistent with the country rock being the source of the negative ε_{Nd} values observed in the Offset and Creek Zones. The presence of rocks with strongly negative ε_{Nd} values in the Marmion terrane (e.g., ε_{Nd} = -6.86 in granodiorites of the Obonga Lake greenstone belt; Tomlinson et al., 2004)

suggests that a crustal contaminant at depth could have imparted negative ε_{Nd} values into the South Lac des Iles Complex. However, the heterogeneity of the tonalitic gneiss complex and the lack of comprehensive isotopic data suggests that more work needs to be done to fully exclude the local country rocks as the principal crustal contaminant.

Sulfur isotope analyses do not provide evidence for crustally derived sulfur in any of the ore zones or lithological domains encompassed in this study. $\delta^{34}S$ values range from -0.37‰ to +3.28‰ VCDT (median = +1.11‰), with values from 52 of 54 analyzed crystals occurring in the range of mantle-derived sulfur (0 ± 2‰; Seal, 2006). The $\Delta^{33}S$ values range from -0.02 to -0.11‰ VCDT, which is entirely within the range of mantle-derived sulfur and thus not indicative of mass-independent fractionation. These results do not support crustal sulfur addition, but are not sufficient to rule it out. Sulfur isotope analyses of tonalitic gneiss country rock samples yielded only slightly higher $\delta^{34}S$ and $\Delta^{33}S$ values compared to the values seen in the SLDIC, implying that even significant addition of country rock sulfur would not result in a mass-independent sulfur signature. Masking of mass-independent sulfur isotope values via high R factor is unlikely, as samples with lower R factors (Cu/Pd and/or S/Se ratios within mantle range) do not display different (i.e. more mass-independent) sulfur isotope values compared to samples with higher R factor. The concordance of sulfur isotope values in all analyzed zones and lithological domains suggests that a similar sulfur source is present in all studied areas. The apparent fractionation of sulfur isotopes in the manner expected in magmatic crystallization suggests that sulfide minerals are of primary magmatic origin, and that hydrothermal crystallization of pyrite and/or remobilization of sulfides did not affect sulfur isotope content.

Whole rock geochemistry also provides evidence that major late-stage remobilization of sulfide minerals and PGEs did not occur.

The strong correlation between low Cu/Pd, low S/Se, and high Pd content in the Offset Zone drill holes suggests that mineralization in the Offset Zone is associated with high R factors. The absence of a direct relationship between Cu/Pd, S/Se, and Pd in the Creek Zone is not easily explained, but it may be due to a lesser quantity of sulfide liquid available in comparison to the Offset Zone as a host for segregation of PGEs from silicate magma. This may suggest that the Roby Central structure being a less significant magma conduit than the Shelby Lake structure, during emplacement of the early magma phase that formed the breccia and norite domains as well as during late-stage magma pulses. Differential crustal sulfur assimilation in the Creek Zone is unlikely due to the similar $\delta^{34}S$ and $\Delta^{33}S$ observed in the Offset Zone, but cannot be ruled out due to the similarity of sulfur isotope content between the SLDIC and the country rock. The Creek Zone may also have been produced via melting of a more depleted mantle source than the Offset Zone, as evidenced by lower Yb-normalized Th and Nb content in the Creek Zone. The similarity of the ε_{Nd} values between the Creek and Offset Zones seems to preclude lesser crustal contamination in the Creek Zone as the source of this variation, but more work should be undertaken to investigate this relationship.

The South Lac des Iles Complex shares several compositional similarities to Alaskan-type intrusions, including magmatic arc affinity and concentric zonation with more melanocratic lithologies at the core of the intrusive complex. Similarities with the Alaskan-type Quetico intrusions, including a temporal and spatial association with the Shebandowan orogeny, indicate that the Lac des Iles suite may be coeval with and formed via similar processes to the

Quetico intrusions. The concentric zonation of many Alaskan-type complexes has been invoked to have formed via flow differentiation during vertical magma flow; the distribution of lithologies and apparently high-energy nature of the South Lac des Iles Complex magma suggest that the breccia and norite domain may have formed via the separation of a flowing magma into a more melanocratic core (the orthopyroxene-rich norite domain) and a more leucocratic margin (the plagioclase-rich breccia domain). Geochemical heterogeneity within equilibrated portions of the South Lac des Iles Complex was likely due to later-stage pulses of a magma with similar source characteristics, which intruded when the intrusive complex was only partially crystallized and thus did not result in textural heterogeneity. Magma infiltration continued until the latest stages of crystallization of the intrusive complex; at these late stages, the portion of the intrusive complex proximal to the feeder structures (Shelby Lake and Roby Central structures) was the only portion that was still partially uncrystallized, and magma pulses were therefore focused in these areas. This late-stage magma influx resulted in brecciation and lithological heterogeneity, which was largely concentrated in the breccia domain but also locally affected the norite domain.

The lack of known economic mineralization distal from the domain boundary contacts and feeder structures suggests that the early, most voluminous pulse of magma that crystallized into the bulk of the breccia and norite domains did not carry significant sulfide liquid. This sulfide liquid may have been locally PGE-enriched, but the presence of PGE-poor sulfide-bearing horizons distal from the domain boundary (i.e., Texas Gulf zone) suggest that this enrichment was not uniform. The association of mineralization with brecciation and proximity to feeder structures seems to indicate that the latest-stage magmas carried the bulk

of the economically PGE-enriched sulfide liquid into its present location, consistent with the model of Barnes and Gomwe (2011). This model provides a reasonable explanation for the concentration of PGE enrichment largely within the breccia domain, and the presence of the bulk of mineralization the Roby/Offset Zones is likely due to the influence of the Shelby Lake structure as a primary feeder structure compared to the lesser influence of the Roby Central structure. The presence of mineralization in the norite domain may be due to the sulfide liquid having mobilized into the intrusive complex by late magma pulses physically settling through the breccia-norite domain boundary. This sulfide liquid was able to move through the lithological contact because the portion of the norite domain proximal to the contact was only partially crystallized as a result of heat from the magma pulses; the sulfide liquid could have then concentrated at the interface between the partially and fully crystallized portions of the norite domain.

References

Andersen, J.C.O., Rasmussen, H., Nielsen, T.F.D., and Ronsbo, J.G., 1998. The Triple Group and the Platinova gold and palladium reefs in the Skaergaard Intrusion: Stratigraphic and petrographic relations. Economic Geology, vol. 93, p. 488-509.

Arndt, N., Lesher, C.M., and Barnes, S.J., 2008. Komatiite. Cambridge University Press, 467p.

Ault, W.U. and Jensen, M.L., 1962. Summary of sulfur isotopic standards, *in* Jensen, M.L., ed., Biogeochemistry of Sulfur Isotopes, National Science Foundation Symposium, Yale University, p. 16-29.

Barnes, S.-J., Couture, J.-F., Sawyer, E.W. and Bouchaib, C., 1993. Nickel-copper occurrences in the Belleterre-Angliers belt of the Pontiac Subprovince and the use of Cu-Pd ratios in interpreting platinum-group element distributions. Economic Geology, vol. 88, p. 1402-1418.

Barnes, S.-J. and Gomwe, T.S., 2010. Composition of the Lac des Iles magma and implications for the origin of the ore. 10th International Platinum Symposium, Program Abstracts, Ontario Geological Survey, Miscellaneous Release, Data 269.

Barnes, S.-J. and Gomwe, T.S., 2011. The Pd deposits of the Lac des Iles complex, northwestern Ontario, *in* Li, C. and Ripley, E.M., eds., Magmatic Ni-Cu and PGE Deposits: Geology, Geochemistry, and Genesis. Reviews in Economic Geology, vol. 17, p. 351-370.

Barriere, M., 1976. Flowage differentiation: Limitation of the “Bagnold effect” to the narrow intrusions. Contributions to Mineralogy and Petrology, vol. 55, p. 139-145.

Beinlich, A., von Heydebrand, A., Klemd, R., Martin, L., and Hicks, J., 2020. Desulphurisation, chromite alteration, and bulk rock PGE redistribution in massive chromitite due to hydrothermal overprint of the Panton Intrusion, east Kimberley, Western Australia. Ore Geology Reviews, vol. 118, 103288.

Bhattacharji, S. and Smith, C.H., 1964. Flowage differentiation. Science, vol. 145, p. 150-153.

Blundy, J.D. and Wood, B.J., 1991. Crystal-chemical controls on the partitioning of Sr and Ba between plagioclase feldspar, silicate melts, and hydrothermal solutions. Geochimica et Cosmochimica Acta, vol. 55, p. 193-209.

Boudreau, A., Djon, M.L., Tchalikian, A., and Corkery, J., 2014. The Lac des Iles palladium deposit, Ontario, Canada part 1: The effect of variable alteration on the Offset Zone. Mineralium Deposita, vol. 49, p. 625-654.

Breeding, C.M., Argue, J.J., and Brocker, M., 2004. Fluid-metasedimentary rock interactions in subduction-related zone melange: Implications for the chemical composition of arc magmas. Geology, vol. 32, p. 1041-1044.

Brugmann, G.E., Naldrett, A.J., and Macdonald, A.J., 1989. Magma mixing and constitution zone refining in the Lac des Iles Complex, Ontario; genesis of platinum-group element mineralization. Economic Geology, vol. 84, p. 1557-1573.

Brugmann, G.E., Reischmann, T., Naldrett, A.J., and Sutcliffe, S.H., 1997. Roots of an Archean volcanic arc complex: the Lac des Iles area in Ontario, Canada. Precambrian Research, vol. 81, p. 223-239.

Brzozowski, M.J., Good, D.J., Wu, C., and Li, W., 2021. Iron isotope fractionation during sulfide liquid evolution in Cu-PGE mineralization of the Eastern Gabbro, Coldwell Complex, Canada. Chemical Geology, vol. 576, article 120282.

Cousins, C.A., and Vermaak, C.F., 1976. The contribution of southern African ore deposits to the geochemistry of the platinum group metals. Economic Geology, vol. 71, p. 287-305.

Campbell, D.A., Jonsson, J.R.B., Bautista, S.Y., Dorland, G., Pettigrew, T.K., and Ferguson, S.A., 2023. Report of Activities 2022, Resident Geologist Program, Thunder Bay South Regional Resident Geologist Report: Thunder Bay South District. Ontario Geological Survey, Open File Report 6401, 199p.

Card, K. D., 1990. A review of the Superior Province of the Canadian Shield, a product of Archean accretion. Precambrian Research, vol. 48, p. 99-156.

Card, K.D. and Ciesielski, A., 1986. Subdivisions of the Superior Province of the Canadian Shield. Geoscience Canada, vol. 13, no. 1, p. 5 – 13.

Chai, G. and Naldrett, A.J., 1992. The Jinchuan ultramafic intrusion: Cumulate of a high-Mg basaltic magma. Journal of Petrology, vol. 33, p. 277-303.

De Waal, S.A., Xu, Z., Li, C., and Mouri, H., 2004. Emplacement of viscous mushes in the Jinchuan ultramafic intrusion, western China. Canadian Mineralogist, vol. 42, p. 371-392.

Decharte, D., Hofton, T., Marrs, G., Olson, S., Peck, D., Perusse, C., Roney, C., Taylor, S., Thibodeau, D., and Young, B., 2018. Feasibility study for Lac des Iles mine incorporating underground mining of the Roby Zone. North American Palladium, NI 43-101 Technical Report, 435p.

DePaolo, D.J., 1981. Neodymium isotopes in the Colorado Front Range and crust-mantle evolution in the Proterozoic. Nature, vol. 291, p. 193-196.

DePaolo, D.J., 1988. Neodymium isotope geochemistry: An introduction. Springer-Verlag, 187p.

DePaolo, D.J. and Wasserburg, G.J., 1976. Nd isotopic variations and petrogenetic models. Geophysical Research Letters, vol. 3, No. 5, p. 249-252.

Dickin, A.P., 2005. Radiogenic isotope geology. Cambridge University Press, 492p.

Djon, M.L., 2017. Petrogenesis and metallogenesis of the ultramafic layered North Lac des Iles intrusion in the Lac des Iles Complex, Ontario, Canada. Unpublished doctoral thesis, Queen's University, p. 1-297.

Djon, M.L. and Barnes, S.-J., 2012. Changes in sulfides and platinum-group minerals with the degree of alteration in the Roby, Twilight, and High Grade Zones of the Lac des Iles Complex, Ontario, Canada. Mineralium Deposita, vol. 47, p. 875-896.

Djon, M.L., Olivo, G.R., Miller, J.D., Peck, D.C., and Joy, B., 2017. Stratiform platinum-group element mineralization in the layered Northern Ultramafic Center of the Lac des Iles Intrusive Complex, Ontario, Canada. Ore Geology Reviews, vol. 90, p. 697-722.

Djon, M.L., Peck, D.C., Olivo, G.R., Miller, J.D., and Joy, B., 2018. Contrasting styles of Pd-rich magmatic sulfide mineralization, Lac des Iles Intrusive Complex, Ontario, Canada. Economic Geology, vol. 113, p. 741-767.

Douglas, R.J.W., 1973. Geological Provinces *in* National Atlas of Canada, 4th edition. Department of Energy, Mines, and Resources Canada, Surveys and Mapping Branch, Map 27-28.

Duran, C.J., Barnes, S.-J., and Corkery, J.T., 2015. Chalcophile and platinum-group element distribution in pyrites from the sulfide-rich pods of the Lac des Iles Pd deposits, Western Ontario, Canada: Implications for post-cumulus re-equilibration of the ore and the use of pyrite compositions in exploration. Journal of Geochemical Exploration, vol. 158, p. 223-242.

Duran, C.J., Barnes, S.-J., and Corkery, J.T., 2016. Geology, petrography, geochemistry, and genesis of sulfide-rich pods in the Lac des Iles palladium deposits, western Ontario, Canada. Mineralium Deposita, vol. 51, p. 509-532.

Durazzo, A. and Taylor, L.A., 1982. Exsolution in the MSS-pentlandite system: Textural and genetic implications for Ni-sulfide ores. Mineralium Deposita, vol. 17, p. 313-332.

Eckstrand, O.R. and Hulbert, L.J., 1987. Selenium and the source of sulfur in magmatic nickel and platinum deposits. Geological Association of Canada – Mineralogical Association of Canada, Program Abstracts, vol. 12, p. 40.

Farahat, E.S. and Helmy, H.M., 2006. Abu Hamamid Neoproterozoic Alaskan-type complex, south Eastern Desert, Egypt. Journal of African Earth Sciences, vol. 45, p. 187-197.

Farquhar, J. and Wing, B.A., 2003. Multiple sulfur isotopes and the evolution of the atmosphere. Earth and Planetary Science Letters, vol. 213, p. 1-13.

Grassineau, N.V., Appel, P.W.U., Fowler, C.M.R., and Nisbet, E.G., 2005. Distinguishing biological from hydrothermal signatures via sulphur and carbon isotopes in Archaean mineralisations at 3.8 and 2.7 Ga, *in*, McDonald, I., Boyce, A.J., Butler, I.B., Herrington, R.J., and Polya, D.A., eds, Mineral Deposits and Earth Evolution. Geological Society of London, Special Publication 248, p. 195-212.

Green, T.H. and Pearson, N.J., 1986. An experimental study of Nb and Ta partitioning between Ti-rich minerals and silicate liquids at high pressure and temperature. Geochimica et Cosmochimica Acta, vol. 51, p. 55-62.

Goodwin, A., 1978. Archean crust in the Superior Geotraverse area: Geologic overview, *in* Smith, I.E.M. and Williams, J.G., eds, Proceedings Archean Geochemistry Conference. University of Toronto press, p. 73-106.

Gupta, V.K. and Sutcliffe, R., 1990. Mafic-ultramafic intrusives and their gravity field: Lac des Iles area, northern Ontario. Geological Society of America Bulletin, 102(11), p. 1471-1483.

Hanley, J.J. and Gladney, E.R., 2011. The presence of carbonic-dominant volatiles during the crystallization of sulfide-bearing mafic pegmatites in the North Roby Zone, Lac des Iles Complex, Ontario. Economic Geology, vol. 106, p. 33-54.

Hattori, K.H., Arai, S., and Clarke, D.B., 2002. Selenium, tellurium, arsenic, and antimony contents of primary mantle sulfides. Canadian Mineralogist, vol. 40, p. 637-650.

Hawkesworth, C.J., McDermott, F.P., Turner, S.P., and Peate, D.W., 1997. U-Th isotopes in arc magmas: Implications for element transfer from the subducted crust. Science, vol. 276, p. 551-555.

Heaman, L.M. and Easton, R.M., 2006. Preliminary U/Pb geochronology results: Lake Nipigon Geoscience Initiative. Ontario Geological Survey, Miscellaneous Release – Data 191.

Helmy, H.M., Abd El-Rahman, Y.M., Yoshikawa, M., Shibata, T., Arai, S., Tamura, A., and Kagami, H., 2014. Petrology and Sm-Nd dating of the Genina Gharbia Alaskan-type complex (Egypt): Insights into deep levels of Neoproterozoic island arcs. Lithos, vols. 198-199, p. 263-280.

Himmelberg, G.R. and Loney, R.A., 1995. Characteristics and petrogenesis of Alaskan-type ultramafic-mafic intrusions, Southeastern Alaska. United States Geological Survey, Professional Paper 1564, 47p.

Hinchey, J.G. and Hattori, K.H., 2005. Magmatic mineralization and hydrothermal enrichment of the High Grade Zone at the Lac des Iles palladium mine, northern Ontario, Canada. Mineralium Deposita, vol. 40, p. 13-23.

Hinchey, J.G. Hattori, K.H. and Lavigne, M.J., 2005. Geology, petrology, and controls on PGE mineralization of the southern Roby and Twilight zones, Lac des Iles mines, Canada. Economic Geology, vol. 100, p. 43-61.

Hofmann, A.W.,1997: Mantle geochemistry: The message from ocean volcanism. Nature, vol. 385, p. 219-229.

Impala Platinum Holdings Limited, 2022. Mineral Resource and Mineral Reserve Statement as at 30 June 2022. Impala Platinum Holdings Limited, 107p.

Ionov, D.A. and Hofmann, A.W., 1995. Nb-Ta-rich mantle amphiboles and micas: Implications for subduction-related metasomatic trace element fractionations. Earth and Planetary Science Letters, vol. 131, p. 341-356.

Keays, R.R. and Lightfoot, P.C., 2010. Crustal sulfur is required to form magmatic Ni-Cu sulfide deposits: Evidence from chalcophile element signatures of Siberian and Deccan Trap basalts. Mineralium Deposita, vol. 45, p. 241-257.

Kelly, D.P. and Vaughan, D.J., 1983. Pyrrhotine-pentlandite ore textures: A mechanistic approach. Mineralogical Magazine, vol. 47, p. 453-463.

Kita, N.T., Ushikubo, T., Fu, B., and Valley, J.W., 2009. High precision SIMS oxygen isotope analysis and the effect of sample topography. Chemical Geology, vol. 264, p. 43-57.

Koenders, C. and Petford, N., 2023. Flow differentiation in dykes and sills not limited by intrusion width. EGU General Assembly 2023, Vienna, Austria, Abstract.

Komar, P., 1972. Mechanical interactions of phenocrysts and flow differentiation of igneous dikes and sills. Geological Society of America Bulletins, vol. 83, p. 973-988.

LaFlamme, C., Martin, L., Jeon, H., Reddy, S.M., Selvaraja, V., Caruso, S., Bui, T.H., Roberts, M.P., Voute, F., Hagemann, S., Wacey, D., Littman, S., Wing, B., Fiorenti, M., and Kilburn, M.R., 2016. In situ multiple sulfur isotope analysis by SIMS of pyrite, chalcopyrite, pyrrhotite, and pentlandite to refine magmatic ore genetic models. Chemical Geology, vol. 444, p. 1-15.

Lavigne, M.J. and Michaud, M.J., 2001. Geology of North American Palladium Ltd.'s Roby Zone deposit, Lac des Iles. Exploration and Mining Geology, vol. 10, p. 1-17.

Li, Y., and Liu, J., 2006. Calculation of sulfur isotope fractionation in sulfides. Geochimica et Cosmochimica Acta, vol. 70, p. 1789-1795.

Lorand, J.P., Alard, O., Luguet, A., and Keays, R.R., 2003. Sulfur and selenium systematics of the subcontinental lithospheric mantle: Inferences from the Massif Central xenolith suite (France). Geochimica et Cosmochimica Acta, vol. 67, p. 4137-4151.

Lu, Y., Lesher, C.M., and Deng, J., 2019. Geochemistry and genesis of magmatic Ni-Cu-(PGE) and PGE-(Cu)-(Ni) deposits in China. Ore Geology Reviews, vol. 107, p. 863-887.

MacTavish, A.D., 1999. The mafic-ultramafic intrusions of the Atikokan-Quetico area, Northwestern Ontario. Ontario Geological Survey, Open File Report 5997, 127p.

Maier, W.D., 2005. Platinum-group element (PGE) deposits and occurrences: Mineralization styles, genetic concepts, and exploration criteria. Journal of African Earth Sciences, vol. 41, p. 165-191.

Maier, W.D., Barnes, S.-J., and de Waal, S.A., 1998. Exploration for magmatic Ni-Cu-PGE sulphide deposits: A review of recent advances in the use of geochemical tools, and their application to some South African ores. South African Journal of Geology, vol. 101, No. 3, p. 237-253.

Maier, W.D., Barnes, S.-J., Chinyepi, G., Barton Jr, J. M., Eglington, B., and Setshedi, I., 2007. The composition of magmatic Ni-Cu-(PGE) sulfide deposits in the Tati and Selebi-Phikwe belts of eastern Botswana. Mineralium Deposita, vol. 43, p. 37-60.

McCollough, M.T. and Gamble, J.A., 1991. Geochemical and geodynamical constraints on subduction zone magmatism. Earth and Planetary Science Letters, vol. 102, p. 358-274.

McDonough, W.F. and Sun, S.S., 1995. The composition of the Earth. Chemical Geology, vol. 120, p. 223-253.

Naldrett, A.J., 1999. World-class Ni-Cu-PGE deposits: Key factors in their genesis. Mineralium Deposita, vol. 34, p. 227-240.

Naldrett, A.J., 2004. Magmatic sulfide deposits: Geology, geochemistry, and exploration. Springer, 730p.

Naldrett, A.J., 2010. Secular variation of magmatic sulfide deposits and their source magmas. Economic Geology, vol. 105, p. 669-688.

Park, Y.-R., Ripley, E.M., Miller, J.D., Li, C., Mariga, J., and Shafer, P., 2004. Stable isotopic constraints on fluid-rock interaction and Cu-PGE-S redistribution in the Sonju Lake intrusion, Minnesota. Economic Geology, vol. 99, p. 325-338

Parks, J., Lin, S., Davis, D., and Corkery, T., 2006. New high-precision U-Pb ages for the Island Lake greenstone belt, northwestern Superior Province: implications for regional stratigraphy and the extent of the North Caribou terrane. Canadian Journal of Earth Sciences, vol. 43, p. 789-803.

Pearce, J.A., 1983. Role of the sub-continental lithosphere in magma genesis at active continental margins, *in* Hawkesworth, C.J. and Norry, M.J., eds., Continental Basalts and Mantle Xenoliths. Shiva Publications, p. 230-249.

Pearce, J.A., 2008. Geochemical fingerprinting of oceanic basalts with applications to ophiolite classification and the search for Archean oceanic crust. Lithos, vol. 100, p. 14-48.

Pearce, J.A. and Peate, D.W., 1995. Tectonic implications of the composition of volcanic arc magmas. Annual Review of Earth and Planetary Sciences, vol. 23, p. 251-285.

Pearce, J.A., Stern, R.J., Bloomer, S.H., and Fryer, F., 2005. Geochemical mapping of the Mariana arc-basin system: Implications for the nature and distribution of subduction components. Geochemistry Geophysics Geosystems, vol. 6, No. 7, p. 1-27.

Peck, D.C., Djon, M.L., McLean, C., DeSchutter, G., Maxwell, J., Privet, K., Decharte, D., Roney, C., Huminicki. M., and Stewart, R., 2016. The Lac des Iles PGE-Cu-Ni Deposit, Canada: An organized mega-breccia unit? Institute on Lake Superior Geology, 62nd Annual Meeting Abstract, p. 115.

Percival, J. A., 2007. Geology and metallogeny of the Superior Province, Canada, *in* Goodfellow, W. D., ed., Mineral Deposits of Canada: A Synthesis of Major Deposit-Types, District Metallogeny, the Evolution of Geological Provinces, and Exploration Methods. Geological Association of Canada, Mineral Deposits Division, Special Publication No. 5, p. 903-928.

Percival, J. A., Sanborn-Barrie, M., Skulski, T., Stott, G. M., Helmstaedt, H., and White, D. J., 2006. Tectonic evolution of the western Superior Province from NATMAP and Lithoprobe studies. Canadian Journal of Earth Sciences, vol. 43, p. 1085-1117.

Percival, J.A., Skulski, T., Sanborn-Barrie, M., Stott, G.M., Leclair, A.D., Corkery, M.T., and Boily, M., 2012. Geology and tectonic evolution of the Superior Province, Canada, *in* Tectonic Styles in Canada: The Lithoprobe Perspective. Geological Association of Canada, Special Paper 49, p. 321-378.

Pettigrew, N.T. and Hattori, K.H., 2006. The Quetico Intrusions of Western Superior Province: Neo-Archean examples of Alaskan/Ural-type mafic-ultramafic intrusions. Precambrian Research, vol. 149, p. 21-42.

Polovina, J.S., Hudson, D.M., and Jones, R.E., 2004. Petrographic and geochemical characteristics of postmagmatic hydrothermal alteration and mineralization in the J-M Reef, Stillwater Complex, Montana. Canadian Mineralogist, vol. 42, p. 261-277.

Queffurus, M. and Barnes, S.-J., 2015. A review of sulfur to selenium ratios in magmatic nickel-copper and platinum-group element deposits. Ore Geology Reviews, vol. 69, p. 301-324.

Ripley, E.M. and Li, C., 2003. Sulfur isotope exchange and metal enrichment in the formation of magmatic Cu-Ni-(PGE) deposits. Economic Geology, vol. 98, p. 635-641.

Ripley, E.M. and Li, C., 2013. Sulfide saturation in mafic magmas: Is external sulfur required for magmatic Ni-Cu-(PGE) ore genesis? Economic Geology, vol. 108, p.45-58.

Rudnick, R.L. and Fountain, D.M., 1995. Nature and composition of the continental crust: A lower crustal perspective. Reviews of Geophysics, vol. 33, No. 3, p. 267-309.

Saunders, A.D., Norry, M.J., and Tarney, J., 1991. Fluid influence on the trace element compositions of subduction zone magmas. Philosophical Transactions of the Royal Society of London, vol. 335, p. 377-392.

Schisa, P., Boudreau, A., Djon, M.L., Tchalikian, A., and Corkery, J., 2015. The Lac des Iles palladium deposit, Ontario, Canada, Part II: Halogen variations in apatite. Mineralium Deposita, vo. 50, p. 339-355.

Schulz, K.J., Chandler, V.W., Nicholson, S.W., Piatak, N., Seal II, R.R., Woodruff, L.G., and Zientek, M.L., 2010. Magmatic sulfide-rich nickel-copper deposits related to picrite and (or) tholeiitic basalt dike-sill complexes: A preliminary deposit model. United States Geological Survey, Open File Report 2010-1179, 25p.

Seabrook, C.L., Prichard, H.M., and Fisher, P.C., 2004. Platinum-group minerals in the Raglan Ni-Cu-(PGE) sulfide deposit, Cape Smith, Quebec, Canada. The Canadian Mineralogist, vol. 42, p. 485-497.

Seal, R.R., 2006. Sulfur isotope geochemistry of sulfide minerals. Reviews in Mineralogy and Geochemistry, vol. 61, p. 633-677.

Seat, Z., Beresford, S.W., Grguric, B.A., Gee, M.A.M., and Grassineau, N.V., 2009. Reevaluation of the role of external sulfur addition in the genesis of Ni-Cu-PGE deposits: Evidence from the Nebo-Babel Ni-Cu-PGE deposit, West Musgrave, Western Australia. Economic Geology, vol. 104, p. 521-538.

Shahabi Far, M., Samson, I.M., Gagnon, J.E., Good, D.J., Linnen, R.L., Layne, G.D., and Wing, B.A., 2018. Identifying externally derived sulfur in conduit-type Cu-platinum group element deposits: The importance of multiple sulfur isotope studies. Geology, vol. 46, No. 3, p. 235-238.

Skulski, T., Corkery, M.T., Stone, D., Whalen, J.B., and Stern, R. A., 2000. Geological and geochemical investigations in the Stull Lake-Edmund Lake greenstone belt and granitoid rocks of the northwestern Superior Province, *in* Report of Activities 2000. Manitoba Industry Trade and Mines, Manitoba Geological Survey, p. 117-128.

Sotiriou, P., Polat, A., Frei, R., Yang, X.-M., and van Vessem, J., 2019. A back-arc origin for the Neoarchean megacrystic anorthosite-bearing Bird River Sill and the associated greenstone belt, Bird River subprovince, Western Superior Province, Manitoba, Canada. International Journal of Earth Sciences, vol. 108, p. 2177-2207.

Sproule, R.A., Lambert, D.D., and Hoatson, D.M., 1999. Re-Os isotopic constraints on the genesis of the Sally Malay Ni-Cu-Co deposit, East Kimberley, Western Australia. Lithos, vol. 47, p. 89-106.

Stockwell, C. H., 1972. Revised Precambrian time scale for the Canadian Shield. Geological Survey of Canada, Paper 72-52.

Stone, D., Lavigne, M.J., Schnieders, B., Scott, J., and Wagner, D., 2003. Regional geology of the Lac des Iles area, *in* Summary of Field Work and Other Activities 2003. Ontario Geological Survey, Open File Report 6120, p. 15-1 to 15-25.

Stone, D. and Davis, D.W., 2006. Revised tectonic domains of the south-central Wabigoon subprovince, *in* Summary of Field Work and Other Activities 2006. Ontario Geological Survey, Open File Report 6192, p. 11-1 to 11-18.

Stott, G. M., 1997. The Superior Province, Canada, *in* de Wit, M.J. and Ashwal, L.D., ed., Greenstone Belts. Oxford Monograph on Geology and Geophysics, vol. 35, p. 480-507.

Stott, G. M., Corkery, M. T., Percival, J. A., Simard, M., and Goutier, J., 2010. A revised terrane subdivision of the Superior Province. Summary of Field Work and Other Activities 2010, Ontario Geological Survey, Open File Report 6260, p. 20-1 to 20-10.

Sun, S. and McDonough, W.F., 1989. Chemical and isotopic systematics of ocean basalts: implications for mantle composition and processes. Geological Society of London, Special Publications, vol. 42, p. 313-345.

Sutcliffe, R.H. and Sweeny, J.M., 1986. Precambrian geology of the Lac des Iles Complex, district of Thunder Bay. Ontario Geological Survey, Preliminary Map P.3047, 1:15840.

Sutcliffe, R.H. and Smith, A.R., 1988. Precambrian geology of the plutonic rocks in the Lac des Iles-Tib Lake area, district of Thunder Bay. Ontario Geological Survey, Preliminary Map P.3098, 1:50000.

Sutcliffe, R.H., Sweeny, J.M., and Edgar, A.D., 1989. The Lac des Iles Complex, Ontario: Petrology and platinum-group-elements mineralization in an Archean mafic intrusion. Canadian Journal of Earth Sciences, vol. 26, p. 1408-1427.

Tanaka, T., Togashi, S., Kamioka, H., Amakawa, H., Kagami, H., Hamamoto, T., Yuhara, M., Orihashi, Y., Yoneda, S., Shimizu, H., Kunimaru, R., Takahashi, K., Yanagi, T., Nakano, T., Fujimaki, H., Shinjo, R., Asahara, Y., Tanimizu, M., and Dragusanu, C., 2000. JNdi-1: a neodymium isotopic reference in consistency with LaJolla neodymium. Chemical Geology, vol. 168, p. 279-281.

Thurston, P. C. and Chivers, K. M., 1990. Secular variation in greenstone sequence development emphasizing Superior Province, Canada. Precambrian Research, vol. 46, p. 21-58.

Thurston, P.C., 1991. Archean geology of Ontario, *in* Thurston, P.C., Williams, H.R., Sutcliffe, R.H., and Stott, G.M., eds., Geology of Ontario. Ontario Geological Survey, Special Volume 4, p. 73-78.

Tomlinson, K.Y., Davis, D.W., Stone, D., and Hart, T.R., 2003. U-Pb age and Nd isotopic evidence for Archean terrane development and crustal recycling in the south-central Wabigoon subprovince, Canada. Contributions to Mineralogy and Petrology, vol. 144, p. 684-702.

Tomlinson, K.Y., Stott, G.M., Percival, J. A., and Stone, D., 2004. Basement terrane correlations and crustal recycling in the western Superior Province: Nd isotopic character of granitoid and felsic volcanic rocks in the Wabigoon subprovince, N. Ontario, Canada. Precambrian Research, vol. 132, p. 245-274.

Tornos, F., Galindo, C., Casquet, C., Rodriguez Pevida, L., Martinez, C., Martinez, E., Velasco, F., and Iriondo, A., 2006. The Aguablanca Ni-(Cu) sulfide deposit, SW Spain: Geologic and geochemical controls and the relationship with a midcrustal layered mafic complex. Mineralium Deposita, vol. 41, p. 737-769.

Turner, S., Hawkesworth, C., van Calsteren, P., Heath, E., Macdonald, R., and Black, S., 1996. U-series isotopes and destructive plate margin magma genesis in the Lesser Antilles. Earth and Planetary Science Letters, vol. 142, p. 191-207.

Turner, S., Bourdon, B., and Gill, J., 2003. Insights into magma genesis at convergent margins from U-series isotopes. Reviews in Mineralogy and Geochemistry, vol. 52, p. 255-315.

Vincent, E.A. and Nightingale, G., 1974. Gallium in rocks and minerals of the Skaergaard intrusion. Chemical Geology, vol. 14, p. 63-73.

Wang, C.Y., Zhou, M.-F., and Keays, R.R., 2006. Geochemical constraints on the origin of the Permian Baimazhai mafic-ultramafic intrusion, SW China. Contributions to Mineralogy and Petrology, vol. 152, p. 309-321.

Wei, B., Wang, C.Y., Lahaye, Y., Xie, L., and Cao, Y., 2019. S and C isotope constraints for mantle-derived sulfur source and organic carbon-induced sulfur saturation of magmatic Ni-Cu sulfide deposits in the Central Asian orogenic belt, north China. Economic Geology, vol. 114, p. 787-806.

Weis, D., Kieffer, B., Maerschalk, C., Barling, J., de Jong, J., Williams, G.A., Hanano, D., Pretorius, W., Mattieli, N., Scoates, J.S., Goolaerts, A., Friedman, R.M., and Mahoney, J.B., 2006. High-precision isotopic characterization of USGS reference materials by TIMS and MC-ICP-MS. Geochemistry, Geophysics, Geosystems, vol. 7, No. 8, p. 1-30.

Yuan, C., Sun, M., Wilde, S., Xiao, W., Xu, Y., Long, X., and Zhao, G., 2010. Post-collisional plutons in the Balikun area, East Chinese Tianshan: Evolving magmatism in response to extension and slab break-off. Lithos, vol. 119, p. 269-288.

Zhang, Z., Mao, J., Chai, F., Yan, S., Chen, B., and Pirajno, F., 2009. Geochemistry of the Permian Kalatongke mafic intrusions, northern Xinjiang, northwest China: Implications for the genesis of magmatic Ni-Cu sulfide deposits. Economic Geology, vol. 104, p. 185-203.

Zhang, Z., Tang, Q., Li, C., Wang, Y., and Ripley, E.M., 2017. Sr-Nd-Os-S isotope and PGE geochemistry of the Xiarihamu magmatic sulfide deposit in the Qinqhai-Tibet plateau, China. Mineralium Deposita, vol. 52, p. 51-68.

Zhao, J.-H. and Zhou, M.-F., 2007. Geochemistry of Neoproterozoic mafic intrusions in the Panzhihua district (Sichuan Province, SW China): Implications for subduction-related metasomatism in the upper mantle. Precambrian Research, vol. 152, p. 27-47.

Appendix A

Petrographic Descriptions

Sample: JJ-TS-001		**Drill hole: 17-804**		**Depth: 117.39 m**
Mineral (interpreted pre-alteration)	%	Mineral (actual)	%	Details
Plagioclase	85	Plagioclase	77	0.2-6.0 mm pre-alteration. ~75% of sample consists of >95% cumulate plagioclase; larger crystals tabular and subhedral to anhedral, smaller crystals (<0.7 mm) anhedral and roughly circular, commonly with polygonal triple junctions. Very weakly fractured, rare deformation twinning. Alteration generally very weak, typically as rims and small patches of very fine grained white mica, less commonly as veinlets and larger patches of fine to very grained chlorite±white mica±epidote. Alteration strongest adjacent to altered pyroxene crystals.
		White mica	4	
		Epidote	tr	
		Quartz	tr	
		Carbonate	tr	
Pyroxene	14	Tremolite-actinolite	10	0.4-3.0 mm pre-alteration. Pyroxene is completely replaced by alteration products. Pre-alteration crystal properties are difficult to determine. Very fine-grained tremolite-actinolite aggregates most common, typically rimmed by very fine-grained tremolite-actinolite±chlorite. Tremolite-actinolite±chlorite±quartz also occurs as the main alteration product replacing a minority of pyroxene crystals. Tremolite-actinolite is rarely present as <0.5 mm discrete crystals. Talc is rarely present as <0.1 mm discrete crystals.
		Chlorite	8	
		Talc	tr	
Sulfides	1	Pyrite	1	<0.01 mm-0.4 mm. Clusters of disseminated monosulfide crystals. Rare ~0.1 mm polysulfide crystals also present. Almost all sulfides occur interstitially to very fine-grained aggregates of silicate alteration minerals.
		Chalcopyrite	tr	
Comments: Sample was chosen to represent cumulate plagioclase and is not representative of surrounding area. Massive, cumulate, equilibrated. Altered pyroxene crystals are connected by <1 mm anastomosing veinlets of alteration minerals cutting through plagioclase, most commonly at ~60° to long axis of thin section. Trace very fine-grained carbonate (likely calcite) is present in one of these altered zones.				

Sample: JJ-TS-009		**Drill hole: 17-804**		**Depth: 155.63 m**
Mineral (interpreted pre-alteration)	%	Mineral (actual)	%	Details
Plagioclase	58	Plagioclase	52	0.1-5.0 mm pre-alteration. Dominantly subhedral and tabular, minority of smaller (>0.7 mm) crystals anhedral and equant. Commonly weakly fractured, dominantly at <10° to long axis of thin section. Very weak to weak patchy alteration to white mica±epidote. Common partial chlorite±white mica rims, especially in contact with altered pyroxene.
		Chlorite	7	
		White mica	4	
		Epidote	tr	
Pyroxene	38	Orthopyroxene	tr	0.2-3.0 mm pre-alteration. Pyroxene completely replaced by alteration products, aside from one tremolite-rimmed orthopyroxene core present as a chadacryst in plagioclase. Pre-alteration crystal properties difficult to determine due to chlorite-dominated alteration at crystal margins that commonly extend into adjacent plagioclase crystals. Alteration most commonly present as fine to fine-grained tremolite-actinolite±chlorite aggregates. Talc is present in
		Tremolite-actinolite	33	
		Talc	tr	
		Anthophyllite	tr	

				a small minority of aggregates and as occasional ~0.1 mm discrete crystals. Few 0.3-1.0 mm optically continuous crystals of tremolite and anthophyllite present.
Biotite	0.5	Biotite	0.5	0.01-0.2 mm subhedral to anhedral crystals and very fine-grained aggregates. Rarely in aggregate with chlorite. Appears to be secondary due to distribution and proximity to tremolite-actinolite-chlorite aggregates.
Sulfides	3.5	Pyrrhotite	1.5	Clusters of disseminated and interstitial crystals. Larger (0.2-1.0 mm) interstitial polysulfide crystals generally dominated by pyrrhotite/ pyrite-dominated. Interstitial crystals commonly surrounded by a <1 cm area of <0.1 mm disseminated monosulfide crystals, (chalcopyrite, pyrite, or pyrrhotite) disseminated in silicate alteration mineral aggregates.
		Pyrite	1	
		Chalcopyrite	0.5	
		Pentlandite	0.5	
Magnetite	tr	Magnetite	tr	~0.1 mm crystals that occur adjacent to interstitial polysulfide crystals in a few locations.
Comments: Equilibrated, cumulate, massive. Anastomosing <0.2 mm-wide chlorite±tremolite-actinolite veinlets crosscut sample at 50-65° to long axis of thin section. Larger crystals of both plagioclase and pre-alteration pyroxene partially to completely enclose smaller crystals of plagioclase and pre-alteration pyroxene.				

Sample: JJ-TS-011		**Drill hole: 17-804**		**Depth: 161.65 m**
Mineral (interpreted pre-alteration)	%	Mineral (actual)	%	Details
Plagioclase	50	Plagioclase	43	0.2-5.0 mm. Cumulate, anhedral. Commonly weakly fractured; few crystals moderately fractured at 70° to long axis of thin section, a few of which show <0.1 mm offset. Deformation twinning present in 10% of crystals. Generally very weakly altered to white mica along fractures and in small patches. Chlorite and/or epidote with rare quartz occasionally present at crystal margins, especially adjacent to altered pyroxene. Few crystals in pyroxene-rich zone completely altered to epidote±white mica. Alteration products very fine-grained aside from occasional fine-grained chlorite.
		White mica	4	
		Epidote	1	
		Quartz	tr	
Pyroxene	48	Orthopyroxene	tr	0.2-10.0 mm pre-alteration. Pyroxene is completely replaced, aside from one partially altered clinopyroxene crystal and a ~6 mm area of several partially altered orthopyroxene crystals. Pre-alteration orthopyroxene/ clinopyroxene proportion not discernible. Alteration present as very fine-grained tremolite-actinolite+talc±chlorite. Chlorite occurs mostly as a minor component in aggregates. Discrete 0.5-2.0 mm chlorite crystals also present.
		Clinopyroxene	tr	
		Tremolite-actinolite	27	
		Chlorite	7	
		Talc	15	
Biotite	0.2	Biotite	0.2	0.1-1.5 mm, mostly as a very fine-grained minor component of chlorite±tremolite-actinolite-dominated aggregates, as well as rare >1.0 mm individual crystals adjacent to altered pyroxene.
Sulfides	2	Pyrite	1	Clusters of disseminated monosulfide and interstitial polysulfide crystals. Disseminated crystals (<0.1 mm) of pyrite and/or chalcopyrite occur adjacent to larger (<2
		Pyrrhotite	0.5	
		Chalcopyrite	0.3	

		Pentlandite	0.2	mm) interstitial crystals but are more commonly scattered throughout the sample, most commonly within silicate alteration mineral aggregates.
Magnetite	tr	Magnetite	tr	0.01-0.2 mm crystals, most commonly as <0.5 mm clusters not adjacent to sulfide minerals. Occasional 0.1-0.2 mm crystals in contact with polysulfide crystals.
Comments: Massive, equilibrated, cumulate, biotite only interstitial phase. Variable grain size throughout, dominantly medium-grained. Plagioclase and pre-alteration pyroxene evenly distributed through most of the sample; one corner of thin section (comprising 10% of thin section) consists of 80% altered pyroxene. Larger (>2 mm) plagioclase crystals occasionally partially or completely enclose small (<0.5 mm) plagioclase and altered pyroxene crystals.				

Sample: JJ-TS-014		**Drill hole: 17-804**		**Depth: 175.03 m**
Mineral (interpreted pre-alteration)	%	Mineral (actual)	%	Details
Plagioclase	55	Plagioclase	14	4-30 mm (pegmatitic portion), crystal size difficult to determine in medium-grained portion – appear to have been <5 mm. Pre-alteration crystal properties difficult to determine due to degree of alteration. In medium-grained portion, zones of chlorite+minor white mica that occur adjacent to pseudomorphed pyroxene are interpreted to have originally been plagioclase. Crystals in pegmatitic portion appear to be anhedral with crystal margins partially encircling pyroxene, moderately altered to very fine-grained white mica± chlorite. Weakly fractured, fractures commonly filled by fine-grained chlorite±epidote. Rare <0.1 mm muscovite crystals present in white mica zones.
		White mica	25	
		Chlorite	20	
		Epidote	tr	
Pyroxene	45	Tremolite-actinolite	36	6-25 mm pre-alteration in pegmatitic portion, 1-4 mm pre-alteration in medium-grained portion. Pyroxene completely replaced by alteration minerals. Degree of alteration obscures pre-alteration crystal properties; appear to have been equant in medium-grained section. Optically continuous >10 mm tremolite-actinolite crystals common in pegmatitic portion, commonly enclosing fine-grained, randomly oriented tremolite-actinolite±talc aggregates. Very fine-grained tremolite-actinolite±chlorite±talc aggregates dominant in medium-grained portion. Single 10 mm optically continuous anthophyllite crystal in pegmatitic section surrounding numerous tremolite-actinolite±chlorite aggregates.
		Anthophyllite	3	
		Talc	2	
Sulfides	tr	Pyrite	tr	Very fine-grained (<0.1 mm) monosulfide disseminations present in silicate alteration aggregates, occasionally as <5 mm clusters.
		Chalcopyrite	tr	
Comments: Massive, cumulate, equilibrated, no interstitial silicates. Pegmatitic section (80% of thin section) bound by sharp, undulating contact with medium-grained section (20% of thin section). Pegmatitic section consists of 65% plagioclase and 35% altered pyroxene. Medium-grained section appears to consist of 90% altered pyroxene and 10% altered plagioclase; intensity of alteration in this portion obscures pre-alteration crystal boundaries.				

Sample: JJ-TS-015		**Drill hole: 17-804**		**Depth: 180.50 m**
Mineral (interpreted pre-alteration)	%	Mineral (actual)	%	Details
Plagioclase	62	Plagioclase	42	0.3-8 mm. Anhedral to rarely subhedral, equant to rarely tabular. Minority of crystals weakly fractured, with fractures sometimes filled by chlorite. Consistent moderate alteration to patches and wispy veinlets of very fine-grained white mica±chlorite. Very fine-grained alteration to lath-shaped chlorite present at some of crystal margins, commonly extending from adjacent altered pyroxene. <0.5 mm basal sections of chlorite rarely present.
		White mica	15	
		Chlorite	10	
		Epidote	tr	
Pyroxene	38	Tremolite-actinolite	32	0.3-4.0 mm. Pyroxene has been completely replaced by alteration products. Alteration is mostly pseudomorphic, with <0.3 mm-wide zones of chlorite-dominated alteration commonly obscuring pre-alteration boundaries. Very fine-grained tremolite-actinolite±talc±chlorite aggregates present throughout, with talc and chlorite commonly occurring as a very minor component.
		Talc	1	
Sulfides	tr	Pyrite	tr	Very fine (<0.1 mm) monosulfide disseminations of chalcopyrite or pyrite within silicate alteration aggregates, occasionally within <3 mm clusters. One 2 mm interstitial pyrite+pentlandite crystal.
		Chalcopyrite	tr	
		Pentlandite	tr	
Comments: Massive, cumulate, equilibrated, no interstitial silicates. Variable crystal size, dominantly medium-grained, <1 mm crystals are rare. Anastomosing discontinuous chlorite-dominated veinlets occur at variable orientations, generally >45° to long axis of thin section. Smaller plagioclase/pyroxene crystals occasionally completely encircled by larger plagioclase crystals.				

Sample: JJ-TS-016		**Drill hole: 17-804**		**Depth: 185.16 m**
Mineral (interpreted pre-alteration)	%	Mineral (actual)	%	Details
Plagioclase	60	Plagioclase	56	0.2-7.0 mm. Anhedral to rarely subhedral. Tabular crystals most common, lesser equant and occasional lath-shaped crystals. Majority of crystals weakly fractured, with fractures typically filled by chlorite+tremolite-actinolite. Very weakly altered to very fine-grained patches and discontinuous veinlets of white mica. Small minority of crystals moderately to strongly altered to very fine grained chlorite±epidote±white mica.
		White mica	1	
		Epidote	tr	
Pyroxene	36	Tremolite-actinolite	32	0.1-4.0 mm. Pyroxene completely replaced by alteration products. Pre-alteration crystal boundaries commonly preserved in smaller (<1 mm) crystals; these appear to have been generally subhedral and equant. Pre-alteration properties of larger crystals difficult to determine due to alteration. Very fine-grained tremolite-actinolite±chlorite aggregates present throughout, occasionally with minor talc. Anthophyllite present as several <0.2 mm optically continuous crystals as well as in aggregates alongside chlorite.
		Chlorite	7	
		Anthophyllite	tr	
		Talc	tr	
Biotite	tr	Biotite	tr	Few <0.4 mm lath-shaped crystals, typically associated with

				chlorite.
Sulfides	4	Pyrrhotite	2	Clusters of 0.3-4 mm interstitial polysulfide crystals, typically surrounded by <5 mm areas of <0.1 mm disseminated monosulfide (pyrite or chalcopyrite) crystals.
		Chalcopyrite	1	
		Pentlandite	1	
		Pyrite	tr	
Magnetite	tr	Magnetite	tr	0.1-2.0 mm, occurring in several <5 mm clusters that occur in contact with or in close proximity to polysulfide crystals.
Comments: Massive, cumulate, equilibrated. Variable crystal size throughout, typically fine to medium-grained. Discontinuous fracturing present throughout, most commonly at 65-75° to long axis of thin section. Larger (>4 mm) crystals of plagioclase and relict pyroxene occasionally completely enclose smaller (<0.3 mm) crystals of plagioclase and relict pyroxene.				

Sample: JJ-TS-017		**Drill hole: 17-804**		**Depth: 190.00 m**
Mineral (interpreted pre-alteration)	%	Mineral	%	Details
Plagioclase	35	Plagioclase	tr	Plagioclase is almost completely replaced by alteration. Few <2.0 mm partially intact crystals present on one corner of the thin section, all of which have been largely altered. Very fine-grained chlorite is by far the dominant alteration product, most commonly as monomineralic aggregates. Chlorite aggregates occasionally contain minor amounts of quartz±white mica. Quartz occurs as very fine to fine-grained monomineralic aggregates, commonly with polygonal triple junctions, on a minority of margins between aggregates of chlorite and tremolite-actinolite.
		Chlorite	31	
		Quartz	4	
		White mica	tr	
Pyroxene	62	Tremolite-actinolite	62	Pyroxene is completely replaced by alteration products. Pre-alteration crystal properties are indiscernible aside from a few <0.5 mm crystals in which relict equant shape has been preserved. Monomineralic tremolite-actinolite aggregates are dominant, with minor quantities of chlorite±talc sometimes present as a minor component. Occasional optically continuous actinolite crystals up to 3 mm in size.
		Talc	tr	
Biotite	tr	Biotite	tr	Few <0.2 mm platy crystals, surrounded by chlorite and/or actinolite.
Sulfides	2.5	Pyrrhotite	1	0.2-3.0 mm interstitial polysulfide crystals commonly surrounded by <5 mm areas of <0.1 mm disseminated monosulfide crystals, the latter of which are also scattered throughout sample within silicate alteration mineral aggregates
		Chalcopyrite	0.5	
		Pentlandite	0.5	
		Pyrite	0.5	
Magnetite	0.5	Magnetite	0.5	Interstitial 0.2-2.0 crystals, generally with sharp straight edges. Occasionally heavily fractured with chalcopyrite filling fractures. Rare disseminated <0.05 mm crystals present alongside sulfides in silicate alteration aggregates.
Comments: No pervasive foliation. Pre-alteration crystal boundaries and texture are very difficult to determine due to intensity of alteration				

Sample: JJ-TS-018	**Drill hole: 17-804**	**Depth: 195.00 m**

Mineral (interpreted pre-alteration)	%	Mineral	%	Details
Plagioclase	75	Plagioclase	71	0.2-8.0 mm. Anhedral, typically equant, rarely tabular. Generally very weakly altered to small patches of white mica±epidote±chlorite. A small minority (~5%) of crystals are moderately to almost completely altered to white mica. Crystal margins generally unaltered, and occasionally altered to <0.1 mm-wide partial rims of white mica. Muscovite occasionally occurs as <0.2 mm platy crystals adjacent to white mica alteration.
		White mica	4	
		Chlorite	tr	
		Epidote	tr	
Ortho-pyroxene	15	Orthopyroxene	12	0.2-4.0 mm. Equant and subhedral throughout. Majority of crystals very weakly altered to <0.1 mm patches of tremolite-actinolite±chlorite± talc. Minority of crystals completely replaced by tremolite-actinolite±chlorite Tremolite-actinolite commonly present as <1 mm optically continuous crystals. Talc also present as very-fine grained monomineralic alteration at crystal margins.
		Tremolite-actinolite	5	
		Talc	tr	
Clino-pyroxene	10	Clinopyroxene	8	3.0-7.0 mm. Typically equant and subhedral, less commonly elongate and irregularly shaped. Weakly to moderately altered to tremolite- actinolite±chlorite±talc.
Sulfides	tr	Pyrite	tr	Sparsely disseminated <0.3 mm pyrite± chalcopyrite crystals, mostly in silicate alteration aggregates. Rare interstitial polysulfide crystals.
		Chalcopyrite	tr	
		Pentlandite	tr	
		Pyrrhotite	tr	
Comments: Cumulate, equilibrated, no interstitial silicates. Massive, no veining or pervasive fracturing present. Highly variable crystal size, commonly with very fine/fine/medium-grained crystals in contact. Larger (>4 mm) pyroxene/altered pyroxene and plagioclase crystals commonly partially to completely enclose <2 mm pyroxene/altered pyroxene and plagioclase crystals.				

Sample: JJ-TS-019		**Drill hole: 17-804**		**Depth: 200.52 m**
Mineral (interpreted pre-alteration)	%	Mineral	%	Details
Plagioclase	60	Plagioclase	52	0.2-4.0 mm. Anhedral, equant to tabular. Contacts between plagioclase crystals, where present, range from straight to wavy and undulating. Plagioclase most commonly weakly altered to patches, and less commonly partial rims, of very fine-grained white mica±epidote. Plagioclase is less commonly moderately to strongly altered to very fine-grained white mica±chlorite±epdiote, typically in more pyroxene-rich portions of the sample.
		White mica	3	
		Epidote	1	
Pyroxene	40	Orthopyroxene	1	Almost all pyroxene crystals completely replaced by alteration minerals. Original crystal shapes generally retained, typically equant and subhedral to anhedral. Few <1.0 mm unaltered orthopyroxene crystals are present on one edge of thin section. Few partially unaltered orthopyroxene crystals present throughout the sample. Alteration present as very fine-grained aggregates of tremolite-actinolite±chlorite±talc. Talc is most common where pyroxene has only been partially replaced.
		Tremolite-actinolite	36	
		Chlorite	6	
		Talc	tr	

				Anthophyllite present as a few <1.5 mm optically continuous crystals.
Biotite	tr	Biotite	tr	<0.2 mm platy crystals, typically associated with tremolite-actinolite and/or chlorite.
Sulfides	tr	Chalcopyrite	tr	Most commonly <0.05 mm disseminated monosulfide chalcopyrite, pyrite, and pentlandite crystals within silicate alteration mineral aggregates. Rare interstitial <0.3 mm polysulfide crystals.
		Pyrite	tr	
		Pentlandite	tr	
		Pyrrhotite	tr	
Magnetite	1	Magnetite	1	Most commonly as 0.3-2.0 mm interstitial crystals with sharp, jagged boundaries. Larger interstitial crystals are heavily fractured. Disseminated <0.05 mm crystals also present within silicate alteration aggregates.
Comments: Cumulate, equilibrated, biotite is the only accessory silicate. Massive, no fracturing or veining present. Variable crystal size; most commonly fine-grained, with gradational transitions to lesser medium-grained material. Larger (>1.5 mm) plagioclase crystals occasionally partially encircle smaller (<0.4 mm) altered pyroxene crystals.				

Sample: JJ-TS-025		**Drill hole: 17-804**		**Depth: 230.70 m**
Mineral (interpreted pre-alteration)	%	Mineral (actual)	%	Details
Plagioclase	65	Plagioclase	63	1-4 mm pre-alteration. Generally unaltered. Anhedral, equant to slightly elongate shape. Commonly moderately fractured. Occasional partial rims/laths of very fine-grained white mica extending from borders of altered pyroxene and rarely filling fractures. Quartz present as trace component of fracture-filling alteration.
		Chlorite	3	
		White mica	1	
		Quartz	tr	
Pyroxene	35	Clinopyroxene	tr	0.5-4 mm pre-alteration. Almost completely replaced by alteration minerals. Pre-alteration texture generally preserved, appearing equant and subhedral. Alteration present as tremolite-actinolite±talc±chlorite. Tremolite-actinolite occasionally occurs as continuous <1.5 mm crystals. Few intact <0.2 mm clinopyroxene cores.
		Tremolite-actinolite	24	
		Talc	8	
		Anthophyllite	1	
Sulfides	tr	Chalcopyrite	tr	0.01-0.2 mm monosulfide crystals, typically in clusters alongside silicate alteration minerals that are interstitial to primary silicate crystals.
		Pyrite	tr	
Comments: Massive, equilibrated, cumulate texture with no accessory minerals aside from sulfides. Plagioclase occasionally partially encloses altered pyroxene. Moderately fractured (2 sets of fractures, perpendicular and 40 degrees to long axis of thin section). Minority of fractures filled with plagioclase±chlorite±quartz±tremolite-actinolite.				

Sample: JJ-TS-026		**Drill hole: 17-804**		**Depth: 236.52 m**
Mineral (interpreted pre-alteration)	%	Mineral (actual)	%	Details
Plagioclase	65	Plagioclase	65	0.2-2.5 mm pre-alteration. Anhedral, smaller crystals are equant, larger crystals are tabular. Rarely fractured, few crystals near fracture display deformation twinning. Typically unaltered. Very minor alteration to white mica±chlorite as occasional pits and along contacts with
		Chlorite	1	
		White mica	tr	

				altered pyroxene.
Ortho-pyroxene	30	Orthopyroxene	22	0.1-1.0 mm pre-alteration. Dominantly subhedral to euhedral, occasionally anhedral. Dominantly equant, minority of crystals are elongate. Pyroxene ranges from unaltered to completely altered, most commonly very weakly altered. Alteration occurs as optically continuous tremolite-actinolite or anthophyllite crystals, and very fine-grained aggregates of actinolite±talc±chlorite.
		Tremolite-actinolite	7	
		Talc	2	
		Anthophyllite	1	
Clino-pyroxene	5	Clinopyroxene	2	0.5-1.0 mm. Similar properties and alteration style to orthopyroxene.
Sulfides	0.2	Chalcopyrite	0.1	>0.01 mm-0.1 mm. Dominantly interstitial polysulfide crystals; pyrite and chalcopyrite also present as very fine-grained monosulfide crystals adjacent to silicate alteration products.
		Pyrite	0.1	
		Pyrrhotite	tr	
Comments: Equilibrated, massive, adcumulate texture with no accessory minerals aside from sulfides. Crystal size is highly variable. Plagioclase commonly partially or completely encloses pyroxene, and occasionally encloses smaller plagioclase crystals. Single anastomosing fracture at 40 degrees to long axis of thin section, filled by chlorite+actinolite+talc.				

Sample: JJ-TS-027		**Drill hole: 17-804**		**Depth: 240.61 m**
Mineral (interpreted pre-alteration)	%	Mineral (actual)	%	Details
Plagioclase	40	Plagioclase	30	0.3-3.0 mm. Equant and anhedral where unaltered. Commonly fractured, with fractures filled by alteration products. Alteration is more pervasive in pegmatitic portion (only two grains in this portion were not completely altered). Alteration present as very fine to fine-grained chlorite±white mica±epidote aggregates that completely replace one or more plagioclase crystals. White mica most commonly occurs as rims or within pits of partially altered plagioclase.
		Chlorite	11	
		White mica	3	
		Epidote	1	
Pyroxene	57	Tremolite-actinolite	45	0.4-15 mm pre-alteration. Pyroxene has been completely altered, with original grain boundaries typically preserved. Alteration most commonly present as fine-grained tremolite-actinolite±talc±chlorite aggregates. Tremolite-actinolite and chlorite also occur as coarser individual crystals (<1 mm). A fine-grained aggregate of anthophyllite+talc was observed in one location.
		Talc	7	
		Anthophyllite	tr	
Sulfides	3	Pyrite	2	Pyrite generally as >0.3 mm crystals, also as disaggregated groups of >0.1 mm crystals. Chalcopyrite and pentlandite occur as disaggregated groups of >0.1 mm crystals. Occasional polysulfide (chalcopyrite+pyrite) crystals. 95% of sulfides occur on pegmatitic portion.
		Chalcopyrite	1	
		Pentlandite	tr	
Oxides	0.3	Magnetite	0.2	0.05-2.0 mm, generally in clusters with/adjacent to sulfides. Ilmenite consistently observed as exsolution from magnetite.
		Ilmenite	0.1	
Comments: Equilibrated, adcumulate texture, no interstitial silicates. 60% of sample is pegmatitic, 40% is medium grained. Contact between pegmatitic and medium grained areas is undulating and equilibrated. Pegmatitic section has a higher proportion of pre-alteration pyroxene (65%) that medium grained section (45%).				

Sample: JJ-TS-028		**Drill hole: 17-804**		**Depth: 242.20 m**
Mineral (interpreted pre-alteration)	%	Mineral (actual)	%	Details
Plagioclase	64	Plagioclase	61	0.3-5.0 mm. Cumulate, generally anhedral. Several <0.5 mm subhedral crystals occur as chadacrysts within an altered pyroxene crystal. Generally equant, occasionally tabular. Typically weakly to moderately fractured. Minor alteration to very fine-grained white mica and/or fine-grained chlorite, with both occurring as partial rims and fracture fill. Chlorite alteration mostly occurs at boundaries to altered pyroxene.
		White mica	2	
		Chlorite	2	
		Epidote	tr	
Pyroxene	35	Tremolite-actinolite	30	0.2-1.5 mm. Primary pyroxene has been completely altered. Boundaries of original crystals are generally recognizable and appear to have been equant. Alteration occurs as fine-grained aggregates of tremolite-actinolite+chlorite±talc, and fine to very fine-grained rims and veinlets of chlorite.
		Talc	5	
Biotite	tr	Biotite	tr	0.1-0.3 mm. Two crystals observed in contact with plagioclase, epidote, and chlorite. Difficult to determine if primary.
Sulfides	0.5	Pyrite	0.3	Mostly present as finely disseminated (<0.1 mm) monosulfide crystals of pyrite or chalcopyrite occurring within silicate alteration aggregates. Rare <0.2 mm blebs pyrite+pentlandite or pyrite+chalcopyrite also present within silicate alteration aggregates.
		Chalcopyrite	0.2	
		Pentlandite	tr	
Magnetite	tr	Magnetite	tr	Very finely disseminated (0.02 mm) crystals rarely occurring as a minor component within silicate alteration aggregates.
Comments: Equilibrated, massive, adcumulate texture. Variable crystal size, ranging from fine to coarse. Larger plagioclase crystals occasionally partially or completely encircle pyroxene and smaller plagioclase crystals, and larger pyroxene crystals occasionally completely encircle smaller plagioclase crystals.				

Sample: JJ-TS-029		**Drill hole: 17-804**		**Depth: 244.40 m**
Mineral (interpreted pre-alteration)	%	Mineral (actual)	%	Details
Plagioclase	60	Plagioclase	50	Cumulate, anhedral, generally equant to occasionally tabular. Weakly to moderately fractured. Larger fractures that extend along the entire thin section commonly filled by white mica±chlorite±actinolite. White mica alteration is present within <0.5 mm pits of most crystals, and less commonly as partial rims. Fine-grained chlorite aggregates commonly replace rims of plagioclase, occasionally replacing entire crystals. Epidote present as <0.3 mm fine to very fine-grained aggregates, generally surrounded by white mica and/or chlorite.
		Chlorite	8	
		White mica	4	
		Epidote	tr	
Pyroxene	40	Tremolite-actinolite	36	Primary pyroxene has been completely altered. Boundaries of original crystals are roughly preserved and appear to have been equant and likely anhedral. Monomineralic fine-grained tremolite-actinolite aggregates most common. Fine to very-fine grained aggregates of tremolite-actinolite±talc±chlorite are also present.
		Talc	2	

Sulfides	tr	Chalcopyrite	tr	Very finely disseminated (<0.1 mm) crystals in silicate mineral alteration aggregates, generally occurring in <3 mm clusters but present throughout sample. Almost always monosulfide chalcopyrite or pyrite crystals, rarely polysulfide chalcopyrite+pyrite crystals.
		Pyrite	tr	
Comments: Equilibrated, adcumulate texture, no interstitial silicates. Crystal size ranges from fine to medium throughout, with no spatial trends observed. Three fractures filled with chlorite and/or tremolite-actinolite crosscut sample at 50-65 degrees to the thin section long axis.				

Sample: JJ-TS-030		**Drill hole: 17-804**		**Depth: 246.56 m**
Mineral (interpreted pre-alteration)	%	Mineral (actual)	%	Details
Plagioclase	60	Plagioclase	53	Cumulate, anhedral, equant. Alteration intensity is directly proportional to proximity to altered pyroxene; weak alteration rims to white mica and/or chlorite are common at boundaries with pyroxene, and crystals in pyroxene-rich areas are mostly completely altered to chlorite±white mica. Plagioclase-plagioclase crystal boundaries are usually unaltered and occasionally very weakly altered to thin rims of white mica and/or chlorite. Pits of weak white mica alteration occur throughout the section, regardless of proximity to pyroxene.
		Chlorite	8	
		White mica	2	
Pyroxene	40	Tremolite-actinolite	35	Primary pyroxene has been completely altered. Boundaries of original crystals are roughly preserved and appear to have been equant. Crystals appear to have been generally anhedral. Alteration mostly occurs as fine to very fine-grained aggregates of tremolite-actinolite± chlorite±talc. A few <0.3 mm optically continuous individual crystals of anthophyllite and tremolite-actinolite are present.
		Talc	2	
		Anthophyllite	0.5	
Sulfides	tr	Chalcopyrite	tr	Very finely disseminated (<0.05 mm) monosulfide (chalcopyrite or pyrite) crystals present in silicate alteration mineral aggregates, typically in <3 mm clusters. Rare <0.1 mm interstitial chalcopyrite+ pyrite crystals.
		Pyrite	tr	
Comments: Weakly developed glomerophyric texture, in which both plagioclase and pyroxene (pre-alteration) most commonly occur in groups of crystals. Groups of pyroxene crystals are weakly aligned roughly perpendicular to the long axis of the thin section. Crystal size ranges from fine to more commonly medium to coarse, with no spatial variation observed. Larger crystals of plagioclase rarely partially or completely enclose smaller plagioclase or pyroxene crystals. Inconsistent fracturing occurs at <20 degrees to long axis of thin section, angled both “NE” and “NW” to long axis.				

Sample: JJ-TS-031		**Drill hole: 17-804**		**Depth: 248.69 m**
Mineral (interpreted pre-alteration)	%	Mineral (actual)	%	Details

Plagioclase	58	Plagioclase	52	Cumulate, anhedral. Equant except for >5 mm crystals, which are tabular. Alteration intensity is weak to locally moderate. Very fine to fine white mica±chlorite occurs as pits and along fractures; alteration rims are not observed. Fine-grained chlorite aggregates occasionally partially or completely replace plagioclase.
		Chlorite	7	
		White mica	1	
Pyroxene	42	Tremolite-actinolite	37	Primary pyroxene is completely replaced by alteration products. Original crystal form is difficult to discern due to alteration. A few altered crystals retain grain boundaries with surrounding plagioclase and appear to have been equant. Fine to very fine-grained tremolite-actinolite±talc±chlorite is the most common alteration product, with original crystal boundaries commonly rimmed by fine-grained chlorite. Fine to very fine-grained monomineralic tremolite-actinolite aggregates are also present.
		Talc	3	
Sulfides	0.3	Chalcopyrite	0.2	Typically <0.05 mm monosulfide chalcopyrite or pyrite crystals, typically in <4 mm clusters. 0.1-0.7 mm interstitial polysulfide crystals also present, typically surrounded by halo of monosulfide crystals.
		Pyrite	0.1	
		Pentlandite	tr	
		Pyrrhotite	tr	
Magnetite	tr	Magnetite	tr	Few <0.02 mm disseminated crystals in silicate alteration aggregates, occurring in sulfide mineral clusters. Crystals are generally tabular with sharp, straight boundaries.
Comments: Cumulate, massive, equilibrated. Variable grain size; plagioclase and altered pyroxene ranging from fine to coarse-grained comprises 65% of thin section, medium-grained to pegmatitic plagioclase and altered pyroxene comprises other 35% of thin section. Boundary between fine and coarse-grained portions is sharp, undulating, and equilibrated.				

Sample: JJ-TS-032		**Drill hole: 17-804**		**Depth: 250.70 m**
Mineral (interpreted pre-alteration)	%	Mineral (actual)	%	Details
Plagioclase	55	Plagioclase	50	0.2-5.0 mm. Equant, generally anhedral; a few subhedral to euhedral crystals occur as chadacrysts within altered pyroxene. Alteration intensity is very weak to locally weak. White mica present mostly as very fine-grained aggregates in pits within plagioclase, occasionally occurring alongside chlorite. Chlorite dominantly occurs as fine-grained partial rims.
		Chlorite	8	
		White mica	1	
Pyroxene	45	Tremolite-actinolite	38	Primary pyroxene has been completely replaced by alteration products. Pre-alteration crystals appear to have been 0.2-8.0 mm, equant and anhedral to subhedral. Alteration present as fine to very fine-grained aggregates of tremolite-actinolite±chlorite±talc. In several locations, optically continuous single tremolite-actinolite crystals occur as rims around tremolite-actinolite±talc±chlorite aggregates.
		Talc	3	
Biotite	tr	Biotite	tr	One 0.2 mm crystal observed, surrounded by chlorite-tremolite-actinolite alteration.
Sulfides	0.2	Chalcopyrite	0.1	Disseminated crystals typically occurring in <3 mm clusters. <0.05 mm monosulfide chalcopyrite and pyrite crystals
		Pyrite	0.1	

		Pentlandite	tr	sometimes surround <0.3 mm polysulfide crystals. Sulfide crystals dominantly occur in silicate alteration mineral aggregates; larger crystals may have originally been interstitial.
		Pyrrhotite	tr	
Comments: Cumulate, equilibrated, massive. Somewhat variable crystal size, typically fine to medium-grained. Three coarse-grained to pegmatitic altered pyroxene crystals are observed, which completely encircle fine-grained plagioclase crystals.				

Sample: JJ-TS-033		**Drill hole: 17-804**		**Depth: 252.72 m**
Mineral (interpreted pre-alteration)	%	Mineral (actual)	%	Details
Plagioclase	60	Plagioclase	3	Plagioclase has been almost completely replaced by alteration assemblage; observed unaltered crystals are present as cores that have been largely altered. Crystal habit, shape, and size are not discernible. Alteration present as very fine-grained white mica±chlorite aggregates and very fine to fine-grained chlorite±quartz. Chlorite commonly occurs as randomly oriented laths, and less commonly as radial laths or >1 mm crystals.
		Chlorite	43	
		White mica	16	
		Quartz	5	
		Epidote	tr	
Pyroxene	40	Tremolite-actinolite	30	Completely replaced by alteration products, pre-alteration shape, size, and habit are not discernible. Alteration present as fine to very fine-grained tremolite-actinolite±chlorite±talc aggregates. Talc is most commonly present as <0.1 mm single crystals or crystal aggregates.
		Talc	3	
Sulfides	tr	Pyrite	tr	<0.1 mm disseminated crystals in silicate alteration mineral aggregates, occurring in <3 mm clusters and lesser discrete crystals. Typically monosulfide pyrite or chalcopyrite crystals, rare chalcopyrite+pyrite crystals.
		Chalcopyrite	tr	
Oxides	tr	Magnetite	tr	<0.5 mm crystals, most commonly within <0.5 mm of sulfide minerals and less commonly occurring without nearby sulfides. Magnetite commonly partially surrounded by irregular rims of ilmenite.
		Ilmenite	tr	
Comments: Degree of alteration makes it very difficult to provide estimates of original mineralogy and texture. Alteration minerals display mm to cm-scale alignment in various directions but no pervasive foliation observed. No fracturing observed. Series of undulating, discontinuous veinlets crosscut sample at 5-10° to the long axis of the thin section, filled by tremolite-actinolite±talc±chlorite.				

Sample: JJ-TS-034		**Drill hole: 17-804**		**Depth: 254.06 m**
Mineral (interpreted pre-alteration)	%	Mineral (actual)	%	Details
Plagioclase	45	Plagioclase	35	0.2-4.0 mm pre alteration. Cumulate, equant to tabular. Crystal shape obscured by alteration but appears to generally be anhedral. Crystals commonly weakly fractured, either at 60-75° to long axis of thin section or along cleavage planes. Majority of crystals weakly altered to patches and veinlets of very fine-grained white mica±chlorite± epidote. Minority of crystals are partially to completely replaced by very fine to fine-grained chlorite. Some crystals that have been dominantly altered by
		Chlorite	12	
		White mica	8	
		Epidote	tr	

				chlorite show undulose extinction. Deformation twinning present in a few crystals.
Pyroxene	50	Tremolite-actinolite	43	0.2-3.0 mm pre-alteration. Pyroxene completely replaced by alteration products. Pre-alteration crystal shape and habit obscured by alteration. Crystal shape is best preserved where present as altered chadacrysts in plagioclase, appearing equant and subhedral. Alteration occurs as very fine to fine-grained tremolite-actinolite±chlorite± talc aggregates, ranging from unidirectional acicular aggregates (more common where surrounded by plagioclase) to randomly oriented crystals (more common in pyroxene clusters).
		Talc	2	
Hornblende	tr	Hornblende	tr	Two adjacent 0.5 mm crystals with light to dark green pleochroism and high first-order birefringence. Partially altered to talc+chlorite+ tremolite-actinolite.
Sulfides	1	Pyrite	0.5	Dominantly disseminated crystals in sulfide alteration mineral aggregates, especially in a 1 cm by 1 cm area in one corner of thin section. Disseminated crystals present as <0.1 mm chalcopyrite and pyrite monosulfide crystals and fine <1.0 mm polysulfide crystals, typically in <3 mm clusters.
		Chalcopyrite	0.3	
		Pyrrhotite	0.2	
		Pentlandite	tr	
Magnetite	tr	Magnetite	tr	Present as <0.3 mm irregularly shaped interstitial crystals, as well as disseminated <0.05 mm crystals in actinolite-dominated silicate alteration aggregates. No association with sulfides.
Comments: Cumulate, equilibrated, massive. Typically fine to medium-grained, with some smaller crystals present as chadacrysts of plagioclase and pyroxene and interstitial plagioclase. ~4 mm-wide anastomosing vein, composed mostly of chlorite alongside lesser tremolite-actinolite, crosscuts sample at ~50° to long axis of thin section. >3.0 mm +plagioclase crystals commonly completely encircle <0.3 mm altered pyroxene crystals.				

Sample: JJ-TS-035		**Drill hole: 17-804**		**Depth: 254.13 m**
Mineral (interpreted pre-alteration)	%	Mineral (actual)	%	Details
Plagioclase	38	Plagioclase	33	0.2-8.0 mm. Smaller crystals are equant, coarse-grained to pegmatitic crystals are tabular. Intact crystals only present on half of the thin section (less altered side of chlorite-quartz veinlet). Weakly altered to white mica±chlorite±epidote as pits and along fractures. Several crystals located <8 mm from veinlet show deformation twinning.
		White mica	2	
		Epidote	tr	
Pyroxene	61	Tremolite-actinolite	48	Primary pyroxene has been completely altered. Aside from few <0.5 mm crystals on plagioclase-bearing portion of sample that appear to have been subhedral and equant, crystal size/shape/ habit are difficult to discern due to degree of alteration. Fine to usually very fine-grained tremolite-actinolite-talc±chlorite aggregates dominate the strongly altered portion of the thin section. In the less altered portion, tremolite-actinolite occurs as fine to medium-grained aggregates and discrete <0.5 mm crystals, and chlorite occurs as fine-grained aggregates. Talc also occurs as discrete <0.5 mm crystals on both sides.
		Chlorite	11	
		Talc	5	

Biotite	tr	Biotite	tr	Few <0.2 mm crystals, surrounded by chlorite-tremolite-actinolite alteration.
Sulfides	1	Pyrite	0.4	Interstitial <0.5 mm polysulfide crystals and monosulfide (pyrrhotite, pyrite, or chalcopyrite) crystals. Disseminated <0.1 mm crystals occur in haloes around polysulfide crystals, and throughout sample.
		Chalcopyrite	0.3	
		Pyrrhotite	0.2	
		Pentlandite	0.1	
Magnetite	tr	Magnetite	tr	Few disseminated <0.2 mm crystals.
Comments: Highly variable crystal size, ranging from fine to coarse. A 1-2 mm-wide fine to very fine-grained chlorite-quartz veinlet bisects sample at 35° to the long axis of the thin section. Several altered pyroxenes (0.3-1.0 mm-wide, pseudomorphed by tremolite-actinolite-chlorite) are present in the veinlet matrix. To one side of the veinlet, primary minerals have been completely replaced by alteration products; appears to have been >90% pyroxene. On the other side of the veinlet, pyroxene is completely replaced and plagioclase is very weakly altered. Original mineral proportion is 75% plagioclase/25% pyroxene on the less altered side. Plagioclase is commonly seen completely encircling very fine (<0.2 mm) crystals of plagioclase and altered pyroxene on the less altered side.				

Sample: JJ-TS-036		**Drill hole: 17-804**		**Depth: 256.44 mm**
Mineral (interpreted pre-alteration)	%	Mineral (actual)	%	Details
Plagioclase	35	Chlorite	22	Plagioclase has been completely replaced by alteration minerals. Pre-alteration crystal shape/habit is not discernible. Pre-alteration crystal size appears to have been 1.0-5.0 mm. Very fine-grained chlorite±white mica replaces plagioclase; chlorite is most commonly dominant, ranging from well-aligned to randomly oriented. Very fine-grained white mica is dominant in a minority of aggregates.
		White mica	15	
Pyroxene	65	Tremolite-actinolite	45	Pyroxene has been completely replaced by alteration minerals. Pre-alteration crystal shape/habit is not discernible. Pre-alteration crystal size appears to be <8 mm; minimum size not discernible. Very fine to fine-grained tremolite-actinolite+talc±chlorite aggregates are most common, with tremolite-actinolite typically well-aligned. Simply twinned <1 mm tremolite crystals are rarely present.
		Talc	18	
Biotite	tr	Biotite	tr	Rare <0.3 mm platy crystals, present within alteration aggregates after both plagioclase and pyroxene.
Sulfides	1	Pyrite	0.3	<2 mm clusters of <0.5 mm polysulfide crystals, rarely surrounded by haloes of <0.05 mm monosulfide (chalcopyrite or pyrite) crystals
		Chalcopyrite	0.3	
		Pyrrhotite	0.2	
		Pyrite	0.2	
Magnetite	tr	Magnetite	tr	<0.3 mm disseminated crystals, sometimes in contact with pyrite/chalcopyrite crystals.
Comments: Massive texture, without fractures or pervasive foliation. Pre-alteration texture not discernible. Pre-alteration crystal size appears to have been variable, ranging from medium to coarse. Alteration minerals after both plagioclase and pyroxene occasionally show local crenulation, which is not consistent over the scale of the sample.				

Sample: JJ-TS-037		**Drill hole: 17-804**		**Depth: 258.29 m**
Mineral (interpreted	%	Mineral (actual)	%	Details

pre-alteration)				
Plagioclase	40	Plagioclase	5	Plagioclase has been mostly replaced by alteration minerals. Pre-alteration crystal shape/habit/size is very difficult to determine. Minority of 0.2-3.0 mm plagioclase crystals are only weakly altered, typically by rims and patches of white mica±chlorite. Where completely replaced, plagioclase is altered to fine to very fine-grained chlorite+white mica±tremolite-actinolite±quartz± epidote.
		White mica	15	
		Chlorite	24	
		Epidote	tr	
		Quartz	tr	
Pyroxene	60	Orthopyroxene	tr	Pyroxene has been almost completely replaced by alteration minerals. Rare <1.0 mm orthopyroxene crystals are only weakly altered by rims of tremolite-actinolite+talc. Alteration present as fine to very fine aggregates of tremolite-actinolite+talc±chlorite. Elongate, optically continuous, twinned tremolite-actinolite crystals up to 7 mm long are rarely present
		Tremolite-actinolite	38	
		Talc	17	
Sulfides	2	Chalcopyrite	0.7	<5 mm clusters of <2 mm polysulfide crystals, commonly aligned in direction of foliation. Very finely disseminated monosulfide (chalcopyrite or pyrite) crystals present throughout.
		Pyrrhotite	0.7	
		Pyrite	0.3	
		Pentlandite	0.3	
Magnetite	tr	Magnetite	tr	Very fine (<0.1 mm) irregularly shaped crystals disseminated throughout.
Comments: Pre-alteration crystal boundaries and proportions are very difficult to discern. Anastomosing foliation present through most of sample, typically at 60-70° to long axis of thin section. Absence of foliation typically occurs within <5 mm areas that are wrapped by foliated sections. Aside from the prevalent foliation, alignment of alteration minerals also occurs on the scale of a single pre-alteration crystal, typically shallower than sample-scale foliation, occasionally deflecting into sample scale foliation at margins. Crenulated <3 mm aggregates rarely present.				

Sample: JJ-TS-038		**Drill hole: 17-804**		**Depth: 260.00 m**
Mineral (interpreted pre-alteration)	%	Mineral (actual)	%	Details
Plagioclase	45	Plagioclase	5	Plagioclase has been mostly replaced by alteration minerals. Crystal shape/habit is not discernible due to degree of alteration. Crystal size is also difficult to determine; weakly altered portions of crystals up to 5 mm are present. Partial plagioclase crystals that are present are commonly fractured and moderately to strongly altered, typically by rims of fine-grained chlorite laths and patches of very fine-grained white mica±chlorite±tremolite-actinolite. Plagioclase is usually completely replaced, chlorite is the dominant alteration mineral, typically in aggregate with white mica±tremolite-actinolite.
		Chlorite	30	
		White mica	13	
Pyroxene	55	Tremolite-actinolite	45	Pyroxene has been completely replaced by alteration minerals. Crystal shape/habit is typically not discernible due to degree of alteration. Few pseudomorphs appear to maintain pre-alteration crystal properties, most typically equant and subhedral in smaller (0.5-1.5 mm) crystals, as well as a single irregular, elongate 4 mm anhedral crystal. Fine to very fine-grained tremolite-actinolite+talc±chlorite aggregates are most common. Actinolite rarely present as
		Talc	6	

				<2 mm irregularly shaped, optically continuous crystals.
Biotite	tr	Biotite	tr	Few <0.5 mm platy crystals, appear to be partially altered, typically surrounded by chlorite.
Sulfides	0.3	Pyrite	0.2	<5 mm clusters of disaggregated <0.5 mm disseminated and interstitial monosulfide (chalcopyrite and pyrite) crystals, and occasional <1 mm polysulfide crystals.
		Chalcopyrite	0.1	
		Pentlandite	tr	
Comments: Massive, no pervasive foliation or fracturing. Pre-alteration crystal size appears to have been dominantly coarse. Discontinuous <1 mm-wide and <1 cm-long chlorite veinlets occasionally extend from altered plagioclase crystals. Books of chlorite crystals are occasionally weakly kinked, typically those that are <1 mm in size.				

Sample: JJ-TS-039		**Drill hole: 17-804**		**Depth: 262.18 m**
Mineral (interpreted pre-alteration)	%	Mineral (actual)	%	Details
Plagioclase	38	Plagioclase	36	0.1-5.0 mm. Equant to tabular, smaller (<1.5 mm) crystals commonly subcircular. Anhedral to rarely subhedral. Crystals occasionally weakly fractured. Alteration present as patches and fractures of white mica±epidote±chlorite. Crystals rarely show deformation twinning.
		White mica	2	
		Chlorite	1	
		Epidote	tr	
Ortho-pyroxene	57	Orthopyroxene	55	0.1-4.0 mm, equant to elongate, subhedral to anhedral. Typically very weakly altered to very fine-grained patches, partial rims, and fracture-filling tremolite-actinolite±talc. Rare 0.5-1.5 mm actinolite crystals.
		Tremolite-actinolite	4	
		Talc	tr	
Clino-pyroxene	5	Clinopyroxene	3	Present as a single 10 mm-wide irregularly shaped oikocryst, encircling several orthopyroxene and plagioclase crystals, and moderately altered to tremolite-actinolite+talc.
Biotite	tr	Biotite	tr	Rare <0.3 mm crystals, typically adjacent to tremolite-actinolite±talc alteration of pyroxene.
Sulfides	0.5	Pyrrhotite	0.2	Interstitial <0.2 mm polysulfide crystals, mostly between unaltered silicates, rarely present along silicate alteration mineral aggregates.
		Chalcopyrite	0.2	
		Pyrite	0.1	
		Pentlandite	tr	
Magnetite	tr	Magnetite	tr	<0.1 mm crystals located in contact with or adjacent to sulfide mineral aggregates.
Comments: Cumulate, equilibrated. Massive, no pervasive foliation. Fractures show weak preferential alignment at 20° to long axis of thin section. Highly variable crystal size, with very fine to medium-grained crystals occurring throughout. Larger (>1.5 mm) plagioclase and pyroxene crystals commonly completely encircle smaller (<0.3 mm) plagioclase and pyroxene crystals.				

Sample: JJ-TS-040		**Drill hole: 17-804**		**Depth: 264.33 m**
Mineral (interpreted pre-alteration)	%	Mineral (actual)	%	Details
Plagioclase	35	Plagioclase	32	0.1-4.0 mm. Most commonly present as <5 mm clusters of crystals. Equant to rarely tabular, anhedral. Deformation twinning, undulose extinction, and fracturing are common. Typically weakly altered to patches and fracture fill of very fine-grained white mica±chlorite±epidote.
		White mica	2	
		Chlorite	2	
		Epidote	tr	

Ortho-pyroxene	61	Orthopyroxene	53	0.3-10.0 mm. Smaller (<3 mm) crystals are equant and subhedral. Larger (3-10 mm) crystals are anhedral and elongate. Larger crystals commonly show slightly kinked cleavage, in which cleavage direction deflects by <10°. Typically present as clusters of crystals. <1 mm-wide, <5 mm-long chlorite aggregates occasionally present at crystal margins. Minority of crystals are completely unaltered. Most crystals are weakly altered by patches, rims, and fracture fill of tremolite-actinolite±talc±chlorite.
		Tremolite-actinolite	7	
		Talc	1	
Clino-pyroxene	4	Clinopyroxene	3	15 mm cluster of several 1.0-8.0 mm irregularly shaped crystals, partially to complete encircling several plagioclase and orthopyroxene crystals and weakly altered to tremolite-actinolite+talc.
Biotite	tr	Biotite	tr	Rare <0.5 mm elongate crystals, typically adjacent to tremolite-actinolite±talc±chlorite alteration of pyroxene.
Sulfides	tr	Pyrrhotite	tr	Few <0.3 mm interstitial polysulfide crystals and very fine (<0.05 mm) disseminated pyrite and chalcopyrite crystals
		Chalcopyrite	tr	
		Pyrite	tr	
		Pentlandite	tr	
Magnetite	0.5	Magnetite	0.5	Very finely disseminated (<0.05 mm) crystals present throughout sample.
Comments: Massive; no foliation or pervasive fracturing or veining. Variable crystal size; commonly medium-grained with lesser fine to very fine-grained crystals dispersed throughout sample. Both plagioclase and pyroxene typically occur as clusters. Larger (>2 mm) pyroxene crystals commonly partially to completely encircle smaller plagioclase and pyroxene crystals.				

Sample: JJ-TS-041		**Drill hole: 17-804**		**Depth: 266.19 m**
Mineral (interpreted pre-alteration)	%	Mineral (actual)	%	Details
Plagioclase	45	Plagioclase	44	0.2-5.0 mm. Almost always present as <10.0 mm clusters of crystals. Equant to rarely tabular, anhedral. Small (<0.4 mm) crystals are usually subcircular. Rare deformation twinning. Unfractured to weakly fractured. Typically very weakly altered to <0.1 mm patches of white mica±chlorite±epidote.
		White mica	1	
		Epidote	tr	
Ortho-pyroxene	45	Orthopyroxene	42	0.2-6.0 mm. Smaller crystals (<1.0 mm) are equant and subhedral, larger crystals (>1.0 mm) are equant to elongate and anhedral. Heavily fractured. Typically very weakly altered to rims and <0.1 mm patches of very fine-grained tremolite-actinolite±talc±chlorite. Occasional 0.2-1.0 mm simply twinned tremolite also present.
		Tremolite-actinolite	4	
		Chlorite	tr	
		Talc	tr	
Clino-pyroxene	9	Clinopyroxene	8	1.0-15.0 mm. Irregularly shaped anhedral chadacrysts that completely enclose smaller orthopyroxene and plagioclase. Commonly contained exsolved elongate <0.2 mm orthopyroxene crystals along cleavage planes. Typically very weakly altered to partial rims and veinlets of tremolite-actinolite±talc.
Biotite	0.5	Biotite	tr	0.1-1.0 mm platy to tabular crystals. Appear to be primary; generally occurring interstitially to orthopyroxene/plagioclase, sometimes without any

				adjacent alteration minerals.
Sulfides	0.5	Chalcopyrite	0.2	Interstitial <0.3 mm polysulfide crystals, rounded and irregularly shaped. Trace very finely (<0.1 mm) disseminated pyrite.
		Pyrrhotite	0.2	
		Pentlandite	0.1	
		Pyrite	tr	
Magnetite	tr	Magnetite	tr	Interstitial <0.1 mm crystals in association with sulfide minerals.
Comment: Cumulate, equilibrated, biotite is only interstitial phase. Massive, no foliation, veining, or pervasive fracturing. Crystal size ranges from very fine to coarse throughout sample. Larger (>2 mm) pyroxene crystals commonly completely encircle smaller (>0.4 mm) plagioclase and pyroxene crystals.				

Sample: JJ-TS-042		**Drill hole: 17-804**		**Depth: 270.23 m**
Mineral (interpreted pre-alteration)	%	Mineral (actual)	%	Details
Plagioclase	42	Plagioclase	41	0.1-4.0 mm. Commonly in <4 mm clusters. Anhedral to rarely subhedral, equant to tabular. Fracturing very weak to absent, rare deformation twinning. Consistently very weakly altered to <0.05 mm patches of very fine-grained white mica±chlorite±epidote.
		White mica	1	
		Epidote	tr	
Ortho-pyroxene	50	Orthopyroxene	44	0.2-3.0 mm. Consistently subhedral and equant. Commonly occurring in <10 mm clusters. Typically very weakly altered to patches/partial rims very fine-grained aggregates of tremolite-actinolite±talc±chlorite. Minority of crystals are strongly altered to rarely completely replaced. Rarely present as <0.5 mm elongate exsolved crystals along clinopyroxene cleavage planes.
		Tremolite-actinolite	5	
		Talc	2	
		Chlorite	tr	
Clino-pyroxene	7	Clinopyroxene	6	Few 1.0-2.0 mm subhedral to anhedral equant crystals, weakly altered by tremolite-actinolite rims. One 5 mm by 11 mm irregularly shaped anhedral chadacryst partially to completely enclosing plagioclase/ pyroxene crystals, and very weakly altered to patches of tremolite-actinolite±talc. Rarely present as <0.2 mm elongate exsolved crystals along orthopyroxene cleavage planes.
Biotite	1	Biotite	1	0.2-1.5 mm crystals, occurring as both primary platy interstitial crystals and as fine-grained aggregates alongside chlorite.
Sulfides	tr	Pyrrhotite	tr	<0.3 mm interstitial polysulfide crystals and very finely disseminated (<0.05 mm) pyrite and chalcopyrite crystals.
		Chalcopyrite	tr	
		Pentlandite	tr	
		Pyrite	tr	
Magnetite	tr	Magnetite	tr	Rare <0.1 mm crystals in contact with sulfides in interstitial aggregates.
Comments: Cumulate, equilibrated, biotite is only interstitial phase. Massive, no foliation, veining, or pervasive fracturing. Crystal size is variable throughout, typically fine to medium. <0.5 mm crystals only occurring as oikocrysts and in clusters of plagioclase crystals. Larger (>2 mm) plagioclase and pyroxene crystals commonly completely encircle smaller (<1 mm) plagioclase and pyroxene crystals.				

Sample: JJ-TS-043		**Drill hole: 17-804**		**Depth: 276.13 m**
Mineral	%	Mineral (actual)	%	Details

(interpreted pre-alteration)				
Plagioclase	40	Plagioclase	35	0.1-3.5 mm. Occasionally in <5 mm clusters. Anhedral, equant to tabular. Weakly fractured, rare deformation twinning. Typically very weakly altered to patches and fracture fill of very fine-grained white mica±chlorite. Rarely strongly to completely altered to chlorite+white mica, especially adjacent to veinlet crosscutting sample.
		White mica	3	
		Chlorite	5	
Ortho-pyroxene	49	Orthopyroxene	40	0.3-3.0 mm. Subhedral to rarely anhedral, equant to rarely elongate. Typically very weakly altered to very fine-grained aggregates of tremolite-actinolite±talc±chlorite. Rarely strongly to completely altered to very fine-grained tremolite-actinolite±chlorite±talc, especially adjacent to veinlet. Tremolite-actinolite rarely present as <2.0 mm single simply twinned crystals and fine-grained monomineralic aggregates .
		Tremolite-actinolite	9	
		Talc	3	
Clino-pyroxene	9	Clinopyroxene	4	Several irregularly shaped anhedral chadacrysts partially to completely enclosing plagioclase/ pyroxene crystals, very weakly altered to partial rims of tremolite-actinolite±chlorite.
Biotite	1	Biotite	1	0.1-1.5 mm, present as platy interstitial crystals and in fine-grained aggregates alongside chlorite and tremolite-actinolite.
Sulfides	tr	Chalcopyrite	tr	<0.1 mm disseminated and interstitial crystals, typically monosulfide (chalcopyrite or pyrite), rarely polysulfide.
		Pyrrhotite	tr	
		Pyrite	tr	
Magnetite	0.3	Magnetite	0.3	Finely disseminated (<0.1 mm) crystals, most commonly associated with silicate alteration.
Comments: Cumulate, equilibrated, biotite is only interstitial phase. Dominantly fine to medium-grained. Massive, no foliation or pervasive fracturing. Anastomosing <0.3 mm-wide veinlet crosscuts sample at ~25° to long axis of thin section, surrounded by ~5 mm-wide halo of increased alteration intensity. Sinistral movement (~0.3 mm of offset) adjacent to veinlet.				

Sample: JJ-TS-044		**Drill hole: 17-804**		**Depth: 280.77 m**
Mineral (interpreted pre-alteration)	%	Mineral (actual)	%	Details
Plagioclase	44	Plagioclase	43	0.1-4.5 mm. Anhedral, equant to tabular. Crystals commonly occur is <8.0 mm clusters. Consistently very weakly fractured, rare deformation twinning. Consistently very weakly altered to patches of very fine-grained white mica. Rare <0.5 mm discrete muscovite crystals present within alteration zones.
		White mica	1	
Ortho-pyroxene	50	Orthopyroxene	40	0.2-3.0 mm. Smaller (<0.7 mm) crystals equant and anhedral to subhedral, larger (>0.7 mm) crystals equant to elongate and anhedral. Typically weakly altered to very fine to fine-grained aggregates of tremolite-actinolite±talc±chlorite. Minority of crystals moderately to completely altered in same style. Tremolite-actinolite rarely present as <1.0 mm discrete, simply twinned crystals.
		Tremolite-actinolite	6	
		Talc	2	
		Chlorite	2	

Clino-pyroxene	6	Clinopyroxene	4	Few 3.0-6.0 mm crystals irregularly shaped chadacrysts partially to completely enclosing smaller plagioclase and orthopyroxene crystals. One crystal is mostly altered to a single ~3 mm optically continuous tremolite crystal; other crystals are weakly altered to rims of tremolite.
Biotite	tr	Biotite	tr	0.1-1.0 mm platy to equant crystals. Present as interstitial crystals in unaltered zones and occasionally completely surrounded by tremolite and/or chlorite alteration. Appear to be primary.
Sulfides	tr	Pyrite	tr	Very finely disseminated pyrite or chalcopyrite crystals and rare <0.2 mm interstitial pyrrhotite± chalcopyrite±pentlandite crystals.
		Pyrrhotite	tr	
		Chalcopyrite	tr	
		Pentlandite	tr	
Magnetite	tr	Magnetite	tr	Very fine disseminated (<0.05 mm) crystals disseminated throughout.
Comments: Cumulate, equilibrated, biotite is only interstitial phase. Fine to medium-grained throughout, rare very fine-grained crystals. Massive, no foliation or pervasive fracturing. ~0.3 mm-wide talc+chlorite(+muscovite?) veinlet crosscuts sample at ~40 degrees to long axis of thin section, with set of anastomosing <0.1 mm-wide veinlets of similar composition occurring within <3 mm of main veinlet. Veinlets surrounded by ~2 mm of strong tremolite+talc+chlorite alteration where cutting through orthopyroxene, mostly replacing crystals. No alteration haloes present where veinlets cut through plagioclase. Pyroxene and plagioclase both occasionally completely encircle smaller (<0.3 mm) plagioclase crystals.				

Sample: JJ-TS-075		**Drill hole: 18-805**		**Depth: 75.26 m**
Mineral (interpreted pre-alteration)	%	Mineral (actual)	%	Details
Plagioclase	60	Plagioclase	40	0.1-4.0 mm. Anhedral, generally equant, >3.0 mm crystals are generally tabular. Typically unfractured; fractures are filled by white mica± chlorite where present. Rare deformation twinning. Dominantly Majority of crystals are weakly to moderately altered to <0.2 mm patches of very fine-grained white mica±chlorite. Very fine to fine-grained chlorite also occurs as partial rims or patches, commonly adjacent to altered pyroxene crystals. Minority of crystals (those surrounded by altered pyroxene and adjacent to pyroxene-dominated zones) are strongly to completely altered to chlorite±white mica. Elongate <0.4 mm muscovite crystals fill fractures in plagioclase in a few locations.
		Chlorite	17	
		White mica	6	
		Epidote	tr	
Pyroxene	39	Tremolite-actinolite	37	Pyroxene has been completed replaced by alteration products. Pre-alteration crystal size, shape, and habit are generally not discernible due to alteration of crystal margins. Minority of crystals have generally discernible size/habit despite alteration intensity; these appear to have been 1.5-4.0 mm and equant to elongate. Alteration typically present as aligned aggregates of very fine to fine-grained tremolite-actinolite± talc. Randomly oriented aggregates and <0.7 discrete tremolite crystals are less common.
		Talc	tr	
Biotite	tr	Biotite	tr	Rare <0.3 mm platy crystals present within chlorite-

				dominated aggregates.
Sulfides	0.4	Pyrite	0.2	Very finely disseminated (<0.1 mm) pyrite, chalcopyrite and pyrite±chalcopyrite±pentlandite crystals, commonly in <2 mm clusters.
		Chalcopyrite	0.2	
		Pentlandite	tr	
Magnetite	tr	Magnetite	tr	Very finely disseminated (<0.1 mm) crystals in association with sulfide minerals.
Comments: Appears to have been cumulate and equilibrated pre-alteration. Massive, no foliation or pervasive fracturing. Where discernible (mostly plagioclase), crystal size appears to be variable throughout, ranging from very fine to medium-grained. Chlorite-dominated aggregates filling fractures in plagioclase most commonly occur at 20-45° to long axis of thin section. >2.0 mm plagioclase and altered pyroxene crystals occasionally encircle <0.3 mm plagioclase crystals.				

Sample: JJ-TS-068		**Drill hole: 18-805**		**Depth: 100.22 m**
Mineral (interpreted pre-alteration)	%	Mineral (actual)	%	Details
Plagioclase	75	Plagioclase	69	0.1-4.0 mm. Anhedral, equant to tabular. Commonly present as <10.0 mm clusters of crystals. Generally unfractured, rare deformation twinning. Generally very weakly altered to <0.05 mm patches of very fine-grained white mica. Minority of crystals moderately to strongly altered to very fine to fine-grained aggregates of chlorite±white mica±epidote. Strongest alteration typically present adjacent to altered pyroxene crystals. Few <0.3 mm discrete crystals of muscovite and chlorite are also present.
		White mica	2	
		Epidote	tr	
Pyroxene	22	Orthopyroxene	tr	Pre-alteration crystal size/shape/habit obscured by degree of alteration and presence of crystals in clusters; alteration mineral aggregates appear to form across multiple pre-alteration crystals. Appear to be 0.3-7.0 mm pre-alteration, equant to possibly elongate. Pyroxene is almost completely replaced by alteration minerals; few <0.5 mm orthopyroxene crystals completely surrounded by plagioclase are only weakly altered. Fine to very fine-grained aggregates of tremolite-actinolite±chlorite±talc and monomineralic aggregates of tremolite-actinolite are most prevalent, occurring as both randomly oriented and aligned aggregates. Discrete <2 mm tremolite-actinolite crystals, commonly surrounding polymineralic aggregates.
		Tremolite-actinolite	17	
		Chlorite	9	
		Talc	tr	
Biotite	tr	Biotite	tr	Few <0.3 mm platy to equant crystals located interstitial to plagioclase crystals, sometimes adjacent to chlorite±tremolite-actinolite alteration.
Sulfide	3	Pyrrhotite	1	Interstitial, irregularly shaped pyrrhotite±chalco-pyrite±pentlandite±pyrite crystals, mostly in plagioclase-rich portion of sample. Disseminated pyrite and chalcopyrite present mostly as <3 mm haloes around interstitial crystals, and less so throughout sample.
		Chalcopyrite	1	
		Pyrite	0.7	
		Pentlandite	0.3	
Magnetite	tr	Magnetite	tr	<0.05 mm disseminated crystals, in silicate alteration aggregates and as inclusions in plagioclase.
Comments: Cumulate, equilibrated, no interstitial minerals aside from possibly biotite. Massive, no foliation or pervasive fracturing. Variable crystal size, ranging from very fine to medium-grained throughout. 50% of sample				

is 90% plagioclase/10% pyroxene, 50% of sample is 65% plagioclase/35% pyroxene. Anastomosing veinlets of chlorite±tremolite-actinolite through sample in no preferred orientation. Smaller (<0.5 mm) plagioclase and pyroxene crystals occasionally partially to completely encircled by larger plagioclase crystals.

Sample: JJ-TS-071		**Drill hole: 18-805**		**Depth: 110.44 m**
Mineral (interpreted pre-alteration)	%	Mineral (actual)	%	Details
Plagioclase	58	Plagioclase	50	0.02-3.0 mm. Significant minority of plagioclase (10% of sample) is present as very fine-grained (<0.1 mm) groups of crystals with polygonal triple junctions; appear to be product of recrystallization. Very fine-grained plagioclase most commonly occurs as rims or along fractures through otherwise unaltered crystals, rarely dominantly to completely replacing coarser crystals. Pre-alteration properties of coarser (>0.5 mm) crystals are obscured by alteration of margins, but appear to be anhedral and equant to tabular. Coarser crystals generally weakly altered to very fine-grained patches of white mica±chlorite and rims/larger patches of chlorite and/or recrystallized plagioclase.
		Chlorite	8	
		White mica	2	
Pyroxene	42	Tremolite-actinolite	37	Pyroxene is completely replaced by alteration minerals. Pre-alteration crystal properties are not discernible due to intensity of alteration of crystal margins. Most commonly very fine-grained aggregates of tremolite-actinolite+chlorite±talc, typically in random orientation and rimmed by very fine-grained chlorite aggregates at boundaries with plagioclase. Tremolite-actinolite present as very fine-grained crystals with polygonal triple junctions in one 4 mm area. Discrete <5 mm tremolite crystals less common. Few <1 mm simply twinned anthophyllite crystals.
		Talc	1	
		Anthophyllite	1	
Biotite	tr	Biotite	tr	<0.1 mm platy crystals in aggregate with tremolite-actinolite and chlorite.
Sulfides	0.2	Chalcopyrite	0.1	Very finely disseminated <0.1 mm, irregularly shaped, interstitial pyrite and/or chalcopyrite crystals, mostly within silicate alteration aggregates.
		Pyrite	0.1	
Magnetite	0.2	Magnetite	0.2	Very finely disseminated (<0.05 mm) crystals distributed throughout sample.
Comments: Alteration obscures majority of crystal boundaries, making pre-alteration crystal relationships difficult to determine. No foliation or pervasive fracturing. Anastomosing zones of strong alteration/recrystallization are generally <20 degrees to long axis of thin section, wrapping around and occasionally cutting through unaltered plagioclase crystals.				

Sample: JJ-TS-072		**Drill hole: 18-805**		**Depth: 115.37 m**
Mineral	%	Mineral (actual)	%	Details

(interpreted pre-alteration)				
Plagioclase	70	Plagioclase	58	0.2-5.0 mm. Anhedral, equant to rarely tabular. Plagioclase typically present as <10 mm clusters. Unfractured to very weakly fractured, 5% of crystals show deformation twinning. Crystals are typically very weakly altered to <0.2 mm patches and fracture fill of very fine-grained white mica±chlorite±epidote. Chlorite typically occurs as very fine to fine-grained monomineralic aggregates occurring as partial rims or <1.0 mm patches extending from adjacent altered pyroxene crystals. Muscovite rarely present as discrete elongate <0.3 mm crystals.
		Chlorite	14	
		White mica	2	
		Epidote	tr	
Pyroxene	30	Tremolite-actinolite	25	Pyroxene has been completely replaced by alteration products. Pre-alteration crystals are generally not discernible due to degree of alteration of crystal margins; altered crystals that are completely surrounded by unaltered plagioclase retain their pre alteration properties, which appear to be equant and subhedral. Alteration typically fine-grained, either as monomineralic tremolite-actinolite aggregates or tremolite-actinolite+chlorite±talc aggregates, both present in random orientation and as aligned crystals. Discrete <2 mm tremolite crystals also present, sometimes with simple twinning. Talc rarely present as <0.2 mm discrete crystals.
		Talc	1	
Sulfides	tr	Pyrite	tr	Very finely disseminated (<0.2 mm) monosulfide pyrite and chalcopyrite crystals, present as irregularly shaped crystals and less commonly as pyrite cubes, mostly in silicate alteration aggregates.
		Chalcopyrite	tr	
Comments: Alteration obscures majority of crystal boundaries, making pre-alteration crystal properties difficult to discern. Appears to be cumulate and equilibrated. Massive, no foliation. Anastomosing set of few <0.05 mm-wide fractures crosscutting sample at <15 degrees to long axis of thin section. Crystal size ranges from fine to medium throughout. Larger (>4.0 mm) plagioclase crystals rarely completely encircle smaller (<0.4 mm) altered pyroxene crystals.				

Sample: JJ-TS-073		**Drill hole: 18-805**		**Depth: 120.72 m**
Mineral (interpreted pre-alteration)	%	Mineral (actual)	%	Details
Plagioclase	56	Plagioclase	47	0.3-3.0 mm pre-alteration. Anhedral, equant to tabular. Fractures rare, irregular, and typically filled by white mica. Crystals typically weakly to moderately altered to patches and fracture-filling white mica, as well as patches and partial rims of chlorite. Minority of crystals are dominantly altered to white mica, generally those that are completely surrounded by altered pyroxene.
		Chlorite	7	
		White mica	4	
Pyroxene	44	Tremolite-actinolite	40	0.3-7.0 mm. Pyroxene has been completely replaced by alteration minerals. Pre-alteration shape/habit is commonly not discernible; some crystals are pseudomorphed, ranging from >5 mm irregularly shaped crystals that wrap around plagioclase crystals, to <1 mm equant, subhedral crystals. Alteration mostly present as very fine to fine-grained
		Anthophyllite	1	
		Talc	1	

				tremolite-actinolite± chlorite±talc aggregates, typically aligned and occasionally in random orientation. Tremolite-actinolite and anthophyllite both occur as 0.2-4.0 mm optically continuous crystals, commonly pseudomorphing pyroxene as rims surrounding tremolite-actinolite±chlorite±talc aggregates.
Sulfides	0.3	Pyrite	0.2	Very finely disseminated monosulfide pyrite and chalcopyrite crystals, mostly associated with alteration aggregates. Less common subhedral <0.5 mm pyrite crystals.
		Chalcopyrite	0.1	
Magnetite	tr	Magnetite	tr	Very finely disseminated (<0.05 mm) crystals present in silicate alteration aggregates.
Comments: Cumulate, equilibrated where primary crystal boundaries preserved, no interstitial minerals observed. Massive, no foliation, pervasive fracturing, or veining. Variable crystal size (very fine to coarse). Coarse-grained section in middle of sample grades to fine to medium-grained portion on the edges. Coarse (>5 mm) altered pyroxene crystals partially to completely enclose fine to medium-grained plagioclase. Medium-grained (<3 mm) plagioclase crystals occasionally completely enclose <0.5 mm plagioclase and altered pyroxene.				

Sample: JJ-TS-074		**Drill hole: 18-805**		**Depth: 125.41 m**
Mineral (interpreted pre-alteration)	%	Mineral (actual)	%	Details
Plagioclase	60	Plagioclase	56	0.1-6.0 mm. Equant to lath-shaped, anhedral to subhedral. Weakly altered to patches and fracture-filling white mica±chlorite±epidote. Margins of crystals altered to patches and partial rims of chlorite, most commonly adjacent to altered pyroxene. Lath-shaped crystals typically ~0.2 mm wide and 0.5-6.0 mm long; those that are <1.0 mm are commonly partially to completely enclosed by altered pyroxene. Rare recrystallized <0.1 mm crystals with polygonal triple junctions (may be quartz?) surrounded by tremolite-actinolite and chlorite.
		Chlorite	4	
		White mica	2	
		Epidote	tr	
Pyroxene	39	Tremolite-actinolite	37	0.2-4.0 mm. Pyroxene has been completely replaced by alteration minerals. Some <0.5 mm pseudomorphed crystals appear to have been subhedral and equant. Shape/habit of some larger crystals obscured by alteration; more commonly pseudomorphed and anhedral, typically irregularly shaped, wrapping around plagioclase crystals. Alteration typically present as very fine-grained tremolite-actinolite±chlorite± talc, typically aligned and less commonly in random orientation. Tremolite-actinolite also present as 0.2-2.0 mm optically continuous crystals, as discrete crystals and as rims surrounding tremolite-actinolite-dominated aggregates.
		Talc	tr	
Biotite	0.5	Biotite	0.5	Few <1.0 mm books of elongate platy crystals, some of which are curvilinear and “kinked”.
Sulfides	0.2	Pyrite	0.1	Very finely disseminated monosulfide pyrite and chalcopyrite crystals throughout sample. Rare <0.2 mm interstitial, irregularly shaped pyrite+ chalcopyrite±pentlandite crystals.
		Chalcopyrite	0.1	
		Pentlandite	tr	
Comments: Cumulate, equilibrated where magmatic crystal margins preserved. No interstitial minerals aside				

from rare biotite crystals. Massive, no foliation, pervasive fracturing, or veining. Variable crystal size, ranging from very fine to medium throughout sample. Medium-grained (>1.5 mm) plagioclase and altered pyroxene crystals occasionally partially to completely enclose fine-grained (<0.5 mm) plagioclase and altered pyroxene crystals.

Sample: JJ-TS-076		**Drill hole: 18-805**		**Depth: 131.20 m**
Mineral (interpreted pre-alteration)	%	Mineral (actual)	%	Details
Plagioclase	62	Plagioclase	58	0.1-3.0 mm. Typically equant and anhedral; some <1.0 mm crystals completely enclosed by other crystals are subhedral and tabular to lath-shaped. Weakly altered to patches of white mica±chlorite± epidote. Chlorite also present as partial rims extending from adjacent altered plagioclase. Crystals weakly fractured, with fractures filled by chlorite±white mica. Few <0.3 mm platy muscovite crystals within altered plagioclase.
		Chlorite	4	
		White mica	2	
		Epidote	tr	
Ortho-pyroxene	30	Orthopyroxene	tr	0.2-2.5 mm. Pre-alteration crystal margins are generally retained and appear to be equant and subhedral to anhedral. Pyroxene has been almost completely replaced by alteration minerals. Few <0.4 mm unaltered cores of orthopyroxene crystals present. Altered to very fine to fine-grained tremolite-actinolite±talc±chlorite and very fine-grained talc aggregates.
		Tremolite-actinolite	18	
		Talc	15	
Clino-pyroxene	8	Clinopyroxene	3	2.0-5.0 mm irregularly shaped crystals that have been partially to completely altered to very fine-grained tremolite-actinolite±talc and discrete, optically continuous rims of tremolite. Altered crystals generally retain original boundaries. Crystals partially to completely enclose smaller plagioclase and altered pyroxenes.
Biotite	tr	Biotite	tr	Few <0.5 mm books of platy crystals present on margin between unaltered plagioclase and altered pyroxene.
Sulfides	0.3	Chalcopyrite	0.2	<3 mm clusters of disaggregated disseminated monosulfide (pyrite and chalcopyrite) and <0.8 mm irregularly shaped interstitial pyrite± pentlandite aggregates.
		Pyrite	0.1	
		Pentlandite	tr	
Magnetite	0.2	Magnetite	0.2	<0.1 mm disseminated crystals, associated with some sulfide mineral clusters.
Comments: Cumulate, equilibrated where magmatic crystal margins preserved, biotite crystals are only possible interstitial phase. Massive, no foliation, pervasive fracturing, or veining. Variable crystal size, ranging from very fine to medium throughout sample. Proportions of pyroxenes pre-alteration is a rough estimate based on shape of unaltered partial crystals and unaltered crystals seen in similar samples (round/oval-shaped orthopyroxene, irregularly shaped clinopyroxene). Larger (>2.0 mm) plagioclase and altered pyroxene commonly completely encircle small (<0.2 mm) plagioclase and pyroxene crystals.				

Sample: JJ-TS-077		**Drill hole: 18-805**		**Depth: 133.36 m**
Mineral	%	Mineral (actual)	%	Details

(interpreted pre-alteration)				
Plagioclase	60	Plagioclase	59	0.1-4.0 mm. Anhedral to rarely subhedral, equant to tabular. Some <0.3 mm crystals completely encircled by orthopyroxene are rectangular and subhedral to euhedral. Rare fractures, sometimes filled by alteration minerals. Very weakly altered to <0.1 mm patches and fracture-filling very fine-grained white mica±chlorite, and rare <0.5 mm patches of very fine-grained chlorite aggregates.
		White mica	1	
		Chlorite	tr	
		Epidote	tr	
Ortho-pyroxene	33	Orthopyroxene	25	0.1-3.0 mm Equant and subhedral to rarely elongate, oval-shaped, and anhedral. Rarely present as <0.2 mm elongate crystals exsolved from clinopyroxene. Minority of <1.0 mm crystals are unaltered. Majority of crystals are weakly to moderately altered to patches and/or partial rims of very fine-grained tremolite-actinolite±talc±chlorite. A few crystals are completely altered to fine-grained tremolite-actinolite+talc.
		Tremolite-actinolite	5	
		Talc	4	
Clino-pyroxene	7	Clinopyroxene	6	0.5-5.0 mm. Majority of crystals are anhedral and irregularly shaped, wrapping around adjacent crystals. Few <1.5 mm crystals are subhedral and equant. Unaltered to weakly altered to <1 mm patches of very fine-grained tremolite-actinolite±talc.
Biotite	tr	Biotite		Few <0.4 mm platy to equant crystals, mostly occurring in one 4 mm cluster adjacent to plagioclase and unaltered pyroxene.
Sulfides	0.2	Pyrrhotite	0.1	Interstitial, irregularly shaped <0.3 mm pyrrhotite± chalcopyrite±pentlandite crystals, sometimes in <2 mm clusters. Occasionally very fine to fine-grained disseminated pyrite and chalcopyrite crystals
		Chalcopyrite	0.1	
		Pentlandite	tr	
		Pyrite	tr	
Comments: Cumulate, equilibrated, biotite is only interstitial phase. Massive, no foliation, pervasive fracturing, or veining. Variable crystal size, varying from very fine to medium throughout. Larger (>2.0 mm) plagioclase, orthopyroxene, and clinopyroxene crystals occasionally completely encircle smaller (<0.2 mm) plagioclase and orthopyroxene crystals.				

Sample: JJ-TS-078		**Drill hole: 18-805**		**Depth: 135.38 m**
Mineral (interpreted pre-alteration)	%	Mineral (actual)	%	Details
Plagioclase	60	Plagioclase	59	0.2-3.5 mm. Anhedral, equant to rarely tabular. Few equant, rectangular, subhedral to euhedral crystals completely encircled by clinopyroxene. Rare deformation twinning. One 3 mm area contains several plagioclase crystals that are heavily fractured, display undulose extinction, and generally do not display polysynthetic twinning. Uniformly very weakly altered to <0.05 mm white mica patches. Rare <0.3 mm discrete muscovite crystals present as plagioclase alteration product. Rare <0.2 mm very fine-grained patches of chlorite aggregates.
		White mica	1	
		Chlorite	tr	

Ortho-pyroxene	31	Orthopyroxene	24	0.1-2.5 mm. Anhedral to subhedral, generally equant. Few <1.0 mm crystals are oval-shaped, elongate, and anhedral. Few >3.0 mm crystals are elongate and irregularly shaped, wrapping around adjacent crystals. Rarely present as <0.1 mm crystals exsolved from clinopyroxene. Rarely unaltered to more commonly weakly altered to patches of very fine-grained talc±tremolite-actinolite. Few crystals are strongly to completely altered to tremolite-actinolite+talc. Few <0.7 mm discrete anthophyllite crystals.
		Talc	5	
		Tremolite-actinolite	3	
		Anthophyllite	tr	
Clino-pyroxene	9	Clinopyroxene	8	0.3-5.0 mm. Majority of crystals are anhedral and irregular, wrapping around adjacent crystals. Few <1.0 mm crystals are equant and subhedral. Unaltered to weakly altered to tremolite-actinolite±talc, in small patches and along fractures.
Biotite	tr	Biotite	tr	<0.5 mm platy crystals, commonly in "books", typically surrounded by pyroxene alteration minerals and less commonly present as inclusions within plagioclase crystals.
Sulfides	0.2	Pyrite	0.1	<0.2 mm irregularly shaped interstitial pyrrhotite+pentlandite ±chalcopyrite±pyrite and very finely disseminated irregularly shaped pyrite and chalcopyrite
		Chalcopyrite	0.1	
		Pyrrhotite	tr	
		Pentlandite	tr	
Comments: Cumulate, equilibrated, biotite is only interstitial phase. Massive, no foliation, pervasive fracturing, or veining. Variable crystal size, varying from very fine to medium throughout. ~5 mm clusters throughout sample composed of 75%+ plagioclase or 75%+ orthopyroxene+clinopyroxene. <0.5 mm plagioclase and orthopyroxene crystals commonly partially to completely encircled by >2.0 mm plagioclase and clinopyroxene crystals.				

Sample: JJ-TS-079		**Drill hole: 18-805**		**Depth: 137.52 m**
Mineral (interpreted pre-alteration)	%	Mineral (actual)	%	Details
Plagioclase	62	Plagioclase	61	0.2-5.0 mm. Anhedral, equant. Several crystals partially to completely encircled by clinopyroxene are euhedral and equant to tabular. Rare deformation twinning. Typically very weakly altered to <0.05 mm patches of very fine-grained white mica. Rarely altered to patches of very fine to fine-grained chlorite.
		White mica	1	
		Chlorite	1	
Ortho-pyroxene	26	Orthopyroxene	21	0.1-3.0 mm. Typically subhedral and equant, >1.5 mm crystals are commonly anhedral, elongate, and oval-shaped. Commonly occur in <4 mm clusters. Rare <0.1 mm elongate crystals exsolved from clinopyroxene. Occasionally unaltered, typically very weakly altered to partial rims and patches of talc±tremolite-actinolite. Rarely strongly to completely altered to very fine-grained tremolite-actinolite+chlorite+talc or monomineralic talc aggregates.
		Tremolite-actinolite	3	
		Talc	3	
Clino-pyroxene	12	Clinopyroxene	11	0.7-5.0 mm. Anhedral and irregularly shaped, wrapping around adjacent crystals. Uniformly very weakly altered to

				partial rims and small patches of very fine-grained talc±tremolite-actinolite.
Biotite	tr	Biotite	tr	0.2-1.2 mm, present as inclusions in plagioclase and alongside pyroxene alteration mineral aggregates.
Sulfides	tr	Pyrite	tr	Interstitial <0.3 mm polysulfide (chalcopyrite± pyrite±pyrrhotite) crystals, typically surrounded by <1 mm haloes of finely disseminated pyrite, pyrrhotite, and/or chalcopyrite crystals.
		Pyrrhotite	tr	
		Chalcopyrite	tr	
Comments: Cumulate, equilibrated, biotite is only interstitial phase. Massive, no foliation or pervasive fracturing. Single anastomosing tremolite-actinolite+chlorite veinlet crosscuts sample at ~45° to long axis of thin section. Variable crystal size; orthopyroxene is typically fine-grained, clinopyroxene is typically medium-grained, and plagioclase generally ranges from fine to medium-grained. <0.5 mm plagioclase and orthopyroxene crystals commonly completely enclosed by >2.0 plagioclase and clinopyroxene.				

Sample: JJ-TS-080		**Drill hole: 18-805**		**Depth: 139.46 m**
Mineral (interpreted pre-alteration)	%	Mineral (actual)	%	Details
Plagioclase	60	Plagioclase	60	0.1-3.5 mm. Generally anhedral and equant. Several crystals partially to completely surrounded by clinopyroxene are subhedral to euhedral and equant to lath-shaped. Rare deformation twinning. Generally very weakly altered to very small patches of very fine-grained white mica and/or chlorite. Minority of crystals appear completely unaltered.
		White mica	tr	
Ortho-pyroxene	22	Orthopyroxene	21	0.1-3.5 mm. Large majority of crystals are <1.0 mm, subhedral, equant, and round. >1.0 mm crystals are typically elongate, oval-shaped and anhedral. Minority of larger (>1.5 mm) crystals are anhedral and irregularly shaped, appearing similar to clinopyroxene aside from birefringence and extinction angle. Rare <0.1 mm equant to elongate crystals exsolved from clinopyroxene. Typically very weakly altered to tremolite-actinolite±talc, as partial rims, along fractures, and as <0.1 mm patches. Crystals adjacent to vein crosscutting sample are moderately to strongly altered to tremolite-actinolite±chlorite±talc.
		Tremolite-actinolite	1	
		Talc	1	
		Chlorite	tr	
Clino-pyroxene	18	Clinopyroxene	17	0.4-6.0 mm. Most crystals are >2.0 mm, anhedral, and irregular, wrapping around adjacent crystals. Minority of crystals are <1.5 mm, equant to elongate, and subhedral. Very weakly altered to partially rims and patches of tremolite-actinolite±talc
Biotite	tr	Biotite	tr	Few <0.3 mm platy to equant crystals, present as inclusions in plagioclase as well as present in chlorite-dominated veinlet.
Sulfides	tr	Pyrite	tr	Interstitial <0.2 mm polysulfide (chalcopyrite± pyrrhotite±pyrite) crystals, commonly in <3 mm clusters. Finely disseminated monosulfide pyrite or chalcopyrite crystals also present throughout.
		Pyrrhotite	tr	
		Chalcopyrite	tr	
Comments: Cumulate, equilibrated, biotite is only interstitial phase. Massive, no foliation or pervasive fracturing. Single ~0.2 mm-wide straight vein crosscuts sample at 10° to long axis of thin section, filled by tremolite-actinolite, chlorite, and biotite, and surrounded by <1.0 cm alteration halo where cutting through				

pyroxene (plagioclase cut by vein shows no halo). <0.5 mm orthopyroxene crystals commonly partially encircled by plagioclase. Variable crystal size; orthopyroxene is typically fine-grained, clinopyroxene is typically medium-grained, and plagioclase generally ranges from fine to medium-grained. <0.5 mm orthopyroxene and <1.5 mm plagioclase crystals commonly partially to completely enclosed by clinopyroxene.

Sample: JJ-TS-081		**Drill hole: 18-805**		**Depth: 141.44 m**
Mineral (interpreted pre-alteration)	%	Mineral (actual)	%	Details
Plagioclase	57	Plagioclase	53	0.2-4.0 mm. Anhedral, equant to tabular. Generally weakly to locally moderately fractured. Few crystals completely surrounded by clinopyroxene are anhedral to euhedral. Typically very weakly altered to <0.05 mm patches of very fine-grained white mica. Less commonly moderately to strongly altered to <0.2 mm patches and veinlets of chlorite±white mica.
		Chlorite	6	
		White mica	1	
Ortho-pyroxene	30	Orthopyroxene	15	0.1-1.5 mm. Typically moderately altered to completely replaced by very fine-grained talc±tremolite-actinolite±chlorite, commonly present as rims and along pre-existing fractures. Minority of crystals are only weakly altered to same assemblage, typically as partial rims. Few <1 mm discrete anthophyllite crystals.
		Talc	12	
		Tremolite-actinolite	5	
		Anthophyllite	5	
Clino-pyroxene	13	Clinopyroxene	8	1.0-10.0 mm. Most crystals weakly to moderately altered to talc±tremolite-actinolite±chlorite. One 8 mm crystal is completely replaced by chlorite+tremolite-actinolite.
Biotite	tr	Biotite	tr	Few <0.5 mm platy crystals, always adjacent to very fine-grained chlorite and/or tremolite-actinolite aggregates.
Sulfides	tr	Pyrite	tr	Finely disseminated <0.05 mm pyrite and chalcopyrite throughout sample, commonly as inclusions/along fractures within plagioclase as well as within silicate alteration mineral aggregates. Rare larger interstitial pyrite crystals up to 0.5 mm.
		Chalcopyrite	tr	
Magnetite	tr	Magnetite	tr	Rare <0.05 crystals in clusters with/in aggregate with finely disseminated pyrite.
Comments: Cumulate, equilibrated, no interstitial minerals aside from possibly biotite, which may be an alteration product. Massive, no foliation or pervasive fracturing. Discontinuous chlorite-dominated veinlets extending from altered pyroxene aggregates and cutting through otherwise weakly altered plagioclase crystals, dominantly at ~50° to long axis of thin section, ranging from 35-80°. Variable crystal size; plagioclase typically fine to medium-grained, orthopyroxene typically fine-grained, clinopyroxene typically coarse-grained. Plagioclase occasionally partially encloses smaller orthopyroxene crystals, clinopyroxene commonly partially to completely encloses smaller orthopyroxene and plagioclase crystals.				

Sample: JJ-TS-082		**Drill hole: 18-805**		**Depth: 142.88 m**
Mineral (interpreted	%	Mineral (actual)	%	Details

pre-alteration)				
Plagioclase	58	Plagioclase	40	Moderately to strongly deformed, common deformation twinning. Commonly crosscut by veinlets, otherwise moderately to heavily fractured. Crystal size/shape/form obscured by deformation, but generally appears to have been equant, anhedral, and <2 mm. One tabular, 4 mm crystal present. Typically weakly altered to <0.1 mm, very fine-grained aggregates of white mica±chlorite. Chlorite and quartz dominantly present in veinlets; difficult to tell if these are plagioclase alteration products or introduced from fluids.
		Chlorite	13	
		White mica	3	
		Quartz	5	
Pyroxene	42	Tremolite-actinolite	39	Pyroxene has been completely replaced by alteration products. Pre-alteration crystal properties are not discernible due to deformation and degree of alteration. Alteration mostly present as fine to fine-grained tremolite-actinolite±chlorite±talc aggregates. Alteration aggregates sometimes deformed in proximity to veinlets. Few <2.0 mm deformed discrete tremolite crystals present.
		Talc	tr	
Sulfides	tr	Chalcopyrite	tr	<0.1 mm crystals very finely disseminated throughout sample.
Appears to have been cumulate and equilibrated but all aspects of primary texture are difficult to discern due to deformation. Biotite is not observed in this sample. Heavily fractured, veinlets that look similar to cataclasite up to 2.5 mm wide crosscut sample at 60-80° to long axis of thin section. Veinlets made up of disaggregated plagioclase and tremolite-actinolite that have been rounded, alongside quartz and chlorite in an aphanitic matrix. Veinlets do not have alteration haloes.				

Sample: JJ-TS-083		**Drill hole: 18-805**		**Depth: 143.05 m**
Mineral (interpreted pre-alteration)	%	Mineral (actual)	%	Details
Plagioclase	30	Plagioclase	5	Pre-alteration crystal properties not discernible due to alteration/deformation. Most crystals strongly altered to veinlets/partial rims of very fine-grained chlorite±white mica and patches of white mica, especially adjacent to fractures. Heavily deformed and very heavily fractured where unaltered. Chlorite also present as major component of fracture fill. Epidote only observed as fracture fill
		Chlorite	22	
		White mica	5	
		Epidote	tr	
Pyroxene	70	Tremolite-actinolite	65	Pyroxene has been completely replaced by alteration minerals. Pre-alteration crystal properties not discernible due to alteration. Alteration dominantly present as fine to fine-grained tremolite-actinolite±chlorite ±talc aggregates. Alteration aggregates commonly kinked/deformed. <4.0 mm discrete tremolite crystals also present, commonly showing undulose extinction.
		Talc	3	
Biotite	tr	Biotite	tr	Few <0.1 mm crystals present as fine-grained aggregates and “ragged” platy crystals within tremolite-actinolite±chlorite aggregates; appears to be alteration/remobilized.
Sulfides	0.2	Chalcopyrite	0.1	Very fine to finely disseminated <0.3 mm chalcopyrite and pyrite crystals typically associated with silicate alteration aggregates, typically irregularly shaped and occasionally
		Pyrite	0.1	

				subhedral.
Magnetite	tr	Magnetite	tr	Very finely disseminated (<0.05 mm) crystals mostly occurring in silicate alteration aggregates.
Pre-alteration mineral proportions and characteristics difficult to discern, but it is clear that pyroxene made up 60%+ of sample prior to alteration. Sample is heavily fractured; anastomosing fractures crosscut sample at 35-60° to long axis of thin section, typically <0.2 mm wide and filled by chlorite/epidote/aphanitic matrix. Crystal deformation is increased adjacent to fractures, though crystal alteration is not.				

Sample: JJ-TS-084		**Drill hole: 18-805**		**Depth: 145.34 m**
Mineral (interpreted pre-alteration)	%	Mineral (actual)	%	Details
Plagioclase	28	Plagioclase	3	Crystal proportions difficult to discern due to alteration; few mostly intact crystals are equant and <3 mm. Mostly strongly to completely altered to chlorite±white mica. Unaltered portions of strongly altered crystals are heavily fractured. Few <1 mm polycrystalline quartz aggregates present adjacent to chlorite aggregates. Few crystals are weakly moderately altered to patches of very fine-grained white mica and partial rims of chlorite are not deformed or heavily fractured.
		Chlorite	26	
		White mica	3	
		Quartz	tr	
Pyroxene	70	Tremolite-actinolite	65	Pyroxene is completely replaced by alteration products. Pre-alteration crystal properties not discernible. Alteration present as very fine to fine-grained tremolite-actinolite±chlorite±talc aggregates and rare <1 mm discrete tremolite crystals. Minority of aggregates are kinked/deformed. Tremolite-actinolite aggregates typically also contain randomly oriented larger (<1 mm) discrete crystals.
		Talc	1	
Biotite	tr	Biotite	tr	Few <2 mm “ragged” platy crystals in contact with chlorite and/or tremolite-actinolite.
Sulfides	2	Chalcopyrite	1.0	<1.0 mm interstitial, irregularly shaped chalcopyrite+pyrite±pentlandite±pyrrhotite aggregates and <0.2 mm disseminated irregularly shaped to subhedral pyrite and chalcopyrite crystals, commonly occurring in <4 mm clusters.
		Pyrite	0.7	
		Pentlandite	0.3	
		Pyrrhotite	0.1	
Magnetite	0.5	Magnetite	0.5	<0.5 mm anhedral to rarely subhedral crystals, occurring throughout sample
Comments: Pre-alteration mineral proportions and characteristics very difficult to discern. Massive, no foliation, pervasive fracturing, or veining. Evident by tremolite-actinolite proportion that pyroxene made up 60%+ of sample pre-alteration.				

Sample: JJ-TS-085		**Drill hole: 18-805**		**Depth: 147.17 m**
Mineral (interpreted	%	Mineral (actual)	%	Details

pre-alteration)				
Plagioclase	54	Chlorite	56	Completely replaced by alteration minerals. Pre-alteration crystal properties not discernible. Alteration typically occurs as monomineralic randomly oriented fine-grained chlorite aggregates. Minor very fine-grained white mica and/or quartz sometimes present as minor component of alteration aggregates.
		White mica	1	
		Quartz	tr	
Pyroxene	45	Tremolite-actinolite	42	Completely replaced by alteration minerals. Pre-alteration crystal properties not discernible. Alteration typically occurs as fine-grained tremolite-actinolite±chlorite aggregates. Talc occasionally present as minor very fine-grained component. Tremolite-actinolite also present as <7 mm discrete crystals, some of which display undulose extinction, which sometimes wrap around tremolite-actinolite+chlorite aggregates
		Talc	tr	
Biotite	0.5	Biotite	0.5	<0.2 mm crystals, present as fine-grained aggregates and "ragged" platy crystals. Always present in contact with chlorite.
Sulfides	tr	Pyrite	tr	Very finely disseminated (<0.05 mm) and elongate (0.5 mm) monosulfide crystals, occurring in silicate alteration aggregates, generally in <3 mm clusters.
		Chalcopyrite	tr	
Magnetite	tr	Magnetite	tr	<0.1 mm disseminated, generally equant crystals, distributed throughout sample.
Comments: Pre-alteration crystal properties are not discernible, though pre-alteration boundaries between plagioclase and pyroxene are mostly discernible. Boundaries commonly partially obscured by chlorite and/or quartz extending across interpreted pre-alteration crystal boundaries. Massive, no foliation, fracturing, or veining.				

Sample: JJ-TS-086		**Drill hole: 18-805**		**Depth: 149.33 m**
Mineral (interpreted pre-alteration)	%	Mineral (actual)	%	Details
Plagioclase	60	Plagioclase	50	0.2-3.0 mm. Anhedral to rarely subhedral, equant to rarely tabular. Typically weakly fractured, with fractures filled by chlorite and/or white mica. Rare deformation twinning. Dominantly weakly to moderately altered to <0.2 mm patches of very fine-grained white mica± chlorite±epidote. Chlorite also present as partial rims of weakly altered crystals. Minority of crystals are mostly replaced by very fine to fine-grained chlorite±white mica. Few <0.2 mm muscovite crystals in areas of white mica alteration.
		Chlorite	8	
		White mica	4	
		Epidote	tr	
Pyroxene	40	Tremolite-actinolite	38	0.2-5.0 mm pre-alteration. Pre-alteration morphology sometimes roughly preserved, generally appearing equant and anhedral. Alteration typically present as very fine to fine-grained tremolite-actinolite±chlorite±talc aggregates, with chlorite occasionally the dominant mineral. Few <2 mm optically continuous tremolite crystals, some showing simple twinning.
		Talc	tr	
Opaques	tr	Pyrite	tr	<0.2 mm very fine to finely disseminated crystals, generally irregularly shaped, occasionally equant and subhedral. Located in silicate alteration mineral aggregates.
		Chalcopyrite	tr	

Magnetite	tr	Magnetite	tr	Very finely disseminated, elongate <0.1 mm crystals, within silicate alteration aggregates.
Comments: Cumulate, equilibrated, no interstitial magmatic minerals. Massive, no foliation, veining, or pervasive fracturing. Biotite not observed in sample. Plagioclase typically fine-grained. Pyroxene mostly appears to have been fine-grained prior to alteration. Altered pyroxene crystals occasionally partially to completely enclose plagioclase crystals.				

Sample: JJ-TS-087		**Drill hole: 18-805**		**Depth: 151.49 m**
Mineral (interpreted pre-alteration)	%	Mineral (actual)	%	Details
Plagioclase	53	Plagioclase	tr	Almost completely replaced by alteration minerals. Pre-alteration crystal size/properties difficult to discern due to intensity of alteration; generally appear to have been <3 mm. Typically altered to fine to very-grained chlorite±white mica aggregates. Partial plagioclase crystals that are present are typically altered to large patches of very fine-grained white mica and fine-grained chlorite rims.
		Chlorite	50	
		White mica	4	
Pyroxene	47	Tremolite-actinolite	44	Completely replaced by alteration minerals. Pre-alteration crystal morphology not discernible due to alteration. Alteration typically present as very fine to fine-grained tremolite-actinolite± chlorite±talc. Few <3 mm discrete tremolite crystals, some of which are simply twinned.
		Talc	2	
Biotite	tr	Biotite	tr	Few <0.1 mm platy crystals surrounded by chlorite.
Sulfides	0.2	Chalcopyrite	0.1	Very finely (<0.1 mm) disseminated pyrite and chalcopyrite, and elongate chalcopyrite crystals up to 2 mm long, occurring in silicate alteration aggregates.
		Pyrite	0.1	
Magnetite	0.5	Magnetite	0.5	Very finely disseminated (<0.1 mm) crystals distributed throughout sample, occurring in silicate alteration aggregates.
Comments: Pre-alteration crystal properties are not discernible, and pre-alteration crystal boundaries are generally vaguely discernible. Massive, no foliation, veining, or fracturing. Interpreted local pre-alteration poikilitic texture occasionally observed, in which altered plagioclase crystals are completely encircled by altered pyroxene crystals.				

Sample: JJ-TS-088		**Drill hole: 18-805**		**Depth: 153.62 m**
Mineral (interpreted pre-alteration)	%	Mineral (actual)	%	Details
Plagioclase	50	Plagioclase	tr	Almost completely replaced by alteration minerals. Pre-alteration crystal properties not discernible due to alteration. Few observed plagioclase crystals are not completely altered; these crystals are largely altered by >1 mm rims of chlorite, with surviving portions heavily altered to patches of white mica. Alteration of completely altered crystals present as very fine-grained chlorite±white mica, and less commonly fine-grained monomineralic chlorite aggregates.
		Chlorite	50	
		White mica	2	
Pyroxene	50	Tremolite-actinolite	48	Completely replaced by alteration minerals. Pre-alteration morphology difficult to discern due to degree of alteration;

		Talc	tr	better pseudomorphed crystals appear to have been equant. Alteration present as very fine to fine-grained tremolite-actinolite±chlorite±talc aggregates. Tremolite occasionally present as discrete <6 mm crystals and rarely present as rims around pyroxene alteration mineral aggregates.
Biotite	tr	Biotite	tr	Few <0.5 mm "ragged", irregularly shaped crystals at margins between altered plagioclase and altered pyroxene.
Sulfides	0.2	Pyrite	0.1	Typically <0.1 mm (rarely up to 2 mm) very finely disseminated monosulfide crystals. Crystals occur in silicate alteration mineral aggregates.
		Chalcopyrite	0.1	
Magnetite	tr	Magnetite	tr	Very finely disseminated <0.1 mm elongate and equant crystals in silicate alteration aggregates.
Comments: Pre-alteration crystal morphology is not discernible, and pre-alteration crystal boundaries are generally somewhat discernible, with chlorite alteration aggregates commonly extending from altered plagioclase to altered pyroxene crystals. Massive, no foliation, fracturing, or veining.				

Sample: JJ-TS-089		**Drill hole: 18-805**		**Depth: 155.39 m**
Mineral (interpreted pre-alteration)	%	Mineral (actual)	%	Details
Plagioclase	50	Plagioclase	tr	Almost completely replaced by alteration minerals. Pre-alteration crystal properties not discernible due to alteration. Two crystals are not completely altered; these partial crystals are surrounded by >1 mm rims of chlorite, with surviving parts of the crystal heavily altered to white mica. Alteration of completely altered crystals present as very fine to fine-grained chlorite±white mica aggregates, with chlorite and white mica most commonly occurring as discrete patches.
		Chlorite	50	
		White mica	2	
		Quartz	tr	
Pyroxene	50	Tremolite-actinolite	46	Completely replaced by alteration minerals. Pre-alteration crystal properties generally not discernible due to alteration; better pseudomorphed crystals appear to have been equant to tabular and mostly <3 mm. Alteration present as very fine-grained tremolite-actinolite±chlorite±talc aggregates. Several 0.5-7 mm optically continuous crystals of tremolite-actinolite present, sometimes surrounding smaller areas of tremolite-actinolite±chlorite aggregates.
		Talc	2	
Biotite	0.2	Biotite	0.2	0.05-1.0 mm crystals irregularly shaped/platy crystals and "books" of crystals, mostly occurring at margins between altered plagioclase and altered pyroxene, and occasionally surrounded by chlorite.
Sulfides	tr	Pyrite	tr	Very fine-grained disseminated monosulfide crystals, generally irregularly shaped, pyrite occasionally subhedral.
		Chalcopyrite	tr	
Magnetite	tr	Magnetite	tr	Rare very fine-grained disseminated crystals, generally in association with sulfide crystals.
Comments: Pre-alteration crystal properties not discernible. Pre-alteration crystal boundaries generally obscured by alteration. Massive, no foliation or fracturing. One anastomosing ~0.1 mm -wide veinlet crosscuts sample at 30-40° to long axis of thin section, filled by talc and minor tremolite.				

Sample: JJ-TS-090		**Drill hole: 18-805**		**Depth: 157.84 m**
Mineral (interpreted pre-alteration)	%	Mineral (actual)	%	Details
Plagioclase	50	Plagioclase	tr	Almost completely replaced by alteration minerals. Pre-alteration crystal properties not discernible; appear to have been <3 mm. Surviving partial plagioclase crystals mostly present in 1 cm area on corner of sample, which range from weakly to strongly altered to white mica and surrounded by chlorite rims. Completely altered crystals replaced by very fine to fine-grained chlorite±white mica. Polycrystalline <0.2 mm mosaic texture quartz crystals present in <0.5 mm patches surrounded by chlorite.
		Chlorite	53	
		White mica	1	
		Quartz		
Pyroxene	50	Tremolite-actinolite	43	Completely replaced by alteration minerals. Minority of crystals are well-pseudomorphed and appear to have been equant, subhedral, and generally <2 mm. Alteration present as fine to very-fine grained tremolite-actinolite±chlorite± talc aggregates and common <2 mm discrete tremolite crystals, which are sometimes simply twinned.
		Talc	3	
Sulfides	tr	Pyrite	tr	Very finely disseminated, irregularly shaped crystals of pyrite and/or chalcopyrite, generally within alteration aggregates after pyroxene.
		Chalcopyrite	tr	
Comments: Pre-alteration crystal properties generally not discernible, though general crystal size appears to have been <3 mm. Massive, no foliation, fracturing, or veining. Biotite not observed in sample. Altered pyroxene crystals occasionally observed partially enclosing partially altered plagioclase crystals.				

Sample: JJ-TS-091		**Drill hole: 18-805**		**Depth: 160.69 m**
Mineral (interpreted pre-alteration)	%	Mineral (actual)	%	Details
Plagioclase	50	Plagioclase	10	Crystal properties somewhat obscured by alteration but generally appear to have been <4 mm, equant to tabular, and anhedral. Majority of crystals are moderately to strongly altered to large patches of very fine-grained white mica and partial to complete chlorite±white mica rims. Minority of plagioclase crystals, typically those mostly bordered by altered pyroxene, are completely altered to chlorite-dominated alteration aggregates, commonly with minor white mica.
		Chlorite	26	
		White mica	18	
		Epidote	tr	
Pyroxene	50	Tremolite-actinolite	44	Completely replaced by alteration minerals. Crystals typically poorly pseudomorphed, and crystal properties aside from size are hard to discern; appear to generally be 1-4 mm. Alteration present as very fine to fine-grained tremolite-actinolite±chlorite±talc aggregates, with talc commonly occurring as discrete patches within aggregates. Occasional discrete <3 mm tremolite crystals, commonly irregularly shaped.
		Talc	2	
Sulfides	tr	Pyrite	tr	Very finely disseminated, irregularly shaped monosulfide crystals, generally within alteration aggregates after pyroxene. Rare interstitial irregularly shaped pyrite+chalcopyrite crystals.
		Chalcopyrite	tr	

Magnetite	tr	Magnetite	tr	Rare <0.05 mm disseminated crystals in silicate alteration aggregates.
Comments: Pre-alteration properties difficult to discern, but appears to be cumulate and equilibrated. Biotite not observed in sample. Massive, no foliation or pervasive fracturing. Two anastomosing veinlets crosscut sample at conjugate angles, both at ~40° to long axis of thin section, filled by tremolite±chlorite±talc. Minor movement (~0.5 mm) seen adjacent to both veinlets (dextral along one veinlet, sinistral along the other). Plagioclase and pyroxene both commonly occur in <1 cm clusters of several crystals.				

Sample: JJ-TS-092		**Drill hole: 18-805**		**Depth: 165.18 m**
Mineral (interpreted pre-alteration)	%	Mineral (actual)	%	Details
Plagioclase	55	Plagioclase	45	0.2-3.5 mm. Anhedral, equant to rarely tabular. Crystals sometimes occur in <7 mm clusters. Majority of crystals weakly to moderately altered to patches of very fine-grained white mica and partial rims of fine-grained chlorite. Minority of crystals, especially those mostly surrounded by altered pyroxene, strongly to completely altered to very fine to fine-grained chlorite±white mica aggregates.
		Chlorite	7	
		White mica	4	
Pyroxene	45	Tremolite-actinolite	41	Completely replaced by alteration minerals. Majority of pre-alteration crystals appear 0.05-0.5 mm, equant, and subhedral to anhedral. Pre-alteration texture of larger crystals is difficult to discern, but it is clear that a smaller population of 0.5-2.0 pre-alteration crystals are present. Smaller crystals pseudomorphed by discrete tremolite crystals or monomineralic very fine-grained tremolite-actinolite aggregates. Larger crystals replaced by very fine to fine-grained tremolite-actinolite±chlorite±talc aggregates, typically randomly oriented and with boundaries with adjacent crystals that are difficult to determine.
		Talc	1	
Sulfides	tr	Pyrite	tr	Very finely disseminated irregularly shaped monosulfide crystals, mostly in pyroxene alteration aggregates.
		Chalcopyrite	tr	
Oxides	tr	Magnetite	tr	<0.2 mm irregularly shaped interstitial magnetite crystals in aggregate with darker-coloured opaque – appears to be ilmenite. Very finely disseminated <0.05 mm magnetite crystals in silicate alteration aggregates also present
		Ilmenite	tr	
Comments: Cumulate, equilibrated, no interstitial minerals present. Biotite not observed in sample. Massive, no foliation, veining, or fracturing. Plagioclase dominantly fine grained, pre-alteration pyroxene dominantly very fine-grained to fine-grained. Plagioclase commonly partially to completely encircles very fine-grained altered pyroxene.				

Sample: JJ-TS-093		**Drill hole: 18-805**		**Depth: 170.22 m**
Mineral (interpreted	%	Mineral (actual)	%	Details

pre-alteration)				
Plagioclase	45	Plagioclase	20	0.3-6.0 mm. Anhedral, smaller crystals are equant, >4 mm crystals are typically tabular. Generally weakly fractured, with fractures filled by very fine-grained and/or white mica. Usually moderately altered, almost always altered to completely very fine-grained to fine-grained chlorite rims, with patches of very fine-grained white mica usually also present. Minority of crystals, mostly those surrounded by plagioclase, are altered to chlorite±white mica.
		Chlorite	25	
		White mica	5	
Pyroxene	55	Tremolite-actinolite	50	Completely replaced by alteration minerals. Pre-alteration crystal properties poorly preserved; appear to have been 0.5-5.0 mm (upper boundary uncertain). <1.0 mm crystals sometimes pseudomorphed, generally appearing equant and subhedral. Altered to tremolite-actinolite± chlorite±talc, with alteration minerals commonly randomly oriented.
		Talc	5	
Biotite	tr	Biotite	tr	Very few "ragged" platy <0.2 mm crystals in contact with tremolite-actinolite and chlorite.
Sulfides	1	Pyrrhotite	0.3	Few interstitial polysulfide crystals and one 15 x 3 mm pyrrhotite+pyrite+pentlandite+chalcopyrite bleb that has been partially remobilized into adjacent silicate alteration aggregates. Very fine disseminate pyrite and chalcopyrite throughout.
		Pyrite	0.3	
		Chalcopyrite	0.2	
		Pyrrhotite	0.2	
Magnetite	tr	Magnetite	tr	Rare disseminated crystals in silicate alteration aggregates.
Comments: Appears to have been cumulate and equilibrated, though pre-alteration texture is difficult to determine. Massive, no foliation or pervasive fracturing. Discontinuous chlorite-dominated veinlets cross cut sample at ~15-30° to long axis of thin section. Plagioclase and pyroxene both appear to have been dominantly medium-grained.				

Sample: JJ-TS-094		**Drill hole: 18-805**		**Depth: 175.14 m**
Mineral (interpreted pre-alteration)	%	Mineral (actual)	%	Details
Plagioclase	45	Plagioclase	8	Crystal properties somewhat difficult to discern due to alteration, but appear to be <3 mm and generally equant. Typically weakly fractured, with fractures filled by chlorite and/or white mica. Typically strongly altered to chlorite rims and patches of white mica and/or chlorite. Minority of crystals completely altered to chlorite.
		Chlorite	38	
		White mica	1	
Pyroxene	55	Tremolite-actinolite	47	Completely replaced by alteration minerals. Pre-alteration properties sometimes preserved, generally appearing to have been equant, and usually <3 mm, with a few altered crystals up to 8 mm present. Altered to very fine to fine-grained tremolite-actinolite±talc±chlorite aggregates. One 8 mm tremolite crystal present, surrounding 4 mm area of talc-dominated alteration.
		Talc	3	
Biotite	tr	Biotite	tr	Few <0.1 ragged platy crystals, typically at margins between altered plagioclase and altered pyroxene crystals.
Sulfides	2	Chalcopyrite	0.7	Interstitial <1 mm pyrrhotite+chalcopyrite±pyrite ±pentlandite crystals. Very finely disseminated pyrite and chalcopyrite, largely as <3 mm clusters, commonly as haloes
		Pyrrhotite	0.5	
		Pentlandite	0.5	

		Pyrite	0.3	around interstitial crystals
Comments: Appears to have been cumulate and equilibrated, with biotite present as the only interstitial mineral. Massive, no foliation or pervasive fracturing. Pre-alteration texture is somewhat difficult to determine, but plagioclase and pyroxene both appear to have been dominantly medium-grained with moderate size variation present. >4 mm altered pyroxene crystals partially to completely encircle altered plagioclase and altered pyroxene crystals.				

Sample: JJ-TS-095		**Drill hole: 18-805**		**Depth: 180.58 m**
Mineral (interpreted pre-alteration)	%	Mineral (actual)	%	Details
Plagioclase	40	Plagioclase	4	Pre-alteration crystal properties not discernible due to alteration; appear to be <4 mm. Majority of crystals are completely altered to very fine to fine-grained to fine-grained chlorite±white mica. Minority of crystals, typically >3 mm crystals, only weakly to moderately altered to complete chlorite rims of chlorite aggregates and very fine-grained patches of white mica.
		Chlorite	36	
		White mica	1	
Pyroxene	60	Tremolite-actinolite	58	Completely replaced by alteration minerals. Pre-alteration properties are generally roughly preserved, though exact position of boundaries is commonly obscured; crystals appear equant to elongate and <4 mm. Alteration present as very fine to fine-grained tremolite-actinolite±talc±chlorite aggregates, with talc present as the dominant mineral in a minority of aggregates.
		Talc	1	
Sulfides	tr	Pyrite	tr	Very finely disseminated irregularly shaped monosulfide crystals, distributed throughout.
		Chalcopyrite	tr	
Comments: Appears to be cumulate textured; no interstitial minerals observed. Biotite not present in sample. Massive, no foliation, fracturing, or veining. Boundaries between pre-alteration difficult to determine in some areas, due to chlorite and sometimes tremolite-actinolite extending between aggregates occurring after plagioclase and after pyroxene.				

Sample: JJ-TS-096		**Drill hole: 18-805**		**Depth: 185.32 m**
Mineral (interpreted pre-alteration)	%	Mineral (actual)	%	Details
Plagioclase	18	Chlorite	20	Plagioclase has been completely replaced by alteration minerals. Pre-alteration morphology cannot be determined; alteration aggregates do not appear to pseudomorph primary plagioclase, generally wrapping around altered pyroxene crystals. Monomineralic very fine to fine-grained chlorite aggregates most common, with chlorite+white mica aggregates also present. Quartz present as few <0.3 mm mosaic texture aggregates.
		White mica	1	
		Quartz	tr	
Pyroxene	80	Tremolite-actinolite	79	Pyroxene has been completely replaced by alteration minerals. Pre-alteration morphology generally roughly discernible, appearing equant and <3 mm. Altered to fine-grained tremolite-actinolite±chlorite±talc aggregates, with chlorite and talc generally present as minor components. Alteration mineral aggregates occasionally weakly
		Talc	tr	

				crenulated. Rare <2 mm discrete simply twinned tremolite crystals.
Sulfides	2	Pyrrhotite	0.7	Most commonly elongate crystals, <0.1 mm wide and up to 3 mm long, within alteration aggregates after pyroxene. Less common very finely disseminated monosulfide and interstitial polysulfide crystals.
		Chalcopyrite	0.5	
		Pyrite	0.5	
		Pentlandite	0.3	
Comments: Sample chosen to represent more melanocratic portion of brecciated zone and is not representative of wider intercept. Appears to have been cumulate and equilibrated, no interstitial minerals observed. Massive, no foliation present. Single 0.2 mm wide quartz-chlorite veinlet crosscutting sample at ~50° to long axis of thin section.				

Sample: JJ-TS-097		**Drill hole: 18-805**		**Depth: 190.21 m**
Mineral (interpreted pre-alteration)	%	Mineral (actual)	%	Details
Plagioclase	62	Plagioclase	53	0.2-8.0 mm. Anhedral, equant to rarely tabular. Crystals commonly occur in <10 mm clusters. Typically weakly fractured, with fractures filled by white mica. Typically weakly altered to patches of very fine-grained white mica. Partial rims of fine-grained chlorite typically present in contact with altered pyroxene. <1 mm epidote crystals (in aggregate or optically continuous) adjacent to white mica alteration aggregates.
		Chlorite	8	
		White mica	4	
		Epidote	1	
Pyroxene	38	Orthopyroxene	4	0.5-7.0 mm pre-alteration. Pre-alteration morphology is somewhat difficult to discern, but smaller (<2 mm) crystals appear to have been equant and subhedral, whereas larger (>2 mm) crystals appear to have been irregularly shaped and anhedral. Most crystals are completely replaced by alteration minerals. A minority of >3 mm crystals are only partially replaced by alteration minerals. Alteration present as very fine to fine grained tremolite-actinolite±talc ±chlorite. Tremolite-actinolite is typically dominant in <2 mm crystals, whereas talc is typically dominant in >2 mm crystals.
		Tremolite-actinolite	22	
		Talc	8	
Sulfides	0.5	Pyrite	0.2	Mostly present as very finely disseminated pyrite and chalcopyrite crystals, generally irregularly shaped and pyrite cubes also present. Less commonly as <0.5 mm polysulfide crystals.
		Pyrrhotite	0.1	
		Chalcopyrite	0.1	
		Pentlandite	0.1	
Magnetite	tr	Magnetite	tr	Very finely disseminated, anhedral to subhedral.
Comments: Cumulate, equilibrated, no interstitial minerals observed. Biotite not present in sample. Massive, no foliation, pervasive fracturing, or veining. Crystal size of plagioclase and pyroxene (pre-alteration) is highly variable, varying from very fine to coarse throughout sample. Larger plagioclase crystals sometimes partially to completely encircle smaller plagioclase and altered pyroxene crystals.				

Sample: JJ-TS-098		**Drill hole: 18-805**		**Depth: 195.63 m**
Mineral (interpreted	%	Mineral (actual)	%	Details

pre-alteration)				
Plagioclase	53	Plagioclase	46	0.2-4.0 mm. Anhedral, equant. Typically weakly fractured, with fractures filled by chlorite and/or white mica. Rare deformation twinning. Typically very weakly to weakly altered; crystals surrounded by altered pyroxene are sometimes strongly to completely altered. Weakly altered crystals altered to <0.2 patches of very fine-grained white mica and partial rims of fine-grained chlorite. Strongly to completely altered crystals altered to fine-grained chlorite, sometimes occurring alongside minor white mica.
		Chlorite	6	
		White mica	3	
Ortho-pyroxene	42	Orthopyroxene	7	0.2-4.0 mm. Anhedral to subhedral, equant. Typically completely replaced by alteration minerals; less commonly very weakly to strongly altered. Partially and completely altered crystals both replaced by very fine to fine-grained tremolite-actinolite±talc±chlorite aggregates; tremolite-actinolite typically more dominant in completely altered crystals, whereas talc typically more dominant in partially altered crystals.
		Tremolite-actinolite	31	
		Talc	5	
Clino-pyroxene	5	Clinopyroxene	2	1.0-6.0 mm. Anhedral, irregularly shaped, wrapping around adjacent crystals. Ranges from weakly to completely altered. Weakly/moderately altered clinopyroxene crystals are altered to tremolite-actinolite±talc as partial/complete rims and along cleavage planes. Completely altered crystals are commonly replaced by discrete <4 mm tremolite crystals, sometimes surrounding <1 mm zones of very fine grained talc±actinolite.
Biotite	tr	Biotite	tr	Two <0.2 mm crystals in contact with chlorite alteration, near edges of plagioclase crystals.
Sulfides	0.5	Pyrrhotite	0.2	Interstitial, irregularly shaped polysulfide crystals and disaggregated crystals that appear to have been interstitial. Rare very finely disseminated pyrite and chalcopyrite.
		Chalcopyrite	0.2	
		Pentlandite	0.1	
		Pyrite	tr	
Cumulate, equilibrated, no interstitial crystal aside from rare biotite. Massive, no foliation, pervasive fracturing or veining. Quantity of pre-alteration pyroxene should be fairly accurate, but relative proportions of orthopyroxene and clinopyroxene difficult to determine due to alteration (mostly determined by shape and size of alteration aggregates occurring after pyroxene).				

Sample: JJ-TS-100		**Drill hole: 18-805**		**Depth: 200.50 m**
Mineral (interpreted pre-alteration)	%	Mineral (actual)	%	Details
Plagioclase	53	Plagioclase	35	0.5-6.5 mm. Anhedral to rarely subhedral, generally equant, >3.0 mm crystals commonly tabular. Crystals commonly in <1.0 mm patches. Rare deformation twinning. Most commonly weakly to moderately altered to patches of very fine-grained white mica±chlorite and partial chlorite rims. Minority of crystals are strongly altered to white mica±chlorite.
		Chlorite	18	
		White mica	3	
Pyroxene	47	Orthopyroxene	tr	Almost completely replaced by alteration minerals. Rare <0.5 mm orthopyroxene cores observed surrounded by
		Tremolite-	44	

		actinolite		alteration minerals. Pre-alteration properties difficult to discern; generally appear to be <3 mm. Typically replaced by tremolite-actinolite±talc±chlorite. Discrete <1.5 mm tremolite crystals occasionally observed.
		Talc	3	
Opaques	tr	Pyrite	tr	<0.3 mm irregularly shaped interstitial polysulfide crystals and very finely disseminated monosulfide crystals.
		Chalcopyrite	tr	
Magnetite	tr	Magnetite	tr	Rare <0.1 mm disseminated crystals, usually in association with sulfide minerals.
Comments: Pre-alteration crystal boundaries commonly difficult to discern due to chlorite and tremolite-actinolite crystals extending across pre-alteration boundaries. Appears to be cumulate, equilibrated. No interstitial minerals observed; biotite not present. Massive, no foliation, veining, or pervasive fracturing. Pre-alteration crystal size somewhat variable, most commonly medium to coarse-grained and less commonly fine-grained				

Sample: JJ-TS-101		**Drill hole: 18-805**		**Depth: 205.00 m**
Mineral (interpreted pre-alteration)	%	Mineral (actual)	%	Details
Plagioclase	37	Plagioclase	3	Pre-alteration morphology generally difficult to discern in altered crystals; less altered crystals are equant, anhedral, and 0.4-7.0 mm. Majority of crystals are completely replaced by alteration minerals, generally present as very fine to fine-grained aggregates of chlorite±white mica. Minority of crystals are only weakly altered to patches of very fine grained-white mica and partial fine-grained chlorite rims.
		Chlorite	32	
		White mica	4	
Pyroxene	63	Tremolite-actinolite	61	Pre-alteration morphology very difficult to discern. Pyroxene appears to have dominantly occurred in clusters, and alteration minerals occurring after these crystals commonly overprint each other. Few pseudomorphs of smaller (<1.5 mm) crystals present, appearing to have been equant. Alteration typically present as fine to very fine-grained tremolite-actinolite±chlorite±talc. Rare discrete <3.0 mm tremolite crystals also present, sometimes showing simple twinning.
		Talc	2	
Biotite	tr	Biotite	tr	Few platy <2.0 mm crystals surrounded by chlorite alteration, appearing to be primary.
Sulfides	tr	Pyrite	tr	Very finely disseminated monosulfide and polysulfide crystals, typically occurring in clusters.
		Chalcopyrite	tr	
Magnetite	tr	Magnetite	tr	Very finely disseminated elongate crystals, mostly within silicate alteration aggregates.
Comments: Pre-alteration properties very difficult to determine due to alteration minerals overprinting boundaries. Alteration mineral aggregates commonly randomly oriented. Massive, no foliation, pervasive fracturing, or veining.				

Sample: JJ-TS-102		**Drill hole: 18-805**		**Depth: 210.36 m**
Mineral (interpreted pre-alteration)	%	Mineral (actual)	%	Details
Plagioclase	55	Plagioclase	12	Pre-alteration morphology difficult to determine, but generally appears to have been 0.5-5.0 mm and equant to tabular. Majority of crystals are strongly altered, and a minority of crystals are completely altered. Alteration is present as very fine to fine-grained chlorite±white mica aggregates, typically as patches that extend across a large portion of a crystal. Chlorite is typically dominant in completely altered crystals and white mica typically dominant in crystals that are not completely altered.
		Chlorite	42	
		White mica	6	
Pyroxene	45	Tremolite-actinolite	40	Pre-alteration morphology somewhat difficult to determine, but generally appears to be equant and <4 mm. Alteration present as very fine to fine-grained tremolite-actinolite±chlorite±talc aggregates. Discrete tremolite-actinolite crystals up to 5 mm also present, sometimes with simple twinning.
		Talc	tr	
Sulfides	tr	Pyrite	tr	Very finely disseminated monosulfide crystals, generally anhedral to less commonly subhedral, typically in <2 mm clusters.
		Chalcopyrite	tr	
Comments: Crystal proportions/properties somewhat difficult to discern due to chlorite and/or tremolite-actinolite aggregates extending across pre-alteration crystal boundaries. No interstitial minerals present. Massive, no foliation, pervasive fracturing, or veining.				

Sample: JJ-TS-103		**Drill hole: 18-805**		**Depth: 215.27 m**
Mineral (interpreted pre-alteration)	%	Mineral (actual)	%	Details
Plagioclase	47	Plagioclase	35	0.1-4.0 mm. Dominantly anhedral and equant; <1.0 mm crystals are occasionally subhedral. No fracturing visible. Crystals typically occur in <10 mm clusters. Majority of crystals are moderately altered to patches of very fine-grained white mica±chlorite± epidote, some also with rims of fine-grained chlorite aggregates. Minority of crystals are completely altered to chlorite±white mica.
		Chlorite	9	
		White mica	7	
		Epidote	tr	
Pyroxene	53	Tremolite-actinolite	46	Pyroxene is completely replaced by alteration minerals. Pre-alteration crystal properties cannot be determined due to alteration aggregates extending across pre-alteration crystals. Crystal size generally appears to have been 1-4 mm. Crystals typically occur in <10 mm clusters. Alteration typically present as very fine to fine-grained tremolite-actinolite±chlorite±talc aggregates. Discrete <0.7 mm tremolite crystals rarely present.
		Talc	2	
Biotite	3	Biotite	3	Platy crystals at pre-alteration crystal margins (as well as between unaltered plagioclase crystals), and very fine-grained aggregates occurring alongside chlorite.
Hornblende	tr	Hornblende	tr	Few <0.7 mm equant, anhedral crystals with good cleavage present in strongly altered, mosaic textured area on margin of sample.

Sulfides	tr	Pyrite	tr	Mostly present as <0.3 mm irregularly shaped interstitial polysulfide crystals. Less commonly present as monosulfide very finely disseminated crystals, typically as <2 mm haloes.
		Pentlandite	tr	
		Chalcopyrite	tr	
Oxides	tr	Magnetite	tr	Rare <0.05 mm interstitial crystals, typically as intergrown magnetite and ilmenite.
		Ilmenite	tr	
Comments: Pre-alteration properties difficult to discern due to alteration, but appears to have been cumulate and equilibrated. Biotite and hornblende both present as accessory phases. Massive, no fracturing or veining. Crystal size is quite variable, ranging from fine to medium throughout. ~6x20 mm area at corner of sample is completely altered and appears to be recrystallized, tremolite-actinolite and biotite commonly showing triple junctions.				

Sample: JJ-TS-104		**Drill hole: 18-805**		**Depth: 220.43 m**
Mineral (interpreted pre-alteration)	%	Mineral (actual)	%	Details
Plagioclase	43	Plagioclase	37	0.2-4.0 mm. Typically anhedral and equant to tabular; crystals partially to completely enclosed by clinopyroxene are subhedral. Commonly weakly to moderately fractured, with fractures usually filled by white mica and/or chlorite.
		Chlorite	10	
		White mica	2	
Ortho-pyroxene	53	Orthopyroxene	7	0.5-5.0 mm. Typically equant and subhedral to anhedral, >3.0 mm crystals are commonly equant. Majority of crystals strongly altered to partial/complete rims and along fractures. Minority of crystals completely altered. Typically altered to very fine-grained tremolite-actinolite± talc±chlorite. Few <1.0 mm discrete tremolite crystals present.
		Tremolite-actinolite	37	
		Talc	6	
Clino-pyroxene	3	Clinopyroxene	2	1.5-4.0 mm. Anhedral and irregularly shaped, with crystals wrapping around adjacent plagioclase and orthopyroxene crystals. Typically weakly altered to rims of tremolite-actinolite that are commonly optically continuous, as well as discontinuous tremolite-actinolite±chlorite along cleavage planes. Less commonly completely altered to tremolite-actinolite±chlorite±talc.
Biotite	tr	Biotite	tr	<1.0 mm platy, irregularly shaped crystals, occurring at boundaries between pre-alteration pyroxene/plagioclase.
Sulfides	0.2	Pyrite	0.1	Irregularly shaped <0.3 mm interstitial polysulfide crystals and very finely disseminated monosulfide crystals, most commonly in clusters
		Pentlandite	0.1	
		Chalcopyrite	tr	
Magnetite	tr	Magnetite	tr	<0.1 mm disseminated anhedral to subhedral crystals, present interstitially and as inclusions in plagioclase.
Comments: Cumulate, equilibrated, biotite is only accessory phase. Massive, no foliation or pervasive veining. Discontinuous fractures typically occur at 20-45° to long axis of thin section. Relative proportion of orthopyroxene and clinopyroxene somewhat difficult to determine; some smaller, completely altered pyroxene crystals classified as orthopyroxene may actually be clinopyroxene. Plagioclase size quite variable, ranging from very fine to medium-grained throughout. Pyroxene is dominantly medium-grained. Clinopyroxene and plagioclase commonly partially to completely encircle smaller orthopyroxene and plagioclase.				

Sample: JJ-TS-105		Drill hole: 18-805		Depth: 225.45 m
Mineral (interpreted pre-alteration)	%	Mineral (actual)	%	Details
Plagioclase	46	Plagioclase	44	0.1-8 mm. <4.0 mm crystals are typically anhedral and equant to rarely tabular; crystals partially to completely enclosed by orthopyroxene/other plagioclase crystals sometimes subhedral. >4.0 mm crystals anhedral and tabular. Crystals sometimes occur in <8 mm clusters containing variable crystal sizes. Alteration is very weak to occasionally absent; typically present as small patches of very fine-grained white mica±chlorite± epidote and monomineralic chlorite aggregates.
		Chlorite	1	
		White mica	1	
		Epidote	tr	
Ortho-pyroxene	46	Orthopyroxene	45	0.2-5.0 mm. Typically equant and euhedral to subhedral; >3.0 mm crystals generally elongate and anhedral. Crystals commonly occur in <8 mm clusters of >80% orthopyroxene. Typically very weakly altered to partial rims and small patches of tremolite-actinolite, typically occurring as discrete crystals. Very fine-grained tremolite-actinolite±talc occur less commonly.
		Tremolite-actinolite	2	
		Talc	tr	
Clino-pyroxene	8	Clinopyroxene	7	0.7-7.0 mm. Typically anhedral and irregularly shaped, partially to completely wrapping around adjacent crystals. >1.5 mm crystals are equant and subhedral to anhedral. Very weakly altered to partial rims of tremolite and very fine-grained aggregates of tremolite-actinolite±chlorite along cleavage planes.
Biotite	tr	Biotite	tr	Few <0.3 mm platy crystals present at boundaries between plagioclase and/or pyroxene.
Sulfides	tr	Pyrrhotite	tr	<0.2 mm interstitial polysulfide crystals, present between silicate crystals and sometimes as inclusions inside silicates.
		Chalcopyrite	tr	
		Pyrite	tr	
		Pentlandite	tr	
Magnetite	tr	Magnetite	tr	<0.1 mm interstitial crystals and disseminated crystals within silicate alteration aggregates.
Comments: Cumulate, equilibrated, biotite is only interstitial phase. Massive, no foliation, pervasive fracturing, or veining. Variable crystal size; plagioclase and orthopyroxene typically range from fine-grained to medium-grained, clinopyroxene typically ranges from medium-grained to coarse-grained. Clinopyroxene and plagioclase commonly partially to completely encircle smaller crystals of orthopyroxene and plagioclase.				

Sample: JJ-TS-106		Drill hole: 18-805		Depth: 230.29 m
Mineral (interpreted pre-alteration)	%	Mineral (actual)	%	Details
Plagioclase	45	Plagioclase	35	0.05-8.0 mm. Typically anhedral and equant, >4.0 mm crystals are typically tabular. <0.1 mm crystals present as groups of mosaic texture crystals at boundaries between larger plagioclase crystals, appearing to be the product of recrystallization. Deformation twinning and undulose extinction are common. Commonly weakly fractured, with
		Chlorite	10	
		White mica	2	
		Epidote	tr	

				some fractures filled by white mica. Most crystals are weakly altered to very fine-grained white mica patches, some with rims of fine-grained chlorite aggregates. Minority of crystals (those surrounded by altered pyroxene) completely altered to chlorite±white mica.
Pyroxene	54	Tremolite-actinolite	53	Completely replaced by alteration minerals. Pre-alteration properties not discernible. Crystals appear to have commonly occurred in <10 mm clusters. Alteration typically present as fine grained tremolite-actinolite±chlorite±talc. Occasional <1.5 mm tremolite crystals present.
		Talc	1	
Biotite	0.5	Biotite	0.5	<1.5 mm crystals, present as discrete platy crystals at margins of pre-alteration crystals, and as very fine-grained aggregates adjacent to chlorite.
Sulfides	0.3	Chalcopyrite	0.2	<0.5 mm interstitial polysulfide crystals and very finely disseminated monosulfide crystals. Disseminated crystals present in silicate alteration aggregates.
		Pyrite	0.1	
		Pentlandite	tr	
Magnetite	tr	Magnetite	tr	Rare <0.1 mm anhedral to subhedral disseminated crystals.
Comments: Pre-alteration crystal quantities are difficult to determine; one 10x20 mm area has no discernible pre-alteration crystal boundaries, but appears to have been pyroxene-dominated due to prevalence of tremolite-actinolite. Appears to have been cumulate, biotite only accessory phase present. Massive, no foliation, veining, or pervasive fracturing. Crystal size is variable; plagioclase crystals range from very fine to medium-grained.				

Sample: JJ-TS-108		**Drill hole: 18-805**		**Depth: 240.78 m**
Mineral (interpreted pre-alteration)	%	Mineral (actual)	%	Details
Plagioclase	55	Plagioclase	40	0.1-5.0 mm. Anhedral and typically equant; >3.0 mm crystals are typically tabular. Crystals in very fine-grained zone are mosaic textured with polygonal triple junctions. Typically weakly altered to very fine-grained white mica±epidote± chlorite patches and partial rims of fine-grained chlorite. Quartz only present in very fine-grained zone.
		Chlorite	15	
		White mica	5	
		Epidote	tr	
		Quartz	tr	
Pyroxene	45	Tremolite-actinolite	40	Completely replaced by alteration minerals. Pre-alteration morphology is generally very difficult to discern; crystals in fine-grained zone are not pseudomorphed. Crystals in coarse-grained zone are generally pseudomorphed, appearing subhedral and equant to elongate. Alteration present as fine to very fine tremolite-actinolite± chlorite±talc aggregates.
		Talc	tr	
Sulfide	0.2	Pyrite	0.1	Very finely disseminated interstitial anhedral to subhedral crystals, present in silicate alteration aggregates.
		Chalcopyrite	0.1	
Magnetite	tr	Magnetite	tr	Very finely disseminated elongate crystals within silicate alteration aggregates.
Comments: Cumulate, equilibrated, no interstitial phases present. Massive, no foliation or pervasive fracturing. Few <0.2 mm-wide tremolite+chlorite veins crosscutting plagioclase crystals in coarse-grained section of sample. Several zones in sample with different grain sizes, each with sharp boundaries. 75% of sample is fine-grained, with occasional medium-grained plagioclase. Two zones on either side of fine-grained zone are coarse-grained, making up 20% of sample. Coarse-grained zones consist of 80% plagioclase. 5% of sample is very fine-grained, with mosaic texture plagioclase and quartz and mosaic-textured/elongate tremolite.				

Sample: JJ-TS-109		**Drill hole: 18-805**		**Depth: 245.31 m**
Mineral (interpreted pre-alteration)	%	Mineral (actual)	%	Details
Plagioclase	50	Plagioclase	38	0.3-5.0 mm. Majority of crystals are anhedral and equant. <0.5 mm crystals enclosed by altered pyroxene and >3.0 mm crystals are typically subhedral and tabular. Typically weakly fractured, with fractures filled by white mica. Typically weakly to moderately altered to patches of very fine-grained white mica aggregates and partial rims of fine-grained chlorite aggregates. Minority of crystals are strongly to completely altered to chlorite±white mica.
		Chlorite	9	
		White mica	6	
Pyroxene	50	Tremolite-actinolite	46	0.5-6.0 mm. Completely replaced by alteration minerals. <3.0 mm pre-alteration crystals are typically equant and subhedral, >3.0 mm pre-alteration crystals are typically irregularly shaped and anhedral, commonly wrapping around adjacent plagioclase/altered pyroxene crystals. Alteration typically present as very fine to fine-grained tremolite-actinolite±chlorite±talc aggregates. Discrete tremolite crystals up to 5 mm in size less commonly present.
		Talc	1	
Biotite	tr	Biotite	tr	0.1-1.0 mm platy crystals at boundaries of pre-alteration plagioclase and pyroxene crystals
Pyrite	tr	Pyrite	tr	Very finely disseminated crystals in silicate alteration aggregates, largely in <1 mm clusters.
		Chalcopyrite	tr	
Oxides	tr	Magnetite	tr	Very finely disseminated crystals as with both minerals present in aggregate.
		Ilmenite	tr	
Comments: Cumulate, equilibrate, biotite is only accessory phase. Massive, no foliation, pervasive fracturing, or veining. Variable crystal size, typically ranging from fine to medium throughout. Altered pyroxene commonly partially to completely encloses plagioclase and other altered pyroxene crystals.				

Sample: JJ-TS-110		**Drill hole: 18-805**		**Depth: 250.54 m**
Mineral (interpreted pre-alteration)	%	Mineral (actual)	%	Details
Plagioclase	63	Plagioclase	58	0.2-10.0 mm. Anhedral to subhedral, equant to tabular. Crystals commonly occur in <15 mm clusters. Typically weakly fractured with some fractures filled by white mica. Rare deformation twinning. Typically very weakly altered to very fine-grained white mica patches. Partial rims of very fine to fine-grained chlorite sometimes present adjacent to altered pyroxene crystals.
		Chlorite	5	
		White mica	2	
Pyroxene	37	Tremolite-actinolite	35	0.5-6.0 mm. Completely replaced by alteration minerals. Typically well pseudomorphed, appearing to have been equant and anhedral to subhedral. Generally replaced by fine grained tremolite-actinolite±chlorite±talc aggregates. Discrete <2 mm tremolite crystals occasionally observed.
		Talc	tr	
Sulfides	tr	Chalcopyrite	tr	Very finely disseminated monosulfide crystals in silicate alteration aggregates, typically in <2 mm clusters.
		Pyrite	tr	

Comments: Cumulate, equilibrated, no accessory phases observed. Massive, no foliation, pervasive fracturing, or veining. Variable crystal size, typically ranging from fine to medium-grained throughout sample. Larger plagioclase crystals occasionally partially to completely enclose smaller plagioclase and altered pyroxene crystals.

Sample: JJ-TS-112		**Drill hole: 18-805**		**Depth: 259.81 m**
Mineral (interpreted pre-alteration)	%	Mineral (actual)	%	Details
Plagioclase	42	Plagioclase	39	0.05-5.0 mm. Anhedral to subhedral, typically equant. >3 mm crystals and crystals surrounded by plagioclase/pyroxene generally subhedral and tabular. ~2% of crystals are <0.1 mm, sometimes anhedral to subhedral and sometimes with polygonal triple junctions, present at margins between other plagioclase crystals. Typically very weakly altered to patches of very fine-grained white mica aggregates and occasional partial rims of chlorite.
		Chlorite	5	
		White mica	1	
Ortho-pyroxene	54	Orthopyroxene	41	0.1-9.0 mm. Typically subhedral and equant; >5 mm crystals are anhedral, elongate, and irregularly shaped, wrapping around adjacent crystals. Typically weakly altered to small patches and partial rims of tremolite-actinolite±chlorite ±talc aggregates and optically continuous tremolite crystals. Minority of crystals are strongly to completely replaced by tremolite-actinolite± chlorite±talc aggregates.
		Tremolite-actinolite	10	
		Talc	2	
Clino-pyroxene	4	Clinopyroxene	2	3.0-7.0 mm. Anhedral, irregularly shaped, wrapping around adjacent crystals. Weakly to strongly altered to very fine-grained aggregates of tremolite-actinolite±talc±chlorite.
Biotite	tr	Biotite	tr	Few <0.2 mm platy crystals at margins between plagioclase and pyroxene crystals.
Sulfide	tr	Chalcopyrite	tr	Very finely disseminated monosulfide, and interstitial polysulfide crystals, present as <0.3 mm irregularly shaped crystals and elongate aggregates up to 5 mm long between plagioclase crystals.
		Pyrite	tr	
		Pyrrhotite	tr	
		Pentlandite	tr	
Magnetite	tr	Magnetite	tr	Very fine equant and elongate crystals, disseminated in silicate alteration aggregates.
Comments: Cumulate, equilibrated, biotite only observed interstitial phase. Massive, no foliation, fracturing, or veining present. Variable crystal size, typically ranging from fine to medium throughout. Larger pyroxene and plagioclase crystals commonly partially to completely enclose smaller orthopyroxene and plagioclase crystals.				

Sample: JJ-TS-118		**Drill hole: 19-025**		**Depth: 340.54 m**
Mineral (interpreted pre-alteration)	%	Mineral (actual)	%	Details
Plagioclase	50	Plagioclase	48	0.2-4.0 mm. Typically anhedral and equant. <0.2 mm crystals sometimes have polygonal triple junctions. >3.0 mm crystals typically subhedral and tabular. Occasionally weakly fractured. Rare deformation twinning. Typically
		Chlorite	1	
		White mica	1	

				very weakly altered to minor very fine-grained white mica±chlorite patches and occasional rims of fine-grained chlorite. Minority of crystals completely unaltered.
Ortho-pyroxene	40	Orthopyroxene	35	0.05-4.0 mm. Typically subhedral to anhedral and equant to rarely elongate. <0.1 mm elongate crystals commonly present along orthopyroxene cleavage planes, appearing to be the product of exsolution. Typically weakly altered to very fine-grained tremolite-actinolite±talc aggregates along fractures/as partial rims.
		Tremolite-actinolite	3	
		Talc	3	
Clino-pyroxene	9	Clinopyroxene	8	1.0-7.0 mm. Anhedral, irregularly shaped, wrapping around adjacent crystals. Typically very weakly altered to tremolite-actinolite±talc aggregates, along cleavage planes and as partial rims.
Sulfides	tr	Pyrite	tr	Very few <0.05 mm finely disseminated crystals, associated with magnetite.
Magnetite	1	Magnetite	1	<0.1 mm interstitial, equant, anhedral crystals.
Comments: Cumulate, equilibrated, no accessory phases present. Massive, no foliation, pervasive fracturing, or veining. Variable crystal size, typically ranging from fine to medium-grained. Plagioclase and clinopyroxene commonly partially to completely enclose smaller plagioclase and orthopyroxene crystals.				

Sample: JJ-TS-123		**Drill hole: 19-025**		**Depth: 360.54 m**
Mineral (interpreted pre-alteration)	%	Mineral (actual)	%	Details
Plagioclase	40	Plagioclase	33	0.2-3.0 mm. Anhedral, equant to tabular. Crystals partially to completely surrounded by other crystals commonly subhedral. Commonly heavily fractured, with fractures commonly filled with white mica and/or chlorite. Most commonly weakly altered to patches of white mica±epidote, with chlorite present as partial to complete rims and veinlets. Minority of crystals completely altered to chlorite.
		Chlorite	8	
		White mica	1	
		Epidote	tr	
Ortho-pyroxene	57	Orthopyroxene	30	0.2-4.0 mm. Typically subhedral and equant to elongate. Most commonly moderately to strongly altered to very fine-grained talc± tremolite-actinolite, present along fractures, cleavage planes, and as partial to complete rims. Less commonly completely altered to fine-grained tremolite-actinolite±talc.
		Talc	15	
		Tremolite-actinolite	11	
Clino-pyroxene	3	Clinopyroxene	2	1.0-3.0 mm. Majority of crystals anhedral and irregularly shaped; ~1 mm crystals are subhedral and equant. Weakly altered to very fine-grained tremolite-actinolite±talc, as partial rims and along cleavage planes.
Sulfides	0.5	Pyrite	0.3	Very finely disseminated monomineralic crystals and disaggregated <0.2 mm pyrite crystals, both typically associated with altered silicates.
		Chalcopyrite	0.2	
Magnetite	tr	Magnetite	tr	Irregularly shaped <0.3 mm crystals, associated with sulfides and typically present in silicate alteration aggregates.
Comments: Cumulate, equilibrated, no interstitial phases observed. Massive, no foliation. Fracturing and veining common throughout sample, with no prevalent orientation. Proportions of orthopyroxene and clinopyroxene somewhat difficult do determine due to alteration. Crystal size quite variable throughout, typically fine to				

medium-grained. Clinopyroxene commonly partially to completely encloses smaller plagioclase and orthopyroxene crystals.

Sample: JJ-TS-126		**Drill hole: 19-025**		**Depth: 372.53 m**
Mineral (interpreted pre-alteration)	%	Mineral (actual)	%	Details
Plagioclase	55	Plagioclase	54	0.1-4.0 mm. Typically equant and anhedral, >2.0 mm crystals are commonly subhedral and tabular, <0.5 mm crystals are commonly circular and sometimes show polygonal triple junctions. Rare deformation twinning, rarely weakly fractured. Typically very weakly altered to very fine-grained white mica±epidote± chlorite aggregates, present as small patches and fracture fill. Minority of crystals appear completely unaltered.
		White mica	1	
		Chlorite	tr	
		Epidote	tr	
Ortho-pyroxene	35	Orthopyroxene	33	0.1-3.0 mm. Equant and subhedral to anhedral. <0.2 mm elongate crystals occasionally present along clinopyroxene cleavage planes, appearing to be exsolved. Typically completely unaltered to very weakly altered, with alteration present as very fine-grained tremolite-actinolite±chlorite patches. Minority of crystals strongly altered to fine-grained tremolite-actinolite±chlorite.
		Tremolite-actinolite	2	
Clino-pyroxene	10	Clinopyroxene	10	0.2-3.0 mm. Typically anhedral and irregularly shaped. <1.0 mm crystals subhedral to anhedral and equant. Typically very weakly altered along cleavage planes to tremolite-actinolite. Minority of crystals completely unaltered.
Biotite	tr	Biotite	tr	Very few <0.1 mm “ragged” crystals, alongside chlorite-dominated alteration aggregates.
Sulfides	tr	Pyrite	tr	<0.1 mm monomineralic crystals, interstitial to primary silicates and associated with silicate alteration
		Chalcopyrite	tr	
Magnetite	0.5	Magnetite	0.5	Equant, subhedral <0.2 mm interstitial crystals.
Comments: Equilibrated, cumulate. No intercumulus minerals; biotite is present but only occurs in association with alteration aggregates. Massive, no foliation, pervasive fracturing, or veining. Variable crystal size, ranging from very fine to medium-grained throughout. Plagioclase and pyroxene occasionally partially to completely encircle <0.5 mm plagioclase and orthopyroxene.				

Sample: JJ-TS-129		**Drill hole: 19-025**		**Depth: 384.86 m**
Mineral (interpreted pre-alteration)	%	Mineral (actual)	%	Details
Plagioclase	36	Plagioclase	34	0.2-4.0 mm. Typically equant and anhedral. Crystals partially to completely enclosed by other crystals are typically tabular and subhedral. Rarely weakly fractured, with some fractures filled by white mica. Rare deformation twinning. Completely unaltered to very weakly altered to very fine-grained white mica±epidote±chlorite patches and/or rare partial rims of very fine-grained chlorite aggregates.
		White mica	1	
		Chlorite	1	
		Epidote	tr	
Ortho-	58	Orthopyroxene	55	0.1-4.0 mm. Typically equant and subhedral, less

pyroxene		Talc	2	commonly elongate and anhedral. Majority of crystals completely unaltered. <0.2 mm elongate crystals present along clinopyroxene cleavage planes, appearing to be exsolved. Minority of crystals weakly to moderately altered by fracture-filling very fine-grained talc±tremolite-actinolite, and/or small patches of fine-grained tremolite-actinolite.
		Tremolite-actinolite	1	
Clino-pyroxene	3	Clinopyroxene	3	1.0-4.0 mm. Anhedral, irregularly shaped. Typically completely unaltered, occasionally very weakly altered to small patches of very fine-grained tremolite-actinolite.
Biotite	tr	Biotite	tr	<0.2 mm platy crystals, present at margins between primary magmatic crystals.
Sulfides	4	Pyrrhotite	2	Irregularly shaped <2 mm interstitial pyrrhotite± chalcopyrite±pentlandite crystals, with pyrite rarely present as a minor component of aggregates.
		Chalcopyrite	1	
		Pentlandite	1	
		Pyrite	tr	
Magnetite	tr	Magnetite	tr	<0.5 mm interstitial crystals associated with sulfides.
Comments: Cumulate, equilibrated, biotite is only interstitial phase. Massive, no foliation or veining. Minor pervasive fracturing at ~70 degrees to long axis of thin section. Crystal size variable throughout, ranging from very fine to medium-grained. Plagioclase and pyroxene occasionally partially to completely enclose <0.3 mm plagioclase and orthopyroxene.				

Sample: JJ-TS-133		**Drill hole: 19-025**		**Depth: 400.44 m**
Mineral (interpreted pre-alteration)	%	Mineral (actual)	%	Details
Plagioclase	35	Plagioclase	29	<0.05 mm-3.0 mm. Majority of plagioclase appears to be recrystallized, present as clusters of <0.5 mm mosaic textured crystals commonly with polygonal triple junctions. Mosaic textured crystal almost always completely unaltered. Minority of crystals are >0.5 mm, anhedral to subhedral, equant to tabular. >0.5 mm crystals typically weakly to moderately altered to patches of white mica, and crosscut by tremolite-actinolite± chlorite±white mica veinlets. Deformation twinning common near veinlets/fractures.
		White mica	3	
		Chlorite	3	
Ortho-pyroxene	63	Orthopyroxene	55	0.1-3.0 mm. Typically equant and subhedral to anhedral, less commonly elongate and anhedral. Typically weakly altered to small rims and/or patches of very fine to fine grained tremolite-actinolite±talc. Crystals near fractures veinlets moderately to completely altered to fine-grained tremolite-actinolite±chlorite±talc.
		Tremolite-actinolite	7	
		Talc	1	
Clino-pyroxene	2	Clinopyroxene	2	0.5-2.0 mm. Equant to elongate, anhedral. Very weakly altered to small patches of tremolite-actinolite.
Sulfides	1	Pyrrhotite	0.4	<1 mm polysulfide interstitial crystals and less common very finely disseminated monosulfide pyrite or chalcopyrite crystals.
		Chalcopyrite	0.4	
		Pentlandite	0.2	
		Pyrite	0.2	
Magnetite	tr	Magnetite	tr	Few <0.3 mm crystals in contact with sulfides.
Comments: Appears to have been equilibrated and cumulate; no interstitial phases present. Massive, no foliation aside from inside veinlets. Discontinuous, anastomosing zones of mosaic textured very fine-grained				

tremolite-actinolite and plagioclase extend across sample at ~30-40° to long axis of thin section. Veinlets filled by very fine-grained tremolite-actinolite±chlorite±talc crosscut sample at 30-60° to long axis of thin section. Veinlets surrounded by <3 mm zones of increased fracturing and alteration.

Sample: JJ-TS-138		**Drill hole: 19-025**		**Depth: 420.10 m**
Mineral (interpreted pre-alteration)	%	Mineral (actual)	%	Details
Plagioclase	55	Plagioclase	48	<0.05-6.0 mm. ~40% of plagioclase is <0.3 mm, anhedral, and equant, commonly with polygonal triple junctions. This very fine-grained plagioclase is typically unaltered to very weakly altered to very fine-grained white mica. Remaining plagioclase is anhedral to subhedral and equant to tabular. Larger plagioclase crystals are weakly to strongly altered to patches of very fine-grained white mica±chlorite±epidote.
		Chlorite	4	
		White mica	3	
		Epidote	tr	
Ortho-pyroxene	33	Orthopyroxene	20	<0.05-4.0 mm. ~65% of crystals are <0.5 mm, anhedral, and equant, sometimes with polygonal triple junctions. Very fine-grained crystals typically unaltered to very weakly altered to very fine-grained talc±tremolite-actinolite aggregates, with a minority of these crystals completely altered to tremolite-actinolite. Coarser crystals typically strongly altered to very fine-grained talc±tremolite-actinolite.
		Tremolite-actinolite	10	
		Talc	9	
Clino-pyroxene	11	Clinopyroxene	5	<0.05-6.0 mm. ~50% of crystals are <0.5 mm, anhedral, and equant, sometimes with polygonal triple junctions. Very fine-grained crystals typically unaltered to weakly altered to very fine-grained talc±tremolite-actinolite. Coarser crystals weakly to strongly altered to very fine-grained talc±tremolite-actinolite
Biotite	tr	Biotite	tr	Few <0.1 mm platy crystals at contacts between primary magmatic crystals.
Sulfides	0.5	Pyrite	0.3	Mostly present as finely disseminated monosulfide pyrite or chalcopyrite crystals in silicate alteration aggregates. Less commonly as <1 mm interstitial pyrrhotite+pentlandite+ chalcopyrite crystals.
		Chalcopyrite	0.1	
		Pyrrhotite	0.1	
		Pentlandite	tr	
Magnetite	tr	Magnetite	tr	Few <0.3 mm interstitial crystals, generally associated with sulfides.
Comments: Cumulate, equilibrated. Massive, no foliation, pervasive fracturing, or veining. 40% of sample is very fine-grained and equigranular, bounded by sharp contacts with adjacent zones of fine to medium-grained, variably sized crystals. Boundaries between equigranular and varitextured zones trend ~30-40° to long axis of thin section. >2 mm clinopyroxene crystals commonly encircle smaller plagioclase and orthopyroxene crystals.				

Sample: JJ-TS-140		**Drill hole: 19-025**		**Depth: 428.42 m**
Mineral	%	Mineral (actual)	%	Details

(interpreted pre-alteration)				
Plagioclase	68	Plagioclase	52	0.05-4.5 mm. Crystals typically equant and anhedral; minority of crystals tabular and anhedral to subhedral. Crystals in plagioclase-rich portion weakly to moderately altered to very fine-grained white mica±chlorite±epidote aggregates and <1 mm epidote crystals. Crystals in pyroxene-rich portion strongly to completely altered to fine-grained chlorite± white mica aggregates.
		Chlorite	13	
		White mica	7	
		Epidote	2	
Pyroxene	32	Tremolite-actinolite	25	Completely replaced by alteration minerals. Appears to have been 0.5-3.0 mm, generally equant to elongate. Alteration present as fine-grained tremolite-actinolite±chlorite aggregates.
		Talc	1	
Sulfides	0.5	Pyrite	0.2	Interstitial, irregularly shaped pyrite±chalcopyrite ±pentlandite crystals and very finely disseminated pyrite and chalcopyrite crystals. Interstitial crystals surrounded by <5 mm haloes of disseminated crystals.
		Chalcopyrite	0.2	
		Pentlandite	0.1	
Magnetite	tr	Magnetite	tr	Rare <0.2 mm interstitial crystals.
Comments: Equilibrated, cumulate, no observed interstitial phases. Massive, no foliation or pervasive fracturing. Few anastomosing chlorite±tremolite veinlets crosscut sample at 45-70° to long axis of thin section. 70% of sample made up of ~85% plagioclase; remaining 30% of sample made up of ~80% altered pyroxene. Boundary between plagioclase and pyroxene-rich zones undulating but otherwise sharp. Crystal size in plagioclase-rich zone highly variable, ranging from very fine to coarse. Crystal size in pyroxene rich-zone obscured by alteration.				

Sample: JJ-TS-148		**Drill hole: 19-025**		**Depth: 460.41 m**
Mineral (interpreted pre-alteration)	%	Mineral (actual)	%	Details
Plagioclase	55	Plagioclase	37	<0.05-12.0 mm. Crystals in plagioclase-rich portion equant to tabular, anhedral to subhedral, weakly to strongly altered to very fine-grained aggregates of white mica±chlorite±epidote. Crystals in pyroxene-rich portion completely altered to fine-grained chlorite aggregates, with boundaries very difficult to discern.
		Chlorite	20	
		White mica	5	
		Epidote	tr	
Pyroxene	45	Tremolite-actinolite	33	Completely replaced by alteration minerals. Pre-alteration morphology not discernible due to alteration intensity. Dominantly replaced by very fine to fine-grained tremolite-actinolite±talc± chlorite aggregates. Discrete, irregularly shaped tremolite crystals up to 7 mm also present.
		Talc	5	
Sulfides	tr	Pyrite	tr	Very finely disseminated monosulfide crystals, usually in <3.0 mm clusters. Generally irregularly shaped, pyrite rarely subhedral.
		Chalcopyrite	tr	
Magnetite	tr	Magnetite	tr	Rare <0.2 mm crystals associated with silicate alteration.
Comments: Sample taken at boundary between plagioclase-rich and pyroxene-rich cumulate zones. No accessory phases present. 50% of sample made up of 95% plagioclase, 5% altered pyroxene. 50% of sample made up of 85% altered pyroxene, 15% altered plagioclase. Chlorite veinlets cut through plagioclase-rich portion at ~15 degrees to thin section axis. Alteration in plagioclase-rich portion increases with proximity to pyroxene-rich portion.				

Sample: JJ-TS-155	**Drill hole: 19-025**	**Depth: 488.30 m**

Mineral (interpreted pre-alteration)	%	Mineral (actual)	%	Details
Plagioclase	60	Plagioclase	52	0.1-7.5mm. <0.3 mm crystals are equant, anhedral, and sometimes have polygonal triple junctions. >0.3 mm crystals are equant to tabular, anhedral to rarely subhedral. Deformation twinning present in ~5% of crystals. Commonly weakly fractured, with fractures filled by chlorite±tremolite±white mica. Typically to moderately altered to very fine-grained white mica±chlorite patches and uncommon partial rims of chlorite. Minority of crystals completely replaced by very fine to fine-grained chlorite+white mica aggregates.
		Chlorite	7	
		White mica	3	
Pyroxene	40	Tremolite-actinolite	37	0.2-10.0 mm. Completely replaced by alteration minerals. Crystals generally well pseudomorphed, appearing to have been equant and subhedral where preserved. Alteration typically present as very fine to fine-grained tremolite-actinolite±talc aggregates. Discrete tremolite crystals up to 8 mm in size also present.
		Talc	1	
Sulfides	tr	Pyrite	tr	Mostly present as disseminate chalcopyrite and pyrite crystals, rarely as interstitial pyrrhotite± chalcopyrite±pentlandite±pyrite crystals. Generally associated with silicate alteration.
		Chalcopyrite	tr	
		Pyrrhotite	tr	
		Pentlandite	tr	
Comments: Cumulate, equilibrated, no accessory phases observed. Massive, no foliation. <0.2 mm-wide chlorite±tremolite-actinolite veinlets crosscut sample at ~20° to long axis of thin section. Fractures in plagioclase also typically occur at ~20° to long axis of thin section. Crystal size is highly variable, ranging from very fine to coarse throughout sample. Plagioclase occasionally partially to completely encircles smaller plagioclase and altered pyroxene crystals.				

Sample: JJ-TS-178		**Drill hole: 19-009**		**Depth: 46.12 m**
Mineral (interpreted pre-alteration)	%	Mineral (actual)	%	Details
Plagioclase	55	Plagioclase	50	0.1-6.5 mm. <0.5 mm crystals typically equant, anhedral, sometimes with polygonal triple junctions. Larger crystals equant to tabular, anhedral to subhedral. Weakly to moderately fractured, with fractures sometimes filled by chlorite±white mica. Very weakly to weakly altered to very fine-grained white mica±chlorite aggregates.
		White mica	3	
		Chlorite	2	
Ortho-pyroxene	25	Orthopyroxene	23	0.1-7.0 mm. Equant, anhedral to subhedral. <0.2 mm crystals commonly present along clinopyroxene cleavage planes, appearing to be exsolved. Very weakly altered to fine-grained tremolite-actinolite±talc aggregates and discrete crystals of tremolite-actinolite as patches and partial rims, and to talc along fractures.
		Tremolite-actinolite	2	
		Talc	tr	
Clino-pyroxene	20	Clinopyroxene	19	0.2-4.0 mm. Anhedral, equant to irregularly shaped, with irregularly shaped crystals commonly wrapping around adjacent crystals. Very weakly altered to very fine to fine-grained tremolite-actinolite±talc as partial rims and along cleavage planes.
Sulfides	tr	Pyrite	tr	Disseminated monosulfide chalcopyrite or pyrite crystals

		Chalcopyrite	tr	associated with silicate alteration, and <0.2 mm interstitial pyrite+chalcopyrite± pentlandite crystals adjacent to magnetite
		Pentlandite	tr	
Magnetite	0.5	Magnetite	0.5	<1.5 mm irregularly shaped interstitial crystals, commonly adjacent to sulfides.
Comments: Cumulate, equilibrated, no interstitial phases observed. Massive, no foliation or veining. Fractures commonly occur at 30-45° to long axis of thin section. Highly variable crystal size, ranging from very fine to coarse throughout sample. Plagioclase and pyroxene crystals commonly partially to completely encircle smaller orthopyroxene and plagioclase crystals.				

Sample: JJ-TS-189		**Drill hole: 19-009**		**Depth: 68.53 m**
Mineral (interpreted pre-alteration)	%	Mineral (actual)	%	Details
Plagioclase	52	Plagioclase	46	0.2-7.0 mm. Typically equant and subhedral to anhedral. >4.0 mm crystals typically subhedral and tabular. Typically weakly altered to patches of very fine-grained white mica±chlorite aggregates. Fine-grained chlorite aggregates occasionally extend from adjacent altered pyroxene crystals. Minority of crystals strongly to completely altered to chlorite±white mica.
		Chlorite	4	
		White mica	2	
Pyroxene	42	Tremolite-actinolite	40	Completely replaced by alteration minerals. Generally very well pseudomorphed. 0.1-5.0 mm. Anhedral to subhedral, equant to elongate. Alteration present as very fine to fine-grained tremolite-actinolite±chlorite±talc aggregates. Tremolite and anthophyllite both rarely present as <2 mm discrete, irregularly shaped crystals.
		Talc	2	
		Anthophyllite	tr	
Sulfides	tr	Pyrite	tr	Trace <0.1 mm disseminated crystals, mostly associated with magnetite. Pyrite is sometimes subhedral.
		Chalcopyrite	tr	
Oxides	6	Magnetite	5	Interstitial irregularly shaped crystals distributed throughout. Ilmenite present as exsolution from magnetite, present as randomly oriented crystal aggregates.
		Ilmenite	1	
Comments: Equilibrated, cumulate, no interstitial phases observed. Massive, no foliation or veining. Weak pervasive fracturing at ~75° to long axis of thin section. Variable crystal size throughout, with pyroxene most commonly fine-grained and plagioclase most commonly medium-grained. Plagioclase occasionally partially to completely encircles altered pyroxene.				

Sample: JJ-TS-193		**Drill hole: 19-009**		**Depth: 76.20 m**
Mineral (interpreted pre-alteration)	%	Mineral (actual)	%	Details
Plagioclase	70	Plagioclase	65	0.2-7.0 mm. Anhedral to rarely subhedral, equant to tabular. Typically moderately fractured in random orientation, with minority of fractures filled by white mica. Typically weakly altered to patches of very fine-grained white mica±epidote±chlorite. Partial rims of fine-grained chlorite aggregates typically present at contacts with altered pyroxene crystals.
		Chlorite	3	
		White mica	3	
		Epidote	tr	
Pyroxene	30	Tremolite-actinolite	29	Completely replaced by alteration minerals. 0.5-7.0 mm. Pre-alteration crystals anhedral to rarely subhedral, equant

		Talc	tr	to irregularly shaped and wrapping around adjacent plagioclase crystals. Alteration typically present as very fine to fine-grained tremolite-actinolite±talc±chlorite aggregates. Discrete <2.0 mm tremolite crystals less commonly present.
Sulfides	tr	Pyrite	tr	Very fine-grained disseminated crystals and few interstitial crystals up to 2 mm in size.
Magnetite	tr	Magnetite	tr	Few <0.1 mm interstitial crystals.
Comments: Equilibrated, cumulate, no interstitial phases observed. Massive, no foliation, pervasive fracturing, or veining. Variable crystal size throughout sample, typically medium to coarse-grained. Altered pyroxene crystals commonly partially encircle adjacent plagioclase crystals.				

Sample: JJ-TS-197		**Drill hole: 19-009**		**Depth: 84.02 m**
Mineral (interpreted pre-alteration)	%	Mineral (actual)	%	Details
Plagioclase	55	Plagioclase	50	0.2-4.0 mm. Equant to tabular, anhedral to subhedral. Crystals commonly occur in <8 mm clusters. Typically weakly to moderately fractured. Generally very weakly altered to very fine-grained patches of white mica±chlorite and partial rims of fine-grained chlorite.
		Chlorite	5	
		White mica	2	
Pyroxene	45	Tremolite-actinolite	42	Generally well-pseudomorphed, appear to have been 0.2-4.0 mm and equant. Alteration most commonly present as very fine to fine-grained tremolite-actinolite±chlorite±talc aggregates. Discrete actinolite crystals up to 8 mm in size also present.
		Talc	1	
Sulfides	0.5	Pyrite	0.5	Typically blebby to interstitial <0.5 mm pyrite± chalcopyrite crystals, euhedral pyrite crystals less common. Very fine-grained disseminated pyrite and chalcopyrite also present.
		Chalcopyrite	tr	
Magnetite	tr	Magnetite	tr	Few <0.2 mm crystals, usually in contact with pyrite, less commonly present as discrete crystals.
Comments: Equilibrated, cumulate, no accessory phases observed. Massive, no foliation. Moderately fractured at ~20° to long axis of thin section, with fractures sometimes filled by very fine-grained chlorite. Variable crystal size throughout, generally ranging from fine to medium-grained.				

Sample: JJ-TS-204		**Drill hole: 19-009**		**Depth: 98.31 m**
Mineral (interpreted pre-alteration)	%	Mineral (actual)	%	Details
Plagioclase	65	Plagioclase	30	0.5-15.0 mm. Equant and anhedral to subhedral. Typically moderately altered to 0.1-1.0 mm very fine-grained white mica±chlorite patches, and altered to partial rims of chlorite aggregates where in contact with altered pyroxene. Crystals surrounded by altered pyroxene completely altered to chlorite.
		Chlorite	30	
		White mica	10	
Pyroxene	35	Tremolite-actinolite	28	1.0-20.0 mm. Anhedral and irregularly shaped, wrapping around adjacent plagioclase crystals. Completely altered to fine to coarse-grained aggregates of tremolite-actinolite±chlorite±talc, which pseudomorph pre-alteration crystals.
		Talc	2	

Sulfides	tr	Pyrite	tr	Trace <0.1 mm subhedral to anhedral crystals present in silicate alteration mineral aggregates.
Comments: Cumulate, equilibrated, no accessory phases observed. Massive, no foliation, veining, or pervasive fracturing. Dominantly coarse-grained to pegmatitic, with lesser fine to medium-grained material. Altered pyroxene crystals commonly partially to completely enclose adjacent plagioclase crystals.				

Appendix B

Whole Rock Geochemical Data

Drill hole #	17-804	17-804	17-804	17-804	17-804	17-804	17-804	17-804	17-804	17-804	17-804	17-804	17-804
Depth From	145	150	155	160	161	165	170	180	185	195	200	205	210
Depth To	146	151	156	161	162	166	171	181	186	196	201	206	211

Rock Type	LGABVT	GABVT	GABVT	GABVT	NOR	NOR	NOR	GABVT	GABVT	GABVT	GABVT	GABVT	GABVT
Lithological Domain	Breccia	Breccia	Breccia	Breccia	Breccia	Breccia	Breccia	Breccia	Breccia	Breccia	Breccia	Breccia	Breccia
Al_2O_3 (%)	20	19.35	15.4	20.5	15.6	18.05	14.85	18	16.2	17.65	15.05	16.65	19.85
CaO (%)	10.8	11.15	9.86	11.2	9.28	10.05	8.22	10.05	9.1	10.35	9.13	11.15	10.8
Cr_2O_3 (%)	0.027	0.034	0.024	0.028	0.035	0.063	0.083	0.059	0.032	0.034	0.031	0.021	0.04
Fe_2O_3 (%)	6.55	6.04	11.6	6.69	10.45	7.15	8.62	6.69	12.3	9.57	11.4	11.25	6.39
K_2O (%)	0.16	0.16	0.24	0.15	0.21	0.15	0.13	0.29	0.24	0.1	0.17	0.13	0.11
MgO (%)	7.67	7.92	9.07	7.75	10.15	11.1	13.75	9.62	9.48	9.65	10.15	8.68	8.24
MnO (%)	0.1	0.1	0.15	0.1	0.15	0.12	0.15	0.11	0.15	0.14	0.16	0.16	0.1
Na_2O (%)	2.08	2.22	1.88	2.23	1.85	1.85	1.82	1.92	1.82	1.97	1.71	2.02	2.08
P_2O_5 (%)	0.01	0.01	0.01	0.005	0.01	0.005	0.01	0.01	0.005	0.01	0.01	0.005	0.005
SiO_2 (%)	49.6	49.7	48.7	50.2	50.5	52.5	53.5	49.7	48.8	50.6	49.2	50.3	49.8
TiO_2 (%)	0.11	0.09	0.21	0.11	0.15	0.11	0.12	0.1	0.25	0.15	0.29	0.31	0.11
LOI (%)	1.43	2.39	2.66	1.24	1.73	0.71	0.62	2.57	1.58	0.35	1.24	0.5	0.65
Total (%)	98.58	99.18	99.83	100.23	100.15	101.88	101.89	99.15	99.98	100.6	98.57	101.2	98.19
Ag (ppm)	0.25	0.25	1.1	0.25	0.25	0.25	0.25	0.25	1.3	0.5	0.25	0.25	0.25
As (ppm)	0.7	0.3	0.5	0.4	0.7	0.3	0.5	0.4	0.7	0.3	0.6	0.5	0.7
Au_ppm	0.082	0.015	0.689	0.086	0.342	0.004	0.002	0.028	0.628	0.29	0.13	0.205	0.028
Ba (ppm)	49.4	48	58.1	49.4	53.7	49.1	40.1	57.4	72	48.3	49.5	47.3	48
Bi (ppm)	0.03	0.04	0.27	0.04	0.1	0.01	0.01	0.29	0.27	0.09	0.06	0.08	0.02
Cd (ppm)	0.25	0.5	0.9	0.25	0.8	0.6	0.6	0.25	0.8	0.25	0.25	0.25	0.5
Ce (ppm)	1.7	1.9	2.5	1.7	3	1.8	4.8	2.9	2.9	3	2.7	2.7	2.9
Co (ppm)	44	42	97	47	81	50	60	46	114	68	79	74	43
Cs (ppm)	1.5	2.14	2.42	1.42	1.71	1.19	1.61	2.55	2.05	0.58	1.2	0.64	0.68
Cu (ppm)	428	173	2770	429	1480	86	89	272	3740	900	655	1010	196
Dy (ppm)	0.35	0.37	0.55	0.4	0.56	0.46	0.48	0.36	0.59	0.48	0.51	0.72	0.4
Er (ppm)	0.25	0.25	0.41	0.29	0.42	0.3	0.32	0.28	0.46	0.35	0.4	0.46	0.33
Eu (ppm)	0.18	0.17	0.23	0.18	0.22	0.18	0.2	0.17	0.31	0.17	0.22	0.27	0.2
Ga (ppm)	12.4	12.5	11.9	12.4	12.1	11.4	10.8	11.6	16.5	11.7	13.1	13.5	13.1
Gd (ppm)	0.26	0.31	0.53	0.32	0.48	0.3	0.46	0.28	0.49	0.34	0.5	0.61	0.3
Ge (ppm)	2.5	2.5	2.5	2.5	2.5	2.5	2.5	2.5	2.5	2.5	2.5	2.5	2.5
Hf (ppm)	0.2	0.1	0.2	0.2	0.2	0.1	0.2	0.2	0.2	0.1	0.2	0.3	0.1
Hg (ppb)													
Ho (ppm)	0.08	0.08	0.13	0.1	0.14	0.09	0.09	0.08	0.12	0.09	0.12	0.16	0.09
In (ppm)	0.005	0.0025	0.016	0.0025	0.009	0.0025	0.0025	0.0025	0.013	0.0025	0.006	0.005	0.0025
La (ppm)	0.9	1.4	1.2	0.9	1.5	0.9	2.2	1.6	1.5	1.7	1.3	1.3	2.5
Li (ppm)	10	10	10	10	10	10	10	10	10	10	10	10	5
Lu (ppm)	0.04	0.04	0.05	0.04	0.06	0.05	0.06	0.05	0.07	0.04	0.08	0.07	0.04
Mo (ppm)	0.5	0.5	0.5	0.5	0.5	0.5	0.5	0.5	0.5	1	0.5	0.5	1
Nb (ppm)	0.1	0.05	0.1	0.1	0.1	0.05	2.2	0.2	0.2	0.2	0.4	0.1	0.3
Ni (ppm)	461	261	2220	464	1500	278	345	359	3010	806	794	946	266
Nd (ppm)	0.9	0.9	1.5	0.9	1.6	0.9	2.4	1.2	1.5	1.3	1.6	1.6	1.5
Pb (ppm)	1	1	1	1	1	2	2	1	1	5	4	5	2
Pd (ppm)	0.902	0.213	6.94	0.856	2.97	0.026	0.003	0.484	5.57	1.95	1.62	2.22	0.336
Pr (ppm)	0.21	0.23	0.33	0.21	0.37	0.21	0.57	0.3	0.36	0.36	0.37	0.39	0.36
Pt (ppm)	0.115	0.028	0.807	0.097	0.417	0.007	0.0025	0.053	0.725	0.281	0.212	0.272	0.055
Rb (ppm)	2.6	4.6	4.4	2.6	3.8	2.2	3.8	10.4	4.6	1.3	2	1.4	1.4
Re (ppm)	0.0005	0.0005	0.004	0.001	0.002	0.0005	0.0005	0.001	0.005	0.001	0.001	0.002	0.0005
S (%)	0.16	0.07	1.1	0.16	0.69	0.04	0.05	0.08	1.42	0.36	0.35	0.52	0.06
Sb (ppm)	0.025	0.025	0.025	0.025	0.025	0.025	0.025	0.36	0.025	0.025	0.025	0.025	0.025
Sc (ppm)	16	19	34	17	29	20	24	19	26	27	31	36	18
Se (ppm)	0.918	0.354	6.87	0.94	4.27	0.149	0.165	0.3 3	8.41	2.07	1.73	2.52	0.334
Sm (ppm)	0.22	0.19	0.42	0.22	0.42	0.25	0.51	0.24	0.41	0.29	0.51	0.46	0.38
Sn (ppm)	0.5	0.5	0.5	0.5	0.5	0.5	0.5	0.5	0.5	0.5	0.5	1	0.5
Sr (ppm)	261	228	191	238	199	204	167	219	307	191.5	204	231	239
Ta (ppm)	0.2	0.05	0.1	0.1	0.1	0.1	0.05	0.1	0.2	0.1	0.05	0.1	0.05
Tb (ppm)	0.05	0.06	0.1	0.06	0.09	0.06	0.07	0.06	0.08	0.06	0.08	0.1	0.07
Te (ppm)	0.27	0.09	2.51	0.25	1.17	0.01	0.01	0.58	2.42	0.79	0.55	0.81	0.11
Th (ppm)	0.05	0.025	0.08	0.05	0.13	0.05	0.38	0.18	0.07	0.16	0.08	0.09	0.18
Tl (ppm)	0.02	0.01	0.07	0.01	0.05	0.01	0.01	0.02	0.06	0.02	0.02	0.01	0.01
Tm (ppm)	0.04	0.03	0.05	0.04	0.07	0.05	0.06	0.04	0.07	0.04	0.06	0.07	0.04
V (ppm)	92	97	168	90	134	98	117	99	236	119	215	229	180
Y (ppm)	2.1	1.9	3.2	2.1	3.6	2.6	2.8	2.2	3.4	2.5	3.3	3.9	2.5
U (ppm)	0.025	0.1	0.025	0.025	0.05	0.025	0.21	0.15	0.025	0.025	0.025	0.025	0.1
W (ppm)	1	1	1	0.5	1	1	1	1	1	0.5	1	0.5	1
Yb (ppm)	0.27	0.18	0.44	0.3	0.42	0.32	0.36	0.31	0.38	0.35	0.42	0.45	0.32
Zr (ppm)	6	3	6	4	8	4	6	4	6	5	6	7	4
Zn (ppm)	42	41	61	42	67	46	55	44	70	59	70	61	41

Drill hole #	17-804	17-804	17-804	17-804	17-804	17-804	17-804	17-804	17-804	17-804	17-804	17-804	17-804
Depth From	215	220	225	230	232	234	236	238	240	242	244	246	248

Depth To	216	221	226	231	233	235	237	239	241	243	245	247	249
Rock Type	GABVT	GABVT	GABVT	GABVT	LGABVT	GABVT	GABVT	GABVT	GABVT	GABVT	GABVT	GABVT	GABVT
Lithological Domain	Breccia	Breccia	Breccia	Breccia	Breccia	Breccia	Breccia	Breccia	Breccia	Breccia	Breccia	Breccia	Breccia
Al_2O_3 (%)	15.1	18	19.05	19.55	18.85	19.05	18.35	18.9	13.8	16.25	18.75	16	18
CaO (%)	9.78	10.3	10.8	10.9	10.5	11.05	10.55	10.95	9.24	9.19	10.15	8.32	9.5
Cr_2O_3 (%)	0.039	0.039	0.035	0.031	0.029	0.038	0.041	0.049	0.038	0.041	0.037	0.033	0.023
Fe_2O_3 (%)	8.02	7.64	6.53	5.49	5.54	6.17	6.62	6.3	9.27	8.54	6.68	8.57	7.43
K_2O (%)	0.16	0.11	0.06	0.1	0.14	0.09	0.11	0.22	0.21	0.13	0.23	0.1	0.12
MgO (%)	10.25	9.56	8.92	7.9	7.75	8.54	9.31	9.15	11.75	10.65	8.79	10.75	8.8
MnO (%)	0.13	0.12	0.11	0.1	0.1	0.11	0.12	0.11	0.15	0.13	0.11	0.13	0.12
Na_2O (%)	1.76	2.06	2.21	2.29	2.42	1.89	1.86	1.81	1.39	1.6	2.09	1.75	2.4
P_2O_5 (%)	0.005	0.005	0.005	0.005	0.005	0.005	0.005	0.01	0.005	0.005	0.01	0.005	0.01
SiO_2 (%)	50.8	50.6	50.8	50.8	52.2	50.5	50.3	47.9	49.6	49.9	48.5	50.6	52.5
TiO_2 (%)	0.13	0.1	0.05	0.05	0.07	0.08	0.09	0.08	0.19	0.13	0.1	0.11	0.15
LOI (%)	2.02	0.81	1.01	1.74	2.17	2.06	1.45	2.54	2.83	2.86	2.75	2.74	2.45
Total (%)	98.2	99.36	99.6	98.97	99.79	99.6	98.82	98.05	98.48	99.43	98.24	99.12	101.52
Ag (ppm)	0.25	0.25	0.25	0.25	0.25	0.25	0.25	0.25	0.25	0.25	0.25	0.25	0.6
As (ppm)	1.1	0.5	0.4	0.3	0.3	0.3	0.3	0.2	0.9	0.4	0.4	0.2	0.5
Au (ppm)	0.293	0.073	0.012	0.008	0.014	0.003	0.021	0.003	0.189	0.238	0.033	0.233	1.1
Ba (ppm)	49.9	41.8	25.6	33.6	42.1	35.8	34	43	40.5	43.5	52.7	37	44.8
Bi (ppm)	0.06	0.03	0.02	0.01	0.05	0.02	0.01	0.02	0.11	0.07	0.02	0.26	0.27
Cd (ppm)	0.25	0.25	0.25	0.25	0.25	0.25	0.25	0.25	0.25	0.25	0.25	0.25	0.25
Ce (ppm)	4.6	2.1	0.7	0.8	1.8	1.1	1.1	1.1	2.7	1.6	1.8	1.5	2.2
Co (ppm)	76	55	47	40	39	42	48	45	73	67	49	72	54
Cs (ppm)	1.2	0.81	0.82	1.27	1.4	0.98	1.13	1.66	1.94	1.54	2.34	1.38	1.39
Cu (ppm)	633	334	229	120	142	93	163	97	736	666	187	670	1020
Dy (ppm)	0.44	0.28	0.17	0.22	0.3	0.3	0.31	0.24	0.58	0.25	0.34	0.24	0.44
Er (ppm)	0.36	0.24	0.16	0.12	0.24	0.28	0.19	0.2	0.34	0.24	0.21	0.2	0.28
Eu (ppm)	0.17	0.18	0.13	0.11	0.14	0.15	0.1	0.12	0.16	0.17	0.14	0.12	0.19
Ga (ppm)	11.6	12.5	12.9	12.3	12.4	11.6	12.4	11.9	10.8	11.6	12.1	12.6	14.3
Gd (ppm)	0.42	0.28	0.16	0.11	0.29	0.3	0.21	0.24	0.44	0.28	0.23	0.23	0.41
Ge (ppm)	2.5	2.5	2.5	2.5	2.5	2.5	2.5	2.5	2.5	2.5	2.5	2.5	2.5
Hf (ppm)	0.4	0.1	0.05	0.1	0.2	0.1	0.1	0.1	0.3	0.2	0.1	0.1	0.2
Hg (ppb)				0.0025	0.0025	0.0025	0.0025	0.0025	0.0025	0.0025	0.0025	0.0025	0.0025
Ho (ppm)	0.1	0.07	0.04	0.04	0.07	0.1	0.07	0.07	0.13	0.09	0.07	0.06	0.09
In (ppm)	0.0025	0.0025	0.0025	0.0025	0.0025	0.0025	0.0025	0.0025	0.005	0.008	0.0025	0.005	0.007
La (ppm)	2.5	1.7	0.4	0.5	1	0.5	0.6	0.6	1.3	0.8	1	0.7	1
Li (ppm)	10	5	5	10	10	10	10	10	10	10	10	10	10
Lu (ppm)	0.06	0.04	0.03	0.03	0.04	0.05	0.03	0.04	0.06	0.04	0.04	0.04	0.04
Mo (ppm)	0.5	1	1	0.5	0.5	0.5	0.5	0.5	0.5	0.5	0.5	1	0.5
Nb (ppm)	0.5	0.1	0.05	0.1	0.4	0.1	0.1	0.1	0.2	0.1	0.1	0.1	0.1
Ni (ppm)	659	428	263	208	266	224	296	262	980	860	379	809	543
Nd (ppm)	2.1	1	0.4	0.4	0.9	0.6	0.6	0.5	1.6	0.8	1	0.8	1.4
Pb (ppm)	3	3	2	1	1	2	1	1	1	1	1	1	3
Pd (ppm)	2.45	0.655	0.088	0.064	0.077	0.004	0.236	0.027	2.66	2.3	0.372	1.88	2.79
Pr (ppm)	0.52	0.22	0.08	0.1	0.2	0.14	0.14	0.13	0.36	0.21	0.22	0.17	0.29
Pt (ppm)	0.338	0.061	0.009	0.005	0.011	0.0025	0.026	0.0025	0.354	0.279	0.042	0.254	0.325
Rb (ppm)	3.1	1.6	0.7	2.1	3	1.8	2.4	3.9	5	3	5	2.1	2.6
Re (ppm)	0.001	0.001	0.0005	0.0005	0.0005	0.0005	0.0005	0.0005	0.001	0.002	0.001	0.001	0.0005
S (%)	0.12	0.15	0.15	0.06	0.04	0.04	0.06	0.03	0.25	0.24	0.06	0.42	0.28
Sb (ppm)	0.07	0.025	0.025	0.025	0.025	0.025	0.025	0.025	0.06	0.025	0.025	0.025	0.07
Sc (ppm)	23	23	20	19	19	21	22	22	25	18	18	13	18
Se (ppm)	1.38	0.78	0.51	0.239	0.221	0.165	0.289	0.173	2.05	1.815	0.434	2.17	1.96
Sm (ppm)	0.54	0.3	0.12	0.07	0.22	0.22	0.19	0.2	0.42	0.22	0.21	0.15	0.36
Sn (ppm)	0.5	0.5	0.5	0.5	0.5	0.5	0.5	0.5	0.5	0.5	0.5	0.5	0.5
Sr (ppm)	181	217	228	234	234	204	201	205	149	176	218	182.5	272
Ta (ppm)	0.05	0.05	0.05	0.05	0.05	0.05	0.05	0.05	0.05	0.05	0.05	0.05	0.05
Tb (ppm)	0.06	0.05	0.03	0.02	0.04	0.04	0.05	0.04	0.09	0.04	0.05	0.03	0.08
Te (ppm)	0.43	0.3	0.08	0.03	0.06	0.01	0.09	0.01	0.78	0.84	0.16	0.65	1.69
Th (ppm)	0.33	0.1	0.025	0.05	0.36	0.11	0.025	0.025	0.12	0.06	0.06	0.12	0.09
Tl (ppm)	0.01	0.01	0.01	0.01	0.01	0.01	0.01	0.01	0.02	0.02	0.01	0.03	0.03
Tm (ppm)	0.05	0.03	0.02	0.02	0.03	0.04	0.03	0.04	0.06	0.02	0.03	0.03	0.05
V (ppm)	127	129	85	68	73	80	88	83	164	117	88	89	110
Y (ppm)	2.8	2	1.2	1	1.7	1.9	1.8	1.6	3.3	1.9	1.7	1.7	2.4
U (ppm)	0.07	0.025	0.025	0.025	0.22	0.12	0.025	0.025	0.07	0.025	0.025	0.29	0.025
W (ppm)	1	1	1	1	1	0.5	0.5	1	0.5	1	1	1	1
Yb (ppm)	0.31	0.27	0.16	0.14	0.25	0.26	0.22	0.26	0.39	0.28	0.2	0.23	0.23
Zr (ppm)	18	4	1	1	5	2	2	2	7	5	4	4	6
Zn (ppm)	60	48	41	35	33	36	37	35	51	48	40	50	44

Drill hole #	17-804	17-804	17-804	17-804	17-804	17-804	17-804	17-804	17-804	17-804	17-804	17-804	17-804

Depth From	250	252	254	256	258	260	262	264	266	268	270	272	274
Depth To	251	253	255	257	259	261	263	265	267	269	271	273	275
Rock Type	GABVT	GABVT	NOR	NOR	NOR	NOR	NOR	NOR	NOR	NOR	NOR	NOR	NOR
Lithological Domain	Breccia	Breccia	Norite	Norite	Norite	Norite	Norite	Norite	Norite	Norite	Norite	Norite	Norite
Al_2O_3 (%)	18.15	16.25	8.42	7.61	6.75	10.35	10.4	10.5	10.95	10.35	11.25	10.5	10.7
CaO (%)	9.07	9.92	5.76	5.32	5.07	6.24	6.33	6.07	6.75	6.6	7.18	6.74	6.7
Cr_2O_3 (%)	0.028	0.019	0.057	0.07	0.074	0.073	0.074	0.07	0.074	0.076	0.074	0.072	0.071
Fe_2O_3 (%)	8.1	7.01	12.15	14.6	15.3	11.6	11.8	11.15	11.6	11.45	11.35	10.85	10.95
K_2O (%)	0.18	0.22	0.14	0.31	0.22	0.25	0.32	0.36	0.13	0.11	0.16	0.1	0.35
MgO (%)	9.47	8.94	15.1	17.45	18.7	15.95	16.75	15.9	16.8	17.65	16.75	17.25	16.45
MnO (%)	0.12	0.12	0.2	0.23	0.21	0.19	0.19	0.19	0.18	0.19	0.18	0.18	0.18
Na_2O (%)	1.84	2.52	1.09	0.6	0.49	0.92	0.94	1.09	1.03	0.95	0.97	0.95	0.94
P_2O_5 (%)	0.01	0.01	0.005	0.005	0.005	0.01	0.005	0.005	0.02	0.005	0.01	0.005	0.005
SiO_2 (%)	48.1	51.1	53.7	48.5	50.2	50	52.1	52.3	52.7	52.8	50.7	52.1	50.4
TiO_2 (%)	0.13	0.11	0.2	0.17	0.19	0.15	0.14	0.14	0.14	0.14	0.13	0.13	0.14
LOI (%)	2.97	3.76	3.01	3.64	2.09	4.27	2.69	1.78	0.83	0.59	1	0.62	3.08
Total (%)	98.21	100.01	99.84	98.51	99.3	100.01	101.74	99.56	101.21	100.92	99.76	99.5	99.98
Ag (ppm)	0.25	0.25	0.5	0.6	0.6	0.5	0.25	0.25	0.25	0.25	0.25	0.25	0.25
As (ppm)	0.4	0.6	0.7	0.9	0.8	0.7	0.4	0.4	0.3	0.3	0.2	0.2	0.4
Au (ppm)	0.129	0.058	0.402	0.52	0.823	0.314	0.172	0.116	0.259	0.078	0.048	0.01	0.007
Ba (ppm)	51.2	65.9	60.1	58.2	35.3	77.1	94.8	94.7	42.7	35.7	36.1	36.4	75.4
Bi (ppm)	0.42	1.73	0.74	0.28	0.13	0.12	0.06	0.05	0.07	0.03	0.02	0.01	0.02
Cd (ppm)	0.25	0.25	0.5	0.5	0.25	0.25	0.25	0.25	0.25	0.25	0.25	0.25	0.25
Ce (ppm)	2.4	16.2	5.7	1.8	1.6	3.5	2.4	2.9	2.3	2.2	2.3	2.5	3.2
Co (ppm)	60	47	98	113	122	87	84	79	89	83	77	80	77
Cs (ppm)	2.05	2.5	1.63	6.37	2.35	2.17	2.94	2.2	1.22	0.87	1.32	0.65	2.24
Cu (ppm)	517	206	1185	1430	1900	680	430	311	773	258	142	63	44
Dy (ppm)	0.27	0.65	0.58	0.55	0.47	0.46	0.46	0.45	0.4	0.37	0.36	0.41	0.42
Er (ppm)	0.21	0.34	0.4	0.4	0.34	0.39	0.29	0.24	0.35	0.29	0.34	0.31	0.28
Eu (ppm)	0.18	0.34	0.14	0.13	0.1	0.18	0.14	0.11	0.12	0.11	0.15	0.12	0.1
Ga (ppm)	13.6	12.4	8.8	8	7.4	9.8	10	9.4	9.8	9.4	9.1	9	9
Gd (ppm)	0.22	0.93	0.46	0.33	0.3	0.41	0.42	0.32	0.35	0.35	0.38	0.41	0.31
Ge (ppm)	2.5	2.5	2.5	2.5	2.5	2.5	2.5	2.5	2.5	2.5	2.5	2.5	2.5
Hf (ppm)	0.1	0.3	0.4	0.2	0.2	0.2	0.3	0.3	0.2	0.2	0.2	0.2	0.4
Hg (ppb)	0.0025	0.0025	0.0025			0.0025	0.0025	0.0025	0.0025	0.0025	0.0025	0.0025	0.0025
Ho (ppm)	0.07	0.12	0.16	0.1	0.1	0.1	0.1	0.12	0.1	0.1	0.12	0.11	0.09
In (ppm)	0.005	0.0025	0.009	0.014	0.013	0.006	0.006	0.0025	0.007	0.0025	0.0025	0.0025	0.0025
La (ppm)	1.3	6.9	3	0.8	0.8	1.7	1.1	1.5	1.2	1.1	1.2	1.3	1.6
Li (ppm)	10	10	10	10	10	20	10	10	5	5	5	5	10
Lu (ppm)	0.03	0.06	0.07	0.08	0.08	0.07	0.06	0.05	0.05	0.06	0.06	0.05	0.06
Mo (ppm)	0.5	0.5	0.5	1	0.5	0.5	0.5	1	1	1	0.5	0.5	0.5
Nb (ppm)	0.2	0.9	1.2	0.1	0.1	0.7	0.2	0.4	0.2	0.1	0.2	0.2	0.4
Ni (ppm)	730	544	1545	1890	2250	1035	883	709	1085	698	567	530	497
Nd (ppm)	1	9	2.3	1.1	1	1.8	1.2	1.2	1.1	1	1.1	1.2	1.4
Pb (ppm)	2	2	1	1	4	3	1	1	2	1	1	1	1
Pd (ppm)	1.96	4.17	4.86	5.99	7.84	2.86	1.97	1.16	2.55	0.762	0.369	0.157	0.112
Pr (ppm)	0.26	2.19	0.6	0.23	0.2	0.42	0.31	0.36	0.29	0.27	0.28	0.29	0.33
Pt (ppm)	0.252	0.125	0.597	0.73	0.899	0.38	0.263	0.156	0.327	0.109	0.069	0.039	0.035
Rb (ppm)	3.5	5.7	3.8	7.8	4.7	6.5	7.9	8.8	3	2.7	2.5	2.3	7.7
Re (ppm)	0.001	0.001	0.001	0.002	0.003	0.001	0.0005	0.0005	0.001	0.001	0.0005	0.0005	0.0005
S (%)	0.15	0.09	0.39	0.51	0.61	0.18	0.18	0.08	0.25	0.09	0.06	0.02	0.01
Sb (ppm)	0.09	0.025	0.09	0.07	0.12	0.1	0.025	0.025	0.025	0.025	0.025	0.025	0.025
Sc (ppm)	14	24	41	39	41	35	34	32	36	37	36	37	36
Se (ppm)	1.38	0.724	3.59	4.04	5.45	1.745	1.51	0.806	2.21	0.72	0.387	0.162	0.08
Sm (ppm)	0.31	1.78	0.47	0.31	0.25	0.41	0.31	0.32	0.32	0.25	0.31	0.31	0.43
Sn (ppm)	0.5	0.5	0.5	0.5	0.5	0.5	0.5	0.5	0.5	0.5	0.5	0.5	0.5
Sr (ppm)	214	257	78.3	65.2	52.7	72.6	101	110	108.5	99.6	105	100	82
Ta (ppm)	0.05	0.05	0.1	0.05	0.05	0.05	0.05	0.05	0.05	0.05	0.05	0.05	0.05
Tb (ppm)	0.04	0.13	0.09	0.05	0.05	0.07	0.07	0.06	0.04	0.06	0.06	0.06	0.06
Te (ppm)	0.66	2.78	1.36	1.47	2.13	0.93	0.64	0.29	0.82	0.23	0.1	0.11	0.06
Th (ppm)	0.12	0.76	0.82	0.1	0.09	0.19	0.12	0.27	0.13	0.13	0.11	0.18	0.24
Tl (ppm)	0.02	0.01	0.04	0.05	0.04	0.01	0.05	0.03	0.02	0.01	0.01	0.01	0.02
Tm (ppm)	0.04	0.05	0.05	0.05	0.06	0.06	0.05	0.04	0.04	0.05	0.03	0.04	0.03
V (ppm)	105	100	166	196	193	138	140	134	145	147	139	136	117
Y (ppm)	1.9	3.4	3.4	2.8	2.8	2.9	2.7	2.6	2.5	2.5	2.4	2.5	2.3
U (ppm)	0.025	0.09	0.27	0.06	0.025	0.1	0.08	0.12	0.025	0.025	0.025	0.025	0.14
W (ppm)	1	3	1	1	2	1	1	1	1	1	1	0.5	1
Yb (ppm)	0.23	0.38	0.4	0.42	0.45	0.41	0.42	0.4	0.38	0.4	0.33	0.37	0.31
Zr (ppm)	5	18	12	6	7	8	9	8	8	8	7	7	16
Zn (ppm)	48	43	72	88	86	69	69	70	68	68	64	67	61
Drill hole #	17-804	17-804	17-804	17-804	17-804	17-804	17-804	17-804	17-804	17-804	17-804	17-804	17-804

Depth From	276	278	280	282	284	286	288	290	292	294	296	298	299.85
Depth To	277	279	281	283	285	287	289	291	293	295	297	299	300.7
Rock Type	NOR	NOR	NOR	NOR	NOR	NOR	NOR	NOR	NOR	NOR	NOR	NOR	NOR
Lithological Domain	Norite	Norite	Norite	Norite	Norite	Norite	Norite	Norite	Norite	Norite	Norite	Norite	Norite
Al2O3 (%)	10.4	10.35	10.6	10.5	10.55	10.3	9.91	10.25	10.2	10.1	10.2	10.1	9.78
CaO (%)	6.75	6.57	7.06	6.57	6.74	6.72	6.47	6.54	6.53	6.61	6.38	6.52	6.45
Cr2O3 (%)	0.073	0.072	0.076	0.074	0.072	0.076	0.071	0.073	0.074	0.076	0.075	0.08	0.082
Fe2O3 (%)	10.8	10.65	11.2	10.55	10.45	10.9	10.25	10.35	10.35	10.75	10.45	10.8	11.05
K2O (%)	0.13	0.18	0.18	0.2	0.14	0.11	0.12	0.11	0.15	0.12	0.18	0.16	0.12
MgO (%)	17.2	17.05	17	17	17.05	17.75	16.7	17.05	17.2	17.9	17.45	18.1	18.6
MnO (%)	0.18	0.18	0.18	0.18	0.18	0.19	0.17	0.18	0.18	0.19	0.18	0.19	0.19
Na2O (%)	0.97	0.95	0.91	1.1	1.02	0.95	0.96	0.94	0.94	0.95	0.97	0.92	0.89
P2O5 (%)	0.005	0.01	0.01	0.005	0.005	0.01	0.005	0.005	0.02	0.005	0.005	0.005	0.01
SiO2 (%)	52	51.5	50.5	53.8	52.5	52.6	52	51.1	51.2	52.6	52	53	53.2
TiO2 (%)	0.13	0.13	0.13	0.13	0.13	0.13	0.13	0.13	0.13	0.13	0.13	0.13	0.14
LOI (%)	1.15	1.02	1	0.9	0.99	0.87	3.5	2.86	2.37	1.42	1.62	1.13	1.15
Total (%)	99.78	98.68	98.86	101.01	99.83	100.62	100.28	99.58	99.35	100.85	99.65	101.14	101.66
Ag (ppm)	0.25	0.25	0.25	0.25	0.25	0.25	0.25	0.25	0.25	0.25	0.25	0.25	0.25
As (ppm)	0.4	0.4	0.7	0.5	0.4	0.2	0.5	0.2	0.2	0.4	0.4	0.1	0.2
Au (ppm)	0.009	0.01	0.009	0.012	0.007	0.007	0.006	0.009	0.007	0.007	0.007	0.007	0.014
Ba (ppm)	38	48.6	44.2	55.7	47	39	33.1	34.5	39.5	34.9	52.2	47.4	37.1
Bi (ppm)	0.01	0.01	0.01	0.01	0.01	0.01	0.03	0.03	0.01	0.01	0.01	0.01	0.01
Cd (ppm)	0.25	0.25	0.25	0.5	0.5	0.25	0.6	0.5	0.25	0.5	0.25	0.25	0.25
Ce (ppm)	2.4	2.6	4.9	3.7	3.5	2.8	3.4	2.6	2.5	2.5	2.8	2.7	2.6
Co (ppm)	79	79	78	76	77	79	76	79	76	79	79	79	79
Cs (ppm)	1.14	1.8	0.88	1.34	1.16	0.96	2.37	2.01	2.16	1.22	2.7	1.76	0.97
Cu (ppm)	66	65	68	62	50	53	44	57	59	58	63	65	60
Dy (ppm)	0.39	0.32	0.43	0.41	0.42	0.44	0.39	0.48	0.41	0.41	0.42	0.39	0.37
Er (ppm)	0.29	0.33	0.36	0.28	0.3	0.33	0.32	0.26	0.26	0.27	0.35	0.33	0.25
Eu (ppm)	0.1	0.1	0.15	0.13	0.12	0.11	0.15	0.1	0.09	0.11	0.13	0.11	0.13
Ga (ppm)	8.9	8.6	8.9	8.9	9	8.7	9	8.8	8.7	8.8	9	9	8.5
Gd (ppm)	0.34	0.33	0.48	0.33	0.36	0.33	0.32	0.26	0.27	0.31	0.29	0.33	0.32
Ge (ppm)	2.5	2.5	2.5	2.5	2.5	2.5	2.5	2.5	2.5	2.5	2.5	2.5	2.5
Hf (ppm)	0.2	0.2	0.2	0.3	0.3	0.2	0.3	0.2	0.2	0.3	0.2	0.3	0.2
Hg (ppb)	0.0025	0.0025	0.0025	0.0025	0.0025	0.0025	0.0025	0.0025	0.0025	0.0025	0.0025	0.0025	0.0025
Ho (ppm)	0.1	0.08	0.11	0.1	0.11	0.09	0.09	0.1	0.08	0.1	0.1	0.11	0.1
In (ppm)	0.0025	0.0025	0.0025	0.0025	0.0025	0.0025	0.0025	0.0025	0.0025	0.0025	0.0025	0.0025	0.0025
La (ppm)	1.2	1.3	2.2	1.9	1.7	1.5	1.7	1.3	1.3	1.2	1.4	1.3	1.3
Li (ppm)	5	5	10	10	5	5	10	10	10	10	10	5	10
Lu (ppm)	0.06	0.06	0.06	0.05	0.05	0.06	0.05	0.07	0.06	0.07	0.05	0.07	0.06
Mo (ppm)	0.5	1	1	0.5	1	0.5	0.5	1	0.5	0.5	1	1	1
Nb (ppm)	0.2	0.3	1.9	0.9	0.7	0.4	0.5	0.4	0.2	0.2	0.5	1.1	0.4
Ni (ppm)	510	521	518	500	499	513	499	517	509	532	517	533	537
Nd (ppm)	1.1	1.2	2.1	1.7	1.6	1.5	1.5	1.3	1.1	1.1	1.3	1.2	1.4
Pb (ppm)	1	1	2	1	1	1	1	5	1	1	3	1	2
Pd (ppm)	0.099	0.103	0.086	0.348	0.087	0.099	0.072	0.121	0.093	0.137	0.094	0.117	0.067
Pr (ppm)	0.28	0.3	0.59	0.42	0.41	0.34	0.37	0.3	0.31	0.3	0.35	0.32	0.32
Pt (ppm)	0.033	0.033	0.032	0.066	0.032	0.033	0.029	0.034	0.03	0.04	0.031	0.034	0.021
Rb (ppm)	2.8	4.4	3.8	4.7	3.7	2.4	3.6	3.2	4.3	2.5	5.5	4.4	3
Re (ppm)	0.0005	0.001	0.0005	0.0005	0.0005	0.0005	0.0005	0.0005	0.0005	0.0005	0.0005	0.0005	0.0005
S (%)	0.02	0.02	0.02	0.02	0.03	0.03	0.02	0.01	0.02	0.03	0.03	0.02	0.02
Sb (ppm)	0.025	0.025	0.025	0.025	0.025	0.025	0.025	0.025	0.025	0.025	0.025	0.025	0.025
Sc (ppm)	37	38	39	37	37	37	37	34	37	39	38	39	39
Se (ppm)	0.182	0.158	0.123	0.111	0.113	0.112	0.082	0.12	0.121	0.127	0.133	0.134	0.125
Sm (ppm)	0.25	0.21	0.46	0.42	0.38	0.28	0.3	0.34	0.26	0.31	0.28	0.25	0.23
Sn (ppm)	0.5	0.5	0.5	0.5	0.5	0.5	0.5	0.5	0.5	0.5	0.5	0.5	0.5
Sr (ppm)	102	99.8	98	103.5	103	100.5	87.4	100.5	98.9	94.2	98.6	95.5	90.8
Ta (ppm)	0.05	0.05	0.05	0.05	0.05	0.05	0.05	0.05	0.05	0.05	0.05	0.05	0.05
Tb (ppm)	0.05	0.05	0.07	0.07	0.05	0.06	0.06	0.05	0.06	0.07	0.05	0.07	0.05
Te (ppm)	0.05	0.04	0.04	0.17	0.04	0.04	0.04	0.03	0.04	0.05	0.05	0.04	0.03
Th (ppm)	0.16	0.17	0.3	0.42	0.31	0.21	0.26	0.18	0.19	0.16	0.21	0.21	0.17
Tl (ppm)	0.02	0.02	0.02	0.02	0.02	0.01	0.01	0.01	0.02	0.01	0.03	0.02	0.02
Tm (ppm)	0.04	0.06	0.04	0.04	0.05	0.05	0.04	0.05	0.05	0.04	0.04	0.04	0.06
V (ppm)	137	128	134	129	129	133	128	128	130	132	128	135	132
Y (ppm)	2.5	2.4	2.7	2.5	2.4	2.4	2.4	2.4	2.4	2.4	2.5	2.4	2.5
U (ppm)	0.025	0.05	0.05	0.11	0.08	0.025	0.05	0.025	0.05	0.05	0.025	0.025	0.025
W (ppm)	1	1	1	1	1	1	1	1	0.5	0.5	1	7	1
Yb (ppm)	0.29	0.36	0.33	0.37	0.33	0.35	0.35	0.34	0.31	0.32	0.36	0.29	0.37
Zr (ppm)	7	9	9	9	9	7	9	7	9	9	8	10	8
Zn (ppm)	64	66	67	63	64	65	60	63	65	67	63	65	66
Drill hole #	18-805	18-805	18-805	18-805	18-805	18-805	18-805	18-805	18-805	18-805	18-805	18-805	18-805

Depth From	0	1	2	3	4	5	6	7	8	9	10	11	12
Depth To	1	2	3	4	5	6	7	8	9	10	11	12	13
Rock Type	GABVT	GABVT	GABVT	GABVT	GABVT	GABVT	GABVT	GABVT	GABVT	GABVT	GABVT	GABVT	GABVT
Lithological Domain	Breccia	Breccia	Breccia	Breccia	Breccia	Breccia	Breccia	Breccia	Breccia	Breccia	Breccia	Breccia	Breccia
Al2O3 (%)	16.7	16.7	16.15	15.5	16.25	15.95	15.65	15.85	14.5	15.6	16.3	15.8	15.65
CaO (%)	10.2	11.25	11	11.25	10.95	11.5	11.45	11.35	10.55	11.15	10.65	9.11	10.95
Cr2O3 (%)	0.014	0.012	0.004	0.008	0.01	0.01	0.008	0.008	0.008	0.009	0.008	0.006	0.01
Fe2O3 (%)	7.39	7.95	8.53	8.63	9.11	9.1	9.48	9.95	10.5	9.75	9.92	7.52	8.6
K2O (%)	0.13	0.15	0.1	0.09	0.1	0.12	0.08	0.11	0.14	0.13	0.65	0.2	0.15
MgO (%)	8.21	8.13	8.87	8.32	8.54	8.32	8.23	8.1	8.46	7.75	7.79	6.05	8.03
MnO (%)	0.13	0.14	0.15	0.15	0.15	0.15	0.16	0.17	0.17	0.16	0.16	0.13	0.16
Na2O (%)	2.32	2.32	2.32	2.14	2.22	2.2	2.09	2.09	1.94	2.05	2.1	3.05	2.24
P2O5 (%)	0.01	0.005	0.005	0.01	0.005	0.01	0.005	0.01	0.01	0.01	0.01	0.005	0.01
SiO2 (%)	51.2	52.8	52	51.4	51.2	52.5	51.9	52.1	51.7	50.4	50.8	57.4	51
TiO2 (%)	0.11	0.14	0.12	0.14	0.13	0.14	0.13	0.14	0.16	0.16	0.14	0.09	0.1
LOI (%)	2.08	1.61	1.42	1.09	1.82	1.63	1.49	1.22	1.26	1.32	2.59	1.78	2.04
Total (%)	98.52	101.23	100.69	98.76	100.51	101.66	100.69	101.12	99.43	98.51	101.15	101.16	98.97
Ag (ppm)	0.25	0.25	0.25	0.25	0.25	0.25	0.25	0.25	0.25	0.25	0.25	0.25	0.25
As (ppm)	0.3	0.3	0.3	0.2	0.5	0.3	0.4	0.1	0.3	0.2	0.3	0.3	0.4
Au (ppm)	0.019	0.027	0.056	0.017	0.035	0.01	0.006	0.003	0.006	0.006	0.005	0.013	0.038
Ba (ppm)	63.9	61.3	48	48.1	44.7	46.6	39.9	44.8	52.6	47.6	104.5	62.5	44.9
Bi (ppm)	0.02	0.03	0.04	0.01	0.08	0.03	0.03	0.02	0.59	0.01	0.04	0.06	0.15
Cd (ppm)	0.5	0.5	0.25	0.7	0.5	0.6	0.6	0.6	0.25	0.6	0.5	0.25	0.7
Ce (ppm)	2.3	3.1	1.8	1.7	1.9	2.1	1.2	0.9	2.1	1.1	1.1	3.8	1.9
Co (ppm)	52	53	65	61	60	55	60	61	68	58	58	50	63
Cs (ppm)	2.24	2.41	1.46	0.94	1.09	0.93	0.76	0.94	1.61	1.17	2.15	1.17	1.16
Cu (ppm)	210	240	381	210	267	193	183	191	278	169	165	174	361
Dy (ppm)	0.39	0.63	0.48	0.65	0.57	0.71	0.6	0.71	0.78	0.8	0.57	0.61	0.4
Er (ppm)	0.28	0.46	0.29	0.51	0.45	0.47	0.44	0.44	0.62	0.51	0.35	0.47	0.35
Eu (ppm)	0.24	0.26	0.2	0.26	0.21	0.25	0.24	0.25	0.25	0.29	0.27	0.2	0.24
Ga (ppm)	14.7	14.9	12.8	13.6	13.1	14	14.9	14.9	13.7	14.5	14.3	14.8	13.4
Gd (ppm)	0.37	0.5	0.39	0.55	0.57	0.69	0.61	0.54	0.51	0.54	0.48	0.57	0.46
Ge (ppm)	2.5	2.5	2.5	2.5	2.5	2.5	2.5	2.5	2.5	2.5	2.5	2.5	2.5
Hf (ppm)	0.2	0.2	0.2	0.2	0.2	0.2	0.2	0.1	0.2	0.2	0.2	0.5	0.1
Hg (ppb)	0.0025	0.0025	0.0025	0.0025	0.0025	0.0025	0.0025	0.0025	0.0025	0.0025	0.0025	0.0025	0.0025
Ho (ppm)	0.1	0.16	0.1	0.13	0.13	0.16	0.14	0.16	0.14	0.19	0.12	0.15	0.1
In (ppm)	0.0025	0.0025	0.005	0.0025	0.005	0.0025	0.006	0.005	0.005	0.005	0.005	0.0025	0.0025
La (ppm)	1.3	1.4	0.9	0.9	0.9	0.9	0.5	0.5	1	0.5	0.5	2	0.8
Li (ppm)	10	10	10	10	10	10	10	10	10	10	20	10	10
Lu (ppm)	0.06	0.07	0.04	0.09	0.05	0.07	0.07	0.1	0.08	0.09	0.07	0.06	0.06
Mo (ppm)	0.5	1	1	0.5	1	0.5	0.5	1	1	0.5	1	1	1
Nb (ppm)	0.1	0.1	0.1	0.1	0.1	0.1	0.1	0.1	0.1	0.1	0.1	0.7	0.1
Ni (ppm)	291	323	363	258	314	252	260	243	308	235	221	194	440
Nd (ppm)	1.3	1.8	1.2	1.3	1.3	1.3	1	0.8	1.4	1.1	0.8	1.7	1.4
Pb (ppm)	2	3	2	2	3	1	4	4	5	1	4	7	1
Pd (ppm)	0.126	0.31	0.385	0.049	0.261	0.021	0.013	0.009	0.005	0.025	0.017	0.097	0.618
Pr (ppm)	0.29	0.44	0.26	0.25	0.26	0.3	0.16	0.16	0.27	0.18	0.16	0.48	0.26
Pt (ppm)	0.02	0.033	0.04	0.008	0.018	0.01	0.008	0.006	0.006	0.01	0.007	0.012	0.068
Rb (ppm)	3.6	3.9	1.5	1.2	2.2	1.8	0.9	1.3	2.8	2.5	18.7	5.6	3.8
Re (ppm)	0.0005	0.001	0.001	0.0005	0.001	0.001	0.0005	0.001	0.0005	0.0005	0.001	0.001	0.001
S (%)	0.09	0.08	0.12	0.07	0.11	0.07	0.06	0.07	0.17	0.07	0.07	0.1	0.21
Sb (ppm)	0.025	0.025	0.025	0.025	0.025	0.025	0.025	0.025	0.025	0.025	0.025	0.025	0.025
Sc (ppm)	26	31	36	35	31	31	37	38	39	34	32	34	29
Se (ppm)	0.486	0.52	0.84	0.445	0.671	0.378	0.396	0.424	0.776	0.365	0.34	0.434	1.135
Sm (ppm)	0.28	0.48	0.29	0.26	0.38	0.3	0.28	0.26	0.35	0.37	0.24	0.43	0.36
Sn (ppm)	0.5	0.5	0.5	0.5	1	1	0.5	0.5	1	0.5	0.5	0.5	0.5
Sr (ppm)	218	222	182.5	187.5	185	191	190	195	173	198.5	189	182	213
Ta (ppm)	0.05	0.05	0.05	0.05	0.05	0.05	0.05	0.05	0.05	0.05	0.05	0.1	0.05
Tb (ppm)	0.07	0.09	0.06	0.09	0.07	0.1	0.1	0.09	0.11	0.09	0.1	0.09	0.08
Te (ppm)	0.13	0.15	0.17	0.06	0.07	0.06	0.05	0.08	0.09	0.06	0.06	0.09	0.29
Th (ppm)	0.06	0.16	0.025	0.025	0.025	0.07	0.025	0.025	0.13	0.025	0.025	0.73	0.06
Tl (ppm)	0.02	0.03	0.02	0.01	0.01	0.01	0.01	0.01	0.02	0.01	0.01	0.01	0.01
Tm (ppm)	0.06	0.07	0.04	0.06	0.07	0.08	0.07	0.07	0.08	0.08	0.06	0.07	0.06
V (ppm)	109	137	133	155	149	161	175	175	171	174	162	118	136
Y (ppm)	2.6	3.6	2.6	3.5	3.4	4.2	3.7	4	4.5	4.7	3.5	3.9	2.9
U (ppm)	0.025	0.025	0.025	0.025	0.025	0.025	0.025	0.025	0.08	0.025	0.025	1.79	0.05
W (ppm)	1	2	1	2	1	3	1	3	1	2	1	2	2
Yb (ppm)	0.29	0.36	0.34	0.42	0.38	0.43	0.52	0.54	0.65	0.6	0.46	0.39	0.37
Zr (ppm)	5	7	4	5	5	5	3	3	5	3	2	11	4
Zn (ppm)	59	56	58	58	56	54	58	59	63	59	58	46	62

Drill hole #	18-805	18-805	18-805	18-805	18-805	18-805	18-805	18-805	18-805	18-805	18-805	18-805	18-805
Depth From	13	14	15	16	17	18	19	20	21	22	23	24	25
Depth To	14	15	16	17	18	19	20	21	22	23	24	25	26
Rock Type	GABVT	GABVT	GABVT	GABVT	GABVT	GABVT	GABVT	GABVT	GABVT	GABVT	GABVT	GABVT	GABVT
Lithological Domain	Breccia	Breccia	Breccia	Breccia	Breccia	Breccia	Breccia	Breccia	Breccia	Breccia	Breccia	Breccia	Breccia
Al_2O_3 (%)	16.4	17.35	17.55	16.8	16.95	18.2	17.95	17.5	19.15	19.2	18.15	16.3	17.1
CaO (%)	10.25	10.7	11	10.15	10.1	10.5	10.95	10.55	9.07	8.79	8.47	6.77	6.91
Cr_2O_3 (%)	0.012	0.014	0.013	0.013	0.012	0.013	0.013	0.013	0.012	0.014	0.013	0.004	0.006
Fe_2O_3 (%)	7.34	7.31	8.14	7.75	6.54	7.25	7.21	6.81	7.65	7.96	8.38	8.52	7.71
K_2O (%)	0.19	0.14	0.13	0.15	0.16	0.16	0.12	0.12	0.15	0.18	0.16	0.19	0.17
MgO (%)	7.59	7.89	7.73	7.96	7.11	7.03	8.14	8.13	7.68	7.88	8	9.02	7.58
MnO (%)	0.13	0.13	0.14	0.14	0.12	0.13	0.14	0.13	0.12	0.13	0.14	0.14	0.12
Na_2O (%)	2.46	2.44	2.34	2.38	2.68	2.54	2.55	2.54	2.74	2.73	2.69	2.73	3.44
P_2O_5 (%)	0.005	0.005	0.005	0.005	0.005	0.005	0.005	0.005	0.01	0.005	0.005	0.005	0.01
SiO_2 (%)	52.4	52.4	52.2	51.8	53.9	50.9	53.5	52	53.4	53.4	53.2	53.6	54.1
TiO_2 (%)	0.1	0.09	0.11	0.09	0.09	0.11	0.09	0.09	0.09	0.09	0.11	0.08	0.1
LOI (%)	2.03	2	1.86	2.1	2.07	1.79	1.13	1.24	1.47	1.55	2.14	3.19	3.1
Total (%)	98.93	100.49	101.24	99.36	99.77	98.66	101.82	99.15	101.58	101.96	101.49	100.58	100.39
Ag (ppm)	0.25	0.25	0.25	0.25	0.25	0.25	0.25	0.25	0.25	0.25	0.25	0.25	0.25
As (ppm)	0.5	0.3	0.3	0.4	0.5	0.3	0.05	0.1	0.3	0.3	0.3	0.4	0.4
Au (ppm)	0.026	0.038	0.02	0.02	0.015	0.026	0.021	0.017	0.031	0.044	0.098	0.023	0.02
Ba (ppm)	75.1	67.2	63.3	72.5	75.8	82.6	71.8	66	65	67.6	79.4	93.5	92.7
Bi (ppm)	0.07	0.02	0.04	0.09	0.07	0.04	0.02	0.02	0.04	0.03	0.05	0.02	0.02
Cd (ppm)	0.7	0.5	0.25	0.5	0.6	0.6	0.6	0.25	0.25	0.25	0.25	0.25	0.25
Ce (ppm)	3.2	2.5	1.9	3.2	3.9	3.4	3.2	3	1.8	1.9	2.2	2.5	6.6
Co (ppm)	51	49	53	51	41	47	48	42	51	48	51	48	44
Cs (ppm)	1.76	1.17	1.18	1.46	1.84	1.44	0.99	1.03	1.32	1.61	1.95	2.48	1.93
Cu (ppm)	243	202	224	193	158	205	199	173	204	213	388	240	154
Dy (ppm)	0.45	0.3	0.57	0.39	0.47	0.43	0.38	0.36	0.22	0.16	0.23	0.16	0.35
Er (ppm)	0.2	0.28	0.33	0.29	0.24	0.29	0.24	0.24	0.15	0.13	0.19	0.11	0.23
Eu (ppm)	0.25	0.23	0.25	0.21	0.3	0.36	0.26	0.29	0.26	0.22	0.26	0.33	0.36
Ga (ppm)	13.8	15.1	15.1	14.5	15.6	16.6	14	14.3	16.2	15.6	15.3	17.8	19.1
Gd (ppm)	0.45	0.46	0.48	0.31	0.4	0.47	0.32	0.39	0.22	0.16	0.2	0.12	0.36
Ge (ppm)	2.5	2.5	2.5	2.5	2.5	2.5	2.5	2.5	2.5	2.5	2.5	2.5	2.5
Hf (ppm)	0.1	0.1	0.1	0.1	0.3	0.1	0.1	0.2	0.1	0.1	0.1	0.1	0.4
Hg (ppb)	0.0025	0.0025	0.0025	0.0025	0.0025	0.0025	0.0025	0.0025	0.0025	0.0025	0.0025	0.0025	0.0025
Ho (ppm)	0.08	0.1	0.12	0.08	0.1	0.12	0.09	0.07	0.06	0.04	0.05	0.04	0.07
In (ppm)	0.0025	0.0025	0.0025	0.0025	0.0025	0.0025	0.0025	0.0025	0.0025	0.0025	0.005	0.0025	0.005
La (ppm)	1.8	1.4	1	1.7	2.1	1.8	1.9	1.5	1.1	1.1	1.3	1.7	4.2
Li (ppm)	10	10	10	10	10	10	10	10	10	10	10	20	20
Lu (ppm)	0.05	0.05	0.04	0.05	0.05	0.05	0.03	0.04	0.03	0.03	0.03	0.02	0.04
Mo (ppm)	0.5	0.5	0.5	0.5	0.5	0.5	0.5	1	0.5	0.5	0.5	0.5	0.5
Nb (ppm)	0.4	0.1	0.1	0.1	0.1	0.1	0.1	0.1	0.1	0.1	0.1	0.1	4.1
Ni (ppm)	345	303	319	304	276	295	306	270	363	315	396	261	214
Nd (ppm)	1.6	1.2	1.1	1.5	1.8	1.6	1.5	1.5	0.8	0.7	0.9	0.8	2.2
Pb (ppm)	1	1	1	1	1	1	1	1	1	1	1	1	1
Pd (ppm)	0.402	0.31	0.287	0.304	0.191	0.454	0.228	0.149	0.355	0.604	1.47	0.118	0.15
Pr (ppm)	0.37	0.3	0.26	0.37	0.46	0.43	0.36	0.34	0.2	0.2	0.23	0.24	0.68
Pt (ppm)	0.045	0.041	0.061	0.059	0.029	0.053	0.032	0.025	0.061	0.076	0.179	0.011	0.017
Rb (ppm)	4.7	2.8	2.7	3.6	4.1	4	1.8	2	2.6	3.8	3.2	4.1	3.8
Re (ppm)	0.001	0.0005	0.001	0.001	0.0005	0.001	0.001	0.001	0.001	0.0005	0.0005	0.001	0.0005
S (%)	0.11	0.1	0.11	0.08	0.07	0.1	0.07	0.06	0.14	0.1	0.16	0.16	0.07
Sb (ppm)	0.025	0.025	0.025	0.025	0.025	0.025	0.025	0.025	0.025	0.025	0.025	0.025	0.025
Sc (ppm)	28	27	29	22	23	22	29	29	13	13	15	12	16
Se (ppm)	0.631	0.569	0.629	0.438	0.389	0.491	0.383	0.358	0.81	0.648	1.305	0.592	0.33
Sm (ppm)	0.4	0.32	0.38	0.34	0.44	0.37	0.44	0.38	0.14	0.11	0.15	0.13	0.3
Sn (ppm)	0.5	0.5	0.5	0.5	0.5	0.5	0.5	0.5	0.5	1	0.5	0.5	1
Sr (ppm)	236	264	224	261	283	304	234	233	318	322	313	314	334
Ta (ppm)	0.05	0.05	0.05	0.05	0.05	0.05	0.05	0.05	0.05	0.05	0.05	0.05	0.4
Tb (ppm)	0.05	0.07	0.07	0.06	0.07	0.07	0.06	0.05	0.02	0.02	0.04	0.02	0.04
Te (ppm)	0.1	0.12	0.08	0.21	0.1	0.17	0.12	0.08	0.19	0.14	0.3	0.09	0.05
Th (ppm)	0.34	0.06	0.05	0.09	0.12	0.07	0.11	0.1	0.05	0.05	0.06	0.05	0.97
Tl (ppm)	0.02	0.02	0.01	0.01	0.02	0.01	0.01	0.01	0.02	0.02	0.02	0.03	0.01
Tm (ppm)	0.04	0.04	0.05	0.04	0.04	0.06	0.04	0.04	0.03	0.02	0.02	0.02	0.05
V (ppm)	111	109	134	109	97	110	98	92	80	75	85	65	73
Y (ppm)	2.3	2.2	2.8	2.2	2.2	2.8	1.9	1.8	1.1	1	1.4	0.8	1.9
U (ppm)	0.1	0.025	0.025	0.025	0.08	0.025	0.025	0.025	0.025	0.025	0.025	0.025	0.21
W (ppm)	1	2	1	1	4	1	2	1	1	4	1	1	2
Yb (ppm)	0.26	0.31	0.33	0.28	0.24	0.29	0.22	0.22	0.19	0.16	0.22	0.15	0.25
Zr (ppm)	6	5	3	6	12	7	5	5	2	2	3	2	10
Zn (ppm)	58	60	56	61	47	54	67	64	60	62	81	99	83

Drill hole #	18-805	18-805	18-805	18-805	18-805	18-805	18-805	18-805	18-805	18-805	18-805	18-805	18-805
Depth From	26	27	28	29	30	31	32	33	34	35	36	37	38
Depth To	27	28	29	30	31	32	33	34	35	36	37	38	39
Rock Type	GABVT	GABVT	GABVT	GABVT	GABVT	GABVT	GABVT	GABVT	GABVT	GABVT	GABVT	GABVT	GABVT
Lithological Domain	Breccia	Breccia	Breccia	Breccia	Breccia	Breccia	Breccia	Breccia	Breccia	Breccia	Breccia	Breccia	Breccia
Al_2O_3 (%)	22.7	23.8	22.7	22.2	21.6	18.9	17.4	23.7	23.1	15.5	13.2	15.1	21
CaO (%)	8.57	9.37	9.96	9.95	9.65	8.82	8.07	10.3	10.15	8.79	6.68	3.86	9.73
Cr_2O_3 (%)	0.008	0.005	0.012	0.007	0.008	0.013	0.023	0.006	0.006	0.016	0.013	0.006	0.008
Fe_2O_3 (%)	3.36	3.15	5.13	5.66	5.93	7.84	7.87	4.31	4.52	9.74	7.9	2.82	6.35
K_2O (%)	0.14	0.18	0.2	0.22	0.2	0.18	0.39	0.24	0.2	0.2	0.33	0.53	0.34
MgO (%)	2.74	2.13	3.88	4.02	4.89	7.24	6.95	3.45	3.45	8.91	7.13	2.21	5.7
MnO (%)	0.05	0.04	0.07	0.07	0.08	0.12	0.12	0.06	0.06	0.14	0.12	0.04	0.1
Na_2O (%)	4.64	4.53	3.6	3.4	3.26	2.57	2.47	3.59	3.51	1.92	2.43	4.33	2.93
P_2O_5 (%)	0.005	0.005	0.005	0.005	0.01	0.005	0.01	0.01	0.005	0.005	0.005	0.005	0.005
SiO_2 (%)	55	53.8	52.7	51.3	52	51.6	52.1	52.1	51.6	50.4	58.8	70.3	51.9
TiO_2 (%)	0.05	0.06	0.09	0.09	0.09	0.12	0.12	0.07	0.08	0.15	0.13	0.04	0.1
LOI (%)	1.29	1.05	1.44	1.74	1.92	2.77	2.73	1.71	1.54	3.01	2.27	1.46	2.36
Total (%)	98.62	98.19	99.84	98.71	99.69	100.21	98.31	99.61	98.27	98.81	99.05	100.73	100.56
Ag (ppm)	0.25	0.25	0.25	0.25	0.25	0.25	0.25	0.25	0.25	0.25	0.25	0.25	0.25
As (ppm)	0.2	0.4	0.2	0.2	0.1	0.3	0.3	0.2	0.3	0.4	0.1	0.4	0.3
Au (ppm)	0.003	0.022	0.081	0.12	0.092	0.121	0.12	0.01	0.04	0.152	0.136	0.025	0.014
Ba (ppm)	99.5	98	81.8	79.1	66.4	65.9	254	79.6	76.6	65	287	85.2	72.9
Bi (ppm)	0.01	0.1	0.26	0.28	0.13	0.07	0.23	0.05	0.15	0.27	0.18	0.24	0.04
Cd (ppm)	0.25	0.25	0.25	0.25	0.25	0.25	0.25	0.25	0.25	0.25	0.25	0.25	0.25
Ce (ppm)	3.6	2.6	2.1	2.6	2.1	2.2	3.4	2	2.1	2.2	9	9.6	2.1
Co (ppm)	13	21	39	53	49	58	60	25	34	80	66	19	40
Cs (ppm)	1.33	1.41	1.85	2.22	2.06	2.11	2.76	2.18	1.81	2.61	2.17	3.32	3.96
Cu (ppm)	49	177	725	798	549	590	713	204	425	944	791	541	214
Dy (ppm)	0.1	0.12	0.18	0.24	0.22	0.27	0.3	0.14	0.19	0.46	0.38	0.49	0.29
Er (ppm)	0.05	0.05	0.11	0.14	0.1	0.19	0.17	0.08	0.13	0.3	0.26	0.3	0.18
Eu (ppm)	0.42	0.32	0.25	0.24	0.23	0.19	0.19	0.2	0.23	0.23	0.27	0.17	0.2
Ga (ppm)	25.2	24.9	20.4	20	19.3	16.2	16	21.1	19.6	14.9	13.6	15.7	17
Gd (ppm)	0.12	0.14	0.15	0.17	0.17	0.2	0.3	0.16	0.16	0.37	0.46	0.47	0.25
Ge (ppm)	2.5	2.5	2.5	2.5	2.5	2.5	2.5	2.5	2.5	2.5	2.5	2.5	2.5
Hf (ppm)	0.1	0.1	0.1	0.1	0.1	0.1	0.2	0.1	0.1	0.1	0.8	1.4	0.1
Hg (ppb)	0.0025	0.0025	0.0025	0.0025	0.0025	0.0025	0.0025	0.0025	0.0025	0.0025	0.0025	0.0025	0.0025
Ho (ppm)	0.02	0.02	0.03	0.04	0.05	0.06	0.07	0.02	0.05	0.1	0.09	0.1	0.05
In (ppm)	0.0025	0.0025	0.0025	0.0025	0.0025	0.005	0.005	0.0025	0.0025	0.009	0.006	0.0025	0.0025
La (ppm)	2.6	1.7	1.2	1.5	1.1	1.3	1.9	1.1	1.2	1.1	5.7	5.9	1.1
Li (ppm)	10	10	10	10	10	10	10	10	10	10	10	10	10
Lu (ppm)	0.02	0.01	0.02	0.02	0.02	0.04	0.04	0.02	0.02	0.06	0.05	0.05	0.03
Mo (ppm)	0.5	0.5	0.5	0.5	0.5	0.5	0.5	0.5	0.5	0.5	0.5	0.5	0.5
Nb (ppm)	0.1	0.1	0.1	0.2	0.1	0.1	0.2	0.1	0.1	0.1	0.9	1.6	0.1
Ni (ppm)	44	216	542	919	640	572	559	166	340	826	738	232	245
Nd (ppm)	1.1	0.8	0.8	1	0.9	1	1.4	0.7	0.9	1.3	2.8	3.2	0.9
Pb (ppm)	1	1	2	1	1	1	1	1	1	1	1	8	1
Pd (ppm)	0.032	0.836	1.86	3.05	1.6	1.13	1.14	0.059	0.719	1.84	1.54	0.57	0.189
Pr (ppm)	0.33	0.24	0.22	0.28	0.23	0.25	0.4	0.21	0.23	0.29	0.86	1.02	0.24
Pt (ppm)	0.0025	0.083	0.189	0.322	0.189	0.119	0.123	0.006	0.075	0.212	0.148	0.058	0.021
Rb (ppm)	3	4.1	5.1	5.8	5.5	5.2	10.6	6.6	5.2	6.5	8.7	18.3	10.5
Re (ppm)	0.0005	0.0005	0.0005	0.0005	0.0005	0.0005	0.0005	0.0005	0.0005	0.001	0.001	0.0005	0.0005
S (%)	0.02	0.16	0.28	0.42	0.25	0.22	0.26	0.07	0.19	0.44	0.4	0.13	0.07
Sb (ppm)	0.025	0.025	0.025	0.025	0.025	0.025	0.025	0.025	0.025	0.025	0.025	0.025	0.025
Sc (ppm)	5	4	8	9	9	14	15	7	8	21	24	6	13
Se (ppm)	0.052	0.817	1.865	3.05	1.91	1.455	1.545	0.402	1.12	2.68	2.29	0.846	0.388
Sm (ppm)	0.12	0.13	0.14	0.19	0.17	0.21	0.28	0.17	0.21	0.34	0.44	0.65	0.22
Sn (ppm)	0.5	1	0.5	0.5	0.5	1	1	0.5	0.5	1	0.5	1	0.5
Sr (ppm)	612	619	468	380	365	312	290	469	449	260	229	231	328
Ta (ppm)	0.05	0.05	0.05	0.05	0.05	0.05	0.05	0.05	0.05	0.05	0.1	0.3	0.05
Tb (ppm)	0.02	0.02	0.03	0.03	0.04	0.04	0.05	0.02	0.03	0.07	0.05	0.08	0.04
Te (ppm)	0.02	0.15	0.38	0.47	0.28	0.31	0.44	0.05	0.18	0.69	0.67	0.17	0.08
Th (ppm)	0.28	0.025	0.06	0.09	0.05	0.09	0.4	0.025	0.05	0.07	0.96	2.04	0.09
Tl (ppm)	0.01	0.03	0.06	0.08	0.04	0.03	0.04	0.02	0.04	0.07	0.09	0.04	0.02
Tm (ppm)	0.02	0.01	0.02	0.02	0.02	0.03	0.03	0.02	0.02	0.06	0.04	0.07	0.03
V (ppm)	28	29	56	65	67	95	91	50	52	146	111	31	88
Y (ppm)	0.5	0.6	0.9	1.1	1.1	1.6	1.6	0.8	1	2.5	2.1	2.7	1.5
U (ppm)	0.06	0.025	0.025	0.025	0.025	0.025	0.08	0.025	0.025	0.025	0.19	1.85	0.025
W (ppm)	4	1	1	1	1	1	1	1	1	1	1	2	1
Yb (ppm)	0.08	0.09	0.11	0.14	0.16	0.2	0.24	0.1	0.1	0.37	0.34	0.38	0.17
Zr (ppm)	3	4	2	4	3	4	7	2	2	5	27	28	3
Zn (ppm)	24	16	27	28	31	50	47	22	24	57	44	17	35

Drill hole #	18-805	18-805	18-805	18-805	18-805	18-805	18-805	18-805	18-805	18-805	18-805	18-805	18-805
Depth From	39	40	41	42	43	44	45	46	47	48	49	50	51
Depth To	40	41	42	43	44	45	46	47	48	49	50	51	52
Rock Type	GABVT	GABVT	GABVT	GABVT	GABVT	GABVT	GABVT	GABVT	GABVT	GABVT	GABVT	GABVT	GABVT
Lithological Domain	Breccia	Breccia	Breccia	Breccia	Breccia	Breccia	Breccia	Breccia	Breccia	Breccia	Breccia	Breccia	Breccia
Al_2O_3 (%)	21.8	23.9	21.4	18.1	21.3	22.4	21.1	24.4	23.1	22.4	22.3	23.4	22.4
CaO (%)	10.25	10.8	10.2	7.25	9.98	10.55	9.58	11.3	11	10.5	10.6	10.65	10.1
Cr_2O_3 (%)	0.007	0.005	0.008	0.006	0.007	0.006	0.008	0.005	0.006	0.007	0.007	0.006	0.006
Fe_2O_3 (%)	5.66	4.18	5.23	3.96	5.78	5.05	6.3	4.64	4.87	6.05	5.66	4.94	5.48
K_2O (%)	0.22	0.35	0.24	0.42	0.21	0.18	0.13	0.24	0.24	0.19	0.17	0.16	0.21
MgO (%)	4.93	3.28	4.74	3.27	5.23	4.51	5.72	3.85	4.15	5.08	5.35	4.44	5.08
MnO (%)	0.09	0.06	0.08	0.06	0.09	0.08	0.1	0.06	0.07	0.08	0.08	0.07	0.08
Na_2O (%)	3.03	3.46	3.12	3.68	2.86	3.1	2.94	3.26	3.14	2.86	2.88	3.15	2.99
P_2O_5 (%)	0.005	0.005	0.005	0.005	0.005	0.005	0.005	0.01	0.01	0.01	0.005	0.01	0.005
SiO_2 (%)	51.7	52	51.5	59.6	51.1	52.2	52.5	51.7	51.7	50.7	51.2	51.2	50.6
TiO_2 (%)	0.1	0.08	0.09	0.06	0.08	0.09	0.07	0.08	0.09	0.08	0.08	0.06	0.07
LOI (%)	1.95	1.96	2.09	2.74	1.99	1.75	2.11	1.79	1.89	2.09	1.92	1.91	2.09
Total (%)	99.79	100.13	98.74	99.2	98.67	99.96	100.6	101.38	100.31	100.09	100.28	100.04	99.15
Ag (ppm)	0.25	0.25	0.25	0.25	0.25	0.25	0.25	0.25	0.25	0.25	0.25	0.25	0.25
As (ppm)	0.2	0.5	0.2	0.05	0.2	0.2	0.2	0.1	0.4	0.5	0.1	0.2	0.4
Au (ppm)	0.009	0.044	0.028	0.006	0.011	0.005	0.011	0.027	0.038	0.063	0.016	0.012	0.032
Ba (ppm)	66.7	91.1	68.1	133.5	67.7	80.2	49.1	71.7	69.2	76.8	57.3	69.4	64.7
Bi (ppm)	0.03	0.1	0.09	0.2	0.11	0.03	0.03	0.04	0.04	0.06	0.02	0.03	0.03
Cd (ppm)	0.25	0.25	0.25	0.25	0.25	0.25	0.25	0.25	0.25	0.25	0.25	0.25	0.25
Ce (ppm)	2.2	5.8	2.4	8	1.9	2.4	2.1	2	5.5	2.7	1.9	2.7	1.8
Co (ppm)	33	33	37	26	38	31	40	26	31	44	36	28	36
Cs (ppm)	2.16	2.78	1.85	2.43	2.56	2.14	2.01	3.2	2.68	2.53	1.89	1.94	2.23
Cu (ppm)	205	594	284	187	162	89	230	222	341	540	199	142	215
Dy (ppm)	0.24	0.32	0.29	0.36	0.21	0.23	0.13	0.17	0.26	0.2	0.26	0.11	0.12
Er (ppm)	0.15	0.16	0.18	0.26	0.14	0.12	0.08	0.16	0.23	0.16	0.11	0.1	0.1
Eu (ppm)	0.25	0.3	0.21	0.18	0.18	0.18	0.16	0.19	0.21	0.22	0.18	0.17	0.18
Ga (ppm)	17.1	18.3	16.9	15.8	16.1	17.9	17.3	19	17.6	19.1	18.1	19	17.8
Gd (ppm)	0.22	0.5	0.22	0.33	0.14	0.24	0.14	0.17	0.37	0.21	0.17	0.13	0.15
Ge (ppm)	2.5	2.5	2.5	2.5	2.5	2.5	2.5	2.5	2.5	2.5	2.5	2.5	2.5
Hf (ppm)	0.1	0.1	0.1	0.8	0.1	0.2	0.1	0.1	0.2	0.2	0.1	0.1	0.1
Hg (ppb)	0.0025	0.0025	0.0025	0.0025	0.0025	0.0025	0.0025	0.0025	0.0025	0.0025	0.0025	0.0025	0.0025
Ho (ppm)	0.05	0.06	0.05	0.08	0.04	0.05	0.03	0.04	0.07	0.06	0.04	0.04	0.04
In (ppm)	0.0025	0.0025	0.0025	0.0025	0.0025	0.0025	0.0025	0.0025	0.0025	0.0025	0.0025	0.0025	0.0025
La (ppm)	1.3	3.2	1.3	5	1	1.3	1.1	1.1	2.6	1.4	1	1.6	1
Li (ppm)	10	10	10	10	10	10	10	10	10	10	10	10	10
Lu (ppm)	0.02	0.03	0.03	0.05	0.02	0.02	0.02	0.02	0.01	0.02	0.02	0.01	0.02
Mo (ppm)	0.5	0.5	0.5	0.5	0.5	0.5	0.5	0.5	0.5	0.5	0.5	0.5	0.5
Nb (ppm)	0.1	0.4	0.2	1.7	0.1	0.2	0.2	0.2	2.9	0.8	0.5	0.4	0.2
Ni (ppm)	224	289	195	208	244	126	217	194	285	466	176	144	210
Nd (ppm)	1	2.6	1	2.5	0.8	1.1	0.8	0.9	2.4	1	0.7	0.9	0.8
Pb (ppm)	1	1	1	2	1	1	1	1	1	1	1	1	1
Pd (ppm)	0.104	0.597	0.201	0.357	0.352	0.048	0.0005	0.253	0.29	0.664	0.009	0.006	0.05
Pr (ppm)	0.25	0.69	0.29	0.77	0.21	0.24	0.22	0.24	0.69	0.29	0.23	0.33	0.23
Pt (ppm)	0.019	0.08	0.016	0.041	0.043	0.008	0.0025	0.041	0.039	0.087	0.0025	0.0025	0.012
Rb (ppm)	6.6	10.6	6.6	13.5	6	5.1	3.6	7	6.8	5.7	4.3	4.2	6
Re (ppm)	0.0005	0.0005	0.0005	0.0005	0.0005	0.0005	0.0005	0.0005	0.0005	0.001	0.0005	0.0005	0.0005
S (%)	0.05	0.19	0.09	0.12	0.06	0.03	0.06	0.07	0.1	0.24	0.05	0.05	0.08
Sb (ppm)	0.025	0.025	0.025	0.025	0.025	0.025	0.025	0.025	0.025	0.025	0.025	0.025	0.025
Sc (ppm)	11	8	12	9	12	11	10	9	11	10	12	9	9
Se (ppm)	0.314	1.075	0.481	0.526	0.401	0.122	0.484	0.408	0.683	1.45	0.326	0.247	0.516
Sm (ppm)	0.26	0.46	0.24	0.4	0.14	0.24	0.11	0.22	0.48	0.23	0.19	0.19	0.15
Sn (ppm)	0.5	0.5	1	0.5	1	0.5	0.5	1	0.5	1	2	0.5	0.5
Sr (ppm)	339	385	326	288	302	342	299	321	295	316	296	322	302
Ta (ppm)	0.05	0.05	0.05	0.1	0.05	0.05	0.05	0.05	0.05	0.05	0.05	0.05	0.05
Tb (ppm)	0.03	0.06	0.04	0.05	0.03	0.04	0.03	0.03	0.06	0.05	0.03	0.02	0.03
Te (ppm)	0.08	0.14	0.13	0.19	0.15	0.04	0.07	0.12	0.16	0.27	0.05	0.04	0.08
Th (ppm)	0.11	0.88	0.18	0.93	0.09	0.19	0.11	0.25	0.44	0.14	0.09	0.2	0.07
Tl (ppm)	0.02	0.03	0.02	0.03	0.02	0.01	0.02	0.02	0.03	0.05	0.01	0.02	0.02
Tm (ppm)	0.03	0.02	0.03	0.05	0.02	0.03	0.02	0.01	0.03	0.02	0.02	0.01	0.01
V (ppm)	76	52	71	46	69	65	61	53	63	69	67	52	57
Y (ppm)	1.3	1.7	1.3	2	1.1	1.3	0.9	1.1	1.6	1.3	1.1	0.9	0.9
U (ppm)	0.025	0.025	0.025	0.85	0.025	0.025	0.025	0.28	0.25	0.025	0.025	0.025	0.025
W (ppm)	1	1	2	1	1	4	3	5	2	1	1	1	1
Yb (ppm)	0.17	0.14	0.14	0.31	0.14	0.15	0.15	0.15	0.18	0.23	0.17	0.13	0.13
Zr (ppm)	3	3	3	18	3	6	3	4	5	6	4	3	3
Zn (ppm)	31	24	27	23	33	29	36	22	24	31	30	25	28

Drill hole #	18-805	18-805	18-805	18-805	18-805	18-805	18-805	18-805	18-805	18-805	18-805	18-805	18-805
Depth From	52	53	54	55	56	57	58	59	60	61	62	63	64
Depth To	53	54	55	56	57	58	59	60	61	62	63	64	65
Rock Type	GABVT	GABVT	GABVT	GABVT	GABVT	GABVT	GABVT	GABVT	LGABVT	LGABVT	LGABVT	LGABVT	LGABVT
Lithological Domain	Breccia	Breccia	Breccia	Breccia	Breccia	Breccia	Breccia	Breccia	Breccia	Breccia	Breccia	Breccia	Breccia
Al_2O_3 (%)	22.3	16.05	21.7	22.4	21.2	22	22.4	23.1	22.4	21.5	21.5	22	21.1
CaO (%)	10.45	3.49	10.55	10.3	10	10.35	10.35	10.65	10.25	10.1	9.97	10.45	10.4
Cr_2O_3 (%)	0.007	0.003	0.008	0.007	0.009	0.01	0.009	0.008	0.009	0.01	0.011	0.009	0.01
Fe_2O_3 (%)	5.61	2	5.9	6.02	6.18	6.01	5.88	5.35	5.5	6.45	6.38	5.91	6.54
K_2O (%)	0.27	1.34	0.36	0.21	0.36	0.24	0.21	0.16	0.2	0.23	0.21	0.19	0.17
MgO (%)	5.2	1.34	5.62	5.51	6.17	6.28	5.95	5.13	5.58	6.08	6.13	5.69	6.42
MnO (%)	0.08	0.03	0.08	0.09	0.09	0.09	0.09	0.08	0.08	0.09	0.09	0.09	0.1
Na_2O (%)	2.9	4.83	2.8	2.87	2.73	2.75	2.84	3.03	2.84	2.66	2.69	2.74	2.57
P_2O_5 (%)	0.005	0.01	0.01	0.005	0.005	0.005	0.005	0.005	0.005	0.01	0.005	0.01	0.005
SiO_2 (%)	51.1	71.1	51.5	51	51.4	51.5	51.7	51.5	50.8	50.7	51	50.6	50.5
TiO_2 (%)	0.08	0.04	0.1	0.07	0.08	0.08	0.07	0.07	0.07	0.1	0.09	0.09	0.1
LOI (%)	2.1	0.9	1.87	1.93	2.45	2.18	2.04	1.74	2.01	2.34	2.39	2.12	2.22
Total (%)	100.14	101.15	100.53	100.44	100.7	101.53	101.58	100.86	99.78	100.3	100.49	99.94	100.17
Ag (ppm)	0.25	0.25	0.25	0.25	0.25	0.25	0.25	0.25	0.25	0.25	0.25	0.25	0.25
As (ppm)	0.3	0.3	0.3	0.3	0.2	0.3	0.4	0.3	0.2	0.2	0.2	0.2	0.2
Au (ppm)	0.031	0.001	0.017	0.013	0.024	0.04	0.025	0.017	0.006	0.026	0.005	0.01	0.007
Ba (ppm)	63.4	79.7	61.2	61.1	63.8	64.2	58.4	53.8	60.1	67.3	60.8	60.9	59.4
Bi (ppm)	0.03	0.36	0.13	0.03	0.05	0.08	0.09	0.11	0.02	0.05	0.03	0.03	0.74
Cd (ppm)	0.25	0.25	0.25	0.25	0.25	0.25	0.25	0.25	0.25	0.25	0.25	0.25	0.25
Ce (ppm)	2	9.5	2.1	1.8	2.6	1.7	1.7	1.9	1.6	1.9	1.6	1.7	1.7
Co (ppm)	37	9	37	37	38	43	41	38	35	43	42	38	40
Cs (ppm)	2.72	3.54	3.3	2.1	3.16	2.4	2.13	1.54	2.06	2.57	2.36	2.24	2.29
Cu (ppm)	232	59	152	209	245	310	217	202	116	211	134	141	157
Dy (ppm)	0.2	0.79	0.3	0.23	0.2	0.21	0.16	0.13	0.15	0.25	0.23	0.15	0.21
Er (ppm)	0.15	0.45	0.19	0.08	0.1	0.14	0.11	0.11	0.08	0.15	0.12	0.16	0.19
Eu (ppm)	0.17	0.19	0.19	0.17	0.15	0.17	0.17	0.15	0.17	0.19	0.16	0.15	0.18
Ga (ppm)	17.3	21	15.8	17.4	17.2	16.8	16.2	16.1	16.4	16.9	15.4	16.5	16.3
Gd (ppm)	0.16	0.69	0.24	0.16	0.23	0.17	0.19	0.13	0.1	0.14	0.19	0.13	0.22
Ge (ppm)	2.5	2.5	2.5	2.5	2.5	2.5	2.5	2.5	2.5	2.5	2.5	2.5	2.5
Hf (ppm)	0.1	1.6	0.2	0.2	0.2	0.1	0.1	0.1	0.1	0.1	0.1	0.1	0.1
Hg (ppb)	0.0025	0.0025	0.0025	0.0025	0.0025	0.0025	0.0025	0.0025	0.0025	0.0025	0.0025	0.0025	0.0025
Ho (ppm)	0.05	0.17	0.07	0.04	0.05	0.04	0.04	0.04	0.04	0.05	0.04	0.06	0.07
In (ppm)	0.0025	0.0025	0.0025	0.0025	0.0025	0.0025	0.0025	0.0025	0.0025	0.0025	0.0025	0.0025	0.0025
La (ppm)	1.1	5.5	1.1	1	1.3	0.9	0.9	1	0.9	1.1	0.9	0.9	0.9
Li (ppm)	10	5	10	10	10	10	10	10	10	10	10	10	10
Lu (ppm)	0.02	0.08	0.03	0.02	0.03	0.02	0.01	0.02	0.02	0.02	0.02	0.03	0.03
Mo (ppm)	0.5	0.5	0.5	0.5	1	0.5	1	0.5	1	0.5	0.5	0.5	0.5
Nb (ppm)	0.2	3.9	0.3	0.3	0.5	0.3	0.1	0.4	0.1	0.1	0.1	0.1	0.1
Ni (ppm)	259	43	294	214	322	337	368	351	182	278	199	195	225
Nd (ppm)	0.9	3.5	1	0.8	0.9	0.7	0.7	0.7	0.6	0.8	0.6	0.7	0.9
Pb (ppm)	1	14	1	1	1	1	1	1	2	1	1	1	1
Pd (ppm)	0.257	0.0005	0.386	0.082	0.376	0.591	0.898	0.668	0.018	0.445	0.044	0.052	0.036
Pr (ppm)	0.26	1.08	0.28	0.2	0.29	0.21	0.18	0.24	0.15	0.23	0.18	0.19	0.19
Pt (ppm)	0.03	0.0025	0.037	0.01	0.056	0.068	0.105	0.084	0.008	0.045	0.012	0.012	0.005
Rb (ppm)	8.1	41.8	10.8	5.9	12.7	6.4	5.4	4.2	5.5	6.5	5.9	5.7	5
Re (ppm)	0.0005	0.0005	0.0005	0.0005	0.001	0.001	0.0005	0.0005	0.0005	0.0005	0.0005	0.0005	0.0005
S (%)	0.1	0.07	0.06	0.05	0.06	0.09	0.07	0.09	0.03	0.07	0.03	0.03	0.03
Sb (ppm)	0.025	0.025	0.025	0.025	0.025	0.025	0.3	0.025	0.025	0.025	0.025	0.025	0.025
Sc (ppm)	11	5	14	11	12	13	12	10	11	13	13	12	15
Se (ppm)	0.626	0.156	0.464	0.399	0.564	0.552	0.455	0.517	0.153	0.409	0.155	0.176	0.183
Sm (ppm)	0.16	0.81	0.24	0.13	0.16	0.21	0.16	0.13	0.18	0.16	0.15	0.13	0.19
Sn (ppm)	0.5	0.5	0.5	0.5	0.5	0.5	0.5	0.5	0.5	0.5	0.5	0.5	1
Sr (ppm)	289	124.5	257	296	277	279	287	286	290	278	261	286	275
Ta (ppm)	0.05	0.4	0.05	0.05	0.05	0.05	0.05	0.05	0.05	0.05	0.05	0.05	0.05
Tb (ppm)	0.03	0.12	0.05	0.03	0.04	0.04	0.02	0.03	0.03	0.03	0.03	0.03	0.04
Te (ppm)	0.12	0.02	0.27	0.07	0.1	0.19	0.17	0.22	0.03	0.11	0.06	0.05	0.43
Th (ppm)	0.1	1.99	0.15	0.07	0.29	0.07	0.05	0.09	0.05	0.09	0.07	0.06	0.11
Tl (ppm)	0.02	0.05	0.05	0.01	0.02	0.03	0.02	0.02	0.02	0.03	0.03	0.02	0.02
Tm (ppm)	0.02	0.07	0.02	0.02	0.03	0.02	0.02	0.02	0.02	0.03	0.02	0.02	0.02
V (ppm)	63	19	71	62	70	67	61	54	57	76	66	70	78
Y (ppm)	1.2	4.5	1.5	0.9	1.3	1.1	0.9	0.9	0.9	1.4	1.1	1	1.4
U (ppm)	0.13	2.47	0.07	0.025	0.11	0.025	0.025	0.025	0.025	0.025	0.025	0.025	0.025
W (ppm)	1	1	1	5	1	1	1	1	1	1	0.5	0.5	3
Yb (ppm)	0.14	0.55	0.18	0.12	0.2	0.12	0.13	0.15	0.09	0.17	0.12	0.17	0.19
Zr (ppm)	4	30	6	4	5	3	4	3	3	5	3	3	4
Zn (ppm)	30	10	31	30	32	36	33	29	33	38	39	35	35

Drill hole #	18-805	18-805	18-805	18-805	18-805	18-805	18-805	18-805	18-805	18-805	18-805	18-805	18-805
Depth From	65	66	67	68	69	70	71	72	73	74	75	76	77
Depth To	66	67	68	69	70	71	72	73	74	75	76	77	78
Rock Type	GABVT	GABVT	GABVT	GABVT	GABVT	GABVT	GABVT	GABVT	GABVT	GABVT	GABVT	GABVT	GABVT
Lithological Domain	Breccia	Breccia	Breccia	Breccia	Breccia	Breccia	Breccia	Breccia	Breccia	Breccia	Breccia	Breccia	Breccia
Al2O3 (%)	20.2	19.55	17.6	17.35	16.9	16.55	17.1	17.85	17.6	17.9	17.55	16.4	16.1
CaO (%)	9.77	8.93	10.15	10.45	10.45	10.35	8.9	8.27	10.3	10.25	8.88	8.64	9.96
Cr2O3 (%)	0.021	0.011	0.009	0.01	0.012	0.008	0.008	0.02	0.025	0.027	0.023	0.024	0.026
Fe2O3 (%)	6.73	6.96	7.89	7.73	8.27	8.77	9.54	7.74	6.98	7.34	9.07	9.89	9.33
K2O (%)	0.17	0.14	0.14	0.13	0.16	0.1	0.11	0.18	0.13	0.13	0.24	0.24	0.18
MgO (%)	6.51	7.15	7.36	6.76	7.66	7.73	7.88	8.68	8.24	8.19	8.58	8.82	8.64
MnO (%)	0.1	0.11	0.13	0.13	0.14	0.15	0.15	0.13	0.13	0.13	0.13	0.14	0.13
Na2O (%)	2.87	3.03	2.72	2.9	2.57	2.59	2.54	2.51	2.53	2.5	2.24	2.08	2.14
P2O5 (%)	0.005	0.005	0.005	0.005	0.01	0.005	0.005	0.01	0.02	0.005	0.01	0.01	0.01
SiO2 (%)	50.9	51.8	50.6	51.5	50.8	51.1	50.4	51.6	51.5	51.6	50.1	48.7	49.1
TiO2 (%)	0.09	0.06	0.08	0.08	0.11	0.09	0.07	0.09	0.1	0.1	0.12	0.14	0.15
LOI (%)	2.85	2.45	2.31	2.79	2.37	2.26	2.67	2.69	2.18	2.26	2.77	3	2.29
Total (%)	100.25	100.23	99.03	99.86	99.48	99.73	99.4	99.8	99.77	100.46	99.74	98.11	98.09
Ag (ppm)	0.25	0.25	0.25	0.25	0.25	0.25	0.25	0.25	0.25	0.25	0.25	0.7	0.5
As (ppm)	0.5	0.2	0.1	0.2	0.2	0.3	0.2	0.05	0.2	0.1	0.3	0.3	0.3
Au (ppm)	0.013	0.002	0.009	0.009	0.019	0.002	0.001	0.0005	0.0005	0.008	0.096	0.128	0.134
Ba (ppm)	52.3	53.3	49.5	49.8	61.5	53.5	53.8	67.3	69.9	57.8	67.6	62.4	60.7
Bi (ppm)	0.06	0.03	0.04	0.05	0.03	0.02	0.03	0.02	0.01	0.02	0.08	3.44	0.12
Cd (ppm)	0.25	0.25	0.25	0.25	0.25	0.25	0.25	0.25	0.25	0.25	0.25	0.5	0.25
Ce (ppm)	1.4	0.9	0.9	6.6	1.3	0.4	0.5	1.5	2.2	2	2	1.9	2.4
Co (ppm)	44	45	52	45	52	51	62	52	41	43	61	75	69
Cs (ppm)	2.09	1.54	1.24	1.57	1.58	1.35	1.77	2.77	1.63	1.71	2.56	3.14	2.25
Cu (ppm)	253	133	204	156	255	98	221	104	63	113	523	958	836
Dy (ppm)	0.13	0.08	0.28	0.28	0.59	0.42	0.14	0.16	0.41	0.31	0.3	0.4	0.51
Er (ppm)	0.13	0.08	0.24	0.2	0.33	0.37	0.08	0.09	0.27	0.28	0.21	0.26	0.34
Eu (ppm)	0.16	0.14	0.17	0.19	0.27	0.24	0.18	0.23	0.31	0.23	0.2	0.17	0.22
Ga (ppm)	17.1	19.9	15.3	16	16.7	14.6	16.7	16	15.3	14.5	13.4	12	13.3
Gd (ppm)	0.18	0.08	0.18	0.24	0.46	0.42	0.07	0.11	0.37	0.3	0.29	0.3	0.46
Ge (ppm)	2.5	2.5	2.5	2.5	2.5	2.5	2.5	2.5	2.5	2.5	2.5	2.5	2.5
Hf (ppm)	0.1	0.1	0.1	0.1	0.1	0.1	0.1	0.1	0.1	0.2	0.1	0.2	0.2
Hg (ppb)	0.0025	0.0025	0.0025	0.0025	0.0025	0.0025	0.0025	0.0025	0.0025	0.0025	0.0025	0.0025	0.0025
Ho (ppm)	0.04	0.02	0.06	0.07	0.12	0.11	0.03	0.04	0.1	0.09	0.06	0.06	0.11
In (ppm)	0.0025	0.0025	0.0025	0.0025	0.005	0.0025	0.0025	0.0025	0.0025	0.0025	0.005	0.009	0.008
La (ppm)	0.9	0.5	0.6	4.2	0.6	0.3	0.3	0.9	1.1	1	1	1	1.2
Li (ppm)	10	10	10	10	10	10	10	10	10	10	10	10	10
Lu (ppm)	0.02	0.02	0.04	0.03	0.06	0.06	0.02	0.03	0.05	0.05	0.04	0.05	0.05
Mo (ppm)	0.5	0.5	0.5	0.5	0.5	0.5	0.5	0.5	0.5	0.5	0.5	0.5	0.5
Nb (ppm)	0.1	0.1	0.1	1.1	0.3	0.1	0.1	0.1	0.1	0.1	0.1	0.2	0.2
Ni (ppm)	221	136	188	154	213	159	191	222	164	180	536	920	899
Nd (ppm)	0.6	0.3	0.4	2	1	0.5	0.1	0.7	1.1	1.1	0.9	1	1.4
Pb (ppm)	1	1	1	1	1	1	1	1	1	1	1	2	2
Pd (ppm)	0.034	0.002	0.001	0.013	0.112	0.001	0.004	0.0005	0.0005	0.001	0.987	1.68	1.5
Pr (ppm)	0.19	0.08	0.1	0.66	0.15	0.08	0.05	0.18	0.3	0.24	0.2	0.23	0.33
Pt (ppm)	0.005	0.0025	0.0025	0.0025	0.012	0.0025	0.0025	0.0025	0.0025	0.0025	0.117	0.189	0.17
Rb (ppm)	4.4	3.4	2.9	3.2	4	2.2	2.9	4.5	3.1	3.3	5.8	5.7	4.8
Re (ppm)	0.0005	0.0005	0.0005	0.0005	0.001	0.0005	0.001	0.001	0.0005	0.0005	0.001	0.001	0.001
S (%)	0.16	0.08	0.12	0.1	0.12	0.17	0.47	0.14	0.06	0.07	0.19	0.45	0.35
Sb (ppm)	0.025	0.025	0.025	0.025	0.025	0.025	0.025	0.025	0.025	0.025	0.025	0.025	0.025
Sc (ppm)	15	14	28	29	34	35	23	17	27	24	20	24	31
Se (ppm)	0.728	0.228	0.256	0.216	0.311	0.279	0.723	0.287	0.121	0.181	0.94	1.83	1.6
Sm (ppm)	0.15	0.11	0.16	0.32	0.3	0.26	0.03	0.09	0.29	0.29	0.28	0.33	0.36
Sn (ppm)	0.5	0.5	0.5	0.5	0.5	0.5	0.5	0.5	0.5	0.5	0.5	0.5	0.5
Sr (ppm)	290	361	274	277	275	259	252	245	250	238	229	207	229
Ta (ppm)	0.05	0.05	0.1	0.05	0.05	0.05	0.05	0.05	0.05	0.05	0.05	0.05	0.05
Tb (ppm)	0.03	0.02	0.05	0.04	0.07	0.08	0.02	0.03	0.06	0.06	0.05	0.06	0.09
Te (ppm)	0.06	0.02	0.03	0.04	0.04	0.02	0.05	0.02	0.02	0.02	0.25	0.97	0.51
Th (ppm)	0.05	0.025	0.025	0.34	0.025	0.025	0.025	0.025	0.025	0.05	0.06	0.08	0.07
Tl (ppm)	0.03	0.02	0.03	0.02	0.02	0.02	0.03	0.03	0.01	0.01	0.04	0.06	0.04
Tm (ppm)	0.02	0.01	0.03	0.03	0.05	0.05	0.01	0.02	0.05	0.05	0.03	0.04	0.05
V (ppm)	72	71	89	98	122	105	85	74	101	96	94	103	133
Y (ppm)	1	0.6	1.6	1.4	3.1	2.8	0.7	1	2.2	1.9	1.6	2	2.9
U (ppm)	0.05	0.025	0.025	0.025	0.025	0.025	0.025	0.025	0.025	0.025	0.025	0.05	0.025
W (ppm)	1	0.5	3	0.5	1	1	1	3	3	2	3	1	1
Yb (ppm)	0.16	0.11	0.21	0.19	0.38	0.39	0.12	0.16	0.23	0.24	0.22	0.3	0.32
Zr (ppm)	2	1	1	2	2	1	1	2	4	5	4	6	6
Zn (ppm)	35	45	50	47	60	72	84	71	70	60	58	62	54

Drill hole #	18-805	18-805	18-805	18-805	18-805	18-805	18-805	18-805	18-805	18-805	18-805	18-805	18-805
Depth From	78	79	80	81	82	83	84	85	86	87	88	89	90
Depth To	79	80	81	82	83	84	85	86	87	88	89	90	91
Rock Type	GABVT	GABVT	GABVT	GABVT	GABVT	GABVT	GABVT	GABVT	GABVT	GABVT	GABVT	GABVT	GABVT
Lithological Domain	Breccia	Breccia	Breccia	Breccia	Breccia	Breccia	Breccia	Breccia	Breccia	Breccia	Breccia	Breccia	Breccia
Al_2O_3 (%)	17.55	16.45	17.1	16.55	16.35	16.85	17.35	17.4	17.65	17.2	17.55	17.85	16.7
CaO (%)	8.76	10.35	10	9.98	10.25	10.5	9.59	9.45	9.21	9.16	9.13	9.72	9.27
Cr_2O_3 (%)	0.022	0.026	0.027	0.021	0.025	0.027	0.026	0.029	0.029	0.029	0.031	0.028	0.034
Fe_2O_3 (%)	8.65	8.09	7.69	7.62	7.94	7.48	7.8	7.68	7.72	7.69	7.59	7.67	8.47
K_2O (%)	0.23	0.18	0.12	0.22	0.16	0.14	0.11	0.12	0.12	0.13	0.15	0.18	0.15
MgO (%)	8.42	8.31	8.22	7.77	8.43	8.15	8.31	8.46	8.45	8.2	8.2	7.97	8.81
MnO (%)	0.13	0.13	0.13	0.13	0.14	0.13	0.13	0.13	0.13	0.13	0.13	0.12	0.14
Na_2O (%)	2.47	2.37	2.4	2.49	2.51	2.65	2.58	2.58	2.58	2.6	2.68	2.73	2.39
P_2O_5 (%)	0.01	0.005	0.005	0.005	0.005	0.005	0.005	0.005	0.01	0.005	0.005	0.005	0.005
SiO_2 (%)	53	51.3	51.6	53.6	53.4	52.5	52.8	53.5	52.7	52.2	53	52.9	52.6
TiO_2 (%)	0.11	0.12	0.09	0.09	0.09	0.09	0.09	0.09	0.09	0.08	0.08	0.1	0.09
LOI (%)	2.58	2.23	2.39	2.44	2.18	1.83	2.26	2.42	2.31	2.27	2.2	2.06	2.36
Total (%)	101.97	99.59	99.8	100.94	101.51	100.39	101.08	101.89	101.03	99.72	100.77	101.37	101.04
Ag (ppm)	0.25	0.25	0.25	0.25	0.25	0.25	0.25	0.25	0.25	0.25	0.25	0.25	0.25
As (ppm)	0.1	0.3	0.2	0.1	0.1	0.1	0.1	0.05	0.05	0.05	0.1	0.2	0.1
Au (ppm)	0.104	0.129	0.068	0.043	0.018	0.016	0.013	0.007	0.005	0.011	0.004	0.005	0.008
Ba (ppm)	59	57	51	58.7	57.2	63.7	61.6	69.9	73.4	64.8	65.1	75.6	65.5
Bi (ppm)	0.08	0.12	0.08	0.9	0.22	0.2	0.08	0.03	0.02	0.02	0.03	0.07	0.05
Cd (ppm)	0.25	0.25	0.25	0.25	0.25	0.25	0.25	0.25	0.25	0.25	0.25	0.25	0.25
Ce (ppm)	2	2.3	2	2.5	2	2	2.2	2.7	2.9	2.2	2.3	2.4	2.3
Co (ppm)	61	55	45	48	43	44	44	46	46	45	44	44	54
Cs (ppm)	2.42	2.35	2.1	2.55	2.52	2.73	2.48	2.46	2.31	1.51	2.03	3.21	2.68
Cu (ppm)	625	572	250	213	143	144	136	101	90	123	103	138	163
Dy (ppm)	0.29	0.38	0.35	0.35	0.43	0.39	0.34	0.32	0.28	0.22	0.26	0.37	0.41
Er (ppm)	0.19	0.34	0.26	0.21	0.23	0.25	0.21	0.24	0.23	0.17	0.2	0.23	0.24
Eu (ppm)	0.22	0.23	0.23	0.21	0.28	0.27	0.27	0.26	0.3	0.26	0.26	0.26	0.32
Ga (ppm)	14.5	14.3	13.8	14.2	14.5	15.1	15.6	15.4	14.9	15.1	14.8	15.2	14.4
Gd (ppm)	0.25	0.35	0.32	0.3	0.38	0.34	0.29	0.33	0.29	0.21	0.23	0.33	0.2
Ge (ppm)	2.5	2.5	2.5	2.5	2.5	2.5	2.5	2.5	2.5	2.5	2.5	2.5	2.5
Hf (ppm)	0.2	0.1	0.1	0.1	0.2	0.1	0.1	0.1	0.1	0.1	0.1	0.1	0.1
Hg (ppb)	0.0025	0.0025	0.0025	0.0025	0.0025	0.0025	0.0025	0.0025	0.0025	0.0025	0.0025	0.0025	0.0025
Ho (ppm)	0.07	0.1	0.06	0.07	0.09	0.09	0.08	0.1	0.08	0.06	0.07	0.08	0.07
In (ppm)	0.006	0.005	0.0025	0.0025	0.0025	0.0025	0.0025	0.0025	0.0025	0.0025	0.0025	0.0025	0.005
La (ppm)	1.1	1.2	1	1.4	1.2	1.1	1.3	1.6	1.7	1.4	1.5	1.5	1.3
Li (ppm)	10	10	10	10	10	10	10	10	10	10	10	10	10
Lu (ppm)	0.04	0.05	0.04	0.04	0.04	0.04	0.04	0.04	0.04	0.04	0.03	0.03	0.04
Mo (ppm)	0.5	0.5	0.5	0.5	0.5	0.5	0.5	0.5	0.5	0.5	0.5	0.5	0.5
Nb (ppm)	0.1	0.1	0.1	0.6	0.2	0.1	0.1	0.1	0.1	0.1	0.1	0.2	0.1
Ni (ppm)	583	581	347	293	249	253	249	233	216	224	225	218	315
Nd (ppm)	1	1.3	1	1.1	1.2	1.2	1.1	1.3	1.4	1.1	1	1.3	1.1
Pb (ppm)	1	3	3	2	1	3	1	2	4	1	2	1	1
Pd (ppm)	0.957	1.76	0.817	0.663	0.253	0.183	0.161	0.06	0.006	0.085	0.003	0.029	0.272
Pr (ppm)	0.25	0.28	0.23	0.35	0.25	0.24	0.3	0.32	0.35	0.26	0.25	0.28	0.29
Pt (ppm)	0.108	0.162	0.057	0.091	0.02	0.024	0.021	0.01	0.0025	0.009	0.0025	0.0025	0.019
Rb (ppm)	5.4	5.5	3.7	7.6	5.5	4.8	3.7	3.9	4.1	3.4	4.6	5.8	5.3
Re (ppm)	0.001	0.001	0.0005	0.0005	0.0005	0.0005	0.0005	0.0005	0.0005	0.0005	0.0005	0.0005	0.0005
S (%)	0.27	0.27	0.11	0.16	0.09	0.07	0.08	0.07	0.06	0.05	0.05	0.08	0.1
Sb (ppm)	0.025	0.025	0.025	0.025	0.025	0.025	0.025	0.025	0.025	0.025	0.025	0.025	0.025
Sc (ppm)	18	27	22	25	28	29	21	23	23	19	18	21	23
Se (ppm)	1.13	1.495	0.524	0.526	0.388	0.234	0.34	0.268	0.213	0.197	0.17	0.265	0.523
Sm (ppm)	0.27	0.36	0.26	0.31	0.28	0.31	0.24	0.38	0.3	0.26	0.21	0.26	0.19
Sn (ppm)	0.5	0.5	2	0.5	1	0.5	0.5	0.5	0.5	0.5	0.5	0.5	0.5
Sr (ppm)	257	253	253	254	256	283	266	256	267	255	265	285	253
Ta (ppm)	0.05	0.05	0.05	0.05	0.05	0.05	0.05	0.05	0.05	0.05	0.05	0.05	0.05
Tb (ppm)	0.04	0.06	0.05	0.05	0.08	0.06	0.05	0.05	0.05	0.05	0.04	0.04	0.04
Te (ppm)	0.33	0.6	0.29	0.28	0.1	0.1	0.05	0.04	0.005	0.05	0.005	0.02	0.1
Th (ppm)	0.11	0.08	0.07	0.09	0.07	0.025	0.025	0.025	0.05	0.025	0.025	0.06	0.05
Tl (ppm)	0.04	0.03	0.02	0.02	0.03	0.03	0.03	0.03	0.02	0.02	0.02	0.02	0.03
Tm (ppm)	0.05	0.04	0.04	0.04	0.05	0.05	0.04	0.03	0.03	0.02	0.03	0.03	0.03
V (ppm)	102	127	103	103	105	101	92	87	85	75	75	86	92
Y (ppm)	1.7	2.5	2	2.1	2.2	2.3	2	2.1	1.8	1.6	1.6	2	1.9
U (ppm)	0.3	0.06	0.025	0.06	0.025	0.025	0.025	0.025	0.025	0.025	0.025	0.025	0.025
W (ppm)	1	1	1	1	2	1	1	1	1	1	3	1	1
Yb (ppm)	0.25	0.31	0.26	0.27	0.24	0.27	0.26	0.19	0.22	0.26	0.13	0.26	0.24
Zr (ppm)	7	5	4	5	3	3	3	3	3	3	2	3	4
Zn (ppm)	55	54	63	58	66	73	71	74	73	67	67	67	76

Drill hole #	18-805	18-805	18-805	18-805	18-805	18-805	18-805	18-805	18-805	18-805	18-805	18-805	18-805
Depth From	91	92	93	94	95	96	97	98	99	100	101	102	103
Depth To	92	93	94	95	96	97	98	99	100	101	102	103	104
Rock Type	GABVT	GABVT	GABVT	GABVT	GABVT	GABVT	GABVT	GABVT	GABVT	GABVT	GABVT	GABVT	GABVT
Lithological Domain	Breccia	Breccia	Breccia	Breccia	Breccia	Breccia	Breccia	Breccia	Breccia	Breccia	Breccia	Breccia	Breccia
Al_2O_3 (%)	16.9	16.9	16.35	17.05	17.5	16.45	16.25	16.05	16.5	17.95	16.05	16	15.85
CaO (%)	10	9.28	9.56	10.1	9.9	9.71	9.39	9.59	9.32	9.76	9.48	9.15	9.57
Cr_2O_3 (%)	0.029	0.034	0.034	0.03	0.027	0.031	0.031	0.036	0.034	0.032	0.039	0.034	0.034
Fe_2O_3 (%)	7.84	8.36	8.6	8.39	8	8.46	8.19	8.96	8.4	7.85	8.53	8.03	8.47
K_2O (%)	0.16	0.18	0.18	0.17	0.17	0.21	0.21	0.24	0.25	0.22	0.2	0.51	0.67
MgO (%)	8.09	8.97	8.84	8.81	8.42	8.95	8.65	9.58	9.17	8.24	9.91	9.25	10.05
MnO (%)	0.13	0.14	0.14	0.14	0.13	0.14	0.13	0.14	0.14	0.12	0.14	0.13	0.13
Na_2O (%)	2.51	2.39	2.22	2.1	2.25	2.15	2.21	2.01	2.13	2.33	2.07	2.35	2.07
P_2O_5 (%)	0.005	0.01	0.005	0.005	0.01	0.005	0.005	0.005	0.005	0.005	0.005	0.01	0.01
SiO_2 (%)	52.6	52	52.2	50.8	51	50.8	52.2	51.8	52.3	50.7	51.5	50.3	50.1
TiO_2 (%)	0.1	0.1	0.1	0.12	0.11	0.12	0.11	0.12	0.11	0.11	0.12	0.11	0.12
LOI (%)	2.25	2.44	2.3	2.2	2.33	2.36	2.36	2.6	2.38	2.19	2.64	3.18	2.89
Total (%)	100.64	100.83	100.55	99.94	99.89	99.41	99.76	101.16	100.76	99.53	100.71	99.09	99.99
Ag (ppm)	0.25	0.25	0.25	0.25	0.25	0.25	0.25	0.25	0.25	0.25	0.25	0.25	0.25
As (ppm)	0.1	0.3	0.3	0.4	0.1	0.2	0.2	0.4	0.3	0.2	0.3	0.3	0.2
Au (ppm)	0.003	0.009	0.005	0.0005	0.003	0.004	0.011	0.007	0.005	0.054	0.002	0.001	0.001
Ba (ppm)	71.2	59.1	63.7	74.1	66.8	61	70.6	79.4	98.8	64.8	53.6	197.5	105.5
Bi (ppm)	0.02	0.05	0.11	0.1	0.03	0.05	0.05	0.09	0.04	0.16	0.05	0.08	0.11
Cd (ppm)	0.25	0.5	0.5	0.6	0.25	0.6	0.5	0.6	0.5	0.25	0.5	0.25	0.25
Ce (ppm)	2.5	2.3	3	2.2	2	2.4	3.1	2.7	3	2	2.4	2.4	2.5
Co (ppm)	45	53	53	55	53	56	53	60	54	63	57	46	53
Cs (ppm)	1.94	2.4	2.31	2.7	2.36	2.26	2.08	2.83	2.29	2.13	2.54	7.96	7.43
Cu (ppm)	97	203	125	108	95	125	142	185	178	727	151	48	117
Dy (ppm)	0.36	0.29	0.43	0.54	0.47	0.54	0.57	0.56	0.51	0.39	0.42	0.6	0.54
Er (ppm)	0.27	0.21	0.24	0.37	0.31	0.41	0.36	0.35	0.39	0.28	0.37	0.38	0.35
Eu (ppm)	0.3	0.23	0.34	0.27	0.29	0.29	0.27	0.23	0.3	0.22	0.21	0.23	0.2
Ga (ppm)	14.9	14.2	13.8	14.5	14.8	15.1	14.4	14.5	14	14.1	13.2	13.6	13.5
Gd (ppm)	0.38	0.36	0.37	0.43	0.48	0.44	0.64	0.53	0.52	0.34	0.54	0.37	0.41
Ge (ppm)	2.5	2.5	2.5	2.5	2.5	2.5	2.5	2.5	2.5	2.5	2.5	2.5	2.5
Hf (ppm)	0.1	0.1	0.1	0.1	0.1	0.1	0.2	0.1	0.2	0.1	0.1	0.1	0.1
Hg (ppb)	0.0025	0.0025	0.0025	0.0025	0.0025	0.0025	0.0025	0.0025	0.0025	0.0025	0.0025	0.0025	0.0025
Ho (ppm)	0.1	0.08	0.09	0.12	0.1	0.13	0.16	0.14	0.13	0.09	0.14	0.11	0.12
In (ppm)	0.0025	0.005	0.005	0.0025	0.0025	0.0025	0.0025	0.0025	0.0025	0.005	0.0025	0.006	0.006
La (ppm)	1.4	1.2	1.6	1.1	1	1.2	1.6	1.4	1.6	1.1	1.1	1.1	1.1
Li (ppm)	10	10	10	20	10	10	10	20	10	10	20	30	20
Lu (ppm)	0.05	0.04	0.06	0.06	0.05	0.06	0.07	0.07	0.05	0.05	0.07	0.04	0.07
Mo (ppm)	0.5	0.5	0.5	0.5	0.5	0.5	0.5	0.5	0.5	0.5	0.5	0.5	0.5
Nb (ppm)	0.1	0.1	0.1	0.1	0.1	0.1	0.3	0.1	0.2	0.1	0.1	0.4	0.1
Ni (ppm)	192	292	274	244	229	266	256	341	282	717	288	323	275
Nd (ppm)	1.3	0.8	1.5	1.3	1.2	1.2	1.8	1.4	1.5	1.2	1.3	1.5	1.4
Pb (ppm)	1	2	2	1	1	1	1	1	3	1	2	2	1
Pd (ppm)	0.013	0.059	0.075	0.003	0.004	0.029	0.006	0.172	0.022	1.3	0.04	0.078	0.002
Pr (ppm)	0.29	0.26	0.39	0.36	0.26	0.31	0.39	0.34	0.38	0.26	0.33	0.38	0.35
Pt (ppm)	0.0025	0.01	0.01	0.0025	0.0025	0.006	0.0025	0.014	0.005	0.155	0.007	0.011	0.0025
Rb (ppm)	5	5.4	5.8	5.8	5.7	6.6	6.6	8.5	8.7	6.9	6.3	21.6	28.1
Re (ppm)	0.0005	0.001	0.001	0.0005	0.0005	0.0005	0.0005	0.0005	0.0005	0.0005	0.001	0.0005	0.0005
S (%)	0.08	0.1	0.11	0.08	0.07	0.08	0.06	0.1	0.07	0.33	0.08	0.03	0.05
Sb (ppm)	0.025	0.025	0.025	0.025	0.025	0.025	0.025	0.025	0.025	0.025	0.025	0.025	0.025
Sc (ppm)	26	20	23	24	26	21	24	22	20	17	20	23	24
Se (ppm)	0.229	0.362	0.328	0.229	0.201	0.241	0.198	0.411	0.251	1.78	0.262	0.077	0.167
Sm (ppm)	0.29	0.3	0.39	0.32	0.47	0.39	0.54	0.36	0.39	0.29	0.32	0.36	0.43
Sn (ppm)	0.5	0.5	0.5	0.5	0.5	0.5	0.5	0.5	0.5	0.5	0.5	0.5	0.5
Sr (ppm)	252	233	225	248	253	248	249	234	235	252	214	200	211
Ta (ppm)	0.05	0.05	0.05	0.05	0.05	0.05	0.05	0.05	0.05	0.05	0.05	0.05	0.05
Tb (ppm)	0.06	0.05	0.06	0.09	0.09	0.1	0.08	0.09	0.07	0.07	0.07	0.06	0.07
Te (ppm)	0.02	0.03	0.04	0.01	0.005	0.03	0.02	0.07	0.02	0.24	0.02	0.1	0.01
Th (ppm)	0.06	0.08	0.19	0.025	0.025	0.025	0.53	0.15	0.18	0.025	0.025	0.07	0.025
Tl (ppm)	0.02	0.03	0.02	0.03	0.02	0.03	0.05	0.05	0.04	0.07	0.02	0.17	0.19
Tm (ppm)	0.03	0.03	0.06	0.07	0.04	0.05	0.06	0.07	0.06	0.04	0.07	0.03	0.06
V (ppm)	100	87	93	102	97	112	102	113	95	81	94	104	93
Y (ppm)	2.5	2.1	2.2	3.3	3.1	3.6	3.3	3.3	3.2	2.7	3.2	3.1	3.1
U (ppm)	0.025	0.025	0.025	0.025	0.025	0.025	0.19	0.08	0.09	0.025	0.025	0.07	0.025
W (ppm)	1	2	2	2	1	1	1	2	1	2	1	1	1
Yb (ppm)	0.29	0.23	0.26	0.36	0.33	0.48	0.49	0.41	0.4	0.33	0.43	0.33	0.31
Zr (ppm)	4	3	5	4	3	4	8	4	6	3	5	6	4
Zn (ppm)	72	74	80	73	60	63	58	67	61	54	60	56	66

Drill hole #	18-805	18-805	18-805	18-805	18-805	18-805	18-805	18-805	18-805	18-805	18-805	18-805	18-805
Depth From	104	105	106	107	108	109	110	111	112	113	114	115	116
Depth To	105	106	107	108	109	110	111	112	113	114	115	116	117
Rock Type	GABVT	GABVT	GABVT	GABVT	GABVT	GABVT	GABVT	GABVT	GABVT	GABVT	GABVT	GABVT	GABVT
Lithological Domain	Breccia	Breccia	Breccia	Breccia	Breccia	Breccia	Breccia	Breccia	Breccia	Breccia	Breccia	Breccia	Breccia
Al_2O_3 (%)	16.65	17.25	18.2	17	17.9	16.8	16.25	16.55	18	16	17.7	17.25	16.05
CaO (%)	10.1	9.85	9.88	9.97	10.2	9.5	9	9.65	10.05	9.87	10.6	10.05	9.96
Cr_2O_3 (%)	0.026	0.023	0.023	0.026	0.024	0.03	0.033	0.031	0.029	0.022	0.02	0.027	0.028
Fe_2O_3 (%)	8.3	8.25	7.96	8.54	8	8.14	8.22	8.37	7.71	8.76	7.76	7.89	7.8
K_2O (%)	0.27	0.3	0.24	0.24	0.21	0.21	0.24	0.26	0.27	0.19	0.15	0.22	0.19
MgO (%)	8.86	8.54	8.42	8.75	8.28	9.06	9.54	9.36	8.09	8.92	7.98	8.3	9.28
MnO (%)	0.14	0.13	0.13	0.14	0.13	0.13	0.13	0.13	0.12	0.13	0.13	0.13	0.13
Na_2O (%)	2.17	2.44	2.44	2.29	2.42	2.27	2.37	2.33	2.43	2.23	2.26	2.31	2.4
P_2O_5 (%)	0.01	0.01	0.005	0.005	0.005	0.01	0.005	0.01	0.005	0.005	0.005	0.005	0.005
SiO_2 (%)	51.3	52.5	51.9	51.5	51.8	50.7	51.6	51.3	51.1	50.6	51	50.7	52.3
TiO_2 (%)	0.12	0.12	0.12	0.14	0.11	0.12	0.12	0.13	0.11	0.14	0.11	0.13	0.12
LOI (%)	2.17	2.27	2.2	2.18	1.84	2.15	2.33	2.36	2.02	2.3	2.15	1.82	2.59
Total (%)	100.15	101.71	101.54	100.81	100.95	99.15	99.86	100.51	99.96	99.19	99.89	98.86	100.87
Ag (ppm)	0.25	0.25	0.25	0.25	0.25	0.25	0.25	0.25	0.25	0.25	0.25	0.25	0.25
As (ppm)	0.2	0.3	0.2	0.4	0.3	0.3	0.3	0.2	0.4	0.5	0.3	0.3	0.4
Au (ppm)	0.011	0.012	0.01	0.027	0.006	0.011	0.002	0.018	0.025	0.074	0.007	0.008	0.003
Ba (ppm)	57.5	61.7	67.4	70	72.6	63.3	56.9	53.8	64.2	47.5	55	68.3	51.2
Bi (ppm)	0.06	0.05	0.02	0.04	0.01	0.01	0.01	0.02	0.02	0.11	0.02	0.01	0.01
Cd (ppm)	0.6	0.6	0.5	0.6	0.6	0.7	0.5	0.9	0.6	1.6	0.6	0.6	0.25
Ce (ppm)	6	3.5	3	2.8	2.3	2.3	3.4	2.9	2.2	2.2	1.8	2.9	3.1
Co (ppm)	54	58	51	58	54	55	54	55	52	64	53	50	50
Cs (ppm)	1.94	2.62	2.05	2.66	2.25	2.49	2.59	2.49	3.31	2.19	1.52	2.16	1.89
Cu (ppm)	239	215	196	344	202	165	155	220	229	466	137	153	116
Dy (ppm)	0.74	0.66	0.54	0.72	0.53	0.56	0.64	0.77	0.48	0.39	0.46	0.62	0.6
Er (ppm)	0.46	0.35	0.34	0.36	0.4	0.34	0.37	0.4	0.31	0.28	0.32	0.44	0.36
Eu (ppm)	0.3	0.28	0.24	0.25	0.33	0.21	0.2	0.29	0.2	0.17	0.23	0.31	0.25
Ga (ppm)	13	15.2	15	14	15.8	14	12.8	12.5	14.7	13.3	14.7	14.6	14.2
Gd (ppm)	0.64	0.56	0.5	0.44	0.4	0.46	0.42	0.55	0.34	0.48	0.35	0.61	0.53
Ge (ppm)	2.5	2.5	2.5	2.5	2.5	2.5	2.5	2.5	2.5	2.5	2.5	2.5	2.5
Hf (ppm)	0.1	0.1	0.1	0.1	0.1	0.2	0.2	0.1	0.1	0.1	0.1	0.1	0.2
Hg (ppb)	0.0025	0.0025	0.0025	0.0025	0.0025	0.0025	0.0025	0.0025	0.0025	0.0025	0.0025	0.0025	0.0025
Ho (ppm)	0.17	0.14	0.11	0.15	0.12	0.12	0.13	0.11	0.1	0.12	0.12	0.13	0.11
In (ppm)	0.0025	0.0025	0.0025	0.006	0.0025	0.0025	0.0025	0.005	0.0025	0.006	0.0025	0.0025	0.0025
La (ppm)	2.6	1.6	1.6	1.3	1.1	1.1	1.6	1.3	1	1.1	0.9	1.3	1.7
Li (ppm)	10	10	10	10	10	20	20	20	20	20	10	10	30
Lu (ppm)	0.06	0.06	0.06	0.06	0.07	0.05	0.08	0.07	0.04	0.06	0.06	0.08	0.05
Mo (ppm)	0.5	0.5	0.5	0.5	0.5	0.5	0.5	0.5	0.5	0.5	0.5	0.5	0.5
Nb (ppm)	3.1	0.9	0.3	0.3	0.1	0.1	0.4	0.3	0.1	0.1	0.1	0.1	0.1
Ni (ppm)	269	326	278	398	246	272	259	272	291	584	255	259	241
Nd (ppm)	3	2	1.4	1.5	1.5	1.4	1.9	1.6	1	1	1	1.5	1.6
Pb (ppm)	1	1	1	3	1	17	1	40	29	32	1	1	2
Pd (ppm)	0.054	0.125	0.183	0.614	0.028	0.029	0.002	0.05	0.127	1.36	0.145	0.044	0.003
Pr (ppm)	0.73	0.45	0.38	0.37	0.33	0.34	0.37	0.42	0.26	0.31	0.26	0.43	0.41
Pt (ppm)	0.007	0.017	0.025	0.048	0.027	0.005	0.0025	0.008	0.015	0.147	0.029	0.0025	0.0025
Rb (ppm)	8	9.3	6.6	7	5.6	5.2	6.3	6	7.6	4.6	3.6	5.3	5
Re (ppm)	0.0005	0.001	0.0005	0.001	0.001	0.0005	0.0005	0.001	0.0005	0.0005	0.0005	0.0005	0.001
S (%)	0.09	0.13	0.09	0.18	0.1	0.07	0.04	0.1	0.1	0.19	0.11	0.06	0.04
Sb (ppm)	0.025	0.025	0.025	0.025	0.025	0.025	0.025	0.025	0.025	0.025	0.025	0.025	0.025
Sc (ppm)	22	23	21	24	24	23	24	28	22	28	27	25	26
Se (ppm)	0.343	0.443	0.342	0.747	0.315	0.252	0.171	0.338	0.388	0.99	0.382	0.258	0.141
Sm (ppm)	0.59	0.51	0.45	0.5	0.38	0.41	0.58	0.47	0.24	0.39	0.46	0.37	0.38
Sn (ppm)	0.5	0.5	0.5	0.5	0.5	0.5	0.5	0.5	0.5	0.5	0.5	0.5	0.5
Sr (ppm)	229	254	261	252	283	241	239	198.5	253	213	240	248	199.5
Ta (ppm)	0.05	0.05	0.05	0.05	0.05	0.05	0.05	0.05	0.05	0.05	0.05	0.05	0.1
Tb (ppm)	0.09	0.1	0.08	0.09	0.06	0.08	0.08	0.11	0.06	0.06	0.06	0.09	0.08
Te (ppm)	0.05	0.08	0.04	0.11	0.02	0.01	0.01	0.04	0.06	0.58	0.05	0.01	0.005
Th (ppm)	0.21	0.05	0.025	0.05	0.025	0.07	0.2	0.06	0.12	0.18	0.06	0.025	0.19
Tl (ppm)	0.02	0.01	0.02	0.02	0.02	0.01	0.01	0.02	0.02	0.03	0.02	0.01	0.01
Tm (ppm)	0.05	0.06	0.07	0.07	0.06	0.07	0.07	0.05	0.04	0.04	0.05	0.07	0.06
V (ppm)	105	108	94	113	106	98	96	112	121	141	114	115	98
Y (ppm)	3.7	3.6	3	3.4	3.2	3.1	3.6	3.6	2.6	2.8	2.5	3.7	3.4
U (ppm)	0.025	0.025	0.025	0.025	0.025	0.18	0.1	0.025	0.05	0.06	0.025	0.05	0.06
W (ppm)	2	3	1	1	1	1	1	1	1	1	2	1	1
Yb (ppm)	0.38	0.45	0.35	0.47	0.33	0.42	0.45	0.42	0.32	0.34	0.35	0.42	0.47
Zr (ppm)	5	6	5	6	4	7	9	5	5	7	4	6	7
Zn (ppm)	55	49	56	71	61	124	60	127	78	344	52	53	47

Drill hole #	18-805	18-805	18-805	18-805	18-805	18-805	18-805	18-805	18-805	18-805	18-805	18-805	18-805
Depth From	117	118	119	120	121	122	123	124	125	126	127	128	129
Depth To	118	119	120	121	122	123	124	125	126	127	128	129	130
Rock Type	GABVT	GABVT	GABVT	GABVT	GABVT	GABVT	GABVT	GABVT	GABVT	GABVT	GABVT	GABVT	GABVT
Lithological Domain	Breccia	Breccia	Breccia	Breccia	Breccia	Breccia	Breccia	Breccia	Breccia	Breccia	Breccia	Breccia	Breccia
Al_2O_3 (%)	16.2	17.25	16.4	17.7	17.55	17.85	18.3	17.05	18.3	17.2	17.35	16.9	17
CaO (%)	9.45	9.18	8.47	10.05	8.88	10.2	10.4	10.25	10.7	10.35	10.25	10.35	10.1
Cr_2O_3 (%)	0.036	0.028	0.027	0.027	0.023	0.026	0.027	0.03	0.025	0.03	0.035	0.032	0.03
Fe_2O_3 (%)	8.18	7.17	6.47	7.2	6	6.66	6.71	8.01	6.05	6.66	6.98	7.83	8.34
K_2O (%)	0.23	0.3	0.33	0.33	0.31	0.27	0.22	0.2	0.24	0.21	0.15	0.19	0.18
MgO (%)	9.84	8.51	8.01	8.55	7.63	8.32	8.53	9.64	8.01	8.83	9.49	9.67	8.86
MnO (%)	0.14	0.12	0.11	0.13	0.1	0.12	0.11	0.13	0.11	0.12	0.12	0.13	0.13
Na_2O (%)	2.19	2.9	2.61	2.47	2.92	2.53	2.49	2.24	2.5	2.3	2.18	2.24	2.34
P_2O_5 (%)	0.005	0.01	0.01	0.005	0.005	0.005	0.01	0.005	0.005	0.005	0.005	0.01	0.005
SiO_2 (%)	51.5	53.8	55.2	51.3	53.8	52.1	51.6	52	50.4	50.3	51.9	51.7	50.9
TiO_2 (%)	0.11	0.12	0.12	0.11	0.1	0.11	0.1	0.12	0.09	0.1	0.1	0.11	0.21
LOI (%)	2.24	1.69	1.2	1.78	1.92	1.82	2.02	2.28	1.91	1.91	2.04	1.96	1.61
Total (%)	100.15	101.11	99	99.68	99.26	100.04	100.55	101.98	98.38	98.04	100.63	101.15	99.73
Ag (ppm)	0.25	0.25	0.25	0.25	0.25	0.25	0.25	0.25	0.25	0.25	0.25	0.25	0.25
As (ppm)	0.2	0.4	0.2	0.3	0.1	0.6	0.4	0.4	0.3	0.1	0.7	0.5	0.2
Au (ppm)	0.002	0.005	0.005	0.006	0.001	0.002	0.002	0.027	0.003	0.003	0.0005	0.042	0.031
Ba (ppm)	66	93.1	166	85.1	85.2	91	57.2	52.8	59.9	55.2	58	57.3	59.3
Bi (ppm)	0.01	0.02	0.06	0.08	0.09	0.03	0.01	0.12	0.01	0.01	0.01	0.04	0.03
Cd (ppm)	0.25	0.6	0.25	0.5	0.25	0.25	0.5	0.5	0.25	0.5	0.25	0.25	0.7
Ce (ppm)	2.6	4.9	5.3	2.3	2.8	8.3	3.3	2.4	2.2	2.1	2.1	2.6	2.9
Co (ppm)	56	51	43	47	38	43	44	54	41	45	48	54	54
Cs (ppm)	2.85	3.01	2.68	2.92	2.89	2.1	1.88	1.67	2.26	2.03	1.78	1.5	1.93
Cu (ppm)	103	180	111	118	64	78	65	264	93	108	126	338	268
Dy (ppm)	0.54	0.57	0.46	0.43	0.47	0.74	0.51	0.43	0.36	0.42	0.38	0.4	0.42
Er (ppm)	0.3	0.32	0.27	0.26	0.38	0.42	0.36	0.33	0.22	0.3	0.28	0.26	0.26
Eu (ppm)	0.17	0.23	0.2	0.24	0.21	0.36	0.23	0.21	0.19	0.17	0.19	0.22	0.18
Ga (ppm)	13.1	13.6	13.7	13.9	12.3	13.7	14	13.1	13.6	13.1	13.3	13	13.7
Gd (ppm)	0.41	0.42	0.38	0.38	0.38	0.71	0.4	0.34	0.29	0.48	0.28	0.34	0.37
Ge (ppm)	2.5	2.5	2.5	2.5	2.5	2.5	2.5	2.5	2.5	2.5	2.5	2.5	2.5
Hf (ppm)	0.2	0.6	0.6	0.2	0.5	0.3	0.2	0.2	0.2	0.2	0.2	0.3	0.3
Hg (ppb)	0.0025	0.006	0.0025	0.0025	0.0025	0.0025	0.0025	0.0025	0.0025	0.0025	0.0025	0.0025	0.0025
Ho (ppm)	0.11	0.13	0.09	0.1	0.11	0.11	0.11	0.11	0.08	0.11	0.09	0.09	0.12
In (ppm)	0.0025	0.0025	0.0025	0.0025	0.0025	0.0025	0.0025	0.0025	0.0025	0.0025	0.0025	0.0025	0.0025
La (ppm)	1.3	2.4	2.8	1.2	1.4	4.1	1.7	1.2	1.1	1	1.1	1.3	1.4
Li (ppm)	20	20	20	20	20	10	10	10	10	10	10	10	10
Lu (ppm)	0.06	0.05	0.06	0.07	0.06	0.07	0.05	0.05	0.05	0.05	0.05	0.04	0.05
Mo (ppm)	0.5	0.5	0.5	0.5	0.5	0.5	0.5	0.5	0.5	0.5	0.5	0.5	0.5
Nb (ppm)	0.1	0.5	0.5	0.1	0.3	0.5	0.1	0.1	0.1	0.1	0.1	0.1	0.1
Ni (ppm)	257	255	236	231	167	199	196	376	197	220	231	400	372
Nd (ppm)	1.5	2.2	2.2	1.2	1.4	4.1	1.5	1.3	1.1	1.1	1.1	1.3	1.6
Pb (ppm)	1	1	1	1	3	2	1	1	1	3	1	1	2
Pd (ppm)	0.002	0.003	0.169	0.208	0.001	0.045	0.001	0.365	0.013	0.012	0.007	0.457	0.364
Pr (ppm)	0.3	0.54	0.54	0.26	0.33	0.99	0.38	0.32	0.26	0.28	0.28	0.29	0.34
Pt (ppm)	0.0025	0.0025	0.025	0.023	0.0025	0.005	0.0025	0.042	0.0025	0.0025	0.0025	0.054	0.042
Rb (ppm)	6.1	7.9	8.7	8.4	8.4	6.7	5.4	4.5	5.5	4.7	2.5	3.4	3.2
Re (ppm)	0.0005	0.0005	0.001	0.0005	0.001	0.0005	0.0005	0.0005	0.001	0.0005	0.001	0.001	0.001
S (%)	0.05	0.06	0.04	0.06	0.03	0.04	0.04	0.13	0.03	0.03	0.04	0.1	0.11
Sb (ppm)	0.025	0.025	0.025	0.025	0.025	0.025	0.025	0.025	0.025	0.025	0.025	0.025	0.025
Sc (ppm)	23	22	19	17	18	21	19	22	20	21	22	24	21
Se (ppm)	0.174	0.107	0.152	0.235	0.109	0.138	0.132	0.621	0.138	0.13	0.164	0.586	0.538
Sm (ppm)	0.39	0.55	0.38	0.33	0.35	0.9	0.42	0.31	0.36	0.28	0.39	0.28	0.41
Sn (ppm)	0.5	0.5	1	0.5	0.5	1	1	0.5	1	0.5	0.5	0.5	0.5
Sr (ppm)	230	262	235	262	238	265	272	244	278	256	234	241	258
Ta (ppm)	0.05	0.1	0.1	0.05	0.05	0.05	0.05	0.05	0.05	0.05	0.05	0.05	0.05
Tb (ppm)	0.08	0.08	0.06	0.06	0.07	0.13	0.08	0.06	0.07	0.06	0.06	0.06	0.07
Te (ppm)	0.01	0.005	0.11	0.1	0.01	0.02	0.01	0.13	0.01	0.02	0.02	0.21	0.1
Th (ppm)	0.025	0.71	1.19	0.025	0.2	1.2	0.2	0.07	0.05	0.025	0.14	0.11	0.12
Tl (ppm)	0.01	0.01	0.02	0.01	0.01	0.01	0.02	0.02	0.01	0.01	0.02	0.02	0.02
Tm (ppm)	0.03	0.06	0.06	0.04	0.05	0.05	0.03	0.04	0.05	0.04	0.04	0.05	0.04
V (ppm)	96	92	82	92	73	88	83	99	79	86	88	108	150
Y (ppm)	3.1	3.4	2.7	2.7	2.9	4	2.7	2.5	2.3	2.7	2.5	2.7	3
U (ppm)	0.025	0.37	0.32	0.025	0.68	0.1	0.025	0.025	0.025	0.025	0.025	0.025	0.025
W (ppm)	2	1	2	2	1	5	1	2	2	2	3	1	1
Yb (ppm)	0.38	0.33	0.33	0.27	0.34	0.43	0.33	0.37	0.25	0.31	0.34	0.31	0.33
Zr (ppm)	5	16	17	5	10	9	6	5	4	5	7	6	8
Zn (ppm)	53	46	39	50	37	42	43	51	40	43	46	49	51

Drill hole #	18-805	18-805	18-805	18-805	18-805	18-805	18-805	18-805	18-805	18-805	18-805	18-805	18-805
Depth From	130	131	132	133	134	135	136	137	138	139	140	141	142
Depth To	131	132	133	134	135	136	137	138	139	140	141	142	143
Rock Type	GABVT	GABVT	GABVT	GABVT	GABVT	GABVT	GABVT	GABVT	GABVT	GABVT	GABVT	GABVT	GABVT
Lithological Domain	Breccia	Breccia	Breccia	Breccia	Breccia	Breccia	Breccia	Breccia	Breccia	Breccia	Breccia	Breccia	Breccia
Al_2O_3 (%)	18.35	18.3	17.5	18.2	18.25	18	17.75	17.55	17.1	17.25	16.6	16.6	15.55
CaO (%)	10.45	10.65	9.97	10.6	10.3	10.2	10.25	10.25	9.98	10.15	9.91	9.49	9.04
Cr_2O_3 (%)	0.03	0.031	0.031	0.033	0.031	0.031	0.032	0.033	0.03	0.033	0.031	0.038	0.041
Fe_2O_3 (%)	6.68	6.69	7.05	6.92	6.86	7.42	7.4	7.38	8.1	7.4	7.42	7.8	8.14
K_2O (%)	0.18	0.18	0.16	0.12	0.12	0.13	0.11	0.12	0.11	0.12	0.32	0.15	0.2
MgO (%)	8.45	8.62	8.9	9.03	8.6	9.38	9.42	9.38	9.41	9.46	9.54	10.3	10.95
MnO (%)	0.11	0.12	0.12	0.12	0.11	0.12	0.13	0.13	0.13	0.13	0.13	0.13	0.14
Na_2O (%)	2.56	2.52	2.4	2.39	2.42	2.37	2.34	2.33	2.21	2.26	2.32	2.08	2.14
P_2O_5 (%)	0.005	0.01	0.01	0.005	0.005	0.01	0.005	0.005	0.005	0.005	0.01	0.005	0.01
SiO_2 (%)	51.7	52.1	51.7	52.1	51.4	52.4	52.2	52	51.1	51.3	51.1	51.5	51.2
TiO_2 (%)	0.1	0.1	0.12	0.1	0.1	0.1	0.11	0.1	0.11	0.11	0.1	0.11	0.11
LOI (%)	1.88	1.7	1.16	0.57	0.39	0.99		0.17	0.24	0.23	2.09	1.84	2.57
Total (%)	100.52	101.06	99.15	100.21	98.61	101.18	99.72	99.47	98.55	98.47	99.6	100.07	100.12
Ag (ppm)	0.25	0.25	0.25	0.25	0.25	0.25	0.25	0.25	0.25	0.25	0.25	0.25	0.25
As (ppm)	0.4	0.4	0.5	0.1	0.4	0.4	0.05	0.4	0.2	0.1	0.2	0.2	0.3
Au (ppm)	0.006	0.004	0.005	0.0005	0.002	0.001	0.0005	0.0005	0.007	0.0005	0.003	0.004	0.011
Ba (ppm)	65.4	61.8	58.1	59.4	59.4	60.1	57.3	55	52.1	55.9	54.6	55.5	61.4
Bi (ppm)	0.01	0.03	0.03	0.01	0.01	0.01	0.01	0.01	0.02	0.01	0.01	0.02	0.02
Cd (ppm)	0.25	0.25	0.25	0.6	0.6	0.6	0.6	0.25	0.7	0.5	0.5	0.25	0.5
Ce (ppm)	2.1	2.4	2.6	2.2	2.1	2	2	2.2	1.8	2	2.6	1.9	1.9
Co (ppm)	46	44	48	46	46	50	49	49	56	50	49	54	55
Cs (ppm)	2.26	1.7	1.64	0.88	1	1.68	0.65	1.09	0.97	0.96	2.63	2.49	4.57
Cu (ppm)	152	97	133	99	139	129	106	97	206	101	87	126	127
Dy (ppm)	0.4	0.49	0.47	0.48	0.34	0.51	0.35	0.46	0.4	0.35	0.36	0.37	0.37
Er (ppm)	0.26	0.28	0.31	0.25	0.21	0.33	0.31	0.32	0.26	0.28	0.23	0.35	0.31
Eu (ppm)	0.14	0.22	0.2	0.19	0.18	0.21	0.22	0.19	0.17	0.19	0.18	0.18	0.19
Ga (ppm)	13.9	14.4	14	14	13.4	13.6	13.6	13.4	14.1	13.4	12.5	12.9	12.3
Gd (ppm)	0.38	0.34	0.38	0.38	0.35	0.3	0.34	0.41	0.29	0.29	0.35	0.28	0.23
Ge (ppm)	2.5	2.5	2.5	2.5	2.5	2.5	2.5	2.5	2.5	2.5	2.5	2.5	2.5
Hf (ppm)	0.2	0.2	0.2	0.2	0.2	0.2	0.2	0.2	0.1	0.1	0.1	0.1	0.1
Hg (ppb)	0.0025	0.0025	0.0025	0.0025	0.0025	0.0025	0.0025	0.0025	0.0025	0.0025	0.0025	0.0025	0.0025
Ho (ppm)	0.09	0.11	0.12	0.11	0.09	0.1	0.1	0.1	0.08	0.12	0.09	0.1	0.09
In (ppm)	0.0025	0.0025	0.0025	0.0025	0.0025	0.0025	0.0025	0.0025	0.0025	0.0025	0.0025	0.0025	0.0025
La (ppm)	1	1.3	1.4	1.1	1.1	1	1	1.2	0.8	1	1.4	1	0.9
Li (ppm)	10	10	10	5	5	10	5	5	5	5	10	10	20
Lu (ppm)	0.05	0.04	0.05	0.05	0.04	0.04	0.04	0.06	0.03	0.03	0.05	0.04	0.05
Mo (ppm)	0.5	0.5	0.5	0.5	0.5	0.5	0.5	0.5	0.5	0.5	0.5	0.5	0.5
Nb (ppm)	0.1	0.5	1.4	0.1	0.1	0.1	0.1	0.1	0.1	0.1	0.1	0.1	0.1
Ni (ppm)	236	226	247	229	222	239	232	225	295	232	235	272	305
Nd (ppm)	1.2	1.4	1.2	1.1	1.1	1.1	1.2	1.1	0.9	1.2	1.4	1	0.8
Pb (ppm)	1	1	1	1	1	1	1	1	1	1	1	2	1
Pd (ppm)	0.038	0.035	0.056	0.001	0.009	0.01	0.001	0.0005	0.062	0.005	0.002	0.017	0.072
Pr (ppm)	0.26	0.3	0.29	0.25	0.22	0.23	0.24	0.32	0.19	0.27	0.31	0.2	0.22
Pt (ppm)	0.007	0.006	0.007	0.0025	0.0025	0.0025	0.0025	0.0025	0.012	0.0025	0.0025	0.0025	0.013
Rb (ppm)	3.6	3.7	3	0.9	1.2	1.9	0.6	1.9	1	0.9	8.4	3.4	5.2
Re (ppm)	0.0005	0.0005	0.0005	0.0005	0.0005	0.001	0.0005	0.0005	0.0005	0.0005	0.0005	0.0005	0.0005
S (%)	0.07	0.05	0.06	0.06	0.08	0.06	0.06	0.05	0.1	0.06	0.03	0.09	0.03
Sb (ppm)	0.025	0.025	0.025	0.025	0.025	0.025	0.025	0.025	0.025	0.025	0.025	0.025	0.025
Sc (ppm)	20	20	23	21	20	21	21	21	22	23	19	22	23
Se (ppm)	0.278	0.195	0.246	0.214	0.25	0.24	0.22	0.21	0.461	0.208	0.113	0.261	0.199
Sm (ppm)	0.27	0.42	0.36	0.29	0.23	0.28	0.31	0.27	0.25	0.23	0.29	0.3	0.22
Sn (ppm)	0.5	0.5	0.5	0.5	0.5	0.5	0.5	0.5	0.5	0.5	0.5	0.5	0.5
Sr (ppm)	288	277	241	262	262	254	251	251	242	246	240	223	228
Ta (ppm)	0.05	0.1	0.1	0.05	0.05	0.05	0.05	0.05	0.05	0.05	0.05	0.05	0.05
Tb (ppm)	0.06	0.07	0.05	0.06	0.06	0.07	0.06	0.07	0.04	0.05	0.06	0.07	0.06
Te (ppm)	0.02	0.05	0.05	0.02	0.02	0.02	0.01	0.01	0.08	0.01	0.005	0.02	0.02
Th (ppm)	0.025	0.09	0.16	0.025	0.025	0.025	0.025	0.06	0.025	0.025	0.025	0.025	0.025
Tl (ppm)	0.02	0.02	0.01	0.01	0.01	0.01	0.01	0.02	0.02	0.01	0.01	0.01	0.01
Tm (ppm)	0.03	0.05	0.04	0.03	0.04	0.04	0.05	0.05	0.04	0.05	0.04	0.04	0.03
V (ppm)	93	90	95	87	85	91	87	89	100	93	87	94	96
Y (ppm)	2.4	2.8	3.1	2.5	2.4	2.7	2.6	2.8	2.3	2.8	2.7	2.5	2.6
U (ppm)	0.025	0.07	0.26	0.025	0.025	0.025	0.025	0.025	0.025	0.025	0.025	0.025	0.025
W (ppm)	4	2	2	3	2	1	1	2	2	1	2	2	1
Yb (ppm)	0.29	0.35	0.4	0.28	0.31	0.34	0.26	0.38	0.25	0.37	0.25	0.38	0.29
Zr (ppm)	5	7	6	5	5	4	4	4	4	4	5	4	4
Zn (ppm)	45	44	51	45	46	50	47	49	52	48	48	53	48

Drill hole #	18-805	18-805	18-805	18-805	18-805	18-805	18-805	18-805	18-805	18-805	18-805	18-805	18-805
Depth From	143	144	145	146	147	148	149	150	151	152	153	154	155
Depth To	144	145	146	147	148	149	150	151	152	153	154	155	156
Rock Type	NOR	NOR	NOR	NOR	NOR	NOR	NOR	NOR	NOR	NOR	NOR	NOR	NOR
Lithological Domain	Norite	Norite	Norite	Norite	Norite	Norite	Norite	Norite	Norite	Norite	Norite	Norite	Norite
Al_2O_3 (%)	7.32	5.33	5.82	12.5	10.95	11.35	16.9	18.45	9.87	10.95	8.96	9.6	9.51
CaO (%)	4.93	4.02	6.39	7.42	6.32	7.86	9.51	9.91	7.18	7.26	7.19	7.46	7.17
Cr_2O_3 (%)	0.063	0.069	0.062	0.039	0.054	0.053	0.04	0.035	0.067	0.06	0.076	0.072	0.071
Fe_2O_3 (%)	17.1	18.45	18.05	12	13.1	12.5	7.64	6.48	12.9	11.95	12.35	11.3	12.05
K_2O (%)	0.14	0.18	0.14	0.36	0.32	0.18	0.35	0.44	0.28	0.28	0.09	0.12	0.2
MgO (%)	16.65	18.4	16.95	10.9	13.9	13.85	9.84	8.94	14.95	13.95	16.15	15.65	15.75
MnO (%)	0.25	0.24	0.28	0.19	0.19	0.21	0.13	0.11	0.21	0.2	0.2	0.19	0.2
Na_2O (%)	0.48	0.24	0.31	2.01	1.4	1.22	2.13	2.45	0.9	1.17	0.57	0.79	0.66
P_2O_5 (%)	0.01	0.01	0.01	0.06	0.02	0.005	0.005	0.005	0.005	0.005	0.005	0.005	0.005
SiO_2 (%)	48.2	48.2	47.5	50.6	51.4	49.7	51.3	52.5	51.4	51.6	50.4	50.1	50.5
TiO_2 (%)	0.2	0.22	0.28	0.36	0.19	0.18	0.12	0.11	0.18	0.16	0.16	0.15	0.17
LOI (%)	3	3.23	2.89	2.29	3.27	3.06	2.64	2.44	3.34	3.44	4.13	4.29	4.27
Total (%)	98.34	98.59	98.68	98.75	101.13	100.17	100.63	101.91	101.29	101.03	100.28	99.72	100.55
Ag (ppm)	0.6	0.8	0.8	0.25	0.25	0.25	0.25	0.25	0.25	0.25	0.25	0.25	0.25
As (ppm)	0.6	0.6	0.3	0.3	0.3	0.4	0.2	0.4	0.4	0.5	0.6	0.6	0.5
Au (ppm)	0.287	0.316	0.297	0.097	0.054	0.077	0.028	0.005	0.241	0.106	0.063	0.037	0.04
Ba (ppm)	21.1	24.9	21.1	114.5	65.3	43.7	76.8	94.4	43	36.1	13.2	19.5	28.4
Bi (ppm)	0.18	0.2	0.42	0.27	0.21	0.37	0.02	0.03	0.08	0.08	0.05	0.03	0.04
Cd (ppm)	0.9	1.1	1.2	0.6	0.8	0.9	0.5	0.6	0.6	0.7	0.7	0.7	0.7
Ce (ppm)	1.8	1.7	2.7	15	4.3	1.7	2.2	2.2	2.1	2	1.6	1.8	2.1
Co (ppm)	133	135	132	74	82	96	54	46	88	84	88	89	90
Cs (ppm)	2.73	3.6	2.3	3.68	4.14	2.69	2.84	2.64	2.35	2.3	1.32	1.29	2.49
Cu (ppm)	1850	1710	1975	660	566	820	155	134	573	301	247	234	230
Dy (ppm)	0.5	0.4	0.61	1.37	0.49	0.41	0.36	0.39	0.6	0.5	0.49	0.5	0.58
Er (ppm)	0.28	0.34	0.48	0.82	0.37	0.37	0.31	0.29	0.39	0.46	0.42	0.43	0.37
Eu (ppm)	0.15	0.11	0.14	0.46	0.16	0.18	0.2	0.2	0.15	0.14	0.16	0.14	0.13
Ga (ppm)	8.7	7.2	8.5	13.1	10.6	10.5	12.2	12.9	9	9.4	7.7	8.1	8.7
Gd (ppm)	0.33	0.47	0.48	1.48	0.52	0.39	0.37	0.3	0.48	0.33	0.35	0.37	0.41
Ge (ppm)	2.5	2.5	2.5	2.5	2.5	2.5	2.5	2.5	2.5	2.5	2.5	2.5	2.5
Hf (ppm)	0.3	0.3	0.2	1.1	0.4	0.2	0.2	0.2	0.3	0.2	0.2	0.2	0.2
Hg (ppb)	0.0025	0.0025	0.0025	0.0025	0.0025	0.0025	0.0025	0.0025	0.0025	0.0025	0.0025	0.0025	0.0025
Ho (ppm)	0.1	0.13	0.15	0.27	0.12	0.11	0.1	0.11	0.12	0.13	0.12	0.12	0.11
In (ppm)	0.016	0.016	0.013	0.008	0.007	0.008	0.0025	0.0025	0.005	0.0025	0.0025	0.0025	0.0025
La (ppm)	0.8	0.8	1.1	7	2	0.8	1.1	1.1	0.9	1	0.7	0.8	1
Li (ppm)	10	10	10	10	10	10	10	10	10	20	20	20	20
Lu (ppm)	0.06	0.07	0.09	0.15	0.07	0.05	0.06	0.06	0.06	0.07	0.06	0.07	0.07
Mo (ppm)	1	0.5	0.5	0.5	0.5	0.5	0.5	0.5	0.5	0.5	0.5	0.5	0.5
Nb (ppm)	0.1	0.1	0.6	1.6	0.5	0.1	0.1	0.1	0.1	0.1	0.1	0.1	0.1
Ni (ppm)	1770	1485	1520	659	721	838	331	275	716	617	624	629	728
Nd (ppm)	0.9	0.7	1.6	6.9	1.9	1.1	1.2	1.1	1.2	1.2	1	1	1.1
Pb (ppm)	1	3	3	1	1	1	1	1	1	1	1	2	1
Pd (ppm)	3.5	2.92	3.14	0.974	0.763	0.987	0.086	0.051	0.809	0.677	0.53	0.498	0.522
Pr (ppm)	0.21	0.24	0.35	1.8	0.49	0.21	0.25	0.25	0.27	0.28	0.21	0.23	0.27
Pt (ppm)	0.471	0.368	0.393	0.146	0.105	0.155	0.012	0.008	0.113	0.081	0.069	0.077	0.073
Rb (ppm)	3.8	4.7	4.1	10.1	10.1	4.9	10.5	12.9	8.1	6.8	2.3	3.5	6.3
Re (ppm)	0.004	0.003	0.002	0.002	0.001	0.001	0.001	0.001	0.0005	0.0005	0.001	0.0005	0.0005
S (%)	0.83	0.64	0.86	0.32	0.2	0.65	0.04	0.06	0.1	0.05	0.06	0.08	0.04
Sb (ppm)	0.025	0.05	0.025	0.025	0.025	0.025	0.025	0.025	0.09	0.08	0.06	0.025	0.025
Sc (ppm)	41	47	47	26	34	35	19	20	41	32	46	37	40
Se (ppm)	4.69	3.95	4.37	1.48	1.06	2.53	0.195	0.284	0.776	0.347	0.331	0.537	0.222
Sm (ppm)	0.3	0.32	0.26	1.33	0.45	0.16	0.3	0.23	0.32	0.29	0.31	0.38	0.34
Sn (ppm)	0.5	0.5	0.5	1	1	0.5	0.5	0.5	0.5	0.5	0.5	0.5	0.5
Sr (ppm)	41.5	15.7	19.4	197.5	135	133	242	274	81.7	98.9	42.1	68.9	59.6
Ta (ppm)	0.05	0.05	0.05	0.1	0.1	0.05	0.05	0.05	0.05	0.05	0.05	0.05	0.05
Tb (ppm)	0.06	0.08	0.08	0.19	0.07	0.05	0.06	0.07	0.07	0.07	0.06	0.07	0.07
Te (ppm)	1.21	0.88	1.04	0.52	0.39	0.5	0.03	0.04	0.2	0.23	0.16	0.14	0.21
Th (ppm)	0.11	0.11	0.12	0.82	0.36	0.1	0.06	0.025	0.1	0.09	0.09	0.08	0.13
Tl (ppm)	0.09	0.08	0.08	0.06	0.07	0.05	0.02	0.01	0.02	0.02	0.01	0.01	0.02
Tm (ppm)	0.05	0.06	0.06	0.12	0.06	0.04	0.04	0.04	0.06	0.06	0.06	0.06	0.06
V (ppm)	172	185	242	160	146	159	99	87	165	150	153	151	151
Y (ppm)	2.9	3.1	3.7	7.4	3.4	2.9	2.5	2.5	3.2	3	2.9	3	3
U (ppm)	0.05	0.025	0.4	0.3	0.13	0.025	0.025	0.025	0.06	0.06	0.025	0.025	0.08
W (ppm)	1	6	5	7	3	3	1	1	0.5	5	1	2	1
Yb (ppm)	0.46	0.54	0.58	0.84	0.48	0.39	0.29	0.34	0.43	0.38	0.38	0.41	0.42
Zr (ppm)	7	9	6	47	18	8	4	4	7	6	5	6	8
Zn (ppm)	99	114	118	73	82	74	53	41	85	83	88	79	87

Drill hole #	18-805	18-805	18-805	18-805	18-805	18-805	18-805	18-805	18-805	18-805	18-805	18-805	18-805
Depth From	156	157	158	159	160	161	162	163	164	165	166	167	168
Depth To	157	158	159	160	161	162	163	164	165	166	167	168	169
Rock Type	NOR	NOR	NOR	NOR	NOR	NOR	NOR	NOR	NOR	NOR	NOR	NOR	NOR
Lithological Domain	Norite	Norite	Norite	Norite	Norite	Norite	Norite	Norite	Norite	Norite	Norite	Norite	Norite
Al2O3 (%)	13.45	14.1	8.97	10.65	12.15	12.3	9.9	14.75	12.5	14.35	14.8	14.1	12.8
CaO (%)	7.73	8.08	6.76	7.22	7.64	7.67	7.15	8.13	7.76	9.12	8.8	9.25	7.66
Cr2O3 (%)	0.051	0.049	0.077	0.067	0.053	0.051	0.068	0.042	0.053	0.053	0.05	0.059	0.056
Fe2O3 (%)	9.68	8.88	11.25	10.5	9.58	8.68	11.8	8.68	9.85	9.09	8.37	8.42	9.57
K2O (%)	0.3	0.3	0.06	0.19	0.31	0.29	0.19	0.3	0.19	0.19	0.22	0.17	0.16
MgO (%)	13	11.9	16.6	15	13.75	13.35	15.5	11.3	13.9	11.95	11.9	12.35	14.25
MnO (%)	0.16	0.15	0.2	0.18	0.16	0.15	0.2	0.14	0.17	0.16	0.14	0.15	0.16
Na2O (%)	1.4	1.75	0.69	0.99	1.12	1.41	0.73	1.84	0.99	1.61	1.64	1.58	1.07
P2O5 (%)	0.02	0.01	0.01	0.005	0.005	0.005	0.005	0.01	0.01	0.01	0.005	0.005	0.005
SiO2 (%)	50	50.3	49.6	50.2	51	52.6	49.7	50.2	49.4	50.8	50.4	51.1	50.1
TiO2 (%)	0.14	0.13	0.14	0.14	0.14	0.11	0.16	0.23	0.13	0.12	0.11	0.11	0.1
LOI (%)	3.37	3.32	4.27	3.55	3.57	3.41	3.6	2.61	3.25	2.51	2.86	1.84	2.69
Total (%)	99.32	99	98.63	98.7	99.49	100.04	99	98.26	98.21	99.98	99.32	99.14	98.63
Ag (ppm)	0.25	0.25	0.25	0.25	0.25	0.25	0.25	0.25	0.25	0.25	0.25	0.25	0.25
As (ppm)	0.3	0.3	0.5	0.5	0.4	0.3	0.3	0.1	0.05	0.05	0.2	0.1	0.05
Au (ppm)	0.016	0.029	0.028	0.035	0.035	0.019	0.054	0.175	0.047	0.039	0.036	0.019	0.082
Ba (ppm)	51.3	52.8	10.9	35.6	50.4	59.1	39.9	81.2	37.3	40.6	40.7	32.4	31.9
Bi (ppm)	0.01	0.08	0.03	0.03	0.03	0.09	0.07	0.12	0.04	0.02	0.06	0.05	0.03
Cd (ppm)	0.6	0.6	0.7	0.5	0.25	0.25	1	0.6	0.25	0.25	0.25	0.25	0.25
Ce (ppm)	2.2	2.8	2.1	2.1	2.4	2.4	2	6.1	1.7	1.9	4.3	1.6	1.6
Co (ppm)	71	67	87	80	73	68	86	69	70	60	60	62	75
Cs (ppm)	3.39	2.38	1.43	2.26	2.37	2.49	2.3	2.49	1.76	1.83	1.92	1.38	1.49
Cu (ppm)	172	296	155	178	150	85	377	597	200	293	242	198	553
Dy (ppm)	0.4	0.45	0.49	0.41	0.47	0.42	0.49	0.55	0.42	0.35	0.36	0.38	0.27
Er (ppm)	0.41	0.39	0.31	0.31	0.37	0.29	0.4	0.35	0.22	0.35	0.26	0.29	0.18
Eu (ppm)	0.15	0.16	0.14	0.14	0.18	0.13	0.16	0.21	0.11	0.11	0.17	0.11	0.15
Ga (ppm)	9.7	9.8	7.8	8.7	9.2	9.2	8.2	11.7	9	10.6	9.5	10.5	8.5
Gd (ppm)	0.33	0.44	0.36	0.36	0.36	0.3	0.44	0.49	0.26	0.34	0.29	0.26	0.21
Ge (ppm)	2.5	2.5	2.5	2.5	2.5	2.5	2.5	2.5	2.5	2.5	2.5	2.5	2.5
Hf (ppm)	0.2	0.3	0.2	0.2	0.3	0.4	0.2	0.7	0.1	0.2	0.2	0.2	0.2
Hg (ppb)	0.0025	0.0025	0.0025	0.0025	0.0025	0.0025	0.0025	0.0025	0.0025	0.0025	0.0025	0.0025	0.0025
Ho (ppm)	0.1	0.11	0.11	0.11	0.12	0.11	0.11	0.11	0.09	0.1	0.1	0.07	0.08
In (ppm)	0.0025	0.0025	0.0025	0.0025	0.0025	0.0025	0.0025	0.0025	0.0025	0.0025	0.0025	0.0025	0.005
La (ppm)	1	1.3	1	0.9	1.1	1.2	1	3	0.8	0.9	2	0.7	0.9
Li (ppm)	10	20	20	10	20	20	10	10	20	10	10	10	10
Lu (ppm)	0.07	0.05	0.06	0.07	0.06	0.06	0.07	0.07	0.04	0.05	0.05	0.05	0.05
Mo (ppm)	0.5	0.5	1	0.5	0.5	0.5	1	0.5	0.5	0.5	0.5	0.5	0.5
Nb (ppm)	0.1	0.1	0.1	0.1	0.2	0.4	0.1	0.8	0.1	0.1	2.2	0.2	0.2
Ni (ppm)	520	554	642	601	549	513	734	677	569	498	514	428	836
Nd (ppm)	1.1	1.3	1.1	1.3	1.2	1.2	1.2	2.5	1	1.1	2	0.8	0.8
Pb (ppm)	2	1	1	1	1	1	1	1	2	2	1	1	1
Pd (ppm)	0.226	0.473	0.411	0.586	0.481	0.392	0.813	0.978	0.658	0.296	0.396	0.514	0.519
Pr (ppm)	0.27	0.34	0.25	0.25	0.29	0.31	0.27	0.71	0.17	0.22	0.52	0.19	0.17
Pt (ppm)	0.031	0.062	0.055	0.088	0.069	0.066	0.092	0.116	0.101	0.034	0.053	0.038	0.084
Rb (ppm)	9.6	10.2	1.9	6.4	10.6	10.1	6.3	9.2	4.8	5.4	5.6	3.8	3.6
Re (ppm)	0.0005	0.0005	0.0005	0.001	0.0005	0.0005	0.001	0.0005	0.001	0.001	0.0005	0.0005	0.0005
S (%)	0.04	0.11	0.05	0.06	0.07	0.03	0.15	0.1	0.02	0.04	0.04	0.07	0.12
Sb (ppm)	0.025	0.025	0.025	0.025	0.025	0.07	0.025	0.025	0.025	0.025	0.025	0.025	0.025
Sc (ppm)	27	24	41	40	34	32	42	22	28	27	25	30	29
Se (ppm)	0.211	0.685	0.34	0.371	0.364	0.19	0.948	0.793	0.222	0.423	0.397	0.465	1.29
Sm (ppm)	0.25	0.31	0.33	0.28	0.27	0.26	0.32	0.54	0.24	0.22	0.26	0.32	0.19
Sn (ppm)	0.5	0.5	0.5	0.5	0.5	0.5	0.5	0.5	0.5	0.5	0.5	0.5	0.5
Sr (ppm)	163.5	198.5	41.9	108.5	116.5	121.5	65	212	112.5	181.5	173	167.5	113.5
Ta (ppm)	0.05	0.05	0.05	0.05	0.05	0.05	0.05	0.05	0.05	0.05	0.05	0.05	0.05
Tb (ppm)	0.06	0.06	0.06	0.06	0.07	0.06	0.08	0.08	0.04	0.08	0.06	0.06	0.05
Te (ppm)	0.06	0.22	0.1	0.13	0.08	0.14	0.27	0.42	0.28	0.09	0.18	0.13	0.37
Th (ppm)	0.15	0.26	0.11	0.16	0.25	0.31	0.12	0.42	0.09	0.15	0.27	0.07	0.1
Tl (ppm)	0.02	0.02	0.01	0.02	0.02	0.02	0.04	0.04	0.01	0.01	0.01	0.02	0.02
Tm (ppm)	0.05	0.04	0.05	0.06	0.05	0.04	0.06	0.06	0.04	0.04	0.05	0.04	0.03
V (ppm)	126	118	134	133	127	108	151	134	127	130	108	120	114
Y (ppm)	2.8	2.9	2.8	2.8	2.9	2.6	3	3.2	2.2	2.5	2.2	2.3	2
U (ppm)	0.06	0.07	0.025	0.05	0.12	0.27	0.025	0.16	0.025	0.05	0.025	0.11	0.025
W (ppm)	0.5	1	1	2	1	2	1	1	0.5	0.5	0.5	2	3
Yb (ppm)	0.36	0.36	0.34	0.4	0.42	0.32	0.35	0.39	0.36	0.33	0.25	0.28	0.25
Zr (ppm)	7	8	6	7	7	8	6	25	5	5	5	4	6
Zn (ppm)	71	66	81	75	68	59	82	62	68	55	52	53	61

Drill hole #	18-805	18-805	18-805	18-805	18-805	18-805	18-805	18-805	18-805	18-805	18-805	18-805	18-805
Depth From	169	170	171	172	173	174	175	176	177	178	179	180	181
Depth To	170	171	172	173	174	175	176	177	178	179	180	181	182
Rock Type	NOR	NOR	NOR	NOR	NOR	NOR	NOR	NOR	NOR	NOR	NOR	NOR	NOR
Lithological Domain	Norite	Norite	Norite	Norite	Norite	Norite	Norite	Norite	Norite	Norite	Norite	Norite	Norite
Al2O3 (%)	9.18	9.66	8.36	10.5	9.05	9.33	9.77	9.21	8.94	9.68	8.92	9.12	9.07
CaO (%)	5.89	6.36	6.41	7.2	6.78	5.9	5.19	6.07	6.2	6.24	5.44	5.32	6.4
Cr2O3 (%)	0.063	0.068	0.071	0.065	0.073	0.071	0.059	0.068	0.072	0.069	0.107	0.117	0.087
Fe2O3 (%)	12	11.4	13.2	12.15	13.45	12.75	10.4	11.35	12.95	12.25	11.5	10.55	11.9
K2O (%)	0.14	0.19	0.18	0.21	0.17	0.16	0.16	0.11	0.18	0.14	0.16	0.11	0.15
MgO (%)	17.45	16.4	16.45	16.25	16.7	16.45	13.4	14.9	16.95	16.3	19.1	18.85	17.15
MnO (%)	0.2	0.19	0.22	0.19	0.19	0.18	0.14	0.16	0.19	0.18	0.18	0.17	0.19
Na2O (%)	0.55	0.57	0.44	0.84	0.66	0.75	1.77	0.77	0.59	0.76	0.53	0.56	0.75
P2O5 (%)	0.01	0.02	0.01	0.005	0.005	0.005	0.01	0.005	0.01	0.005	0.005	0.01	0.005
SiO2 (%)	50.1	49.6	49.9	50.2	48.6	49.5	55.1	49	48.9	49.5	50.5	48.9	49
TiO2 (%)	0.13	0.13	0.17	0.14	0.14	0.13	0.11	0.15	0.14	0.13	0.13	0.11	0.12
LOI (%)	3.67	3.71	3.48	3.45	3.82	3.85	3.45	4.11	3.89	4.06	4.09	4.45	3.98
Total (%)	99.38	98.3	98.89	101.21	99.63	99.07	99.58	95.9	99.01	99.32	100.66	98.27	98.8
Ag (ppm)	0.6	0.25	0.25	0.5	1.4	1.1	1.4	1.3	1.2	1.4	0.25	0.25	0.5
As (ppm)	0.4	0.05	0.6	0.5	1.7	1.5	3	3.2	1.2	0.9	0.5	0.05	2.6
Au (ppm)	0.577	0.239	0.157	0.486	1.9	1.73	1.95	2.03	2.11	2.23	0.372	0.156	1.02
Ba (ppm)	27.3	33	27.7	35.6	25.3	37.5	55.1	18.8	24.9	24.3	21.4	11.8	16.2
Bi (ppm)	0.11	0.04	0.03	0.1	0.25	0.39	0.34	0.42	0.24	0.23	0.06	0.03	0.92
Cd (ppm)	0.6	0.25	0.25	0.5	0.8	0.6	0.6	0.7	0.7	0.7	0.5	0.6	0.8
Ce (ppm)	1.4	1.5	1.9	1.6	1.5	3.1	9.8	5	2.3	2.2	1.6	1.1	1.6
Co (ppm)	105	87	89	92	126	121	107	113	116	120	95	85	117
Cs (ppm)	1.8	3.22	2.94	1.86	2.16	1.54	1.18	1.25	1.71	1.5	1.29	0.95	1.14
Cu (ppm)	1770	620	388	1280	3280	3160	3230	3030	3190	3590	1320	427	1930
Dy (ppm)	0.39	0.36	0.55	0.42	0.34	0.38	0.48	0.41	0.4	0.38	0.37	0.37	0.32
Er (ppm)	0.21	0.24	0.28	0.26	0.25	0.28	0.28	0.29	0.35	0.23	0.39	0.28	0.29
Eu (ppm)	0.06	0.11	0.15	0.11	0.12	0.14	0.13	0.15	0.13	0.13	0.08	0.08	0.08
Ga (ppm)	7.9	8.3	8.3	8.8	8.2	9.1	8.7	9.2	8	8.7	7.1	7.5	7.9
Gd (ppm)	0.16	0.28	0.3	0.38	0.34	0.32	0.47	0.54	0.35	0.27	0.24	0.27	0.29
Ge (ppm)	2.5	2.5	2.5	2.5	2.5	2.5	2.5	2.5	2.5	2.5	2.5	2.5	2.5
Hf (ppm)	0.2	0.2	0.3	0.2	0.1	0.4	0.9	0.4	0.3	0.2	0.2	0.2	0.1
Hg (ppb)	0.0025	0.0025	0.0025	0.0025	0.0025	0.0025	0.0025	0.0025	0.0025	0.0025	0.0025	0.0025	0.0025
Ho (ppm)	0.08	0.07	0.12	0.09	0.09	0.11	0.11	0.13	0.1	0.07	0.1	0.07	0.1
In (ppm)	0.011	0.007	0.005	0.008	0.017	0.017	0.015	0.013	0.015	0.014	0.008	0.0025	0.009
La (ppm)	0.7	0.7	0.8	0.8	0.7	1.4	5.4	2.3	1.1	1.1	0.7	0.5	0.8
Li (ppm)	10	10	10	10	10	10	10	20	10	10	10	20	20
Lu (ppm)	0.06	0.06	0.05	0.06	0.06	0.05	0.07	0.07	0.05	0.06	0.04	0.06	0.05
Mo (ppm)	0.5	0.5	0.5	0.5	0.5	0.5	0.5	0.5	0.5	0.5	0.5	1	0.5
Nb (ppm)	0.2	0.2	0.2	0.1	0.1	0.4	0.6	0.9	0.3	0.2	0.2	0.1	0.2
Ni (ppm)	1890	970	787	1365	3320	3650	3760	3710	3860	4320	1700	804	3360
Nd (ppm)	0.7	0.9	1	1	0.9	1.1	2.9	2.2	1	1.2	0.8	0.7	0.9
Pb (ppm)	1	1	1	1	2	1	1	1	1	1	1	2	1
Pd (ppm)	3.56	1.35	1.115	4.58	20.4	19	20.9	22	20.5	21.4	4.87	0.958	18.5
Pr (ppm)	0.17	0.19	0.22	0.21	0.18	0.28	0.94	0.6	0.22	0.25	0.18	0.13	0.21
Pt (ppm)	0.464	0.203	0.146	0.532	2.32	2.13	2.17	2.38	2.23	2.39	0.542	0.099	2.06
Rb (ppm)	3.7	5.1	4.9	5.9	4.3	3.9	3.7	3.2	4.4	3.4	3.6	2	3.5
Re (ppm)	0.002	0.0005	0.0005	0.001	0.004	0.003	0.003	0.003	0.003	0.004	0.001	0.0005	0.001
S (%)	0.5	0.15	0.06	0.37	1.09	0.98	1	0.85	0.95	0.99	0.34	0.1	0.65
Sb (ppm)	0.025	0.025	0.38	0.025	0.025	0.025	0.08	0.27	0.025	0.025	0.025	0.025	0.37
Sc (ppm)	37	34	36	38	39	34	29	35	37	36	35	30	38
Se (ppm)	5.05	1.68	0.653	3.26	10.25	10.6	11.4	10.6	11.2	11.85	3.73	0.982	7.7
Sm (ppm)	0.2	0.22	0.25	0.13	0.22	0.31	0.57	0.6	0.32	0.28	0.19	0.22	0.19
Sn (ppm)	0.5	0.5	0.5	0.5	0.5	0.5	0.5	0.5	0.5	0.5	0.5	0.5	0.5
Sr (ppm)	50.6	56.2	35.8	98.6	62.8	74.9	91.4	52.3	51.8	70.1	50.3	41.6	47.7
Ta (ppm)	0.05	0.05	0.05	0.05	0.05	0.05	0.2	0.1	0.05	0.05	0.05	0.05	0.05
Tb (ppm)	0.04	0.04	0.07	0.05	0.03	0.05	0.06	0.09	0.05	0.06	0.05	0.05	0.04
Te (ppm)	1.25	0.37	0.19	1.07	4.38	5.29	5.65	5.23	4.84	5.29	1.06	0.31	4.97
Th (ppm)	0.11	0.09	0.15	0.1	0.11	0.22	2.82	0.52	0.19	0.12	0.13	0.05	0.11
Tl (ppm)	0.06	0.04	0.04	0.03	0.08	0.07	0.09	0.04	0.07	0.06	0.02	0.01	0.03
Tm (ppm)	0.05	0.05	0.06	0.07	0.05	0.06	0.05	0.05	0.04	0.06	0.05	0.05	0.05
V (ppm)	140	139	160	148	143	133	107	130	136	120	123	106	122
Y (ppm)	2.2	2.3	2.8	2.5	2.5	2.4	2.9	3.3	2.7	2.3	2.6	2.2	2.2
U (ppm)	0.025	0.025	0.025	0.025	0.025	0.05	0.8	0.17	0.06	0.025	0.025	0.025	0.06
W (ppm)	1	1	1	1	0.5	2	2	2	1	1	0.5	0.5	0.5
Yb (ppm)	0.36	0.35	0.49	0.38	0.36	0.36	0.47	0.48	0.35	0.25	0.4	0.3	0.28
Zr (ppm)	6	5	7	6	5	12	29	13	12	8	8	5	5
Zn (ppm)	70	73	89	73	75	71	55	67	71	68	69	64	59

Drill hole #	18-805	18-805	18-805	18-805	18-805	18-805	18-805	18-805	18-805	18-805	18-805	18-805	18-805
Depth From	182	183	184	185	186	187	188	189	190	191	192	193	194
Depth To	183	184	185	186	187	188	189	190	191	192	193	194	195
Rock Type	NOR	NOR	NOR	NOR	NOR	NOR	NOR	NOR	NOR	NOR	NOR	NOR	NOR
Lithological Domain	Norite	Norite	Norite	Norite	Norite	Norite	Norite	Norite	Norite	Norite	Norite	Norite	Norite
Al2O3 (%)	10.15	8.81	13.15	14.4	11.9	11.75	14.8	14.6	15.1	12.45	13.35	15	13.85
CaO (%)	6.88	6.82	7.65	8.91	7.82	7.89	10.05	9.29	9.02	7.2	8.85	8.49	7.79
Cr2O3 (%)	0.064	0.075	0.057	0.044	0.055	0.048	0.037	0.04	0.037	0.049	0.044	0.049	0.051
Fe2O3 (%)	11.55	12.65	10.15	9.46	11.05	10.7	8.73	9.63	9.81	11.15	10.9	9.39	9.81
K2O (%)	0.13	0.05	0.16	0.43	0.27	0.12	0.13	0.13	0.11	0.12	0.1	0.12	0.11
MgO (%)	16.25	17	13.7	12.1	14.6	14.15	12.1	13	12.1	14.7	12.7	12.95	14.6
MnO (%)	0.18	0.18	0.15	0.14	0.18	0.17	0.15	0.15	0.15	0.17	0.16	0.14	0.16
Na2O (%)	0.74	0.59	1.84	1.48	1.18	1.15	1.49	1.41	1.51	1.12	1.4	1.41	1.25
P2O5 (%)	0.01	0.01	0.02	0.005	0.005	0.02	0.01	0.01	0.01	0.005	0.005	0.005	0.01
SiO2 (%)	49.6	49	51.3	49.6	51.1	49.7	51.2	51.5	50.7	49.5	50.9	50.7	51.4
TiO2 (%)	0.11	0.12	0.13	0.12	0.14	0.14	0.13	0.12	0.13	0.12	0.17	0.11	0.11
LOI (%)	4.22	4.35	3.14	2.88	2.39	2.26	2.14	1.79	1.36	2.53	2.05	1.48	0.96
Total (%)	99.88	99.66	101.47	99.58	100.71	98.11	100.98	101.68	100.06	99.12	100.63	99.85	100.11
Ag (ppm)	1.4	1	0.25	0.25	0.25	0.25	0.25	0.25	0.25	0.6	0.25	0.25	0.25
As (ppm)	2.7	5	1.3	1	1.1	0.7	0.6	0.2	0.2	0.3	0.4	0.4	0.4
Au (ppm)	1.6	2.47	0.577	0.391	0.363	0.528	0.096	0.39	0.328	0.55	0.629	0.682	0.416
Ba (ppm)	19.5	7.6	48.5	76.7	48.6	37.1	39.4	39.4	42	36.7	40.3	43	34.7
Bi (ppm)	0.99	2.14	1	0.36	0.17	0.15	0.11	0.13	0.09	0.19	0.18	0.14	0.08
Cd (ppm)	0.7	0.6	0.6	0.5	0.5	0.25	0.25	0.5	0.6	0.25	0.5	0.25	0.25
Ce (ppm)	1.7	2.3	4	2.4	3.1	2.9	2.8	1.9	2.1	1.6	3.1	2.2	2
Co (ppm)	118	153	81	73	83	87	66	84	79	103	91	89	86
Cs (ppm)	0.99	0.72	2.24	3.07	1.83	1.33	1.13	0.99	0.77	1.23	1.04	1.15	0.75
Cu (ppm)	2570	4020	1290	812	871	1180	368	1140	1000	1710	1520	1660	934
Dy (ppm)	0.37	0.31	0.51	0.42	0.53	0.47	0.44	0.37	0.39	0.33	0.53	0.34	0.36
Er (ppm)	0.26	0.33	0.34	0.32	0.35	0.33	0.3	0.28	0.25	0.27	0.36	0.26	0.27
Eu (ppm)	0.14	0.13	0.19	0.13	0.16	0.16	0.18	0.13	0.13	0.11	0.17	0.17	0.15
Ga (ppm)	8.6	8.3	10.9	11.7	10.1	10	11.3	10.6	12	9.5	12	12.4	11.2
Gd (ppm)	0.32	0.29	0.4	0.44	0.4	0.43	0.32	0.34	0.27	0.25	0.56	0.26	0.27
Ge (ppm)	2.5	2.5	2.5	2.5	2.5	2.5	2.5	2.5	2.5	2.5	2.5	2.5	2.5
Hf (ppm)	0.2	0.2	0.4	0.2	0.2	0.3	0.3	0.2	0.3	0.2	0.3	0.2	0.2
Hg (ppb)	0.0025	0.0025	0.0025	0.0025	0.0025	0.0025	0.0025	0.0025	0.0025	0.0025	0.0025	0.0025	0.0025
Ho (ppm)	0.08	0.1	0.11	0.11	0.12	0.1	0.1	0.11	0.09	0.07	0.13	0.07	0.07
In (ppm)	0.012	0.016	0.007	0.005	0.006	0.009	0.0025	0.007	0.007	0.012	0.009	0.01	0.007
La (ppm)	0.8	1.1	2.1	1	1.3	1.4	1.3	0.9	1.1	0.9	1.5	1.1	0.9
Li (ppm)	20	20	10	10	10	10	10	10	10	10	10	10	5
Lu (ppm)	0.05	0.05	0.06	0.06	0.07	0.05	0.07	0.06	0.05	0.05	0.06	0.05	0.05
Mo (ppm)	1	0.5	0.5	1	1	0.5	0.5	0.5	1	0.5	1	1	1
Nb (ppm)	0.2	0.3	0.4	0.2	0.3	0.3	0.2	0.2	0.2	0.1	0.2	0.2	0.2
Ni (ppm)	3470	5210	1820	1210	1330	1290	655	1310	1100	1820	1620	1780	1280
Nd (ppm)	0.8	1.4	2	1.3	1.6	1.6	1.4	1.1	1.1	0.7	1.9	0.9	0.9
Pb (ppm)	5	6	3	2	4	5	6	5	7	4	2	5	6
Pd (ppm)	18.4	29.2	8.99	5.02	5.33	4.93	1.175	4.93	3.34	5.95	6.94	7.12	4.2
Pr (ppm)	0.19	0.29	0.5	0.29	0.38	0.36	0.32	0.23	0.28	0.2	0.39	0.26	0.22
Pt (ppm)	1.95	3.22	1	0.517	0.568	0.607	0.12	0.568	0.369	0.618	0.783	0.86	0.502
Rb (ppm)	4.9	1.3	5.1	13.9	7.7	2.7	2.8	2.6	1.9	2.3	1.7	2.2	1.7
Re (ppm)	0.002	0.002	0.002	0.001	0.001	0.001	0.001	0.001	0.001	0.001	0.001	0.002	0.001
S (%)	0.81	1.19	0.36	0.3	0.21	0.3	0.08	0.35	0.31	0.49	0.53	0.47	0.26
Sb (ppm)	0.3	1.01	0.49	0.17	0.09	0.05	0.025	0.025	0.025	0.025	0.08	0.025	0.025
Sc (ppm)	36	38	29	22	31	33	25	27	26	32	31	24	27
Se (ppm)	9.73	16.1	4.22	3.02	2.38	3.02	0.81	3.5	2.76	4.67	4.43	4.79	2.83
Sm (ppm)	0.2	0.26	0.34	0.25	0.42	0.3	0.4	0.26	0.32	0.16	0.42	0.14	0.2
Sn (ppm)	1	0.5	0.5	0.5	0.5	1	0.5	0.5	0.5	0.5	0.5	0.5	0.5
Sr (ppm)	60.7	30.6	218	167	130.5	137	164.5	164.5	182	121	161.5	168.5	147
Ta (ppm)	0.05	0.05	0.6	0.05	0.05	0.05	0.05	0.05	0.05	0.05	0.05	0.05	0.05
Tb (ppm)	0.05	0.06	0.07	0.06	0.07	0.06	0.06	0.06	0.06	0.04	0.09	0.04	0.06
Te (ppm)	4.72	8.05	2.44	1.04	1.18	1.25	0.44	1.46	0.97	1.8	1.76	2.13	1.18
Th (ppm)	0.11	0.15	0.27	0.1	0.21	0.2	0.18	0.12	0.12	0.1	0.19	0.12	0.11
Tl (ppm)	0.03	0.05	0.03	0.02	0.02	0.03	0.01	0.01	0.01	0.03	0.02	0.02	0.01
Tm (ppm)	0.05	0.04	0.06	0.05	0.05	0.07	0.04	0.05	0.04	0.03	0.06	0.05	0.05
V (ppm)	113	112	108	118	122	124	115	120	124	111	148	97	103
Y (ppm)	2.3	2.6	2.8	2.7	3	3	2.9	2.2	2.5	2	3.5	2	1.9
U (ppm)	0.025	0.025	0.09	0.05	0.08	0.05	0.05	0.025	0.025	0.025	0.05	0.025	0.025
W (ppm)	1	1	1	2	3	1	2	2	1	3	2	2	1
Yb (ppm)	0.42	0.36	0.34	0.43	0.34	0.46	0.32	0.34	0.29	0.29	0.39	0.27	0.31
Zr (ppm)	5	7	13	7	8	10	9	8	9	6	12	7	7
Zn (ppm)	56	54	54	49	62	61	51	54	58	65	61	56	58

Drill hole #	18-805	18-805	18-805	18-805	18-805	18-805	18-805	18-805	18-805	18-805	18-805	18-805	18-805
Depth From	195	196	197	198	199	200	201	202	203	204	206	207	208
Depth To	196	197	198	199	200	201	202	203	204	205	207	208	209
Rock Type	NOR	NOR	NOR	NOR	NOR	NOR	NOR	NOR	NOR	NOR	NOR	NOR	NOR
Lithological Domain	Norite	Norite	Norite	Norite	Norite	Norite	Norite	Norite	Norite	Norite	Norite	Norite	Norite
Al2O3 (%)	12.9	16.9	14.95	11.05	17.85	12.6	13.7	14.1	18.8	14.25	18.5	17.55	14.6
CaO (%)	7.76	9.16	8.21	6.59	9.54	7.07	7.27	7.84	9.81	8.18	10.6	9.34	8.45
Cr2O3 (%)	0.057	0.042	0.047	0.061	0.04	0.065	0.055	0.055	0.045	0.061	0.026	0.034	0.047
Fe2O3 (%)	10.25	8.35	8.98	11.4	7.64	9.87	8.19	8.99	7.16	8.84	7.1	7.52	9.44
K2O (%)	0.13	0.11	0.2	0.28	0.28	0.22	0.58	0.24	0.23	0.24	0.49	0.34	0.29
MgO (%)	15.25	12.15	13.8	16.8	11.15	15.7	13.4	14.4	11.35	14.55	8.94	10.15	13.05
MnO (%)	0.17	0.13	0.15	0.18	0.12	0.16	0.14	0.15	0.12	0.15	0.12	0.12	0.14
Na2O (%)	1.14	1.5	1.35	0.88	1.71	1.04	1.37	1.25	1.49	1.19	2.12	1.89	1.24
P2O5 (%)	0.005	0.02	0.01	0.005	0.01	0.01	0.01	0.01	0.01	0.01	0.02	0.01	0.02
SiO2 (%)	50.7	51.6	51.6	50.9	51.5	50.4	51.6	51.8	50.6	51.7	51.5	49.7	50.9
TiO2 (%)	0.12	0.11	0.11	0.13	0.12	0.12	0.1	0.11	0.09	0.11	0.15	0.11	0.12
LOI (%)	1.4	0.79	1.88	2.25	1.81	2.08	2.16	1.53	1.61	1.8	1.99	2.79	3.42
Total (%)	99.89	100.88	101.31	100.54	101.8	99.35	98.6	100.5	101.35	101.1	101.59	99.58	101.74
Ag (ppm)	0.25	0.25	0.25	0.5	0.25	0.25	0.25	0.25	0.25	0.25	0.25	0.25	0.25
As (ppm)	0.05	0.05	0.1	0.5	0.1	0.05	0.05	0.1	0.2	0.2	0.5	0.3	1.5
Au (ppm)	0.498	0.457	0.401	0.8	0.164	0.261	0.042	0.175	0.037	0.092	0.033	0.094	0.564
Ba (ppm)	33.4	41.1	47.4	47.4	56.1	40.2	84.3	50.9	46	44.9	99.3	72.1	58.8
Bi (ppm)	0.08	0.08	0.13	0.29	0.13	0.08	0.04	0.09	0.06	0.03	0.17	0.42	0.25
Cd (ppm)	0.8	0.6	0.5	0.7	0.25	0.5	0.5	0.25	0.25	0.25	0.25	0.25	0.25
Ce (ppm)	2.7	2.2	2.3	2.3	2.7	2.2	3.6	2.3	1.8	3.3	6	2.9	2.4
Co (ppm)	93	73	82	111	65	83	66	74	51	68	45	55	75
Cs (ppm)	0.98	1.05	1.51	1.84	1.88	1.01	3.49	1.43	1.76	1.28	2.73	2.64	1.94
Cu (ppm)	1070	1110	1140	2180	665	656	84	373	67	352	96	302	816
Dy (ppm)	0.29	0.32	0.38	0.38	0.33	0.35	0.39	0.35	0.26	0.39	0.51	0.38	0.42
Er (ppm)	0.29	0.24	0.31	0.36	0.2	0.26	0.27	0.27	0.18	0.25	0.46	0.3	0.29
Eu (ppm)	0.14	0.12	0.16	0.14	0.2	0.12	0.18	0.16	0.14	0.15	0.3	0.14	0.16
Ga (ppm)	10.5	12.4	11.9	9.4	12.6	9.2	11.3	11.3	11.6	10.5	15	14.4	12.1
Gd (ppm)	0.32	0.24	0.3	0.3	0.35	0.25	0.36	0.36	0.2	0.44	0.52	0.44	0.27
Ge (ppm)	2.5	2.5	2.5	2.5	2.5	2.5	2.5	2.5	2.5	2.5	2.5	2.5	2.5
Hf (ppm)	0.3	0.2	0.2	0.3	0.3	0.2	0.3	0.3	0.1	0.2	0.4	0.2	0.2
Hg (ppb)	0.0025	0.0025	0.0025	0.0025	0.0025	0.0025	0.0025	0.0025	0.0025	0.0025	0.0025	0.0025	0.0025
Ho (ppm)	0.1	0.09	0.08	0.09	0.09	0.09	0.09	0.09	0.06	0.09	0.14	0.08	0.09
In (ppm)	0.007	0.007	0.008	0.014	0.005	0.007	0.0025	0.005	0.0025	0.005	0.0025	0.005	0.007
La (ppm)	1.4	1.1	1.2	1.1	1.4	1.1	1.7	1.2	1	1.5	3	1.4	1.2
Li (ppm)	10	10	10	10	10	10	10	10	10	10	10	20	20
Lu (ppm)	0.05	0.04	0.06	0.06	0.05	0.07	0.06	0.05	0.04	0.05	0.07	0.05	0.05
Mo (ppm)	0.5	1	0.5	0.5	0.5	1	0.5	0.5	1	1	1	1	0.5
Nb (ppm)	0.8	0.1	0.2	0.2	0.3	0.2	0.5	0.3	0.2	1.4	0.7	0.4	0.3
Ni (ppm)	1470	1290	1430	2500	1070	1080	518	695	406	581	353	639	969
Nd (ppm)	1.3	1.1	1	1	1.3	1	1.4	0.9	0.8	1.5	2.6	1.2	1.2
Pb (ppm)	5	5	3	6	1	2	4	2	7	3	6	5	2
Pd (ppm)	4.88	4.1	4.52	9.69	3.05	3.04	0.478	2.14	0.805	1.21	0.996	2.37	5.99
Pr (ppm)	0.39	0.26	0.26	0.27	0.31	0.22	0.42	0.28	0.23	0.39	0.73	0.36	0.3
Pt (ppm)	0.578	0.442	0.48	1.05	0.339	0.293	0.073	0.263	0.071	0.151	0.09	0.237	0.596
Rb (ppm)	2.6	2.1	5.4	7.9	8.1	5.4	18.2	6.7	5.6	5.6	14	10	9.8
Re (ppm)	0.002	0.001	0.001	0.002	0.0005	0.0005	0.001	0.0005	0.0005	0.0005	0.0005	0.0005	0.001
S (%)	0.31	0.3	0.28	0.59	0.2	0.19	0.02	0.08	0.02	0.1	0.03	0.07	0.19
Sb (ppm)	0.025	0.025	0.025	0.025	0.025	0.025	0.025	0.025	0.025	0.025	0.025	0.16	0.3
Sc (ppm)	32	22	24	34	18	26	24	26	18	26	20	18	21
Se (ppm)	3.29	3.15	3.47	7.08	2.42	2.15	0.152	0.967	0.123	0.735	0.17	0.669	2.19
Sm (ppm)	0.3	0.27	0.22	0.22	0.32	0.21	0.27	0.2	0.18	0.29	0.63	0.2	0.26
Sn (ppm)	0.5	0.5	0.5	0.5	1	0.5	0.5	0.5	0.5	0.5	1	0.5	0.5
Sr (ppm)	132	184.5	165	105	211	117.5	147	160	190.5	142	252	214	153
Ta (ppm)	0.05	0.05	0.05	0.05	0.05	0.05	0.05	0.05	0.05	0.05	0.05	0.05	0.05
Tb (ppm)	0.05	0.05	0.05	0.05	0.04	0.06	0.05	0.07	0.04	0.06	0.1	0.05	0.04
Te (ppm)	1.43	1.38	1.4	2.21	0.76	0.82	0.16	0.51	0.28	0.26	0.54	1.16	1.13
Th (ppm)	0.18	0.12	0.14	0.17	0.15	0.16	0.37	0.2	0.08	0.18	0.4	0.17	0.14
Tl (ppm)	0.02	0.02	0.03	0.08	0.03	0.03	0.09	0.04	0.02	0.02	0.03	0.01	0.02
Tm (ppm)	0.03	0.05	0.05	0.07	0.04	0.05	0.05	0.06	0.03	0.05	0.06	0.05	0.04
V (ppm)	105	89	94	122	86	91	84	104	75	91	109	93	116
Y (ppm)	2.2	2.1	2.1	2.6	2.3	2.1	2.4	2.4	1.6	2.3	3.5	2.2	2.5
U (ppm)	0.025	0.025	0.025	0.08	0.05	0.025	0.2	0.06	0.025	0.05	0.17	0.08	0.06
W (ppm)	2	1	1	2	2	4	1	1	3	1	2	3	2
Yb (ppm)	0.31	0.25	0.36	0.37	0.28	0.34	0.31	0.34	0.2	0.3	0.38	0.21	0.28
Zr (ppm)	7	5	8	10	8	7	9	10	6	8	15	7	8
Zn (ppm)	59	49	50	62	41	57	52	55	44	54	44	51	58

Drill hole #	18-805	18-805	18-805	18-805	18-805	18-805	18-805	18-805	18-805	18-805	18-805	18-805	18-805
Depth From	209	210	211	212	213	214	215	216	217	218	219	220	221
Depth To	210	211	212	213	214	215	216	217	218	219	220	221	222
Rock Type	NOR	NOR	NOR	NOR	NOR	NOR	NOR	NOR	NOR	NOR	NOR	NOR	NOR
Lithological Domain	Norite	Norite	Norite	Norite	Norite	Norite	Norite	Norite	Norite	Norite	Norite	Norite	Norite
Al2O3 (%)	18	17.65	13.35	14	15.1	12.5	15.4	14.15	13.95	13.7	13.55	13.7	13.4
CaO (%)	10.5	9.49	8.29	8.3	8.21	7.03	8.73	7.91	8.65	8.96	8.46	8.58	8.9
Cr2O3 (%)	0.029	0.037	0.056	0.043	0.052	0.062	0.049	0.054	0.056	0.055	0.051	0.05	0.051
Fe2O3 (%)	7.02	7.3	8.93	10	8.26	9.39	8.16	9.07	8.82	8.73	8.75	9.51	9.18
K2O (%)	0.57	0.46	0.15	0.16	0.23	0.45	0.45	0.24	0.25	0.18	0.34	0.32	0.2
MgO (%)	9.14	10.45	14.35	12.9	13.15	15.45	12.05	13.7	13.95	13.7	13.2	13.9	13.75
MnO (%)	0.11	0.12	0.15	0.16	0.14	0.16	0.14	0.16	0.15	0.15	0.16	0.17	0.16
Na2O (%)	2.23	2.03	1.18	1.33	1.36	1.11	1.79	1.18	1.2	1.26	1.48	1.36	1.29
P2O5 (%)	0.02	0.005	0.005	0.01	0.01	0.01	0.01	0.01	0.01	0.01	0.01	0.01	0.01
SiO2 (%)	51.3	50.9	50.8	50.4	50.4	49.9	51.9	50.9	50.6	51.5	50.8	51.3	51.8
TiO2 (%)	0.15	0.11	0.12	0.14	0.11	0.12	0.1	0.1	0.12	0.12	0.12	0.15	0.13
LOI (%)	2.64	2.81	1.61	1.61	2.16	2.42	2.28	2.87	2.66	1.09	1.99	2.26	1.42
Total (%)	101.74	101.39	99	99.06	99.21	98.62	101.08	100.36	100.44	99.47	98.93	101.33	100.31
Ag (ppm)	0.25	0.25	0.25	0.25	0.25	0.25	0.25	0.25	0.25	0.25	0.25	0.25	0.25
As (ppm)	0.4	0.3	0.3	0.3	0.05	0.8	1.1	0.2	0.8	0.05	0.1	0.4	0.05
Au (ppm)	0.076	0.029	0.061	0.177	0.137	0.144	0.38	0.269	0.307	0.033	0.012	0.07	0.031
Ba (ppm)	102.5	83.7	38.8	44	48.6	66.1	71.6	51.7	50.2	45	67	60.7	52.5
Bi (ppm)	0.17	0.09	0.02	0.07	0.09	0.2	0.51	0.03	0.05	0.01	0.01	0.05	0.03
Cd (ppm)	0.25	0.25	0.25	0.6	0.5	0.25	0.6	0.25	0.5	0.25	0.25	0.25	0.25
Ce (ppm)	3.8	2.8	2	2	2.2	2.4	2.9	1.6	1.8	1.8	2.9	2.1	5.3
Co (ppm)	52	54	71	79	70	75	69	70	71	66	68	75	72
Cs (ppm)	2.63	2.38	0.96	1.17	1.75	3.05	2.99	1.55	1.42	0.79	1.53	1.41	1.02
Cu (ppm)	282	129	255	657	524	275	546	350	440	153	81	387	191
Dy (ppm)	0.47	0.33	0.4	0.47	0.28	0.38	0.35	0.28	0.43	0.39	0.37	0.38	0.6
Er (ppm)	0.27	0.3	0.29	0.36	0.23	0.3	0.23	0.23	0.3	0.27	0.29	0.35	0.33
Eu (ppm)	0.25	0.17	0.2	0.18	0.15	0.16	0.17	0.14	0.18	0.15	0.15	0.14	0.24
Ga (ppm)	14.3	13.9	10.9	12.3	11.8	10.1	12.2	12.2	10.7	11.4	11.5	9.5	11
Gd (ppm)	0.51	0.3	0.33	0.37	0.27	0.32	0.24	0.25	0.24	0.3	0.35	0.35	0.53
Ge (ppm)	2.5	2.5	2.5	2.5	2.5	2.5	2.5	2.5	2.5	2.5	2.5	2.5	2.5
Hf (ppm)	0.4	0.2	0.2	0.1	0.1	0.2	0.2	0.1	0.2	0.2	0.2	0.2	0.2
Hg (ppb)	0.0025	0.0025	0.0025	0.0025	0.0025	0.0025	0.0025	0.0025	0.0025	0.0025	0.0025	0.0025	0.0025
Ho (ppm)	0.12	0.07	0.09	0.11	0.08	0.08	0.07	0.07	0.08	0.09	0.09	0.08	0.11
In (ppm)	0.0025	0.0025	0.0025	0.007	0.006	0.005	0.0025	0.0025	0.005	0.0025	0.0025	0.0025	0.0025
La (ppm)	1.9	1.4	1	1	1.1	1.2	1.5	0.9	0.9	1	1.4	1.1	2.6
Li (ppm)	20	20	10	10	10	10	10	10	10	10	10	10	5
Lu (ppm)	0.06	0.06	0.06	0.06	0.05	0.05	0.05	0.04	0.04	0.04	0.04	0.04	0.06
Mo (ppm)	0.5	1	0.5	0.5	0.5	0.5	1	0.5	0.5	0.5	0.5	1	0.5
Nb (ppm)	0.5	0.3	0.2	0.2	0.2	0.2	0.3	0.1	0.1	0.1	0.3	0.2	0.4
Ni (ppm)	580	546	587	824	827	869	1150	725	789	487	495	641	515
Nd (ppm)	2.1	1.4	1	1.1	1.2	1	1.5	0.8	0.8	0.9	1.2	1.1	2.7
Pb (ppm)	5	2	1	1	5	1	4	5	5	2	4	2	2
Pd (ppm)	1.35	0.645	0.514	1.585	1.24	2.61	7.46	2.59	3.81	0.241	0.168	1.07	0.433
Pr (ppm)	0.45	0.36	0.23	0.24	0.25	0.27	0.31	0.18	0.19	0.2	0.28	0.28	0.63
Pt (ppm)	0.14	0.1	0.076	0.212	0.156	0.286	0.701	0.256	0.363	0.037	0.03	0.123	0.059
Rb (ppm)	18.6	14.8	3.4	3.9	6.4	13.1	14.1	7	7	4.3	10.1	8.9	5
Re (ppm)	0.0005	0.0005	0.0005	0.001	0.0005	0.0005	0.0005	0.0005	0.0005	0.0005	0.0005	0.0005	0.0005
S (%)	0.07	0.04	0.07	0.21	0.13	0.05	0.14	0.1	0.1	0.04	0.02	0.09	0.05
Sb (ppm)	0.07	0.025	0.025	0.025	0.025	0.025	0.24	0.025	0.025	0.025	0.025	0.025	0.025
Sc (ppm)	25	19	30	30	22	24	21	22	29	32	30	32	33
Se (ppm)	0.629	0.344	0.591	1.69	1.405	0.899	1.785	1.055	1.355	0.408	0.174	0.959	0.423
Sm (ppm)	0.38	0.28	0.33	0.25	0.25	0.18	0.23	0.17	0.18	0.25	0.29	0.16	0.5
Sn (ppm)	1	1	0.5	0.5	0.5	1	0.5	0.5	0.5	0.5	0.5	0.5	0.5
Sr (ppm)	249	223	147	168.5	162.5	123	198.5	153	130	147	161	126	145.5
Ta (ppm)	0.05	0.05	0.05	0.05	0.05	0.05	0.05	0.05	0.05	0.05	0.05	0.05	0.05
Tb (ppm)	0.08	0.05	0.06	0.07	0.05	0.06	0.04	0.06	0.04	0.05	0.06	0.04	0.08
Te (ppm)	0.6	0.26	0.24	0.54	0.7	0.63	2.25	0.51	0.95	0.12	0.11	0.33	0.22
Th (ppm)	0.25	0.16	0.09	0.09	0.11	0.16	0.28	0.09	0.1	0.1	0.12	0.1	0.74
Tl (ppm)	0.01	0.01	0.02	0.02	0.02	0.06	0.07	0.03	0.02	0.01	0.02	0.02	0.02
Tm (ppm)	0.05	0.03	0.05	0.05	0.05	0.06	0.05	0.05	0.04	0.04	0.05	0.05	0.06
V (ppm)	110	91	105	135	91	101	100	113	105	107	111	107	118
Y (ppm)	3.1	2.2	2.5	2.6	2.1	2.2	1.9	1.9	2.1	2.4	2.3	2.3	2.9
U (ppm)	0.1	0.05	0.025	0.025	0.025	0.08	0.12	0.025	0.025	0.025	0.08	0.025	0.025
W (ppm)	4	3	2	2	3	1	3	2	1	2	1	3	1
Yb (ppm)	0.37	0.27	0.32	0.33	0.34	0.24	0.35	0.25	0.25	0.33	0.31	0.37	0.46
Zr (ppm)	14	8	7	6	6	7	7	5	6	6	7	6	7
Zn (ppm)	42	44	54	61	50	59	47	54	51	51	54	58	55

Drill hole #	18-805	18-805	18-805	18-805	18-805	18-805	18-805	18-805	18-805	18-805	18-805	18-805	18-805
Depth From	222	223	224	225	226	227.95	229	230	231	232	233	234	235
Depth To	223	224	225	226	227	229	230	231	232	233	234	235	236
Rock Type	NOR	NOR	NOR	NOR	NOR	NOR-Bx	NOR-Bx	NOR-Bx	NOR-Bx	NOR-Bx	NOR-Bx	NOR-Bx	NOR-Bx
Lithological Domain	Norite	Norite	Norite	Norite	Norite	Norite	Norite	Norite	Norite	Norite	Norite	Norite	Norite
Al2O3 (%)	13.85	13.7	13.65	13.9	12.1	16.75	14.6	12.75	14.65	15.4	15.75	19.1	12.3
CaO (%)	8.94	8.94	9.11	9.03	8.48	10.2	9.47	8.68	9.49	9.69	10.1	11.05	7.74
Cr2O3 (%)	0.051	0.05	0.052	0.051	0.052	0.036	0.032	0.046	0.035	0.044	0.038	0.031	0.049
Fe2O3 (%)	9.25	9.3	9.32	9.44	10.55	7.45	11.25	10.35	9.88	8.86	8.57	7.42	11.5
K2O (%)	0.19	0.14	0.12	0.16	0.19	0.53	0.35	0.29	0.44	0.21	0.22	0.22	0.2
MgO (%)	13.65	13.8	13.85	13.85	14.2	8.78	9.94	11.65	11.7	11.55	10.7	8.62	14.25
MnO (%)	0.16	0.16	0.16	0.16	0.17	0.11	0.15	0.16	0.16	0.14	0.14	0.12	0.18
Na2O (%)	1.34	1.34	1.33	1.37	1.22	1.88	1.73	1.45	1.73	1.62	1.72	2.06	1.22
P2O5 (%)	0.02	0.01	0.01	0.02	0.005	0.01	0.01	0.01	0.005	0.005	0.005	0.01	0.01
SiO2 (%)	52.3	52.4	52.4	52.9	51.5	51.5	50.6	51.4	51.6	50.7	51.1	51.7	51.8
TiO2 (%)	0.11	0.12	0.12	0.12	0.13	0.12	0.25	0.14	0.14	0.12	0.12	0.1	0.13
LOI (%)	1.24	0.94	0.81	0.65	1.25	1.88	1.94	1.64	2.12	1.78	1.59	1.49	1.2
Total (%)	101.12	100.91	100.94	101.67	99.86	99.28	100.34	98.59	101.97	100.13	100.07	101.95	100.6
Ag (ppm)	0.25	0.25	0.25	0.25	0.25	0.25	1	0.25	0.25	0.25	0.25	0.25	0.25
As (ppm)	0.05	0.1	0.3	0.3	0.2	0.7	0.5	0.3	0.5	0.4	0.2	0.4	0.4
Au (ppm)	0.025	0.024	0.025	0.025	0.095	0.111	1.54	0.231	0.106	0.085	0.095	0.109	0.171
Ba (ppm)	49.1	42.5	37.6	48.5	47	114.5	90.5	64.3	67	60.7	54.7	64.9	47.5
Bi (ppm)	0.01	0.01	0.01	0.01	0.04	0.11	0.24	0.05	0.08	0.04	0.05	0.07	0.06
Cd (ppm)	0.6	0.5	0.6	0.25	0.6	0.5	0.9	0.6	0.25	0.7	0.6	0.25	0.7
Ce (ppm)	2.4	2.3	2	2	2.3	4.1	5	3.4	3.6	2.3	2.4	1.9	2.2
Co (ppm)	71	74	75	75	82	61	167	78	72	68	71	59	93
Cs (ppm)	0.95	0.89	0.48	0.7	0.94	1.54	1.21	1.12	1.43	1.21	1.01	1.12	0.81
Cu (ppm)	176	161	160	181	496	965	2200	700	501	495	702	617	671
Dy (ppm)	0.46	0.39	0.41	0.41	0.41	0.58	0.71	0.42	0.45	0.47	0.44	0.35	0.39
Er (ppm)	0.29	0.26	0.28	0.36	0.36	0.36	0.48	0.32	0.37	0.23	0.34	0.16	0.3
Eu (ppm)	0.16	0.14	0.16	0.16	0.15	0.18	0.21	0.13	0.12	0.14	0.14	0.17	0.16
Ga (ppm)	11.5	10.7	11.5	11.2	10.4	12.8	13	11.4	10.8	10.7	11.9	13.2	10
Gd (ppm)	0.32	0.31	0.26	0.25	0.31	0.34	0.55	0.35	0.41	0.27	0.39	0.4	0.26
Ge (ppm)	2.5	2.5	2.5	2.5	2.5	2.5	2.5	2.5	2.5	2.5	2.5	2.5	2.5
Hf (ppm)	0.2	0.2	0.2	0.2	0.2	0.4	0.6	0.3	0.3	0.2	0.3	0.2	0.2
Hg (ppb)	0.0025	0.0025	0.0025	0.0025	0.0025	0.0025	0.0025	0.0025	0.0025	0.0025	0.0025	0.0025	0.0025
Ho (ppm)	0.06	0.08	0.09	0.08	0.09	0.12	0.13	0.11	0.11	0.09	0.08	0.07	0.07
In (ppm)	0.0025	0.0025	0.0025	0.0025	0.005	0.005	0.015	0.005	0.0025	0.0025	0.006	0.0025	0.006
La (ppm)	1.2	1.2	0.9	1	1.2	2.1	2.5	1.9	1.8	1.2	1.1	1.1	1
Li (ppm)	5	5	5	5	10	10	10	10	10	10	10	10	10
Lu (ppm)	0.05	0.05	0.04	0.05	0.06	0.06	0.08	0.05	0.05	0.04	0.05	0.04	0.04
Mo (ppm)	0.5	1	1	0.5	0.5	1	0.5	1	1	1	1	1	0.5
Nb (ppm)	0.1	0.1	0.1	0.1	0.1	0.4	0.7	0.2	0.5	0.1	0.1	0.1	0.2
Ni (ppm)	465	454	466	468	709	675	3680	792	777	620	713	558	923
Nd (ppm)	1	1.2	1.1	1	1	2	2.3	1.6	1.6	1.2	1.2	1	0.8
Pb (ppm)	1	3	7	4	2	4	6	2	2	2	4	2	3
Pd (ppm)	0.2	0.177	0.17	0.225	1.46	1.04	5.74	1.72	1.325	0.578	0.442	0.72	1.435
Pr (ppm)	0.27	0.26	0.26	0.24	0.3	0.51	0.6	0.41	0.45	0.24	0.3	0.25	0.28
Pt (ppm)	0.036	0.035	0.033	0.037	0.25	0.178	0.596	0.211	0.176	0.072	0.063	0.122	0.15
Rb (ppm)	4.4	2.9	2.1	3.5	4.5	13	8.7	6.3	10.5	4.8	4.8	4.6	4.2
Re (ppm)	0.0005	0.0005	0.0005	0.001	0.001	0.001	0.003	0.001	0.001	0.001	0.001	0.001	0.001
S (%)	0.05	0.04	0.04	0.04	0.13	0.17	1.25	0.2	0.11	0.14	0.18	0.16	0.2
Sb (ppm)	0.025	0.025	0.025	0.025	0.025	0.025	0.05	0.025	0.025	0.025	0.025	0.025	0.025
Sc (ppm)	31	34	34	35	38	26	28	29	25	24	27	20	29
Se (ppm)	0.411	0.328	0.333	0.332	1.08	1.355	7.1	1.69	1.07	1.12	1.465	1.275	1.64
Sm (ppm)	0.17	0.27	0.21	0.25	0.33	0.29	0.56	0.31	0.32	0.21	0.27	0.17	0.18
Sn (ppm)	0.5	0.5	0.5	0.5	1	1	1	0.5	1	0.5	0.5	0.5	0.5
Sr (ppm)	151	148	152.5	157.5	140	199.5	182.5	152.5	140	157	185.5	237	136
Ta (ppm)	0.05	0.05	0.05	0.05	0.05	0.05	0.05	0.05	0.05	0.05	0.05	0.05	0.05
Tb (ppm)	0.07	0.05	0.05	0.04	0.04	0.07	0.12	0.06	0.06	0.04	0.06	0.03	0.06
Te (ppm)	0.11	0.12	0.11	0.15	0.42	0.36	1.7	0.31	0.41	0.2	0.26	0.31	0.44
Th (ppm)	0.19	0.17	0.13	0.13	0.15	0.82	0.43	0.57	1.13	0.49	0.11	0.08	0.14
Tl (ppm)	0.01	0.02	0.01	0.01	0.02	0.02	0.07	0.02	0.03	0.02	0.02	0.02	0.03
Tm (ppm)	0.04	0.05	0.04	0.04	0.05	0.06	0.07	0.05	0.05	0.04	0.05	0.04	0.04
V (ppm)	109	112	115	122	132	104	181	140	124	112	120	97	124
Y (ppm)	2.4	2.4	2.3	2.4	2.7	3	3.8	2.6	2.8	2.2	2.4	1.9	2.3
U (ppm)	0.025	0.025	0.025	0.025	0.06	0.28	0.19	0.53	0.41	0.07	0.06	0.025	0.06
W (ppm)	1	2	2	2	2	3	1	2	2	4	2	3	2
Yb (ppm)	0.31	0.28	0.31	0.26	0.3	0.37	0.44	0.39	0.29	0.21	0.24	0.25	0.31
Zr (ppm)	6	7	6	7	7	12	23	10	7	6	7	5	6
Zn (ppm)	54	56	56	58	65	45	56	61	55	50	51	44	69

Drill hole #	18-805	18-805	18-805	18-805	18-805	18-805	18-805	18-805	18-805	18-805	18-805	18-805	18-805
Depth From	236	237	238	239	240	241	242	243	244	246	247	248	249
Depth To	237	238	239	240	241	242	243	244	245	247	248	249	250
Rock Type	NOR-Bx	NOR-Bx	NOR-Bx	NOR-Bx	NOR-Bx	NOR-Bx	NOR-Bx	NOR-Bx	NOR-Bx	NOR-Bx	NOR-Bx	NOR-Bx	NOR-Bx
Lithological Domain	Norite	Norite	Norite	Norite	Norite	Norite	Norite	Norite	Norite	Norite	Norite	Norite	Norite
Al2O3 (%)	13.3	14.9	15.95	17.35	17.95	15.35	16.35	16.2	15.4	16	20.1	10.2	14
CaO (%)	8.2	8.28	8.69	9.41	10.4	9.8	9.6	9.6	9.57	9.21	10.4	5.91	8.46
Cr2O3 (%)	0.04	0.041	0.038	0.035	0.028	0.031	0.038	0.038	0.038	0.041	0.029	0.054	0.045
Fe2O3 (%)	11.25	9.44	8.91	8.35	7.46	8.41	8	8.44	9.51	8.82	6.03	12.55	10.6
K2O (%)	0.2	0.22	0.17	0.21	0.21	0.36	0.23	0.23	0.17	0.3	0.25	0.22	0.22
MgO (%)	13.15	12.75	12	11.05	9.34	9.77	11.15	11.45	11.6	11.65	7.85	15.4	12.9
MnO (%)	0.18	0.16	0.15	0.14	0.12	0.13	0.14	0.14	0.15	0.14	0.1	0.19	0.16
Na2O (%)	1.35	1.42	1.49	1.71	1.96	1.88	1.75	1.58	1.54	1.54	2.28	1.17	1.5
P2O5 (%)	0.005	0.005	0.005	0.01	0.01	0.005	0.005	0.01	0.005	0.01	0.01	0.005	0.005
SiO2 (%)	49.3	49.3	49.1	51.1	49.2	51.4	50.6	50.5	50.7	50.5	50.5	51.7	51
TiO2 (%)	0.15	0.1	0.11	0.11	0.12	0.13	0.11	0.11	0.14	0.12	0.09	0.15	0.14
LOI (%)	1.76	1.61	1.36	1.25	1.6	1.75	1.84	1.46	1.42	2.13	1.71	2.05	1.91
Total (%)	98.9	98.24	98	100.76	98.43	99.04	99.84	99.79	100.27	100.49	99.39	99.61	100.97
Ag (ppm)	0.25	0.25	0.25	0.25	0.25	0.25	0.25	0.25	0.25	0.25	0.25	0.25	0.25
As (ppm)	0.9	0.5	0.3	0.2	0.2	0.7	0.1	0.3	1.4	0.2	0.5	0.4	0.2
Au (ppm)	0.141	0.075	0.059	0.046	0.058	0.098	0.007	0.01	0.084	0.049	0.035	0.273	0.213
Ba (ppm)	102	55.7	41.2	45.4	52.5	73.3	58	40.3	43.2	63.6	68.1	56.5	51.2
Bi (ppm)	0.06	0.04	0.02	0.02	0.03	0.04	0.01	0.01	0.03	0.02	0.02	0.14	0.1
Cd (ppm)	0.7	0.25	0.25	0.25	0.5	0.5	0.25	0.25	0.25	0.6	0.25	0.7	0.5
Ce (ppm)	2.9	2.4	1.8	1.9	2.2	4	2.8	1.8	2.1	1.9	2	3.9	2.2
Co (ppm)	84	73	70	60	58	61	55	58	67	63	43	99	85
Cs (ppm)	0.85	1.1	0.81	0.79	0.97	1.19	1.16	0.72	0.72	1.26	1.19	1.2	0.89
Cu (ppm)	902	289	315	190	280	425	60	81	363	266	293	1310	1190
Dy (ppm)	0.44	0.29	0.31	0.28	0.39	0.49	0.47	0.31	0.42	0.39	0.25	0.43	0.41
Er (ppm)	0.27	0.26	0.24	0.27	0.25	0.41	0.28	0.25	0.29	0.29	0.18	0.39	0.36
Eu (ppm)	0.17	0.14	0.15	0.13	0.18	0.18	0.16	0.13	0.19	0.17	0.16	0.13	0.17
Ga (ppm)	11.7	12.5	12	13.5	13.4	12	13.5	12.6	11.9	12	12.4	9.8	11.1
Gd (ppm)	0.46	0.25	0.25	0.28	0.34	0.43	0.29	0.28	0.39	0.28	0.22	0.36	0.39
Ge (ppm)	2.5	2.5	2.5	2.5	2.5	2.5	2.5	2.5	2.5	2.5	2.5	2.5	2.5
Hf (ppm)	0.2	0.4	0.1	0.1	0.1	0.3	0.3	0.1	0.2	0.1	0.1	0.3	0.3
Hg (ppb)	0.01	0.0025	0.006	0.0025	0.0025	0.0025	0.0025	0.0025	0.0025	0.0025	0.0025	0.0025	0.0025
Ho (ppm)	0.08	0.08	0.06	0.06	0.09	0.08	0.08	0.06	0.09	0.09	0.05	0.1	0.08
In (ppm)	0.009	0.005	0.005	0.0025	0.0025	0.005	0.0025	0.0025	0.0025	0.0025	0.0025	0.01	0.007
La (ppm)	1.5	1.2	1	1.1	1.3	2.1	1.5	0.9	1.1	1	1.1	1.9	1.1
Li (ppm)	10	10	10	10	10	10	10	10	10	10	10	10	10
Lu (ppm)	0.06	0.05	0.04	0.04	0.05	0.06	0.05	0.03	0.05	0.05	0.03	0.07	0.08
Mo (ppm)	0.5	0.5	1	1	0.5	0.5	0.5	0.5	0.5	0.5	1	0.5	3
Nb (ppm)	0.9	0.6	0.3	0.3	0.3	0.8	0.4	0.1	0.1	0.1	0.1	0.6	0.2
Ni (ppm)	850	582	522	424	500	539	301	315	520	416	340	1330	1060
Nd (ppm)	1.5	0.9	1	1	1.2	1.9	1.4	0.9	1.1	0.9	0.8	1.6	1.3
Pb (ppm)	3	5	2	1	2	3	1	1	3	4	2	5	3
Pd (ppm)	1.33	0.923	0.566	0.521	0.812	1.035	0.073	0.101	1.1	0.399	0.157	2.84	1.965
Pr (ppm)	0.35	0.32	0.2	0.25	0.3	0.46	0.32	0.24	0.24	0.22	0.25	0.49	0.3
Pt (ppm)	0.162	0.115	0.072	0.057	0.099	0.12	0.014	0.018	0.11	0.048	0.021	0.338	0.197
Rb (ppm)	4.4	4.9	3.2	3.5	4	8	5	3.1	2.8	6.3	5.3	4.9	4.7
Re (ppm)	0.001	0.001	0.0005	0.0005	0.0005	0.001	0.001	0.0005	0.001	0.0005	0.001	0.002	0.002
S (%)	0.26	0.06	0.09	0.06	0.09	0.14	0.03	0.04	0.13	0.08	0.07	0.41	0.4
Sb (ppm)	0.05	0.025	0.025	0.025	0.025	0.025	0.025	0.025	0.025	0.025	0.025	0.025	0.025
Sc (ppm)	28	23	22	21	24	29	19	22	26	23	16	34	28
Se (ppm)	1.79	0.667	0.651	0.386	0.727	0.984	0.103	0.153	0.88	0.516	0.5	3.19	2.84
Sm (ppm)	0.33	0.22	0.17	0.18	0.3	0.43	0.17	0.16	0.28	0.23	0.17	0.48	0.26
Sn (ppm)	0.5	0.5	0.5	0.5	0.5	1	1	0.5	0.5	0.5	0.5	0.5	0.5
Sr (ppm)	151	166.5	174	190	208	178	201	171	165.5	179	241	116.5	161
Ta (ppm)	0.05	0.05	0.05	0.05	0.05	0.1	0.05	0.05	0.05	0.05	0.05	0.1	0.05
Tb (ppm)	0.07	0.04	0.03	0.05	0.06	0.07	0.05	0.05	0.05	0.04	0.03	0.07	0.07
Te (ppm)	0.4	0.2	0.18	0.15	0.2	0.26	0.05	0.05	0.21	0.11	0.13	0.97	0.64
Th (ppm)	0.3	0.2	0.1	0.11	0.1	0.3	0.24	0.11	0.09	0.06	0.14	0.55	0.14
Tl (ppm)	0.03	0.03	0.02	0.01	0.01	0.02	0.02	0.01	0.01	0.02	0.01	0.05	0.02
Tm (ppm)	0.05	0.05	0.04	0.03	0.05	0.04	0.04	0.04	0.05	0.05	0.04	0.05	0.05
V (ppm)	147	106	101	92	104	118	105	98	121	106	67	136	125
Y (ppm)	2.6	2	1.7	1.8	2.3	3	2.4	2	2.4	2.3	1.6	2.8	2.6
U (ppm)	0.1	0.23	0.025	0.05	0.07	0.1	0.1	0.025	0.025	0.025	0.06	0.16	0.06
W (ppm)	0.5	0.5	0.5	0.5	0.5	1	0.5	0.5	1	0.5	0.5	0.5	0.5
Yb (ppm)	0.35	0.31	0.22	0.2	0.3	0.38	0.36	0.23	0.29	0.23	0.22	0.4	0.36
Zr (ppm)	6	17	5	6	6	11	9	5	6	5	4	14	11
Zn (ppm)	66	60	56	49	42	49	48	52	54	51	33	67	56

Drill hole #	18-805	18-805	18-805	18-805	18-805	18-805	18-805	18-805	18-805	18-805	18-805	18-805	18-805
Depth From	250	251	252	253	254	255	256	257	258	259	260	261	262
Depth To	251	252	253	254	255	256	257	258	259	260	261	262	263
Rock Type	NOR-Bx	NOR-Bx	NOR-Bx	NOR-Bx	NOR-Bx	NOR-Bx	NOR-Bx	NOR-Bx	NOR-Bx	NOR-Bx	NOR-Bx	NOR-Bx	NOR-Bx
Lithological Domain	Norite	Norite	Norite	Norite	Norite	Norite	Norite	Norite	Norite	Norite	Norite	Norite	Norite
Al2O3 (%)	22.1	17.95	14.5	19.05	21.4	16.65	16.75	18.55	13.6	10.4	13.3	13.65	11.25
CaO (%)	10.95	9.69	8.79	9.95	11	9.3	9.62	10.15	8.48	7.61	10.3	10.05	8.5
Cr2O3 (%)	0.027	0.033	0.037	0.035	0.028	0.042	0.041	0.037	0.053	0.062	0.042	0.038	0.058
Fe2O3 (%)	5.32	8.33	10.35	7.45	5.81	8.7	8.72	7.76	10.1	12.5	10.7	10.15	10.9
K2O (%)	0.4	0.24	0.13	0.18	0.27	0.25	0.21	0.23	0.33	0.27	0.11	0.12	0.1
MgO (%)	7.12	9.45	12.55	9.75	7.42	10.85	11.1	10.25	13.55	16.05	11.7	11.75	14.6
MnO (%)	0.09	0.12	0.16	0.12	0.1	0.14	0.14	0.13	0.16	0.2	0.16	0.16	0.18
Na2O (%)	2.7	2.12	1.58	2.11	2.65	1.96	1.75	1.95	1.43	0.98	1.53	1.57	1.21
P2O5 (%)	0.005	0.01	0.005	0.01	0.005	0.005	0.01	0.005	0.01	0.01	0.01	0.01	0.02
SiO2 (%)	50.7	51.1	49.8	50.2	50.9	51	49.1	50.6	50.7	49.4	50.9	51.5	51.4
TiO2 (%)	0.07	0.12	0.13	0.08	0.08	0.1	0.1	0.1	0.11	0.16	0.19	0.14	0.14
LOI (%)	1.89	1.81	1.48	1.93	1.65	1.81	1.94	1.36	1.53	0.98	1.28	0.91	0.89
Total (%)	101.41	101	99.53	100.9	101.35	100.83	99.5	101.15	100.08	98.64	100.23	100.06	99.26
Ag (ppm)	0.25	0.25	0.25	0.25	0.25	0.25	0.25	0.25	0.25	0.25	0.7	0.25	0.25
As (ppm)	0.2	0.4	0.2	0.6	0.1	0.1	0.2	0.3	0.2	0.1	0.5	0.4	0.3
Au (ppm)	0.012	0.138	0.091	0.052	0.019	0.06	0.075	0.028	0.037	0.167	0.224	0.182	0.087
Ba (ppm)	75.2	44.1	41.2	50	60	46.7	48.7	46.3	47	50.7	39.1	36.7	34.8
Bi (ppm)	0.03	0.06	0.06	0.04	0.02	0.07	0.06	0.03	0.03	0.07	0.14	0.08	0.04
Cd (ppm)	0.25	0.25	0.8	0.25	0.25	0.25	0.25	0.25	0.25	0.7	0.7	0.25	0.6
Ce (ppm)	2.2	2.2	2.4	1.6	2.5	3	1.9	2.2	1.8	2.6	2.6	1.9	3
Co (ppm)	36	60	83	55	44	66	71	56	71	99	92	79	82
Cs (ppm)	1.45	0.95	0.53	1.06	1.05	1.27	1.1	0.8	1.18	0.86	0.33	0.36	0.53
Cu (ppm)	158	666	913	467	272	378	675	316	245	889	1800	828	445
Dy (ppm)	0.28	0.43	0.37	0.22	0.29	0.34	0.25	0.32	0.31	0.55	0.63	0.5	0.55
Er (ppm)	0.23	0.3	0.38	0.18	0.24	0.28	0.23	0.21	0.29	0.34	0.44	0.39	0.32
Eu (ppm)	0.18	0.16	0.18	0.18	0.19	0.14	0.18	0.16	0.15	0.16	0.2	0.18	0.18
Ga (ppm)	14.6	13.8	11.9	13.5	14.7	12	13.9	13.4	11.5	10.1	10.3	10.6	11
Gd (ppm)	0.23	0.34	0.39	0.19	0.33	0.35	0.26	0.28	0.29	0.38	0.46	0.4	0.41
Ge (ppm)	2.5	2.5	2.5	2.5	2.5	2.5	2.5	2.5	2.5	2.5	2.5	2.5	2.5
Hf (ppm)	0.1	0.2	0.2	0.1	0.1	0.1	0.1	0.1	0.1	0.1	0.3	0.2	0.2
Hg (ppb)	0.0025	0.0025	0.0025	0.0025	0.0025	0.0025	0.0025	0.0025	0.0025	0.0025	0.0025	0.0025	0.0025
Ho (ppm)	0.05	0.09	0.09	0.05	0.07	0.06	0.05	0.08	0.09	0.1	0.14	0.11	0.1
In (ppm)	0.0025	0.007	0.007	0.0025	0.0025	0.0025	0.005	0.0025	0.0025	0.008	0.015	0.006	0.0025
La (ppm)	1.2	1.1	1.2	0.9	1.4	1.5	1	1.2	1	1.1	1.2	0.9	1.5
Li (ppm)	10	10	10	10	10	10	10	10	10	10	10	5	10
Lu (ppm)	0.03	0.06	0.06	0.04	0.04	0.05	0.05	0.03	0.04	0.05	0.06	0.06	0.07
Mo (ppm)	2	1	1	0.5	0.5	1	1	1	0.5	1	1	1	1
Nb (ppm)	0.1	0.1	0.2	0.1	0.1	0.2	0.1	0.1	0.1	0.3	0.2	0.1	0.3
Ni (ppm)	267	623	1000	599	384	727	788	468	558	1170	1220	822	675
Nd (ppm)	1.1	1.1	1.1	0.7	0.9	1.2	0.9	0.9	0.9	1.3	1.5	1.1	1.6
Pb (ppm)	2	2	3	2	6	2	4	4	6	4	6	8	5
Pd (ppm)	0.21	1.145	0.951	0.663	0.209	0.722	0.872	0.604	0.441	2.4	1.795	1.29	0.974
Pr (ppm)	0.23	0.29	0.33	0.18	0.26	0.39	0.23	0.3	0.24	0.3	0.34	0.25	0.39
Pt (ppm)	0.019	0.14	0.096	0.074	0.036	0.086	0.101	0.079	0.052	0.217	0.183	0.145	0.128
Rb (ppm)	10.6	4.4	2.2	4.4	6.5	4.7	4.7	5.2	7.9	7.2	1.8	1.7	1.5
Re (ppm)	0.001	0.001	0.001	0.001	0.0005	0.0005	0.001	0.0005	0.0005	0.002	0.002	0.002	0.001
S (%)	0.03	0.23	0.39	0.18	0.08	0.08	0.19	0.09	0.05	0.24	0.59	0.34	0.16
Sb (ppm)	0.025	0.025	0.025	0.025	0.025	0.025	0.025	0.07	0.025	0.025	0.025	0.025	0.025
Sc (ppm)	14	20	26	18	17	25	27	22	30	41	39	37	40
Se (ppm)	0.168	1.475	2.32	1.18	0.541	0.734	1.53	0.607	0.422	2.4	3.74	1.935	1.095
Sm (ppm)	0.28	0.24	0.28	0.13	0.25	0.18	0.26	0.2	0.21	0.38	0.48	0.39	0.42
Sn (ppm)	0.5	0.5	0.5	0.5	0.5	0.5	0.5	0.5	0.5	0.5	0.5	0.5	0.5
Sr (ppm)	290	225	177.5	249	287	207	201	227	166.5	109.5	157.5	158	132
Ta (ppm)	0.05	0.05	0.05	0.05	0.05	0.05	0.05	0.05	0.05	0.05	0.05	0.05	0.05
Tb (ppm)	0.03	0.07	0.05	0.04	0.05	0.05	0.04	0.05	0.04	0.07	0.1	0.08	0.07
Te (ppm)	0.12	0.48	0.52	0.3	0.12	0.33	0.36	0.16	0.12	0.43	1.03	0.45	0.35
Th (ppm)	0.07	0.07	0.15	0.06	0.07	0.26	0.1	0.06	0.08	0.11	0.13	0.09	0.3
Tl (ppm)	0.01	0.02	0.01	0.01	0.01	0.02	0.02	0.02	0.03	0.04	0.01	0.01	0.01
Tm (ppm)	0.04	0.05	0.05	0.04	0.03	0.04	0.04	0.03	0.04	0.07	0.07	0.05	0.07
V (ppm)	61	95	130	85	69	96	112	101	122	166	149	128	135
Y (ppm)	1.5	2.6	2.3	1.7	1.9	1.9	2	1.9	2.2	3.1	3.4	2.8	3
U (ppm)	0.07	0.05	0.025	0.025	0.025	0.1	0.05	0.08	0.08	0.07	0.05	0.025	0.025
W (ppm)	0.5	8	0.5	0.5	0.5	1	0.5	0.5	0.5	0.5	1	1	1
Yb (ppm)	0.19	0.31	0.33	0.22	0.22	0.27	0.31	0.29	0.28	0.43	0.39	0.41	0.34
Zr (ppm)	4	5	6	4	4	5	5	4	5	7	7	5	6
Zn (ppm)	27	43	56	36	30	50	48	43	55	71	58	56	64

Drill hole #	18-805	18-805	18-805	18-805	18-805	18-805	18-805	18-805	18-805	18-805	18-805	18-805	18-805
Depth From	263	264	265	266	267	268	269	270	271	272	273	274	275
Depth To	264	265	266	267	268	269	270	271	272	273	274	275	276
Rock Type	NOR-Bx	NOR-Bx	NOR-Bx	NOR-Bx	NOR-Bx	NOR-Bx	NOR-Bx	NOR-Bx	NOR-Bx	NOR-Bx	NOR-Bx	NOR-Bx	NOR-Bx
Lithological Domain	Norite	Norite	Norite	Norite	Norite	Norite	Norite	Norite	Norite	Norite	Norite	Norite	Norite
Al2O3 (%)	7.56	11.1	15.25	17.5	19.65	17.2	18.6	16.85	17.15	17.15	13.3	9.75	17.05
CaO (%)	6.14	7.57	9.77	10.95	11.7	10.6	11.5	10.75	11.45	10.85	9.31	7.26	10.55
Cr2O3 (%)	0.074	0.053	0.04	0.027	0.023	0.025	0.02	0.024	0.024	0.025	0.039	0.049	0.038
Fe2O3 (%)	14.35	12.3	9.19	6.49	5.42	7.73	6.5	8.03	7.25	7.74	10.7	13.35	8.04
K2O (%)	0.09	0.18	0.12	0.19	0.12	0.13	0.13	0.14	0.11	0.14	0.12	0.09	0.1
MgO (%)	18.1	14.4	10.7	8.33	7.07	9.68	7.54	9.41	9.25	9.48	13	15.45	10.3
MnO (%)	0.22	0.19	0.14	0.11	0.09	0.13	0.11	0.12	0.12	0.12	0.16	0.2	0.13
Na2O (%)	0.73	1.24	1.73	2.09	2.35	2.02	2.28	2.11	2.17	2.1	1.52	1.03	1.97
P2O5 (%)	0.01	0.005	0.01	0.01	0.005	0.005	0.005	0.005	0.01	0.005	0.005	0.01	0.01
SiO2 (%)	51.8	52.1	50.5	51.5	50.7	51.1	50.7	51.1	52.6	51	51.1	51.1	52.6
TiO2 (%)	0.16	0.15	0.12	0.09	0.08	0.11	0.1	0.11	0.1	0.11	0.13	0.16	0.11
LOI (%)	0.75	1.38	1.43	1.59	1.36	1.18	1.41	1.41	1.07	1.28	1.14	1.05	1.06
Total (%)	99.98	100.67	99.02	98.91	98.6	99.93	98.91	100.07	101.32	100.04	100.54	99.51	101.98
Ag (ppm)	0.25	0.25	0.25	0.25	0.25	0.25	0.25	0.25	0.25	0.25	0.25	0.25	0.25
As (ppm)	0.4	0.3	0.4	0.1	0.3	0.05	0.1	0.3	0.1	0.2	0.3	0.3	0.6
Au (ppm)	0.464	0.241	0.178	0.013	0.01	0.048	0.038	0.056	0.021	0.042	0.165	0.216	0.069
Ba (ppm)	29.8	41.7	41.7	45.9	48.2	39.3	45.9	41.9	44.2	42.5	32.9	24.7	45.1
Bi (ppm)	0.1	0.12	0.1	0.02	0.01	0.03	0.03	0.03	0.03	0.04	0.11	0.13	0.06
Cd (ppm)	1	0.25	0.25	0.25	0.25	0.25	0.25	0.25	0.5	0.25	0.5	0.7	0.25
Ce (ppm)	2	2.9	1.9	4.3	2.2	1.6	2	2	1.9	1.9	1.7	1.6	2.1
Co (ppm)	114	96	76	48	39	55	48	65	58	63	92	111	61
Cs (ppm)	0.4	0.74	0.61	1.02	0.63	0.39	0.55	0.56	0.53	0.91	0.76	0.94	1.17
Cu (ppm)	1090	1270	972	206	134	341	457	662	293	514	1150	1230	447
Dy (ppm)	0.51	0.56	0.43	0.72	0.33	0.41	0.44	0.45	0.43	0.4	0.53	0.48	0.4
Er (ppm)	0.34	0.34	0.25	0.42	0.27	0.28	0.24	0.28	0.37	0.26	0.32	0.3	0.28
Eu (ppm)	0.11	0.14	0.15	0.23	0.2	0.12	0.15	0.2	0.2	0.19	0.16	0.14	0.14
Ga (ppm)	10.7	9.9	12.2	13.2	13.7	12.6	14	12.5	13.7	11.5	10.2	9	12.7
Gd (ppm)	0.35	0.34	0.4	0.62	0.28	0.28	0.39	0.28	0.37	0.28	0.34	0.35	0.26
Ge (ppm)	2.5	2.5	2.5	2.5	2.5	2.5	2.5	2.5	2.5	2.5	2.5	2.5	2.5
Hf (ppm)	0.2	0.2	0.1	0.3	0.1	0.1	0.1	0.1	0.1	0.1	0.1	0.1	0.1
Hg (ppb)	0.0025	0.0025	0.016	0.012	0.008	0.015	0.011	0.008	0.0025	0.006	0.0025	0.0025	0.005
Ho (ppm)	0.11	0.14	0.11	0.12	0.09	0.07	0.1	0.1	0.09	0.09	0.09	0.11	0.09
In (ppm)	0.008	0.009	0.006	0.0025	0.0025	0.0025	0.0025	0.0025	0.0025	0.0025	0.005	0.008	0.0025
La (ppm)	0.9	1.6	1	2.1	1	0.8	1	1	0.9	0.9	0.8	0.6	1
Li (ppm)	5	10	10	10	10	10	10	10	10	10	10	10	10
Lu (ppm)	0.07	0.06	0.07	0.05	0.04	0.05	0.03	0.05	0.04	0.06	0.04	0.07	0.05
Mo (ppm)	0.5	1	1	1	1	1	0.5	0.5	1	1	1	0.5	2
Nb (ppm)	0.2	0.1	0.1	1	0.1	0.1	0.1	0.1	0.1	0.1	0.1	0.1	0.1
Ni (ppm)	1330	1270	863	273	194	362	380	576	345	499	1040	1190	488
Nd (ppm)	1.1	1.6	1.3	2.1	1	1	1	1.1	1	1.2	0.9	1.2	0.9
Pb (ppm)	4	3	4	5	5	4	5	6	4	4	4	3	2
Pd (ppm)	3.55	2.51	1.665	0.122	0.049	0.284	0.266	0.371	0.249	0.301	1.51	2.36	0.826
Pr (ppm)	0.25	0.35	0.27	0.52	0.23	0.23	0.27	0.25	0.25	0.23	0.26	0.17	0.2
Pt (ppm)	0.41	0.261	0.19	0.013	0.0025	0.034	0.031	0.041	0.042	0.025	0.147	0.256	0.086
Rb (ppm)	2	5.1	3.1	8.5	3	1.5	1.5	1.6	0.9	1.6	1.3	1.4	1.1
Re (ppm)	0.001	0.002	0.002	0.0005	0.0005	0.001	0.0005	0.001	0.001	0.001	0.002	0.002	0.0005
S (%)	0.41	0.43	0.31	0.07	0.05	0.13	0.14	0.3	0.17	0.24	0.46	0.49	0.15
Sb (ppm)	0.025	0.025	0.025	0.025	0.025	0.025	0.025	0.025	0.025	0.025	0.025	0.025	0.025
Sc (ppm)	44	37	29	25	19	26	22	30	28	28	36	42	27
Se (ppm)	3.09	3.01	2.07	0.264	0.19	0.639	0.741	1.31	0.699	1.065	2.38	3.35	1.01
Sm (ppm)	0.32	0.34	0.25	0.41	0.32	0.24	0.19	0.21	0.26	0.29	0.28	0.38	0.35
Sn (ppm)	0.5	0.5	0.5	0.5	0.5	0.5	0.5	0.5	0.5	0.5	0.5	0.5	1
Sr (ppm)	81	129	203	230	271	209	254	220	237	219	154.5	109.5	222
Ta (ppm)	0.1	0.05	0.05	0.1	0.05	0.05	0.05	0.05	0.05	0.05	0.05	0.05	0.05
Tb (ppm)	0.07	0.08	0.06	0.1	0.06	0.06	0.05	0.07	0.08	0.05	0.07	0.06	0.07
Te (ppm)	0.86	0.89	0.53	0.04	0.02	0.08	0.12	0.13	0.08	0.13	0.53	0.67	0.21
Th (ppm)	0.12	0.18	0.07	0.67	0.13	0.08	0.06	0.07	0.05	0.06	0.06	0.07	0.06
Tl (ppm)	0.02	0.03	0.01	0.02	0.01	0.01	0.01	0.01	0.01	0.01	0.02	0.01	0.01
Tm (ppm)	0.06	0.07	0.04	0.06	0.03	0.04	0.04	0.04	0.04	0.03	0.04	0.07	0.05
V (ppm)	159	137	113	87	73	95	92	102	100	94	123	148	100
Y (ppm)	3	3	2.3	3.6	2.2	2	2.1	2.3	2.6	2.5	2.4	2.8	2.3
U (ppm)	0.025	0.05	0.025	0.44	0.025	0.025	0.025	0.025	0.025	0.025	0.025	0.025	0.025
W (ppm)	2	3	2	4	4	1	3	2	10	1	1	1	1
Yb (ppm)	0.4	0.41	0.25	0.47	0.31	0.22	0.31	0.27	0.29	0.29	0.33	0.39	0.26
Zr (ppm)	6	9	5	7	5	4	5	5	6	5	5	5	5
Zn (ppm)	83	67	51	33	29	41	36	41	40	42	57	79	46

Drill hole #	18-805	18-805	18-805	18-805	18-805	18-805	18-805	18-805	18-805	18-805	18-805	18-805	18-805
Depth From	276	277	278	279	280	281	282	283	284	285	286	287	288
Depth To	277	278	279	280	281	282	283	284	285	286	287	288	289
Rock Type	NOR-Bx	NOR-Bx	NOR-Bx	NOR-Bx	NOR-Bx	NOR-Bx	NOR-Bx	NOR-Bx	NOR-Bx	NOR-Bx	NOR-Bx	NOR-Bx	NOR-Bx
Lithological Domain	Norite	Norite	Norite	Norite	Norite	Norite	Norite	Norite	Norite	Norite	Norite	Norite	Norite
Al2O3 (%)	15.75	16.35	19.1	19.65	14.7	14.5	13.9	13.65	13.1	12.15	13.85	13.85	13.6
CaO (%)	9.71	10.65	10.95	10.35	8.93	8.47	8	7.93	7.78	7.71	8.49	8.25	8.28
Cr2O3 (%)	0.033	0.034	0.027	0.029	0.039	0.037	0.037	0.036	0.038	0.041	0.038	0.04	0.039
Fe2O3 (%)	8.88	8.19	6.97	6.7	10.6	9.06	8.95	8.71	9.87	11.45	9.6	9.41	9.95
K2O (%)	0.12	0.09	0.11	0.1	0.14	0.14	0.11	0.1	0.14	0.1	0.12	0.09	0.09
MgO (%)	10.9	10.55	8.29	8.47	11.7	12.85	13.05	12.45	13.5	14.35	12.95	13.05	13.45
MnO (%)	0.14	0.13	0.11	0.1	0.16	0.15	0.15	0.15	0.16	0.18	0.16	0.15	0.16
Na2O (%)	1.82	1.87	2.33	2.31	1.69	1.61	1.55	1.85	1.42	1.39	1.61	1.62	1.6
P2O5 (%)	0.005	0.005	0.005	0.005	0.01	0.005	0.01	0.01	0.01	0.02	0.01	0.01	0.01
SiO2 (%)	50.3	51.4	51.9	52.3	51.9	52.3	51.2	50.2	50.9	52	52	51.7	52.1
TiO2 (%)	0.11	0.11	0.1	0.09	0.13	0.1	0.09	0.09	0.1	0.12	0.12	0.11	0.15
LOI (%)	1.15	1.44	1.62	1.81	1.89	2.34	3.07	3.23	2.74	0.58	1.08	0.63	0.7
Total (%)	98.94	100.83	101.55	101.95	101.92	101.59	100.14	98.43	99.77	100.1	100.05	98.93	100.15
Ag (ppm)	0.25	0.25	0.25	0.25	0.25	0.25	0.25	0.25	0.25	0.25	0.25	0.25	0.25
As (ppm)	0.6	0.3	0.4	0.2	0.4	0.4	0.4	0.4	0.5	0.2	0.3	0.1	0.1
Au (ppm)	0.152	0.105	0.066	0.032	0.259	0.042	0.006	0.033	0.017	0.084	0.017	0.008	0.008
Ba (ppm)	43.9	40.3	51	56	45.6	46.9	36.7	36.2	45.1	37.1	46.3	41	40.4
Bi (ppm)	0.1	0.12	0.06	0.02	0.11	0.02	0.01	0.01	0.05	0.06	0.01	0.01	0.01
Cd (ppm)	0.25	0.25	0.25	0.25	0.7	0.25	0.5	0.25	0.25	0.7	0.25	0.6	0.25
Ce (ppm)	2.2	1.9	2	2	1.7	2.1	1.5	1.3	1.7	1.4	1.7	1.7	1.5
Co (ppm)	73	65	53	45	82	67	66	66	86	94	69	68	76
Cs (ppm)	0.87	0.78	1.01	1.07	0.98	1.5	1.06	0.82	1.53	0.74	1.14	0.75	0.96
Cu (ppm)	764	627	462	310	955	263	136	259	906	783	179	167	171
Dy (ppm)	0.39	0.48	0.33	0.27	0.36	0.36	0.29	0.41	0.38	0.42	0.45	0.42	0.42
Er (ppm)	0.31	0.27	0.25	0.24	0.28	0.23	0.26	0.2	0.28	0.25	0.31	0.34	0.31
Eu (ppm)	0.13	0.13	0.21	0.17	0.16	0.14	0.13	0.12	0.16	0.15	0.15	0.14	0.17
Ga (ppm)	11.9	12.5	13.8	14.5	11.6	11	9.7	10.5	10.9	10.6	11.9	11.3	11.2
Gd (ppm)	0.35	0.3	0.29	0.22	0.24	0.24	0.29	0.2	0.26	0.31	0.33	0.3	0.3
Ge (ppm)	2.5	2.5	2.5	2.5	2.5	2.5	2.5	2.5	2.5	2.5	2.5	2.5	2.5
Hf (ppm)	0.1	0.2	0.1	0.1	0.1	0.2	0.1	0.1	0.1	0.1	0.1	0.1	0.1
Hg (ppb)	0.007	0.0025	0.005	0.0025	0.005	0.007	0.0025	0.0025	0.006	0.0025	0.0025	0.007	0.0025
Ho (ppm)	0.08	0.11	0.09	0.05	0.08	0.09	0.08	0.07	0.07	0.09	0.08	0.08	0.08
In (ppm)	0.005	0.0025	0.0025	0.0025	0.008	0.0025	0.0025	0.0025	0.008	0.005	0.0025	0.0025	0.0025
La (ppm)	1.2	0.9	1	1	0.9	1.1	0.7	0.7	0.9	0.7	0.9	0.9	0.8
Li (ppm)	5	10	10	10	10	10	10	10	10	5	5	10	10
Lu (ppm)	0.04	0.05	0.04	0.05	0.05	0.05	0.05	0.04	0.05	0.07	0.04	0.06	0.05
Mo (ppm)	1	0.5	0.5	0.5	1	0.5	1	0.5	0.5	1	1	1	0.5
Nb (ppm)	0.1	0.1	0.1	0.1	0.1	0.1	0.1	0.1	0.1	0.1	0.1	0.1	0.1
Ni (ppm)	744	666	539	411	968	503	445	561	1020	905	413	420	447
Nd (ppm)	1.1	1	0.9	0.8	1	0.9	0.9	0.7	0.8	0.7	0.9	0.8	0.8
Pb (ppm)	4	5	1	2	4	2	3	8	1	1	3	5	3
Pd (ppm)	1.135	1.1	0.747	0.21	2.39	0.351	0.009	0.023	0.031	0.566	0.278	0.076	0.068
Pr (ppm)	0.23	0.22	0.27	0.24	0.2	0.21	0.2	0.18	0.2	0.15	0.22	0.2	0.17
Pt (ppm)	0.147	0.128	0.09	0.072	0.27	0.04	0.0025	0.0025	0.007	0.065	0.021	0.01	0.009
Rb (ppm)	1.4	1.1	1.5	1.6	2.1	2.2	2	2	2.6	1.3	1.9	1	1
Re (ppm)	0.001	0.001	0.001	0.0005	0.001	0.001	0.0005	0.001	0.001	0.001	0.001	0.0005	0.001
S (%)	0.31	0.23	0.17	0.08	0.32	0.09	0.05	0.09	0.3	0.28	0.06	0.06	0.06
Sb (ppm)	0.025	0.025	0.025	0.025	0.025	0.025	0.025	0.025	0.025	0.025	0.025	0.025	0.025
Sc (ppm)	27	30	19	17	27	25	26	27	29	36	32	30	33
Se (ppm)	2.06	1.63	1.305	0.629	2.38	0.616	0.297	0.661	2.2	1.955	0.371	0.38	0.367
Sm (ppm)	0.2	0.24	0.36	0.21	0.25	0.23	0.17	0.16	0.18	0.21	0.24	0.19	0.24
Sn (ppm)	0.5	0.5	0.5	0.5	0.5	0.5	0.5	0.5	0.5	0.5	0.5	0.5	0.5
Sr (ppm)	199	215	259	267	184	186.5	172	190.5	168.5	154	191.5	191.5	179.5
Ta (ppm)	0.05	0.05	0.05	0.05	0.05	0.05	0.05	0.05	0.05	0.05	0.05	0.05	0.05
Tb (ppm)	0.07	0.06	0.05	0.05	0.07	0.05	0.04	0.04	0.05	0.05	0.07	0.07	0.06
Te (ppm)	0.37	0.51	0.27	0.11	0.58	0.15	0.02	0.04	0.21	0.27	0.06	0.04	0.05
Th (ppm)	0.09	0.05	0.025	0.07	0.05	0.08	0.08	0.025	0.1	0.025	0.025	0.025	0.025
Tl (ppm)	0.01	0.01	0.01	0.01	0.01	0.01	0.01	0.01	0.02	0.01	0.01	0.01	0.01
Tm (ppm)	0.03	0.04	0.03	0.03	0.04	0.03	0.03	0.03	0.04	0.05	0.05	0.04	0.05
V (ppm)	103	111	85	69	120	92	82	78	98	114	113	105	126
Y (ppm)	2.2	2.5	1.9	1.7	2.2	2	1.9	1.9	2.1	2.3	2.4	2.1	2.3
U (ppm)	0.025	0.025	0.025	0.025	0.025	0.025	0.025	0.025	0.06	0.025	0.025	0.025	0.025
W (ppm)	2	3	1	2	1	1	3	2	1	3	1	5	2
Yb (ppm)	0.26	0.28	0.24	0.23	0.35	0.31	0.28	0.23	0.27	0.32	0.31	0.36	0.38
Zr (ppm)	5	6	4	4	4	11	3	3	4	4	4	4	4
Zn (ppm)	52	45	38	40	61	56	54	54	61	69	59	59	65

Drill hole #	18-805	18-805	18-805	18-805	18-805	18-805	18-805	18-805	18-805	18-805	18-805	18-805	18-805
Depth From	289	290	291	292	293	294	295	296	297	298	299	300	301
Depth To	290	291	292	293	294	295	296	297	298	299	300	301	302
Rock Type	NOR-Bx	NOR-Bx	NOR-Bx	NOR-Bx	NOR-Bx	NOR-Bx	NOR-Bx	NOR-Bx	NOR-Bx	NOR-Bx	NOR-Bx	NOR-Bx	NOR-Bx
Lithological Domain	Norite	Norite	Norite	Norite	Norite	Norite	Norite	Norite	Norite	Norite	Norite	Norite	Norite
Al2O3 (%)	12.6	13.5	13	12.8	12.4	12.65	12.6	13.1	13.3	13.3	12.7	14.5	13.25
CaO (%)	8.4	8.06	7.92	7.39	7.08	6.96	6.91	7.1	7.11	6.99	6.84	7.63	7.09
Cr2O3 (%)	0.038	0.043	0.045	0.044	0.046	0.047	0.047	0.048	0.045	0.046	0.05	0.045	0.046
Fe2O3 (%)	10.9	9.59	9.66	9.72	9.67	9.99	10.1	9.97	9.68	9.77	10.05	9.14	9.34
K2O (%)	0.12	0.09	0.06	0.1	0.1	0.07	0.07	0.08	0.07	0.07	0.07	0.11	0.09
MgO (%)	13.05	14.25	14.65	14.85	15.4	15.8	15.9	15.7	15.15	15.2	15.75	14.25	14.6
MnO (%)	0.17	0.16	0.16	0.16	0.17	0.17	0.17	0.17	0.17	0.17	0.17	0.16	0.16
Na2O (%)	1.53	1.55	1.42	1.43	1.39	1.38	1.38	1.43	1.45	1.45	1.37	1.63	1.44
P2O5 (%)	0.005	0.02	0.01	0.005	0.01	0.005	0.005	0.005	0.005	0.005	0.005	0.005	0.005
SiO2 (%)	51.3	53.1	52.5	52.7	51	53.2	53.2	53.8	52.9	53	52.9	53	51.7
TiO2 (%)	0.15	0.1	0.09	0.1	0.1	0.1	0.1	0.1	0.11	0.1	0.1	0.1	0.09
LOI (%)	1.35	0.58	0.26	0.32	4.39	0.2		0.25	0.24	0.07	0.35	0.34	0.27
Total (%)	99.63	101.05	99.8	99.63	101.77	100.58	100.45	101.76	100.24	100.18	100.36	100.93	98.09
Ag (ppm)	0.25	0.25	0.25	0.25	0.25	0.25	0.25	0.25	0.25	0.25	0.25	0.25	0.25
As (ppm)	0.3	0.4	0.4	0.05	0.1	0.1	0.1	0.2	0.3	0.2	0.05	0.05	0.3
Au (ppm)	0.129	0.005	0.012	0.006	0.003	0.002	0.009	0.002	0.01	0.003	0.006	0.016	0.03
Ba (ppm)	39.6	37.7	30.4	38.1	36.6	35.4	32.1	35.3	34.6	36.6	36.5	46.5	36.7
Bi (ppm)	0.04	0.01	0.01	0.01	0.01	0.01	0.02	0.01	0.01	0.01	0.03	0.03	0.03
Cd (ppm)	0.25	0.25	0.25	0.5	0.25	0.25	0.25	0.25	0.25	0.25	0.25	0.5	0.25
Ce (ppm)	1.4	1.5	1.2	1.9	1.7	1.3	1.2	1.3	1.4	1.4	1.5	2	1.9
Co (ppm)	86	67	70	72	72	76	79	71	71	72	80	71	75
Cs (ppm)	1.34	0.85	0.38	0.67	1.05	0.51	0.31	0.6	0.49	0.45	0.58	0.81	0.67
Cu (ppm)	519	123	160	148	164	217	247	168	160	181	456	340	340
Dy (ppm)	0.38	0.33	0.29	0.33	0.33	0.28	0.26	0.26	0.32	0.24	0.32	0.3	0.22
Er (ppm)	0.25	0.23	0.24	0.2	0.28	0.18	0.21	0.21	0.23	0.2	0.22	0.26	0.18
Eu (ppm)	0.14	0.14	0.09	0.13	0.12	0.13	0.15	0.13	0.14	0.14	0.13	0.16	0.12
Ga (ppm)	11.6	10.7	9.9	10.4	10	10.7	10	10.3	10.8	10.6	10.1	11.2	10.8
Gd (ppm)	0.27	0.22	0.15	0.24	0.27	0.26	0.19	0.19	0.21	0.23	0.22	0.19	0.22
Ge (ppm)	2.5	2.5	2.5	2.5	2.5	2.5	2.5	2.5	2.5	2.5	2.5	2.5	2.5
Hf (ppm)	0.1	0.1	0.1	0.1	0.2	0.1	0.1	0.1	0.1	0.1	0.1	0.1	0.2
Hg (ppb)	0.0025	0.0025	0.0025	0.0025	0.0025	0.0025	0.0025	0.0025	0.0025	0.005	0.0025	0.0025	0.0025
Ho (ppm)	0.08	0.07	0.06	0.09	0.09	0.06	0.07	0.08	0.06	0.06	0.08	0.08	0.07
In (ppm)	0.006	0.0025	0.0025	0.0025	0.0025	0.0025	0.0025	0.0025	0.0025	0.0025	0.0025	0.0025	0.0025
La (ppm)	0.7	0.8	0.7	1	0.8	0.7	0.7	0.7	0.7	0.7	0.8	1	0.9
Li (ppm)	10	5	10	10	5	5	5	5	5	5	10	10	10
Lu (ppm)	0.06	0.04	0.05	0.05	0.05	0.05	0.05	0.05	0.05	0.06	0.06	0.04	0.04
Mo (ppm)	1	0.5	1	0.5	0.5	0.5	0.5	0.5	0.5	0.5	0.5	0.5	0.5
Nb (ppm)	0.1	0.1	0.1	0.1	0.2	0.1	0.1	0.1	0.1	0.1	0.1	0.2	0.1
Ni (ppm)	666	416	457	452	473	528	555	472	477	504	723	602	654
Nd (ppm)	0.8	0.8	0.7	0.8	0.8	0.5	0.6	0.6	0.5	0.7	0.5	0.9	0.8
Pb (ppm)	2	1	1	1	1	1	1	1	1	1	1	1	1
Pd (ppm)	1.295	0.054	0.113	0.038	0.02	0.002	0.102	0.01	0.105	0.011	0.003	0.145	0.338
Pr (ppm)	0.16	0.17	0.14	0.19	0.19	0.12	0.15	0.14	0.17	0.15	0.18	0.23	0.21
Pt (ppm)	0.151	0.005	0.029	0.005	0.0025	0.0025	0.01	0.0025	0.011	0.0025	0.0025	0.018	0.039
Rb (ppm)	2.1	1.3	0.4	2.1	1.7	0.7	0.5	0.8	0.7	0.8	0.9	2.2	1.4
Re (ppm)	0.001	0.0005	0.001	0.0005	0.0005	0.001	0.0005	0.0005	0.0005	0.0005	0.0005	0.0005	0.0005
S (%)	0.16	0.04	0.05	0.05	0.06	0.07	0.07	0.05	0.05	0.06	0.12	0.1	0.11
Sb (ppm)	0.025	0.025	0.025	0.025	0.025	0.025	0.025	0.025	0.025	0.025	0.025	0.025	0.025
Sc (ppm)	39	25	30	25	28	24	25	24	21	20	23	25	22
Se (ppm)	1.22	0.257	0.385	0.333	0.392	0.528	0.58	0.401	0.39	0.434	1.115	0.838	1.005
Sm (ppm)	0.27	0.19	0.16	0.18	0.21	0.13	0.18	0.15	0.19	0.21	0.14	0.2	0.24
Sn (ppm)	0.5	0.5	0.5	0.5	0.5	1	0.5	0.5	0.5	0.5	0.5	0.5	0.5
Sr (ppm)	176.5	172	158	166.5	161.5	157	161	167.5	173	172	163.5	179	169.5
Ta (ppm)	0.05	0.05	0.05	0.05	0.05	0.05	0.05	0.05	0.05	0.05	0.05	0.05	0.05
Tb (ppm)	0.07	0.05	0.04	0.05	0.03	0.04	0.04	0.04	0.04	0.05	0.05	0.04	0.04
Te (ppm)	0.28	0.05	0.05	0.03	0.05	0.09	0.06	0.03	0.07	0.04	0.13	0.12	0.13
Th (ppm)	0.025	0.05	0.025	0.12	0.24	0.05	0.025	0.025	0.025	0.025	0.025	0.19	0.09
Tl (ppm)	0.02	0.01	0.01	0.01	0.01	0.01	0.01	0.01	0.01	0.01	0.01	0.01	0.02
Tm (ppm)	0.04	0.03	0.03	0.05	0.04	0.04	0.03	0.03	0.04	0.04	0.04	0.04	0.04
V (ppm)	140	91	86	94	94	90	91	91	90	91	93	90	90
Y (ppm)	2.4	2.1	1.8	1.8	2	1.9	1.7	1.9	1.7	1.9	1.9	2	1.7
U (ppm)	0.025	0.025	0.025	0.025	0.22	0.025	0.025	0.025	0.025	0.025	0.025	0.025	0.025
W (ppm)	2	2	1	1	3	2	1	4	2	1	3	1	2
Yb (ppm)	0.42	0.27	0.28	0.33	0.27	0.3	0.33	0.28	0.28	0.35	0.34	0.33	0.28
Zr (ppm)	4	4	3	5	6	3	3	3	3	4	5	4	4
Zn (ppm)	67	61	62	62	64	66	68	64	63	65	66	62	62

Drill hole #	18-805	18-805	18-805	18-805	18-805	18-805	19-009	19-009	19-009	19-009	19-009	19-009	19-009
Depth From	302	303	303.85	304.7	305.35	306	20	22	24	26	28	30	32
Depth To	303	303.85	304.7	305.35	306	307	21	23	25	27	29	31	33
Rock Type	NOR-Bx	NOR-Bx	NOR-Bx	NOR-Bx	NOR-Bx	NOR-Bx	NOR	NOR	NOR	NOR	NOR	NOR	NOR
Lithological Domain	Norite	Norite	Norite	Norite	Norite	Norite	Norite	Norite	Norite	Norite	Norite	Norite	Norite
Al2O3 (%)	13.45	15.1	13.7	13.2	12.15	13.95	16.45	16.5	16.05	17	17.6	15.5	16.8
CaO (%)	7.38	9.21	7.32	7	6.57	9.2	11.15	10.65	9.44	10.1	10.85	9.17	9.68
Cr2O3 (%)	0.047	0.036	0.051	0.049	0.055	0.026	0.009	0.008	0.009	0.008	0.009	0.022	0.009
Fe2O3 (%)	9.62	10.25	9.38	9.02	9.65	12.85	8.83	8.76	9.05	8.68	9.24	9.92	10.45
K2O (%)	0.08	0.14	0.1	0.18	0.12	0.14	0.39	0.35	0.31	0.34	0.31	0.34	0.25
MgO (%)	15.4	11.55	15.05	14.2	15.2	9.84	7.95	8.04	8.33	8.18	7.97	9.88	8.79
MnO (%)	0.16	0.16	0.16	0.15	0.16	0.16	0.14	0.15	0.15	0.13	0.14	0.15	0.15
Na2O (%)	1.47	1.68	1.47	1.42	1.32	1.9	2.31	2.35	3.07	2.63	2.45	2.15	2.25
P2O5 (%)	0.005	0.005	0.005	0.005	0.005	0.01	0.005	0.01	0.005	0.005	0.005	0.005	0.01
SiO2 (%)	52.5	51	53.1	50.5	50.9	46.9	49.4	49.2	50.8	49.2	49.5	50	48.1
TiO2 (%)	0.1	0.22	0.1	0.1	0.1	0.74	0.24	0.23	0.26	0.25	0.25	0.18	0.33
LOI (%)	0.61	0.97	0.56	3.43	3.48	2.52	1.83	1.75	2.32	3.12	2.41	2.92	3.51
Total (%)	100.84	100.35	101	99.26	99.72	98.26	98.73	98.03	99.82	99.67	100.76	100.26	100.35
Ag (ppm)	0.25	0.25	0.25	0.25	0.25	0.25	0.25	0.25	0.25	0.25	0.25	0.25	0.25
As (ppm)	0.1	0.6	0.1	0.1	0.2	0.3	0.5	0.6	0.4	0.6	0.3	0.2	0.4
Au (ppm)	0.025	0.274	0.015	0.028	0.031	0.015	0.005	0.008	0.004	0.002	0.0005	0.0005	0.007
Ba (ppm)	30.4	38.9	30.5	37.4	24.4	36	72.3	75.1	57.9	56.2	60.7	55.7	39.5
Bi (ppm)	0.02	0.08	0.02	0.05	0.05	0.04	0.01	0.01	0.01	0.03	0.08	0.01	0.02
Cd (ppm)	0.25	0.5	0.25	0.25	0.25	0.5	0.25	0.25	0.25	0.5	0.25	0.25	0.5
Ce (ppm)	2	2	1.4	2.6	1.6	2.1	2.9	2.5	3.1	2.3	2.7	2.3	3
Co (ppm)	71	77	73	76	79	71	52	53	51	50	52	61	62
Cs (ppm)	1.55	2.04	1.01	2.47	1.41	1.57	1.25	1.46	1.14	1.08	1.25	1.16	0.72
Cu (ppm)	222	983	303	615	577	216	233	203	126	121	30	26	52
Dy (ppm)	0.37	0.42	0.3	0.3	0.33	0.65	0.76	0.78	0.74	0.75	0.77	0.49	0.88
Er (ppm)	0.25	0.35	0.21	0.21	0.23	0.38	0.45	0.5	0.44	0.53	0.48	0.41	0.54
Eu (ppm)	0.12	0.21	0.1	0.09	0.11	0.2	0.23	0.27	0.23	0.21	0.24	0.2	0.28
Ga (ppm)	8.7	10.4	8.9	9.3	9	14	13.4	14.1	12.7	14.1	14.7	13.2	13.8
Gd (ppm)	0.32	0.4	0.18	0.2	0.16	0.48	0.61	0.6	0.6	0.56	0.63	0.46	0.71
Ge (ppm)	2.5	2.5	2.5	2.5	2.5	2.5	2.5	2.5	2.5	2.5	2.5	2.5	2.5
Hf (ppm)	0.1	0.2	0.1	0.1	0.1	0.2	0.3	0.3	0.2	0.3	0.3	0.2	0.3
Hg (ppb)	0.0025	0.0025	0.0025	0.0025	0.0025	0.0025	0.0025	0.0025	0.0025	0.0025	0.0025	0.0025	0.0025
Ho (ppm)	0.09	0.11	0.07	0.05	0.06	0.14	0.15	0.15	0.16	0.14	0.15	0.12	0.18
In (ppm)	0.0025	0.007	0.0025	0.008	0.008	0.005	0.0025	0.0025	0.0025	0.005	0.0025	0.0025	0.0025
La (ppm)	1	1	0.7	1.5	0.9	0.9	1.3	1.1	1.6	1.1	1.6	1.2	1.5
Li (ppm)	10	5	5	10	10	10	30	40	40	60	40	30	40
Lu (ppm)	0.05	0.06	0.05	0.06	0.05	0.07	0.07	0.06	0.07	0.06	0.07	0.06	0.09
Mo (ppm)	0.5	0.5	0.5	0.5	0.5	0.5	1	0.5	0.5	0.5	0.5	1	0.5
Nb (ppm)	0.1	0.2	0.1	0.1	0.1	0.1	0.1	0.1	0.1	0.1	0.1	0.05	0.1
Ni (ppm)	533	990	621	914	912	369	184	182	162	151	162	239	159
Nd (ppm)	0.8	1.1	0.6	0.9	0.8	1.4	1.6	1.6	1.8	1.2	1.5	1.4	1.8
Pb (ppm)	1	1	1	1	1	4	4	1	3	1	7	3	4
Pd (ppm)	0.131	2.36	0.062	0.041	0.045	0.111	0.013	0.013	0.011	0.011	0.005	0.03	0.007
Pr (ppm)	0.22	0.24	0.17	0.27	0.19	0.3	0.39	0.34	0.39	0.29	0.35	0.31	0.38
Pt (ppm)	0.016	0.293	0.011	0.009	0.011	0.016	0.0025	0.0025	0.0025	0.0025	0.0025	0.009	0.0025
Rb (ppm)	1.6	2.8	1.4	4.7	2.8	3.1	7	6.2	5.4	5.1	4.9	5.2	4.4
Re (ppm)	0.0005	0.001	0.0005	0.001	0.001	0.001	0.001	0.0005	0.0005	0.0005	0.0005	0.0005	0.0005
S (%)	0.05	0.38	0.08	0.18	0.16	0.22	0.06	0.03	0.02	0.02	0.005	0.005	0.04
Sb (ppm)	0.025	0.025	0.025	0.025	0.025	0.025	0.025	0.025	0.025	0.025	0.025	0.025	0.025
Sc (ppm)	22	24	20	22	25	26	39	40	40	38	36	34	47
Se (ppm)	0.469	2.51	0.699	1.545	1.46	0.549	0.328	0.201	0.073	0.308	0.241	0.226	0.369
Sm (ppm)	0.31	0.3	0.14	0.19	0.18	0.41	0.41	0.46	0.44	0.4	0.45	0.3	0.5
Sn (ppm)	0.5	0.5	0.5	0.5	0.5	0.5	0.5	0.5	0.5	1	0.5	0.5	0.5
Sr (ppm)	147	172	149.5	144	127	214	245	232	205	185	204	179.5	230
Ta (ppm)	0.05	0.05	0.05	0.05	0.05	0.05	0.1	0.1	0.1	0.1	0.1	0.1	0.1
Tb (ppm)	0.04	0.07	0.04	0.04	0.04	0.09	0.12	0.11	0.1	0.11	0.1	0.08	0.12
Te (ppm)	0.08	0.62	0.1	0.26	0.3	0.04	0.04	0.05	0.04	0.05	0.05	0.05	0.04
Th (ppm)	0.1	0.08	0.05	0.13	0.025	0.025	0.07	0.06	0.05	0.025	0.025	0.025	0.06
Tl (ppm)	0.02	0.03	0.02	0.04	0.03	0.01	0.01	0.01	0.01	0.01	0.01	0.01	0.01
Tm (ppm)	0.04	0.06	0.03	0.04	0.05	0.06	0.06	0.07	0.06	0.07	0.06	0.06	0.08
V (ppm)	97	173	91	93	99	525	250	247	266	261	251	167	307
Y (ppm)	2	2.7	1.9	1.8	1.9	3.6	3.7	4	3.8	3.8	4	2.9	4.7
U (ppm)	0.025	0.025	0.025	0.025	0.025	0.025	0.025	0.025	0.025	0.025	0.05	0.025	0.025
W (ppm)	0.5	1	1	0.5	0.5	5	1	1	1	1	1	1	1
Yb (ppm)	0.24	0.35	0.25	0.23	0.36	0.46	0.42	0.45	0.46	0.43	0.44	0.29	0.58
Zr (ppm)	5	7	4	4	4	6	9	8	7	7	7	6	9
Zn (ppm)	60	60	62	63	66	68	52	52	51	53	53	62	59

Drill hole #	19-009	19-009	19-009	19-009	19-009	19-009	19-009	19-009	19-009	19-009	19-009	19-009	19-009
Depth From	34	36	38	40	42	44	46	48	50	52	54	56	58
Depth To	35	37	39	41	43	45	47	49	51	53	55	57	59
Rock Type	NOR	NOR	NOR	NOR	NOR	NOR	NOR	NOR	NOR	NOR	NOR	NOR	NOR
Lithological Domain	Norite	Norite	Norite	Norite	Norite	Norite	Norite	Norite	Norite	Norite	Norite	Norite	Norite
Al2O3 (%)	16.7	15.9	16	16.1	17.05	16.3	16.15	16.3	16.55	16	16.35	16.6	16.4
CaO (%)	9.87	12.1	11.65	11.2	11.45	11.05	11.6	11.75	12.2	11.8	11.6	11.65	11.55
Cr2O3 (%)	0.009	0.01	0.009	0.009	0.008	0.009	0.01	0.01	0.009	0.009	0.008	0.008	0.008
Fe2O3 (%)	9.24	10.25	10	9.5	9.49	9.38	9.55	9.77	10.15	9.67	9.88	10	10.4
K2O (%)	0.38	0.32	0.38	0.43	0.35	0.43	0.28	0.23	0.18	0.25	0.3	0.21	0.19
MgO (%)	8.55	8.47	8.26	8.03	7.88	7.74	7.82	7.76	7.82	7.62	7.54	7.76	7.76
MnO (%)	0.14	0.16	0.16	0.16	0.15	0.16	0.16	0.16	0.15	0.16	0.15	0.15	0.15
Na2O (%)	2.79	2.08	2.15	2.33	2.41	2.33	2.03	2.09	1.99	2.05	2.15	2.15	1.98
P2O5 (%)	0.005	0.005	0.02	0.005	0.01	0.01	0.005	0.005	0.01	0.005	0.01	0.005	0.01
SiO2 (%)	49.8	50.3	49.1	50	49.9	49.9	49.7	50	50.7	49.5	49.6	50.3	49.6
TiO2 (%)	0.29	0.31	0.3	0.29	0.29	0.28	0.26	0.28	0.28	0.27	0.26	0.25	0.27
LOI (%)	2.55	1.13	2.21	2.01	2.11	1.89	0.96	1.07	0.67	1.2	1.76	1.66	1.17
Total (%)	100.35	101.06	100.27	100.09	101.13	99.52	98.55	99.46	100.73	98.56	99.64	100.77	99.52
Ag (ppm)	0.25	0.25	0.25	0.25	0.25	0.25	0.25	0.25	0.25	0.25	0.25	0.25	0.25
As (ppm)	0.3	0.6	0.4	0.3	0.3	0.5	0.4	0.5	0.3	0.5	0.3	0.2	0.5
Au (ppm)	0.002	0.002	0.004	0.002	0.004	0.002	0.002	0.001	0.002	0.006	0.001	0.004	0.002
Ba (ppm)	59	58	66.8	67.4	63	79.1	61.4	51.8	50.5	55.4	59.2	55.1	48.6
Bi (ppm)	0.02	0.01	0.02	0.06	0.03	0.01	0.005	0.01	0.005	0.005	0.01	0.005	0.01
Cd (ppm)	0.25	0.25	0.25	0.25	0.5	0.25	0.25	0.25	0.25	0.5	0.7	0.25	0.25
Ce (ppm)	2.4	2.6	2.6	2.6	2.6	3.3	2.6	2.6	2.6	2.7	2.5	2.8	2.8
Co (ppm)	56	61	63	60	56	58	59	58	60	59	58	56	59
Cs (ppm)	1	1.19	1.29	1.25	1.17	1.12	1	0.85	0.8	0.89	0.89	1.03	0.95
Cu (ppm)	101	138	155	172	129	126	125	119	130	137	135	128	110
Dy (ppm)	0.83	0.88	0.93	0.84	0.75	0.89	0.79	0.84	0.91	0.88	0.85	0.87	0.76
Er (ppm)	0.52	0.64	0.56	0.58	0.54	0.62	0.55	0.45	0.59	0.51	0.61	0.64	0.57
Eu (ppm)	0.24	0.26	0.22	0.22	0.22	0.24	0.25	0.28	0.26	0.29	0.26	0.28	0.29
Ga (ppm)	13.7	14.6	13.9	13.8	14.2	14	14.4	13.9	14.3	14.4	14.4	14	14.2
Gd (ppm)	0.69	0.72	0.72	0.68	0.65	0.66	0.67	0.73	0.83	0.75	0.77	0.68	0.82
Ge (ppm)	2.5	2.5	2.5	2.5	2.5	2.5	2.5	2.5	2.5	2.5	2.5	2.5	2.5
Hf (ppm)	0.3	0.3	0.3	0.3	0.3	0.3	0.3	0.3	0.3	0.4	0.3	0.4	0.4
Hg (ppb)	0.0025	0.0025	0.0025	0.0025	0.0025	0.0025	0.0025	0.0025	0.0025	0.0025	0.0025	0.0025	0.0025
Ho (ppm)	0.17	0.21	0.18	0.16	0.17	0.18	0.18	0.17	0.18	0.19	0.19	0.21	0.16
In (ppm)	0.006	0.0025	0.0025	0.0025	0.0025	0.0025	0.0025	0.0025	0.0025	0.0025	0.0025	0.0025	0.0025
La (ppm)	1.1	1.1	1.1	1.1	1.1	1.6	1.2	1.2	1.1	1.3	1.1	1.2	1.3
Li (ppm)	40	10	30	30	30	20	10	10	10	10	20	20	20
Lu (ppm)	0.07	0.1	0.08	0.08	0.07	0.05	0.06	0.08	0.11	0.09	0.08	0.09	0.08
Mo (ppm)	1	0.5	0.5	1	1	0.5	0.5	0.5	1	1	0.5	1	1
Nb (ppm)	0.1	0.1	0.1	0.1	0.1	0.2	0.1	0.1	0.1	0.1	0.1	0.1	0.1
Ni (ppm)	149	160	156	152	143	148	151	149	155	154	149	149	156
Nd (ppm)	1.6	1.7	1.7	1.5	1.5	1.9	1.8	1.7	1.8	1.6	1.6	1.8	1.8
Pb (ppm)	2	3	2	1	1	5	2	1	1	4	1	5	3
Pd (ppm)	0.011	0.012	0.011	0.012	0.013	0.012	0.012	0.013	0.013	0.012	0.011	0.011	0.011
Pr (ppm)	0.3	0.37	0.35	0.35	0.31	0.41	0.41	0.4	0.4	0.38	0.39	0.39	0.39
Pt (ppm)	0.0025	0.0025	0.0025	0.0025	0.0025	0.0025	0.0025	0.0025	0.0025	0.0025	0.0025	0.0025	0.0025
Rb (ppm)	6.3	5.5	6.8	8.2	6.8	7	4.4	3	2.4	3.3	4.7	3.4	2.5
Re (ppm)	0.0005	0.001	0.001	0.001	0.001	0.001	0.001	0.001	0.001	0.001	0.0005	0.0005	0.0005
S (%)	0.08	0.09	0.13	0.06	0.11	0.07	0.08	0.08	0.08	0.09	0.07	0.07	0.06
Sb (ppm)	0.025	0.025	0.025	0.025	0.025	0.025	0.025	0.025	0.025	0.025	0.025	0.025	0.025
Sc (ppm)	41	46	49	47	43	42	48	44	48	46	42	41	42
Se (ppm)	0.246	0.225	0.31	0.213	0.287	0.226	0.241	0.243	0.28	0.278	0.24	0.256	0.278
Sm (ppm)	0.47	0.56	0.52	0.53	0.44	0.58	0.46	0.47	0.43	0.47	0.5	0.53	0.49
Sn (ppm)	0.5	0.5	0.5	0.5	1	0.5	0.5	0.5	0.5	0.5	0.5	0.5	0.5
Sr (ppm)	191.5	194.5	200	225	207	226	203	207	199	204	220	227	203
Ta (ppm)	0.1	0.1	0.1	0.1	0.1	0.1	0.1	0.1	0.1	0.1	0.1	0.1	0.1
Tb (ppm)	0.11	0.13	0.11	0.12	0.11	0.14	0.11	0.11	0.13	0.11	0.11	0.13	0.15
Te (ppm)	0.05	0.04	0.05	0.06	0.05	0.03	0.05	0.06	0.04	0.04	0.06	0.04	0.04
Th (ppm)	0.025	0.07	0.05	0.025	0.025	0.11	0.025	0.025	0.025	0.025	0.025	0.025	0.025
Tl (ppm)	0.02	0.01	0.01	0.01	0.01	0.01	0.01	0.01	0.01	0.01	0.01	0.01	0.01
Tm (ppm)	0.08	0.09	0.08	0.08	0.07	0.08	0.09	0.09	0.07	0.09	0.08	0.07	0.1
V (ppm)	282	325	285	274	264	237	264	261	258	254	225	231	254
Y (ppm)	4.3	5.1	4.8	4.5	4.2	4.5	4.4	4.5	4.9	4.8	4.6	4.8	4.5
U (ppm)	0.025	0.025	0.025	0.025	0.025	0.025	0.025	0.025	0.025	0.025	0.025	0.025	0.025
W (ppm)	1	1	1	1	1	1	1	1	1	2	1	1	1
Yb (ppm)	0.5	0.56	0.55	0.53	0.53	0.5	0.54	0.53	0.58	0.56	0.52	0.53	0.59
Zr (ppm)	9	9	9	8	8	10	9	8	9	11	8	9	8
Zn (ppm)	52	50	52	53	50	54	51	54	53	54	53	53	54

Drill hole #	19-009	19-009	19-009	19-009	19-009	19-009	19-009	19-009	19-009	19-009	19-009	19-009	19-009
Depth From	60	62	64	66	68	70	72	74	76	80	82	84	86
Depth To	61	63	65	67	69	71	73	75	77	81	83	85	87
Rock Type	NOR	NOR	NOR	NOR	NOR	LGABVT	LGABVT	LGABVT	LGABVT	LGABVT	LGABVT	LGABVT	LGABVT
Lithological Domain	Norite	Norite	Norite	Norite	Norite	Breccia	Breccia	Breccia	Breccia	Breccia	Breccia	Breccia	Breccia
Al_2O_3 (%)	16.15	16.15	16.25	16.05	15.05	15.45	20.4	20.7	21	21	20.8	18.8	20.4
CaO (%)	10.85	11.2	11.7	11.45	10	10.45	10.05	10.55	10.55	10.25	10.65	11.1	10.95
Cr_2O_3 (%)	0.008	0.01	0.008	0.008	0.007	0.173	0.023	0.015	0.02	0.025	0.015	0.009	0.019
Fe_2O_3 (%)	10.45	11.05	11.35	10.85	15	8.24	6.38	6.41	5.84	5.32	6.24	7.84	6.66
K_2O (%)	0.18	0.2	0.25	0.22	0.17	0.36	0.47	0.42	0.54	0.55	0.36	0.27	0.35
MgO (%)	8.37	8.01	7.76	8.21	7.81	11.6	8.83	8.27	8.66	9.1	8.29	7.51	7.95
MnO (%)	0.14	0.16	0.16	0.17	0.21	0.14	0.1	0.11	0.09	0.09	0.09	0.11	0.1
Na_2O (%)	2.11	2.07	2.07	2.14	2.21	1.23	1.63	1.91	1.61	1.52	1.78	2.32	1.92
P_2O_5 (%)	0.005	0.005	0.01	0.02	0.005	0.005	0.01	0.005	0.01	0.02	0.005	0.02	0.005
SiO_2 (%)	48.3	49.9	50.4	50.8	46.3	49	48.2	50.2	48.9	48.3	49.3	50.5	49.7
TiO_2 (%)	0.3	0.38	0.33	0.26	0.95	0.15	0.13	0.1	0.07	0.06	0.09	0.16	0.1
LOI (%)	2.97	1.29	0.66	1.61	2.48	2.56	2.66	2.03	2.26	2.75	2.16	1.78	2.14
Total (%)	99.86	100.45	100.98	101.82	100.22	99.38	98.91	100.76	99.58	99.02	99.81	100.46	100.32
Ag (ppm)	0.25	0.25	0.25	0.25	0.25	0.25	0.25	0.25	0.25	0.25	0.25	0.25	0.25
As (ppm)	0.4	0.5	0.3	0.4	0.7	0.4	0.3	0.6	0.6	0.4	0.8	1.1	0.3
Au (ppm)	0.001	0.003	0.002	0.002	0.003	0.0005	0.002	0.019	0.002	0.0005	0.016	0.029	0.014
Ba (ppm)	47.6	54.1	58.5	65	46	98.1	98.1	76	77	86.7	61.5	62.7	63.6
Bi (ppm)	0.05	0.01	0.01	0.01	0.03	0.01	0.02	0.03	0.04	0.02	0.03	0.05	0.02
Cd (ppm)	0.25	0.25	0.6	0.25	0.25	0.7	0.25	0.25	0.25	0.25	0.6	0.7	0.25
Ce (ppm)	3.3	3.3	3	5.9	3.5	2.3	1.9	2.1	1.8	1.2	1.7	3	1.9
Co (ppm)	60	59	59	55	72	60	47	46	40	40	50	60	42
Cs (ppm)	0.99	0.87	0.97	1.31	0.88	1.1	2.01	1.46	1.19	1.38	1.17	0.9	1.22
Cu (ppm)	96	125	136	63	180	14	50	55	24	15	134	543	141
Dy (ppm)	0.78	0.98	0.91	1.23	0.93	0.48	0.3	0.37	0.25	0.22	0.31	0.68	0.35
Er (ppm)	0.51	0.58	0.58	0.67	0.55	0.32	0.16	0.22	0.19	0.13	0.2	0.33	0.3
Eu (ppm)	0.24	0.26	0.32	0.37	0.31	0.2	0.17	0.17	0.13	0.12	0.16	0.26	0.19
Ga (ppm)	14.4	14.7	14.9	14.1	17.4	9.7	12.3	12.4	11.4	10.5	12.6	14.3	12.9
Gd (ppm)	0.73	0.64	0.83	1.01	0.9	0.41	0.23	0.33	0.22	0.15	0.34	0.56	0.37
Ge (ppm)	2.5	2.5	2.5	2.5	2.5	2.5	2.5	2.5	2.5	2.5	2.5	2.5	2.5
Hf (ppm)	0.3	0.3	0.3	0.3	0.3	0.2	0.1	0.1	0.1	0.1	0.1	0.2	0.2
Hg (ppb)	0.0025	0.0025	0.0025	0.0025	0.0025	0.0025	0.0025	0.0025	0.0025	0.0025	0.0025	0.0025	0.0025
Ho (ppm)	0.2	0.21	0.21	0.22	0.23	0.09	0.06	0.07	0.06	0.05	0.08	0.14	0.08
In (ppm)	0.006	0.0025	0.0025	0.0025	0.0025	0.0025	0.0025	0.0025	0.0025	0.0025	0.0025	0.0025	0.0025
La (ppm)	1.9	1.5	1.2	2.9	1.6	1	1	1.1	0.9	0.6	0.9	1.5	1
Li (ppm)	50	20	10	30	40	20	30	20	20	30	30	20	30
Lu (ppm)	0.07	0.07	0.1	0.09	0.1	0.05	0.03	0.04	0.02	0.02	0.04	0.06	0.04
Mo (ppm)	1	0.5	1	1	0.5	1	0.5	0.5	0.5	0.5	0.5	0.5	0.5
Nb (ppm)	0.1	0.1	0.1	0.3	0.2	0.1	0.1	0.1	0.1	0.1	0.1	0.1	0.05
Ni (ppm)	166	168	150	152	153	349	290	285	266	287	388	320	254
Nd (ppm)	1.9	2.2	2.1	3.8	2.2	1.5	1	1.1	0.8	0.6	0.8	1.6	1.1
Pb (ppm)	7	2	4	3	2	1	1	1	1	1	1	1	1
Pd (ppm)	0.009	0.013	0.011	0.009	0.029	0.051	0.13	0.268	0.715	0.187	0.558	0.258	0.103
Pr (ppm)	0.5	0.51	0.44	0.85	0.47	0.3	0.24	0.27	0.21	0.13	0.19	0.43	0.26
Pt (ppm)	0.0025	0.0025	0.0025	0.0025	0.0025	0.014	0.038	0.072	0.143	0.044	0.126	0.056	0.019
Rb (ppm)	2.5	2.6	3.4	3.2	2.5	6.7	9	7	10.4	11.3	7.3	4.2	6
Re (ppm)	0.0005	0.001	0.001	0.0005	0.002	0.0005	0.001	0.001	0.0005	0.0005	0.001	0.0005	0.001
S (%)	0.04	0.1	0.11	0.03	0.22	0.01	0.02	0.03	0.01	0.01	0.16	0.27	0.07
Sb (ppm)	0.025	0.025	0.025	0.025	0.025	0.025	0.025	0.025	0.025	0.025	0.025	0.025	0.025
Sc (ppm)	39	40	46	45	47	21	15	15	14	12	16	24	17
Se (ppm)	0.622	0.256	0.294	0.21	0.415	0.066	0.095	0.154	0.049	0.039	0.487	1.035	0.343
Sm (ppm)	0.54	0.72	0.5	1.01	0.68	0.43	0.21	0.2	0.2	0.15	0.17	0.5	0.25
Sn (ppm)	0.5	0.5	0.5	0.5	0.5	0.5	0.5	0.5	0.5	0.5	0.5	0.5	0.5
Sr (ppm)	189.5	222	219	212	199.5	151	203	211	205	190	211	252	221
Ta (ppm)	0.1	0.1	0.1	0.1	0.1	0.1	0.1	0.05	0.1	0.1	0.1	0.1	0.1
Tb (ppm)	0.13	0.14	0.12	0.18	0.13	0.06	0.05	0.06	0.04	0.02	0.04	0.08	0.05
Te (ppm)	0.05	0.03	0.04	0.05	0.04	0.02	0.05	0.07	0.09	0.05	0.12	0.06	0.08
Th (ppm)	0.025	0.025	0.05	0.67	0.07	0.1	0.08	0.1	0.06	0.07	0.06	0.06	0.05
Tl (ppm)	0.01	0.01	0.01	0.01	0.01	0.01	0.01	0.01	0.01	0.01	0.07	0.06	0.08
Tm (ppm)	0.09	0.1	0.09	0.1	0.09	0.05	0.03	0.04	0.03	0.02	0.04	0.04	0.05
V (ppm)	283	328	288	230	651	142	114	84	68	64	84	147	100
Y (ppm)	4.6	5	5.1	5.8	5.1	2.7	1.6	2	1.4	1.1	1.7	3.4	2.1
U (ppm)	0.22	0.025	0.025	0.025	0.025	0.025	0.025	0.05	0.025	0.025	0.025	0.025	0.025
W (ppm)	1	1	1	2	1	1	1	1	1	1	1	1	1
Yb (ppm)	0.46	0.58	0.57	0.6	0.59	0.32	0.19	0.23	0.16	0.12	0.23	0.43	0.25
Zr (ppm)	8	8	8	8	8	5	4	4	4	3	4	5	5
Zn (ppm)	58	59	61	62	66	65	45	42	34	30	34	37	39

Drill hole #	19-009	19-009	19-009	19-009	19-009	19-009	19-009	19-009	19-025	19-025	19-025	19-025	19-025
Depth From	88	90	92	94	96	98	100	102	320	322	324	326	328
Depth To	89	91	93	95	97	99	101	103	321	323	325	327	329
Rock Type	LGABVT	LGABVT	LGABVT	LGABVT	LGABVT	LGABVT	LGABVT	LGABVT	NOR	NOR	NOR	NOR	NOR
Lithological Domain	Breccia	Breccia	Breccia	Breccia	Breccia	Breccia	Breccia	Breccia	Norite	Norite	Norite	Norite	Norite
Al_2O_3 (%)	22.7	24.5	23.4	22	22.9	8.81	10.3	4.49	16.4	13.8	15.1	12.05	16.25
CaO (%)	11.7	12.15	11.95	11.05	9.42	12.15	13.35	15.45	9.4	7.96	7.95	6.93	8.52
Cr_2O_3 (%)	0.033	0.017	0.029	0.032	0.032	0.197	0.217	0.425	0.035	0.049	0.068	0.092	0.046
Fe_2O_3 (%)	4.43	4.25	4.28	4.7	4.33	6.94	6.59	8.07	8.33	10.2	9.24	11.8	8.83
K_2O (%)	0.39	0.61	0.29	0.65	0.83	0.11	0.3	0.08	0.13	0.11	0.15	0.11	0.14
MgO (%)	7.97	6.05	8.09	8.28	9.3	17.45	15.1	19.1	10.05	13.25	12.1	14.85	10.4
MnO (%)	0.08	0.07	0.07	0.08	0.07	0.18	0.14	0.15	0.14	0.17	0.14	0.19	0.15
Na_2O (%)	1.55	1.98	1.45	1.72	2.08	0.96	0.94	0.4	1.87	1.51	1.52	1.25	2.05
P_2O_5 (%)	0.005	0.01	0.01	0.005	0.005	0.005	0.02	0.01	0.005	0.02	0.005	0.01	0.005
SiO_2 (%)	48.7	49.3	49	49.8	48.5	47.9	50.8	49.5	50.1	51.3	50.2	51.5	51.5
TiO_2 (%)	0.06	0.06	0.04	0.06	0.05	0.23	0.2	0.23	0.13	0.15	0.13	0.14	0.13
LOI (%)	1.79	2.06	1.5	2.22	3.8	5.32	2.79	2.42	1.47	1.46	2.19	1.15	1.67
Total (%)	99.44	101.1	100.13	100.63	101.36	100.26	100.78	100.33	98.09	100.01	98.8	100.08	99.72
Ag (ppm)	0.25	0.25	0.25	0.25	0.25	0.25	0.25	0.25	0.25	0.25	0.25	0.25	0.25
As (ppm)	0.2	0.5	0.4	0.8	1	0.9	0.6	0.4	0.8	0.9	1.4	0.4	0.6
Au (ppm)	0.001	0.0005	0.0005	0.0005	0.0005	0.0005	0.001	0.011	0.021	0.004	0.083	0.0005	0.007
Ba (ppm)	53.9	89.4	44.6	98.8	164	12.9	45.8	28.6	48.1	36.5	40.8	37.7	55.9
Bi (ppm)	0.01	0.02	0.01	0.02	0.03	0.1	0.01	0.005	0.02	0.01	0.14	0.01	0.01
Cd (ppm)	0.25	0.25	0.5	0.25	0.25	0.25	0.25	0.9	0.6	0.6	0.6	0.8	0.6
Ce (ppm)	1.2	1.7	1.1	2.2	1.1	4.2	8.3	5.3	2.4	2.1	2	2.1	3.5
Co (ppm)	33	29	34	37	32	51	46	61	62	75	80	92	63
Cs (ppm)	1.17	1.52	0.65	1.25	3.04	0.25	1.14	0.52	0.66	0.63	0.79	0.59	0.56
Cu (ppm)	29	15	22	14	9	7	4	18	161	55	394	45	44
Dy (ppm)	0.2	0.27	0.13	0.21	0.18	1.08	1.05	1.3	0.43	0.47	0.33	0.44	0.4
Er (ppm)	0.15	0.11	0.08	0.12	0.15	0.68	0.52	0.76	0.27	0.24	0.23	0.33	0.3
Eu (ppm)	0.12	0.16	0.13	0.15	0.09	0.25	0.3	0.41	0.21	0.17	0.17	0.14	0.24
Ga (ppm)	11.4	13.2	11.5	11.2	10.8	7.6	7.2	5	12.6	10.5	11.9	10.6	13.3
Gd (ppm)	0.17	0.18	0.13	0.19	0.14	1.17	1.15	1.57	0.3	0.4	0.18	0.33	0.32
Ge (ppm)	2.5	2.5	2.5	2.5	2.5	2.5	2.5	2.5	2.5	2.5	2.5	2.5	2.5
Hf (ppm)	0.1	0.1	0.1	0.1	0.1	0.4	0.5	0.7	0.2	0.1	0.2	0.3	0.3
Hg (ppb)	0.0025	0.0025	0.0025	0.0025	0.0025	0.0025	0.0025	0.0025	0.0025	0.0025	0.0025	0.0025	0.0025
Ho (ppm)	0.04	0.04	0.03	0.04	0.04	0.25	0.21	0.28	0.1	0.06	0.07	0.08	0.09
In (ppm)	0.0025	0.0025	0.0025	0.0025	0.0025	0.0025	0.0025	0.0025	0.0025	0.0025	0.0025	0.0025	0.0025
La (ppm)	0.6	0.9	0.6	1.2	0.7	1.7	3.4	1.8	1.3	1.2	1.1	1.1	1.8
Li (ppm)	10	30	10	30	100	100	30	20	10	10	10	10	10
Lu (ppm)	0.01	0.02	0.03	0.03	0.02	0.09	0.08	0.1	0.05	0.05	0.04	0.07	0.04
Mo (ppm)	0.5	0.5	0.5	1	0.5	0.5	0.5	0.5	0.5	0.5	0.5	0.5	0.5
Nb (ppm)	0.05	0.05	0.05	0.1	0.1	0.1	0.4	0.1	0.05	0.1	0.1	0.1	0.2
Ni (ppm)	269	192	266	265	272	396	376	562	356	388	590	447	312
Nd (ppm)	0.6	0.8	0.4	0.9	0.5	3.6	5	4.6	1.3	1.2	1	1.1	1.5
Pb (ppm)	1	1	1	1	1	7	3	3	1	1	3	1	4
Pd (ppm)	0.116	0.094	0.134	0.134	0.061	0.009	0.043	0.066	0.14	0.038	0.373	0.017	0.051
Pr (ppm)	0.14	0.21	0.11	0.22	0.14	0.72	1.08	0.89	0.27	0.27	0.26	0.25	0.4
Pt (ppm)	0.023	0.027	0.028	0.026	0.016	0.007	0.026	0.039	0.027	0.013	0.067	0.0025	0.007
Rb (ppm)	6	10.1	4.7	11.1	15.4	1.8	5.5	2.3	1.5	1.2	2	1.6	2
Re (ppm)	0.001	0.0005	0.0005	0.0005	0.001	0.0005	0.0005	0.0005	0.0005	0.0005	0.0005	0.0005	0.0005
S (%)	0.02	0.02	0.01	0.01	0.01	0.005	0.005	0.03	0.08	0.02	0.15	0.01	0.03
Sb (ppm)	0.025	0.025	0.025	0.025	0.025	0.025	0.025	0.025	0.025	0.025	0.025	0.025	0.025
Sc (ppm)	11	10	10	12	11	53	46	52	22	22	18	22	18
Se (ppm)	0.07	0.066	0.038	0.037	0.133	0.626	0.028	0.044	0.382	0.076	0.775	0.07	0.087
Sm (ppm)	0.13	0.15	0.09	0.17	0.1	1.09	1.13	1.37	0.27	0.2	0.17	0.28	0.38
Sn (ppm)	0.5	0.5	0.5	0.5	0.5	0.5	0.5	0.5	0.5	0.5	0.5	0.5	0.5
Sr (ppm)	211	259	209	229	295	40.7	147.5	79.8	201	149	163.5	134.5	235
Ta (ppm)	0.1	0.05	0.1	0.6	0.1	0.1	0.1	0.1	0.1	0.1	0.1	0.2	0.1
Tb (ppm)	0.03	0.03	0.02	0.02	0.03	0.17	0.19	0.25	0.05	0.05	0.05	0.05	0.07
Te (ppm)	0.02	0.04	0.02	0.03	0.04	0.07	0.04	0.01	0.1	0.03	0.3	0.03	0.04
Th (ppm)	0.025	0.025	0.025	0.07	0.025	0.11	0.31	0.13	0.06	0.06	0.06	0.11	0.11
Tl (ppm)	0.06	0.05	0.04	0.09	0.02	0.01	0.04	0.24	0.01	0.01	0.02	0.01	0.01
Tm (ppm)	0.02	0.02	0.02	0.02	0.02	0.08	0.08	0.1	0.05	0.05	0.03	0.06	0.03
V (ppm)	54	57	49	56	57	181	156	182	120	138	127	147	115
Y (ppm)	1.2	1.1	1	1.2	1.1	5.2	5.2	6.6	2.5	2.2	2	2.6	2.3
U (ppm)	0.025	0.025	0.025	0.025	0.025	0.14	0.07	0.025	0.12	0.05	0.025	0.025	0.025
W (ppm)	1	1	1	1	1	1	1	1	1	0.5	1	1	1
Yb (ppm)	0.14	0.16	0.15	0.17	0.14	0.52	0.51	0.63	0.28	0.21	0.19	0.26	0.25
Zr (ppm)	3	2	2	2	2	13	14	22	4	4	4	7	10
Zn (ppm)	27	25	24	26	24	44	34	44	56	66	62	78	61

Drill hole #	19-025	19-025	19-025	19-025	19-025	19-025	19-025	19-025	19-025	19-025	19-025	19-025	19-025
Depth From	330	332	334	336	338	340	342	344	346	348	350	352	354
Depth To	331	333	335	337	339	341	343	345	347	349	351	353	355
Rock Type	NOR	NOR	NOR	NOR	NOR	NOR	NOR	NOR	NOR	NOR	NOR	NOR	NOR
Lithological Domain	Norite	Norite	Norite	Norite	Norite	Norite	Norite	Norite	Norite	Norite	Norite	Norite	Norite
Al_2O_3 (%)	17	17.1	13.65	15.7	15.4	13.65	18.25	17.7	16.05	14.3	14.4	13.2	10.3
CaO (%)	8.66	8.56	7.96	9.16	9.56	9.24	9.97	8.78	8.5	8.2	8.89	8.39	7.37
Cr_2O_3 (%)	0.052	0.045	0.059	0.044	0.037	0.041	0.038	0.066	0.068	0.075	0.033	0.036	0.037
Fe_2O_3 (%)	9.21	9.11	11.2	10.25	10.95	11.1	8.88	9.88	13.25	14.9	12.4	12.45	14.65
K_2O (%)	0.13	0.17	0.08	0.11	0.11	0.09	0.22	0.11	0.09	0.11	0.1	0.1	0.11
MgO (%)	10.55	10.2	12.55	10.5	11.45	12.15	8.51	9.53	10.35	10.9	11.25	12.1	14.4
MnO (%)	0.15	0.14	0.17	0.15	0.16	0.17	0.15	0.14	0.15	0.16	0.16	0.18	0.23
Na_2O (%)	1.82	1.92	1.43	1.74	1.59	1.43	2.36	2.12	1.67	1.63	1.58	1.57	1.23
P_2O_5 (%)	0.02	0.005	0.03	0.005	0.005	0.005	0.01	0.01	0.02	0.005	0.005	0.01	0.01
SiO_2 (%)	51	50.9	50.4	50	51.9	50.3	51.2	51.5	49.8	48.5	50.5	50.4	51.5
TiO_2 (%)	0.12	0.12	0.15	0.13	0.13	0.15	0.12	0.13	0.24	0.31	0.17	0.17	0.19
LOI (%)	0.77	1.05	0.92	1.14	0.51	0.81	2.2	1.1	1.06	0.47	0.38	1.01	0.19
Total (%)	99.49	99.35	98.61	98.95	101.81	99.15	101.95	101.11	101.27	99.59	99.87	99.64	100.23
Ag (ppm)	0.25	0.25	0.25	0.25	0.25	0.25	0.25	0.25	0.25	0.25	0.25	0.25	0.25
As (ppm)	0.6	0.6	0.7	0.5	0.4	0.4	0.6	0.5	1	0.7	0.5	0.3	0.5
Au (ppm)	0.0005	0.0005	0.0005	0.003	0.0005	0.0005	0.0005	0.0005	0.0005	0.0005	0.002	0.412	0.037
Ba (ppm)	46.9	55.1	34.7	39.5	36.9	35.3	61.9	56.3	38.9	42.1	35.2	41.9	37.7
Bi (ppm)	0.005	0.01	0.005	0.01	0.005	0.005	0.005	0.005	0.02	0.05	0.005	0.01	0.02
Cd (ppm)	0.6	0.6	0.8	0.6	0.6	0.5	0.7	0.25	0.5	0.25	0.8	0.9	0.25
Ce (ppm)	2	2.3	2	1.9	1.9	2.2	2.3	3.1	1.8	6.6	2	2.1	2.4
Co (ppm)	67	68	88	75	77	83	60	70	81	86	77	79	99
Cs (ppm)	0.4	0.43	0.48	0.52	0.55	0.64	1.25	0.51	0.68	0.62	0.39	0.56	0.55
Cu (ppm)	17	24	9	21	11	17	5	2	28	20	21	66	351
Dy (ppm)	0.29	0.25	0.46	0.42	0.41	0.51	0.27	0.31	0.29	0.45	0.4	0.48	0.63
Er (ppm)	0.24	0.24	0.3	0.28	0.34	0.31	0.31	0.2	0.2	0.32	0.32	0.33	0.43
Eu (ppm)	0.19	0.14	0.14	0.12	0.18	0.16	0.16	0.19	0.12	0.23	0.13	0.17	0.19
Ga (ppm)	13.3	13.5	11.3	11.5	12.1	11.7	14.1	14.9	14.7	15.3	13.3	12.3	10.3
Gd (ppm)	0.18	0.19	0.37	0.28	0.29	0.48	0.39	0.28	0.32	0.48	0.24	0.33	0.61
Ge (ppm)	2.5	2.5	2.5	2.5	2.5	2.5	2.5	2.5	2.5	2.5	2.5	2.5	2.5
Hf (ppm)	0.1	0.2	0.2	0.1	0.2	0.2	0.2	0.1	0.2	0.3	0.1	0.2	0.3
Hg (ppb)	0.0025	0.0025	0.0025	0.0025	0.0025	0.0025	0.0025	0.0025	0.0025	0.0025	0.0025	0.0025	0.0025
Ho (ppm)	0.07	0.08	0.1	0.06	0.1	0.11	0.08	0.07	0.06	0.1	0.09	0.12	0.13
In (ppm)	0.0025	0.0025	0.0025	0.0025	0.0025	0.0025	0.0025	0.0025	0.0025	0.0025	0.0025	0.0025	0.005
La (ppm)	1.1	1.2	1.1	1	0.9	1	1.2	1.8	1	2.8	1	1.2	1.1
Li (ppm)	5	10	5	10	10	10	20	10	10	5	5	10	5
Lu (ppm)	0.06	0.04	0.06	0.04	0.05	0.06	0.05	0.04	0.05	0.06	0.06	0.05	0.07
Mo (ppm)	0.5	0.5	0.5	0.5	0.5	0.5	0.5	0.5	0.5	0.5	0.5	0.5	0.5
Nb (ppm)	0.1	0.1	0.1	0.05	0.1	0.1	0.2	0.1	0.1	3.1	0.4	0.3	0.2
Ni (ppm)	309	321	409	351	347	393	264	329	375	384	333	379	542
Nd (ppm)	0.9	0.9	1.2	0.9	0.9	1.4	1.1	1.3	0.8	3	1	1	1.5
Pb (ppm)	1	1	1	1	1	1	1	1	1	1	1	1	3
Pd (ppm)	0.058	0.052	0.041	0.082	0.116	0.06	0.09	0.056	0.117	0.189	0.212	0.268	0.648
Pr (ppm)	0.21	0.23	0.24	0.26	0.21	0.33	0.29	0.31	0.22	0.86	0.24	0.28	0.32
Pt (ppm)	0.0025	0.009	0.0025	0.005	0.006	0.0025	0.0025	0.0025	0.013	0.065	0.053	0.067	0.168
Rb (ppm)	1.7	1.9	1.2	1.8	1.3	1.2	3.1	1.3	1.3	1.5	1.1	1.4	1.7
Re (ppm)	0.0005	0.001	0.0005	0.0005	0.0005	0.0005	0.0005	0.0005	0.0005	0.0005	0.0005	0.0005	0.0005
S (%)	0.01	0.01	0.01	0.01	0.005	0.005	0.005	0.01	0.02	0.02	0.01	0.01	0.08
Sb (ppm)	0.025	0.025	0.025	0.025	0.025	0.025	0.025	0.025	0.025	0.025	0.025	0.025	0.025
Sc (ppm)	14	15	19	21	19	21	23	18	22	29	28	26	49
Se (ppm)	0.029	0.027	0.014	0.03	0.013	0.02	0.005	0.008	0.036	0.017	0.018	0.245	0.659
Sm (ppm)	0.17	0.23	0.3	0.29	0.21	0.39	0.31	0.27	0.25	0.68	0.26	0.26	0.44
Sn (ppm)	0.5	0.5	0.5	0.5	0.5	0.5	0.5	0.5	0.5	0.5	0.5	0.5	0.5
Sr (ppm)	199	200	151	170.5	170.5	157	255	256	193	191	178.5	178	121.5
Ta (ppm)	0.2	0.1	0.1	0.1	0.1	0.1	0.1	0.1	0.1	0.1	0.1	0.1	0.1
Tb (ppm)	0.04	0.03	0.07	0.06	0.06	0.09	0.06	0.03	0.03	0.07	0.05	0.06	0.09
Te (ppm)	0.01	0.01	0.01	0.02	0.01	0.01	0.005	0.005	0.01	0.01	0.01	0.14	0.2
Th (ppm)	0.07	0.09	0.06	0.06	0.05	0.06	0.05	0.09	0.025	0.29	0.06	0.07	0.1
Tl (ppm)	0.01	0.01	0.01	0.01	0.01	0.01	0.01	0.01	0.01	0.01	0.01	0.01	0.02
Tm (ppm)	0.04	0.04	0.05	0.04	0.05	0.04	0.04	0.03	0.03	0.04	0.05	0.06	0.07
V (ppm)	116	112	151	127	159	169	120	134	317	532	243	233	215
Y (ppm)	1.9	1.8	2.6	2	2.5	3	2	1.7	1.9	2.5	2.3	2.9	3.7
U (ppm)	0.025	0.025	0.025	0.025	0.025	0.025	0.025	0.025	0.025	0.025	0.025	0.025	0.025
W (ppm)	1	1	1	0.5	1	1	1	1	1	1	1	1	1
Yb (ppm)	0.2	0.25	0.37	0.28	0.29	0.34	0.22	0.19	0.2	0.23	0.25	0.49	0.45
Zr (ppm)	4	6	6	5	5	6	4	5	4	8	5	7	7
Zn (ppm)	57	55	70	60	60	68	58	64	69	80	70	73	97

Drill hole #	19-025	19-025	19-025	19-025	19-025	19-025	19-025	19-025	19-025	19-025	19-025	19-025	19-025
Depth From	356	358	360	362	364	366	368	370	372	374	378	380	382
Depth To	357	359	361	363	365	367	369	371	373	375	379	381	383
Rock Type	NOR	NOR	NOR	NOR	NOR	NOR	NOR	NOR	NOR	NOR	NOR	NOR	NOR
Lithological Domain	Norite	Norite	Norite	Norite	Norite	Norite	Norite	Norite	Norite	Norite	Norite	Norite	Norite
Al2O3 (%)	12	14.6	12.15	16.85	16.1	15.95	18.3	17	18.25	17.65	8.71	7.89	6.39
CaO (%)	7.72	8.59	7.8	9.63	11.95	11.8	12.75	12.45	13.25	13.05	5.75	5.47	5.07
Cr2O3 (%)	0.03	0.023	0.029	0.022	0.023	0.022	0.016	0.018	0.015	0.014	0.037	0.039	0.043
Fe2O3 (%)	12.55	11.7	12.4	9.92	8.84	9.95	8.5	7.91	7.66	7.06	15.4	14.75	16.5
K2O (%)	0.12	0.18	0.18	0.33	0.16	0.11	0.11	0.11	0.1	0.08	0.08	0.17	0.09
MgO (%)	13.95	11.5	13.35	9.76	9.55	9.75	7.47	8.16	7.83	7.8	17.25	17.9	19.35
MnO (%)	0.19	0.17	0.18	0.14	0.14	0.14	0.12	0.12	0.12	0.12	0.23	0.23	0.24
Na2O (%)	1.3	1.68	1.16	1.95	1.73	1.69	2.1	1.94	2.05	2.1	0.87	0.82	0.68
P2O5 (%)	0.02	0.005	0.01	0.01	0.005	0.01	0.005	0.005	0.01	0.01	0.005	0.005	0.005
SiO2 (%)	51.2	50.5	49.7	50.3	50.5	50.5	50.6	49.8	51.2	50.6	50.9	50.8	51.7
TiO2 (%)	0.16	0.2	0.17	0.16	0.23	0.23	0.23	0.22	0.22	0.18	0.19	0.2	0.22
LOI (%)	1.01	0.89	2.36	2.69	1.97	0.74	1	0.88	0.2	0.65	0.26	1.34	0.36
Total (%)	100.26	100.06	99.5	101.8	101.21	100.91	101.22	98.63	100.93	99.33	99.68	99.61	100.65
Ag (ppm)	0.25	0.25	0.25	0.5	0.25	1.1	0.9	0.25	0.25	0.25	0.7	0.25	0.25
As (ppm)	0.5	0.4	0.6	0.8	0.4	0.6	0.2	0.5	0.5	0.7	0.5	0.4	0.2
Au (ppm)	0.041	0.055	0.076	0.071	0.064	0.127	0.119	0.024	0.018	0.009	0.101	0.012	0.087
Ba (ppm)	36.5	45.6	39.1	68.3	61	34.1	43.1	43.6	40	44.7	26.9	42	22.5
Bi (ppm)	0.07	0.06	0.19	0.18	0.04	0.1	0.12	0.03	0.01	0.01	0.09	0.02	0.07
Cd (ppm)	0.6	0.7	0.9	0.7	0.25	0.8	0.7	0.5	0.5	0.25	1	0.6	1
Ce (ppm)	1.7	1.9	1.8	2	2.6	2.2	2.3	2.2	2.2	2.7	1.5	1.6	1.7
Co (ppm)	89	77	89	74	62	84	70	54	48	49	131	109	136
Cs (ppm)	0.7	0.96	1.26	1.04	1.2	0.38	0.35	0.43	0.19	0.27	0.34	1.6	0.5
Cu (ppm)	469	503	770	927	638	1905	1940	337	215	172	1295	149	1145
Dy (ppm)	0.46	0.46	0.53	0.51	0.91	0.7	0.65	0.67	0.71	0.63	0.54	0.55	0.58
Er (ppm)	0.23	0.3	0.39	0.43	0.57	0.39	0.48	0.42	0.49	0.52	0.39	0.45	0.36
Eu (ppm)	0.14	0.21	0.14	0.21	0.28	0.21	0.23	0.22	0.17	0.28	0.13	0.11	0.17
Ga (ppm)	10.7	12.8	10.9	13.2	13.4	11.6	14.6	14.5	14.3	15	9.4	9	8.6
Gd (ppm)	0.33	0.33	0.42	0.42	0.67	0.53	0.57	0.68	0.42	0.52	0.33	0.27	0.38
Ge (ppm)	2.5	2.5	2.5	2.5	2.5	2.5	2.5	2.5	2.5	2.5	2.5	2.5	2.5
Hf (ppm)	0.2	0.2	0.2	0.2	0.4	0.2	0.3	0.3	0.2	0.3	0.2	0.3	0.2
Hg (ppb)	0.0025	0.0025	0.0025	0.0025	0.0025	0.0025	0.0025	0.0025	0.0025	0.0025	0.0025	0.0025	0.0025
Ho (ppm)	0.08	0.11	0.1	0.08	0.19	0.15	0.14	0.13	0.14	0.15	0.11	0.12	0.14
In (ppm)	0.0025	0.005	0.0025	0.0025	0.0025	0.005	0.0025	0.0025	0.0025	0.0025	0.0025	0.0025	0.005
La (ppm)	0.9	1	0.8	1	1.1	0.9	1.1	1	1	1.3	0.7	0.7	0.7
Li (ppm)	10	10	20	20	10	10	10	10	10	10	10	10	20
Lu (ppm)	0.03	0.05	0.06	0.06	0.08	0.06	0.08	0.05	0.06	0.06	0.08	0.08	0.09
Mo (ppm)	0.5	0.5	0.5	0.5	0.5	0.5	0.5	0.5	0.5	0.5	0.5	0.5	0.5
Nb (ppm)	0.2	0.1	0.1	0.1	0.1	0.2	0.1	0.1	0.1	0.1	0.1	0.1	0.1
Ni (ppm)	635	560	780	824	646	1385	1395	415	311	284	1335	570	1345
Nd (ppm)	1	1.2	1	1.2	2	1.3	1.7	1.4	1.5	1.7	0.8	1	1.1
Pb (ppm)	2	1	1	1	1	1	2	1	1	1	3	3	2
Pd (ppm)	0.429	0.489	0.689	0.962	0.466	1.09	1.075	0.207	0.096	0.065	1.12	0.226	1.095
Pr (ppm)	0.19	0.22	0.24	0.23	0.39	0.32	0.31	0.31	0.31	0.37	0.22	0.21	0.22
Pt (ppm)	0.06	0.068	0.097	0.135	0.063	0.152	0.137	0.029	0.016	0.01	0.138	0.036	0.131
Rb (ppm)	2.3	2.9	4.7	6.3	3.4	1.2	1.1	1	0.7	0.8	1.3	6.4	2.1
Re (ppm)	0.0005	0.0005	0.0005	0.001	0.001	0.002	0.002	0.0005	0.0005	0.001	0.001	0.0005	0.0005
S (%)	0.11	0.2	0.17	0.35	0.19	0.56	0.6	0.11	0.07	0.06	0.45	0.06	0.46
Sb (ppm)	0.025	0.025	0.025	0.025	0.025	0.025	0.025	0.025	0.025	0.025	0.025	0.025	0.025
Sc (ppm)	40	29	36	23	40	35	37	41	39	42	40	48	51
Se (ppm)	0.827	1.095	1.625	2.08	1.245	3.81	4.07	0.699	0.426	0.289	2.69	0.271	2.53
Sm (ppm)	0.31	0.33	0.35	0.35	0.58	0.31	0.5	0.49	0.53	0.41	0.2	0.23	0.27
Sn (ppm)	0.5	0.5	0.5	0.5	0.5	0.5	0.5	0.5	0.5	0.5	0.5	0.5	0.5
Sr (ppm)	151.5	188	122	202	191	155	211	202	203	247	88	81.7	66.4
Ta (ppm)	0.1	0.1	0.1	0.1	0.1	0.1	0.1	0.1	0.1	0.1	0.1	0.1	0.1
Tb (ppm)	0.03	0.07	0.07	0.06	0.12	0.09	0.1	0.11	0.11	0.1	0.06	0.07	0.07
Te (ppm)	0.27	0.34	0.51	0.64	0.3	0.92	0.84	0.18	0.1	0.08	0.57	0.07	0.5
Th (ppm)	0.05	0.05	0.07	0.025	0.025	0.05	0.025	0.025	0.05	0.06	0.05	0.08	0.025
Tl (ppm)	0.01	0.02	0.03	0.01	0.01	0.02	0.01	0.01	0.01	0.01	0.02	0.04	0.02
Tm (ppm)	0.05	0.04	0.06	0.05	0.07	0.07	0.06	0.06	0.07	0.06	0.06	0.07	0.07
V (ppm)	203	194	223	170	271	218	229	245	246	221	242	238	263
Y (ppm)	2.4	2.7	2.8	2.7	4.4	3.5	3.8	4	4.1	4.1	3.1	3.2	3.4
U (ppm)	0.025	0.025	0.025	0.025	0.025	0.025	0.025	0.025	0.025	0.025	0.025	0.025	0.025
W (ppm)	1	1	1	1	1	1	1	1	1	1	1	1	1
Yb (ppm)	0.32	0.33	0.47	0.26	0.48	0.37	0.57	0.42	0.48	0.44	0.47	0.38	0.55
Zr (ppm)	4	4	5	4	10	6	7	6	6	6	5	5	7
Zn (ppm)	77	74	71	51	47	51	42	43	38	39	91	88	94

Drill hole #	19-025	19-025	19-025	19-025	19-025	19-025	19-025	19-025	19-025	19-025	19-025	19-025	19-025
Depth From	384	386	388	390	392	394	396	398	400	402	404	406	408
Depth To	385	387	389	391	393	395	397	399	401	403	405	407	409
Rock Type	NOR	NOR	NOR	NOR	NOR	NOR	NOR	NOR	NOR	NOR	NOR	NOR	NOR
Lithological Domain	Norite	Norite	Norite	Norite	Norite	Norite	Norite	Norite	Norite	Norite	Norite	Norite	Norite
Al2O3 (%)	8.98	8.68	11.25	10.65	9.27	10.9	11.3	9.54	9.7	10.35	10.15	9.09	9.7
CaO (%)	5.5	5.39	6.36	6.51	6.53	6.38	6.56	5.96	6.25	6.37	5.8	6.75	6.69
Cr2O3 (%)	0.04	0.04	0.035	0.036	0.035	0.036	0.033	0.038	0.038	0.037	0.031	0.037	0.036
Fe2O3 (%)	16.7	16.2	12.65	12.75	12.5	12.6	11.85	13.45	13.35	12.05	12.25	13.65	13.35
K2O (%)	0.09	0.12	0.52	0.22	0.3	0.18	0.25	0.1	0.07	0.17	0.21	0.1	0.1
MgO (%)	16.6	16.95	15.45	15.65	15.7	16.2	14.8	17.05	17.1	16.35	14.2	16.95	16.4
MnO (%)	0.21	0.2	0.18	0.2	0.19	0.19	0.19	0.2	0.21	0.19	0.19	0.21	0.2
Na2O (%)	0.93	0.78	1.2	0.96	0.9	1.2	1.4	1.02	0.94	1.03	1.61	0.92	0.99
P2O5 (%)	0.01	0.005	0.005	0.005	0.01	0.01	0.005	0.005	0.005	0.02	0.005	0.02	0.02
SiO2 (%)	48.4	48.7	49.1	49	50.4	51.5	50.4	50.8	50	50.6	52.7	51.3	49.9
TiO2 (%)	0.21	0.17	0.17	0.18	0.23	0.18	0.16	0.19	0.19	0.17	0.21	0.21	0.22
LOI (%)	0.68	0.82	2.28	2.94	3.44	1.89	2.37	1.38	0.31	1.37	2.44	0.78	1.65
Total (%)	98.35	98.06	99.22	99.1	99.53	101.29	99.33	99.74	98.16	98.72	99.81	100.02	99.26
Ag (ppm)	1.9	1.8	0.25	0.25	0.25	0.25	0.25	0.25	0.25	0.25	0.25	0.25	0.25
As (ppm)	0.1	0.4	0.4	0.4	0.6	0.3	0.8	0.6	0.4	0.4	0.7	0.5	0.6
Au (ppm)	0.349	0.332	0.072	0.02	0.01	0.009	0.019	0.032	0.037	0.014	0.018	0.007	0.01
Ba (ppm)	24.2	24.8	79.3	42.1	61.3	47.7	61.6	37.4	29.4	48.6	96.3	26.8	31.9
Bi (ppm)	0.3	0.37	0.08	0.04	0.07	0.02	0.04	0.04	0.03	0.02	0.07	0.02	0.03
Cd (ppm)	1.1	1	0.5	0.8	0.7	0.7	0.7	0.8	0.6	0.5	0.6	0.8	0.8
Ce (ppm)	1.2	1.2	1.4	1.7	2.2	2.1	2.4	2.2	1.9	1.6	3	1.7	1.9
Co (ppm)	165	165	101	92	91	89	82	96	98	88	84	95	94
Cs (ppm)	0.51	0.52	2.6	0.77	2.1	1.25	0.95	0.75	0.42	0.83	0.89	0.46	0.96
Cu (ppm)	4200	4540	958	343	166	182	295	424	435	139	326	159	146
Dy (ppm)	0.45	0.36	0.35	0.52	0.49	0.45	0.44	0.51	0.55	0.44	0.54	0.59	0.57
Er (ppm)	0.32	0.37	0.26	0.34	0.35	0.35	0.27	0.38	0.41	0.27	0.33	0.32	0.41
Eu (ppm)	0.13	0.14	0.13	0.11	0.11	0.14	0.19	0.18	0.12	0.17	0.14	0.15	0.1
Ga (ppm)	9.3	9	10.1	10.4	10.2	10.2	11.1	9.8	9.3	9	10.7	9.4	9.6
Gd (ppm)	0.27	0.25	0.27	0.29	0.37	0.4	0.22	0.34	0.37	0.35	0.33	0.33	0.32
Ge (ppm)	2.5	2.5	2.5	2.5	2.5	2.5	2.5	2.5	2.5	2.5	2.5	2.5	2.5
Hf (ppm)	0.1	0.1	0.1	0.2	0.3	0.2	0.2	0.1	0.2	0.1	0.4	0.2	0.2
Hg (ppb)	0.0025	0.009	0.0025	0.0025	0.0025	0.0025	0.0025	0.0025	0.0025	0.006	0.0025	0.0025	0.0025
Ho (ppm)	0.1	0.07	0.07	0.09	0.1	0.1	0.08	0.11	0.1	0.1	0.12	0.12	0.14
In (ppm)	0.011	0.014	0.009	0.005	0.0025	0.0025	0.0025	0.005	0.0025	0.005	0.005	0.005	0.005
La (ppm)	0.6	0.6	0.8	0.7	1.1	1	1.3	1.2	0.8	0.8	1.7	0.8	0.8
Li (ppm)	10	10	20	20	30	10	10	10	10	10	10	5	10
Lu (ppm)	0.07	0.05	0.06	0.07	0.07	0.07	0.07	0.08	0.08	0.06	0.06	0.06	0.07
Mo (ppm)	0.5	0.5	0.5	0.5	0.5	0.5	0.5	0.5	0.5	0.5	0.5	0.5	0.5
Nb (ppm)	0.05	0.1	0.1	0.1	0.2	0.1	0.1	0.1	0.1	0.1	0.4	0.1	0.05
Ni (ppm)	3230	3540	1075	640	541	472	542	687	734	493	547	491	469
Nd (ppm)	0.9	0.8	0.8	0.8	1.2	0.9	1.5	1.2	1	0.9	1.3	0.9	0.9
Pb (ppm)	1	1	1	1	1	1	1	1	4	1	1	1	4
Pd (ppm)	3.64	3.63	0.814	0.24	0.199	0.138	0.219	0.441	0.427	0.208	0.347	0.09	0.136
Pr (ppm)	0.15	0.17	0.2	0.2	0.3	0.24	0.28	0.29	0.26	0.19	0.34	0.24	0.22
Pt (ppm)	0.422	0.42	0.105	0.035	0.035	0.025	0.035	0.06	0.057	0.03	0.053	0.017	0.019
Rb (ppm)	2.1	2.8	21.2	6.4	9	5.5	7	2.2	1.5	3.8	5	1.9	2.5
Re (ppm)	0.005	0.004	0.002	0.001	0.0005	0.0005	0.0005	0.0005	0.001	0.0005	0.0005	0.0005	0.0005
S (%)	1.51	1.6	0.32	0.14	0.06	0.08	0.09	0.18	0.2	0.06	0.09	0.07	0.07
Sb (ppm)	0.025	0.025	0.025	0.025	0.025	0.025	0.025	0.025	0.025	0.025	0.025	0.025	0.025
Sc (ppm)	41	41	32	36	41	38	29	38	42	40	36	46	45
Se (ppm)	9.4	9.69	2.03	0.748	0.39	0.372	0.494	0.95	1.02	0.255	0.479	0.294	0.307
Sm (ppm)	0.17	0.22	0.18	0.26	0.31	0.29	0.36	0.42	0.23	0.2	0.35	0.35	0.29
Sn (ppm)	0.5	0.5	0.5	0.5	0.5	0.5	0.5	0.5	0.5	0.5	0.5	0.5	0.5
Sr (ppm)	101.5	86.7	115	88.6	82.4	130	162	118	103	105.5	129.5	88	94.4
Ta (ppm)	0.05	0.05	0.05	0.1	0.1	0.05	0.1	0.05	0.05	0.05	0.1	0.05	0.05
Tb (ppm)	0.06	0.06	0.04	0.06	0.08	0.05	0.07	0.06	0.06	0.06	0.07	0.07	0.07
Te (ppm)	2.54	2.37	0.54	0.19	0.17	0.09	0.12	0.19	0.22	0.06	0.24	0.09	0.07
Th (ppm)	0.06	0.025	0.05	0.06	0.07	0.07	0.09	0.09	0.05	0.05	0.24	0.06	0.06
Tl (ppm)	0.07	0.07	0.12	0.03	0.06	0.04	0.04	0.03	0.02	0.02	0.02	0.02	0.02
Tm (ppm)	0.05	0.05	0.05	0.05	0.08	0.05	0.06	0.05	0.06	0.06	0.07	0.06	0.05
V (ppm)	217	209	188	198	222	197	181	194	208	191	199	237	222
Y (ppm)	2.6	2.6	2.4	2.7	3	2.8	2.7	3.1	3	2.6	3.1	3.6	3.4
U (ppm)	0.025	0.025	0.025	0.025	0.025	0.025	0.025	0.15	0.025	0.025	0.11	0.025	0.025
W (ppm)	1	1	1	1	1	1	1	1	1	1	1	1	1
Yb (ppm)	0.33	0.4	0.3	0.38	0.43	0.43	0.35	0.46	0.4	0.29	0.39	0.45	0.55
Zr (ppm)	5	5	6	5	8	8	6	7	6	6	18	7	6
Zn (ppm)	87	83	68	73	63	75	77	87	82	73	68	79	80

Drill hole #	19-025	19-025	19-025	19-025	19-025	19-025	19-025	19-025	19-025	19-025	19-025	19-025	19-025
Depth From	410	412	414	416	418	420.33	422	424	426	428	430	432	434
Depth To	411	413	415	417	419	421	423	425	427	429	431	433	435
Rock Type	NOR	NOR	NOR	NOR	NOR	GABVT-Bx	GABVT-Bx	GABVT-Bx	GABVT-Bx	GABVT-Bx	GABVT-Bx	GABVT-Bx	GABVT-Bx
Lithological Domain	Norite	Norite	Norite	Norite	Norite	Breccia	Breccia	Breccia	Breccia	Breccia	Breccia	Breccia	Breccia
Al2O3 (%)	12.6	11.75	8.56	13.8	14.6	19.8	19.2	18.75	21.1	16.95	9.44	6.98	21.2
CaO (%)	7.54	7.05	6.85	7.74	8.44	10.6	11.2	10.65	10.55	8.82	10.05	8.03	12.1
Cr2O3 (%)	0.032	0.033	0.034	0.031	0.026	0.019	0.024	0.04	0.028	0.025	0.117	0.135	0.052
Fe2O3 (%)	11.95	11.5	11.4	10.35	11	6.9	8.13	7.26	5.41	8.44	11.05	12.75	5.23
K2O (%)	0.19	0.12	0.15	0.2	0.2	0.23	0.26	0.42	0.39	0.42	0.1	0.05	0.15
MgO (%)	14.6	15.8	16.65	14.85	12.55	8.78	8.42	8.91	8.98	11	15.8	18.85	8.44
MnO (%)	0.18	0.18	0.2	0.17	0.17	0.1	0.12	0.12	0.09	0.13	0.18	0.21	0.09
Na2O (%)	1.17	1.03	0.74	1.18	1.43	1.56	1.7	2.2	1.77	1.64	0.71	0.39	1.53
P2O5 (%)	0.03	0.02	0.02	0.02	0.02	0.01	0.01	0.01	0.02	0.01	0.005	0.01	0.005
SiO2 (%)	50.5	51.1	51.4	51.8	50.7	48	48.4	51	49.3	48.8	49	49.7	48
TiO2 (%)	0.18	0.14	0.17	0.16	0.15	0.09	0.32	0.13	0.08	0.13	0.19	0.18	0.08
LOI (%)	1.35	0.78	3.56	1.59	2.64	1.95	2.11	2.47	2.83	3.27	2.13	2.65	2.04
Total (%)	100.33	99.51	99.73	101.91	101.94	98.06	99.93	102	100.59	99.67	98.78	99.95	98.93
Ag (ppm)	0.25	0.25	0.25	0.25	0.6	0.6	0.25	0.25	0.25	0.5	1	0.7	0.25
As (ppm)	0.6	0.5	0.4	0.6	0.6	0.5	0.8	0.7	0.5	0.7	1	1	0.9
Au (ppm)	0.02	0.012	0.007	0.009	0.094	0.062	0.021	0.038	0.004	0.089	0.123	0.177	0.026
Ba (ppm)	33.9	29.1	24.7	33.5	39.4	50.1	55.1	101	74.8	71	24.5	10.7	44.2
Bi (ppm)	0.03	0.01	0.01	0.01	0.08	0.08	0.03	0.12	0.01	0.09	0.13	0.16	0.04
Cd (ppm)	0.6	0.8	0.5	0.6	0.8	0.25	0.25	0.25	0.25	0.5	0.8	0.8	0.25
Ce (ppm)	1.3	1.3	1.8	1.6	1.6	1.3	1.6	3	1.5	4.1	3.4	3	1.7
Co (ppm)	96	84	85	76	91	72	53	54	41	69	91	103	40
Cs (ppm)	1.13	0.71	0.88	1.57	1.66	1.14	1.4	1.87	2.82	2.44	1.08	0.37	1.39
Cu (ppm)	378	110	101	131	1090	859	330	585	74	699	1260	1335	212
Dy (ppm)	0.38	0.36	0.51	0.53	0.44	0.24	0.49	0.38	0.23	0.48	0.79	0.72	0.31
Er (ppm)	0.27	0.29	0.39	0.31	0.33	0.16	0.34	0.35	0.19	0.26	0.44	0.54	0.19
Eu (ppm)	0.15	0.11	0.16	0.13	0.13	0.14	0.23	0.22	0.16	0.22	0.33	0.17	0.16
Ga (ppm)	10.5	9.7	8.3	10.3	10.5	12	13.8	12.5	12	11.2	8.6	6.7	11.4
Gd (ppm)	0.31	0.23	0.35	0.34	0.35	0.2	0.36	0.43	0.27	0.52	0.89	0.69	0.33
Ge (ppm)	2.5	2.5	2.5	2.5	2.5	2.5	2.5	2.5	2.5	2.5	2.5	2.5	2.5
Hf (ppm)	0.1	0.1	0.2	0.2	0.2	0.1	0.1	0.2	0.1	0.2	0.3	0.2	0.1
Hg (ppb)	0.0025	0.005	0.0025	0.007	0.0025	0.0025	0.0025	0.005	0.0025	0.0025	0.0025	0.0025	0.0025
Ho (ppm)	0.09	0.08	0.11	0.12	0.08	0.04	0.11	0.08	0.05	0.12	0.18	0.15	0.06
In (ppm)	0.005	0.0025	0.0025	0.0025	0.007	0.006	0.0025	0.0025	0.0025	0.006	0.011	0.014	0.0025
La (ppm)	0.7	0.7	0.8	0.9	0.8	0.7	0.7	1.5	0.8	2.2	1.2	1.1	0.8
Li (ppm)	10	5	20	10	10	10	10	10	20	20	5	5	10
Lu (ppm)	0.05	0.04	0.06	0.06	0.06	0.03	0.05	0.04	0.02	0.05	0.08	0.08	0.04
Mo (ppm)	0.5	0.5	0.5	0.5	0.5	0.5	0.5	0.5	0.5	0.5	0.5	0.5	0.5
Nb (ppm)	0.1	0.1	0.3	0.1	0.1	0.05	0.1	0.2	0.1	0.2	0.1	0.1	0.05
Ni (ppm)	870	446	450	380	1120	1135	449	648	285	863	1175	1435	414
Nd (ppm)	0.7	0.8	1.1	1	0.9	0.8	1	1.7	0.6	2	3.1	2.2	1.2
Pb (ppm)	3	1	4	1	1	1	1	1	1	5	1	1	2
Pd (ppm)	0.311	0.149	0.123	0.204	0.938	0.875	0.286	0.676	0.102	1.13	1.46	2.02	0.394
Pr (ppm)	0.15	0.19	0.25	0.2	0.21	0.15	0.23	0.41	0.16	0.47	0.51	0.46	0.23
Pt (ppm)	0.042	0.026	0.024	0.031	0.12	0.138	0.048	0.082	0.026	0.154	0.214	0.323	0.079
Rb (ppm)	4.7	2.6	3.6	4.1	5.5	5.9	5.5	9.3	9.3	11.2	2.4	0.9	4.2
Re (ppm)	0.001	0.001	0.0005	0.0005	0.002	0.002	0.001	0.001	0.0005	0.001	0.002	0.001	0.0005
S (%)	0.37	0.06	0.02	0.05	0.48	0.41	0.28	0.19	0.02	0.26	0.52	0.56	0.1
Sb (ppm)	0.025	0.025	0.025	0.025	0.025	0.025	0.025	0.025	0.025	0.025	0.025	0.025	0.025
Sc (ppm)	33	31	41	26	21	17	22	19	14	18	43	41	16
Se (ppm)	1.49	0.266	0.179	0.206	2.66	2.41	0.943	1.165	0.097	1.815	3.1	3.1	0.508
Sm (ppm)	0.33	0.31	0.32	0.23	0.22	0.18	0.34	0.46	0.13	0.54	0.93	0.77	0.3
Sn (ppm)	0.5	0.5	0.5	0.5	0.5	0.5	0.5	0.5	0.5	0.5	0.5	0.5	0.5
Sr (ppm)	127	111.5	55.5	128.5	149.5	194	236	277	223	184	141.5	54.6	210
Ta (ppm)	0.05	0.05	0.1	0.1	0.05	0.1	0.1	0.1	0.05	0.05	0.05	0.1	0.05
Tb (ppm)	0.08	0.05	0.05	0.06	0.05	0.04	0.07	0.07	0.04	0.08	0.16	0.12	0.04
Te (ppm)	0.15	0.06	0.06	0.07	0.67	0.59	0.14	0.2	0.02	0.43	0.63	0.82	0.11
Th (ppm)	0.06	0.05	0.1	0.08	0.11	0.025	0.025	0.24	0.05	0.5	0.13	0.05	0.07
Tl (ppm)	0.05	0.02	0.01	0.04	0.12	0.1	0.04	0.07	0.01	0.14	0.17	0.11	0.03
Tm (ppm)	0.05	0.05	0.06	0.06	0.05	0.03	0.06	0.05	0.03	0.03	0.08	0.07	0.02
V (ppm)	203	167	184	154	160	87	195	106	76	133	181	159	71
Y (ppm)	2.5	2.3	3.1	2.9	2.4	1.6	2.3	2.6	1.7	2.8	4.9	3.8	1.9
U (ppm)	0.025	0.025	0.025	0.025	0.65	0.05	0.025	0.14	0.025	0.025	0.025	0.17	0.025
W (ppm)	1	1	1	1	1	1	1	1	2	1	1	1	1
Yb (ppm)	0.44	0.32	0.39	0.43	0.33	0.18	0.28	0.29	0.21	0.32	0.51	0.47	0.21
Zr (ppm)	5	5	7	6	5	3	4	6	4	4	9	7	4
Zn (ppm)	67	68	69	59	62	41	43	39	30	52	66	76	30

Drill hole #	19-025	19-025	19-025	19-025	19-025	19-025	19-025	19-025	19-025	19-025	19-025	19-025	19-025
Depth From	436	438	440	442	444	446	448	450	452	454	456	458	460
Depth To	437	439	441	443	445	447	449	451	453	455	457	459	461
Rock Type	GABVT-Bx	GABVT-Bx	GABVT-Bx	GABVT-Bx	GABVT-Bx	GABVT-Bx	GABVT-Bx	GABVT-Bx	GABVT-Bx	GABVT-Bx	GABVT-Bx	GABVT-Bx	GABVT-Bx
Lithological Domain	Breccia	Breccia	Breccia	Breccia	Breccia	Breccia	Breccia	Breccia	Breccia	Breccia	Breccia	Breccia	Breccia
Al2O3 (%)	16.5	18.3	21.6	16.1	17.55	14.75	18.5	9.31	4.92	7.54	4.34	9.73	11.4
CaO (%)	11.15	10.6	11.25	9.24	9.8	8.83	10.05	10.6	11	8.88	10.4	8.72	10.5
Cr2O3 (%)	0.085	0.032	0.037	0.021	0.036	0.042	0.028	0.186	0.358	0.219	0.386	0.226	0.23
Fe2O3 (%)	7.41	7.43	4.67	11.6	8.83	9.89	7.37	11.1	11.45	10.3	11.6	11.65	9.57
K2O (%)	0.22	0.17	0.26	0.18	0.17	0.22	0.25	0.11	0.11	0.12	0.05	0.11	0.34
MgO (%)	11.25	9.5	8.8	8.87	9.92	11.65	7.92	15.45	17.8	14.65	17.85	15.2	14.9
MnO (%)	0.13	0.12	0.08	0.16	0.14	0.16	0.12	0.2	0.22	0.18	0.2	0.19	0.17
Na2O (%)	1.28	1.73	1.57	1.81	1.86	1.37	2.78	0.91	0.46	1.13	0.36	0.77	1.01
P2O5 (%)	0.005	0.005	0.005	0.01	0.01	0.005	0.01	0.005	0.005	0.005	0.005	0.01	0.005
SiO2 (%)	48.6	48.7	48	49.4	49.7	49.5	52.2	50.2	52.2	53.5	49.8	49.9	50.5
TiO2 (%)	0.12	0.11	0.06	0.38	0.12	0.13	0.11	0.21	0.26	0.21	0.26	0.21	0.17
LOI (%)	2.61	2.56	2.68	2.52	2.7	3.23	1.93	2.7	2.32	2.66	2.81	3.69	2.95
Total (%)	99.39	99.28	99.04	100.33	100.88	99.8	101.33	100.98	101.1	99.4	98.06	100.42	101.76
Ag (ppm)	0.25	0.6	0.25	0.25	0.25	0.6	0.25	0.25	0.25	0.25	0.25	0.25	0.25
As (ppm)	0.6	0.4	0.4	0.5	0.6	0.7	0.3	0.7	0.4	0.5	0.05	0.3	0.4
Au (ppm)	0.071	0.071	0.001	0.011	0.007	0.028	0.004	0.004	0.001	0.0005	0.0005	0.0005	0.001
Ba (ppm)	48.3	51.1	57.2	50.5	49.5	42.6	70.1	22.9	8.9	38.3	7.3	21.8	71.2
Bi (ppm)	0.11	0.22	0.01	0.04	0.03	0.09	0.03	0.08	0.06	0.13	0.1	0.06	0.12
Cd (ppm)	0.6	0.25	0.25	0.5	0.8	0.6	0.6	0.6	0.9	0.7	0.8	0.6	0.6
Ce (ppm)	2.3	2.3	1.3	2.1	1.6	1.7	2.6	2.6	3.2	4.5	3.6	2.8	3.2
Co (ppm)	60	61	36	68	55	68	44	67	67	58	73	71	62
Cs (ppm)	1.48	1.35	1.74	1.69	0.96	1.21	1.31	0.75	0.76	0.86	0.33	1.2	3.21
Cu (ppm)	595	919	30	183	100	266	109	84	44	41	46	45	98
Dy (ppm)	0.59	0.34	0.18	0.47	0.31	0.37	0.31	0.79	1.08	0.94	1.15	0.74	0.72
Er (ppm)	0.37	0.21	0.13	0.31	0.19	0.24	0.17	0.54	0.69	0.63	0.8	0.51	0.6
Eu (ppm)	0.21	0.21	0.14	0.23	0.24	0.23	0.27	0.24	0.33	0.24	0.24	0.21	0.28
Ga (ppm)	9.8	11.6	11.9	14.8	13.5	12	14.9	9.1	5.8	7.8	6.3	8.3	7.8
Gd (ppm)	0.42	0.4	0.18	0.35	0.27	0.31	0.22	0.8	1.1	0.89	1.43	0.81	0.92
Ge (ppm)	2.5	2.5	2.5	2.5	2.5	2.5	2.5	2.5	2.5	2.5	2.5	2.5	2.5
Hf (ppm)	0.1	0.2	0.05	0.2	0.1	0.1	0.2	0.3	0.9	1.6	0.4	0.3	0.3
Hg (ppb)	0.0025	0.0025	0.0025	0.0025	0.0025	0.0025	0.0025	0.0025	0.0025	0.0025	0.0025	0.0025	0.0025
Ho (ppm)	0.1	0.08	0.04	0.08	0.05	0.08	0.06	0.19	0.23	0.18	0.25	0.15	0.17
In (ppm)	0.0025	0.005	0.0025	0.005	0.0025	0.005	0.0025	0.0025	0.0025	0.0025	0.0025	0.0025	0.0025
La (ppm)	0.9	1	0.7	1.2	0.8	0.8	1.5	1	1.1	1.8	1.1	1	1.2
Li (ppm)	10	10	10	20	10	20	10	10	10	10	5	20	20
Lu (ppm)	0.04	0.05	0.03	0.06	0.03	0.05	0.03	0.07	0.1	0.09	0.11	0.05	0.07
Mo (ppm)	0.5	0.5	0.5	0.5	0.5	0.5	0.5	0.5	0.5	0.5	0.5	0.5	0.5
Nb (ppm)	0.05	0.05	0.05	0.1	0.05	0.05	0.1	0.05	0.3	0.3	0.2	0.1	0.1
Ni (ppm)	664	729	274	302	288	455	282	380	412	338	432	378	409
Nd (ppm)	1.8	1.2	0.7	1.1	0.9	1.1	1.2	2.2	3.1	2.9	3.4	2.4	2.5
Pb (ppm)	1	1	1	1	1	1	1	1	1	1	2	2	1
Pd (ppm)	0.833	0.843	0.139	0.123	0.066	0.373	0.024	0.096	0.023	0.062	0.027	0.061	0.155
Pr (ppm)	0.39	0.26	0.17	0.25	0.21	0.24	0.31	0.44	0.55	0.62	0.67	0.47	0.49
Pt (ppm)	0.147	0.139	0.028	0.026	0.021	0.075	0.01	0.019	0.015	0.023	0.017	0.014	0.027
Rb (ppm)	6.1	4.9	8.3	4.2	4.9	5.2	5.3	3	3.8	3.1	0.8	2.7	10.3
Re (ppm)	0.001	0.001	0.0005	0.0005	0.0005	0.001	0.0005	0.0005	0.0005	0.0005	0.001	0.0005	0.001
S (%)	0.22	0.22	0.01	0.21	0.03	0.12	0.03	0.06	0.05	0.04	0.14	0.04	0.04
Sb (ppm)	0.025	0.11	0.025	0.025	0.025	0.025	0.025	0.025	0.025	0.025	0.025	0.025	0.025
Sc (ppm)	25	21	13	25	18	19	19	44	48	40	51	40	36
Se (ppm)	1.35	1.535	0.029	0.56	0.135	0.555	0.127	0.208	0.168	0.142	0.181	0.111	0.196
Sm (ppm)	0.56	0.41	0.2	0.25	0.23	0.31	0.28	0.64	0.98	0.87	0.99	0.72	0.67
Sn (ppm)	0.5	0.5	0.5	0.5	0.5	0.5	0.5	0.5	0.5	0.5	0.5	0.5	0.5
Sr (ppm)	188	239	226	218	284	208	340	105	25.6	94.5	21.8	89.9	149.5
Ta (ppm)	0.05	0.05	0.05	0.05	0.05	0.05	0.05	0.05	0.1	0.1	0.1	0.1	0.1
Tb (ppm)	0.1	0.06	0.02	0.06	0.04	0.04	0.05	0.14	0.17	0.13	0.2	0.14	0.13
Te (ppm)	0.3	0.39	0.01	0.04	0.03	0.1	0.04	0.06	0.04	0.09	0.05	0.04	0.1
Th (ppm)	0.05	0.025	0.05	0.05	0.025	0.025	0.07	0.025	0.09	0.24	0.025	0.05	0.06
Tl (ppm)	0.08	0.04	0.01	0.03	0.01	0.03	0.01	0.01	0.03	0.01	0.03	0.01	0.01
Tm (ppm)	0.05	0.04	0.03	0.06	0.04	0.05	0.04	0.08	0.1	0.1	0.12	0.06	0.07
V (ppm)	104	109	64	297	126	139	109	202	209	191	226	175	166
Y (ppm)	2.9	2.1	1.3	2.8	1.8	2.3	1.9	4.5	5.8	4.9	6.4	4	3.9
U (ppm)	0.025	0.025	0.025	0.025	0.025	0.025	0.025	0.09	0.24	0.15	0.025	0.025	0.025
W (ppm)	1	1	1	1	1	1	1	1	3	1	2	1	1
Yb (ppm)	0.31	0.26	0.14	0.29	0.26	0.32	0.27	0.55	0.59	0.62	0.71	0.53	0.42
Zr (ppm)	5	4	3	6	2	3	7	7	36	66	10	8	7
Zn (ppm)	41	47	27	68	56	73	41	70	84	68	76	75	62

Drill hole #	19-025	19-025	19-025	19-025	19-025	19-025	19-025	19-025	19-025	19-025	19-025	19-025	19-025
Depth From	462	464	466	468	470	472	474	476	478	480	482	484	486
Depth To	463	465	467	469	471	473	475	477	479	481	483	485	487
Rock Type	GABVT-Bx	GABVT-Bx	GABVT-Bx	GABVT-Bx	GABVT-Bx	GABVT-Bx	GABVT-Bx	GABVT-Bx	GABVT-Bx	GABVT-Bx	GABVT-Bx	GABVT-Bx	GABVT-Bx
Lithological Domain	Breccia	Breccia	Breccia	Breccia	Breccia	Breccia	Breccia	Breccia	Breccia	Breccia	Breccia	Breccia	Breccia
Al2O3 (%)	15	18.6	20.3	16.3	17.35	15.65	18.45	20	20.5	18.75	20.5	17.8	17.9
CaO (%)	11.05	9.87	11.15	12.4	11.9	10.55	10.85	11.8	11.4	10.4	11.6	10.45	10.85
Cr2O3 (%)	0.067	0.026	0.023	0.026	0.019	0.018	0.02	0.012	0.01	0.04	0.014	0.045	0.018
Fe2O3 (%)	9.27	7.38	6.47	7.09	5.5	6.05	6.51	5.2	5.23	5.21	5.39	6.76	7.63
K2O (%)	0.19	0.26	0.22	0.17	0.07	0.1	0.09	0.14	0.16	0.16	0.13	0.25	0.12
MgO (%)	11.5	9.18	8.48	9.22	9.4	8.45	8.15	6.67	6.51	6.83	6.78	8.96	9.06
MnO (%)	0.15	0.12	0.11	0.13	0.11	0.11	0.11	0.09	0.09	0.09	0.09	0.12	0.13
Na2O (%)	1.53	1.97	2.01	1.45	2.24	1.91	2.54	2.69	2.82	2.83	2.78	2.33	2.18
P2O5 (%)	0.005	0.01	0.02	0.01	0.01	0.02	0.02	0.02	0.005	0.01	0.02	0.005	0.01
SiO2 (%)	50.1	50.1	50.2	50.1	51.5	55	49.9	51.1	51.1	52.3	51.6	51	51.3
TiO2 (%)	0.16	0.09	0.09	0.13	0.08	0.07	0.1	0.08	0.08	0.1	0.09	0.1	0.1
LOI (%)	2.45	2.81	2.4	3.45	1.54	2.11	1.74	1.15	1.53	1.56	1.33	2.27	1.87
Total (%)	101.5	100.46	101.52	100.51	99.75	100.08	98.53	98.99	99.48	98.33	100.37	100.13	101.21
Ag (ppm)	0.25	0.25	0.25	0.25	0.25	0.6	0.25	0.25	0.25	0.25	0.25	0.25	0.25
As (ppm)	0.2	0.3	0.6	0.05	0.1	0.2	0.05	0.1	0.4	0.1	0.2	0.2	0.3
Au (ppm)	0.012	0.005	0.017	0.01	0.001	0.004	0.004	0.001	0.02	0.0005	0.002	0.0005	0.006
Ba (ppm)	50.2	61.8	71.7	44.9	42.2	44.9	64.2	67.1	69.9	78.2	72.6	75.5	56.1
Bi (ppm)	0.13	0.04	0.1	0.15	0.14	0.62	0.15	0.11	0.11	0.14	0.08	0.07	0.09
Cd (ppm)	0.5	0.25	0.25	0.25	0.7	0.6	0.25	0.25	0.25	0.25	0.25	0.5	0.25
Ce (ppm)	2.3	1.8	2.2	2.1	1.5	1.2	2.3	1.9	2	4.8	2.5	2.4	1.9
Co (ppm)	60	51	46	51	45	57	57	41	43	37	38	48	57
Cs (ppm)	2.22	3.47	2.34	0.85	0.65	0.93	0.75	1	1.93	1.99	1.4	2.66	1.16
Cu (ppm)	176	46	152	172	285	683	558	214	227	94	116	135	188
Dy (ppm)	0.79	0.27	0.29	0.64	0.4	0.3	0.32	0.35	0.31	0.47	0.34	0.47	0.4
Er (ppm)	0.48	0.24	0.25	0.38	0.29	0.25	0.28	0.29	0.32	0.33	0.3	0.29	0.33
Eu (ppm)	0.25	0.19	0.24	0.26	0.15	0.17	0.22	0.21	0.23	0.26	0.2	0.2	0.23
Ga (ppm)	11.1	12.4	12.2	11.1	11.5	11.1	13.6	13.6	14	12.6	14	12.1	12.3
Gd (ppm)	0.83	0.34	0.43	0.65	0.38	0.3	0.4	0.25	0.4	0.48	0.43	0.41	0.41
Ge (ppm)	2.5	2.5	2.5	2.5	2.5	2.5	2.5	2.5	2.5	2.5	2.5	2.5	2.5
Hf (ppm)	0.2	0.1	0.1	0.2	0.2	0.1	0.2	0.1	0.1	0.4	0.2	0.2	0.1
Hg (ppb)	0.0025	0.0025	0.005	0.0025	0.0025	0.0025	0.0025	0.0025	0.006	0.0025	0.0025	0.005	0.0025
Ho (ppm)	0.13	0.07	0.06	0.13	0.1	0.08	0.06	0.08	0.07	0.1	0.1	0.1	0.08
In (ppm)	0.0025	0.0025	0.0025	0.0025	0.0025	0.0025	0.0025	0.0025	0.0025	0.0025	0.0025	0.0025	0.0025
La (ppm)	0.8	0.8	1	0.8	0.6	0.5	1.1	0.8	1	2.5	1.1	1.2	0.8
Li (ppm)	20	20	20	20	10	10	10	10	10	10	10	20	10
Lu (ppm)	0.07	0.02	0.04	0.05	0.04	0.04	0.03	0.04	0.02	0.05	0.03	0.05	0.04
Mo (ppm)	0.5	0.5	0.5	0.5	0.5	1	0.5	0.5	0.5	0.5	0.5	0.5	0.5
Nb (ppm)	0.1	0.1	0.1	0.05	0.1	0.1	0.1	0.1	0.1	0.3	0.1	0.1	0.1
Ni (ppm)	367	250	277	339	275	720	463	261	241	247	230	293	293
Nd (ppm)	2.1	0.9	1.1	1.8	0.8	0.8	1.2	1.1	1.1	2.3	1.2	1.4	0.9
Pb (ppm)	2	1	1	1	3	1	1	1	1	1	1	1	1
Pd (ppm)	0.358	0.058	0.346	0.244	0.031	0.428	0.082	0.083	0.07	0.051	0.037	0.066	0.075
Pr (ppm)	0.4	0.21	0.25	0.32	0.2	0.2	0.3	0.23	0.26	0.56	0.29	0.36	0.19
Pt (ppm)	0.062	0.012	0.056	0.044	0.012	0.073	0.014	0.015	0.016	0.011	0.01	0.016	0.013
Rb (ppm)	4.6	6.8	4.9	3.7	1.2	1.9	1.4	2.2	3.5	3.6	2.5	6	2.5
Re (ppm)	0.0005	0.0005	0.001	0.0005	0.001	0.005	0.001	0.0005	0.001	0.001	0.0005	0.0005	0.0005
S (%)	0.11	0.02	0.04	0.06	0.03	0.13	0.08	0.05	0.1	0.02	0.03	0.02	0.07
Sb (ppm)	0.025	0.025	0.025	0.025	0.025	0.025	0.025	0.025	0.025	0.025	0.025	0.025	0.025
Sc (ppm)	28	20	18	34	30	26	21	23	20	23	21	23	26
Se (ppm)	0.43	0.124	0.264	0.392	0.254	1.405	0.945	0.46	0.71	0.213	0.255	0.194	0.43
Sm (ppm)	0.6	0.28	0.28	0.44	0.33	0.2	0.36	0.23	0.15	0.43	0.28	0.35	0.25
Sn (ppm)	0.5	0.5	0.5	0.5	0.5	0.5	0.5	0.5	0.5	0.5	0.5	0.5	0.5
Sr (ppm)	221	255	297	214	252	234	282	275	306	300	313	275	233
Ta (ppm)	0.1	0.1	0.1	0.2	0.1	0.2	0.2	0.1	0.1	0.2	0.1	0.2	0.1
Tb (ppm)	0.11	0.05	0.04	0.11	0.08	0.06	0.05	0.07	0.05	0.05	0.05	0.07	0.06
Te (ppm)	0.12	0.03	0.1	0.12	0.08	0.61	0.13	0.12	0.13	0.1	0.06	0.07	0.08
Th (ppm)	0.025	0.025	0.025	0.025	0.05	0.025	0.05	0.07	0.07	0.75	0.07	0.06	0.025
Tl (ppm)	0.01	0.01	0.01	0.02	0.01	0.08	0.04	0.02	0.02	0.02	0.01	0.02	0.02
Tm (ppm)	0.07	0.03	0.03	0.05	0.04	0.04	0.04	0.04	0.03	0.04	0.04	0.04	0.04
V (ppm)	162	107	92	133	110	94	98	90	88	88	87	99	120
Y (ppm)	3.8	1.6	1.8	3.4	2.3	2.1	2.2	2	2.1	2.6	2.1	2.4	2.3
U (ppm)	0.025	0.025	0.025	0.025	0.025	0.025	0.025	0.025	0.025	0.15	0.025	0.025	0.025
W (ppm)	1	1	1	1	1	1	1	3	1	23	1	1	20
Yb (ppm)	0.45	0.32	0.22	0.39	0.3	0.32	0.28	0.23	0.27	0.35	0.29	0.28	0.27
Zr (ppm)	5	3	3	5	3	3	4	4	3	15	5	5	4
Zn (ppm)	54	45	37	41	35	48	40	29	27	41	33	43	49

Drill hole #	19-025	19-025	19-025	19-025	19-025	19-025	19-025	19-025	19-025
Depth From	488	490	492	494	496	498	500	502	504.2
Depth To	489	491	493	495	497	499	501	503	505.44
Rock Type	GABVT-Bx	GABVT-Bx	GABVT-Bx	GABVT-Bx	GABVT-Bx	GABVT-Bx	GABVT-Bx	GABVT-Bx	GABVT-Bx
Lithological Domain	Breccia	Breccia	Breccia	Breccia	Breccia	Breccia	Breccia	Breccia	Breccia
Al_2O_3 (%)	16.6	19	17.55	18.1	18.9	18.2	22.1	16.95	20.4
CaO (%)	10.1	11.05	10.55	10.75	9.81	10.8	10.05	9.65	9.58
Cr_2O_3 (%)	0.021	0.011	0.013	0.014	0.016	0.021	0.007	0.026	0.019
Fe_2O_3 (%)	8.47	5.2	8.04	6.64	6.98	6.8	4.52	7.33	5.79
K_2O (%)	0.15	0.12	0.12	0.1	0.14	0.14	0.17	0.15	0.27
MgO (%)	9.98	6.68	8.6	8.33	8.51	8.82	5.1	9.27	7.64
MnO (%)	0.14	0.09	0.13	0.12	0.12	0.12	0.07	0.13	0.1
Na_2O (%)	1.92	3.03	2.51	2.79	2.69	2.46	3.52	2.63	2.91
P_2O_5 (%)	0.01	0.01	0.005	0.005	0.01	0.005	0.005	0.01	0.02
SiO_2 (%)	51.2	55.2	51.3	51.6	52.2	51.5	51.7	53.2	52
TiO_2 (%)	0.11	0.08	0.1	0.1	0.08	0.1	0.05	0.08	0.08
LOI (%)	2.42	1.02	1.7	1.52	2.06	1.76	1.72	1.92	2.02
Total (%)	101.16	101.54	100.65	100.1	101.56	100.76	99.06	101.4	100.9
Ag (ppm)	0.25	0.25	0.25	0.25	0.25	0.25	0.25	0.25	0.25
As (ppm)	0.1	0.1	0.6	0.1	0.3	0.2	0.2	0.05	0.1
Au (ppm)	0.074	0.001	0.028	0.007	0.002	0.011	0.044	0.003	0.019
Ba (ppm)	56	72.6	60.5	73.1	60.9	67.7	75.2	59.2	84.4
Bi (ppm)	0.56	0.01	0.13	0.03	0.05	0.05	0.03	0.05	0.14
Cd (ppm)	0.6	0.25	0.25	0.25	0.25	0.25	0.25	0.25	0.5
Ce (ppm)	2.1	6	2.2	2.8	1.7	2.3	1.7	2.2	2.1
Co (ppm)	68	36	62	44	47	46	33	50	40
Cs (ppm)	1.05	0.63	0.95	0.92	1.15	1.27	1.32	1.15	2.79
Cu (ppm)	672	36	398	130	96	112	132	103	249
Dy (ppm)	0.43	0.46	0.37	0.46	0.26	0.48	0.25	0.33	0.19
Er (ppm)	0.33	0.3	0.28	0.36	0.24	0.29	0.11	0.18	0.14
Eu (ppm)	0.17	0.26	0.21	0.23	0.19	0.27	0.22	0.23	0.25
Ga (ppm)	11.9	12.8	13.2	13.2	12.7	13	17.1	12.5	13.9
Gd (ppm)	0.41	0.45	0.41	0.44	0.26	0.34	0.12	0.27	0.21
Ge (ppm)	2.5	2.5	2.5	2.5	2.5	2.5	2.5	2.5	2.5
Hf (ppm)	0.1	0.2	0.1	0.2	0.1	0.1	0.1	0.1	0.1
Hg (ppb)	0.005	0.0025	0.0025	0.0025	0.0025	0.0025	0.0025	0.0025	0.0025
Ho (ppm)	0.09	0.07	0.1	0.09	0.04	0.06	0.03	0.04	0.05
In (ppm)	0.0025	0.0025	0.0025	0.0025	0.0025	0.0025	0.0025	0.0025	0.0025
La (ppm)	1	2.7	1	1.2	0.8	1	0.9	1	1
Li (ppm)	20	10	10	10	20	10	10	20	20
Lu (ppm)	0.04	0.04	0.05	0.05	0.02	0.05	0.01	0.03	0.03
Mo (ppm)	0.5	0.5	0.5	0.5	0.5	0.5	0.5	0.5	0.5
Nb (ppm)	0.2	2.4	0.6	0.4	0.1	0.2	0.1	0.1	0.1
Ni (ppm)	680	175	344	221	227	240	185	242	285
Nd (ppm)	1.2	2.9	1.3	1.6	0.9	1.2	0.7	1	0.9
Pb (ppm)	2	1	1	1	1	1	1	1	1
Pd (ppm)	0.794	0.006	0.09	0.01	0.033	0.059	0.015	0.07	0.189
Pr (ppm)	0.29	0.71	0.28	0.35	0.18	0.29	0.14	0.27	0.22
Pt (ppm)	0.136	0.0025	0.018	0.008	0.013	0.012	0.0025	0.016	0.037
Rb (ppm)	2.9	1.3	2.5	2.2	2.9	3.4	4.1	3.4	7.3
Re (ppm)	0.001	0.0005	0.001	0.001	0.0005	0.001	0.0005	0.001	0.001
S (%)	0.2	0.01	0.15	0.03	0.02	0.04	0.06	0.05	0.09
Sb (ppm)	0.06	0.025	0.025	0.025	0.025	0.025	0.025	0.025	0.025
Sc (ppm)	27	25	26	25	19	22	10	21	12
Se (ppm)	1.675	0.1	1.005	0.226	0.186	0.233	0.392	0.309	0.617
Sm (ppm)	0.26	0.47	0.34	0.38	0.17	0.41	0.15	0.15	0.22
Sn (ppm)	0.5	0.5	0.5	0.5	0.5	0.5	0.5	0.5	0.5
Sr (ppm)	208	294	253	316	274	328	411	299	437
Ta (ppm)	0.2	0.2	0.2	0.2	0.1	0.2	0.1	0.2	0.1
Tb (ppm)	0.05	0.06	0.06	0.07	0.04	0.05	0.03	0.04	0.05
Te (ppm)	0.52	0.02	0.14	0.03	0.05	0.09	0.05	0.07	0.13
Th (ppm)	0.05	0.43	0.05	0.12	0.025	0.025	0.025	0.025	0.025
Tl (ppm)	0.09	0.01	0.04	0.01	0.02	0.02	0.04	0.02	0.05
Tm (ppm)	0.05	0.05	0.05	0.04	0.03	0.04	0.01	0.02	0.01
V (ppm)	126	85	126	111	79	106	49	95	74
Y (ppm)	2.5	2.2	2.3	2.6	1.5	2.2	0.8	1.6	1.3
U (ppm)	0.025	0.025	0.025	0.025	0.025	0.025	0.025	0.025	0.025
W (ppm)	1	1	1	1	1	1	1	1	1
Yb (ppm)	0.29	0.27	0.37	0.38	0.2	0.32	0.14	0.25	0.33
Zr (ppm)	4	6	3	5	3	4	1	3	2
Zn (ppm)	55	46	54	39	44	44	31	53	43

Appendix C

Sulfur Isotope Data

Sample #	Drill hole	Depth (m)	Assemblage	Mineral	Crystal ID	Analysis #	δ34S (‰)	δ34S error	Δ33S (‰)	Δ33S error	Δ36S (‰)	Δ36S error
TS-009	17-804	155.63	Py-Po-Pn-Ccp	Pyrite	Py4	1	0.96	0.11	-0.13	0.08	0.2	0.57
TS-009	17-804	155.63	Py-Po-Pn-Ccp	Pyrite	Py4	2	0.78	0.11	-0.08	0.08	0.1	0.52
TS-009	17-804	155.63	Py-Po-Pn-Ccp	Pyrite	Py4	3	1.04	0.11	-0.09	0.08	0.3	0.48
TS-009	17-804	155.63	Py-Po-Pn-Ccp	Pyrite	Py4	4	0.41	0.11	-0.07	0.08	0.1	0.51
TS-009	17-804	155.63	Py-Po-Pn-Ccp	Pyrite	Py4	5	1.16	0.11	-0.12	0.08	0.3	0.56
TS-009	17-804	155.63	Py-Po-Pn-Ccp	Pyrite	Py4	6	2.38	0.11	-0.07	0.08	0.2	0.65
TS-009	17-804	155.63	Py-Po-Pn-Ccp	Pyrite	Py4	7	2.07	0.11	-0.09	0.08	0.5	0.50
TS-009	17-804	155.63	Py-Po-Pn-Ccp	Pyrite	Py4	8	1.78	0.11	-0.08	0.08	0.3	0.65
TS-009	17-804	155.63	Py-Po-Pn-Ccp	Pyrite	Py4	9	2.45	0.11	-0.07	0.08	0.4	0.57
TS-009	17-804	155.63	Py-Po-Pn-Ccp	Pyrite	Py4	10	1.91	0.11	-0.09	0.08	0.1	0.60
TS-009	17-804	155.63	Py-Po-Pn-Ccp	Chalcopyrite	Ccp3	1	1.09	0.12	-0.10	0.11	0.3	0.23
TS-009	17-804	155.63	Py-Po-Pn-Ccp	Chalcopyrite	Ccp3	2	-0.40	0.22	-0.09	0.15	0.2	0.23
TS-009	17-804	155.63	Py-Po-Pn-Ccp	Chalcopyrite	Ccp3	3	0.59	0.13	-0.06	0.11	0.2	0.23
TS-009	17-804	155.63	Py-Po-Pn-Ccp	Chalcopyrite	Ccp3	4	0.93	0.12	-0.11	0.11	0.3	0.23
TS-009	17-804	155.63	Py-Po-Pn-Ccp	Chalcopyrite	Ccp3	5	1.05	0.12	-0.07	0.11	0.5	0.23
TS-009	17-804	155.63	Py-Po-Pn-Ccp	Chalcopyrite	Ccp3	6	0.93	0.12	-0.10	0.11	0.3	0.23
TS-009	17-804	155.63	Py-Po-Pn-Ccp	Chalcopyrite	Ccp3	7	0.91	0.12	-0.09	0.11	0.3	0.23
TS-009	17-804	155.63	Py-Po-Pn-Ccp	Chalcopyrite	Ccp3	8	0.72	0.12	-0.05	0.11	0.4	0.23
TS-009	17-804	155.63	Py-Po-Pn-Ccp	Chalcopyrite	Ccp3	9	1.07	0.12	-0.08	0.10	0.4	0.23
TS-009	17-804	155.63	Py-Po-Pn-Ccp	Chalcopyrite	Ccp3	10	0.89	0.13	-0.07	0.11	0.1	0.23
TS-009	17-804	155.63	Py-Po-Pn-Ccp	Chalcopyrite	Ccp3	11	0.73	0.13	-0.10	0.11	0.2	0.23
TS-009	17-804	155.63	Py-Po-Pn-Ccp	Chalcopyrite	Ccp3	12	0.90	0.12	-0.03	0.11	0.7	0.23
TS-009	17-804	155.63	Py-Po-Pn-Ccp	Chalcopyrite	Ccp3	14	1.02	0.13	-0.04	0.11	0.4	0.23
TS-009	17-804	155.63	Py-Po-Pn-Ccp	Chalcopyrite	Ccp3	15	0.87	0.14	-0.07	0.11	0.3	0.23
TS-009	17-804	155.63	Py-Po-Pn-Ccp	Pyrrhotite	Po1	1	1.59	0.16	-0.01	0.14	0.5	0.39
TS-009	17-804	155.63	Py-Po-Pn-Ccp	Pyrrhotite	Po1	2	2.28	0.16	-0.12	0.17	-2.9	0.39
TS-009	17-804	155.63	Py-Po-Pn-Ccp	Pyrrhotite	Po1	3	1.47	0.16	-0.02	0.14	0.3	0.39
TS-009	17-804	155.63	Py-Po-Pn-Ccp	Pyrrhotite	Po1	4	1.60	0.16	-0.06	0.14	0.3	0.39
TS-009	17-804	155.63	Py-Po-Pn-Ccp	Pyrrhotite	Po1	5	1.44	0.17	-0.01	0.14	0.2	0.39
TS-009	17-804	155.63	Py-Po-Pn-Ccp	Pyrrhotite	Po1	6	1.48	0.16	-0.06	0.14	-0.1	0.39
TS-009	17-804	155.63	Py-Po-Pn-Ccp	Pyrrhotite	Po1	7	1.44	0.16	-0.07	0.14	0.4	0.39
TS-009	17-804	155.63	Py-Po-Pn-Ccp	Pyrrhotite	Po1	8	1.54	0.16	0.02	0.14	0.8	0.39
TS-009	17-804	155.63	Py-Po-Pn-Ccp	Pyrrhotite	Po1	9	1.58	0.16	-0.05	0.14	0.4	0.39
TS-009	17-804	155.63	Py-Po-Pn-Ccp	Pyrrhotite	Po1	10	1.43	0.16	-0.05	0.14	0.4	0.39
TS-009	17-804	155.63	Py-Po-Pn-Ccp	Pyrrhotite	Po1	11	1.46	0.16	-0.03	0.14	0.2	0.39
TS-009	17-804	155.63	Py-Po-Pn-Ccp	Pyrrhotite	Po1	12	1.60	0.16	-0.09	0.14	0.3	0.39
TS-009	17-804	155.63	Py-Po-Pn-Ccp	Pyrrhotite	Po1	13	1.47	0.17	0.01	0.14	0.2	0.39
TS-009	17-804	155.63	Py-Po-Pn-Ccp	Pyrrhotite	Po1	14	1.02	0.18	0.03	0.15	0.8	0.39
TS-009	17-804	155.63	Py-Po-Pn-Ccp	Pyrrhotite	Po1	15	1.66	0.16	-0.04	0.14	0.3	0.39
TS-009	17-804	155.63	Py-Po-Pn-Ccp	Pyrrhotite	Po2	1	1.59	0.16	-0.05	0.14	0.3	0.39
TS-009	17-804	155.63	Py-Po-Pn-Ccp	Pyrrhotite	Po2	2	1.34	0.16	0.00	0.14	0.2	0.39
TS-009	17-804	155.63	Py-Po-Pn-Ccp	Pyrrhotite	Po2	3	1.49	0.16	-0.05	0.14	0.4	0.39
TS-009	17-804	155.63	Py-Po-Pn-Ccp	Pyrrhotite	Po2	4	1.33	0.16	-0.06	0.15	0.1	0.39
TS-009	17-804	155.63	Py-Po-Pn-Ccp	Pyrrhotite	Po2	5	1.47	0.16	-0.01	0.14	0.4	0.39
TS-009	17-804	155.63	Py-Po-Pn-Ccp	Pyrrhotite	Po2	6	1.54	0.16	0.01	0.15	0.3	0.39
TS-009	17-804	155.63	Py-Po-Pn-Ccp	Pyrrhotite	Po2	7	1.58	0.16	-0.03	0.14	0.3	0.39
TS-009	17-804	155.63	Py-Po-Pn-Ccp	Pyrrhotite	Po2	8	1.63	0.16	-0.01	0.14	0.4	0.39
TS-009	17-804	155.63	Py-Po-Pn-Ccp	Pyrrhotite	Po2	9	1.40	0.16	0.03	0.15	0.5	0.39
TS-009	17-804	155.63	Py-Po-Pn-Ccp	Pyrrhotite	Po2	10	1.43	0.16	-0.02	0.14	0.3	0.39
TS-016	17-804	185.16	Py-Po-Pn-Ccp	Pyrite	Py8	1	2.40	0.11	-0.15	0.08	0.0	0.49
TS-016	17-804	185.16	Py-Po-Pn-Ccp	Pyrite	Py8	2	1.72	0.11	-0.07	0.08	0.0	0.53
TS-016	17-804	185.16	Py-Po-Pn-Ccp	Pyrite	Py8	3	0.73	0.11	-0.09	0.08	0.3	0.54
TS-016	17-804	185.16	Py-Po-Pn-Ccp	Pyrite	Py8	4	0.59	0.11	-0.05	0.08	0.3	0.59
TS-016	17-804	185.16	Py-Po-Pn-Ccp	Pyrite	Py8	5	0.54	0.11	-0.08	0.08	0.1	0.56
TS-016	17-804	185.16	Py-Po-Pn-Ccp	Pyrite	Py8	6	0.93	0.11	-0.09	0.08	0.4	0.58
TS-016	17-804	185.16	Py-Po-Pn-Ccp	Chalcopyrite	Ccp6	1	1.02	0.13	-0.05	0.11	0.0	0.23
TS-016	17-804	185.16	Py-Po-Pn-Ccp	Chalcopyrite	Ccp6	2	1.08	0.12	-0.12	0.10	0.3	0.23
TS-016	17-804	185.16	Py-Po-Pn-Ccp	Chalcopyrite	Ccp6	3	1.11	0.13	-0.09	0.10	0.2	0.23
TS-016	17-804	185.16	Py-Po-Pn-Ccp	Chalcopyrite	Ccp6	4	1.22	0.12	-0.08	0.11	0.4	0.23
TS-016	17-804	185.16	Py-Po-Pn-Ccp	Chalcopyrite	Ccp6	5	1.07	0.12	-0.04	0.11	0.3	0.23
TS-016	17-804	185.16	Py-Po-Pn-Ccp	Chalcopyrite	Ccp6	6	1.12	0.12	-0.09	0.10	0.3	0.23

Sample #	Drill hole	Depth (m)	Assemblage	Mineral	Crystal ID	Analysis #	δ34S (‰)	δ34S error	Δ33S (‰)	Δ33S error	Δ36S (‰)	Δ36S error
TS-016	17-804	185.16	Py-Po-Pn-Ccp	Chalcopyrite	Ccp6	7	0.94	0.13	-0.09	0.11	0.5	0.23
TS-016	17-804	185.16	Py-Po-Pn-Ccp	Chalcopyrite	Ccp6	8	1.15	0.12	-0.04	0.11	0.5	0.23
TS-016	17-804	185.16	Py-Po-Pn-Ccp	Chalcopyrite	Ccp6	9	1.11	0.12	-0.10	0.10	0.5	0.23
TS-016	17-804	185.16	Py-Po-Pn-Ccp	Chalcopyrite	Ccp6	10	1.22	0.12	-0.11	0.10	0.2	0.23
TS-016	17-804	185.16	Py-Po-Pn-Ccp	Chalcopyrite	Ccp6	11	1.12	0.12	-0.07	0.11	0.1	0.23
TS-016	17-804	185.16	Py-Po-Pn-Ccp	Chalcopyrite	Ccp6	12	1.13	0.11	-0.05	0.10	0.5	0.23
TS-016	17-804	185.16	Py-Po-Pn-Ccp	Pyrrhotite	Po5	1	1.36	0.16	0.00	0.14	0.5	0.39
TS-016	17-804	185.16	Py-Po-Pn-Ccp	Pyrrhotite	Po5	2	1.83	0.16	-0.03	0.14	0.3	0.39
TS-016	17-804	185.16	Py-Po-Pn-Ccp	Pyrrhotite	Po5	3	1.61	0.16	-0.02	0.14	0.7	0.39
TS-016	17-804	185.16	Py-Po-Pn-Ccp	Pyrrhotite	Po5	4	1.68	0.16	-0.10	0.14	0.3	0.39
TS-016	17-804	185.16	Py-Po-Pn-Ccp	Pyrrhotite	Po5	5	1.76	0.16	-0.09	0.14	0.6	0.39
TS-016	17-804	185.16	Py-Po-Pn-Ccp	Pyrrhotite	Po5	6	1.65	0.16	-0.07	0.14	0.4	0.39
TS-016	17-804	185.16	Py-Po-Pn-Ccp	Pyrrhotite	Po5	7	1.82	0.16	-0.05	0.14	0.5	0.39
TS-016	17-804	185.16	Py-Po-Pn-Ccp	Pyrrhotite	Po5	8	1.67	0.16	-0.09	0.14	0.5	0.39
TS-016	17-804	185.16	Py-Po-Pn-Ccp	Pyrrhotite	Po5	9	1.74	0.16	-0.03	0.14	0.3	0.39
TS-016	17-804	185.16	Py-Po-Pn-Ccp	Pyrrhotite	Po5	10	1.82	0.16	-0.03	0.14	0.4	0.39
TS-016	17-804	185.16	Py-Po-Pn-Ccp	Pyrrhotite	Po5	11	1.79	0.16	-0.08	0.14	0.5	0.39
TS-016	17-804	185.16	Py-Po-Pn-Ccp	Pyrrhotite	Po5	12	1.69	0.16	-0.07	0.14	0.3	0.39
TS-016	17-804	185.16	Py-Po-Pn-Ccp	Pyrrhotite	Po5	13	1.78	0.16	-0.03	0.14	0.6	0.39
TS-016	17-804	185.16	Py-Po-Pn-Ccp	Pyrrhotite	Po5	14	1.72	0.16	-0.01	0.14	0.6	0.39
TS-016	17-804	185.16	Py-Po-Pn-Ccp	Pyrrhotite	Po5	15	1.87	0.16	-0.04	0.14	0.4	0.39
TS-016	17-804	185.16	Py-Po-Pn-Ccp	Pyrrhotite	Po7	1	1.46	0.16	0.00	0.14	0.7	0.39
TS-016	17-804	185.16	Py-Po-Pn-Ccp	Pyrrhotite	Po7	2	1.49	0.16	-0.05	0.14	0.5	0.39
TS-016	17-804	185.16	Py-Po-Pn-Ccp	Pyrrhotite	Po7	3	1.65	0.16	-0.02	0.14	0.5	0.39
TS-016	17-804	185.16	Py-Po-Pn-Ccp	Pyrrhotite	Po7	4	1.66	0.16	-0.04	0.14	0.8	0.39
TS-016	17-804	185.16	Py-Po-Pn-Ccp	Pyrrhotite	Po7	5	1.65	0.16	-0.05	0.14	0.3	0.39
TS-016	17-804	185.16	Py-Po-Pn-Ccp	Pyrrhotite	Po7	6	1.69	0.16	-0.01	0.14	0.4	0.39
TS-016	17-804	185.16	Py-Po-Pn-Ccp	Pyrrhotite	Po7	7	1.59	0.16	0.06	0.14	0.6	0.39
TS-016	17-804	185.16	Py-Po-Pn-Ccp	Pyrrhotite	Po7	8	1.56	0.16	-0.04	0.14	0.2	0.39
TS-016	17-804	185.16	Py-Po-Pn-Ccp	Pyrrhotite	Po7	9	1.73	0.16	-0.09	0.14	0.5	0.39
TS-016	17-804	185.16	Py-Po-Pn-Ccp	Pyrrhotite	Po7	10	1.70	0.16	-0.11	0.14	0.6	0.39
TS-016	17-804	185.16	Py-Po-Pn-Ccp	Pyrrhotite	Po7	11	1.64	0.16	0.00	0.14	0.3	0.39
TS-016	17-804	185.16	Py-Po-Pn-Ccp	Pyrrhotite	Po7	12	1.73	0.16	-0.05	0.14	0.3	0.39
TS-016	17-804	185.16	Py-Po-Pn-Ccp	Pentlandite	Pn9	1	0.68	0.17	-0.07	0.09	0.1	0.28
TS-016	17-804	185.16	Py-Po-Pn-Ccp	Pentlandite	Pn9	2	0.39	0.18	-0.13	0.10	0.4	0.28
TS-016	17-804	185.16	Py-Po-Pn-Ccp	Pentlandite	Pn9	3	0.64	0.16	-0.03	0.10	0.4	0.28
TS-016	17-804	185.16	Py-Po-Pn-Ccp	Pentlandite	Pn9	4	-0.07	0.21	-0.07	0.11	0.0	0.28
TS-016	17-804	185.16	Py-Po-Pn-Ccp	Pentlandite	Pn9	5	-0.99	0.21	-0.10	0.12	0.3	0.28
TS-016	17-804	185.16	Py-Po-Pn-Ccp	Pentlandite	Pn9	6	0.34	0.17	-0.05	0.09	-0.1	0.28
TS-016	17-804	185.16	Py-Po-Pn-Ccp	Pentlandite	Pn9	7	0.60	0.16	-0.10	0.10	0.2	0.28
TS-016	17-804	185.16	Py-Po-Pn-Ccp	Pentlandite	Pn9	8	0.67	0.17	-0.11	0.10	0.2	0.28
TS-016	17-804	185.16	Py-Po-Pn-Ccp	Pentlandite	Pn9	9	0.57	0.16	-0.11	0.09	0.0	0.28
TS-016	17-804	185.16	Py-Po-Pn-Ccp	Pentlandite	Pn9	10	0.91	0.17	0.00	0.10	0.6	0.28
TS-016	17-804	185.16	Py-Po-Pn-Ccp	Pentlandite	Pn9	11	0.58	0.18	-0.13	0.11	0.3	0.28
TS-016	17-804	185.16	Py-Po-Pn-Ccp	Pentlandite	Pn9	12	0.80	0.16	-0.07	0.09	0.6	0.28
TS-016	17-804	185.16	Py-Po-Pn-Ccp	Pentlandite	Pn9	13	0.95	0.16	-0.10	0.09	0.1	0.28
TS-016	17-804	185.16	Py-Po-Pn-Ccp	Pentlandite	Pn9	14	0.87	0.16	-0.10	0.09	-0.1	0.28
TS-018	17-804	195.00	Py-Po-Pn-Ccp	Pyrrhotite	Po10	1	1.15	0.15	-0.16	0.15		
TS-018	17-804	195.00	Py-Po-Pn-Ccp	Pyrrhotite	Po10	2	1.38	0.15	-0.08	0.15		
TS-018	17-804	195.00	Py-Po-Pn-Ccp	Pyrrhotite	Po10	3	1.29	0.15	-0.11	0.14		
TS-018	17-804	195.00	Py-Po-Pn-Ccp	Pyrrhotite	Po10	4	1.15	0.15	-0.07	0.14		
TS-018	17-804	195.00	Py-Po-Pn-Ccp	Pyrrhotite	Po10	5	1.33	0.15	-0.09	0.14		
TS-018	17-804	195.00	Py-Po-Pn-Ccp	Pyrrhotite	Po10	6	1.23	0.15	0.01	0.14		
TS-018	17-804	195.00	Py-Po-Pn-Ccp	Pyrrhotite	Po10	7	1.35	0.15	-0.02	0.15		
TS-018	17-804	195.00	Py-Po-Pn-Ccp	Pyrrhotite	Po10	8	0.96	0.15	0.00	0.14		
TS-018	17-804	195.00	Py-Po-Pn-Ccp	Pyrrhotite	Po10	9	1.28	0.15	-0.02	0.15		
TS-018	17-804	195.00	Py-Po-Pn-Ccp	Pyrrhotite	Po10	10	0.96	0.15	-0.03	0.14		
TS-018	17-804	195.00	Py-Po-Pn-Ccp	Pyrrhotite	Po10	11	1.02	0.16	0.00	0.15		
TS-018	17-804	195.00	Py-Po-Pn-Ccp	Pyrrhotite	Po10	12	1.02	0.15	-0.02	0.15		
TS-018	17-804	195.00	Py-Po-Pn-Ccp	Pyrrhotite	Po10	13	1.12	0.15	-0.13	0.15		
TS-018	17-804	195.00	Py-Po-Pn-Ccp	Pyrrhotite	Po10	14	1.33	0.16	-0.07	0.15		

Sample #	Drill hole	Depth (m)	Assemblage	Mineral	Crystal ID	Analysis #	δ34S (‰)	δ34S error	Δ33S (‰)	Δ33S error	Δ36S (‰)	Δ36S error
TS-018	17-804	195.00	Py-Po-Pn-Ccp	Pyrrhotite	Po10	15	1.07	0.16	-0.02	0.14		
TS-018	17-804	195.00	Py-Po-Pn-Ccp	Pyrrhotite	Po12	1	0.76	0.15	-0.03	0.14		
TS-018	17-804	195.00	Py-Po-Pn-Ccp	Pyrrhotite	Po12	2	1.01	0.16	-0.08	0.14		
TS-018	17-804	195.00	Py-Po-Pn-Ccp	Pyrrhotite	Po12	3	0.96	0.16	-0.11	0.14		
TS-018	17-804	195.00	Py-Po-Pn-Ccp	Pyrrhotite	Po12	4	1.08	0.15	-0.09	0.15		
TS-018	17-804	195.00	Py-Po-Pn-Ccp	Pyrrhotite	Po12	5	1.00	0.15	-0.08	0.15		
TS-018	17-804	195.00	Py-Po-Pn-Ccp	Pyrrhotite	Po12	6	0.89	0.16	-0.04	0.15		
TS-018	17-804	195.00	Py-Po-Pn-Ccp	Pyrrhotite	Po12	7	1.13	0.16	-0.07	0.15		
TS-018	17-804	195.00	Py-Po-Pn-Ccp	Pyrrhotite	Po12	8	1.08	0.15	-0.04	0.14		
TS-018	17-804	195.00	Py-Po-Pn-Ccp	Pyrrhotite	Po12	9	0.72	0.16	-0.06	0.15		
TS-018	17-804	195.00	Py-Po-Pn-Ccp	Pyrrhotite	Po12	10	1.11	0.15	-0.10	0.14		
TS-018	17-804	195.00	Py-Po-Pn-Ccp	Pyrrhotite	Po12	11	0.56	0.16	-0.10	0.14		
TS-018	17-804	195.00	Py-Po-Pn-Ccp	Pyrrhotite	Po12	12	0.95	0.15	-0.10	0.14		
TS-018	17-804	195.00	Py-Po-Pn-Ccp	Pyrrhotite	Po12	13	1.12	0.15	-0.03	0.14		
TS-018	17-804	195.00	Py-Po-Pn-Ccp	Pyrrhotite	Po12	14	1.00	0.15	-0.03	0.14		
TS-018	17-804	195.00	Py-Po-Pn-Ccp	Pyrrhotite	Po12	15	1.14	0.15	-0.10	0.14		
TS-018	17-804	195.00	Py-Po-Pn-Ccp	Pyrrhotite	Po16	1	1.14	0.15	-0.06	0.14		
TS-018	17-804	195.00	Py-Po-Pn-Ccp	Pyrrhotite	Po16	2	1.15	0.15	-0.10	0.15		
TS-018	17-804	195.00	Py-Po-Pn-Ccp	Pyrrhotite	Po16	3	1.14	0.15	-0.03	0.14		
TS-018	17-804	195.00	Py-Po-Pn-Ccp	Pyrrhotite	Po16	4	1.34	0.15	-0.01	0.15		
TS-018	17-804	195.00	Py-Po-Pn-Ccp	Pyrrhotite	Po16	5	1.07	0.15	-0.14	0.15		
TS-018	17-804	195.00	Py-Po-Pn-Ccp	Pyrrhotite	Po16	6	1.17	0.15	-0.01	0.14		
TS-018	17-804	195.00	Py-Po-Pn-Ccp	Pyrrhotite	Po16	7	1.07	0.15	-0.04	0.14		
TS-018	17-804	195.00	Py-Po-Pn-Ccp	Pyrrhotite	Po16	8	0.96	0.15	-0.02	0.14		
TS-018	17-804	195.00	Py-Po-Pn-Ccp	Pyrrhotite	Po16	9	1.05	0.16	-0.02	0.14		
TS-018	17-804	195.00	Py-Po-Pn-Ccp	Pyrrhotite	Po16	10	1.04	0.15	-0.04	0.14		
TS-018	17-804	195.00	Py-Po-Pn-Ccp	Pyrrhotite	Po16	11	1.11	0.15	-0.07	0.15		
TS-018	17-804	195.00	Py-Po-Pn-Ccp	Pyrrhotite	Po16	12	1.01	0.15	-0.01	0.15		
TS-018	17-804	195.00	Py-Po-Pn-Ccp	Pyrrhotite	Po16	13	1.18	0.15	0.01	0.14		
TS-018	17-804	195.00	Py-Po-Pn-Ccp	Pyrrhotite	Po16	14	1.17	0.15	-0.06	0.14		
TS-018	17-804	195.00	Py-Po-Pn-Ccp	Pyrrhotite	Po16	15	1.17	0.15	-0.03	0.15		
TS-018	17-804	195.00	Py-Po-Pn-Ccp	Chalcopyrite	Ccp11	1	1.01	0.13	-0.12	0.09	-0.1	2.46
TS-018	17-804	195.00	Py-Po-Pn-Ccp	Chalcopyrite	Ccp11	2	0.96	0.13	-0.07	0.08	0.5	2.61
TS-018	17-804	195.00	Py-Po-Pn-Ccp	Chalcopyrite	Ccp11	3	1.01	0.13	-0.05	0.09	0.3	2.59
TS-018	17-804	195.00	Py-Po-Pn-Ccp	Chalcopyrite	Ccp11	4	0.86	0.13	-0.06	0.09	0.3	2.33
TS-018	17-804	195.00	Py-Po-Pn-Ccp	Chalcopyrite	Ccp11	5	0.91	0.13	-0.09	0.09	0.2	2.59
TS-018	17-804	195.00	Py-Po-Pn-Ccp	Chalcopyrite	Ccp11	6	0.98	0.12	-0.15	0.09	0.5	2.45
TS-018	17-804	195.00	Py-Po-Pn-Ccp	Chalcopyrite	Ccp11	7	0.90	0.13	-0.16	0.09	0.0	2.59
TS-018	17-804	195.00	Py-Po-Pn-Ccp	Chalcopyrite	Ccp11	8	0.82	0.12	-0.10	0.08	0.0	2.24
TS-018	17-804	195.00	Py-Po-Pn-Ccp	Chalcopyrite	Ccp11	9	0.89	0.13	-0.18	0.10	0.2	2.23
TS-018	17-804	195.00	Py-Po-Pn-Ccp	Chalcopyrite	Ccp11	10	1.00	0.13	-0.12	0.09	0.1	2.45
TS-018	17-804	195.00	Py-Po-Pn-Ccp	Chalcopyrite	Ccp11	11	0.96	0.13	-0.10	0.09	0.4	2.76
TS-018	17-804	195.00	Py-Po-Pn-Ccp	Chalcopyrite	Ccp11	12	0.11	0.20	-0.09	0.12	0.6	2.33
TS-018	17-804	195.00	Py-Po-Pn-Ccp	Chalcopyrite	Ccp11	13	0.92	0.13	-0.15	0.09	0.6	2.51
TS-018	17-804	195.00	Py-Po-Pn-Ccp	Chalcopyrite	Ccp11	14	0.95	0.13	-0.09	0.09	0.4	2.29
TS-018	17-804	195.00	Py-Po-Pn-Ccp	Chalcopyrite	Ccp11	15	0.94	0.13	-0.08	0.09	0.3	2.35
TS-018	17-804	195.00	Py-Po-Pn-Ccp	Chalcopyrite	Ccp13	1	0.61	0.13	-0.09	0.09	0.3	2.42
TS-018	17-804	195.00	Py-Po-Pn-Ccp	Chalcopyrite	Ccp13	2	1.00	0.13	-0.13	0.09	0.3	2.29
TS-018	17-804	195.00	Py-Po-Pn-Ccp	Chalcopyrite	Ccp13	3	1.00	0.13	-0.09	0.09	0.4	2.61
TS-018	17-804	195.00	Py-Po-Pn-Ccp	Chalcopyrite	Ccp13	4	0.12	0.17	-0.04	0.11	0.2	2.51
TS-018	17-804	195.00	Py-Po-Pn-Ccp	Chalcopyrite	Ccp13	5	0.95	0.13	-0.09	0.09	0.5	2.55
TS-018	17-804	195.00	Py-Po-Pn-Ccp	Chalcopyrite	Ccp13	6	0.92	0.13	-0.08	0.09	0.0	2.37
TS-018	17-804	195.00	Py-Po-Pn-Ccp	Chalcopyrite	Ccp13	7	1.11	0.12	-0.13	0.09	0.9	2.39
TS-018	17-804	195.00	Py-Po-Pn-Ccp	Chalcopyrite	Ccp13	8	0.59	0.14	-0.03	0.10	0.2	2.11
TS-018	17-804	195.00	Py-Po-Pn-Ccp	Chalcopyrite	Ccp13	9	0.49	0.14	-0.11	0.09	0.3	1.99
TS-018	17-804	195.00	Py-Po-Pn-Ccp	Chalcopyrite	Ccp13	10	0.96	0.12	-0.10	0.08	0.4	2.36
TS-018	17-804	195.00	Py-Po-Pn-Ccp	Chalcopyrite	Ccp13	11	0.89	0.13	-0.08	0.09	0.6	2.25
TS-018	17-804	195.00	Py-Po-Pn-Ccp	Chalcopyrite	Ccp13	12	0.93	0.13	-0.07	0.09	0.3	2.42
TS-018	17-804	195.00	Py-Po-Pn-Ccp	Chalcopyrite	Ccp13	13	0.91	0.13	-0.08	0.09	0.4	2.23
TS-018	17-804	195.00	Py-Po-Pn-Ccp	Chalcopyrite	Ccp13	14	1.04	0.12	-0.05	0.09	0.3	2.25

Sample #	Drill hole	Depth (m)	Assemblage	Mineral	Crystal ID	Analysis #	δ34S (‰)	δ34S error	Δ33S (‰)	Δ33S error	Δ36S (‰)	Δ36S error
TS-018	17-804	195.00	Py-Po-Pn-Ccp	Chalcopyrite	Ccp13	15	0.69	0.12	-0.07	0.08	0.7	1.52
TS-018	17-804	195.00	Py-Po-Pn-Ccp	Chalcopyrite	Ccp17	1	1.00	0.12	-0.10	0.09	0.7	2.61
TS-018	17-804	195.00	Py-Po-Pn-Ccp	Chalcopyrite	Ccp17	2	0.51	0.14	-0.06	0.09	0.6	2.37
TS-018	17-804	195.00	Py-Po-Pn-Ccp	Chalcopyrite	Ccp17	3	0.71	0.12	-0.07	0.08	0.5	2.64
TS-018	17-804	195.00	Py-Po-Pn-Ccp	Chalcopyrite	Ccp17	4	0.62	0.12	-0.08	0.08	0.8	2.47
TS-018	17-804	195.00	Py-Po-Pn-Ccp	Chalcopyrite	Ccp17	5	0.61	0.13	-0.08	0.09	0.4	2.62
TS-018	17-804	195.00	Py-Po-Pn-Ccp	Chalcopyrite	Ccp17	6	-0.98	0.20	-0.05	0.11	0.4	1.91
TS-018	17-804	195.00	Py-Po-Pn-Ccp	Chalcopyrite	Ccp17	7	0.34	0.16	-0.09	0.10	0.8	2.11
TS-018	17-804	195.00	Py-Po-Pn-Ccp	Chalcopyrite	Ccp17	8	0.72	0.13	-0.01	0.08	0.1	2.83
TS-018	17-804	195.00	Py-Po-Pn-Ccp	Chalcopyrite	Ccp17	9	0.34	0.14	-0.08	0.10	0.3	2.11
TS-018	17-804	195.00	Py-Po-Pn-Ccp	Chalcopyrite	Ccp17	10	-0.56	0.20	-0.06	0.13	0.7	1.60
TS-018	17-804	195.00	Py-Po-Pn-Ccp	Chalcopyrite	Ccp17	11	0.44	0.13	-0.13	0.09	0.1	1.90
TS-018	17-804	195.00	Py-Po-Pn-Ccp	Chalcopyrite	Ccp17	12	0.43	0.14	-0.12	0.10	0.3	2.03
TS-018	17-804	195.00	Py-Po-Pn-Ccp	Pentlandite	Pn14	1	0.15	0.20	-0.13	0.14	0.0	0.41
TS-018	17-804	195.00	Py-Po-Pn-Ccp	Pentlandite	Pn14	2	0.05	0.21	-0.14	0.14	0.5	0.66
TS-018	17-804	195.00	Py-Po-Pn-Ccp	Pentlandite	Pn14	3	0.11	0.21	-0.11	0.14	0.3	0.53
TS-018	17-804	195.00	Py-Po-Pn-Ccp	Pentlandite	Pn14	4	0.22	0.20	-0.15	0.13	0.0	0.49
TS-018	17-804	195.00	Py-Po-Pn-Ccp	Pentlandite	Pn14	5	0.25	0.21	-0.09	0.15	0.0	0.48
TS-018	17-804	195.00	Py-Po-Pn-Ccp	Pentlandite	Pn14	6	-0.56	0.24	-0.10	0.15	0.2	2.21
TS-018	17-804	195.00	Py-Po-Pn-Ccp	Pentlandite	Pn14	7	-0.06	0.20	-0.12	0.14	0.1	0.50
TS-018	17-804	195.00	Py-Po-Pn-Ccp	Pentlandite	Pn14	8	0.22	0.19	0.02	0.13	0.1	0.42
TS-018	17-804	195.00	Py-Po-Pn-Ccp	Pentlandite	Pn14	9	0.23	0.21	-0.05	0.14	0.4	0.59
TS-018	17-804	195.00	Py-Po-Pn-Ccp	Pentlandite	Pn14	10	0.06	0.20	-0.11	0.13	0.3	0.56
TS-018	17-804	195.00	Py-Po-Pn-Ccp	Pentlandite	Pn14	11	0.60	0.20	-0.05	0.13	0.2	0.46
TS-018	17-804	195.00	Py-Po-Pn-Ccp	Pentlandite	Pn14	12	0.36	0.20	0.00	0.13	0.3	0.45
TS-018	17-804	195.00	Py-Po-Pn-Ccp	Pentlandite	Pn14	13	0.67	0.21	-0.01	0.14	0.4	0.49
TS-018	17-804	195.00	Py-Po-Pn-Ccp	Pentlandite	Pn14	14	0.42	0.20	-0.11	0.14	0.7	0.48
TS-018	17-804	195.00	Py-Po-Pn-Ccp	Pentlandite	Pn14	15	0.28	0.24	-0.08	0.15	0.6	0.92
TS-018	17-804	195.00	Py-Po-Pn-Ccp	Pentlandite	Pn18	1	0.17	0.19	-0.08	0.13	0.6	0.52
TS-018	17-804	195.00	Py-Po-Pn-Ccp	Pentlandite	Pn18	2	0.18	0.19	-0.08	0.13	0.8	0.45
TS-018	17-804	195.00	Py-Po-Pn-Ccp	Pentlandite	Pn18	3	-0.18	0.19	-0.06	0.13	0.7	1.75
TS-018	17-804	195.00	Py-Po-Pn-Ccp	Pentlandite	Pn18	4	-0.72	0.23	-0.10	0.14	0.8	2.42
TS-018	17-804	195.00	Py-Po-Pn-Ccp	Pentlandite	Pn18	5	-0.23	0.20	-0.08	0.14	0.5	0.99
TS-018	17-804	195.00	Py-Po-Pn-Ccp	Pentlandite	Pn18	6	0.02	0.19	0.00	0.13	0.6	0.51
TS-018	17-804	195.00	Py-Po-Pn-Ccp	Pentlandite	Pn18	7	0.53	0.19	-0.08	0.14	0.9	0.44
TS-018	17-804	195.00	Py-Po-Pn-Ccp	Pentlandite	Pn18	8	-0.09	0.21	-0.11	0.15	0.7	0.91
TS-018	17-804	195.00	Py-Po-Pn-Ccp	Pentlandite	Pn18	9	0.23	0.19	-0.06	0.13	0.5	0.51
TS-027	17-804	240.61	Py-Pn-Ccp	Pyrite	Py22	1	0.70	0.16	-0.07	0.15	0.7	0.61
TS-027	17-804	240.61	Py-Pn-Ccp	Pyrite	Py22	2	0.74	0.16	-0.10	0.15	0.5	0.62
TS-027	17-804	240.61	Py-Pn-Ccp	Pyrite	Py22	3	0.44	0.16	-0.04	0.15	0.5	0.61
TS-027	17-804	240.61	Py-Pn-Ccp	Pyrite	Py22	4	1.13	0.16	-0.09	0.15	0.4	0.61
TS-027	17-804	240.61	Py-Pn-Ccp	Pyrite	Py22	5	0.05	0.17	-0.06	0.15	0.2	2.52
TS-027	17-804	240.61	Py-Pn-Ccp	Pyrite	Py22	6	0.49	0.16	-0.10	0.15	0.9	1.95
TS-027	17-804	240.61	Py-Pn-Ccp	Pyrite	Py22	7	1.05	0.16	-0.06	0.15	0.6	0.62
TS-027	17-804	240.61	Py-Pn-Ccp	Pyrite	Py22	8	0.91	0.16	-0.06	0.15	0.4	0.60
TS-027	17-804	240.61	Py-Pn-Ccp	Pyrite	Py22	9	0.59	0.16	-0.08	0.15	0.5	0.61
TS-027	17-804	240.61	Py-Pn-Ccp	Pyrite	Py22	10	0.65	0.16	-0.03	0.15	0.8	0.91
TS-027	17-804	240.61	Py-Pn-Ccp	Pyrite	Py22	11	1.20	0.16	-0.08	0.15	0.7	0.60
TS-027	17-804	240.61	Py-Pn-Ccp	Pyrite	Py22	12	0.44	0.16	-0.06	0.15	0.8	0.69
TS-027	17-804	240.61	Py-Pn-Ccp	Pyrite	Py22	13	0.62	0.16	0.01	0.15	0.9	0.67
TS-027	17-804	240.61	Py-Pn-Ccp	Pyrite	Py22	14	0.59	0.17	-0.05	0.15	0.3	0.52
TS-027	17-804	240.61	Py-Pn-Ccp	Pyrite	Py22	15	0.69	0.16	-0.07	0.15	0.0	0.58
TS-027	17-804	240.61	Py-Pn-Ccp	Chalcopyrite	S5Ccp	1	0.53	0.18	-0.11	0.15	1.1	1.30
TS-027	17-804	240.61	Py-Pn-Ccp	Chalcopyrite	S5Ccp	2	0.52	0.19	-0.10	0.15	0.8	1.33
TS-027	17-804	240.61	Py-Pn-Ccp	Chalcopyrite	S5Ccp	3	0.96	0.18	-0.09	0.15	1.0	1.55
TS-027	17-804	240.61	Py-Pn-Ccp	Chalcopyrite	S5Ccp	4	-0.31	0.20	-0.04	0.16	0.4	1.18
TS-027	17-804	240.61	Py-Pn-Ccp	Chalcopyrite	S5Ccp	5	0.46	0.18	-0.09	0.15	0.5	1.35
TS-027	17-804	240.61	Py-Pn-Ccp	Chalcopyrite	S5Ccp	6	-0.21	0.19	-0.05	0.15	0.8	1.19
TS-027	17-804	240.61	Py-Pn-Ccp	Chalcopyrite	S5Ccp	7	0.55	0.17	-0.13	0.15	0.3	0.84
TS-027	17-804	240.61	Py-Pn-Ccp	Chalcopyrite	S5Ccp	8	0.06	0.18	-0.05	0.15	0.6	1.34

Sample #	Drill hole	Depth (m)	Assemblage	Mineral	Crystal ID	Analysis #	δ34S (‰)	δ34S error	Δ33S (‰)	Δ33S error	Δ36S (‰)	Δ36S error
TS-027	17-804	240.61	Py-Pn-Ccp	Chalcopyrite	S5Ccp	9	0.33	0.19	-0.08	0.15	0.2	1.27
TS-027	17-804	240.61	Py-Pn-Ccp	Chalcopyrite	S5Ccp	10	0.81	0.17	-0.03	0.15	0.2	0.97
TS-027	17-804	240.61	Py-Pn-Ccp	Chalcopyrite	S5Ccp	11	0.39	0.18	-0.08	0.15	0.0	1.14
TS-027	17-804	240.61	Py-Pn-Ccp	Pentlandite	Pn23	1	3.11	0.23	-0.09	0.18	0.1	0.56
TS-027	17-804	240.61	Py-Pn-Ccp	Pentlandite	Pn23	2	3.37	0.23	-0.15	0.19	0.1	0.50
TS-027	17-804	240.61	Py-Pn-Ccp	Pentlandite	Pn23	3	2.85	0.23	-0.04	0.19	0.1	0.75
TS-027	17-804	240.61	Py-Pn-Ccp	Pentlandite	Pn23	4	2.96	0.23	-0.15	0.19	0.3	0.81
TS-027	17-804	240.61	Py-Pn-Ccp	Pentlandite	Pn23	5	2.69	0.24	-0.09	0.19	0.3	1.03
TS-027	17-804	240.61	Py-Pn-Ccp	Pentlandite	Pn23	6	2.31	0.25	-0.12	0.19	0.0	1.51
TS-027	17-804	240.61	Py-Pn-Ccp	Pentlandite	Pn23	7	3.06	0.23	-0.08	0.19	0.0	0.52
TS-027	17-804	240.61	Py-Pn-Ccp	Pentlandite	Pn23	8	2.65	0.23	-0.03	0.19	0.1	0.65
TS-027	17-804	240.61	Py-Pn-Ccp	Pentlandite	Pn23	9	4.59	0.17	-0.08	0.17	0.3	0.57
TS-027	17-804	240.61	Py-Pn-Ccp	Pentlandite	Pn23	10	3.12	0.23	-0.11	0.19	-0.1	0.60
TS-027	17-804	240.61	Py-Pn-Ccp	Pentlandite	Pn23	11	2.89	0.23	-0.10	0.19	-0.1	0.71
TS-027	17-804	240.61	Py-Pn-Ccp	Pentlandite	Pn23	12	3.07	0.23	-0.04	0.18	0.1	0.83
TS-027	17-804	240.61	Py-Pn-Ccp	Pentlandite	Pn23	13	3.04	0.23	-0.07	0.18	0.4	0.74
TS-027	17-804	240.61	Py-Pn-Ccp	Pentlandite	Pn23	14	2.70	0.26	-0.12	0.20	0.4	0.90
TS-027	17-804	240.61	Py-Pn-Ccp	Pentlandite	S5Pn	1	2.86	0.24	-0.04	0.19	0.4	0.54
TS-027	17-804	240.61	Py-Pn-Ccp	Pentlandite	S5Pn	2	3.03	0.23	-0.06	0.19	0.1	0.52
TS-027	17-804	240.61	Py-Pn-Ccp	Pentlandite	S5Pn	3	4.33	0.17	0.01	0.17	0.3	0.58
TS-027	17-804	240.61	Py-Pn-Ccp	Pentlandite	S5Pn	4	4.65	0.17	-0.03	0.17	0.5	0.54
TS-027	17-804	240.61	Py-Pn-Ccp	Pentlandite	S5Pn	5	3.15	0.23	-0.04	0.19	0.3	0.52
TS-027	17-804	240.61	Py-Pn-Ccp	Pentlandite	S5Pn	6	3.31	0.23	-0.07	0.19	0.0	0.50
TS-027	17-804	240.61	Py-Pn-Ccp	Pentlandite	S5Pn	7	3.17	0.23	-0.07	0.19	0.3	0.52
TS-027	17-804	240.61	Py-Pn-Ccp	Pentlandite	S5Pn	8	2.96	0.22	-0.13	0.19	-0.1	0.50
TS-027	17-804	240.61	Py-Pn-Ccp	Pentlandite	S5Pn	9	3.53	0.22	-0.01	0.19	0.0	0.49
TS-027	17-804	240.61	Py-Pn-Ccp	Pentlandite	S5Pn	10	3.27	0.24	-0.07	0.19	0.1	0.50
TS-027	17-804	240.61	Py-Pn-Ccp	Pentlandite	S5Pn	11	2.65	0.23	-0.22	0.20	0.7	0.49
TS-027	17-804	240.61	Py-Pn-Ccp	Pentlandite	S5Pn	12	2.46	0.25	-0.07	0.19	0.2	1.03
TS-032	17-804	250.70	Py-Po-Pn-Ccp	Pyrite	Py31	1	0.77	0.07	-0.06	0.07		
TS-032	17-804	250.70	Py-Po-Pn-Ccp	Pyrite	Py31	2	0.70	0.07	-0.05	0.07		
TS-032	17-804	250.70	Py-Po-Pn-Ccp	Pyrite	Py31	3	2.13	0.07	-0.05	0.07		
TS-032	17-804	250.70	Py-Po-Pn-Ccp	Pyrite	Py31	4	1.79	0.07	-0.03	0.07		
TS-032	17-804	250.70	Py-Po-Pn-Ccp	Pyrite	Py31	5	0.95	0.07	-0.10	0.07		
TS-032	17-804	250.70	Py-Po-Pn-Ccp	Pyrite	Py31	6	1.39	0.07	-0.05	0.07		
TS-032	17-804	250.70	Py-Po-Pn-Ccp	Pyrite	Py31	7	0.61	0.07	-0.09	0.07		
TS-032	17-804	250.70	Py-Po-Pn-Ccp	Pyrite	Py31	8	0.63	0.07	-0.02	0.07		
TS-032	17-804	250.70	Py-Po-Pn-Ccp	Pyrite	Py31	9	1.07	0.07	-0.11	0.07		
TS-032	17-804	250.70	Py-Po-Pn-Ccp	Pyrite	Py31	10	2.00	0.07	-0.08	0.07		
TS-032	17-804	250.70	Py-Po-Pn-Ccp	Pyrite	Py31	11	0.55	0.07	-0.13	0.07		
TS-032	17-804	250.70	Py-Po-Pn-Ccp	Pyrite	Py31	12	1.58	0.07	-0.14	0.07		
TS-032	17-804	250.70	Py-Po-Pn-Ccp	Pyrite	Py31	13	0.01	0.07	-0.11	0.07		
TS-032	17-804	250.70	Py-Po-Pn-Ccp	Pyrite	Py31	14	1.25	0.07	-0.10	0.07		
TS-032	17-804	250.70	Py-Po-Pn-Ccp	Pyrite	Py31	15	1.77	0.07	-0.08	0.07		
TS-032	17-804	250.70	Py-Po-Pn-Ccp	Chalcopyrite	Ccp29	1	0.67	0.12	-0.04	0.10	0.0	1.32
TS-032	17-804	250.70	Py-Po-Pn-Ccp	Chalcopyrite	Ccp29	2	0.75	0.12	-0.07	0.10	0.3	1.55
TS-032	17-804	250.70	Py-Po-Pn-Ccp	Chalcopyrite	Ccp29	3	0.81	0.13	-0.06	0.10	0.1	1.62
TS-032	17-804	250.70	Py-Po-Pn-Ccp	Chalcopyrite	Ccp29	4	0.72	0.13	-0.10	0.10	-0.1	1.88
TS-032	17-804	250.70	Py-Po-Pn-Ccp	Chalcopyrite	Ccp29	5	0.74	0.13	-0.05	0.10	0.3	2.16
TS-032	17-804	250.70	Py-Po-Pn-Ccp	Chalcopyrite	Ccp29	6	-0.70	0.14	-0.04	0.11	0.3	1.09
TS-032	17-804	250.70	Py-Po-Pn-Ccp	Chalcopyrite	Ccp29	7	-0.91	0.17	-0.09	0.11	-0.4	1.48
TS-032	17-804	250.70	Py-Po-Pn-Ccp	Pentlandite	Pn30	1	1.11	0.23	-0.12	0.18	-0.1	0.66
TS-032	17-804	250.70	Py-Po-Pn-Ccp	Pentlandite	Pn30	2	1.32	0.23	-0.13	0.18	-0.1	0.57
TS-032	17-804	250.70	Py-Po-Pn-Ccp	Pentlandite	Pn30	3	0.78	0.23	0.03	0.18	0.1	0.90
TS-032	17-804	250.70	Py-Po-Pn-Ccp	Pentlandite	Pn30	4	1.11	0.23	-0.10	0.18	-0.4	0.54
TS-032	17-804	250.70	Py-Po-Pn-Ccp	Pentlandite	Pn30	5	0.94	0.23	-0.02	0.18	0.6	0.61
TS-032	17-804	250.70	Py-Po-Pn-Ccp	Pentlandite	Pn30	6	0.78	0.24	-0.04	0.18	0.1	0.56
TS-032	17-804	250.70	Py-Po-Pn-Ccp	Pentlandite	Pn30	7	5.20	0.16	-0.05	0.15	-0.3	0.69
TS-032	17-804	250.70	Py-Po-Pn-Ccp	Pentlandite	Pn30	8	0.61	0.24	-0.05	0.18	0.1	1.31
TS-032	17-804	250.70	Py-Po-Pn-Ccp	Pentlandite	Pn30	9	0.75	0.24	-0.01	0.18	0.2	0.97

Sample #	Drill hole	Depth (m)	Assemblage	Mineral	Crystal ID	Analysis #	δ34S (‰)	δ34S error	Δ33S (‰)	Δ33S error	Δ36S (‰)	Δ36S error
TS-032	17-804	250.70	Py-Po-Pn-Ccp	Pentlandite	Pn30	10	0.66	0.23	-0.12	0.18	0.0	0.66
TS-032	17-804	250.70	Py-Po-Pn-Ccp	Pentlandite	Pn30	11	0.80	0.23	-0.02	0.17	0.0	0.90
TS-032	17-804	250.70	Py-Po-Pn-Ccp	Pentlandite	Pn30	12	0.83	0.23	0.00	0.17	0.2	0.67
TS-032	17-804	250.70	Py-Po-Pn-Ccp	Pentlandite	Pn30	13	0.39	0.23	-0.07	0.17	-0.2	0.71
TS-032	17-804	250.70	Py-Po-Pn-Ccp	Pentlandite	Pn30	14	1.12	0.24	-0.11	0.17	-0.1	0.62
TS-032	17-804	250.70	Py-Po-Pn-Ccp	Pentlandite	Pn30	15	0.51	0.23	-0.04	0.18	-0.2	0.71
TS-037	17-804	258.29	Py-Po-Pn-Ccp	Pyrite	Py34	1	0.70	0.07	-0.06	0.07		
TS-037	17-804	258.29	Py-Po-Pn-Ccp	Pyrite	Py34	2	0.78	0.07	-0.06	0.07		
TS-037	17-804	258.29	Py-Po-Pn-Ccp	Pyrite	Py34	3	1.11	0.07	-0.02	0.07		
TS-037	17-804	258.29	Py-Po-Pn-Ccp	Pyrite	Py34	4	1.01	0.07	-0.08	0.07		
TS-037	17-804	258.29	Py-Po-Pn-Ccp	Pyrite	Py34	5	0.90	0.07	-0.07	0.07		
TS-037	17-804	258.29	Py-Po-Pn-Ccp	Pyrite	Py34	6	0.54	0.07	-0.12	0.07		
TS-037	17-804	258.29	Py-Po-Pn-Ccp	Pyrite	Py34	7	0.86	0.07	-0.05	0.08		
TS-037	17-804	258.29	Py-Po-Pn-Ccp	Pyrite	Py34	8	1.33	0.07	-0.13	0.07		
TS-037	17-804	258.29	Py-Po-Pn-Ccp	Pyrite	Py34	9	0.19	0.07	-0.06	0.07		
TS-037	17-804	258.29	Py-Po-Pn-Ccp	Pyrite	Py34	10	1.18	0.07	-0.07	0.07		
TS-037	17-804	258.29	Py-Po-Pn-Ccp	Pyrite	Py34	11	1.52	0.07	-0.11	0.08		
TS-037	17-804	258.29	Py-Po-Pn-Ccp	Pyrite	Py34	12	1.38	0.07	-0.08	0.08		
TS-037	17-804	258.29	Py-Po-Pn-Ccp	Pyrite	Py34	13	0.99	0.07	-0.09	0.07		
TS-037	17-804	258.29	Py-Po-Pn-Ccp	Pyrite	Py34	14	0.54	0.06	-0.06	0.07		
TS-037	17-804	258.29	Py-Po-Pn-Ccp	Pyrite	Py34	15	0.47	0.07	-0.08	0.07		
TS-037	17-804	258.29	Py-Po-Pn-Ccp	Chalcopyrite	Ccp32	1	0.38	0.13	-0.05	0.10	-0.1	1.47
TS-037	17-804	258.29	Py-Po-Pn-Ccp	Chalcopyrite	Ccp32	2	0.50	0.12	-0.10	0.10	0.0	1.18
TS-037	17-804	258.29	Py-Po-Pn-Ccp	Chalcopyrite	Ccp32	3	0.59	0.13	-0.09	0.10	0.0	1.87
TS-037	17-804	258.29	Py-Po-Pn-Ccp	Chalcopyrite	Ccp32	4	0.38	0.13	-0.08	0.10	-0.5	1.37
TS-037	17-804	258.29	Py-Po-Pn-Ccp	Chalcopyrite	Ccp32	5	0.71	0.13	-0.05	0.10	0.4	2.01
TS-037	17-804	258.29	Py-Po-Pn-Ccp	Chalcopyrite	Ccp32	6	0.30	0.14	-0.06	0.10	-0.1	1.39
TS-037	17-804	258.29	Py-Po-Pn-Ccp	Chalcopyrite	Ccp32	7	0.32	0.14	-0.08	0.10	0.0	1.48
TS-037	17-804	258.29	Py-Po-Pn-Ccp	Chalcopyrite	Ccp32	8	0.47	0.14	-0.07	0.10	-0.2	1.74
TS-037	17-804	258.29	Py-Po-Pn-Ccp	Pentlandite	Pn33	1	-0.24	0.24	-0.04	0.17	-0.5	1.17
TS-037	17-804	258.29	Py-Po-Pn-Ccp	Pentlandite	Pn33	2	-0.25	0.25	-0.07	0.18	-0.1	0.81
TS-037	17-804	258.29	Py-Po-Pn-Ccp	Pentlandite	Pn33	3	-0.08	0.24	-0.07	0.18	-0.6	1.02
TS-037	17-804	258.29	Py-Po-Pn-Ccp	Pentlandite	Pn33	4	-0.04	0.25	-0.05	0.18	-0.7	1.78
TS-037	17-804	258.29	Py-Po-Pn-Ccp	Pentlandite	Pn33	5	-0.38	0.24	-0.08	0.18	-0.1	1.10
TS-037	17-804	258.29	Py-Po-Pn-Ccp	Pentlandite	Pn33	6	-0.36	0.25	-0.08	0.18	0.1	1.01
TS-037	17-804	258.29	Py-Po-Pn-Ccp	Pentlandite	Pn33	7	-1.22	0.24	-0.01	0.18	0.1	3.32
TS-041	17-804	266.19	Py-Po-Pn-Ccp	Chalcopyrite	Ccp36	1	1.24	0.19	-0.07	0.18	0.5	0.81
TS-041	17-804	266.19	Py-Po-Pn-Ccp	Chalcopyrite	Ccp36	2	0.74	0.19	-0.06	0.18	0.1	0.52
TS-041	17-804	266.19	Py-Po-Pn-Ccp	Chalcopyrite	Ccp36	3	1.11	0.19	-0.08	0.18	0.4	0.82
TS-041	17-804	266.19	Py-Po-Pn-Ccp	Chalcopyrite	Ccp36	4	0.99	0.20	0.00	0.18	0.2	1.10
TS-041	17-804	266.19	Py-Po-Pn-Ccp	Chalcopyrite	Ccp36	5	0.91	0.19	-0.13	0.18	0.4	1.12
TS-041	17-804	266.19	Py-Po-Pn-Ccp	Chalcopyrite	Ccp36	6	0.99	0.19	-0.07	0.18	0.7	1.07
TS-041	17-804	266.19	Py-Po-Pn-Ccp	Chalcopyrite	Ccp36	7	1.13	0.19	-0.06	0.18	0.4	0.88
TS-041	17-804	266.19	Py-Po-Pn-Ccp	Chalcopyrite	Ccp36	8	0.77	0.19	-0.05	0.18	0.6	0.83
TS-041	17-804	266.19	Py-Po-Pn-Ccp	Chalcopyrite	Ccp36	9	0.99	0.19	-0.06	0.18	0.1	1.42
TS-041	17-804	266.19	Py-Po-Pn-Ccp	Chalcopyrite	Ccp36	10	0.38	0.19	-0.03	0.18	-0.2	0.84
TS-041	17-804	266.19	Py-Po-Pn-Ccp	Chalcopyrite	Ccp37	1	0.56	0.20	-0.10	0.18	0.4	0.89
TS-041	17-804	266.19	Py-Po-Pn-Ccp	Chalcopyrite	Ccp37	2	0.79	0.19	-0.10	0.18	0.6	0.74
TS-041	17-804	266.19	Py-Po-Pn-Ccp	Chalcopyrite	Ccp37	3	0.68	0.19	-0.03	0.18	0.6	0.86
TS-041	17-804	266.19	Py-Po-Pn-Ccp	Chalcopyrite	Ccp37	4	0.82	0.19	-0.07	0.18	0.2	0.89
TS-041	17-804	266.19	Py-Po-Pn-Ccp	Chalcopyrite	Ccp37	5	0.76	0.19	-0.02	0.18	0.4	1.08
TS-041	17-804	266.19	Py-Po-Pn-Ccp	Chalcopyrite	Ccp37	6	0.67	0.19	-0.03	0.18	0.5	1.10
TS-041	17-804	266.19	Py-Po-Pn-Ccp	Chalcopyrite	Ccp37	7	0.62	0.19	-0.05	0.18	0.4	1.05
TS-041	17-804	266.19	Py-Po-Pn-Ccp	Pyrrhotite	Po35	1	0.75	0.14	0.00	0.13		
TS-041	17-804	266.19	Py-Po-Pn-Ccp	Pyrrhotite	Po35	2	0.59	0.14	-0.02	0.13		
TS-041	17-804	266.19	Py-Po-Pn-Ccp	Pyrrhotite	Po35	3	0.82	0.14	0.02	0.13		
TS-041	17-804	266.19	Py-Po-Pn-Ccp	Pyrrhotite	Po35	4	0.63	0.14	-0.05	0.13		
TS-041	17-804	266.19	Py-Po-Pn-Ccp	Pyrrhotite	Po35	5	0.90	0.14	-0.08	0.13		
TS-041	17-804	266.19	Py-Po-Pn-Ccp	Pyrrhotite	Po35	6	0.64	0.14	-0.02	0.13		
TS-041	17-804	266.19	Py-Po-Pn-Ccp	Pyrrhotite	Po35	7	0.84	0.14	-0.01	0.13		

Sample #	Drill hole	Depth (m)	Assemblage	Mineral	Crystal ID	Analysis #	δ34S (‰)	δ34S error	Δ33S (‰)	Δ33S error	Δ36S (‰)	Δ36S error
TS-041	17-804	266.19	Py-Po-Pn-Ccp	Pyrrhotite	Po35	8	0.79	0.15	-0.03	0.13		
TS-041	17-804	266.19	Py-Po-Pn-Ccp	Pyrrhotite	Po35	9	0.81	0.14	-0.07	0.13		
TS-041	17-804	266.19	Py-Po-Pn-Ccp	Pyrrhotite	Po35	10	0.84	0.14	-0.02	0.13		
TS-041	17-804	266.19	Py-Po-Pn-Ccp	Pyrrhotite	Po35	11	0.56	0.14	-0.02	0.13		
TS-041	17-804	266.19	Py-Po-Pn-Ccp	Pyrrhotite	Po35	12	0.60	0.14	-0.01	0.13		
TS-041	17-804	266.19	Py-Po-Pn-Ccp	Pyrrhotite	Po35	13	0.67	0.14	-0.05	0.13		
TS-041	17-804	266.19	Py-Po-Pn-Ccp	Pyrrhotite	Po35	14	0.70	0.14	-0.02	0.13		
TS-068	18-805	100.22	Py-Po-Pn-Ccp	Pyrite	Py27	1	0.35	0.16	-0.12	0.15	-0.1	0.59
TS-068	18-805	100.22	Py-Po-Pn-Ccp	Pyrite	Py27	2	0.95	0.16	-0.04	0.15	0.4	0.57
TS-068	18-805	100.22	Py-Po-Pn-Ccp	Pyrite	Py27	3	1.28	0.16	-0.07	0.15	0.0	0.57
TS-068	18-805	100.22	Py-Po-Pn-Ccp	Pyrite	Py27	4	1.87	0.16	-0.02	0.15	0.0	0.61
TS-068	18-805	100.22	Py-Po-Pn-Ccp	Pyrite	Py27	5	2.02	0.16	-0.04	0.15	-0.1	0.58
TS-068	18-805	100.22	Py-Po-Pn-Ccp	Chalcopyrite	Cpy28	1	1.10	0.12	-0.05	0.09	0.1	0.79
TS-068	18-805	100.22	Py-Po-Pn-Ccp	Chalcopyrite	Cpy28	2	1.27	0.12	-0.10	0.10	0.3	0.82
TS-068	18-805	100.22	Py-Po-Pn-Ccp	Chalcopyrite	Cpy28	3	1.28	0.11	-0.05	0.09	-0.1	0.73
TS-068	18-805	100.22	Py-Po-Pn-Ccp	Chalcopyrite	Cpy28	4	1.22	0.12	-0.04	0.09	-0.1	0.69
TS-068	18-805	100.22	Py-Po-Pn-Ccp	Chalcopyrite	Cpy28	5	1.16	0.11	-0.10	0.10	-0.1	0.62
TS-068	18-805	100.22	Py-Po-Pn-Ccp	Chalcopyrite	Cpy28	6	1.13	0.12	-0.04	0.10	-0.1	0.37
TS-068	18-805	100.22	Py-Po-Pn-Ccp	Chalcopyrite	Cpy28	7	1.13	0.12	-0.11	0.10	-0.4	0.47
TS-068	18-805	100.22	Py-Po-Pn-Ccp	Chalcopyrite	Cpy28	8	1.23	0.12	-0.11	0.10	-0.3	0.86
TS-068	18-805	100.22	Py-Po-Pn-Ccp	Chalcopyrite	Cpy25	1	1.11	0.11	-0.10	0.10	0.2	0.77
TS-068	18-805	100.22	Py-Po-Pn-Ccp	Chalcopyrite	Cpy25	2	1.21	0.12	-0.06	0.09	0.0	0.73
TS-068	18-805	100.22	Py-Po-Pn-Ccp	Chalcopyrite	Cpy25	3	1.52	0.11	-0.06	0.10	0.4	0.78
TS-068	18-805	100.22	Py-Po-Pn-Ccp	Chalcopyrite	Cpy25	4	1.07	0.12	-0.14	0.10	-0.3	0.55
TS-068	18-805	100.22	Py-Po-Pn-Ccp	Chalcopyrite	Cpy25	5	1.20	0.11	-0.09	0.09	-0.1	0.64
TS-068	18-805	100.22	Py-Po-Pn-Ccp	Chalcopyrite	Cpy25	6	1.36	0.11	-0.12	0.09	0.1	0.61
TS-068	18-805	100.22	Py-Po-Pn-Ccp	Chalcopyrite	Cpy25	7	1.19	0.12	-0.07	0.10	0.1	0.73
TS-068	18-805	100.22	Py-Po-Pn-Ccp	Chalcopyrite	Cpy25	8	1.39	0.11	-0.07	0.09	0.5	0.72
TS-068	18-805	100.22	Py-Po-Pn-Ccp	Chalcopyrite	Cpy25	9	1.15	0.11	-0.09	0.10	-0.2	0.58
TS-068	18-805	100.22	Py-Po-Pn-Ccp	Chalcopyrite	Cpy25	10	1.10	0.12	0.00	0.09	-0.2	0.61
TS-068	18-805	100.22	Py-Po-Pn-Ccp	Chalcopyrite	Cpy25	11	1.16	0.11	-0.06	0.09	0.1	0.39
TS-068	18-805	100.22	Py-Po-Pn-Ccp	Chalcopyrite	Cpy25	12	0.86	0.12	-0.07	0.10	0.1	0.45
TS-068	18-805	100.22	Py-Po-Pn-Ccp	Pyrrhotite	Po26	1	1.31	0.17	-0.02	0.15	0.2	0.50
TS-068	18-805	100.22	Py-Po-Pn-Ccp	Pyrrhotite	Po26	2	1.44	0.17	-0.04	0.15	0.2	0.49
TS-068	18-805	100.22	Py-Po-Pn-Ccp	Pyrrhotite	Po26	3	-0.21	0.18	-0.06	0.16	0.4	1.15
TS-068	18-805	100.22	Py-Po-Pn-Ccp	Pyrrhotite	Po26	4	1.18	0.17	-0.07	0.15	0.1	0.50
TS-068	18-805	100.22	Py-Po-Pn-Ccp	Pyrrhotite	Po26	5	1.16	0.17	-0.03	0.15	0.0	0.49
TS-068	18-805	100.22	Py-Po-Pn-Ccp	Pyrrhotite	Po26	6	1.28	0.17	-0.10	0.15	0.3	0.49
TS-068	18-805	100.22	Py-Po-Pn-Ccp	Pyrrhotite	Po26	7	1.20	0.17	0.00	0.15	0.7	0.49
TS-068	18-805	100.22	Py-Po-Pn-Ccp	Pyrrhotite	Po26	8	1.36	0.17	0.02	0.15	0.4	0.50
TS-068	18-805	100.22	Py-Po-Pn-Ccp	Pyrrhotite	Po26	9	1.30	0.17	-0.05	0.15	0.6	0.50
TS-068	18-805	100.22	Py-Po-Pn-Ccp	Pyrrhotite	Po26	10	1.21	0.17	-0.05	0.15	0.7	0.53
TS-068	18-805	100.22	Py-Po-Pn-Ccp	Pyrrhotite	Po26	11	1.24	0.17	-0.07	0.15	0.5	0.51
TS-068	18-805	100.22	Py-Po-Pn-Ccp	Pyrrhotite	Po26	12	1.20	0.17	-0.07	0.15	0.6	0.61
TS-068	18-805	100.22	Py-Po-Pn-Ccp	Pyrrhotite	Po26	13	1.32	0.17	-0.06	0.15	0.6	0.50
TS-068	18-805	100.22	Py-Po-Pn-Ccp	Pyrrhotite	Po26	14	1.27	0.18	-0.04	0.15	0.7	0.49
TS-068	18-805	100.22	Py-Po-Pn-Ccp	Pyrrhotite	Po24	1	0.96	0.17	-0.02	0.15	-0.4	0.50
TS-068	18-805	100.22	Py-Po-Pn-Ccp	Pyrrhotite	Po24	2	1.17	0.17	-0.03	0.15	-0.2	0.48
TS-068	18-805	100.22	Py-Po-Pn-Ccp	Pyrrhotite	Po24	3	1.09	0.17	-0.01	0.15	-0.5	0.50
TS-068	18-805	100.22	Py-Po-Pn-Ccp	Pyrrhotite	Po24	4	1.25	0.17	-0.01	0.15	-0.2	0.49
TS-068	18-805	100.22	Py-Po-Pn-Ccp	Pyrrhotite	Po24	5	1.24	0.17	-0.06	0.15	-0.2	0.49
TS-068	18-805	100.22	Py-Po-Pn-Ccp	Pyrrhotite	Po24	6	1.16	0.17	-0.14	0.15	-0.2	0.49
TS-068	18-805	100.22	Py-Po-Pn-Ccp	Pyrrhotite	Po24	7	1.26	0.17	-0.06	0.16	-0.2	0.49
TS-068	18-805	100.22	Py-Po-Pn-Ccp	Pyrrhotite	Po24	8	1.35	0.17	-0.09	0.15	0.1	0.49
TS-068	18-805	100.22	Py-Po-Pn-Ccp	Pyrrhotite	Po24	9	1.14	0.17	-0.08	0.15	-0.1	0.49
TS-068	18-805	100.22	Py-Po-Pn-Ccp	Pyrrhotite	Po24	10	1.24	0.17	-0.05	0.15	0.1	0.49
TS-068	18-805	100.22	Py-Po-Pn-Ccp	Pyrrhotite	Po24	11	1.13	0.17	-0.04	0.15	0.1	0.52
TS-068	18-805	100.22	Py-Po-Pn-Ccp	Pyrrhotite	Po24	12	1.29	0.17	-0.05	0.15	-0.2	0.50
TS-068	18-805	100.22	Py-Po-Pn-Ccp	Pyrrhotite	Po24	13	1.22	0.17	-0.05	0.15	0.7	0.48
TS-068	18-805	100.22	Py-Po-Pn-Ccp	Pyrrhotite	Po24	14	1.15	0.17	-0.07	0.15	-0.3	0.49

Sample #	Drill hole	Depth (m)	Assemblage	Mineral	Crystal ID	Analysis #	δ34S (‰)	δ34S error	Δ33S (‰)	Δ33S error	Δ36S (‰)	Δ36S error
TS-068	18-805	100.22	Py-Po-Pn-Ccp	Pyrrhotite	Po24	15	1.15	0.17	-0.05	0.15	0.1	0.59
TS-093	18-805	170.22	Py-Po-Pn-Ccp	Pyrite	Py47	1	0.70	0.08	-0.02	0.08		
TS-093	18-805	170.22	Py-Po-Pn-Ccp	Pyrite	Py47	2	0.79	0.08	-0.06	0.08		
TS-093	18-805	170.22	Py-Po-Pn-Ccp	Pyrite	Py47	3	-0.26	0.09	-0.05	0.08		
TS-093	18-805	170.22	Py-Po-Pn-Ccp	Pyrite	Py47	4	0.59	0.08	-0.05	0.08		
TS-093	18-805	170.22	Py-Po-Pn-Ccp	Pyrite	Py47	5	0.25	0.08	-0.08	0.08		
TS-093	18-805	170.22	Py-Po-Pn-Ccp	Pyrite	Py47	6	0.26	0.08	-0.07	0.08		
TS-093	18-805	170.22	Py-Po-Pn-Ccp	Pyrite	Py47	7	0.32	0.08	-0.08	0.08		
TS-093	18-805	170.22	Py-Po-Pn-Ccp	Pyrite	Py47	8	0.33	0.08	-0.05	0.08		
TS-093	18-805	170.22	Py-Po-Pn-Ccp	Pyrite	Py47	9	0.40	0.08	-0.09	0.08		
TS-093	18-805	170.22	Py-Po-Pn-Ccp	Pyrite	Py47	10	0.39	0.08	-0.04	0.08		
TS-093	18-805	170.22	Py-Po-Pn-Ccp	Pyrite	Py47	11	0.26	0.08	-0.08	0.08		
TS-096	18-805	185.32	Py-Po-Pn-Ccp	Pyrite	Py49	1	0.63	0.07	0.03	0.05		
TS-096	18-805	185.32	Py-Po-Pn-Ccp	Pyrite	Py49	2	0.76	0.07	-0.02	0.06		
TS-096	18-805	185.32	Py-Po-Pn-Ccp	Pyrite	Py49	3	0.34	0.07	-0.08	0.05		
TS-096	18-805	185.32	Py-Po-Pn-Ccp	Pyrite	Py49	4	0.44	0.07	-0.12	0.05		
TS-096	18-805	185.32	Py-Po-Pn-Ccp	Pyrite	Py49	5	0.43	0.07	-0.02	0.05		
TS-096	18-805	185.32	Py-Po-Pn-Ccp	Pyrite	Py49	6	0.27	0.07	-0.08	0.05		
TS-096	18-805	185.32	Py-Po-Pn-Ccp	Pyrite	Py49	7	0.39	0.07	-0.12	0.05		
TS-096	18-805	185.32	Py-Po-Pn-Ccp	Pyrite	Py49	8	0.36	0.07	-0.16	0.06		
TS-096	18-805	185.32	Py-Po-Pn-Ccp	Pyrite	Py49	9	0.29	0.07	-0.10	0.05		
TS-096	18-805	185.32	Py-Po-Pn-Ccp	Pyrite	Py49	10	0.36	0.07	-0.09	0.06		
TS-096	18-805	185.32	Py-Po-Pn-Ccp	Pyrite	Py49	11	0.32	0.07	-0.09	0.06		
TS-096	18-805	185.32	Py-Po-Pn-Ccp	Pyrite	Py49	12	0.59	0.07	-0.04	0.05		
TS-112	18-805	259.81	Py-Po-Pn-Ccp	Pyrite	Py52	1	1.35	0.07	-0.11	0.05		
TS-112	18-805	259.81	Py-Po-Pn-Ccp	Pyrite	Py52	2	1.46	0.07	-0.09	0.06		
TS-112	18-805	259.81	Py-Po-Pn-Ccp	Pyrite	Py52	3	1.64	0.07	-0.08	0.06		
TS-112	18-805	259.81	Py-Po-Pn-Ccp	Pyrite	Py52	4	1.02	0.07	-0.13	0.05		
TS-112	18-805	259.81	Py-Po-Pn-Ccp	Pyrite	Py52	5	0.97	0.07	-0.12	0.05		
TS-112	18-805	259.81	Py-Po-Pn-Ccp	Chalcopyrite	Ccp51	1	1.28	0.08	-0.11	0.06		
TS-112	18-805	259.81	Py-Po-Pn-Ccp	Chalcopyrite	Ccp51	2	0.87	0.08	0.01	0.07		
TS-112	18-805	259.81	Py-Po-Pn-Ccp	Chalcopyrite	Ccp51	3	1.29	0.08	-0.03	0.06		
TS-112	18-805	259.81	Py-Po-Pn-Ccp	Chalcopyrite	Ccp51	4	0.94	0.07	-0.07	0.06		
TS-112	18-805	259.81	Py-Po-Pn-Ccp	Chalcopyrite	Ccp51	5	1.15	0.07	-0.03	0.06		
TS-112	18-805	259.81	Py-Po-Pn-Ccp	Chalcopyrite	Ccp51	6	1.30	0.07	0.00	0.06		
TS-112	18-805	259.81	Py-Po-Pn-Ccp	Chalcopyrite	Ccp51	7	1.08	0.07	-0.10	0.07		
TS-112	18-805	259.81	Py-Po-Pn-Ccp	Chalcopyrite	Ccp51	9	1.08	0.07	-0.07	0.06		
TS-112	18-805	259.81	Py-Po-Pn-Ccp	Chalcopyrite	Ccp51	10	0.96	0.07	-0.05	0.07		
TS-112	18-805	259.81	Py-Po-Pn-Ccp	Chalcopyrite	Ccp51	11	1.15	0.07	-0.10	0.06		
TS-112	18-805	259.81	Py-Po-Pn-Ccp	Chalcopyrite	Ccp51	12	1.11	0.08	-0.08	0.06		
TS-112	18-805	259.81	Py-Po-Pn-Ccp	Chalcopyrite	Ccp51	13	1.21	0.07	-0.10	0.06		
TS-112	18-805	259.81	Py-Po-Pn-Ccp	Chalcopyrite	Ccp53	1	1.11	0.07	-0.06	0.06		
TS-112	18-805	259.81	Py-Po-Pn-Ccp	Chalcopyrite	Ccp53	2	1.07	0.06	-0.01	0.06		
TS-112	18-805	259.81	Py-Po-Pn-Ccp	Chalcopyrite	Ccp53	3	1.06	0.07	-0.02	0.06		
TS-112	18-805	259.81	Py-Po-Pn-Ccp	Chalcopyrite	Ccp53	4	1.16	0.07	-0.06	0.06		
TS-112	18-805	259.81	Py-Po-Pn-Ccp	Chalcopyrite	Ccp53	5	1.14	0.07	-0.08	0.07		
TS-112	18-805	259.81	Py-Po-Pn-Ccp	Chalcopyrite	Ccp53	6	1.11	0.07	-0.07	0.06		
TS-112	18-805	259.81	Py-Po-Pn-Ccp	Chalcopyrite	Ccp53	7	1.21	0.07	-0.07	0.07		
TS-112	18-805	259.81	Py-Po-Pn-Ccp	Chalcopyrite	Ccp53	8	0.92	0.07	-0.06	0.07		
TS-112	18-805	259.81	Py-Po-Pn-Ccp	Chalcopyrite	Ccp53	9	1.05	0.07	-0.06	0.06		
TS-112	18-805	259.81	Py-Po-Pn-Ccp	Chalcopyrite	Ccp53	10	1.03	0.07	-0.04	0.07		
TS-112	18-805	259.81	Py-Po-Pn-Ccp	Chalcopyrite	Ccp53	11	1.05	0.07	-0.04	0.07		
TS-112	18-805	259.81	Py-Po-Pn-Ccp	Chalcopyrite	Ccp53	12	0.97	0.08	-0.04	0.06		
TS-112	18-805	259.81	Py-Po-Pn-Ccp	Chalcopyrite	Ccp53	13	1.10	0.07	-0.06	0.06		
TS-112	18-805	259.81	Py-Po-Pn-Ccp	Chalcopyrite	Ccp53	14	1.02	0.08	-0.08	0.07		
TS-112	18-805	259.81	Py-Po-Pn-Ccp	Chalcopyrite	Ccp53	15	1.12	0.08	-0.08	0.07		
TS-123	19-025	360.54	Py-Ccp	Pyrite	Py54	1	1.72	0.08	-0.09	0.08		
TS-123	19-025	360.54	Py-Ccp	Pyrite	Py54	2	1.63	0.08	-0.08	0.08		
TS-123	19-025	360.54	Py-Ccp	Pyrite	Py54	3	1.70	0.08	-0.02	0.08		
TS-123	19-025	360.54	Py-Ccp	Pyrite	Py54	4	1.49	0.08	-0.02	0.08		

Sample #	Drill hole	Depth (m)	Assemblage	Mineral	Crystal ID	Analysis #	δ34S (‰)	δ34S error	Δ33S (‰)	Δ33S error	Δ36S (‰)	Δ36S error
TS-123	19-025	360.54	Py-Ccp	Pyrite	Py54	5	1.54	0.08	-0.06	0.08		
TS-123	19-025	360.54	Py-Ccp	Pyrite	Py54	6	1.53	0.08	-0.03	0.08		
TS-123	19-025	360.54	Py-Ccp	Pyrite	Py54	7	1.57	0.08	-0.03	0.08		
TS-123	19-025	360.54	Py-Ccp	Pyrite	Py54	8	1.56	0.08	-0.04	0.08		
TS-123	19-025	360.54	Py-Ccp	Pyrite	Py54	9	1.69	0.08	-0.05	0.08		
TS-123	19-025	360.54	Py-Ccp	Pyrite	Py54	10	1.55	0.08	-0.13	0.08		
TS-123	19-025	360.54	Py-Ccp	Pyrite	Py54	11	1.74	0.08	-0.06	0.08		
TS-123	19-025	360.54	Py-Ccp	Pyrite	Py54	12	1.70	0.08	-0.09	0.08		
TS-123	19-025	360.54	Py-Ccp	Pyrite	Py54	13	1.65	0.08	-0.10	0.08		
TS-123	19-025	360.54	Py-Ccp	Pyrite	Py54	14	1.64	0.08	-0.06	0.08		
TS-123	19-025	360.54	Py-Ccp	Pyrite	Py54	15	1.68	0.08	-0.05	0.08		
TS-129	19-025	384.86	Py-Po-Pn-Ccp	Chalcopyrite	Ccp56	1	0.79	0.13	-0.07	0.10		
TS-129	19-025	384.86	Py-Po-Pn-Ccp	Chalcopyrite	Ccp56	2	0.99	0.11	-0.12	0.10		
TS-129	19-025	384.86	Py-Po-Pn-Ccp	Chalcopyrite	Ccp56	3	0.98	0.11	-0.08	0.10		
TS-129	19-025	384.86	Py-Po-Pn-Ccp	Chalcopyrite	Ccp56	4	0.99	0.11	-0.06	0.10		
TS-129	19-025	384.86	Py-Po-Pn-Ccp	Chalcopyrite	Ccp56	5	0.98	0.11	-0.04	0.10		
TS-129	19-025	384.86	Py-Po-Pn-Ccp	Chalcopyrite	Ccp56	6	1.01	0.11	-0.03	0.10		
TS-129	19-025	384.86	Py-Po-Pn-Ccp	Chalcopyrite	Ccp56	7	0.62	0.14	-0.07	0.11		
TS-129	19-025	384.86	Py-Po-Pn-Ccp	Chalcopyrite	Ccp56	8	0.88	0.12	-0.07	0.10		
TS-129	19-025	384.86	Py-Po-Pn-Ccp	Chalcopyrite	Ccp56	9	0.96	0.11	-0.02	0.10		
TS-129	19-025	384.86	Py-Po-Pn-Ccp	Chalcopyrite	Ccp56	10	1.10	0.11	-0.07	0.10		
TS-129	19-025	384.86	Py-Po-Pn-Ccp	Chalcopyrite	Ccp56	11	0.97	0.11	-0.08	0.10		
TS-129	19-025	384.86	Py-Po-Pn-Ccp	Chalcopyrite	Ccp56	12	0.83	0.12	-0.11	0.11		
TS-129	19-025	384.86	Py-Po-Pn-Ccp	Chalcopyrite	Ccp56	13	0.98	0.11	-0.03	0.09		
TS-129	19-025	384.86	Py-Po-Pn-Ccp	Chalcopyrite	Ccp56	14	1.02	0.11	-0.13	0.10		
TS-129	19-025	384.86	Py-Po-Pn-Ccp	Chalcopyrite	Ccp56	15	0.89	0.11	-0.08	0.10		
TS-129	19-025	384.86	Py-Po-Pn-Ccp	Pyrrhotite	Po55	1	1.23	0.13	-0.10	0.13		
TS-129	19-025	384.86	Py-Po-Pn-Ccp	Pyrrhotite	Po55	2	1.21	0.13	-0.04	0.13		
TS-129	19-025	384.86	Py-Po-Pn-Ccp	Pyrrhotite	Po55	3	1.38	0.13	-0.07	0.13		
TS-129	19-025	384.86	Py-Po-Pn-Ccp	Pyrrhotite	Po55	4	1.04	0.13	-0.11	0.13		
TS-129	19-025	384.86	Py-Po-Pn-Ccp	Pyrrhotite	Po55	5	1.23	0.13	0.00	0.13		
TS-129	19-025	384.86	Py-Po-Pn-Ccp	Pyrrhotite	Po55	6	1.02	0.13	-0.06	0.13		
TS-129	19-025	384.86	Py-Po-Pn-Ccp	Pyrrhotite	Po55	7	1.08	0.13	-0.09	0.13		
TS-129	19-025	384.86	Py-Po-Pn-Ccp	Pyrrhotite	Po55	8	1.18	0.13	-0.05	0.13		
TS-129	19-025	384.86	Py-Po-Pn-Ccp	Pyrrhotite	Po55	9	0.99	0.13	-0.03	0.13		
TS-129	19-025	384.86	Py-Po-Pn-Ccp	Pyrrhotite	Po55	10	1.11	0.13	-0.04	0.13		
TS-129	19-025	384.86	Py-Po-Pn-Ccp	Pyrrhotite	Po55	11	1.29	0.13	-0.12	0.13		
TS-129	19-025	384.86	Py-Po-Pn-Ccp	Pyrrhotite	Po55	12	1.05	0.13	-0.08	0.13		
TS-129	19-025	384.86	Py-Po-Pn-Ccp	Pyrrhotite	Po55	13	1.05	0.13	-0.03	0.13		
TS-129	19-025	384.86	Py-Po-Pn-Ccp	Pyrrhotite	Po55	14	1.11	0.13	-0.10	0.13		
TS-129	19-025	384.86	Py-Po-Pn-Ccp	Pyrrhotite	Po55	15	1.07	0.13	-0.06	0.13		
TS-129	19-025	384.86	Py-Po-Pn-Ccp	Pentlandite	Pn57	1	-0.18	0.15	-0.06	0.10	1.1	0.84
TS-129	19-025	384.86	Py-Po-Pn-Ccp	Pentlandite	Pn57	2	0.34	0.13	-0.13	0.11	0.7	0.50
TS-129	19-025	384.86	Py-Po-Pn-Ccp	Pentlandite	Pn57	3	0.31	0.15	0.02	0.11	1.4	0.41
TS-129	19-025	384.86	Py-Po-Pn-Ccp	Pentlandite	Pn57	4	-0.16	0.14	-0.05	0.12	1.2	0.44
TS-129	19-025	384.86	Py-Po-Pn-Ccp	Pentlandite	Pn57	5	-0.23	0.15	0.00	0.10	0.5	0.51
TS-133	19-025	400.44	Py-Po-Pn-Ccp	Chalcopyrite	Ccp59	1	1.22	0.15	-0.10	0.14		
TS-133	19-025	400.44	Py-Po-Pn-Ccp	Chalcopyrite	Ccp59	2	1.40	0.15	-0.09	0.14		
TS-133	19-025	400.44	Py-Po-Pn-Ccp	Chalcopyrite	Ccp59	3	1.20	0.15	-0.06	0.14		
TS-133	19-025	400.44	Py-Po-Pn-Ccp	Chalcopyrite	Ccp59	4	1.14	0.15	-0.11	0.14		
TS-133	19-025	400.44	Py-Po-Pn-Ccp	Chalcopyrite	Ccp59	5	1.52	0.15	-0.04	0.14		
TS-133	19-025	400.44	Py-Po-Pn-Ccp	Chalcopyrite	Ccp59	6	1.46	0.15	-0.06	0.14		
TS-133	19-025	400.44	Py-Po-Pn-Ccp	Chalcopyrite	Ccp59	7	1.35	0.15	-0.05	0.14		
TS-133	19-025	400.44	Py-Po-Pn-Ccp	Chalcopyrite	Ccp59	8	0.54	0.16	-0.06	0.14		
TS-133	19-025	400.44	Py-Po-Pn-Ccp	Chalcopyrite	Ccp59	9	1.39	0.15	-0.02	0.14		
TS-133	19-025	400.44	Py-Po-Pn-Ccp	Chalcopyrite	Ccp59	10	1.07	0.15	-0.06	0.14		
TS-133	19-025	400.44	Py-Po-Pn-Ccp	Chalcopyrite	Ccp59	11	1.32	0.15	-0.09	0.14		
TS-133	19-025	400.44	Py-Po-Pn-Ccp	Chalcopyrite	Ccp59	12	1.13	0.15	-0.07	0.14		
TS-133	19-025	400.44	Py-Po-Pn-Ccp	Chalcopyrite	Ccp59	13	1.52	0.15	-0.03	0.14		
TS-133	19-025	400.44	Py-Po-Pn-Ccp	Chalcopyrite	Ccp59	14	1.20	0.15	-0.04	0.14		

Sample #	Drill hole	Depth (m)	Assemblage	Mineral	Crystal ID	Analysis #	δ34S (‰)	δ34S error	Δ33S (‰)	Δ33S error	Δ36S (‰)	Δ36S error
TS-133	19-025	400.44	Py-Po-Pn-Ccp	Chalcopyrite	Ccp59	15	1.09	0.15	-0.01	0.14		
TS-133	19-025	400.44	Py-Po-Pn-Ccp	Pentlandite	Pn60	1	1.25	0.13	-0.07	0.11		
TS-133	19-025	400.44	Py-Po-Pn-Ccp	Pentlandite	Pn60	2	0.87	0.13	-0.13	0.11		
TS-133	19-025	400.44	Py-Po-Pn-Ccp	Pentlandite	Pn60	3	1.02	0.13	-0.09	0.10		
TS-133	19-025	400.44	Py-Po-Pn-Ccp	Pentlandite	Pn60	4	0.56	0.14	-0.09	0.11		
TS-133	19-025	400.44	Py-Po-Pn-Ccp	Pentlandite	Pn60	5	0.66	0.13	-0.12	0.11		
TS-133	19-025	400.44	Py-Po-Pn-Ccp	Pentlandite	Pn60	6	1.18	0.13	-0.07	0.10		
TS-133	19-025	400.44	Py-Po-Pn-Ccp	Pentlandite	Pn60	7	0.95	0.13	-0.05	0.11		
TS-133	19-025	400.44	Py-Po-Pn-Ccp	Pentlandite	Pn60	8	1.22	0.13	-0.08	0.11		
TS-133	19-025	400.44	Py-Po-Pn-Ccp	Pentlandite	Pn60	9	0.88	0.13	-0.05	0.10		
TS-133	19-025	400.44	Py-Po-Pn-Ccp	Pentlandite	Pn60	10	0.90	0.13	-0.08	0.10		
TS-141	19-025	432.44	Po-Pn-Ccp	Chalcopyrite	Ccp62	4	1.20	0.15	0.01	0.14		
TS-141	19-025	432.44	Po-Pn-Ccp	Chalcopyrite	Ccp62	5	1.80	0.15	-0.09	0.14		
TS-141	19-025	432.44	Po-Pn-Ccp	Chalcopyrite	Ccp62	6	2.07	0.15	-0.09	0.14		
TS-141	19-025	432.44	Po-Pn-Ccp	Chalcopyrite	Ccp62	7	1.88	0.15	-0.04	0.14		
TS-141	19-025	432.44	Po-Pn-Ccp	Chalcopyrite	Ccp62	8	1.96	0.15	-0.07	0.14		
TS-141	19-025	432.44	Po-Pn-Ccp	Chalcopyrite	Ccp62	9	2.15	0.15	-0.11	0.14		
TS-141	19-025	432.44	Po-Pn-Ccp	Chalcopyrite	Ccp62	10	2.04	0.15	-0.11	0.14		
TS-141	19-025	432.44	Po-Pn-Ccp	Chalcopyrite	Ccp62	11	2.07	0.15	-0.06	0.14		
TS-141	19-025	432.44	Po-Pn-Ccp	Chalcopyrite	Ccp62	12	1.76	0.15	-0.13	0.14		
TS-141	19-025	432.44	Po-Pn-Ccp	Chalcopyrite	Ccp62	13	1.87	0.15	-0.12	0.14		
TS-141	19-025	432.44	Po-Pn-Ccp	Chalcopyrite	Ccp62	14	1.84	0.15	-0.06	0.14		
TS-141	19-025	432.44	Po-Pn-Ccp	Chalcopyrite	Ccp62	15	1.54	0.15	-0.06	0.14		
TS-155	19-025	488.30	Py-Po-Pn-Ccp	Pyrite	Py39	1	1.14	0.15	-0.12	0.13		
TS-155	19-025	488.30	Py-Po-Pn-Ccp	Pyrite	Py39	2	1.48	0.15	-0.11	0.13		
TS-155	19-025	488.30	Py-Po-Pn-Ccp	Pyrite	Py39	3	0.92	0.15	-0.12	0.13		
TS-155	19-025	488.30	Py-Po-Pn-Ccp	Pyrite	Py39	4	0.93	0.15	-0.12	0.13		
TS-155	19-025	488.30	Py-Po-Pn-Ccp	Pyrite	Py39	5	0.63	0.15	-0.09	0.13		
TS-155	19-025	488.30	Py-Po-Pn-Ccp	Pyrite	Py39	6	1.87	0.15	-0.07	0.13		
TS-155	19-025	488.30	Py-Po-Pn-Ccp	Pyrite	Py39	7	1.72	0.15	-0.04	0.13		
TS-155	19-025	488.30	Py-Po-Pn-Ccp	Pyrite	Py39	8	0.89	0.15	-0.07	0.13		
TS-155	19-025	488.30	Py-Po-Pn-Ccp	Pyrite	Py39	9	1.57	0.15	-0.04	0.13		
TS-155	19-025	488.30	Py-Po-Pn-Ccp	Pyrite	Py39	10	1.16	0.15	-0.04	0.13		
TS-155	19-025	488.30	Py-Po-Pn-Ccp	Pyrite	Py39	11	0.53	0.15	-0.07	0.13		
TS-155	19-025	488.30	Py-Po-Pn-Ccp	Pyrite	Py39	12	1.06	0.15	-0.06	0.13		
TS-155	19-025	488.30	Py-Po-Pn-Ccp	Pyrite	Py39	13	0.79	0.15	-0.02	0.13		
TS-155	19-025	488.30	Py-Po-Pn-Ccp	Pyrrhotite	Po38	1	1.28	0.15	-0.03	0.13		
TS-155	19-025	488.30	Py-Po-Pn-Ccp	Pyrrhotite	Po38	2	1.35	0.14	-0.02	0.13		
TS-155	19-025	488.30	Py-Po-Pn-Ccp	Pyrrhotite	Po38	3	1.21	0.14	-0.03	0.13		
TS-155	19-025	488.30	Py-Po-Pn-Ccp	Pyrrhotite	Po38	4	1.12	0.14	-0.02	0.13		
TS-155	19-025	488.30	Py-Po-Pn-Ccp	Pyrrhotite	Po38	5	1.06	0.15	-0.03	0.13		
TS-155	19-025	488.30	Py-Po-Pn-Ccp	Pyrrhotite	Po38	6	0.81	0.15	-0.05	0.13		
TS-155	19-025	488.30	Py-Po-Pn-Ccp	Pyrrhotite	Po38	7	0.27	0.14	-0.01	0.13		
TS-155	19-025	488.30	Py-Po-Pn-Ccp	Pyrrhotite	Po38	8	0.79	0.14	0.01	0.13		
TS-155	19-025	488.30	Py-Po-Pn-Ccp	Pyrrhotite	Po38	9	0.93	0.14	-0.06	0.13		
TS-155	19-025	488.30	Py-Po-Pn-Ccp	Pyrrhotite	Po38	10	1.03	0.14	-0.04	0.13		
TS-155	19-025	488.30	Py-Po-Pn-Ccp	Pyrrhotite	Po38	11	1.04	0.14	-0.04	0.13		
TS-155	19-025	488.30	Py-Po-Pn-Ccp	Pyrrhotite	Po38	12	1.10	0.14	-0.04	0.13		
TS-155	19-025	488.30	Py-Po-Pn-Ccp	Pyrrhotite	Po38	13	1.15	0.14	-0.05	0.13		
TS-155	19-025	488.30	Py-Po-Pn-Ccp	Pyrrhotite	Po38	14	1.49	0.14	-0.06	0.13		
TS-155	19-025	488.30	Py-Po-Pn-Ccp	Pyrrhotite	Po38	15	1.25	0.14	-0.05	0.13		
TS-155	19-025	488.30	Py-Po-Pn-Ccp	Pyrrhotite	Po40	1	0.85	0.14	-0.04	0.13		
TS-155	19-025	488.30	Py-Po-Pn-Ccp	Pyrrhotite	Po40	2	1.20	0.14	-0.03	0.13		
TS-155	19-025	488.30	Py-Po-Pn-Ccp	Pyrrhotite	Po40	3	1.27	0.14	-0.02	0.13		
TS-155	19-025	488.30	Py-Po-Pn-Ccp	Pyrrhotite	Po40	4	1.31	0.14	-0.05	0.13		
TS-155	19-025	488.30	Py-Po-Pn-Ccp	Pyrrhotite	Po40	5	1.12	0.14	-0.05	0.13		
TS-155	19-025	488.30	Py-Po-Pn-Ccp	Pyrrhotite	Po40	6	1.12	0.14	-0.01	0.13		
TS-155	19-025	488.30	Py-Po-Pn-Ccp	Pyrrhotite	Po40	7	1.19	0.15	0.03	0.13		
TS-155	19-025	488.30	Py-Po-Pn-Ccp	Pyrrhotite	Po40	8	1.09	0.15	-0.03	0.13		
TS-155	19-025	488.30	Py-Po-Pn-Ccp	Pyrrhotite	Po40	9	1.12	0.14	-0.02	0.13		

Sample #	Drill hole	Depth (m)	Assemblage	Mineral	Crystal ID	Analysis #	δ34S (‰)	δ34S error	Δ33S (‰)	Δ33S error	Δ36S (‰)	Δ36S error
TS-155	19-025	488.30	Py-Po-Pn-Ccp	Pyrrhotite	Po40	10	1.15	0.14	-0.03	0.13		
TS-155	19-025	488.30	Py-Po-Pn-Ccp	Pyrrhotite	Po40	11	1.22	0.15	-0.03	0.13		
TS-189	19-009	68.00	Py-Ccp	Pyrite	Py64	1	0.92	0.09	-0.04	0.11		
TS-189	19-009	68.00	Py-Ccp	Pyrite	Py64	2	0.17	0.09	-0.04	0.11		
TS-189	19-009	68.00	Py-Ccp	Pyrite	Py64	3	1.07	0.09	-0.08	0.11		
TS-189	19-009	68.00	Py-Ccp	Pyrite	Py64	4	1.08	0.09	-0.02	0.11		
TS-189	19-009	68.00	Py-Ccp	Pyrite	Py64	5	1.19	0.09	-0.12	0.11		
TS-189	19-009	68.00	Py-Ccp	Pyrite	Py64	6	0.99	0.09	-0.06	0.11		
TS-189	19-009	68.00	Py-Ccp	Pyrite	Py64	7	0.90	0.10	-0.10	0.11		
TS-189	19-009	68.00	Py-Ccp	Pyrite	Py64	8	0.86	0.09	-0.05	0.11		
TS-189	19-009	68.00	Py-Ccp	Chalcopyrite	Ccp65	1	-0.27	0.12	-0.03	0.11		
TS-189	19-009	68.00	Py-Ccp	Chalcopyrite	Ccp65	2	-0.22	0.12	-0.08	0.11		
TS-189	19-009	68.00	Py-Ccp	Chalcopyrite	Ccp65	3	-0.39	0.12	-0.07	0.11		
TS-197	19-009	84.00	Py-Ccp	Pyrite	Py66	1	1.70	0.09	-0.09	0.11		
TS-197	19-009	84.00	Py-Ccp	Pyrite	Py66	2	1.71	0.09	-0.09	0.11		
TS-197	19-009	84.00	Py-Ccp	Pyrite	Py66	3	1.70	0.09	-0.07	0.11		
TS-197	19-009	84.00	Py-Ccp	Pyrite	Py66	4	1.64	0.09	-0.05	0.11		
TS-197	19-009	84.00	Py-Ccp	Pyrite	Py66	5	1.41	0.09	-0.06	0.11		
TS-197	19-009	84.00	Py-Ccp	Pyrite	Py66	6	1.56	0.09	-0.09	0.11		
TS-197	19-009	84.00	Py-Ccp	Pyrite	Py66	7	1.55	0.10	0.00	0.11		
TS-197	19-009	84.00	Py-Ccp	Pyrite	Py66	8	1.73	0.09	-0.11	0.11		
TS-197	19-009	84.00	Py-Ccp	Pyrite	Py66	9	1.58	0.09	-0.03	0.11		
TS-197	19-009	84.00	Py-Ccp	Pyrite	Py66	10	1.60	0.09	-0.04	0.11		
TS-197	19-009	84.00	Py-Ccp	Pyrite	Py66	11	1.49	0.09	-0.04	0.11		
TS-197	19-009	84.00	Py-Ccp	Pyrite	Py66	12	1.88	0.09	-0.02	0.11		
TS-197	19-009	84.00	Py-Ccp	Pyrite	Py66	13	1.87	0.09	-0.05	0.11		
TS-197	19-009	84.00	Py-Ccp	Pyrite	Py66	14	1.68	0.09	-0.04	0.11		
TS-197	19-009	84.00	Py-Ccp	Pyrite	Py66	15	1.50	0.09	-0.05	0.11		
TS-197	19-009	84.00	Py-Ccp	Pyrite	Py67	1	1.73	0.09	-0.10	0.11		
TS-197	19-009	84.00	Py-Ccp	Pyrite	Py67	2	1.69	0.09	-0.08	0.11		
TS-197	19-009	84.00	Py-Ccp	Pyrite	Py67	3	1.91	0.09	-0.09	0.11		
TS-197	19-009	84.00	Py-Ccp	Pyrite	Py67	4	1.36	0.10	-0.04	0.11		
TS-197	19-009	84.00	Py-Ccp	Pyrite	Py67	5	1.41	0.09	-0.08	0.11		
TS-197	19-009	84.00	Py-Ccp	Pyrite	Py67	6	1.62	0.09	-0.10	0.11		
TS-197	19-009	84.00	Py-Ccp	Pyrite	Py67	7	1.46	0.09	-0.01	0.11		
TS-197	19-009	84.00	Py-Ccp	Pyrite	Py67	8	1.59	0.09	-0.09	0.11		
TS-197	19-009	84.00	Py-Ccp	Pyrite	Py67	9	1.50	0.09	-0.06	0.11		
TS-197	19-009	84.00	Py-Ccp	Pyrite	Py67	10	1.51	0.09	-0.12	0.11		
TS-197	19-009	84.00	Py-Ccp	Pyrite	Py67	11	1.60	0.09	-0.04	0.11		
TS-197	19-009	84.00	Py-Ccp	Pyrite	Py67	12	1.56	0.09	-0.08	0.11		
TON-01	N/A	N/A	Py	Pyrite	Py68	1	2.07	0.09	-0.07	0.10		
TON-01	N/A	N/A	Py	Pyrite	Py68	2	2.28	0.09	-0.08	0.10		
TON-01	N/A	N/A	Py	Pyrite	Py68	3	2.46	0.09	-0.09	0.10		
TON-01	N/A	N/A	Py	Pyrite	Py68	4	1.71	0.09	-0.09	0.10		
TON-01	N/A	N/A	Py	Pyrite	Py68	5	2.21	0.09	-0.11	0.10		
TON-01	N/A	N/A	Py	Pyrite	Py68	6	3.12	0.09	-0.03	0.10		
TON-01	N/A	N/A	Py	Pyrite	Py68	7	2.15	0.09	-0.07	0.10		
TON-01	N/A	N/A	Py	Pyrite	Py68	8	2.40	0.09	-0.08	0.10		
TON-01	N/A	N/A	Py	Pyrite	Py68	9	1.89	0.09	-0.04	0.10		
TON-01	N/A	N/A	Py	Pyrite	Py68	10	2.53	0.09	-0.09	0.10		
TON-01	N/A	N/A	Py	Pyrite	Py68	11	2.47	0.09	-0.05	0.10		
TON-01	N/A	N/A	Py	Pyrite	Py68	12	2.79	0.09	-0.09	0.10		
TON-01	N/A	N/A	Py	Pyrite	Py68	13	2.70	0.09	-0.10	0.10		
TON-01	N/A	N/A	Py	Pyrite	Py68	14	2.82	0.09	-0.12	0.10		
TON-01	N/A	N/A	Py	Pyrite	Py68	15	2.43	0.10	-0.09	0.10		
TON-02	N/A	N/A	Py	Pyrite	Py69	1	2.16	0.10	-0.11	0.08		
TON-02	N/A	N/A	Py	Pyrite	Py69	2	1.21	0.10	-0.14	0.08		
TON-02	N/A	N/A	Py	Pyrite	Py69	3	2.14	0.10	-0.15	0.08		
TON-02	N/A	N/A	Py	Pyrite	Py69	4	2.13	0.10	-0.06	0.08		
TON-02	N/A	N/A	Py	Pyrite	Py69	5	1.93	0.10	-0.18	0.08		

Sample #	Drill hole	Depth (m)	Assemblage	Mineral	Crystal ID	Analysis #	δ34S (‰)	δ34S error	Δ33S (‰)	Δ33S error	Δ36S (‰)	Δ36S error
TON-02	N/A	N/A	Py	Pyrite	Py69	6	1.88	0.10	-0.10	0.08		
TON-02	N/A	N/A	Py	Pyrite	Py69	7	1.95	0.10	-0.08	0.08		
TON-02	N/A	N/A	Py	Pyrite	Py69	8	1.61	0.10	-0.09	0.08		
TON-02	N/A	N/A	Py	Pyrite	Py69	9	1.77	0.10	-0.05	0.08		
TON-02	N/A	N/A	Py	Pyrite	Py69	10	2.08	0.10	-0.07	0.08		
TON-02	N/A	N/A	Py	Pyrite	Py69	11	1.70	0.10	-0.07	0.08		
TON-02	N/A	N/A	Py	Pyrite	Py69	12	1.93	0.10	-0.09	0.08		
TON-02	N/A	N/A	Py	Pyrite	Py69	13	1.56	0.10	-0.11	0.08		
TON-02	N/A	N/A	Py	Pyrite	Py69	14	1.60	0.10	-0.09	0.08		
TON-02	N/A	N/A	Py	Pyrite	Py69	15	1.93	0.10	-0.09	0.08		

Appendix D

Neodymium Isotope Data

Sample	LDI-JJ-Nd-01	LDI-JJ-Nd-02	LDI-JJ-Nd-03	LDI-JJ-Nd-04	LDI-JJ-Nd-05	LDI-JJ-Nd-06
Drill hole	17-804	17-804	17-804	17-804	17-804	17-804
Depth from	145	155	185	200	240	258
Depth to	146	156	186	201	241	259
Domain	Breccia	Breccia	Breccia	Breccia	Breccia	Norite
Age	2689	2689	2689	2689	2689	2689
Nd (ppm)	1.816	2.944	2.284	2.625	3.588	1.806
Sm (ppm)	1.463	2.692	1.898	2.331	3.115	1.547
Current $^{143}Nd/^{144}Nd$ (Sm corr.)	0.511999	0.512195	0.511961	0.512178	0.512073	0.512137
$^{143}Nd/^{144}Nd$ error (2SE)	0.0000154	0.0000070	0.0000076	0.0000074	0.0000050	0.0000064
Current $^{144}Nd/^{145}Nd$ (Sm corr.)	0.348409	0.348400	0.348409	0.348409	0.348408	0.348404
$^{144}Nd/^{145}Nd$ error (2SE)	0.0000092	0.0000037	0.0000042	0.0000042	0.0000027	0.0000035
$^{147}Sm/^{144}Nd$	0.159578	0.181097	0.164585	0.175915	0.171952	0.169727
Initial $^{143}Nd/^{144}Nd$	0.50917	0.50898	0.50904	0.50906	0.50902	0.50913
εNd	0.384	-3.271	-2.099	-1.787	-2.469	-0.437

Sample	LDI-JJ-Nd-07	LDI-JJ-Nd-08	LDI-JJ-Nd-09	LDI-JJ-Nd-10	LDI-JJ-Nd-11	LDI-JJ-Nd-12
Drill hole	17-804	17-804	17-804	19-025	19-025	19-025
Depth from	266	280	298	334	364	384
Depth to	267	281	299	335	365	385
Domain	Norite	Norite	Norite	Norite	Norite	Norite
Age	2689	2689	2689	2689	2689	2689
Nd (ppm)	2.339	2.510	2.411	2.235	3.202	1.425
Sm (ppm)	1.822	1.981	1.789	1.841	2.904	1.295
Current $^{143}Nd/^{144}Nd$ (Sm corr.)	0.511772	0.511744	0.511700	0.511935	0.512270	0.512247
$^{143}Nd/^{144}Nd$ error (2SE)	0.0000086	0.0000061	0.0000076	0.0000166	0.0000068	0.0000194
Current $^{144}Nd/^{145}Nd$ (Sm corr.)	0.348404	0.348411	0.348408	0.348416	0.348414	0.348411
$^{144}Nd/^{145}Nd$ error (2SE)	0.0000042	0.0000030	0.0000039	0.0000094	0.0000029	0.0000103
$^{147}Sm/^{144}Nd$	0.154335	0.156283	0.146958	0.163164	0.179640	0.180105
Initial $^{143}Nd/^{144}Nd$	0.50903	0.50897	0.50909	0.50904	0.50908	0.50905
εNd	-2.247	-3.472	-1.094	-2.129	-1.293	-1.890

Sample	LDI-JJ-Nd-13	LDI-JJ-Nd-14	LDI-JJ-Nd-15	LDI-JJ-Nd-16	LDI-JJ-Nd-17	LDI-JJ-Nd-18
Drill hole	19-025	19-025	19-009	19-009	19-009	19-009
Depth from	398	482	22	46	64	70
Depth to	399	483	23	47	65	71
Domain	Norite	Breccia	Norite	Norite	Norite	Breccia
Age	2689	2689	2689	2689	2689	2689
Nd (ppm)	2.490	1.131	1.475	1.606	1.846	1.243
Sm (ppm)	2.041	0.289	0.448	0.467	0.572	0.361
Current $^{143}Nd/^{144}Nd$ (Sm corr.)	0.511913	0.511781	0.512282	0.512230	0.512325	0.512138
$^{143}Nd/^{144}Nd$ error (2SE)	0.0000070	0.0000144	0.0000085	0.0000058	0.0000051	0.0000073
Current $^{144}Nd/^{145}Nd$ (Sm corr.)	0.348411	0.348416	0.348410	0.348412	0.348412	0.348406
$^{144}Nd/^{145}Nd$ error (2SE)	0.0000036	0.0000085	0.0000041	0.0000031	0.0000027	0.0000043
$^{147}Sm/^{144}Nd$	0.162374	0.154394	0.183830	0.175958	0.187493	0.175778
Initial $^{143}Nd/^{144}Nd$	0.50903	0.50904	0.50902	0.50911	0.50900	0.50902
εNd	-2.278	-2.093	-2.504	-0.793	-2.933	-2.530

Sample	LDI-JJ-Nd-19
Drill hole	19-009
Depth from	76
Depth to	77
Domain	Breccia
Age	2689
Nd (ppm)	0.771
Sm (ppm)	0.183
Current $^{143}Nd/^{144}Nd$ (Sm corr.)	0.511573
$^{143}Nd/^{144}Nd$ error (2SE)	0.0000173
Current $^{144}Nd/^{145}Nd$ (Sm corr.)	0.348407
$^{144}Nd/^{145}Nd$ error (2SE)	0.0000100
$^{147}Sm/^{144}Nd$	0.143316
Initial $^{143}Nd/^{144}Nd$	0.50903
εNd	-2.320